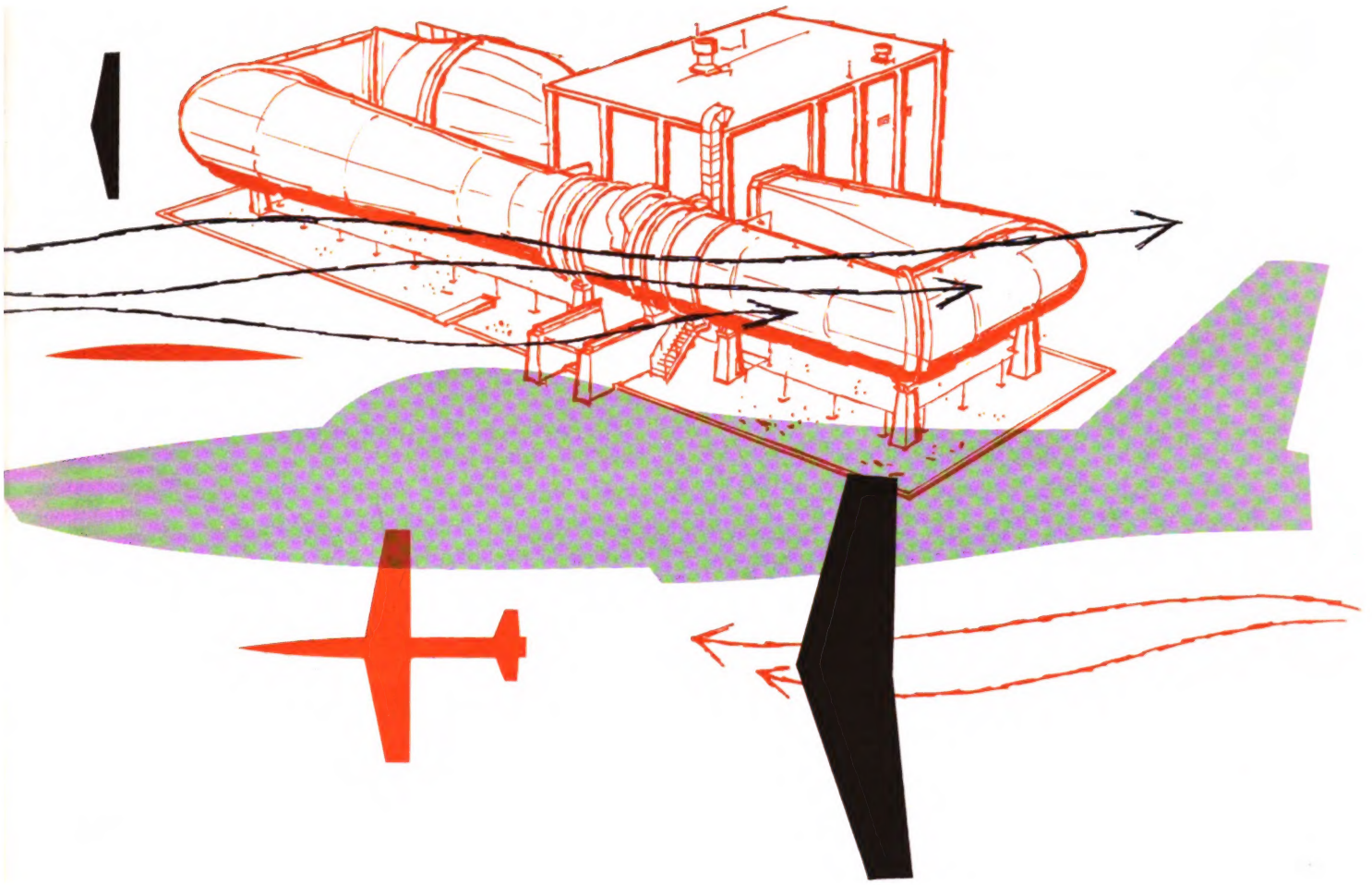

DYNAMICS OF THE AIRFRAME

AE-6-4-II

NORAIR A DIVISION OF NORTHROP CORPORATION

BUREAU OF AERONAUTICS
FLIGHT CONTROL SYSTEM MANUALS

This series was originally prepared by Norair under Bureau of Aeronautics sponsorship to correlate the new and expanding techniques of automatic, powered control systems.

Continuing interest in these manuals, expressed by educational and industrial agencies, affirms the need for authoritative documents presenting technology of this scientific area.

In response Norair is offering, with Bureau of Aeronautics permission and encouragement, special reprints of the entire series of manuals to all interested individuals and agencies. Our objective is to contribute to understanding and advancing the state-of-the-art.

A list of the other volumes in this series, including printing costs, may be found on the last page of this manual.

BU AER

REPORT AE-61-4 II

DYNAMICS OF THE AIRFRAME

BASIC VOLUME

WRITTEN AND EDITED BY SERVOMECHANISMS SECTION AND AERODYNAMICS SECTION

NORTHROP AIRCRAFT, INC.

CONTRIBUTIONS TO VOLUME BY OTHER AUTHORS ARE NOTED IN INDIVIDUAL SECTIONS IN ACCORDANCE WITH "IMPORTANT NOTE" ON FOLLOWING PAGE

PREPARATION OF VOLUME SPONSORED BY

BUREAU OF AERONAUTICS, NAVY DEPARTMENT

SEPTEMBER, 1952

IMPORTANT NOTE

This volume was written by and for engineers and scientists who are concerned with the analysis and synthesis of piloted aircraft flight control systems. The Bureau of Aeronautics undertook the sponsorship of this project when it become apparent that many significant advances were being made in this extremely technical field and that the presentation and dissemination of information concerning such advances would be of benefit to the Services, to the airframe companies, and to the individuals concerned.

A contract for collecting, codifying, and presenting this scattered material was awarded to Northrop Aircraft, Inc., and the present basic volume represents the the results of these efforts.

The need for such a volume as this is obvious to those working in the field. It is equally apparent that the rapid changes and refinements in the techniques used make it essential that new material be added as it becomes available. The best way of maintaining and improving the usefulness of this volume is therefore by frequent revisions to keep it as complete and as up-to-date as possible.

For these reasons, the Bureau of Aeronautics solicits suggestions for revisions and additions from those who make use of the volume. In some cases, these suggestions might be simply that the wording of a paragraph be changed for clarification; in other cases, whole sections outlining new techniques might be submitted.

Each suggestion will be acknowledged and will receive careful study. For those which are approved, revision pages will be prepared and distributed. Each of these will contain notations as necessary to give full credit to the person and organization responsible.

This cooperation on the part of the readers of this volume is vital. Suggestions forwarded to the Chief, Bureau of Aeronautics, (Attention AE-612), Washington 25, D. C., will be most welcome.

L. M. Chattler
Head, Actuating & Flight Controls Systems Section
Airborne Equipment Division
Bureau of Aeronautics

PREFACE

This volume, "Dynamics of the Airframe," has been written under BuAer Contract NO as 51-514(c), in order to present to those concerned with the problems of designing integrated aircraft controls systems certain basic information regarding aerodynamic stability and control.

The purpose of this volume is to present those elements of aerodynamic stability and control that describe the airframe as a dynamic component of a control system. This volume is written for the college graduate who has had training in system engineering with the intent of providing him with the basic knowledge of rigid body airframe dynamics that bears directly on aircraft control system design. No attempt has been made to give anywhere near complete coverage to the subject of aerodynamic stability and control; but rather, the attempt has been to give the system designer enough of the fundamentals so that he may work more closely with skilled aerodynamicists.

The approach used in this volume has been to describe the transient behavior of the airframe through the transfer function. Special attention has been given to the use of an analog computer as a design tool and the Bode chart method of presenting results. Also included is a detailed discussion of the stability derivatives that enter the transfer functions. In these respects, it is hoped that this volume may also be of some value to the practicing aerodynamicist.

D. T. McRuer, Supervisor
Servomechanisms Section

C. L. Bates, Director
Mechanical Design Department

I. L. Ashkenas, Director
Aerodynamics Department

CONTRIBUTING AUTHORS

F. R. Nelson
W. Koerner
R. E. Trudel

EDITORIAL BOARD

A. M. Eichen
R. Halliday
J. Moser
E. Moness
K. B. Tuttle

TABLE OF CONTENTS

CHAPTER I

INTRODUCTION

The airframe is a prime unalterable component of the aircraft control system. The control system also contains various mechanical and electrical components and includes a human pilot. The basic purpose of this volume is to construct and to discuss a mathematical model, of use to the system designer, of the airframe component of the overall system.

The motion of an airframe in flight is determined by the propulsive forces supplied by the power plant, the force of gravity, the inertial characteristics of the airplane and aerodynamic forces. To derive the equations of motion of the airframe, it is necessary to equate the forces and moments acting on the airframe to the craft reactions, according to Newton's laws. The transfer functions relating to motion of the airframe to a given force can then be determined by solving the equations of motion. The transfer functions completely describe the transient motion of the airframe within the limits of the approximations made during their derivation. The transfer functions for various control deflections are derived in Chapter II.

Chapter III is devoted to an investigation of the characteristic motions of the airframe by analysis of the transfer functions, which are expressed as ratios of polynomials in the complex variable s. Useful approximations to the time constants, natural frequencies and dampings contained in these polynomials will be presented, along with a comparison of the exact and approximate results. These approximate results will then be used to demonstrate the effects of various factors contained in the transfer functions on the characteristic motions of the airframe. The effect of the flight condition of the airframe on motions caused by control surface deflections will be investigated by analyzing results of solutions of the equations of motion from an analog computer.

Chapter IV presents a detailed discussion of the aerodynamic coefficients which are included in the transfer functions. These coefficients are analyzed in relation to the various factors that must be considered in their determination.

Methods of obtaining numerical values for the aerodynamic coefficients are discussed in Chapter V.

CHAPTER II

DERIVATION OF THE AIRFRAME TRANSFER FUNCTIONS

SECTION 1 – INTRODUCTION

In this chapter, the transfer functions relating airframe motion to control deflection are derived. The controls considered are elevator, ailerons, rudder, throttle, flaps, and dive brakes.

The equations of motion of an airframe are written by equating the forces and moments acting on the airframe to the craft reactions, in accordance with Newton's laws. It is shown that a set of Eulerian axes may be used advantageously as a frame of reference for writing such equations, and the properties of this axis system are then discussed. The theory of small perturbations is introduced into the derivation to arrive at linear equations, and the restrictions that must be imposed on these equations to permit consideration of the so-called longitudinal motions of the airframe independently of the lateral motions are described.

Laplace transforms and determinants are used to solve the equations of motion for the transfer functions. Throughout the derivation of these transfer functions, assumptions are made that partially restrict the range of validity of these transfer functions. The assumptions are discussed when introduced and are restated at the end of the chapter.

SECTION 2 – EQUATIONS OF MOTION OF AN AIRFRAME WITH RESPECT TO AXES FIXED IN SPACE

In this section, the equations of motion of an airframe are derived according to Newton's laws, that is, with reference to axes fixed in space.

ASSUMPTION I. The airframe is assumed to be a rigid body.

A rigid body is defined as one in which the distances between any specified points in the body are invariant. This assumption eliminates consideration of forces acting between individual elements of mass, and it allows the airframe motion to be described completely by a translation of the center of gravity and by a rotation about this point.

The derivation of the equations of motion incorporates this assumption, and later some of the effects of aeroelastic deflection are discussed. (An example of aeroelastic deflection is wing bending caused by the aerodynamic loads.)

Since all motion is relative, a suitable frame of reference describing airframe motion must be selected; to meet this requirement, the following assumption is made:

ASSUMPTION II. The earth is assumed to be fixed in space, and, unless specifically stated otherwise, the earth's atmosphere is assumed to be fixed with respect to the earth.

This assumption provides the needed frame of reference without imposing any practical limitations on the equations to be derived.

Consider the motion of an airplane referred to a right-hand system of Cartesian axes fixed in space. The airplane has a mass m, a linear velocity $\bar{V}$, and an angular velocity $\bar{\omega}$. The component quantities related to these inertial axes are illustrated in Figure II-1 and tabulated in Table II-1.

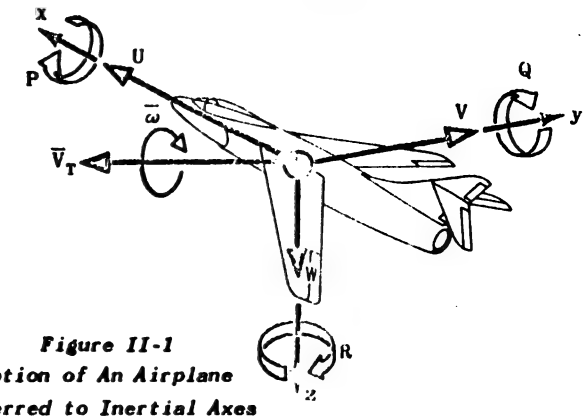

Figure II-1
Motion of An Airplane
Referred to Inertial Axes

Newton's second law of motion states that the rate of change of momentum of a body is proportional to the force applied to the body and that the rate of change of the moment of momentum is proportional to the torque applied to the body. (II-1) and (II-2) are mathematical statements of this law:

(II-1)
$$\Sigma F_x = \frac{d}{dt}(mU)$$
$$\Sigma F_y = \frac{d}{dt}(mV)$$
$$\Sigma F_z = \frac{d}{dt}(mW)$$

(II-2)
$$\Sigma L = \frac{dh_x}{dt}$$
$$\Sigma M = \frac{dh_y}{dt}$$
$$\Sigma N = \frac{dh_z}{dt}$$

where ΣF_x, ΣF_y, and ΣF_z are the summations of the components of applied force parallel to the x, y, and z axes respectively; where ΣL, ΣM, and ΣN are the summations of the components of the applied moment about the x, y, and z axes respectively; and where h_x, h_y, and h_z are the components of the moment of momentum about the x, y, and z axes respectively.

airplane after all fuel is expended, but the time rate of change of mass due to fuel consumption is relatively small and may be safely neglected for the periods of time required for most analyses. (The effect of firing ammunition and dropping external stores is considered in Section 4 of Chapter IV.)

Many of the following pages are devoted to an expansion of equations (II-2) by investigating the dynamics of an infinitesimal element of mass dm of the airplane shown in Figure II-1.

Figure II-2 shows the components of linear velocity of dm due to angular velocity $\bar{\omega}$. The accuracy of this representation can be verified by multiplying the proper components of angular velocity and displacement according to the right-hand rule for vector quantities.

The components of the moment of momentum are calculated by summing the moments of these velocity vectors about each axis and multiplying by the mass dm.

Axis	Linear Velocity Along Axis	Angular Velocity Along Axis	Summation of Moments About Axis	Summation of Forces Along Axis	Displacements About Axis	Moments of Momentum About Axis	Moment of Inertia
x	U	P Rolling Vel.	ΣL	ΣF_x	Φ	h_x	I_{xx}
y	V	Q Pitching Vel.	ΣM	ΣF_y	θ	h_y	I_{yy}
z	W	R Yawing Vel.	ΣN	ΣF_z	Ψ	h_z	I_{zz}

Table II-1 Notation

To allow the mass of the airplane to be written outside the differentiation sign in (II-1), another assumption is made:

ASSUMPTION III. The mass of the airplane is assumed to remain constant for the duration of any particular dynamic analysis.

Actually, there is considerable difference in mass between an airplane carrying a full fuel load and the same

For example:

$$dh_x = y(yP)dm + z(zP)dm - z(xR)dm - y(xQ)dm$$

The set of equations obtained in this way consists of:

(II-3)
$$dh_x = (y^2 + z^2)\,P\,dm - zx\,R\,dm - yx\,Q\,dm$$
$$dh_y = (z^2 + x^2)\,Q\,dm - xy\,P\,dm - yz\,R\,dm$$
$$dh_z = (x^2 + y^2)\,R\,dm - zx\,P\,dm - zy\,Q\,dm$$

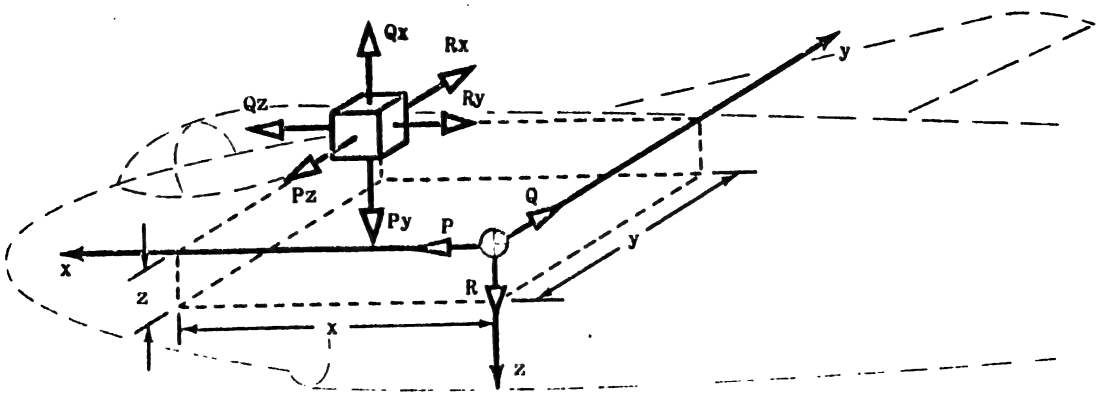

Figure II-2 Linear Velocity Components of an Element of Mass Due to an Angular Velocity $\bar{\omega}$ Having Components P, Q, and R

For a finite mass, the components of the moment of momentum are the integrals of (II-3) over the entire mass:

$$(II\text{-}4)\qquad \begin{aligned} h_x &= P\int(y^2+z^2)\,dm - Q\int xy\,dm - R\int xz\,dm \\ h_y &= Q\int(z^2+x^2)\,dm - R\int yz\,dm - P\int yx\,dm \\ h_z &= R\int(x^2+y^2)\,dm - P\int zx\,dm - Q\int zy\,dm \end{aligned}$$

The integral $\int(y^2+z^2)\,dm$ is defined as the moment of inertia, I_{xx}, of the entire mass of the airplane about the x-axis. Similarly, the integral $\int xy\,dm$ is defined as the product of inertia, I_{xy}. The remaining integrals in (II-4) are similarly defined and the equations may be rewritten as:

$$(II\text{-}5)\qquad \begin{aligned} h_x &= P I_{xx} - Q I_{xy} - R I_{xz} \\ h_y &= Q I_{yy} - R I_{yz} - P I_{xy} \\ h_z &= R I_{zz} - P I_{xz} - Q I_{yz} \end{aligned}$$

where $I_{yz} = I_{zy}$, from the form of the integrals.

The derivative $\frac{dh}{dt}$ may be found by differentiating each of (II-5) with respect to time. When these rates of change of moment of momentum of an aircraft are substituted in (II-2), the equations of motion relative to inertial axes become:

$$(II\text{-}6)\qquad \begin{aligned} \Sigma F_x &= m\frac{dU}{dt} \\ \Sigma F_y &= m\frac{dV}{dt} \\ \Sigma F_z &= m\frac{dW}{dt} \end{aligned}$$

$$\Sigma L = \frac{dh_x}{dt} = \dot{P}I_{xx} + P\dot{I}_{xx} - \dot{Q}I_{xy} - Q\dot{I}_{xy} - \dot{R}I_{xz} - R\dot{I}_{xz}$$

$$\Sigma M = \frac{dh_y}{dt} = \dot{Q}I_{yy} + Q\dot{I}_{yy} - \dot{R}I_{yz} - R\dot{I}_{yz} - \dot{P}I_{xy} - P\dot{I}_{xy}$$

$$\Sigma N = \frac{dh_z}{dt} = \dot{R}I_{zz} + R\dot{I}_{zz} - \dot{P}I_{xz} - P\dot{I}_{xz} - \dot{Q}I_{zy} - Q\dot{I}_{zy}$$

SECTION 3 – EQUATIONS OF MOTION WITH RESPECT TO EULERIAN AXES

The equations of motion written with respect to fixed axes, (II-6), could be used to describe the motion of an airplane as a function of time, but there are reasons why it is expedient for this purpose to use an Eulerian axis system. In this section, the nature of Eulerian axes and the reasons for their use are discussed, and the equations of motion of an airframe are expressed in terms of quantities measured relative to these axes.

Consider an airplane flying with an absolute linear velocity, $\bar{V}_T$, and an angular velocity, $\bar{\omega}$, about its center of gravity. At every instant, another right-hand system of orthogonal coordinate axes (x_1, y_1, z_1), fixed in space, and originating at the center of gravity, can be superimposed on the airframe. At each instant, the orientation of these axes relative to the airframe is the same. With respect to this axis system, the airframe has linear and angular velocities and accelerations but no displacements. Figure II-3 shows the airframe with superimposed axes at three different instants along its flight path. It may be noticed that the velocity vector is not necessarily aligned with any particular axis.

Suppose three instruments which read absolute linear velocity are mounted in the airframe at the center of gravity. If these instruments are aligned with the three axes, x_1, y_1, z_1, they resolve the absolute linear velocity, $\bar{V}_T$, into its three components along these axes. According to the notation in Table II-1, these component velocities are U_1, V_1, and W_1, along the x_1, y_1, and z_1 axes respectively.

At any instant during the flight of the airplane, these instruments measure the linear velocity of the airplane relative to fixed space. However, because these instruments and their axes are fixed to the airframe, they have the same instantaneous angular velocity as the airplane, a factor which must be taken into account when writing the expression for the absolute acceleration of the airplane in terms of the velocity measured by these instruments. For instance, suppose an airplane is flying at constant speed with a constant angular velocity. These conditions are met when an airplane flies in a circular flight path as in Figure II-4.

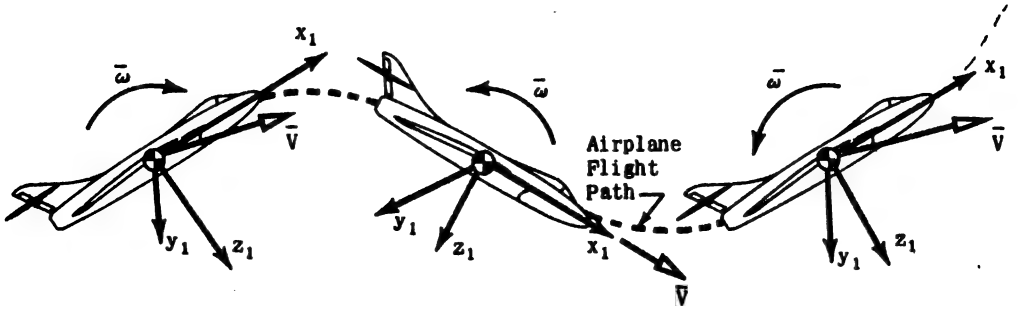

Figure II-3 Motion of Airplane with Superimposed Axes

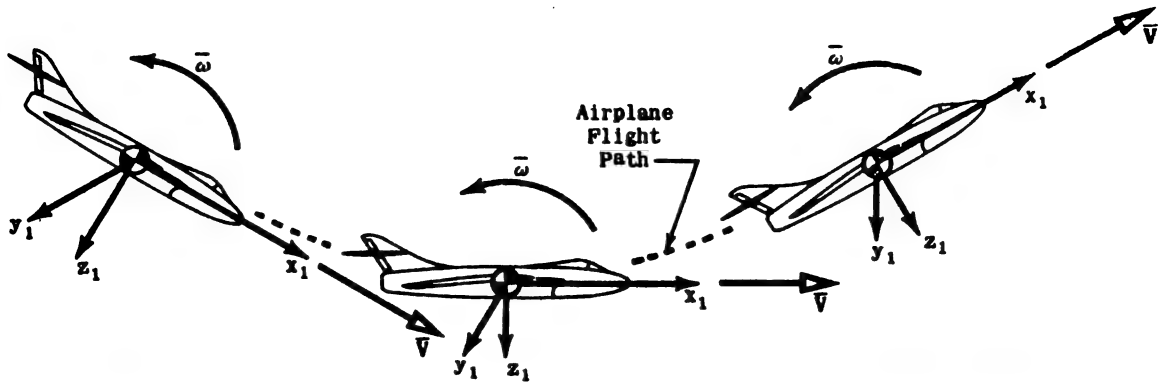

Figure II-4 Airplane in Flight with Constant Speed and Constant Angular Velocity

It may be seen from this figure that the velocity vector measured by the instruments is invariant relative to the x_1, y_1, and z_1 axes.

However, the airplane is in accelerated flight because of its circular flight path and must therefore have a centripetal acceleration. For the conditions shown in Figure II-4, this centripetal acceleration is the only acceleration of the airplane, and it can be expressed as the vector cross product of the angular velocity $\bar{\omega}$ and the linear velocity $\bar{V}_T$:

$$\bar{a} = \bar{\omega} \times \bar{V}_T \qquad \text{(II-7)}$$

where the instantaneous linear velocity, $\bar{V}_T$, is measured relative to the x_1, y_1, and z_1 axes.

An airplane flying with varying linear velocity and zero angular velocity corresponds to an airplane flying along a straight flight path with varying speed as in Figure II-5.

where $\bar{V}_T$ is again measured relative to x_1, y_1, and z_1 axes.

For an airplane having both an angular velocity and a varying linear velocity measured with respect to axes such as x_1, y_1, z_1, the expression for the absolute acceleration (i.e., the acceleration measured relative to inertial axes) can be determined by combining (II-7) and (II-8) to form the equation:

$$\bar{a}_{abs} = \frac{d\bar{V}_T}{dt} + \bar{\omega} \times V_T \qquad \text{(II-9)}$$

An expression for the rate of change of the moment of momentum in terms of quantities measured relative to the x_1, y_1, and z_1 axes can be determined in a similar way. Suppose three rate gyroscopes are mounted in the airplane at the center of gravity so that they are aligned with the x_1, y_1, and z_1 axes. These gyroscopes then measure the three components of the instantaneous angular velocity of the airplane relative to fixed space. By using the notation in Table II-1 again, these component velocities are called P_1, Q_1, and R_1 about the

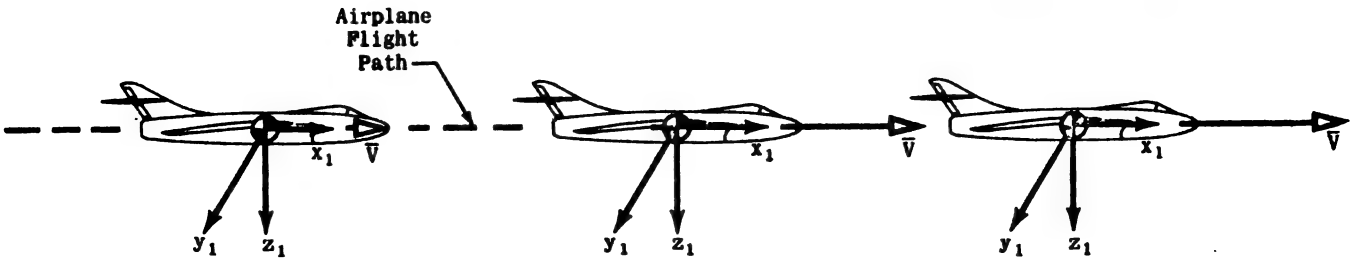

Figure II-5 Airplane in Flight with Varying Forward Velocity and Zero Angular Velocity

The forward velocity vector measured relative to the x_1, y_1, and z_1 axes varies with time. The airplane is thus in accelerated flight, and this acceleration is equal to the rate of change of the velocity as expressed in the equation:

$$\bar{a} = \frac{d\bar{V}_T}{dt} \qquad \text{(II-8)}$$

x_1, y_1, and z_1 axes respectively. Since these velocities are the instantaneous absolute angular velocities of the airplane, the expressions for the components of the moment of momentum derived in Section II-1 and written in (II-5) are applicable to the x_1, y_1, and z_1 axes.

Equations (II-5) are rewritten below in terms of quantities referred to the x_1, y_1, and z_1 axes.

(II-10)
$$h_x = P_1 I_{xx} - Q_1 I_{xy} - R_1 I_{xz}$$
$$h_y = Q_1 I_{yy} - R_1 I_{yz} - P_1 I_{xy}$$
$$h_z = R_1 I_{zz} - P_1 I_{xz} - Q_1 I_{yz}$$

where the total moment of momentum $\bar{h}$ is defined as $\bar{I}h_x + \bar{J}h_y + \bar{k}h_z$ and where $\bar{I}$, $\bar{J}$, and $\bar{k}$ are unit vectors along the x_1, y_1, and z_1 axes respectively.

Each of these instantaneous axis systems along the flight path, such as x_1, y_1, and z_1 in the discussion above, is called an Eulerian axis system. Thus an Eulerian axis system is a right-hand system of orthogonal coordinate axes which has its origin at the center of gravity of the airplane and its orientation fixed with respect to the airplane. Velocities of the airplane measured relative to these axes are absolute velocities, since, at any instant, the Eulerian axes are considered to be fixed in space.

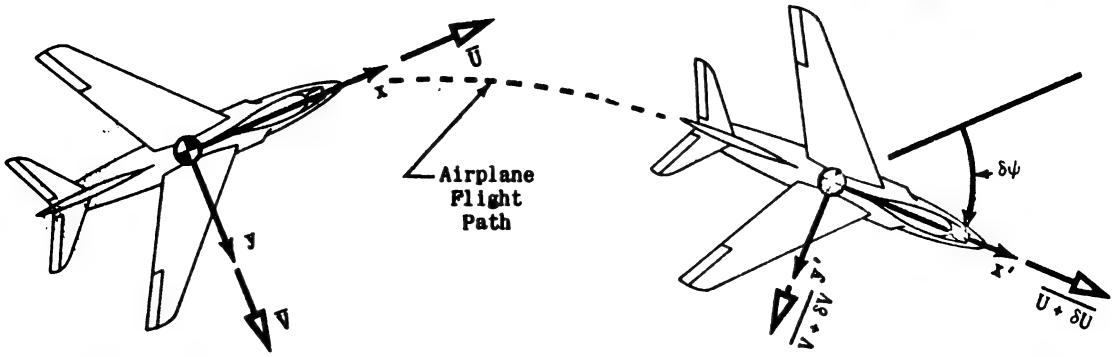

Figure II-6 Airplane Before and After Being Accelerated

Equations (II-10) show relations between the components of the moment of momentum and the components of the instantaneous angular velocity. Since the instruments measuring these angular velocities are aligned with the x_1, y_1, and z_1 axes and have the same instantaneous angular velocity as the airplane, the moment of momentum vector, $\bar{h}$, has the same angular velocity with respect to the x_1, y_1, and z_1 axes. This is exactly parallel to that for the linear velocity vector. Again, the absolute rate of change of the moment of momentum (relative to inertial axes) is composed of two terms, as in:

(II-11)
$$\frac{d\bar{h}_{abs}}{dt} = \frac{d\bar{h}}{dt} + \bar{\omega} \times \bar{h}$$

The term $\frac{d\bar{h}}{dt}$ on the right side of (II-11) arises from the fact that the moment of momentum is changing instantaneously relative to the x_1, y_1, z_1 axes, and the term $\bar{\omega} \times \bar{h}$ arises from the fact that the x_1, y_1, z_1 axes have an instantaneous angular velocity, $\bar{\omega}$, with respect to the x, y, z axes.

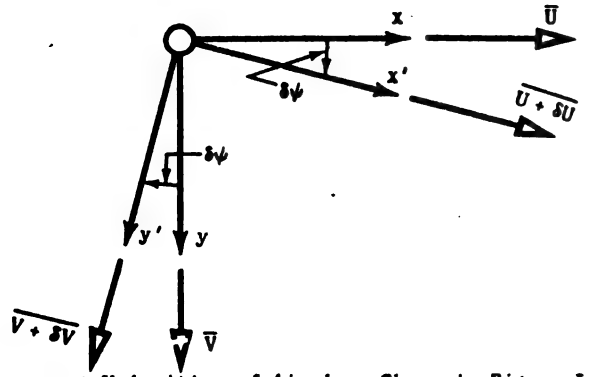

Component Velocities of Airplane Shown in Figure II-6
Figure II-7

One reason why Eulerian axes are particularly useful in the study of airframe dynamics is that velocities measured with respect to these axes are the same as the velocities that would be measured by instruments mounted in the airplane. This point, demonstrated in the discussion above, has been very valuable in airframe controller design. Another reason is that moments and products of inertia measured relative to Eulerian axes are independent of time in view of Assumption III because these axes do not move with respect to the airframe. The moments and products of inertia are, however, functions of the weight loading of the airframe and the orientation of the axes with respect to the airframe. (This point is discussed in a later section.)

A simple two dimensional example which is helpful in the intuitive understanding of (II-9) and (II-11) is presented next, and the equations of motion referred to Eulerian axes are then expanded in terms of the component velocities.

Figure II-6 shows the plan view of an airplane at two points along its flight path. The drawing at the left represents the airplane in an unaccelerated flight condition and the drawing at the right represents the same airplane some time after it has passed through rough air which has caused it to accelerate. The Eulerian axes at the two instants pictured are represented by x, y and x', y'. At the first instant, the velocity components of the airplane are $\bar{U}$ and $\bar{V}$ along the x and y axes respectively; a small increment of time, δt, later, when the airplane has rotated through an angle $\delta\psi$, the linear velocity components are $\overline{U + \delta U}$ and $\overline{V + \delta V}$ with respect to the x', y' axes (see Figure II-7).

When the acceleration is written as the time rate of change of the velocity, the components of acceleration with respect to the original x, y axes become:

(II-12)
$$a_x = \lim_{\delta t \to 0} \frac{(U + \delta U)\cos\delta\psi - (V + \delta V)\sin\delta\psi - U}{\delta t}$$

By considering $\delta\psi$ to be a small angle, by setting $\sin\delta\psi = \delta\psi$ and $\cos\delta\psi = 1$, and by neglecting products of deltas, the x component of acceleration becomes:

(II-13) $$a_x = \lim_{\delta t \to 0} \frac{\delta U - V\delta\psi}{\delta t} = \frac{dU}{dt} - V\frac{d\psi}{dt}$$

The rate of change of ψ is an angular velocity about the z axis. Table II-1 shows that $\frac{d\psi}{dt}$ is equal to R. Making this substitution in (II-13) yields:

(II-14) $$a_x = \frac{dU}{dt} - VR$$

Similarly,

(II-15) $$a_y = \frac{dV}{dt} + UR$$

In this restricted two dimensional example, P and Q, the angular velocity components about the x and y axes respectively, and W, the component of linear velocity along the z axis, were purposely selected to be zero. Thus, the total angular velocity $\bar{\omega}$ is equal to R, and the total linear velocity $\bar{V}_T$ is the vector sum of the two components of linear velocity along the x and y axes. By using the relationships:

(II-16) $$\bar{\omega} = \bar{R}$$

and

(II-17) $$\bar{V}_T = \bar{U} + \bar{V}$$

and by keeping in mind the rules for vector cross multiplication, the results of (II-14) and (II-15) can be combined into the single equation:

(II-18) $$\bar{a}_{abs} = \frac{d\bar{V}_T}{dt} + \bar{\omega} \times \bar{V}_T$$

Equations (II-18) and (II-9) are then identical.

In the actual case of three dimensions, (II-9) applies. Recalling that the components of the linear velocity $\bar{V}_T$ are defined as $\bar{U}$, $\bar{V}$, and $\bar{W}$, and that the components of the angular velocity $\bar{\omega}$ are defined as $\bar{P}$, $\bar{Q}$, and $\bar{R}$ along and about the x, y, and z axes respectively, (II-9) may be expanded as the cross product of two vectors.

(II-19) $$\bar{\omega} \times \bar{V}_T = \begin{vmatrix} i & j & k \\ P & Q & R \\ U & V & W \end{vmatrix}$$

(II-20) $$\bar{\omega} \times \bar{V}_T = i(QW - RV) + j(RU - PW) + k(PV - QU)$$

By substituting the results of (II-20) into (II-7), the components of acceleration can then be written as:

(II-21) $$a_x = \dot{U} + QW - RV$$
$$a_y = \dot{V} + RU - PW$$
$$a_z = \dot{W} + PV - QU$$

Equation (II-11) is repeated for reference:

(II-22) $$\frac{d\bar{h}}{dt}_{abs} = \frac{d\bar{h}}{dt} + \bar{\omega} \times \bar{h}$$

This expression can be written in component form as:

(II-23) $$\left.\frac{dh_x}{dt}\right|_{abs} = \frac{dh_x}{dt} + h_zQ - h_yR$$
$$\left.\frac{dh_y}{dt}\right|_{abs} = \frac{dh_y}{dt} + h_xR - h_zP$$
$$\left.\frac{dh_z}{dt}\right|_{abs} = \frac{dh_z}{dt} + h_yP - h_xQ$$

Substituting (II-10) into (II-23) and performing the indicated differentiations yield (II-24). It should be noted that since the moments and products of inertia measured with respect to Eulerian axes are constant, (II-24) do not contain the terms similar to $\dot{I}_{xx}$ and $\dot{I}_{xz}$ which appeared in (II-6):

(II-24)

$$\left.\frac{dh_x}{dt}\right|_{abs} = \dot{P}I_{xx} - \dot{Q}I_{xy} - \dot{R}I_{xz} + QR(I_{zz} - I_{yy}) - PQI_{xz} - Q^2I_{zy} + R^2I_{yz} + PRI_{xy}$$

$$\left.\frac{dh_y}{dt}\right|_{abs} = \dot{Q}I_{yy} - \dot{R}I_{yz} - \dot{P}I_{xy} + PR(I_{xx} - I_{zz}) - QRI_{xy} - R^2I_{xz} + P^2I_{xz} + PQI_{zy}$$

$$\left.\frac{dh_z}{dt}\right|_{abs} = \dot{R}I_{zz} - \dot{P}I_{xz} - \dot{Q}I_{zy} + PQ(I_{yy} - I_{xx}) - PRI_{yz} - P^2I_{xy} + Q^2I_{xy} + QRI_{xz}$$

In the discussion up to this point, the orientation of the of the Eulerian axes with respect to the airframe has been arbitrary, and (II-24) are in general form. There are several factors which influence the orientation chosen for the Eulerian axes, but these factors are discussed, for the most part, in a later section.

Because the geometry of the airframe is conventional, a simplification of (II-24) can be made immediately by choosing a particular orientation of the y axis, but before considering an axis system oriented as the one in Figure II-8, another assumption is made:

ASSUMPTION IV. The xz plane is assumed to be a plane of symmetry.

Assumption IV is a very good approximation for most airplanes, and in the light of this assumption, it can be seen from Figure II-8 that there is both a positive and a negative value of y for each value of z; consequently, $I_{yz} = \int yz\,dm = 0$, and similarly, $I_{xy} = \int xy\,dm = 0$.

The expanded form of the equations of motion of an airframe referred to Eulerian axes can then be written as:

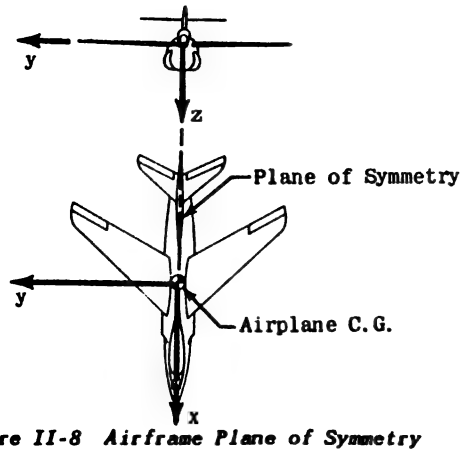

Figure II-8 Airframe Plane of Symmetry

(II-25)

$$\Sigma F_x = m[\dot{U} + QW - RV]$$

$$\Sigma F_y = m[\dot{V} + RU - PW]$$

$$\Sigma F_z = m[\dot{W} + PV - QU]$$

$$\Sigma L = \dot{P}I_{xx} - \dot{R}I_{xz} + QR(I_{zz} - I_{yy}) - PQI_{xz}$$

$$\Sigma M = \dot{Q}I_{yy} + PR(I_{xx} - I_{zz}) - R^2I_{xz} + P^2I_{xz}$$

$$\Sigma N = \dot{R}I_{zz} - \dot{P}I_{xz} + PQ(I_{yy} - I_{xx}) + QRI_{xz}$$

SECTION 4 – EXPANSION OF APPLIED FORCES AND MOMENTS

The left sides of (II-25) are the summations of the external forces and moments applied to the airplane in flight. The external forces can be classified as gravity forces, aerodynamic forces, and thrust forces. Before describing these forces, some explanation of how they are included in the equations of motion is given.

Equilibrium flight is defined as unaccelerated flight, that is, flight along a straight flight path during which the linear velocity vector measured relative to fixed space is invariant and the angular velocity is zero. For the purposes of the following discussion, a condition called steady flight is defined as flight during which vectors measured with respect to Eulerian axes are invariant. According to this definition, equilibrium flight and flight with constant angular velocity are also steady flight. Thus, flight at a constant rate of turn could be classified as steady flight.

The disturbed motion of an airplane at any instant can always be considered the result of disturbing the airplane from some steady flight condition. This motion may be referred to as disturbed flight and the Eulerian axes under these conditions are referred to as disturbed axes. The forces acting on an airplane during disturbed flight can consequently be considered equal to the sum of the forces acting during the steady flight condition and the increments of force caused by the disturbance. As shown later, writing the forces according to this convention permits a simplification of the resulting equation of motion.

SECTION 5 – EXPANSION OF THE GRAVITY FORCE

The gravity force can be considered to act at the center of gravity of the airplane, but since the origin of the Eulerian axes system is also located at the center of gravity, this force makes no contribution to the summation of external moments. However, it will contribute components to the summation of external forces.

To find the expressions for the components of gravity forces to be used in the equations of motion for an airplane disturbed from some steady flight condition, a general direction cosine matrix is derived which can be used to express the vectors in any Eulerian axis system as vectors in another Eulerian axis system displaced from the first by the Eulerian angles ψ, θ, and ϕ.

Eulerian angles are defined as those angles through which one axis system must be rotated to superimpose it upon another having an initial angular displacement from the first. In the following pages, these angles are defined more completely by rotating an axis system

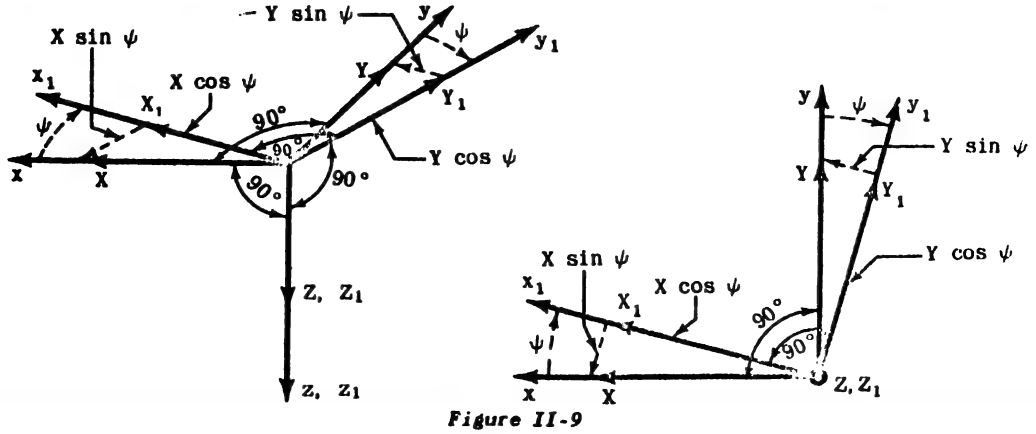

Figure II-9

through each of the Eulerian angles in the derivation of the general direction cosine matrix which follows. The order of rotation and the axes about which these rotations are made are shown. This order of rotation is important because all subsequent rotations must have the same order if the indicated operations are to give correct results.

Figure II-9 shows a vector in the x, y, z axis system with components X, Y, Z. The x and y axes are rotated in accordance with the right-hand rule through a positive angle, ψ, about the z axis into the position of the x_1, y_1, z_1 axes. The components of the vector along these axes are:

(II-26)
$$\bar{X}_1 = \bar{X}\cos\psi + \bar{Y}\sin\psi$$
$$\bar{Y}_1 = \bar{Y}\cos\psi - \bar{X}\sin\psi$$
$$\bar{Z}_1 = \bar{Z}$$

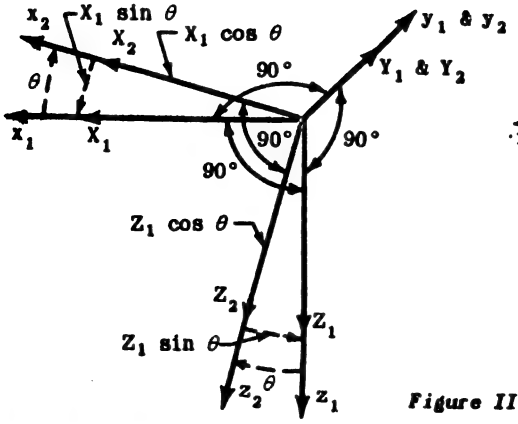

Figure II-10

In Figure II-10, the x_1, and z_1 axes are rotated through a positive angle, θ, about the y_1 axis into the position of the x_2 y_2, z_2 axes. The components of the vector in the new system are:

(II-27)
$$X_2 = X_1\cos\theta - Z_1\sin\theta$$
$$Y_2 = Y_1$$
$$Z_2 = Z_1\cos\theta + X_1\sin\theta$$

Finally, as shown in Figure II-11, the y_2 and z_2 axes are rotated through a positive angle, ϕ, about the z_2 axis into the position of the x_3, y_3, z_3 axes. The components of the vector is this new system are:

(II-28)
$$X_3 = X_2$$
$$Y_3 = Y_2\cos\phi + Z_2\sin\phi$$
$$Z_3 = Z_2\cos\phi - Y_2\sin\phi$$

Substituting (II-26) and (II-27) into (II-28) yields the following equations:

(II-29)
$$\bar{X}_3 = \bar{X}\cos\theta\cos\psi + \bar{Y}\cos\theta\sin\psi - \bar{Z}\sin\theta$$
$$\bar{Y}_3 = \bar{X}(\cos\psi\sin\theta\sin\phi - \sin\psi\cos\phi) + \bar{Y}(\cos\psi\cos\phi + \sin\psi\sin\theta\sin\phi) + \bar{Z}(\cos\theta\sin\phi)$$
$$\bar{Z}_3 = \bar{X}(\cos\psi\sin\theta\cos\phi + \sin\psi\sin\phi) + \bar{Y}(\sin\psi\sin\theta\cos\phi - \cos\psi\sin\phi) + \bar{Z}(\cos\theta\cos\phi)$$

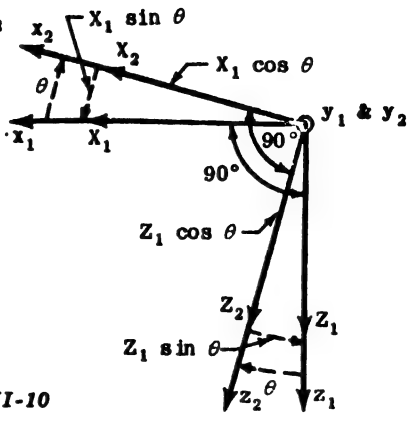

This set of equations may be conveniently written in the following matrix form:

General Direction Cosine Matrix

(II-30)

$$\begin{bmatrix} \cos\theta\cos\psi & \cos\theta\sin\psi & -\sin\theta \\ \cos\psi\sin\theta\sin\phi - \sin\psi\cos\phi & \cos\psi\cos\phi + \sin\psi\sin\theta\sin\phi & \cos\theta\sin\phi \\ \cos\psi\sin\theta\cos\phi + \sin\psi\sin\phi & \sin\psi\sin\theta\cos\phi - \cos\psi\sin\phi & \cos\theta\cos\phi \end{bmatrix} \begin{bmatrix} \bar{X} \\ \bar{Y} \\ \bar{Z} \end{bmatrix} = \begin{bmatrix} \bar{X}_3 \\ \bar{Y}_3 \\ \bar{Z}_3 \end{bmatrix}$$

Initial System — Final System

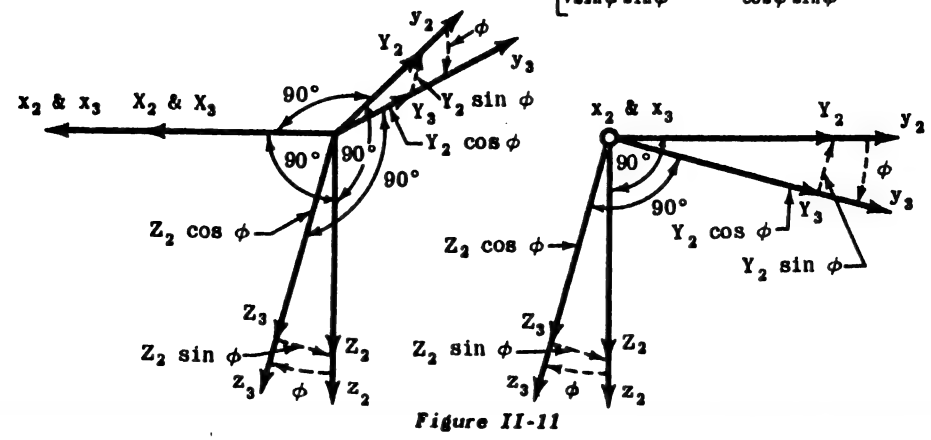

Figure II-11

The components of gravity acting along the axes of a disturbed airframe are now determined in terms of the gravity components acting along the steady flight axes (initial axes) and the Eulerian angles.

The components of force due to gravity acting on an airplane which is in steady flight and which has initial angles θ_o and ϕ_o with respect to the gravity vector can be found from Figure II-12 by direct resolution of the gravity force along the x_o, y_o, and z_o (steady flight) axes.

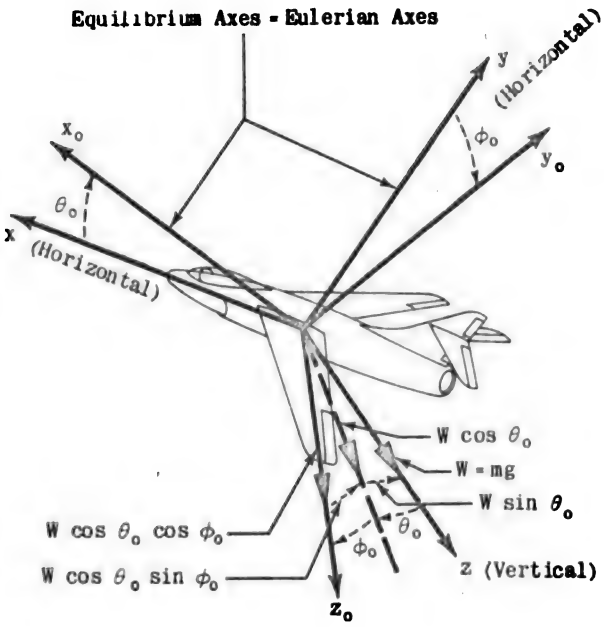

Figure II-12

(II-31)
$$X_o = -W \sin\theta_o$$
$$Y_o = W \cos\theta_o \sin\phi_o$$
$$Z_o = W \cos\theta_o \cos\phi_o$$

The components of gravity acting along the disturbed Eulerian axes can then be determined by substituting (II-31) into (II-29):

(II-32)
$$X_3 = (-W \sin\theta_o)\cos\theta\cos\psi + (W\cos\theta_o\sin\phi_o)\cos\theta\sin\psi - (W\cos\theta_o\cos\phi_o)\sin\theta$$
$$Y_3 = (-W\sin\theta_o)(\cos\psi\sin\theta\sin\phi - \sin\psi\cos\phi) + (W\cos\theta_o\sin\phi_o)(\cos\psi\cos\theta + \sin\psi\sin\theta\sin\phi) + (W\cos\theta_o\cos\phi_o)(\cos\theta\sin\phi)$$
$$Z_3 = (-W\sin\theta_o)(\cos\psi\sin\theta\cos\phi + \sin\psi\sin\phi) + (W\cos\theta_o\sin\phi_o)(\sin\psi\sin\theta\cos\phi - \cos\psi\sin\phi) + (W\cos\theta_o\cos\phi_o)(\cos\theta\cos\phi)$$

The left sides of the first three equations of (II-25) are the summations of the aerodynamic, thrust, and gravity forces applied to the airplane at any instant during flight. Each of these summations may be rewritten as:

(II-33)
$$\Sigma F_x = \Sigma F'_x + f_x(\text{Gravity})$$
$$\Sigma F_y = \Sigma F'_y + f_y(\text{Gravity})$$
$$\Sigma F_z = \Sigma F'_z + f_z(\text{Gravity})$$

The primed quantities in (II-33) are the summations of the aerodynamic and thrust forces; the gravity force enters the equations explicitly as f (Gravity); and the subscripts denote the axis along which the component of the gravity force is acting. Equations (II-32) express the components of gravity acting along the Eulerian axes at any instant as X_3, Y_3, and Z_3. It should be noted that if the instant under consideration occurs during the steady flight condition, then $\theta = \phi = \psi = 0$, and the components X_3, Y_3, and Z_3 reduce to (II-31). (II-33) can now be written as:

(II-34)
$$\Sigma F_x = \Sigma F'_x + X_3$$
$$\Sigma F_y = \Sigma F'_y + Y_3$$
$$\Sigma F_z = \Sigma F'_z + Z_3$$

The force relations from (II-25), with the gravity terms transposed to the right side, are rewritten as:

(II-35)
$$\Sigma F'_x = m[\dot{U} + QW - RV] - X_3$$
$$\Sigma F'_y = m[\dot{V} + RU - PW] - Y_3$$
$$\Sigma F'_z = m[\dot{W} + PV - QU] - Z_3$$

By substituting (II-32) in (II-35), the equations of (II-25) may be written in the form:

(II-36)
$$\Sigma F'_x = m[\dot{U} + QW - RV] + (W\sin\theta_o)\cos\theta\cos\psi - (W\cos\theta_o\sin\phi_o)\cos\theta\sin\psi + (W\cos\theta_o\cos\phi_o)\sin\theta$$

$$\Sigma F'_y = m[\dot{V} + RU - PW] + (W\sin\theta_o)(\cos\psi\sin\theta\sin\phi - \sin\psi\cos\phi) - (W\cos\theta_o\sin\phi_o)(\cos\psi\cos\phi + \sin\psi\sin\theta\sin\phi) - (W\cos\theta_o\cos\phi_o)(\cos\theta\sin\phi)$$

$$\Sigma F'_z = m[\dot{W} + PV - QU] + (W\sin\theta_o)(\cos\psi\sin\theta\cos\phi + \sin\psi\sin\phi) - (W\cos\theta_o\sin\phi_o)(\sin\psi\sin\theta\cos\phi - \cos\psi\sin\phi) - (W\cos\theta_o\cos\phi_o)(\cos\theta\cos\phi)$$

$$\Sigma L = \dot{P}I_{xx} - \dot{R}I_{xz} + QR(I_{zz} - I_{yy}) - PQI_{xz}$$
$$\Sigma M = \dot{Q}I_{yy} + PR(I_{xx} - I_{zz}) - R^2I_{xz} + P^2I_{xz}$$
$$\Sigma N = \dot{R}I_{zz} - \dot{P}I_{xz} + PQ(I_{yy} - I_{xx}) + QRI_{xz}$$

These equations are now complete except for the external forces and moments on the left side which will include aerodynamic and thrust forces as well as moments due to control surface deflection.

SECTION 6 – RELATION BETWEEN THE RATES OF CHANGE OF THE EULERIAN ANGLES AND THE INSTANTANEOUS ANGULAR VELOCITIES

Equations (II-36) are to be linearized before they are expanded to include the aerodynamic and thrust forces. But first, the relation between the rates of change of the Eulerian angles and the instantaneous angular velocities is derived.

Consider an airplane with axes in the instantaneous position of the x_3, y_3, z_3 axes displaced from the steady flight axes by the Eulerian angles ψ, θ, and ϕ. The instantaneous angular velocities are P, Q, and R, and the vectors representing these angular velocities are directed along the x_3, y_3, and z_3 axes respectively. In the derivation of the general direction cosine matrix, (II-30), it was shown that the Eulerian angle ψ was a rotation about the z axis (see Figure II-9) and that the Eulerian angles θ and ϕ were rotations about the y_1 and x_2 axes respectively (see Figures II-10 and II-11). The rates of change of these Eulerian angles can be represented as vectors pointed along the axes about which the individual rotations take place. Thus $\dot{\psi}$, $\dot{\theta}$, and $\dot{\phi}$ are represented as vectors along the z, y_1, and x_2 axes, respectively. Figure II-13 shows a composite picture of the axes with the vectors representing both the rates of change of the Eulerian angles and the instantaneous angular velocities. It can be seen that the vectors $\dot{\psi}$, $\dot{\theta}$, and $\dot{\phi}$ are not orthogonal.

The positions of the vectors in Figure II-13 can be checked by performing the actual rotations. The following relations can be obtained by direct resolution:

(II-37)
$$\begin{aligned} P &= \dot{\phi} - \dot{\psi}\sin\theta \\ Q &= \dot{\theta}\cos\phi + \dot{\psi}\sin\phi\cos\theta \\ R &= \dot{\psi}\cos\phi\cos\theta - \dot{\theta}\sin\phi \end{aligned}$$

The rates of change of the Eulerian angles can be most easily expressed as functions of the instantaneous angular velocities by solving (II-37) with the aid of determinants. This procedure yields the following results:

(II-38)
$$\begin{aligned} \dot{\phi} &= P + Q\tan\theta\sin\phi + R\tan\theta\cos\phi \\ \dot{\theta} &= Q\cos\phi - R\sin\phi \\ \dot{\psi} &= R\left(\frac{\cos\phi}{\cos\theta}\right) + Q\left(\frac{\sin\phi}{\cos\theta}\right) \end{aligned}$$

These relations are presented here for two reasons. First, they are needed to evaluate the approximations made when the equations are linearized, and second, they are potentially useful in the solution of trajectory problems.

SECTION 7 – LINEARIZATION OF THE EQUATIONS OF MOTION

Equations (II-36) equate the aerodynamic and thrust forces acting on an airplane to the gravity forces and to the resulting inertia forces. These equations are nonlinear since they contain products of the dependent variables and also because the dependent variables appear as transcendental functions.

In Section II-4 it was stated that airframe motion could always be considered the result of disturbing the airframe from some steady flight condition. Accordingly, each of the total instantaneous velocity components of the airframe can be written as the sum of a velocity component during the steady flight condition and a change in velocity caused by the disturbance:

(II-39)
$$\begin{aligned} U &= U_0 + u \\ V &= V_0 + v \\ W &= W_0 + w \\ P &= P_0 + p \\ Q &= Q_0 + q \\ R &= R_0 + r \end{aligned}$$

The zero subscripts in (II-39) indicate the steady flight velocities, and the lower case letters represent the changes in the velocities (disturbance velocities). By substituting (II-39) in (II-36) and by considering that

$$\frac{dU_0}{dt} = \frac{dP_0}{dt} = 0, \text{ etc.},$$

(II-40)
$$\begin{aligned} \Sigma F'_x &= m[\dot{u} + Q_0W_0 + W_0q + Q_0w + wq \\ &\quad - R_0V_0 - R_0v - V_0r - vr \\ &\quad + (g\sin\theta_0)\cos\theta\cos\psi - (g\cos\theta_0\sin\phi_0)\cos\theta\sin\psi \\ &\quad + (g\cos\theta_0\cos\phi_0)\sin\theta] \\ \Sigma F'_y &= m[\dot{v} + U_0R_0 + U_0r + R_0u + ru - P_0W_0 - P_0w - W_0p \\ &\quad - wp + (g\sin\theta_0)(\cos\psi\sin\theta\sin\phi - \sin\psi\cos\phi) \\ &\quad - (g\cos\theta_0\sin\phi_0)(\cos\psi\cos\phi + \sin\psi\sin\theta\sin\phi) \\ &\quad - (g\cos\theta_0\cos\phi_0)(\cos\theta\sin\phi)] \\ \Sigma F'_z &= m[\dot{w} + P_0V_0 + P_0v + V_0p + pv \\ &\quad - Q_0U_0 - Q_0u - U_0q - qu \\ &\quad + (g\sin\theta_0)(\cos\psi\sin\theta\cos\phi + \sin\psi\sin\phi) \\ &\quad - (g\cos\theta_0\sin\phi_0)(\sin\psi\sin\theta\cos\phi - \cos\psi\sin\phi) \\ &\quad - g(\cos\theta_0\cos\phi_0)(\cos\theta\cos\phi)] \\ \Sigma L &= \dot{p}I_{xx} - \dot{r}I_{xz} + (Q_0R_0 + Q_0r + R_0q + qr)(I_{zz} - I_{yy}) \\ &\quad - (P_0Q_0 + P_0q + Q_0p + pq)I_{xz} \\ \Sigma M &= \dot{q}I_{yy} + (P_0R_0 + P_0r + R_0p + pr)(I_{xx} - I_{zz}) \\ &\quad - (R_0^2 + 2R_0r + r^2)I_{xz} + (P_0^2 + 2P_0p + p^2)I_{xz} \\ \Sigma N &= \dot{r}I_{zz} - \dot{p}I_{xz} + (P_0Q_0 + P_0q + Q_0p + pq)(I_{yy} - I_{xx}) \\ &\quad + (Q_0R_0 + Q_0r + R_0q + qr)I_{xz} \end{aligned}$$

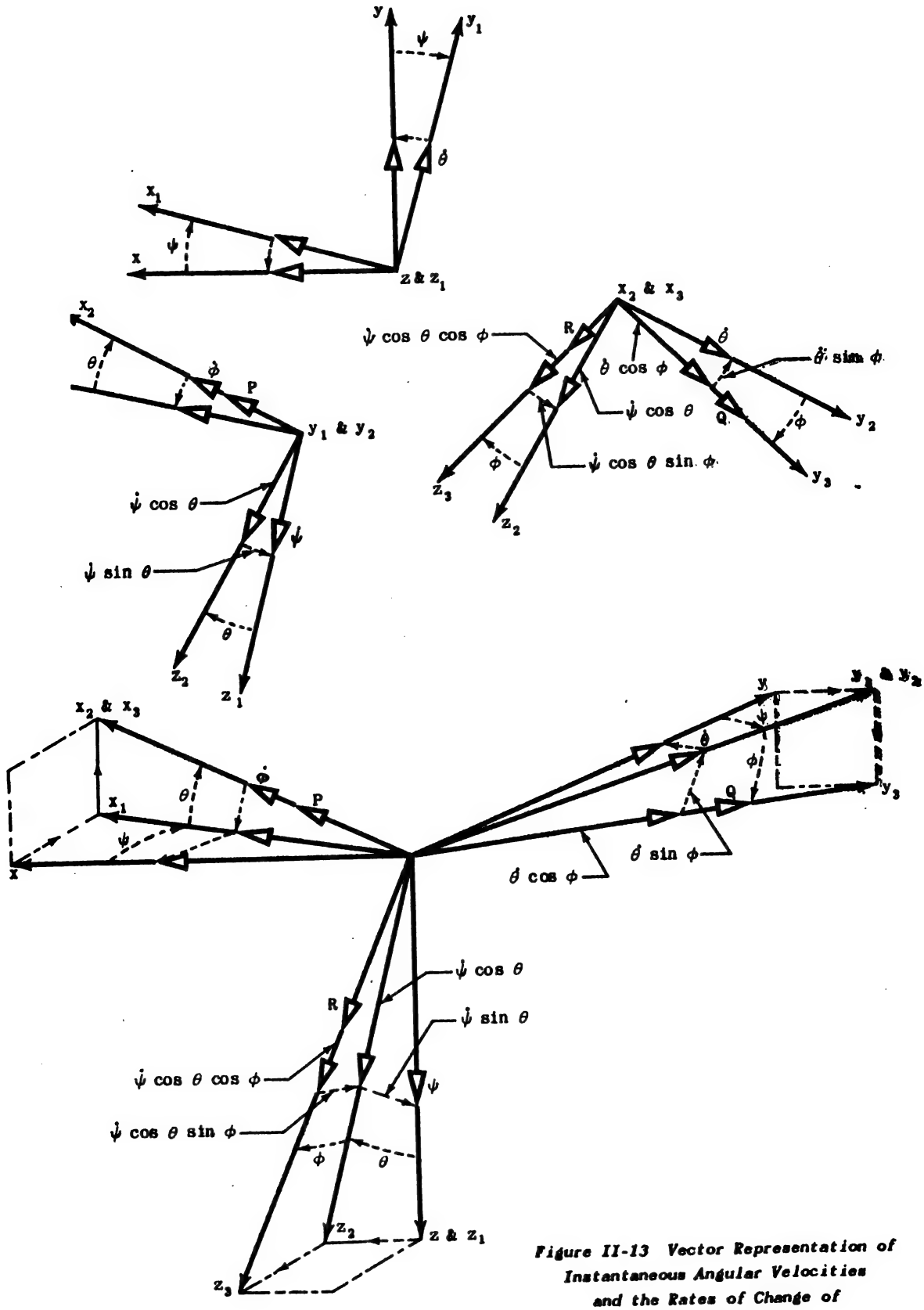

Figure II-13 Vector Representation of Instantaneous Angular Velocities and the Rates of Change of the Eulerian Axes

ASSUMPTION V. The disturbances from the steady flight condition are assumed to be small enough so that the products and squares of the changes in velocities are negligible in comparison with the changes themselves. Also, the disturbance angles are assumed to be small enough so that the sines of these angles may be set equal to the angles and the cosines set equal to one. Products of these angles are also approximately zero and can be neglected. And, since the disturbances are small, the change in air density encountered by the airplane during any disturbance can be considered zero.

Thus, terms similar to qr and $\sin\psi \sin\phi$ may be set equal to zero, and (II-40) then reduce to:

(II-41)

$$\Sigma F_x' = m[\dot{u} + Q_0 W_0 + W_0 q + Q_0 w - R_0 V_0 - R_0 v - V_0 r + g \sin\theta_0 - (g \cos\theta_0 \sin\phi_0)\psi + (g \cos\theta_0 \cos\phi_0)\theta]$$
$$\Sigma F_y' = m[\dot{v} + U_0 R_0 + U_0 r + R_0 u - P_0 W_0 - P_0 w - W_0 p - (g \sin\theta_0)\psi - g \cos\theta_0 \sin\phi - (g \cos\theta_0 \cos\phi_0)\phi]$$
$$\Sigma F_z' = m[\dot{w} + P_0 V_0 + P_0 v + V_0 p - Q_0 U_0 - Q_0 u - U_0 q + (g \sin\theta_0)\theta + (g \cos\theta_0 \sin\phi_0)\phi - (g \cos\theta_0 \cos\phi_0)]$$
$$\Sigma L = \dot{p} I_{xx} - \dot{r} I_{xz} + (Q_0 R_0 + Q_0 r + R_0 q)(I_{zz} - I_{yy}) - (P_0 Q_0 + P_0 q + Q_0 p) I_{xz}$$
$$\Sigma M = \dot{q} I_{yy} + (P_0 R_0 + P_0 r + R_0 p)(I_{xx} - I_{zz}) - (R_0^2 + 2R_0 r) I_{xz} + (P_0^2 + 2P_0 p) I_{xz}$$
$$\Sigma N = \dot{r} I_{zz} - \dot{p} I_{xz} + (P_0 Q_0 + P_0 q + Q_0 p)(I_{yy} - I_{xx}) + (Q_0 R_0 + Q_0 r + R_0 q) I_{xz}$$

Assumption V not only limits the applicability of (II-41) to what are called small perturbations, but reduces (II-41) to linear equations and yields a simplification of the mathematical methods necessary for the analysis of complicated airplane motions. In the rigorous mathematical sense, (II-41) are applicable only to infinitesimal disturbances; however, experience has shown that quite accurate results can be obtained by applying these equations to disturbances of finite, non-zero magnitude. An additional result of the assumption of small perturbations is the reduction of equations (II-37) which are repeated here for reference:

(II-42)

$$P = \dot{\phi} - \dot{\psi} \sin\theta$$
$$Q = \dot{\theta} \cos\phi + \dot{\psi} \sin\phi \cos\theta$$
$$R = \dot{\psi} \cos\phi \cos\theta - \dot{\theta} \sin\phi$$

These equations reduce to:

(II-43)

$$P = \dot{\phi} - \dot{\psi}\theta$$
$$Q = \dot{\theta} + \dot{\psi}\phi$$
$$R = \dot{\psi} - \dot{\theta}\phi$$

and, neglecting the products of perturbations, to:

(II-44)

$$P = \dot{\phi}$$
$$Q = \dot{\theta}$$
$$R = \dot{\psi}$$

Equations (II-44) show that within the limits of small perturbation theory, the instantaneous angular velocities may be set equal to the rates of change of the Eulerian angles.

Equations (II-41) are more complete than generally required for a particular analysis. They can be used, for example, to describe the motions of an airplane that is disturbed from a complicated steady flight condition of steady state rolling, pitching, and yawing velocities as well as of constant sideslip and forward speed. For the purposes of this volume, however, the following assumption is made:

ASSUMPTION VI. During the steady flight condition, the airplane is assumed to be flying with wings level and with all components of velocity zero except U_0 and W_0.

$$(V_0 = P_0 = Q_0 = R_0 = \phi_0 = \psi_0 = 0)$$

An airplane in steady flight with only U_0 and W_0 as velocity components is flying along a straight flight path at constant linear velocity and zero angular velocity. The airplane may be flying horizontally or it may be climbing or diving. This behavior is, of course, unaccelerated flight, and therefore corresponds to equilibrium flight as previously defined (see Section II-4).

By eliminating the quantities assumed zero in Assumption VI, equations (II-41) may be rewritten as:

(II-45)
$$\Sigma F_x' = m[\dot{u} + W_0 q + g \sin\theta_0 + g\theta \cos\theta_0]$$
$$\Sigma F_y' = m[\dot{v} + U_0 r - W_0 p - g\psi \sin\theta_0 - g\phi \cos\theta_0]$$
$$\Sigma F_z' = m[\dot{w} - U_0 q + g\theta \sin\theta_0 - g \cos\theta_0]$$
$$\Sigma L = \dot{p} I_{xx} - \dot{r} I_{xz}$$
$$\Sigma M = \dot{q} I_{yy}$$
$$\Sigma N = \dot{r} I_{zz} - \dot{p} I_{xz}$$

Assumption VI restricts (II-45) to an airplane whose flight condition is disturbed only slightly from equilibrium flight with U_0 and W_0 as the only component velocities. This is no great restriction because most airplanes are flown in such an equilibrium flight condition over 90% of the time. Much of the necessary design information can be obtained by investigating the dynamic response of an airplane to small disturbances from this equilibrium condition. The equations can be altered to apply to an airplane disturbed from a steady turn or from other steady flight conditions by following the procedure used in the derivation of (II-45).

SECTION 8 – EXPANSION OF THE AERODYNAMIC FORCES AND MOMENTS

The aerodynamic forces acting on an airplane in flight are the forces exerted by the surrounding atmosphere in resisting the motion of the airplane. These forces are present at all times during flight and, of course, vary with the flight conditions. Since deflection of the control surfaces changes the flight condition, aerodynamic forces are therefore functions of control surface deflection.

The aerodynamic forces and moments acting on an airplane at any instant during its flight are shown in Figure II-14:

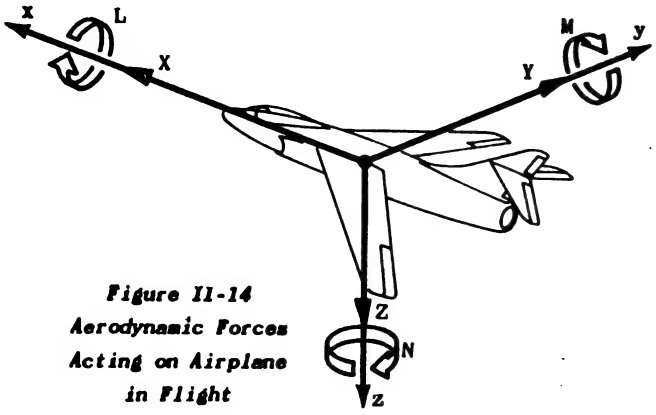

Figure II-14 Aerodynamic Forces Acting on Airplane in Flight

For convenience, aerodynamic forces along the individual Eulerian axes are designated by the capital letters X, Y, and Z to associate them with the axes along which they act, and the moments are denoted as L, M, and N about the x, y, and z axes respectively.

It can be shown by dimensional analysis* that the forces acting on solids moving through fluids can be expressed in the form:

(II-46)

$$F = C_F \tfrac{1}{2} \rho V^2 S$$

C_F = A dimensionless coefficient
ρ = Density of fluid
V = Velocity of the solid relative to the fluid
S = Characteristic area of the solid

Since a moment is the product of a force by a moment arm, the expression for a moment could be written in a form similar to that of (II-46); the moments and forces acting on an airplane in flight may then be written as:

(II-47)

$L = C_L \tfrac{1}{2}\rho V^2 S$	= Lift
$D = C_D \tfrac{1}{2}\rho V^2 S$	= Drag
$X = C_x \tfrac{1}{2}\rho V^2 S$	= Aerodynamic Force Along x Axis
$Y = C_y \tfrac{1}{2}\rho V^2 S$	= Aerodynamic Force Along y Axis
$Z = C_z \tfrac{1}{2}\rho V^2 S$	= Aerodynamic Force Along z Axis
$L = C_l \tfrac{1}{2}\rho V^2 Sb$	= Rolling Moment
$M = C_m \tfrac{1}{2}\rho V^2 Sc$	= Pitching Moment
$N = C_n \tfrac{1}{2}\rho V^2 Sb$	= Yawing Moment

where

S = Wing Area
c = Mean Aerodynamic Chord = The wing chord which has the average characteristics of all chords in the wing.
b = Wing span

(See Figure II-15.)

Two new quantities are introduced in (II-47); they are given in the first two relations which are the equations of lift, L, and drag, D, respectively. The lift is the force acting normal to the flight path (i.e., to the relative wind), and the drag is the force acting parallel to the flight path (see Figure II-16). The X, Y, and Z forces are actually functions of the lift and drag.

* Millikan, C. B., 'Aerodynamics of the Airplane,' John Wiley and Sons, Inc., New York, 1941.

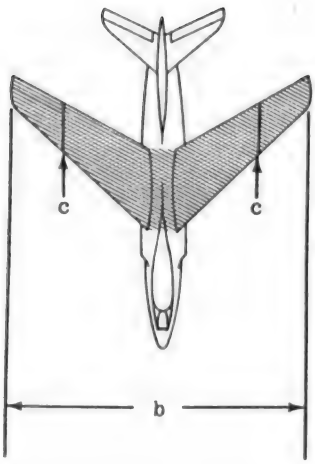

Shaded Area = S

Figure II-15 S, b, and c of Wing

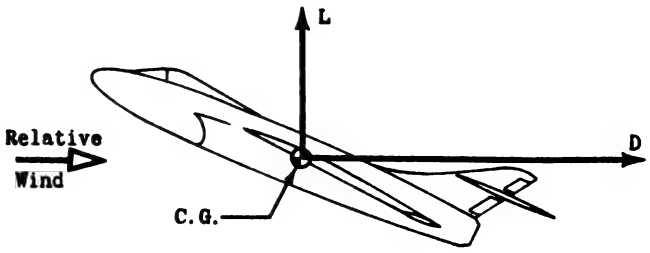

Figure II-16 Lift and Drag Acting on an Airplane

The other quantities appearing in (II-47) have been previously defined.

In general, each of the dimensionless coefficients of (II-47) varies with each of the variables in (II-40) and their derivatives. (More will be said about this variation in subsequent sections of this chapter.) To avoid confusion, it should be noted that the dimensionless coefficient in the lift equation is written with a capital L while a lower case l is used in the rolling moment coefficient.

Each of the forces (X, Y, and Z) and the moments (L, M, and N) can be expressed as a function of the variables by expanding the forces in a Taylor series. These series have the form:

(II-48)
$$F = (F)_o + \left(\frac{\partial F}{\partial \alpha}\right)_o \alpha + \left(\frac{\partial F}{\partial \beta}\right)_o \beta + \left(\frac{\partial F}{\partial \gamma}\right)_o \gamma + \cdots\cdots$$

where α, β, and γ are variables, and the subscript zero indicates the quantities are evaluated at the steady flight condition.

In (II-48), terms of the order $\left(\frac{\partial^2 F}{\partial \alpha^2}\right)_o \frac{\alpha^2}{2!}$ and all higher order terms have been omitted in accordance with Assumption V.

Before proceeding with the actual expansion of (II-48), a simplification can be made. Because the xz plane is a plane of symmetry, the rate of change of the X and Z forces and of the moment M, with respect to the disturbance velocities p, r, and v, is indentically zero. That this is true may be seen by considering the rate of change of the X force with respect to the side velocity v; that is, $(\partial X/\partial v)$.

From (II-48), the increment of force along the x axis caused by the disturbance velocity v, can be written in the form:

(II-49)
$$\Delta X = \left(\frac{\partial X}{\partial v}\right) v$$

Examine the X force caused by a side velocity v. If, for the purposes of this discussion, the airplane is assumed to have a side velocity to the right (i.e., if v is positive), a positive X force is produced as shown in Figure II-17. If, in addition, this force is assumed proportional to the magnitude of v, a plot of X versus v might then appear as in Figure II-18.

Because the xz plane is a plane of symmetry, the X force produced by a side velocity v has the same magnitude and direction regardless of whether v is positive or negative. Consequently, for negative values of v, the curve of X versus v is a mirror image of Figure II-18. The complete curve of X versus v might then appear as in Figure II-19.

It was stated that the zero subscript of quantities similar to $(\partial X/\partial v)_o$ means that this quantity should be evaluated at the steady flight condition. Assumption VI stated that $V_o = 0$ during the steady flight condition. Figure II-19 shows that the slope of X versus v at (v = 0) is zero. Thus, because the xz plane is a plane of symmetry, $(\partial X/\partial v)_o$ is identically equal to zero. It should be noted that this conclusion does not depend on whether the X force produced by a side velocity v was positive or negative. It can be shown by similar analysis that if the steady flight condition is chosen when P = V = R = Q = 0, X, Z, and M are functions of only u, w, and q and their derivatives, whereas Y, L, and N are functions of only v, p, and r and their derivatives.

This brings to light an important consideration. If, instead of specifying steady state flight with zero sideslip velocity, one were to specify steady state flight with sideslip velocity V_o, then there would be an X component of force caused by this velocity. The preceding analysis proved only that the slope of this force with respect to v was zero when v = 0 during the steady flight condition. From Figure II-19 it can be seen that $(\partial X/\partial v)_o$ is equal to zero at $V_o = 0$ and only then. Therefore, the magnitude of $(\partial X/\partial v)_o$ and similar derivatives must be investigated if the equilibrium condition is chosen when velocities other than U_o and W_o exist.

For the steady flight condition of Assumption VI, forces and moments acting on a disturbed airplane can be expressed in one form of (II-48) as:

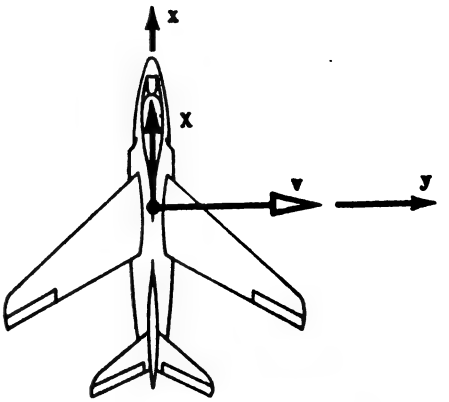

Figure II-17 Force Caused by Side Velocity

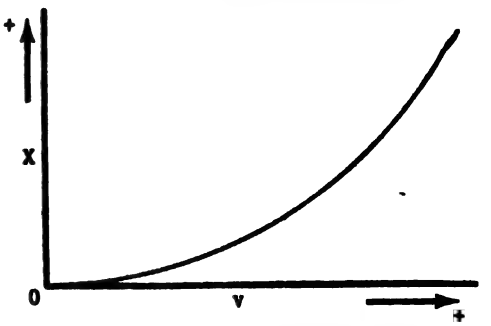

Figure II-18 Force Caused by Positive Side Velocity

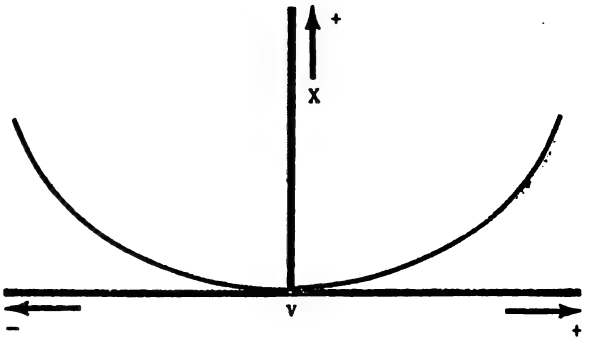

Figure II-19 Force Caused by Side Velocity

(II-50)

$$X = X_o + \frac{\partial X}{\partial u} u + \frac{\partial X}{\partial \dot{u}} \dot{u} + \frac{\partial X}{\partial q} q + \frac{\partial X}{\partial \dot{q}} \dot{q} + \frac{\partial X}{\partial w} w + \frac{\partial X}{\partial \dot{w}} \dot{w} + \frac{\partial X}{\partial \delta_E} \delta_E$$
$$+ \frac{\partial X}{\partial \dot{\delta}_E} \dot{\delta}_E + \frac{\partial X}{\partial \ddot{\delta}_E} \ddot{\delta}_E + \frac{\partial X}{\partial \delta_F} \delta_F + \frac{\partial X}{\partial \dot{\delta}_F} \dot{\delta}_F + \frac{\partial X}{\partial \delta_B} \delta_B + \frac{\partial X}{\partial \dot{\delta}_B} \dot{\delta}_B + \frac{\partial X}{\partial \ddot{\delta}_B} \ddot{\delta}_B$$

$$Y = Y_o + \frac{\partial Y}{\partial r} r + \frac{\partial Y}{\partial \dot{r}} \dot{r} + \frac{\partial Y}{\partial v} v + \frac{\partial Y}{\partial \dot{v}} \dot{v} + \frac{\partial Y}{\partial p} p + \frac{\partial Y}{\partial \dot{p}} \dot{p} + \frac{\partial Y}{\partial \delta_A} \delta_A$$
$$+ \frac{\partial Y}{\partial \dot{\delta}_A} \dot{\delta}_A + \frac{\partial Y}{\partial \ddot{\delta}_A} \ddot{\delta}_A + \frac{\partial Y}{\partial \delta_R} \delta_R + \frac{\partial Y}{\partial \dot{\delta}_R} \dot{\delta}_R + \frac{\partial Y}{\partial \ddot{\delta}_R} \ddot{\delta}_R$$

$$Z = Z_o + \frac{\partial Z}{\partial u} u + \frac{\partial Z}{\partial \dot{u}} \dot{u} + \frac{\partial Z}{\partial q} q + \frac{\partial Z}{\partial \dot{q}} \dot{q} + \frac{\partial Z}{\partial w} w + \frac{\partial Z}{\partial \dot{w}} \dot{w} + \frac{\partial Z}{\partial \delta_E} \delta_E$$
$$+ \frac{\partial Z}{\partial \dot{\delta}_E} \dot{\delta}_E + \frac{\partial Z}{\partial \ddot{\delta}_E} \ddot{\delta}_E + \frac{\partial Z}{\partial \delta_F} \delta_F + \frac{\partial Z}{\partial \dot{\delta}_F} \dot{\delta}_F + \frac{\partial Z}{\partial \delta_B} \delta_B + \frac{\partial Z}{\partial \dot{\delta}_B} \dot{\delta}_B + \frac{\partial Z}{\partial \ddot{\delta}_B} \ddot{\delta}_B$$

$$L = L_o + \frac{\partial L}{\partial r} r + \frac{\partial L}{\partial \dot{r}} \dot{r} + \frac{\partial L}{\partial v} v + \frac{\partial L}{\partial \dot{v}} \dot{v} + \frac{\partial L}{\partial p} p + \frac{\partial L}{\partial \dot{p}} \dot{p} + \frac{\partial L}{\partial \delta_A} \delta_A$$
$$+ \frac{\partial L}{\partial \dot{\delta}_A} \dot{\delta}_A + \frac{\partial L}{\partial \ddot{\delta}_A} \ddot{\delta}_A + \frac{\partial L}{\partial \delta_R} \delta_R + \frac{\partial L}{\partial \dot{\delta}_R} \dot{\delta}_R + \frac{\partial L}{\partial \ddot{\delta}_R} \ddot{\delta}_R$$

$$M = M_o + \frac{\partial M}{\partial u} u + \frac{\partial M}{\partial \dot{u}} \dot{u} + \frac{\partial M}{\partial q} q + \frac{\partial M}{\partial \dot{q}} \dot{q} + \frac{\partial M}{\partial w} w + \frac{\partial M}{\partial \dot{w}} \dot{w} + \frac{\partial M}{\partial \delta_E} \delta_E$$
$$+ \frac{\partial M}{\partial \dot{\delta}_E} \dot{\delta}_E + \frac{\partial M}{\partial \ddot{\delta}_E} \ddot{\delta}_E + \frac{\partial M}{\partial \delta_F} \delta_F + \frac{\partial M}{\partial \dot{\delta}_F} \dot{\delta}_F + \frac{\partial M}{\partial \delta_B} \delta_B + \frac{\partial M}{\partial \dot{\delta}_B} \dot{\delta}_B + \frac{\partial M}{\partial \ddot{\delta}_B} \ddot{\delta}_B$$

$$N = N_o + \frac{\partial N}{\partial v} v + \frac{\partial N}{\partial \dot{v}} \dot{v} + \frac{\partial N}{\partial r} r + \frac{\partial N}{\partial \dot{r}} \dot{r} + \frac{\partial N}{\partial p} p + \frac{\partial N}{\partial \dot{p}} \dot{p} + \frac{\partial N}{\partial \delta_R} \delta_R$$
$$+ \frac{\partial N}{\partial \dot{\delta}_R} \dot{\delta}_R + \frac{\partial N}{\partial \ddot{\delta}_R} \ddot{\delta}_R + \frac{\partial N}{\partial \delta_A} \delta_A + \frac{\partial N}{\partial \dot{\delta}_A} \dot{\delta}_A + \frac{\partial N}{\partial \ddot{\delta}_A} \ddot{\delta}_A$$

WHERE: δ_E = Angle of deflection of elevator
δ_B = Angle of deflection of dive brakes
δ_F = Angle of deflection of flaps
δ_A = Angle of deflection of ailerons
δ_R = Angle of deflection of rudder

Each of the terms in (II-50) has a physical significance; X_o, Y_o, and Z_o, and L_o, M_o, and N_o are the forces and moments acting along and about the x, y, and z axes respectively while the airplane is in the steady flight condition. The terms similar to $\left(\frac{\partial X}{\partial u}\right)_o u$ express the change in the given force or moment caused by the given disturbance quantity. A more detailed explanation of these quantities is given in a later section of this chapter.

It should be emphasized that the relations in (II-50) are valid only for small disturbances from the steady flight condition of Assumption VI, which states that the airplane is initially flying in unaccelerated flight along a straight flight path (i.e., U_o and W_o are the only component velocities not equal to zero).

SECTION 9 – EXPANSION OF THE THRUST FORCE

In this section, the thrust effects are introduced into the equations of motion. (The influence of thrust on the aerodynamic forces and moments due to such phenomena as the change in flow pattern over the horizontal tail caused by the jet blast will be discussed qualitatively in Chapter IV.)

For the present analysis, the thrust is considered a function of: 1) the power plant revolutions per minute, 2) the forward speed of the airplane, and 3) the altitude. With a power plant arrangement as shown in Figure II-20, the thrust contributes to the X and Z forces and to the moment M.

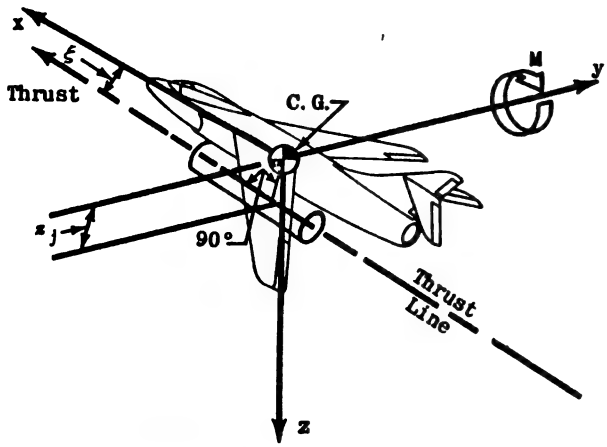

ξ = angle between x axis and thrust line
z_j = perpendicular distance from C.G. to thrust line

Figure II-20

By setting the steady flight thrust equal to T_o, the equations for the steady flight condition become:

(II-51)
$$X_o = T_o \cos \xi$$
$$Z_o = -T_o \sin \xi$$
$$M_o = T_o z_j$$

Since the Eulerian axes remain fixed with reference to the airplane during a disturbance, the thrust components relative to disturbed axes become:

(II-52)
$$X = T_1 \cos \xi$$
$$Z = -T_1 \sin \xi$$
$$M = T_1 z_j$$

where T_1 (the thrust during the disturbance) $= T_o + \Delta T$

The air density remains constant during the small disturbances under consideration, and ΔT can be determined to a good degree of approximation by considering it dependent only upon the change in forward speed and upon the change in power plant rpm. Thus:

(II-53)

$$\Delta T = \frac{\partial T}{\partial u} u + \frac{\partial T}{\partial \delta_{RPM}} \delta_{RPM}$$

and

(II-54)

$$X = T_o \cos \xi + (\cos \xi)\frac{\partial T}{\partial u} u + (\cos \xi)\frac{\partial T}{\partial \delta_{RPM}} \delta_{RPM}$$

$$Z = -T_o \sin \xi - (\sin \xi)\frac{\partial T}{\partial u} u - (\sin \xi)\frac{\partial T}{\partial \delta_{RPM}} \delta_{RPM}$$

$$M = T_o z_j + z_j \frac{\partial T}{\partial u} u + z_j \frac{\partial T}{\partial \delta_{RPM}} \delta_{RPM}$$

The thrust force due to change in power plant rpm. is actually an input force similar to a control surface deflection and would arise from a throttle deflection. Since there would be a time lag between the throttle deflection and the resulting change in rpm of the power plant, the analysis is somewhat simplified by considering the partial derivative $\partial T/\partial \delta_{RPM}$ rather than $\partial T/\partial \delta_{throttle}$

SECTION 10 – COMPLETE EQUATIONS OF MOTION

Now that the individual contributions to the equations of motion have been examined in some small detail, the complete equations of motion of the airframe can be written. The equations for the steady flight condition can be found by substituting the steady flight values of the aerodynamic and thrust forces and moments into (II-45) and setting the disturbance terms equal to zero:

(II-55)

$$\begin{aligned} X_o - W\sin\theta_o + T_o \cos\xi &= 0 \\ Y_o + 0 + 0 &= 0 \\ Z_o + W\cos\theta_o - T_o \sin\xi &= 0 \\ L_o + 0 + 0 &= 0 \\ M_o + 0 + T_o z_j &= 0 \\ N_o + 0 + 0 &= 0 \end{aligned}$$

The equations of motion for the disturbed airplane are found by substituting the disturbed values of the forces and moments, (II-50) and (II-54), into (II-45):

(II-56)

$$m[\dot{u} + W_o q + \boxed{+ g \sin\theta_o} + g\,\theta \cos\theta_o] = \boxed{X_o} + \frac{\partial X}{\partial u} u + \frac{\partial X}{\partial \dot{u}} \dot{u}$$
$$+ \frac{\partial X}{\partial q} q + \frac{\partial X}{\partial \dot{q}} \dot{q} + \frac{\partial X}{\partial w} w + \frac{\partial X}{\partial \dot{w}} \dot{w} + \frac{\partial X}{\partial \delta_E} \delta_E + \frac{\partial X}{\partial \dot{\delta}_E} \dot{\delta}_E + \frac{\partial X}{\partial \ddot{\delta}_E} \ddot{\delta}_E + \frac{\partial X}{\partial \delta_P} \delta_P$$
$$+ \frac{\partial X}{\partial \dot{\delta}_P} \dot{\delta}_P + \frac{\partial X}{\partial \delta_B} \delta_B + \frac{\partial X}{\partial \dot{\delta}_B} \dot{\delta}_B + \frac{\partial X}{\partial \ddot{\delta}_B} \ddot{\delta}_B + \boxed{T_o \cos\xi} + (\cos\xi)\frac{\partial T}{\partial u} u + (\cos\xi)\frac{\partial T}{\partial \delta_{RPM}} \delta_{RPM}$$

$$m[\dot{v} + U_o r - W_o p - g\psi \sin\theta_o - (g\cos\theta_o)\phi] + \boxed{Y_o} + \frac{\partial Y}{\partial r} r + \frac{\partial Y}{\partial \dot{r}} \dot{r} + \frac{\partial Y}{\partial v} v$$
$$+ \frac{\partial Y}{\partial \dot{v}} \dot{v} + \frac{\partial Y}{\partial p} p + \frac{\partial Y}{\partial \dot{p}} \dot{p} + \frac{\partial Y}{\partial \delta_A} \delta_A + \frac{\partial Y}{\partial \dot{\delta}_A} \dot{\delta}_A + \frac{\partial Y}{\partial \ddot{\delta}_A} \ddot{\delta}_A + \frac{\partial Y}{\partial \delta_R} \delta_R + \frac{\partial Y}{\partial \dot{\delta}_R} \dot{\delta}_R + \frac{\partial Y}{\partial \ddot{\delta}_R} \ddot{\delta}_R$$

$$m[\dot{w} - U_o q + g\theta \sin\theta_o \boxed{- g\cos\theta_o}] + \boxed{Z_o} + \frac{\partial Z}{\partial u} u + \frac{\partial Z}{\partial \dot{u}} \dot{u} + \frac{\partial Z}{\partial q} q + \frac{\partial Z}{\partial \dot{q}} \dot{q}$$
$$+ \frac{\partial Z}{\partial w} w + \frac{\partial Z}{\partial \dot{w}} \dot{w} + \frac{\partial Z}{\partial \delta_E} \delta_E + \frac{\partial Z}{\partial \dot{\delta}_E} \dot{\delta}_E + \frac{\partial Z}{\partial \ddot{\delta}_E} \ddot{\delta}_E + \frac{\partial Z}{\partial \delta_P} \delta_P + \frac{\partial Z}{\partial \dot{\delta}_P} \dot{\delta}_P + \frac{\partial Z}{\partial \delta_B} \delta_B + \frac{\partial Z}{\partial \dot{\delta}_B} \dot{\delta}_B$$
$$+ \frac{\partial Z}{\partial \ddot{\delta}_B} \ddot{\delta}_B \boxed{- T_o \sin\xi} - (\sin\xi)\frac{\partial T}{\partial u} u - (\sin\xi)\frac{\partial T}{\partial \delta_{RPM}} \delta_{RPM}$$

$$\dot{p} I_{xx} - \dot{r} I_{xz} = \boxed{L_o} + \frac{\partial L}{\partial r} r + \frac{\partial L}{\partial \dot{r}} \dot{r} + \frac{\partial L}{\partial v} v + \frac{\partial L}{\partial \dot{v}} \dot{v} + \frac{\partial L}{\partial p} p + \frac{\partial L}{\partial \dot{p}} \dot{p} + \frac{\partial L}{\partial \delta_A} \delta_A$$
$$+ \frac{\partial L}{\partial \dot{\delta}_A} \dot{\delta}_A + \frac{\partial L}{\partial \ddot{\delta}_A} \ddot{\delta}_A + \frac{\partial L}{\partial \delta_R} \delta_R + \frac{\partial L}{\partial \dot{\delta}_R} \dot{\delta}_R + \frac{\partial L}{\partial \ddot{\delta}_R} \ddot{\delta}_R$$

$$\dot{q} I_{yy} = \boxed{M_o} + \frac{\partial M}{\partial u} u + \frac{\partial M}{\partial \dot{u}} \dot{u} + \frac{\partial M}{\partial q} q + \frac{\partial M}{\partial \dot{q}} \dot{q} + \frac{\partial M}{\partial w} w + \frac{\partial M}{\partial \dot{w}} \dot{w} + \frac{\partial M}{\partial \delta_E} \delta_E + \frac{\partial M}{\partial \dot{\delta}_E} \dot{\delta}_E$$
$$+ \frac{\partial M}{\partial \ddot{\delta}_E} \ddot{\delta}_E + \frac{\partial M}{\partial \delta_P} \delta_P + \frac{\partial M}{\partial \dot{\delta}_P} \dot{\delta}_P + \frac{\partial M}{\partial \delta_B} \delta_B + \frac{\partial M}{\partial \dot{\delta}_B} \dot{\delta}_B + \frac{\partial M}{\partial \ddot{\delta}_B} \ddot{\delta}_B + \boxed{T_o z_j} + z_j \frac{\partial T}{\partial u} u + z_j \frac{\partial T}{\partial \delta_{RPM}} \delta_{RPM}$$

$$\dot{r} I_{zz} - \dot{p} I_{xz} = \boxed{N_o} + \frac{\partial N}{\partial v} v + \frac{\partial N}{\partial \dot{v}} \dot{v} + \frac{\partial N}{\partial r} r + \frac{\partial N}{\partial \dot{r}} \dot{r} + \frac{\partial N}{\partial p} p + \frac{\partial N}{\partial \dot{p}} \dot{p} + \frac{\partial N}{\partial \delta_R} \delta_R$$
$$+ \frac{\partial N}{\partial \dot{\delta}_R} \dot{\delta}_R + \frac{\partial N}{\partial \ddot{\delta}_R} \ddot{\delta}_R + \frac{\partial N}{\partial \delta_A} \delta_A + \frac{\partial N}{\partial \dot{\delta}_A} \dot{\delta}_A + \frac{\partial N}{\partial \ddot{\delta}_A} \ddot{\delta}_A$$

The quantities in the boxes disappear because of the steady flight conditions of (II-55). Dividing the force equations by the mass m and the moment equations by the appropriate moments of inertia yields terms of the form:

$$\frac{1}{m}\frac{\partial X}{\partial u} u \qquad \text{and} \qquad \frac{1}{I_{xx}}\frac{\partial L}{\partial r} r$$

Replacing $\frac{1}{m}\frac{\partial X}{\partial u}$ by X_u and $\frac{1}{I_{xx}}\frac{\partial L}{\partial r}$ by L_r simplifies the notation. These quantities are called either "dimensional stability derivatives "or simply "stability derivatives." By eliminating those terms whose sum, in accordance with equations (II-55), is zero because of the steady flight conditions, and by using the previous shorthand notation, (II-56) are reduced to the form:

(II-57)

$$\dot{u} + W_o q + g\theta \cos\theta_o = X_u u + X_{\dot{u}}\dot{u} + X_q q + X_{\dot{q}}\dot{q} + X_w w + X_{\dot{w}}\dot{w}$$
$$+ X_{\delta_E}\delta_E + X_{\dot{\delta}_E}\dot{\delta}_E + X_{\ddot{\delta}_E}\ddot{\delta}_E + X_{\delta_P}\delta_P + X_{\dot{\delta}_P}\dot{\delta}_P + X_{\delta_B}\delta_B + X_{\dot{\delta}_B}\dot{\delta}_B$$
$$+ X_{\ddot{\delta}_B}\ddot{\delta}_B + \cos\xi\, T_u u + \cos\xi\, T_{\delta_{RPM}}\delta_{RPM}$$

$$\dot{v} + U_o r - W_o p - g\psi \sin\theta_o - g\phi \cos\theta_o = Y_r r + Y_{\dot{r}}\dot{r} + Y_v v$$
$$+ Y_{\dot{v}}\dot{v} + Y_p p + Y_{\dot{p}}\dot{p} + Y_{\delta_A}\delta_A + Y_{\dot{\delta}_A}\dot{\delta}_A + Y_{\ddot{\delta}_A}\ddot{\delta}_A + Y_{\delta_R}\delta_R + Y_{\dot{\delta}_R}\dot{\delta}_R$$
$$+ Y_{\ddot{\delta}_R}\ddot{\delta}_R$$

$$\dot{w} - U_o q + g\theta \sin\theta_o = Z_u u + Z_{\dot{u}}\dot{u} + Z_q q + Z_{\dot{q}}\dot{q} + Z_w w + Z_{\dot{w}}\dot{w}$$
$$+ Z_{\delta_E}\delta_E + Z_{\dot{\delta}_E}\dot{\delta}_E + Z_{\ddot{\delta}_E}\ddot{\delta}_E + Z_{\delta_P}\delta_P + Z_{\dot{\delta}_P}\dot{\delta}_P + Z_{\delta_B}\delta_B + Z_{\dot{\delta}_B}\dot{\delta}_B$$
$$+ Z_{\ddot{\delta}_B}\ddot{\delta}_B - (\sin\xi)T_u u - (\sin\xi)T_{\delta_{RPM}}\delta_{RPM}$$

$$\dot{p} - \dot{r}\frac{I_{xz}}{I_{xx}} = L_r r + L_{\dot{r}}\dot{r} + L_v v + L_{\dot{v}}\dot{v} + L_p p + L_{\dot{p}}\dot{p} + L_{\delta_A}\delta_A$$
$$+ L_{\dot{\delta}_A}\dot{\delta}_A + L_{\ddot{\delta}_A}\ddot{\delta}_A + L_{\delta_R}\delta_R + L_{\dot{\delta}_R}\dot{\delta}_R + L_{\ddot{\delta}_R}\ddot{\delta}_R$$

$$\dot{q} = M_u u + M_{\dot{u}}\dot{u} + M_q q + M_{\dot{q}}\dot{q} + M_w w + M_{\dot{w}}\dot{w} + M_{\delta_E}\delta_E + M_{\dot{\delta}_E}\dot{\delta}_E + M_{\ddot{\delta}_E}\ddot{\delta}_E$$
$$+ M_{\delta_P}\delta_P + M_{\dot{\delta}_P}\dot{\delta}_P + M_{\delta_B}\delta_B + M_{\dot{\delta}_B}\dot{\delta}_B + M_{\ddot{\delta}_B}\ddot{\delta}_B + \frac{z_j}{I_{yy}}T_u u$$
$$+ \frac{z_j}{I_{yy}}T_{\delta_{RPM}}\delta_{RPM}$$

$$\dot{r} - \dot{p}\frac{I_{xz}}{I_{zz}} = N_v v + N_{\dot{v}}\dot{v} + N_r r + N_{\dot{r}}\dot{r} + N_p p + N_{\dot{p}}\dot{p} + N_{\delta_R}\delta_R$$
$$+ N_{\dot{\delta}_R}\dot{\delta}_R + N_{\ddot{\delta}_R}\ddot{\delta}_R + N_{\delta_A}\delta_A + N_{\dot{\delta}_A}\dot{\delta}_A + N_{\ddot{\delta}_A}\ddot{\delta}_A$$

SECTION 11 – UNSTEADY FLOW

In the classical derivation of the equations of motion of an airplane, it is assumed that the aerodynamic forces and moments acting on the airplane are dependent only on the velocities of the airplane relative to the air mass. This assumption implies that these forces acting on an airplane at any instant during accelerated flight are the same as those that would be acting on the airplane if it were in steady flight with the velocities prevailing at that instant. In other words, if an airplane were to change its orientation suddenly with respect to its flight path, the flow around the airplane would instantaneously change to a steady state flow pattern without any transition period. This sort of flow is called quasi-steady flow and is used to simplify the problems.

The resultant force on an airplane is also dependent on the rate of change of the velocities. A so-called "apparent mass effect" arises from the fact that the airplane must accelerate a finite mass of air when the airplane itself is in accelerated motion. Even after the airplane returns to steady flight, it is possible that local flow disturbances caused by the accelerated motion of the airplane previous to its return to steady flight may be close enough to the airplane to produce forces on it. That is to say, the forces acting on an airplane at any instant are also dependent upon the history of the motion. In the light in these facts, quasi-steady theory does not truly represent the forces acting on an airframe in accelerated motion.

Until recently, motions of an airplane predicted by the use of quasi-steady theory were in satisfactory agreement with flight test data. However, the behavior of some modern high speed jet airplanes has exhibited marked discrepancies between the predicted damping and the observed flight test damping of high frequency oscillatory modes. These discrepancies increase with increasing Mach number; as a result, the development of equations to account for unsteady flow effects must necessarily be based on compressible flow theory. Several excellent papers have recently appeared treating non-steady flow, but as yet, research on the subject is still in the developmental stages. For the rest of this volume, flow is assumed to be quasi-steady.

ASSUMPTION VII. The flow is assumed to be quasi-steady.

Because of Assumption VII, all derivatives with respect to the rates of change of velocities are omitted with the exception of those with respect to $\dot{w}$, which are retained to account for the effect on the horizontal tail of the downwash from the wing. This effect is explained later on the basis of purely quasi-steady considerations.

Downwash can be briefly described as follows: A wing producing lift on an airplane in flight has a greater resultant pressure acting on the lower surface than on the upper. Because of this pressure differential, air from the bottom surface (high pressure area) flows around the wing tips to the upper surface (low pressure area) as shown by the arrows in Figure II-21. As the airplane proceeds along its flight path it leaves two trails of air in circular motion. These air masses are referred to as "tip vortices" and are shown in Figure II-22.

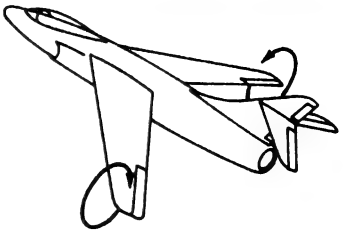

Figure II-21 Flow Around Wing Tips from High to Low Pressure Area

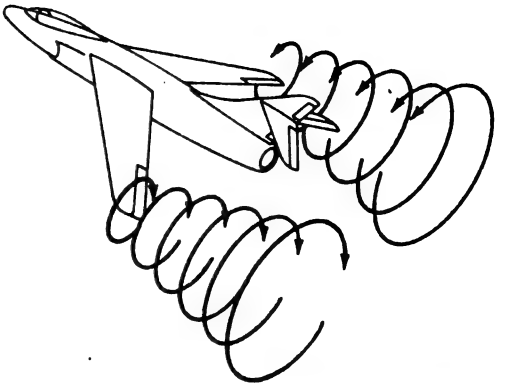

Figure II-22 Airplane with Tip Vortices

Figure II-22 shows that these vortices produce a downward flow of air at the horizontal tail. The velocity with which this air flows around the wing tip has been shown to be proportional to the angle of attack of the wing.

The angle of attack is defined as the angle between the wing chord line and the relative wind vector as shown in Figure II-23.

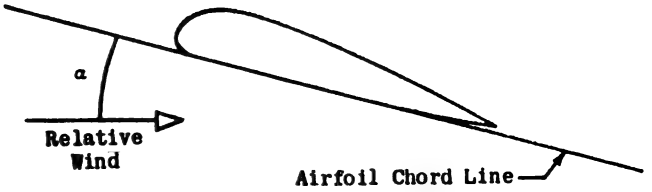

α = Angle of Attack

Figure II-23 Wing Angle of Attack

If a wing moving through an air mass with an angle of attack α_o and a steady forward velocity U_o is suddenly given a vertical velocity w without changing the forward velocity, the angle of attack changes as shown in Figure II-24:

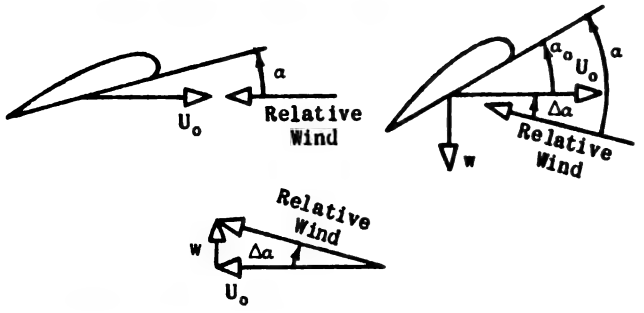

Figure II-24 Change in Angle of Attack Due to Vertical Velocity

The changes in angle of attack are proportional to the vertical velocity w. From Figure II-24 the following relations may be derived:

$\tan \Delta\alpha = \frac{w}{U_o}$; considering $\Delta\alpha$ to be small:

$$\Delta\alpha \cong \frac{w}{U_o}$$

Since downwash is a downward flow of air, it effectively reduces the angle of attack of the tail.

If it is assumed that the wing tip vortices change abruptly with disturbances in wing angle of attack (quasi-steady flow) the effect of such a disturbance will not be apparent at the tail until the tail reaches the position in the air mass held by the wing at the time of the disturbance. That is, there will exist a time lag between the cause and effect of downwash.

Figure II-25 shows an airplane at two instants along its flight path.

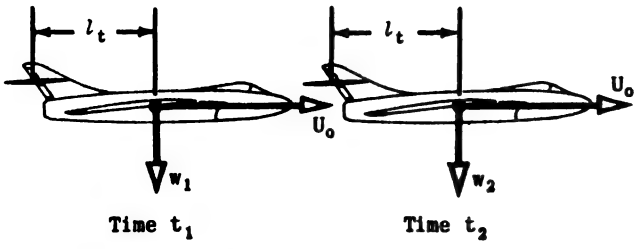

l_t = Distance from wing to horizontal tail

Figure II-25 Airplane at Two Instants During Flight

At the time t_2, the airplane has a downward velocity w_2 that is different from the downward velocity w_1 of the airplane at time t_1. The angle of attack of the wing has changed; consequently, the downwash at the wing has changed. The airplane will travel the distance l_t in $\frac{l_t}{U_o}$ seconds. If the difference between t_2 and t_1, say Δt, is equal to $\frac{l_t}{U_o}$, the tail at time t_2 will occupy the position occupied by the wing at time t_1.

For small intervals of time, the expression for w_2 may be written as:

$$w_2 = w_1 + \frac{dw}{dt}\,\Delta t \qquad \text{(II-58)}$$

Since $\frac{l_t}{U_o}$ is numerically small:

$$w_2 = w_1 + \frac{dw}{dt}\,\frac{l_t}{U_o} \qquad \text{(II-59)}$$

The downwash at the tail is proportional to the downwash at the wing which is proportional to the angle of attack of the wing. The angle of attack of the wing, in turn, is proportional to the vertical velocity of the wing. Thus, (II-60) may be written:

$$(DW)_T = k\,w = \text{Downwash at the tail due to downwash from wing} \qquad \text{(II-60)}$$

Since equation (II-60) shows that the downwash at the tail is proportional to the vertical velocity of the airplane, the change of the value of the downwash at the tail is then proportional to the change of vertical velocity.

The change of vertical velocity, Δw, which can be obtained from (II-59), may be written:

$$\Delta w = w_2 - w_1 = \frac{dw}{dt}\,\frac{l_t}{U_o} \qquad \text{(II-61)}$$

The change of downwash at the tail due to the wing is then equal to $k\,\Delta w$.

$$(\Delta DW)_T = k\,\frac{l_t}{U_o}\,\frac{dw}{dt} = \text{Change of downwash at tail due to downwash from wing} \qquad \text{(II-62)}$$

This change in downwash produces a change in the angle of attack of the tail which in turn causes a change in the resultant aerodynamic force which acts on the tail and which is proportional to $\dot{w}$, the rate of change of the vertical velocity of the airplane. Thus it may be seen that aerodynamic partial derivatives with respect to $\dot{w}$ can be included in the equations of motion on the basis of purely quasi-steady considerations.

SECTION 12 – CHOICE OF AXIS SYSTEM

The only restrictions thus far imposed on the orientation of the Eulerian axes with respect to the airplane are that the y axis be a principal axis and that the origin be located at the center of gravity of the airplane. When the x axis is oriented so that it is a principal axis, the Eulerian axes are referred to as principal axes, but when the x axis is so oriented in the airplane during the steady flight condition that it is parallel to the relative wind, the Eulerian axes are referred to as stability axes. It is important to remember that the stability axes are oriented with the x axis parallel to the relative wind during the steady flight condition. When the airframe is disturbed from the steady flight condition, the Eulerian axes rotate with the airframe and do not change direction with respect to the airplane, consequently, the disturbed x axis may or may not be parallel to the relative wind while the airplane is in the disturbed flight condition (see Figure II-26).

fixed with respect to the airplane. If the instrument axes are aligned with principal airplane axes, flight test data yield stability derivatives with respect to principal axes.

The use of stability axes eliminates the terms containing W_o from (II-57), but now the product of inertia, I_{xz}, is different from zero, and the moments and the product of inertia vary with the equilibrium flight condition as well as with the airplane weight loading. Wind tunnel test results are measured in terms of lift and drag forces which are measured perpendicular and parallel to the relative wind and which are logically referred to stability axes. Stability derivatives calculated from subsonic flow theory are also calculated with reference to stability axes.

The various methods of obtaining stability derivatives

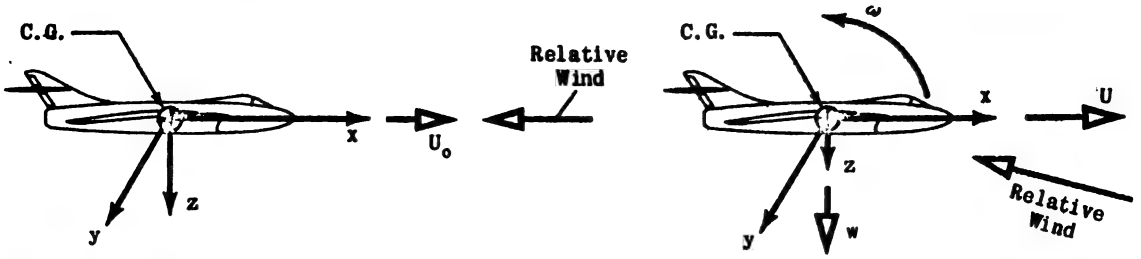

Figure II-26 Direction of Stability Axes with Respect to the Relative Wind During the Steady Flight and Disturbed Flight Conditions

Several factors must be considered in determining which axis system is more suitable for a given analysis.

If the equations of motion are written in terms of motion along the principal axes, these equations are somewhat simplified because the product of inertia, I_{xz}, is identically zero. In addition, the moments of inertia in a principal axis system of an airplane are not dependent upon the steady flight condition. On the other hand, the location of the principal axes is a function of the distribution of the airplane's mass and consequently varies according to the loading. In general, the principal x axis very nearly coincides with the longitudinal fuselage reference line which, in most cases, is only slightly different from the wing chord line (see Figure II-27).

In calculating stability derivatives for supersonic flight, it is convenient to orient the x axis along the wing chord line. When the disturbance is small, the pressure difference between the upper and lower wing surfaces is determined from the general Bernoulli equation, and the stability derivatives are determined from integrations of the forces and moments over the wing. Since the wing chord line is only slightly displaced from the principal axis in this case, it is convenient to use principal axes.

Flight test data are generally measured by instruments

are discussed in a later section of this volume. The important points to be noted here are that stability derivatives are referred either to principal axes or to stability axes, according to the method of derivation, and that the equations of motion can easily be altered to apply to either axis system. Throughout the remainder of this volume, the stability axis system is used since stability derivatives are most commonly obtained with respect to this system. It should be emphasized, however, that the equations of motion differ only slightly

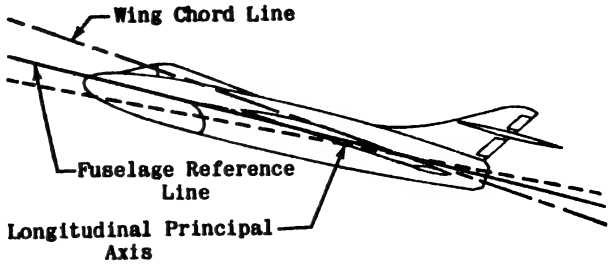

Figure II-27

when referenced to either axis system and that the mathematical techniques employed in their solution are identical.

SECTION 13 – EQUATIONS OF MOTION REFERRED TO STABILITY AXES

The equations of motion referred to stability axes with the flow considered to be quasi-steady can be obtained from (II-57) by eliminating the following quantities:

1. All terms containing W_o, which disappears because of the direction of the stability axes.
2. All aerodynamic partial derivatives with respect to rates of change of velocities except those with respect to w.
3. All aerodynamic partial derivatives with respect to rates of change of control surface deflections.

Equations (II-57) then reduce to (II-63) and (II-64).

(II-63)
$$\dot{u} + g\theta\cos\theta_o = T_u(\cos\xi)u + T_{\delta_{RPM}}\delta_{RPM}\cos\xi + X_u u + X_q q + X_w w + X_{\dot{w}}\dot{w} + X_{\delta_E}\delta_E + X_{\delta_F}\delta_F + X_{\delta_B}\delta_B$$

$$\dot{w} - U_o q + g\theta\sin\theta_o = -T_u(\sin\xi)u - T_{\delta_{RPM}}\delta_{RPM}\sin\xi + Z_u u + Z_q q + Z_w w + Z_{\dot{w}}\dot{w} + Z_{\delta_E}\delta_E + Z_{\delta_F}\delta_F + Z_{\delta_B}\delta_B$$

$$\dot{q} = \frac{z_T m}{I_{yy}} T_u u + \frac{z_T m}{I_{yy}} T_{\delta_{RPM}}\delta_{RPM} + M_u u + M_q q + M_w w + M_{\dot{w}}\dot{w} + M_{\delta_E}\delta_E + M_{\delta_F}\delta_F + M_{\delta_B}\delta_B$$

(II-64)
$$\dot{v} + U_o r - g\psi\sin\theta_o - g\phi\cos\theta_o = Y_r r + Y_v v + Y_p p + Y_{\delta_A}\delta_A + Y_{\delta_R}\delta_R$$

$$\dot{p} - \frac{I_{xz}}{I_{xx}}\dot{r} = L_r r + L_v v + L_p p + L_{\delta_A}\delta_A + L_{\delta_R}\delta_R$$

$$\dot{r} - \frac{I_{xz}}{I_{zz}}\dot{p} = N_r r + N_v v + N_p p + N_{\delta_A}\delta_A + N_{\delta_R}\delta_R$$

An examination of these equations shows that (II-63) are functions of the variables u, θ, and w, whereas (II-64) are functions of the variables v, r, and p. Thus, as a result of the assumptions made in the previous analysis, the equations of motion can be treated as two independent sets of three equations. Equations (II-63) are referred to as the longitudinal or symmetrical equations because, when these motions occur, the plane of symmetry of the airplane remains in the plane it occupied in the steady flight condition. Equations (II-64) are referred to as the lateral or asymmetrical equations.

Since the longitudinal motions are independent of the lateral motions, they are treated separately in the rest of this volume.

SECTION 14 – DESCRIPTION OF THE DIMENSIONAL STABILITY DERIVATIVES

The adoption of Assumption VII has greatly reduced the number of stability derivatives appearing in the equations of motion. In this section, each of the dimensional stability derivatives in (II-63) and (II-64) is first given a brief physical interpretation, then expanded into a more basic form, and shown to be a function of what are called "basic non-dimensional stability derivatives." (A detailed discussion of these basic non-dimensional stability derivatives is given in Chapter V.) The longitudinal stability derivatives, which appear in the equations of motion given in (II-63), are treated first and the lateral stability derivatives, which appear in (II-64), are treated later. Equations (II-47), used in the discussion, are repeated here for reference:

(II-65)

$L = C_L \frac{1}{2}\rho V^2 S$ $\qquad$ $Z = C_z \frac{1}{2}\rho V^2 S$

$D = C_D \frac{1}{2}\rho V^2 S$ $\qquad$ $L = C_l \frac{1}{2}\rho V^2 Sb$

$X = C_x \frac{1}{2}\rho V^2 S$ $\qquad$ $M = C_m \frac{1}{2}\rho V^2 Sc$

$Y = C_y \frac{1}{2}\rho V^2 S$ $\qquad$ $N = C_n \frac{1}{2}\rho V^2 Sb$

It should be noted that the quantity V^2, which appears in (II-65), is the square of the total linear velocity. In the stability axis system, the total linear velocity during the steady flight condition is equal to U_o, which is the velocity in the direction of the x axis. When disturbed from steady flight, the airplane can have velocity components $U_o + u$, v, and w directed along the x, y and z axes respectively. During disturbed flight, the magnitude of the total linear velocity, can be expressed as:

(II-66)
$$|\bar{V}| = \sqrt{(U_o + u)^2 + v^2 + w^2}$$

or

(II-67)
$$|\bar{V}| = \sqrt{U_o^2 + 2U_o u + u^2 + v^2 + w^2}$$

In Assumption V, u, v, and w were assumed to be very small so that their products and squares could be neglected. Thus:

(II-68)
$$|\bar{V}| \simeq \sqrt{U_o^2 + 2U_o u}$$

Also, since U_o^2 is very much greater than $2U_o u$, a very good approximation can be given in:

(II-69)
$$|\bar{V}| \simeq U_o \simeq U$$

Therefore, the magnitude of the total linear velocity $\bar{V}$ at any instant is approximately equal to the x component of linear velocity, U, at that instant. Since $U = U_o + u$, the magnitude of $\bar{V}$ at any instant is approximately equal also to the linear velocity during the steady

flight condition, U_o. Thus V, U_o, and U can be used somewhat interchangeably.

LONGITUDINAL STABILITY DERIVATIVES

Effect of u, The Change in Forward Speed

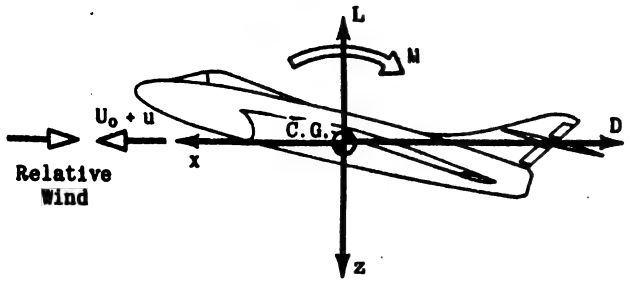

Figure II-28 Variation of Lift, Drag and Pitching Moment with Change in Forward Velocity

As an airplane increases its forward speed, the lift, L, drag, D, and moment, M, change. Generally, but not always, each of these quantities increases.

Since drag acts along the negative x axis, an increase in drag contributes a negative X force. The change in X force due to a change in forward speed can be expressed mathematically in the form:

(II-70) $$\Delta X = \frac{\partial X}{\partial u} u = -\frac{\partial D}{\partial u} u$$

(II-71) $$X_u = \frac{1}{m}\frac{\partial X}{\partial u} = -\frac{1}{m}\frac{\partial D}{\partial u}$$

Using the drag equation from (II-65), equation (II-71) can be written as:

(II-72) $$X_u = -\frac{1}{m}\frac{\partial D}{\partial u} = -\frac{1}{m}\frac{\partial(\frac{1}{2}\rho U^2 S C_D)}{\partial u}$$

When the indicated differentiation is performed, (II-72) yields:

(II-73) $$X_u = -\frac{\rho S}{2m}\left[U^2\frac{\partial C_D}{\partial u} + 2U C_D\right]$$

and

(II-74) $$X_u = -\frac{\rho S U}{m}\left[\frac{U}{2}\frac{\partial C_D}{\partial u} + C_D\right]$$

Since lift acts along the negative z axis, an increase in lift due to a change in forward speed contributes a negative Z force:

(II-75) $$\Delta Z = \frac{\partial Z}{\partial u} u = -\frac{\partial L}{\partial u} u$$

(II-76) $$Z_u = \frac{1}{m}\frac{\partial Z}{\partial u} = -\frac{1}{m}\frac{\partial L}{\partial u}$$

By noting the similarity between (II-76) and (II-71) and between the lift and drag equations of (II-75), equation (II-77) can be written immediately:

(II-77) $$Z_u = -\frac{\rho S U}{m}\left[\frac{U}{2}\frac{\partial C_L}{\partial u} + C_L\right]$$

The change in moment caused by a change in forward speed can be expressed as:

(II-78) $$\Delta M = \frac{\partial M}{\partial u} u$$

(II-79) $$M_u = \frac{1}{I_{yy}}\frac{\partial M}{\partial u}$$

The same mechanics used in the expansion of X_u can be used to derive M_u:

(II-80) $$M_u = \frac{\rho S U c}{I_{yy}}\left[\frac{U}{2}\frac{\partial C_m}{\partial u} + C_m\right]$$

The equation for thrust can be written in a form similar to that of the lift and drag equations in (II-65):

(II-81) $$T = \frac{1}{2}\rho U^2 S C_T$$

The change in thrust due to a change in forward speed is:

(II-82) $$\Delta T = \frac{\partial T}{\partial u} u$$

According to the mechanics used in the expansion of X_u, the stability derivative T_u can be written as:

(II-83) $$T_u = \frac{\rho S U}{m}\left[\frac{U}{2}\frac{\partial C_T}{\partial u} + C_T\right]$$

Some new symbols are now defined. The quantity C_{m_u} is equal by definition to $\frac{U}{2}\frac{\partial C_m}{\partial u}$:

(II-84) $$\frac{U}{2}\frac{\partial C_m}{\partial u} = C_{m_u}$$

Similarly,

(II-85) $$\frac{U}{2}\frac{\partial C_L}{\partial u} = C_{L_u}$$

(II-86) $$\frac{U}{2}\frac{\partial C_D}{\partial u} = C_{D_u}$$

(II-87) $$\frac{U}{2}\frac{\partial C_T}{\partial u} = C_{T_u}$$

In Figure II-29, the quantities L_o and D_o represent the lift and drag acting on the airplane during the steady flight condition. The lift and drag always act respectively normal and parallel to the relative wind. According

Effect of w, The Change in Speed Along the z Axis

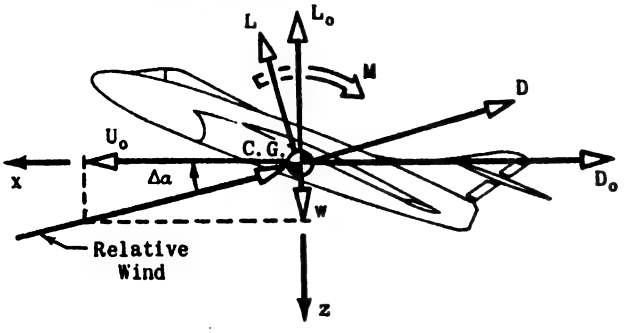

Figure II-29

to the definition of stability axes, the relative wind during the steady flight condition is parallel to the x axis. Therefore the only component of linear velocity during the steady flight condition is U_o. Thus, L_o and D_o are respectively perpendicular and parallel to the x axis. When the airplane is disturbed from steady flight so that it has a component of velocity along the z axis, w, as well as a forward velocity, U_o, the relative wind shifts to a new position as shown in Figure II-29. This shift results in an increase in angle of attack denoted by the angle $\Delta\alpha$. The quantities L and D, in Figure II-29, represent the lift and drag acting on the airplane during the disturbed flight condition, and they act normal and parallel to the relative wind. The relative wind acts in the direction opposite to the vector which represents the sum of $\bar{U}_o$ and $\bar{w}$.

The change in X and Z forces caused by w, the change in speed along the z axis, can be found by resolving L and D along the x and z axes:

(II-88) $$\frac{\partial X}{\partial w} = \underset{w \to 0}{\text{Limit}} \frac{\Delta X}{w}$$

$$w = U_o \tan \Delta\alpha \approx U_o \Delta\alpha$$

(II-89) $$\frac{\partial X}{\partial w} = \underset{\Delta\alpha \to 0}{\text{Limit}} \frac{1}{U_o} \frac{\Delta X}{\Delta\alpha}$$

From Figure II-29,

(II-90) $$\Delta X = L \sin \Delta\alpha - D \cos \Delta\alpha - (-D_o)$$

L and D can be written as:

(II-91) $$L = L_o + \Delta L$$
$$D = D_o + \Delta D$$

Since, according to Assumption V, disturbances from steady flight are considered small, ΔL, ΔD, and $\Delta\alpha$ are small. By setting $\sin \Delta\alpha = \Delta\alpha$ and $\cos \Delta\alpha = 1$, and using (II-91), equation (II-90) can be rewritten as:

(II-92) $$\Delta X = (L_o + \Delta L)\, \Delta\alpha - (D_o + \Delta D) + D_o$$

Neglecting products of small quantities,

(II-93) $$\Delta X = L_o \Delta\alpha - \Delta D$$

Substituting (II-93) into (II-89) yields:

(II-94) $$\frac{\partial X}{\partial w} = \underset{\Delta\alpha \to 0}{\text{Limit}} \frac{1}{U_o} \frac{L\Delta\alpha - \Delta D}{\Delta\alpha}$$

And in the limit:

(II-95) $$\frac{\partial X}{\partial w} = \frac{1}{U_o}\left(L - \frac{\partial D}{\partial \alpha}\right)$$

Also

(II-96) $$X_w = \frac{1}{m} \frac{\partial X}{\partial w} = \frac{1}{m U_o}\left(L - \frac{\partial D}{\partial \alpha}\right)$$

Substitution of the values of lift and drag from (II-65) into (II-96) yields:

(II-97) $$X_w = \frac{1}{m U_o}\left[\frac{1}{2}\rho S U^2 C_L - \frac{\partial}{\partial \alpha}\left(\frac{1}{2}\rho S U^2 C_D\right)\right]$$

(II-98) $$X_w = \frac{\rho S U}{2m}\left(C_L - C_{D_\alpha}\right)$$

where $$C_{D_\alpha} = \frac{\partial C_D}{\partial \alpha}$$

The change in the Z force due to w can be found by resolving the forces in Figure II-29 along the z axis and performing operations similar to those used in the derivation of (II-98):

(II-99) $$Z_w = -\frac{\rho S U}{2m}\left(C_{L_\alpha} + C_D\right)$$

The change in moment due to w is most easily visualized by observing the components of the total lift and drag that act on the wing and the horizontal tail. Figure II-30 shows these components.

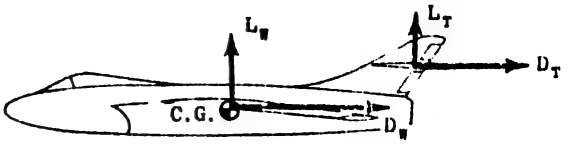

Figure II-30 Lift and Drag Acting on the Wing and the Horizontal Tail

The subscripts W and T refer to wing and tail. A vertical velocity, w, causes a change in angle of attack of both the wing and the horizontal tail and consequently changes the lift and drag acting on these lifting surfaces. The resulting moment can be found by summing the moments caused by each of these forces about the center of gravity. It may be seen that this moment is dependent upon the location of the center of gravity with respect to the wing. The moment equation from (II-65) is rewritten:

(II-100) $$M = \frac{1}{2}\rho U^2 S c C_m$$

(II-101) $$\frac{\partial M}{\partial w} = \frac{\rho U^2 S c}{2}\frac{\partial C_m}{\partial w}$$

Substituting $w = U_o\Delta\alpha$ in (II-101) yields:

$$\frac{\partial M}{\partial w} = \frac{\rho U^2 S c}{2}\frac{1}{U_o}\frac{\partial C_m}{\partial \alpha} \quad \text{Since} \quad M_w = \frac{1}{I_{yy}}\frac{\partial M}{\partial w}$$

(II-102) $$M_w = \frac{\rho S U c}{2 I_{yy}} C_{m_\alpha} \quad \text{where} \quad C_{m_\alpha} = \frac{\partial C_m}{\partial \alpha}$$

Effect of $\dot{w}$, the Rate of Change of Speed along the z Axis

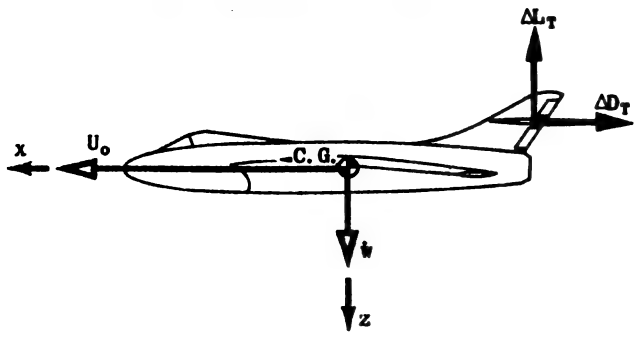

Figure II-31

In the discussion of unsteady flow (Section II-10), the existence of a force due to $\dot{w}$ was explained on the basis of quasi-steady flow considerations. It was pointed out that this rate of change of speed along the axis results in an effective change of the angle of attack of the horizontal tail. This change in angle of attack causes changes in the lift and drag acting on the horizontal tail. These are incremental forces and are represented by ΔL_T and ΔD_T in Figure II-31.

The change in drag on the horizontal tail is the main contributor to the change in the X force. Because the drag on the horizontal tail is generally small in comparison with that on the total airplane, this force is not considered. Therefore, $X_{\dot{w}}$ is considered zero in the first approximation. However, the change in lift on the horizontal tail causes a change both in the Z force and in the moment. The lift on the horizontal tail acts in the negative z direction, and therefore:

(II-103) $$\Delta Z = \frac{\partial Z}{\partial \dot{w}}\dot{w} = -\frac{\partial L}{\partial \dot{w}}\dot{w}$$

(II-104) $$\frac{\partial L}{\partial \dot{w}} = \frac{\rho S U^2}{2}\frac{\partial C_L}{\partial \dot{w}} = \frac{\rho S U}{2}\frac{\partial C_L}{\partial \dot{\alpha}}$$

since $$\dot{w} = U_o\dot{\alpha}$$

since $$Z_{\dot{w}} = \frac{1}{m}\frac{\partial Z}{\partial \dot{w}}$$

(II-105) $$Z_{\dot{w}} = -\frac{\rho S U}{2m}\frac{\partial C_L}{\partial \dot{\alpha}}$$

To form a non-dimensional coefficient, (II-105) is multiplied and divided by $\frac{c}{2U}$.

(II-106) $$Z_{\dot{w}} = -\frac{\rho S U}{2m}\frac{c}{2U}\frac{\partial C_L}{\partial\left(\frac{\dot{\alpha}c}{2U}\right)}$$

(II-107) $$Z_{\dot{w}} = -\frac{\rho S c}{4m} C_{L_{\dot{\alpha}}} \quad \text{where} \quad C_{L_{\dot{\alpha}}} = \frac{\partial C_L}{\partial\left(\frac{\dot{\alpha}c}{2U}\right)}$$

$M_{\dot{w}}$ can be expressed as:

(II-108) $$\Delta M = \frac{\partial M}{\partial \dot{w}}\dot{w}$$

(II-109) $$\frac{\partial M}{\partial \dot{w}} = \frac{\rho S U^2 c}{2}\frac{\partial C_m}{\partial \dot{w}}$$

$$M_{\dot{w}} = \frac{1}{I_{yy}}\frac{\partial M}{\partial \dot{w}}$$

(II-110) $$M_{\dot{w}} = \frac{\rho S c^2}{4 I_{yy}} C_{m_{\dot{\alpha}}} \quad \text{where} \quad C_{m_{\dot{\alpha}}} = \frac{\partial C_m}{\partial\left(\frac{\dot{\alpha}c}{2U}\right)}$$

Effect of q, the Pitching Velocity

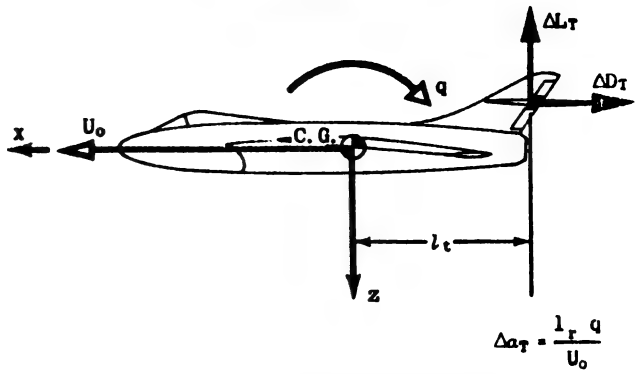

Figure II-32

In the light of the quasi-steady flow assumption (Assumption VII) the major effect of the airplane's pitching about its center of gravity is to cause an increase in the angle of attack of the horizontal tail. As in the case of the effect of $\dot{w}$, the resulting drag increase is neglected in the first approximation and X_q is set equal to zero.

The incremental lift produces a change both in the Z force and in pitching moment. The expressions for Z_q and M_q can be derived as follows:

(II-111) $$\Delta Z = \frac{\partial Z}{\partial q}q = -\frac{\partial L}{\partial q}q$$

(II-112) $$\frac{\partial L}{\partial q} = \frac{\rho S U^2}{2}\frac{\partial C_L}{\partial q} = \frac{\rho S U^2}{2}\frac{c}{2U}\frac{\partial C_L}{\partial\left(\frac{qc}{2U}\right)}$$

$$Z_q = \frac{1}{m}\frac{\partial Z}{\partial q}$$

(II-113) $Z_q = -\frac{\rho S U c}{4m} C_{L_q}$ where $C_{L_q} = \frac{\partial C_L}{\partial \left(\frac{qc}{2U}\right)}$

and

(II-114) $\Delta M = \frac{\partial M}{\partial q} q$

(II-115) $\frac{\partial M}{\partial q} = \frac{\rho S U^2 c}{2} \frac{\partial C_m}{\partial q} = \frac{\rho S U^2 c}{2} \frac{c}{2U} \frac{\partial C_m}{\partial \left(\frac{qc}{2U}\right)}$

$M_q = \frac{1}{I_{yy}} \frac{\partial M}{\partial q}$

(II-116) $M_q = \frac{\rho S U c^2}{4 I_{yy}} C_{m_q}$ where $C_{m_q} = \frac{\partial C_m}{\partial \left(\frac{qc}{2U}\right)}$

Effects of δ_{RPM}, the Change of Power Plant Revolutions per Minute

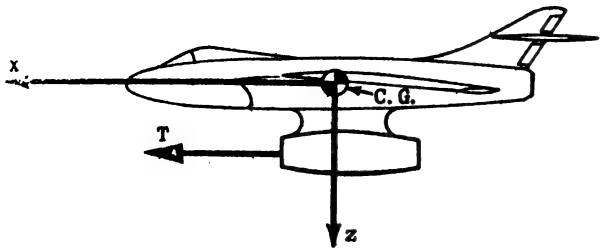

Figure II-33

An increase in power plant revolutions per minute yields an increase in thrust. By using equation (II-81), the increment of thrust can be expressed as:

(II-117) $\Delta T = \frac{\partial T}{\partial \delta_{RPM}} \delta_{RPM}$

(II-118) $\frac{\partial T}{\partial \delta_{RPM}} = \frac{1}{2} \rho S U^2 \frac{\partial C_T}{\partial \delta_{RPM}}$

To form a non-dimensional coefficient, (II-118) is multiplied and divided by $\frac{60c}{2u}$, where the coefficient 60 is used to convert u from feet per second to feet per minute.

Since $T_{\delta_{RPM}} = \frac{1}{m} \frac{\partial T}{\partial \delta_{RPM}}$

(II-119) $T_{\delta_{RPM}} = \frac{30 \rho S U c}{m} C_{T_{\delta_{RPM}}}$

where $C_{T_{\delta_{RPM}}} = \frac{\partial C_T}{\partial \left(\frac{30 c \delta_{RPM}}{U}\right)}$

Effect of δ_E, the Elevator Deflection

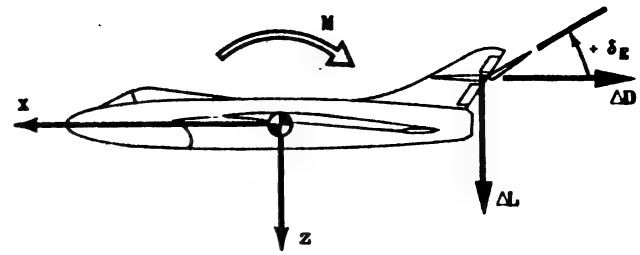

Figure II-34

Deflecting the elevator up is defined as the positive direction of elevator deflection, as shown in Figure II-34. The most important effect of an elevator deflection is to produce a change in lift which acts on the horizontal tail and which causes a pitching moment. It can be seen from Figure II-34 that a positive elevator deflection decreases the effective angle of attack of the horizontal tail thus causing a positive Z force and a positive moment M. The increment of Z force can be expressed as:

(II-120) $\Delta Z = \frac{\partial Z}{\partial \delta_E} \delta_E = \frac{\partial L}{\partial \delta_E} \delta_E$

(II-121) $\frac{\partial L}{\partial \delta_E} = \frac{1}{2} \rho U^2 S \frac{\partial C_L}{\partial \delta_E}$

$Z_{\delta_E} = \frac{1}{m} \frac{\partial C_L}{\partial \delta_E}$

(II-122) $Z_{\delta_E} = \frac{1}{2} \frac{\rho U^2 S}{m} C_{L_{\delta_E}}$ where $C_{L_{\delta_E}} = \frac{\partial C_L}{\partial \delta_E}$

The increment of moment has a similar form:

(II-123) $\Delta M = \frac{\partial M}{\partial \delta_E} \delta_E$

(II-124) $\frac{\partial M}{\partial \delta_E} = \frac{1}{2} \rho U^2 S c \frac{\partial C_m}{\partial \delta_E}$

$M_{\delta_E} = \frac{1}{I_{yy}} \frac{\partial M}{\partial \delta_E}$

(II-125) $M_{\delta_E} = \frac{\rho U^2 S c}{2 I_{yy}} C_{m_{\delta_E}}$ where $C_{m_{\delta_E}} = \frac{\partial C_m}{\partial \delta_E}$

The change in the X force due to elevator deflection is caused by the change in drag. Thus:

(II-126) $\Delta X = \frac{\partial X}{\partial \delta_E} \delta_E = -\frac{\partial D}{\partial \delta_E} \delta_E$

(II-127) $\frac{\partial D}{\partial \delta_E} = \frac{1}{2} \rho U^2 S \frac{\partial C_D}{\partial \delta_E}$

$X_{\delta_E} = \frac{1}{m} \frac{\partial X}{\partial \delta_E}$

(II-128) $X_{\delta_E} = -\frac{\rho U^2 S}{2m} C_{D_{\delta_E}}$ where $C_{D_{\delta_E}} = \frac{\partial C_D}{\partial \delta_E}$

Effect of δ_F, the Flap Deflection

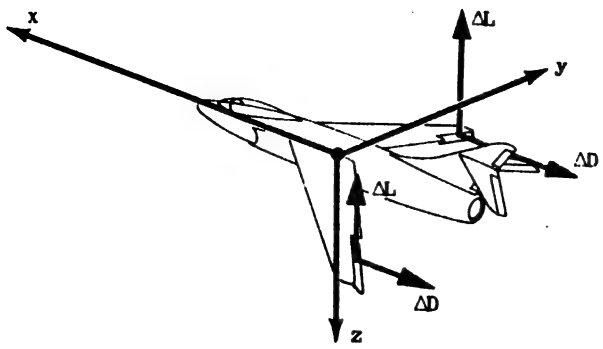

Figure II-35

"Flaps down" is defined as the positive direction of flap deflection as shown in Figure II-35. This flap deflection increases the effective angle of attack of a section of the wing thus increasing the lift and drag acting on this section of the wing. The increase in drag produces a negative X force.

The incremental X force can be expressed as:

(II-129) $$\Delta X = \frac{\partial X}{\partial \delta_F} \delta_F = - \frac{\partial D}{\partial \delta_F} \delta_F$$

(II-130) $$\frac{\partial D}{\partial \delta_F} = \frac{1}{2} \rho U^2 S \frac{\partial C_D}{\partial \delta_F}$$

$$X_{\delta_F} = \frac{1}{m} \frac{\partial X}{\partial \delta_F}$$

(II-131) $$X_{\delta_F} = - \frac{\rho U^2 S}{2m} C_{D_{\delta_F}} \quad \text{where} \quad C_{D_{\delta_F}} = \frac{\partial C_D}{\partial \delta_F}$$

The incremental Z force is:

(II-132) $$\Delta Z = \frac{\partial Z}{\partial \delta_F} \delta_F = - \frac{\partial L}{\partial \delta_F} \delta_F$$

(II-133) $$\frac{\partial L}{\partial \delta_F} = \frac{1}{2} \rho U^2 S \frac{\partial C_D}{\partial \delta_F}$$

$$Z_{\delta_F} = \frac{1}{m} \frac{\partial Z}{\partial \delta_F}$$

(II-134) $$Z_{\delta_F} = - \frac{\rho U^2 S}{2m} C_{L_{\delta_F}} \quad \text{where} \quad C_{L_{\delta_F}} = \frac{\partial C_L}{\partial \delta_F}$$

The moment produced by a flap deflection is dependent on the location of the c.g. with respect to the wing. The expression for the incremental moment is:

(II-135) $$\Delta M = \frac{\partial M}{\partial \delta_F} \delta_F$$

(II-136) $$\frac{\partial M}{\partial \delta_F} = \frac{1}{2} \rho U^2 S c \frac{\partial C_m}{\partial \delta_F}$$

$$M_{\delta_F} = \frac{1}{I_{yy}} \frac{\partial M}{\partial \delta_F}$$

(II-137) $$M_{\delta_F} = \frac{\rho U^2 S c}{2 I_{yy}} C_{m_{\delta_F}} \quad \text{where} \quad C_{m_{\delta_F}} = \frac{\partial C_m}{\partial \delta_F}$$

Effect of δ_B, the Dive Brake Deflection

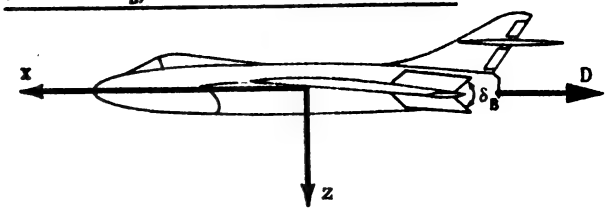

Figure II-36

Dive brakes are generally designed to produce only a drag force as shown in Figure II-36. Assuming that a dive brake deflection also produces some small amount of lift and moment, the expressions for the stability derivatives have a form similar to those related to flap deflection and can be written immediately as:

(II-138) $$X_{\delta_B} = - \frac{\rho U^2 S}{2m} C_{D_{\delta_B}} \quad \text{where} \quad C_{D_{\delta_B}} = \frac{\partial C_D}{\partial \delta_B}$$

(II-139) $$Z_{\delta_B} = - \frac{\rho U^2 S}{2m} C_{L_{\delta_B}} \quad \text{where} \quad C_{L_{\delta_B}} = \frac{\partial C_L}{\partial \delta_B}$$

(II-140) $$M_{\delta_B} = \frac{\rho U^2 S}{2 I_{yy}} C_{m_{\delta_B}} \quad \text{where} \quad C_{m_{\delta_B}} = \frac{\partial C_m}{\partial \delta_B}$$

LATERAL STABILITY DERIVATIVES

Effect of v, the Change in Side Velocity

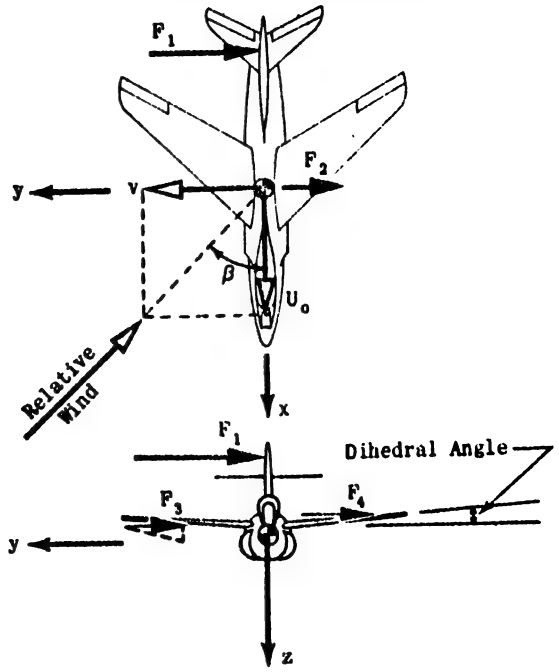

Figure II-37

When an airplane is disturbed from steady flight so that it has a side velocity, v, a force along the y axis and moments about the x and z axes are developed. The major forces caused by the side velocity are labeled F_1, F_2, F_3, and F_4 in Figure II-37. F_1 arises from the change of the angle of attack of the vertical tail. F_2 is the side force acting on the fuselage, and F_3 and F_4 are forces acting on each semi-span of the wing, due to the effective dihedral of the wing. From (II-65), the side force equation may be seen to have the form:

$$Y = \frac{1}{2} \rho U^2 S C_y$$

The change in side force due to a change in side velocity, v, can be found by differentiation:

(II-141) $$\Delta Y = \frac{\partial Y}{\partial v} v$$

(II-142) $$\frac{\partial Y}{\partial v} = \frac{1}{2} \rho U^2 S \frac{\partial C_y}{\partial v}$$

(II-143) $$Y_v = \frac{1}{m} \frac{\partial Y}{\partial v} = \frac{\rho U^2 S}{2m} \frac{\partial C_y}{\partial v}$$

From Figure II-37, it may be seen that the angle of sideslip, β, is related to the sideslip velocity, v:

(II-144) $$\tan \beta = \frac{v}{U_o}$$

Since v has been assumed to be a small quantity

(II-145) $$\beta \approx \frac{v}{U_o}$$

and

(II-146) $$v = U_o \beta$$

Substituting (II-146) in (II-143) yields:

(II-147) $$Y_v = \frac{\rho U^2 S}{2m} \frac{\partial C_y}{U_o \partial \beta}$$

(II-148) $$Y_v = \frac{\rho U S}{2m} C_{y_\beta} \quad \text{where} \quad \frac{\partial C_y}{\partial \beta} = C_{y_\beta}$$

The rolling moment about the x axis is caused mainly by F_1, which acts above the x axis, and by the components of F_3 and F_4 which act normal to the wing. The equation for L, from (II-65), is rewritten:

$$L = \frac{1}{2} \rho U^2 S b C_l$$

The change in L due to a side velocity, v, can be expressed as:

(II-149) $$\Delta L = \frac{\partial L}{\partial v} v$$

(II-150) $$\frac{\partial L}{\partial v} = \frac{1}{2} \rho U^2 S b \frac{\partial C_l}{\partial v}$$

$$L_v = \frac{1}{I_{xx}} \frac{\partial L}{\partial v}$$

(II-151) $$L_v = \frac{\rho U^2 S b}{2 I_{xx}} \frac{\partial C_l}{\partial v}$$

Substituting the value of v from (II-146) into (II-151) yields:

(II-152) $$L_v = \frac{\rho U S b}{2 I_{xx}} C_{l_\beta} \quad \text{where} \quad C_{l_\beta} = \frac{\partial C_l}{\partial \beta}$$

Also, since $v = U_o \beta$

$$L_v = \frac{1}{U_o} L_\beta \quad \text{and} \quad L_v v = L_\beta \beta$$

(The quantity L_β is used later in the chapter.)

The yawing moment due to a side velocity, v, is caused mainly by the force on the vertical tail, F_1. The form of the stability derivative N_v is similar to (II-152):

(II-153) $$N_v = \frac{\rho U S b}{2 I_{zz}} C_{n_b}$$

also $$N_v = \frac{1}{U_o} N_\beta$$

Effect of p, the Change in Rolling Velocity

A rolling velocity, p, causes a force to act on the vertical tail. This force is illustrated as F_1 in Figure II-38. The change in the Y force due to p is expressed as:

(II-154) $$\Delta Y = \frac{\partial Y}{\partial p} p$$

(II-155) $$\frac{\partial Y}{\partial p} = \frac{\rho U^2 S}{2} \frac{\partial C_y}{\partial \left(\frac{pb}{2U}\right)}$$

(II-156) $$Y_p = \frac{1}{m} \frac{\partial Y}{\partial p} = \frac{\rho U^2 S}{2m} \frac{\partial C_y}{\partial p}$$

To form a non-dimensional coefficient, (II-156) is multiplied and divided by $\frac{b}{2U}$. Thus:

$$Y_p = \frac{\rho U^2 S}{2m} \frac{b}{2U} \frac{\partial C_y}{\partial \left(\frac{pb}{2U}\right)}$$

(II-157) $$Y_p = \frac{\rho U S b}{4m} C_{y_p} \quad \text{where} \quad C_{y_p} = \frac{\partial C_y}{\partial \left(\frac{pb}{2U}\right)}$$

There are also incremental forces acting on the wing. These forces are illustrated as F_1 and F_2 in Figure II-38. The vertical velocity of the downgoing wing at any station a distance l_1 from the xz plane, is pl_1. This vertical velocity increases the effective angle of attack at this station by an amount $\Delta\alpha_1$ (where $\Delta\alpha_1 \approx \frac{pl_1}{U_o}$).

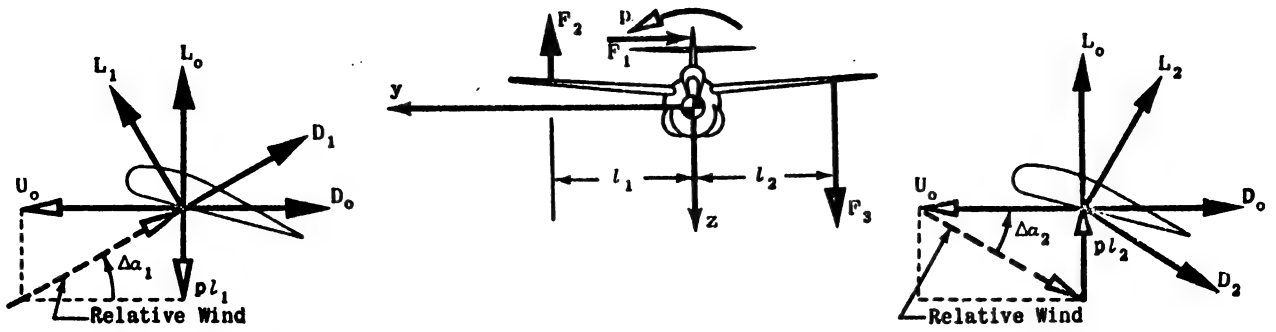

Figure II-38

This increase in angle of attack increases the lift and drag acting on the wing. The effective angle of attack of the upgoing wing at a station a distance l_2 from the xz plane is decreased by an amount $\Delta\alpha_2$ (where $\Delta\alpha_2 \simeq pl_2/U_o$). This decrease in effective angle of attack decreases the lift and drag acting on the wing at this station

Usually the change in drag force is relatively small and is neglected for the purposes of this discussion. In the preceding discussion, it is stated that the lift on the downgoing wing is increased and the lift on the upgoing wing is decreased resulting in a change in the rolling moment, L. The change in rolling moment due to p is expressed:

(II-158) $$\Delta L = \frac{\partial L}{\partial p} p$$

(II-159) $$\frac{\partial L}{\partial p} = \frac{1}{2} \rho U^2 S b \frac{\partial C_l}{\partial p}$$

(II-160) $$L_p = \frac{1}{I_{xx}} \frac{\partial L}{\partial p}$$

Multiplying and dividing (II-159) by $\frac{b}{2U}$, and substituting the result into (II-160) yield:

(II-161) $$L_p = \frac{\rho U S b^2}{4 I_{xx}} C_{l_p} \quad \text{where} \quad C_{l_p} = \frac{\partial C_l}{\partial \left(\frac{pb}{2U}\right)}$$

In addition to the change in magnitude of the lift forces acting on each semi-span of the wing, it may be seen from Figure II-38 that the lift forces acting on the downgoing and upgoing semi-spans are rotated forward and backward respectively. The change in direction of these forces results in a negative yawing moment about the z axis.

Figure II-38 represents the general case. However, for flight near the stall, the drag forces may become important and result in a yawing moment of opposite sign. The change in yawing moment due to p is expressed as:

(II-162) $$\Delta N = \frac{\partial N}{\partial p} p$$

By noting the similarity between (II-162) and (II-158) and between the equations for L and N in (II-65), equation (II-163) can be written immediately:

(II-163) $$N_p = \frac{\rho U S b^2}{4 I_{zz}} C_{n_p} \quad \text{where} \quad C_{n_p} = \frac{\partial C_n}{\partial \left(\frac{pb}{2U}\right)}$$

Effect of r, the Change in Yawing Velocity

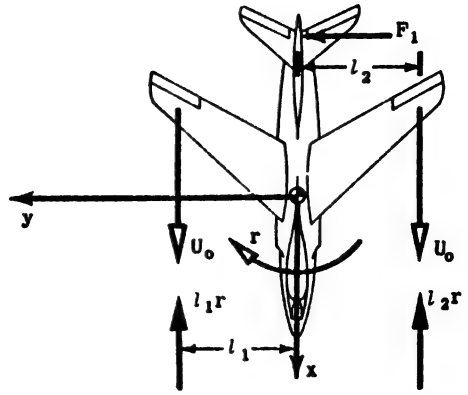

Figure II-39

A side force, F_1, is caused by a yawing velocity, r, which is mainly due to the fact that the effective angle of attack of the vertical tail is increased. This side force is generally positive and can be expressed as:

(II-164) $$\Delta Y = \frac{\partial Y}{\partial r} r$$

By analogy with Y_p, derived in equation (II-57), it is possible to write:

(II-165) $$Y_r = \frac{\rho U S b}{4 m} C_{y_r} \quad \text{where} \quad C_{y_r} = \frac{\partial C_y}{\partial \left(\frac{rb}{2U}\right)}$$

As shown in Figure II-39, the forward speed of a station which is a distance l_1 from the xz plane on the semi-span of the wing is decreased an amount $l_1 r$, resulting in a decrease in lift at this section. Similarly, the forward speed of a station a distance l_2 normal to the z axis on the semi-span of the wing is increased an amount $l_2 r$ resulting in an increase in lift at this section. The result of the changes in lift acting on each semi-span is then a moment about the x axis. This moment is usually positive and can be expressed as:

(II-166) $$\Delta L = \frac{\partial L}{\partial r} r$$

By analogy with L_p, derived in equation (II-57), equation (II-167) can be immediately written:

(II-167) $$L_r = \frac{\rho U S b^2}{4 I_{xx}} C_{l_r} \quad \text{where} \quad C_{l_r} = \frac{\partial C_l}{\partial \left(\frac{rb}{2U}\right)}$$

The side force F_1 in Figure II-39 also causes a moment about the z axis since the vertical tail is some distance aft of the center of gravity. This moment is usually negative and can be expressed as:

(II-168) $$\Delta N = \frac{\partial N}{\partial r} r$$

(II-169) $$\frac{\partial N}{\partial r} = \frac{\rho U^2 S b}{2} \frac{\partial C_n}{\partial r}$$

(II-170) $$N_r = \frac{1}{I_{zz}} \frac{\partial N}{\partial r}$$

Multiplying and dividing (II-169) by $\frac{b}{2U}$, and substituting this result in (II-170) yield:

(II-171) $$N_r = \frac{\rho U S b^2}{4 I_{zz}} C_{n_r} \quad \text{where} \quad C_{n_r} = \frac{\partial C_n}{\partial \left(\frac{rb}{2U}\right)}$$

Effect of δ_R, the Rudder Deflection

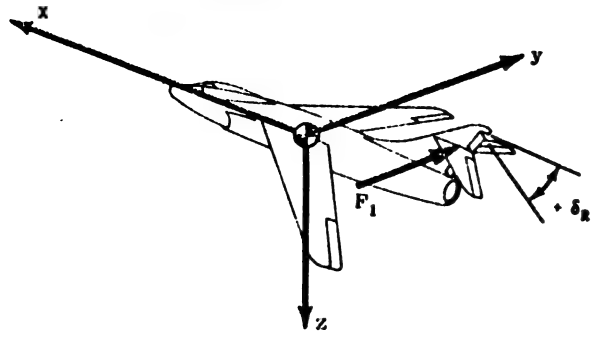

Figure II-40

A positive rudder deflection causes a force to act in the positive y direction as illustrated by F_1 in Figure II-40. The rudder deflection changes the effective angle of attack of the vertical tail, which in turn produces a force proportional to this change in angle of attack.

(II-172) $$\Delta Y = \frac{\partial Y}{\partial \delta_R} \delta_R$$

(II-173) $$\frac{\partial Y}{\partial \delta_R} = \frac{1}{2} \rho U^2 S \frac{\partial C_y}{\partial \delta_R}$$

since

$$Y_{\delta_R} = \frac{1}{m} \frac{\partial Y}{\partial \delta_R}$$

(II-174) $$Y_{\delta_R} = \frac{\rho U^2 S}{2 m} C_{y_{\delta_R}} \quad \text{where} \quad C_{y_{\delta_R}} = \frac{\partial C_y}{\partial \delta_R}$$

By referring to Figure II-40 again, it can be seen that F_1 causes a negative moment, N, about the z axis.

(II-175) $$\Delta N = \frac{\partial N}{\partial \delta_R} \delta_R$$

(II-176) $$\frac{\partial N}{\partial \delta_R} = \frac{\rho U^2 S b}{2} \frac{\partial C_n}{\partial \delta_R}$$

Since $$N_{\delta_R} = \frac{1}{I_{zz}} \frac{\partial N}{\partial \delta_R}$$

(II-177) $$N_{\delta_R} = \frac{\rho U^2 S b}{2 I_{zz}} C_{n_{\delta_R}} \quad \text{where} \quad C_{n_{\delta_R}} = \frac{\partial C_n}{\partial \delta_R}$$

Depending on whether the center of pressure, that is, the point at which F_1 can be considered to act, is above or below the x axis, a positive rudder deflection can cause either a positive or a negative rolling moment ΔL. This increment of rolling moment can be expressed as follows:

(II-178) $$\Delta L = \frac{\partial L}{\partial \delta_R} \delta_R$$

(II-179) $$\frac{\partial L}{\partial \delta_R} = \frac{1}{2} \rho U^2 S b \frac{\partial C_l}{\partial \delta_R} \quad \text{since} \quad L_{\delta_R} = \frac{1}{I_{xx}} \frac{\partial L}{\partial \delta_R}$$

(II-180) $$L_{\delta_R} = \frac{\rho U^2 S b}{2 I_{xx}} C_{l_{\delta_R}} \quad \text{where} \quad C_{l_{\delta_R}} = \frac{\partial C_l}{\partial \delta_R}$$

Effect of δ_A, the Aileron Deflection

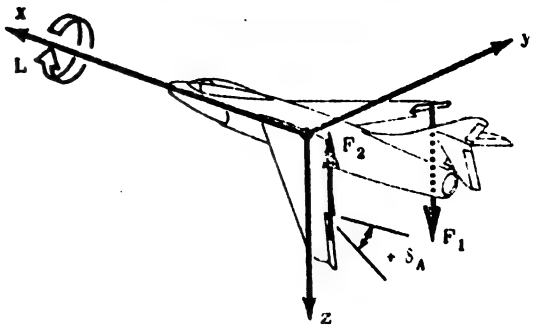

Figure II-41

Positive aileron deflection is defined as the upward deflection of the aileron on the semi-span of the wing lying along the positive y axis and the downward deflection of the other aileron as shown in Figure II-41. The aileron which is deflected up decreases the effective angle of attack of a section of the wing and generally causes a decrease in lift and drag acting on that section of the wing, whereas the aileron which is deflected down usually causes a corresponding increase in the lift and drag acting on that section of the wing.

The changes in lift produce a positive rolling moment, ΔL. This change is rolling moment can be expressed as:

(II-181) $$\Delta L = \frac{\partial L}{\partial \delta_A} \delta_A$$

(II-182) $$\frac{\partial L}{\partial \delta_A} = \frac{\rho U^2 S b}{2} \frac{\partial C_l}{\partial \delta_A}$$

Since $$L_{\delta_A} = \frac{1}{I_{xx}} \frac{\partial L}{\partial \delta_A}$$

(II-183) $$L_{\delta_A} = \frac{\rho U^2 S b}{2 I_{xx}} C_{l_{\delta_A}} \quad \text{where} \quad C_{l_{\delta_A}} = \frac{\partial C_l}{\partial \delta_A}$$

The change in drag generally produces a negative yawing moment about the z axis. The increment of yawing moment can be written as:

(II-184) $$\Delta N = \frac{\partial N}{\partial \delta_A} \delta_A$$

(II-185) $$\frac{\partial N}{\partial \delta_A} = \frac{\rho U^2 S b}{2} \frac{\partial C_n}{\partial \delta_A}$$

Since $$N_{\delta_A} = \frac{1}{I_{zz}} \frac{\partial N}{\partial \delta_A}$$

(II-186) $$N_{\delta_A} = \frac{\rho U^2 S b}{2 I_{zz}} C_{n_{\delta_A}} \quad \text{where} \quad C_{n_{\delta_A}} = \frac{\partial C_n}{\partial \delta_A}$$

There is generally no side force due to aileron deflection, but if one did exist, it could be expressed as:

(II-187) $$\Delta Y = \frac{\partial Y}{\partial \delta_A} \delta_A$$

(II-188) $$\frac{\partial Y}{\partial \delta_A} = \frac{\rho U^2 S}{2} \frac{\partial C_Y}{\partial \delta_A} \quad \text{Since} \quad Y_{\delta_A} = \frac{1}{m} \frac{\partial Y}{\partial \delta_A}$$

(II-189) $$Y_{\delta_A} = \frac{\rho U^2 S}{2 m} C_{y_{\delta_A}} \quad \text{where} \quad C_{y_{\delta_A}} = \frac{\partial C_Y}{\partial \delta_A}$$

The longitudinal and lateral stability derivatives discussed above are tabulated in (II-190) and (II-191) respectively. All of the dimensionless coefficients of the form C_{n_p}, $C_{n_{\delta_F}}$, etc., in (II-190) and (II-191) are referred to as basic non-dimensional stability derivatives.

Longitudinal Stability Derivatives

(II-190)

$$X_u = \frac{\rho U S}{m}(-C_{D_u} - C_D) \qquad M_q = \frac{\rho U S c^2}{4 I_{yy}} C_{m_q}$$

$$Z_u = \frac{\rho U S}{m}(-C_{L_u} - C_L) \qquad T_{\delta_{RPM}} = \frac{30 \rho U S c}{m} C_{T_{\delta_{RPM}}}$$

$$M_u = \frac{\rho U S c}{I_{yy}}(C_{m_u} + C_m) \qquad X_{\delta_E} = -\frac{\rho U^2 S}{2 m} C_{D_{\delta_E}}$$

$$T_u = \frac{\rho U S}{m}(C_{T_u} + C_T) \qquad Z_{\delta_E} = \frac{\rho U^2 S}{2 m} C_{L_{\delta_E}}$$

$$X_w = \frac{\rho U S}{2 m}(C_L - C_{D_\alpha}) \qquad M_{\delta_E} = \frac{\rho U^2 S c}{2 I_{yy}} C_{m_{\delta_E}}$$

$$Z_w = \frac{\rho U S}{2 m}(-C_{L_\alpha} - C_D) \qquad X_{\delta_F} = -\frac{\rho U^2 S}{2 m} C_{D_{\delta_F}}$$

$$M_w = \frac{\rho U S c}{2 I_{yy}} C_{m_\alpha} \qquad Z_{\delta_F} = -\frac{\rho U^2 S c}{2 m} C_{L_{\delta_F}}$$

$$X_{\dot{w}} \cong 0 \qquad M_{\delta_F} = \frac{\rho U^2 S c}{2 I_{yy}} C_{m_{\delta_F}}$$

$$Z_{\dot{w}} = -\frac{\rho S c}{4 m} C_{L_{\dot{\alpha}}} \qquad X_{\delta_B} = -\frac{\rho U^2 S}{2 m} C_{D_{\delta_B}}$$

$$M_{\dot{w}} = \frac{\rho S c^2}{4 I_{yy}} C_{m_{\dot{\alpha}}} \qquad Z_{\delta_B} = -\frac{\rho U^2 S}{2 m} C_{L_{\delta_B}}$$

$$X_q \cong 0 \qquad M_{\delta_B} = \frac{\rho U^2 S c}{2 I_{yy}} C_{m_{\delta_B}}$$

$$Z_q = -\frac{\rho U S c}{4 m} C_{L_q}$$

Lateral Stability Derivatives

(II-191)

$$Y_v = \frac{\rho U S}{2 m} C_{y_\beta} \qquad L_r = \frac{\rho U S b^2}{4 I_{xx}} C_{l_r}$$

$$L_v = \frac{\rho U S b}{2 I_{xx}} C_{l_\beta} \qquad N_r = \frac{\rho U S b^2}{4 I_{zz}} C_{n_r}$$

$$L_\beta = U_o L_v \qquad Y_{\delta_R} = \frac{\rho U^2 S}{2 m} C_{y_{\delta_R}}$$

$$N_v = \frac{\rho U S b}{2 I_{zz}} C_{n_\beta} \qquad L_{\delta_R} = \frac{\rho U^2 S b}{2 I_{xx}} C_{l_{\delta_R}}$$

$$N_\beta = U_o N_v \qquad N_{\delta_R} = \frac{\rho U^2 S b}{2 I_{zz}} C_{n_{\delta_R}}$$

$$Y_p = \frac{\rho U S b}{4 m} C_{y_p} \qquad Y_{\delta_A} = \frac{\rho U^2 S}{2 m} C_{y_{\delta_A}}$$

$$L_p = \frac{\rho U S b^2}{4 I_{xx}} C_{l_p} \qquad L_{\delta_A} \frac{\rho U^2 S b}{2 I_{xx}} C_{l_{\delta_A}}$$

$$N_p = \frac{\rho U S b^2}{4 I_{zz}} C_{n_p} \qquad N_{\delta_A} = \frac{\rho U^2 S b}{2 I_{zz}} C_{n_{\delta_A}}$$

$$Y_r = \frac{\rho U S b}{4 m} C_{y_r}$$

SECTION 15 – TRANSFER FUNCTIONS

In this section, (II-63) and (II-64) are converted by the use of determinants into the transfer functions considered in the rest of this volume. Some preliminary discussion of the quantities involved in these equations is given first. Although most of these quantities have been defined in the preceding text, they are redefined here for the sake of clarity. The longitudinal quantities are treated first.

The angle of attack, α, is defined as the angle between the wing chord line and the relative wind. It is equal to the sum of the steady flight angle of attack, α_o, and the perturbation angle of attack, $\Delta\alpha$: $\alpha = \alpha_o + \Delta\alpha$.

The angle between the flight path and the horizontal is defined as the flight path angle γ and is equal to $\gamma_o + \Delta\gamma$ (the sum of the steady flight angle γ_o and the perturbation angle $\Delta\gamma$). In the stability axis system, γ_o is equal to the angle between the x axis and the horizontal, when the airplane is in the steady flight condition.

The pitch angle, θ, is also composed of a steady flight value, θ_o, and a perturbation value, θ. It is the angle between the wing chord line and the horizontal: $\theta = \theta_o + \theta$.

In the derivation of the expressions for the components of gravity acting along the disturbed Eulerian axes in

Section II-5, the angle between the horizontal and the Eulerian x axis in the steady flight position was defined as θ_o.

At that point in the derivation of the equations of motion, the orientation of the Eulerian x axis with respect to both the airplane and the relative wind was arbitrary.

If the Eulerian x axis had been aligned parallel to the wing chord line, the definitions of θ_o given in Section II-5 and immediately above would have been consistent. However, the substitution of γ_o for θ_o in the equations of motion should not lead to any difficulty if stability axes are used as reference axes and the above definitions are used.

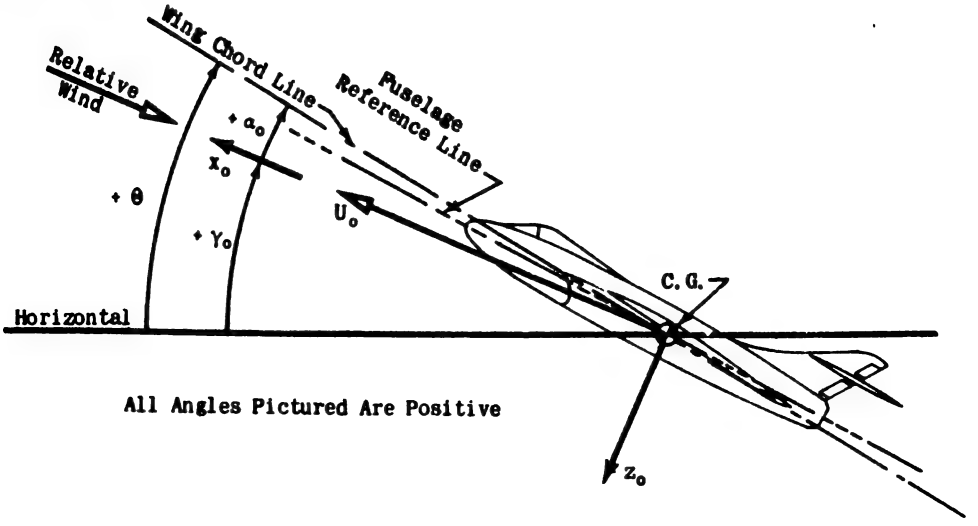

Figure II-42 Airframe in Equilibrium Condition

It was not until Assumption VI was made that stability axes were selected as the reference axes. In the stability axis system, the x axis in the steady flight position is parallel to the relative wind. Therefore, when stability axes are used as reference axes, the angle called θ_o in previous sections is equal to γ_o according to the definitions given above.

The components of velocity along the x and z axes are U and W respectively, and each is composed of steady flight and perturbation values defined as: $U = U_o + u$ and $W = W_o + w$. However, according to Assumption VI, W_o is equal to zero; therefore: $W_o = 0$ and $W = w$.

The steady flight values of the above variables and the

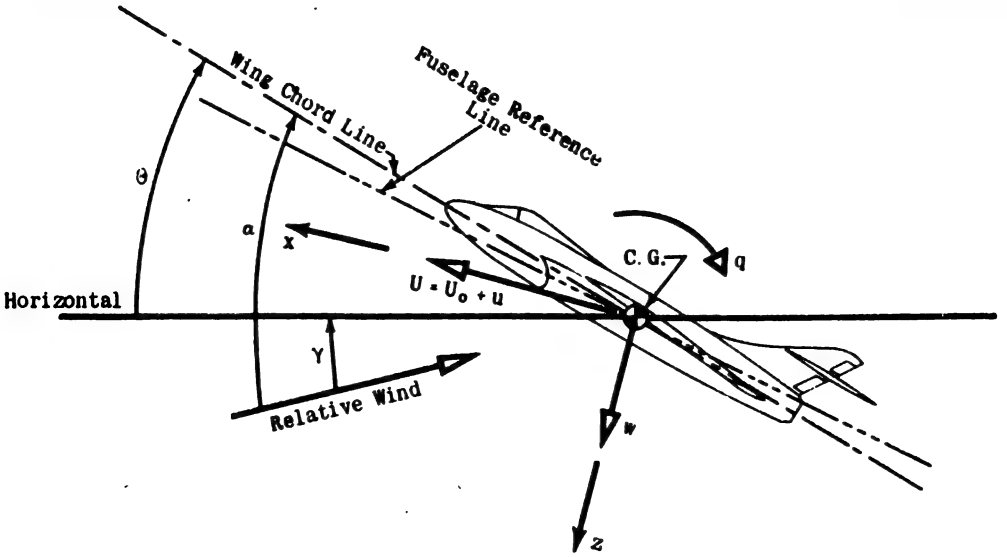

Figure II-43 Airframe in Disturbed Condition

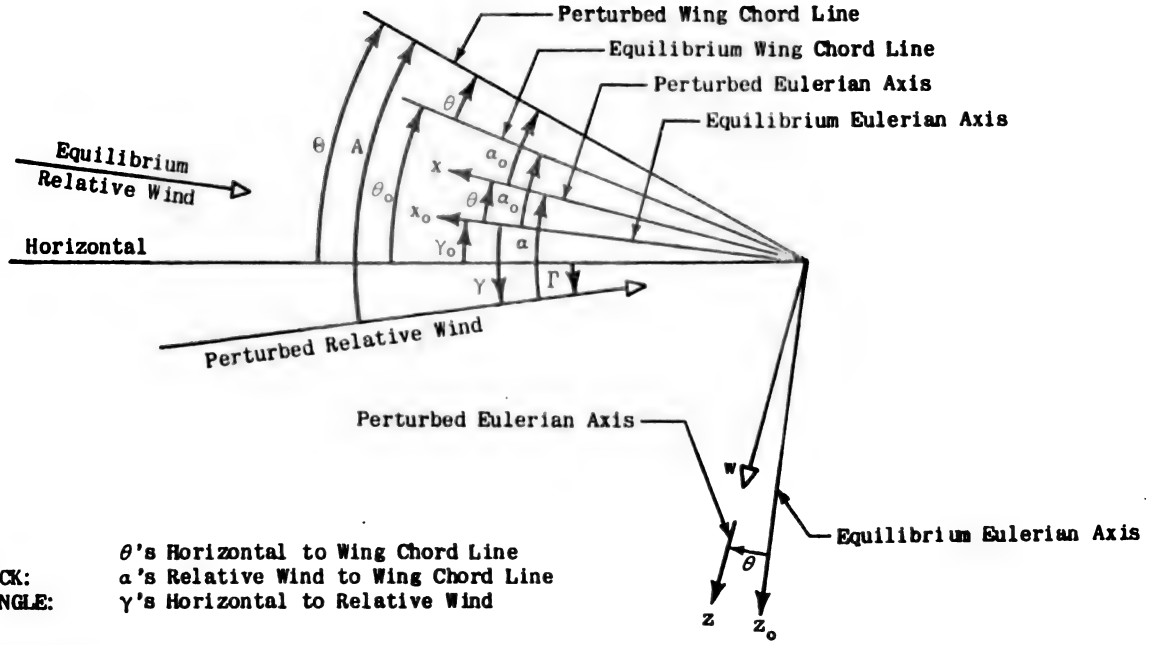

PITCH ANGLE: θ's Horizontal to Wing Chord Line
ANGLE OF ATTACK: α's Relative Wind to Wing Chord Line
FLIGHT PATH ANGLE: γ's Horizontal to Relative Wind

Total Perturbed Quantities minus Equilibrium Quantities give magnitude of Perturbations:

$$\theta - \theta_o = \theta$$
$$A - \alpha_o = \alpha$$
$$\Gamma - \gamma_o = \gamma$$

Figure II-44

x and z axes during the steady flight condition are shown in Figure II-42. The subscript o is used to denote axes during the steady flight condition.

By recalling that once the axes are fixed to the airframe during the steady flight condition they remain fixed with respect to the airframe during any particular analysis, the airframe in a disturbed condition and the disturbed x and z axes would appear as in Figure II-43. It should be noted that the relative wind does not necessarily lie along the disturbed axis.

To present a complete picture of the longitudinal angles, it is necessary to superimpose Figure II-42 on Figure II-43, as in Figure II-44, with the fuselage reference line and the airframe outline omitted.

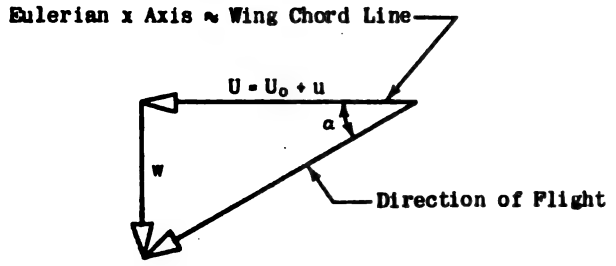

Figure II-45

From Figure II-44, it can be seen that the flight path angle γ is equal to the pitch angle, θ, minus the angle of attack α:

(II-192) $$\gamma = \theta - \alpha$$

The change in angle of attack, $\Delta\alpha$, can be expressed as a function of the component velocities.

From Figure II-45, the following relation can be derived:

$$\tan \Delta\alpha = \frac{w}{u} = \frac{w}{U_o + u}$$

Since both w and u are small:

$$\tan \Delta\alpha \cong \frac{w}{U_o} \cong \Delta\alpha \quad \text{and} \quad w \cong U_o \Delta\alpha$$

The lateral angles are shown in Figure II-46. The angle of yaw, ψ, is the angle between the steady flight x_o axis and the disturbed x axis and is positive as shown. The angle of sideslip, β, is the angle between the flightpath and the disturbed x axis and is related to the lateral velocities by: $\tan \beta = \frac{v}{u} = \frac{v}{U_o + u}$

By noting in the figures the correspondence between β and the perturbation angle of attack, $\Delta\alpha$, it may be concluded that:

$$\beta \cong \frac{v}{U_o}$$

The roll angle, ϕ, is of course not shown, but is defined as the rotation about the disturbed x axis. The angle

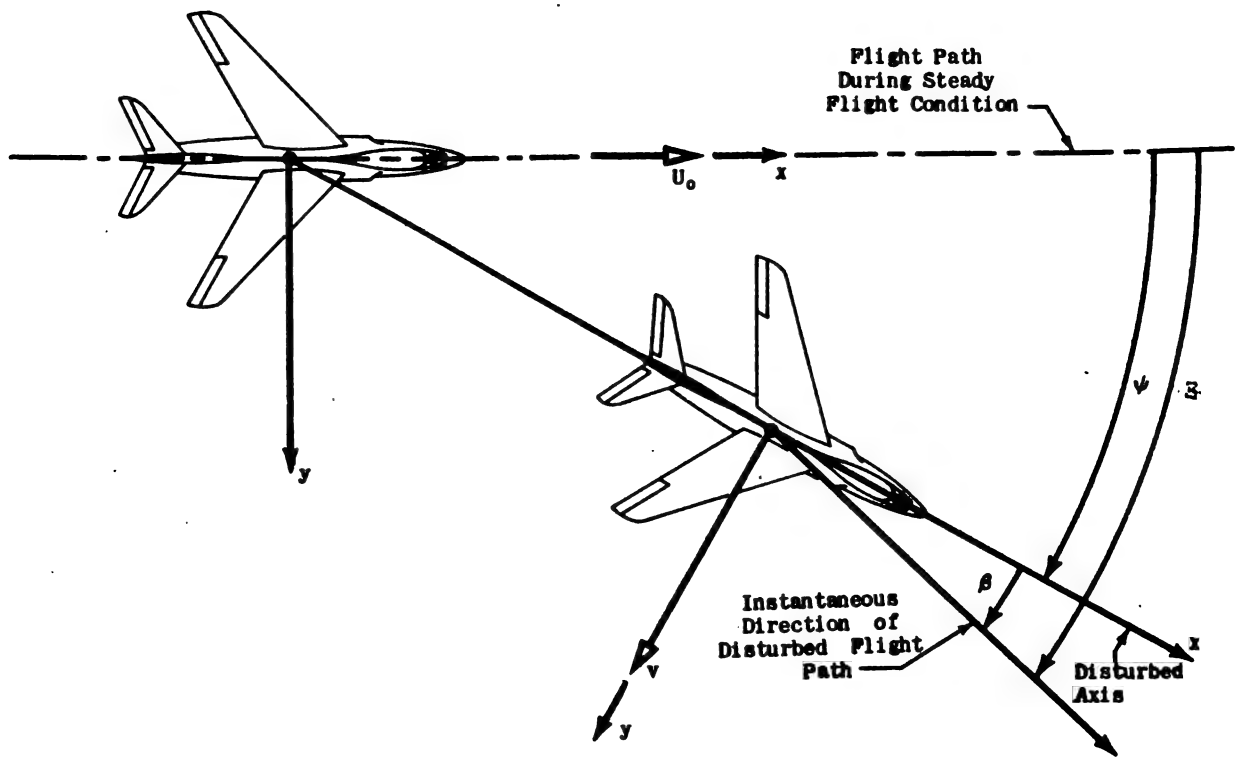

Figure II-46

Ξ is defined as the angle between the equilibrium flight path and the disturbed flight path.

It should be pointed out that only when Ξ is equal to zero is the sidelip angle β, equal to the negative of the yaw angle (see Figure II-47).

The equations of motion are now used to derive the transfer functions. (II-63) and (II-64) are rewritten below with γ_o substituted for θ_o:

(II-193)

$$\dot{u} - X_u u - \left(T_u \cos\xi\right)u - X_q q + g\theta\cos\gamma_o - X_{\dot{w}}\dot{w} - X_w w = X_{\delta_E}\delta_E + X_{\delta_B}\delta_B + T_{\delta_{RPM}}\delta_{RPM} + X_{\delta_P}\delta_P$$

$$-Z_u u + \left(T_u \sin\xi\right)u - U_o q - Z_q q + g\theta\sin\gamma_o + \dot{w} - Z_{\dot{w}}\dot{w} - Z_w w = Z_{\delta_E}\delta_E + Z_{\delta_B}\delta_B - \left(T_{\delta_{RPM}}\sin\xi\right)\delta_{RPM} + Z_{\delta_P}\delta_P$$

$$-M_u u - \frac{z_{TH}}{I_{yy}} T_u u + \dot{q} - M_q q - M_{\dot{w}}\dot{w} - M_w w = M_{\delta_E}\delta_E + M_{\delta_B}\delta_B + \frac{z_{TH}}{I_{yy}} T_{\delta_{RPM}}\delta_{RPM}$$

(II-194)

$$\dot{v} - Y_v v - Y_p p - g\left(\cos\gamma_o\right)\phi + U_o r - Y_r r - g\left(\sin\gamma_o\right)\psi = Y_{\delta_A}\delta_A + Y_{\delta_R}\delta_R$$

$$-L_v v + \dot{p} - L_p p - \frac{I_{xz}}{I_{xx}}\dot{r} - L_r r = L_{\delta_A}\delta_A + L_{\delta_R}\delta_R$$

$$-N_v v - \frac{I_{xz}}{I_{zz}}\dot{p} - N_p p + \dot{r} - N_r r = N_{\delta_A}\delta_A + N_{\delta_R}\delta_R$$

The variable, β, is substituted for v in (II-194) using the relation $\beta = \frac{v}{U_o}$. Thus:

(II-195)

$$U_o\dot{\beta} - Y_v U_o\beta - Y_p p - \left(g\cos\gamma_o\right)\phi + U_o r - Y_r r - \left(g\sin\gamma_o\right)\psi = Y_{\delta_A}\delta_A + Y_{\delta_R}\delta_R$$

$$-L_\beta\beta + \dot{p} - L_p p - \frac{I_{xz}}{I_{xx}}\dot{r} - L_r r = L_{\delta_A}\delta_A + L_{\delta_R}\delta_R$$

$$-N_\beta\beta - \frac{I_{xz}}{I_{zz}}\dot{p} - N_p p + \dot{r} - N_r r = N_{\delta_A}\delta_A + N_{\delta_R}\delta_R$$

Dividing the first equation of (II-195) by U_o yields:

(II-196)

$$\dot{\beta} - Y_v\beta - Y_p^* p - \left(\frac{g}{U_o}\cos\gamma_o\right)\phi + r - Y_r^* r - \left(\frac{g}{U_o}\sin\gamma_o\right)\psi = Y_{\delta_A}^*\delta_A + Y_{\delta_R}^*\delta_R \quad \text{where } Y_p^* = \frac{Y_p}{U_o}, \text{ etc.}$$

(II-195) can therefore be written as:

$$\dot{\beta} - Y_v\beta - Y_p^* p - \left(\frac{g}{U_o}\cos\gamma_o\right)\phi + r - Y_r^* r - \left(\frac{g}{U_o}\sin\gamma_o\right)\psi = Y_{\delta_A}^*\delta_A + Y_{\delta_R}^*\delta_R$$

(II-197)

$$-L_\beta\beta + \dot{p} - L_p p - \frac{I_{xz}}{I_{xx}}\dot{r} - L_r r = L_{\delta_A}\delta_A + L_{\delta_R}\delta_R$$

$$-N_\beta\beta - \frac{I_{xz}}{I_{zz}}\dot{p} - N_p p + \dot{r} - N_r r = N_{\delta_A}\delta_A + N_{\delta_R}\delta_R$$

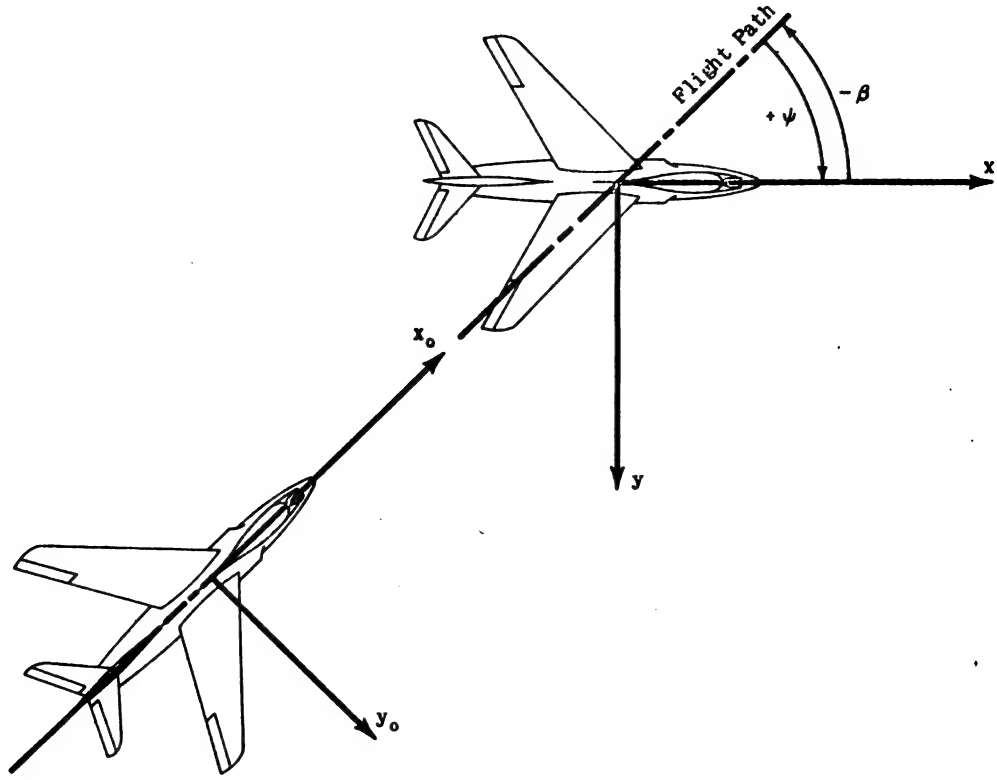

Figure II-47

The right sides of (II-193) and (II-197) are the control forces and represent the means by which either the human pilot or an autopilot can control the motion of the airframe. The motion is also influenced by rough air (such as gusts), but this is not a phenomenon which the pilot can control; he can only try to avoid flying through such rough air. Once he is in rough air, the pilot has only the controls mentioned above to control to any degree the motion resulting from disturbances.

The thrust and the control surface inputs are the forcing functions which determine the resultant motion of the airframe. Since the airframe equations of motion are linear equations, the principle of superposition may be used to obtain a solution. For instance, the response to simultaneous application of elevator and dive brake deflections can be determined by calculating the response to each of these deflections separately and then adding together the results to arrive at the complete solution.

In this volume only the longitudinal response to elevator deflection and the lateral response to rudder and aileron deflection are given detailed analysis. It should be emphasized however, that the mathematical techniques of solution for the other control inputs are identical.

The Laplace transform method* of solution is used throughout this volume. Equations (II-193) and (II-197) transformed, become:

* Gardner, M.F., and Barnes, J.L., 'Transients in Linear Systems,' John Wiley and Sons, New York, 1942.

(II-198)

$$[s-(X_u+A')]u(s)-(sX_{\dot{w}}+X_w)w(s)-(sX_q-g\cos\gamma_o)\theta(s)$$
$$= X_{\delta_E}\delta_E(s)+X_{\delta_B}\delta_B(s)+B'\delta_{RPM}(s)+X_{\delta_F}\delta_F(s)$$

$$-(Z_u-C')u(s)+[s(1-Z_{\dot{w}})-Z_w]w(s)-[s(U_o+Z_q)-g\sin\gamma_o]\theta(s)$$
$$= Z_{\delta_E}\delta_E(s)+Z_{\delta_B}\delta_B(s)-D'\delta_{RPM}(s)+Z_{\delta_F}\delta_F(s)$$

$$-(M_u+E')u(s)-(sM_{\dot{w}}+M_w)w(s)+(s^2-M_qs)\theta(s)$$
$$= M_{\delta_E}\delta_E(s)+M_{\delta_B}\delta_B(s)+F'\delta_{RPM}(s)+M_{\delta_F}\delta_F(s)$$

$$(s-Y_u)\beta(s)-(s\frac{Y_{\dot{R}}}{U_o}+\frac{g}{U_o}\cos\gamma_o)\phi(s)+[s(1-\frac{Y_{\dot{r}}}{U_o})-\frac{g}{U_o}\sin\gamma_o]\psi(s)$$
$$= [Y_{\delta_A}\delta_A(s)+Y_{\delta_R}\delta_R(s)]\frac{1}{U_o}$$

$$-L_\beta\beta(s)+(s^2-sL_p)\phi(s)-(A_1s^2+sL_{\dot{r}})\psi(s)$$
$$= L_{\delta_A}\delta_A(s)+L_{\delta_R}\delta_R(s)$$

$$-N_\beta\beta(s)-(B_1s^2+sN_p)\phi(s)+(s^2-sN_{\dot{r}})\psi(s)$$
$$= N_{\delta_A}\delta_A(s)+N_{\delta_R}\delta_R(s)$$

where

$$A' = T_u\cos\xi \qquad F' = \frac{z_1 m}{I_{yy}}T_{\delta_{RPM}}$$
$$B' = T_{\delta_{RPM}}\cos\xi$$
$$C' = T_u\sin\xi$$
$$D' = T_{\delta_{RPM}}\sin\xi \qquad A_1 = \frac{I_{xz}}{I_{xx}}$$
$$E' = \frac{z_1 m}{I_{yy}}T_u \qquad B_1 = \frac{I_{xz}}{I_{zz}}$$

The longitudinal transfer functions written in determinant form for the response to elevator deflection ($\delta_B = \delta_P = \delta_{RPM} = 0$) are:

(II-199)

$$\frac{u(s)}{\delta_E(s)} = \frac{\begin{vmatrix} X_{\delta_E} & -(sX_{\dot{w}}+X_w) & -(sX_q - g\cos\gamma_o) \\ Z_{\delta_E} & [s(1-Z_{\dot{w}})-Z_w] & -[s(U_o+Z_q)-g\sin\gamma_o] \\ M_{\delta_E} & -(sM_{\dot{w}}+M_w) & (s^2-M_q s) \end{vmatrix}}{\begin{vmatrix} [s-(X_u+A')] & -(sX_{\dot{w}}+X_w) & -(sX_q - g\cos\gamma_o) \\ -(Z_u-C') & [s(1-Z_{\dot{w}})-Z_w] & -[s(U_o+Z_q)-g\sin\gamma_o] \\ -(M_u+E') & -(sM_{\dot{w}}+M_w) & (s^2-M_q s) \end{vmatrix}} = \frac{N_u}{D_1}$$

D_1 is the determinant of the homogeneous equations and is expanded in (II-200).

(II-200) $D_1 = As^4 + Bs^3 + Cs^2 + Ds + E$

where $A = 1 - Z_{\dot{w}}$

$B = -(1-Z_{\dot{w}})[(X_u + A') + M_q] - Z_w - M_{\dot{w}}(U_o + Z_q) - X_{\dot{w}}(Z_u - C')$

$C = (X_u+A')[M_q(1-Z_{\dot{w}}) + Z_w + M_{\dot{w}}(U_o+Z_q)] - (M_u+E')[X_{\dot{w}}(U_o+Z_q) + X_q(1-Z_{\dot{w}})] + M_q Z_w + (Z_u - C')[M_q X_{\dot{w}} - X_w) - X_q M_{\dot{w}}] + M_{\dot{w}} g \sin\gamma_o - M_w(U_o + Z_q)$

$D = g\sin\gamma_o[(M_u+E)X_{\dot{w}} + M_w - M_{\dot{w}}(X_u+A')] + g\cos\gamma_o[(Z_u - C')M_{\dot{w}} + (M_u+E')(1-Z_{\dot{w}})] + (M_u+E')[-X_w(U_o+Z_q) + Z_w X_q] + (Z_u - C')[X_w M_q - X_q M_w] + (X_u+A')[M_w(U_o+Z_q) - M_q Z_w]$

$E = g\cos\gamma_o[M_w(Z_u - C') - Z_w(M_u+E')] + g\sin\gamma_o[(M_u+E')X_w - (X_u+A')M_w]$

The numerator determinant N_u is expanded in (II-201):

(II-201) $N_u = A_u s^3 + B_u s^2 + C_u s + D_u$

where $A_u = X_{\delta_E}(1-Z_{\dot{w}}) + Z_{\delta_E} X_{\dot{w}}$

$B_u = -X_{\delta_E}[(1-Z_{\dot{w}})M_q + Z_w + M_{\dot{w}}(U_o+Z_q)] + Z_{\delta_E}[X_q M_{\dot{w}} - X_{\dot{w}} M_q + X_w] + M_{\delta_E}[X_{\dot{w}}(U_o+Z_q) + (1-Z_{\dot{w}})X_q]$

$C_u = X_{\delta_E}[M_q Z_w + M_{\dot{w}} g\sin\gamma_o - M_w(U_o+Z_q)] + Z_{\delta_E}[X_q M_w - M_{\dot{w}} g\cos\gamma_o - X_w M_q] + M_{\delta_E}[-X_{\dot{w}} g\sin\gamma_o + X_w(U_o+Z_q) - (1-Z_{\dot{w}})g\cos\gamma_o - Z_w X_q]$.

$D_u = X_{\delta_E}(M_w g\sin\gamma_o) - Z_{\delta_E}(M_w g\cos\gamma_o) + M_{\delta_E}(Z_w g\cos\gamma_o - X_w g\sin\gamma_o)$

Similarly,

(II-202)

$$\frac{w(s)}{\delta_E(s)} = \frac{\begin{vmatrix} [s-(X_u+A')] & X_{\delta_E} & -(sX_q - g\cos\gamma_o) \\ -(Z_u-C') & Z_{\delta_E} & -[s(U_o+Z_q)-g\sin\gamma_o] \\ -(M_u+E) & M_{\delta_E} & (s^2-M_q s) \end{vmatrix}}{D_1} = \frac{N_w}{D_1}$$

(II-203) $N_w = A_w s^3 + B_w s^2 + C_w s + D_w$

where

$A_w = Z_{\delta_E}$

$B_w = X_{\delta_E}(Z_u - C') + Z_{\delta_E}[-M_q - (X_u+A')] + M_{\delta_E}(U_o+Z_q)$

$C_w = X_{\delta_E}[(U_o+Z_q)(M_u+E') - M_q(Z_u-C')] + Z_{\delta_E}[M_q(X_u+A') - (M_u+E')X_q] + M_{\delta_E}[X_q(Z_u-C') - g\sin\gamma_o - (U_o+Z_q)(X_u+A')]$

$D_w = -X_{\delta_E}(M_u+E')(g\sin\gamma_o) + Z_{\delta_E}(M_u+E')g\cos\gamma_o + M_{\delta_E}[(X_u+A')g\sin\gamma_o - (Z_u-C')g\cos\gamma_o]$

and

(II-204)

$$\frac{\theta(s)}{\delta_E(s)} = \frac{\begin{vmatrix} [s-(X_u+A')] & -(sX_{\dot{w}}+X_w) & X_{\delta_E} \\ -(Z_u-C') & [s(1-Z_{\dot{w}})-Z_w] & Z_{\delta_E} \\ -(M_u+E') & -(sM_{\dot{w}}+M_w) & M_{\delta_E} \end{vmatrix}}{D_1} = \frac{N_\theta}{D_1}$$

(II-205) where $N_\theta = A_\theta s^2 + B_\theta s + C_\theta$

$A_\theta = Z_{\delta_E} M_{\dot{w}} + M_{\delta_E}(1-Z_{\dot{w}})$

$B_\theta = X_{\delta_E}[(Z_u-C')M_{\dot{w}} + (1-Z_{\dot{w}})(M_u+E')] + Z_{\delta_E}[M_w - M_{\dot{w}}(X_u+A') + (M_u+E')X_{\dot{w}}] + M_{\delta_E}[-Z_w - (1-Z_{\dot{w}})(X_u+A') - X_{\dot{w}}(Z_u-C')]$

$C_\theta = X_{\delta_E}[M_w(Z_u-C') - Z_w(M_u+E')] + M_{\delta_E}[Z_w(X_u+A') - X_w(Z_u-C')] + Z_{\delta_E}[-M_w(X_u+A) + X_w(M_u+E')]$

It should be noted from the mechanics of the above derivation that had it been desirable to derive the transfer functions for any one of the other control inputs, it would have been necessary only to replace δ_E by the appropriate derivative whenever δ_E appeared in the above transfer functions. This useful knowledge can also be applied to the lateral transfer functions about to be derived. To make the following transfer functions applicable to aileron deflection δ_A instead of rudder deflection δ_R it is necessary only to replace δ_R by δ_A wherever δ_R appears, and to replace the quantities Y_{δ_R}, L_{δ_R}, and N_{δ_R} by Y_{δ_A}, L_{δ_A}, and N_{δ_A} respectively.

The lateral transfer functions for rudder deflection, ($\delta_R = 0$), can be derived as follows:

(II-206)

$$\frac{\beta(s)}{\delta_R(s)} = \frac{\begin{vmatrix} Y^*_{\delta_R} & -(sY^*_p + \frac{g}{U_o}\cos\gamma_o) & [s(1-Y^*_r) - \frac{g}{U_o}\sin\gamma_o] \\ L_{\delta_R} & (s^2 - sL_p) & -(A_1 s^2 + sL_r) \\ N_{\delta_R} & -(B_1 s^2 + sN_p) & (s^2 - sN_r) \end{vmatrix}}{\begin{vmatrix} (s-Y_v) & -(sY^*_p + \frac{g}{U_o}\cos\gamma_o) & [s(1-Y^*_r) - \frac{g}{U_o}\sin\gamma_o] \\ -L_\beta & (s^2 - sL_p) & -(A_1 s^2 + sL_r) \\ -N_\beta & -(B_1 s^2 + sN_p) & (s^2 - sN_r) \end{vmatrix}}$$

$$= \frac{N_{(\beta/\delta_R)}}{D_2}$$

Note that: $Y^*_{\delta_R} = \frac{Y_{\delta_R}}{U_o}$ similarly $Y^*_p = \frac{Y_p}{U_o}$ and $Y^*_r = \frac{Y_r}{U_o}$

(II-207) $D_2 = s(As^4 + Bs^3 + Cs^2 + Ds + E)$

$A = 1 - A_1B_1$

$B = -Y_v(1-A_1B_1) - L_p - N_r - A_1N_p - B_1L_r$

$C = N_\beta(1-Y^*_r) + L_p(Y_v + N_r) - Y^*_p(A_1N_\beta + L_\beta)$
$\quad + N_p(A_1Y_v - L_r) + Y_v(B_1L_r + N_r) + L_\beta B_1(1-Y^*_r)$

$D = -N_\beta[(1-Y^*_r)L_p + L_rY^*_p + A_1\frac{g}{U_o}\cos\gamma_o + \frac{g}{U_o}\sin\gamma_o]$
$\quad + N_p[L_\beta(1-Y^*_r) + Y_vL_r] - L_pN_rY_v$
$\quad + L_\beta[N_rY^*_p - \frac{g}{U_o}\cos\gamma_o - B_1\frac{g}{U_o}\sin\gamma_o]$

$E = \frac{g}{U_o}\cos\gamma_o(L_\beta N_r - N_\beta L_r) + \frac{g}{U_o}\sin\gamma_o(N_\beta L_p - L_\beta N_p)$

(II-208) $N_{(\beta/\delta_R)} = s(A_\beta s^3 + B_\beta s^2 + C_\beta s + D_\beta)$

where

$A_\beta = Y^*_{\delta_R}(1-A_1B_1)$

$B_\beta = Y^*_{\delta_R}[-L_p - N_r - A_1N_p - B_1L_r] + L_{\delta_R}[Y^*_p - B_1(1-Y^*_r)]$
$\quad + N_{\delta_R}[A_1Y^*_p - (1-Y^*_r)]$

$C_\beta = Y^*_{\delta_R}[L_pN_r - N_pL_r] + L_{\delta_R}[\frac{g}{U_o}\cos\gamma_o - N_rY^*_p - N_p(1-Y^*_r)$
$\quad + B_1\frac{g}{U_o}\sin\gamma_o] + N_{\delta_R}[Y^*_pL_r + A_1\frac{g}{U_o}\cos\gamma_o + L_p(1-Y^*_r)$
$\quad + \frac{g}{U_o}\sin\gamma_o]$

$D_\beta = L_{\delta_R}\frac{g}{U_o}[-N_r\cos\gamma_o + N_p\sin\gamma_o]$
$\quad + N_{\delta_R}\frac{g}{U_o}[L_r\cos\gamma_o - L_p\sin\gamma_o]$

(II-209)

$$\frac{\phi(s)}{\delta_R(s)} = \frac{\begin{vmatrix} (s-Y_v) & Y^*_{\delta_R} & [s(1-Y^*_r) - \frac{g}{U_o}\sin\gamma_o] \\ -L_\beta & L_{\delta_R} & -(A_1s^2 - sL_r) \\ -N_\beta & N_{\delta_R} & (s^2 - sN_r) \end{vmatrix}}{D_2}$$

$$= \frac{N_{(\phi/\delta_R)}}{D_2}$$

(II-210) $N_{(\phi/\delta_R)} = s(A_\phi s^2 + B_\phi s + C_\phi + \frac{D_\phi}{s})$

where

$A_\phi = L_{\delta_R} + N_{\delta_R}A_1$

$B_\phi = Y^*_{\delta_R}(L_\beta + A_1N_\beta) + L_{\delta_R}(-N_r - Y_v) + N_{\delta_R}(L_r - A_1Y_v)$

$C_\phi = Y^*_{\delta_R}[-L_rN_\beta - L_\beta N_r] + L_{\delta_R}[Y_vN_r + N_\beta(1-Y^*_r)]$
$\quad + N_{\delta_R}[-L_\beta(1-Y^*_r) + Y_vL_r]$

$D_\phi = (N_{\delta_R}L_\beta - L_{\delta_R}N_\beta)\frac{g}{U_o}\sin\gamma_o$

(II-211)

$$\frac{\psi(s)}{\delta_R(s)} = \frac{\begin{vmatrix} (s-Y_v) & -(sY^*_p + \frac{g}{U_o}\cos\gamma_o) & Y^*_{\delta_R} \\ -L_\beta & (s^2 - sL_p) & L_{\delta_R} \\ -N_\beta & -(B_1s^2 + sN_p) & N_{\delta_R} \end{vmatrix}}{D_2}$$

$$= \frac{N_{(\psi/\delta_R)}}{D_2}$$

(II-212) $N_{(\psi/\delta_R)} = A_\psi s^3 + B_\psi s^2 + C_\psi s + D_\psi$

where

$A_\psi = N_{\delta_R} + B_1L_{\delta_R}$

$B_\psi = Y^*_{\delta_R}(N_\beta + B_1L_\beta) + L_{\delta_R}(N_p - B_1Y_v) + N_{\delta_R}(-Y_v - L_p)$

$C_\psi = Y^*_{\delta_R}(L_\beta N_p - N_\beta L_p) + L_{\delta_R}(Y^*_pN_\beta - Y_vN_p)$
$\quad + N_{\delta_R}(L_pY_v - Y^*_pL_\beta)$

$D_\psi = (L_{\delta_R}N_\beta - N_{\delta_R}L_\beta)\frac{g}{U_o}\cos\gamma_o$

The above transfer functions, which are used as the basis of discussion in Chapter III, completely describe the airframe within the limits of the assumptions made in their derivation. The assumptions are repeated here for reference.

ASSUMPTIONS.

I. The airframe is assumed to be a rigid body.

II. The earth is assumed to be fixed in space, and, unless specifically stated otherwise, the earth's atmosphere is assumed to be fixed with respect to the earth.

III. The mass of the airplane is assumed to remain constant for the duration of any particular dynamic analysis.

IV. The x-z plane is assumed to be a plane of symmetry.

V. The disturbances from the steady flight condition are assumed to be small enough so that the products and squares of the changes in velocities are negligible in comparison with the changes themselves. Also, the disturbance angles are assumed to be small enough so

that the sines of these angles may be set equal to the angles and the cosines set equal to one. Products of these angles are also approximately zero and can be neglected. And, since the disturbances are small, the change in air density encountered by the airplane during any disturbance can be considered to be zero.

VI. During the steady flight condition, the airplane is assumed to be flying with wings level and all components of velocity zero except U_o. Since stability axes are now used as reference axes, $W_o = 0$.

VII. The flow is assumed to be quasi-steady.

The main problem associated with the use of these transfer functions is the determination of the numerical values of the stability derivatives. Over a period of years, considerable experience in the application of these equations to many varied airframe configurations flying at low subsonic speeds has been gained. For the low subsonic speed range, it may be said, in general, that there is good agreement between the results of theoretical analyses and of experimental flight tests.

Experience in the correlation of experimental flight test results and theoretical analyses of the dynamics of airplanes flying in the transonic and supersonic speed ranges is definitely limited at this time. In view of this lack of experience, no attempt is made to draw any firm conclusions regarding the dynamic behavior of aircraft flying at these speeds; however, some rather general remarks can be made. The assumption of quasi-steady flow does not appear to be very accurate for airplanes flying at transonic speeds; consequently, unsteady flow effects may have to be introduced into the transfer functions for the results of an analysis to have practical value. The outlook seems to be more favorable for purely supersonic flow. The time lags for the forces to approach steady values appear to be of the same order of magnitude as in subsonic flow with at least one exception, this being the lag in the damping of a wing in pitch for the lower supersonic Mach numbers. In general, the basic theory used in the derivation of the transfer functions can be applied to an airplane flying at either subsonic, transonic or supersonic speeds, but caution must be used to ensure that all of the necessary stability derivatives are included.

CHAPTER III

DISCUSSION OF TRANSFER FUNCTIONS

SECTION 1 – INTRODUCTION

In this chapter, the transfer functions previously derived are analyzed with the aim of promoting an intuitive understanding of the aircraft motions represented by these transfer functions and of showing how an analog computer may be used in the analysis.

Some comments relating to transfer functions in general are presented first; the rest of the chapter is devoted to a detailed discussion of the longitudinal and lateral transfer functions.

The transfer functions derived in Chapter II are simplified by neglecting relatively unimportant terms; they are then evaluated numerically for a representative high-performance jet aircraft at a typical flight condition, that is, for an airframe which has dynamic characteristics similar to those occurring during most flight conditions.

Complete three degree of freedom responses to a control surface deflection for the longitudinal motions are analyzed first; then some lesser degree of freedom solutions and approximate factors of analytical value are determined by inspection of Bode plots and analog computer solutions of the complete case. The lateral motions are treated similarly. The simplified solutions are used to determine the relative importance of the individual stability derivatives to the various modes of motion.

Analog computer solutions are given which demonstrate the effect of flight conditions and of individual dimensional and basic non-dimensional stability derivatives.

SECTION 2 – GENERAL DISCUSSION OF TRANSFER FUNCTIONS

This section presents certain general information regarding transfer functions in preparation for the detailed analyses in the remainder of the chapter. Methods of presenting the results obtained by working with the transfer functions are also considered at this point.

These transfer functions have already been derived in Chapter II and shown to be of the form $N(s)/D(s)$, where both N and D are rational polynomials in the complex variable s. $D(s)$ is the expansion of the system determinant, that is, the expansion of the determinant of the coefficients in the homogeneous equations of motion. The conditional equality, $D(s) = 0$, is referred to as the characteristic equation of the system and is related to the functional form of the transient motion of the airframe. The roots of this characteristic equation determine the functional form of the transient motions of the aircraft. For example, if $D(s) = As^4 + Bs^3 + Cs^2 + Ds + E = A(s + \alpha_1)(s + \alpha_2)(s + \alpha_3)(s + \alpha_4)$, the time histories of the transient motions of the craft are of the form:

$$K_1e^{-\alpha_1 t} + K_2e^{-\alpha_2 t} + K_3e^{-\alpha_3 t} + K_4e^{-\alpha_4 t}$$

where the K's depend upon both numerator and denominator quantities in the transfer function and where the α's may be complex as well as pure real quantities.

If two of the α's, say α_3 and α_4, are complex conjugates, the time histories may be written in the form $K_1e^{-\alpha_1 t} + K_2e^{-\alpha_2 t} + K_3'e^{-at}\sin(\omega t + \phi)$ where a, ω, and ϕ are functions of the real and imaginary parts of α_3 and α_4.

When the time histories are written in this way by combining any complex conjugate terms, they consist of subsidences (real exponentials with $\alpha > 0$), divergences (real exponentials with $\alpha < 0$), and oscillations (complex exponentials).

Each term of these types (subsidences, divergences, and oscillations) is referred to as a mode of the aircraft transient motion. In the example considered, the term $K_1e^{-\alpha_1 t}$ is one mode; $K_2e^{-\alpha_2 t}$, another; and $K_3'e^{-at}\sin(\omega t + \phi)$, a third.

Since the major concern of this volume is the transient response of the airframe, much of the discussion is in terms of the modes of the transient motion.

The complete solution of the system of linear differential equations which describe the motion of a dynamic system is the sum of a steady-state and a transient solution, provided that a steady state exists, a condition which occurs only if the system is stable. The stability or instability of a system can be determined by applying Routh's criterion to the coefficients in the characteristic equation, and the degree of stability (or instability) can be determined by finding the roots of the characteristic equation.

A system is stable if, and only if, the transfer function has no poles in the right half of the complex s-plane. If N(s) and D(s) have no common factor, the last statement is equivalent to saying: A system is stable if, and only if, the characteristic equation has no zeros in the right half of the complex s-plane. (If N and D do have common factors, these must, of course, be cancelled out before applying this second test for stability.) The steady-state solution for a stable system corresponds to the system response to a sinusoidal forcing function after a sufficiently long time has elapsed from the application of the sinusoid so that the transient response has damped out to a negligibly small amount.

The frequency response, or Bode plot, is a valuable design tool for the determination of the system transient characteristics. It consists of two parts: one, a plot of transfer function amplitude in decibels, and the other, a plot of transfer function phase angle, both plotted against the logarithm of the frequency. The Bode plot can be obtained from the transfer function by substituting $j\omega$ for s.

Whether the system represented by the transfer function is stable or unstable, this substitution leads to a result mathematically identical to the solution of the non-homogeneous equations of motion of the system with a sinusoidal forcing function.

If the system is stable, the information required for plotting a Bode chart can be obtained experimentally by exciting the physical system with a sinewave of variable frequency and measuring the responses after the transients have died out. For a stable system, only one plot is essential, since the phase angle is a known function of the amplitude. Bode diagrams can also be obtained by reduction of transient data, but much more analytical work is required.

Results of analyses in this chapter are to be presented both as Bode charts and as functions of time by means of analog computer recordings.

Although the Bode chart is basically a system design tool, it also yields information concerning transient responses; this latter use is the one emphasized in this chapter. These Bode charts of airframe transfer functions give data in a form which the control systems designer can readily use.

The analog computer is an especially valuable tool for analyzing the dynamic response of complicated systems because it yields large amounts of quantitative data quickly and easily. The analog computer traces are plots of certain variables as functions of time. Identical results could be obtained by taking the inverse Laplace transform of the transfer functions and plotting the resulting expressions against time, but this procedure would require far more time and effort.

LONGITUDINAL TRANSFER FUNCTIONS

SECTION 3 – COMPLETE THREE DEGREE OF FREEDOM RESPONSE TO ELEVATOR DEFLECTION

In this section, the complete three degree of freedom response of an airframe to an elevator deflection is examined. As mentioned previously, the transfer functions derived in Chapter II are to be simplified before proceeding with the analysis.

In comparison with other terms appearing in (II-198), several terms are small in magnitude because they contain stability derivatives, such as $X_{\dot{w}}$, X_q, $Z_{\dot{w}}$, X_{δ_E}, and T_u, which are usually very small. The derivative Z_q is relatively unimportant because it appears as an addition to U_o in the Z force equation of motion and is always small in comparison with U_o.

ASSUMPTION VIII. It is assumed that:

$$X_{\dot{w}} = X_q = Z_{\dot{w}} = X_{\delta_E} = Z_q = T_u = T_{\delta_{RPM}} = 0$$

Perhaps the best general evidence in justification of Assumption VIII is that the derivatives named in it rarely appear in the technical literature concerned with aircraft dynamics. The inference here is that although individual investigators have evaluated the effects of these derivatives for a multitude of various airframe configurations, they have found them to be of only secondary importance. The adoption of Assumption VIII does not in any way alter the methods of analysis applied in the remainder of this chapter, but it must be remembered that if any of these derivatives were actually of primary importance for a particular airframe, erroneous quantitative data might result from the use of this assumption in the analysis of that airframe.

In general, any stability derivative may be neglected if it is first determined that the term containing the given derivative is small in comparison with other terms in the same equations.

ASSUMPTION IX. In the steady flight condition, the flight path of the airplane is assumed to be horizontal: $\gamma_o = 0$.

Assumption IX is introduced solely to simplify the mechanics of the analysis. When the flight path of an airplane is initially inclined to the horizontal, γ_o must of course be included in the transfer functions.

The longitudinal transfer functions derived in Chapter II are simplified into the following forms by the use of Assumptions VIII and IX:

(III-1)
$$\frac{u(s)}{\delta_E(s)} = \frac{N_u}{D_1} = \frac{B_u s^2 + C_u s + D_u}{D_1}$$

$$B_u = Z_{\delta_E} X_w$$

$$C_u = -Z_{\delta_E}(gM_{\dot{w}} + M_q X_w) + M_{\delta_E}(U_o X_w - g)$$

$$D_u = g(M_{\delta_E} Z_w - M_w Z_{\delta_E})$$

(III-2) $$\frac{w(s)}{\delta_E(s)} = \frac{N_w}{D_1} = \frac{A_w s^3 + B_w s^2 + C_w s + D_w}{D_1}$$

$$A_w = Z_{\delta_E}$$

$$B_w = -Z_{\delta_E}(M_q + X_u) + M_{\delta_E} U_o$$

$$C_w = X_u(Z_{\delta_E} M_q - M_{\delta_E} U_o)$$

$$D_w = g(Z_{\delta_E} M_u - M_{\delta_E} Z_u)$$

(III-3) $$\frac{\theta(s)}{\delta_E(s)} = \frac{N_\theta}{D_1} = \frac{A_\theta s^2 + B_\theta s + C_\theta}{D_1}$$

$$A_\theta = Z_{\delta_E} M_{\dot{w}} + M_{\delta_E}$$

$$B_\theta = Z_{\delta_E}(M_w - M_{\dot{w}} X_u) - M_{\delta_E}(X_u + Z_w)$$

$$C_\theta = Z_{\delta_E}(M_u X_w - M_w \check{X}_u) + M_{\delta_E}(X_u \check{Z}_w - X_w \check{Z}_u)$$

(III-4) $$D_1 = As^4 + Bs^3 + Cs^2 + Ds + E$$

$$A = 1$$

$$B = -(M_q + X_u + Z_w + U_o M_{\dot{w}})$$

$$C = M_q \check{Z}_w - U_o M_w + X_u(\check{M}_q + \check{Z}_w + U_o \check{M}_{\dot{w}}) - X_w \check{Z}_u$$

$$D = -X_u(M_q \check{Z}_w - U_o \check{M}_w) - M_u U_o X_w + M_q \check{X}_w Z_u + g(M_w \check{Z}_u + \check{M}_u)$$

$$E = g(M_w Z_u - M_u Z_w)$$

For the numerical analysis in this section, the data in Table III-1 are used.

Altitude (ft)		20,000
Weight (lbs)		30,500
Mach Number		.638
True Airspeed (ft/sec)		660
	X_u	-.0097
	X_w	+.0016
	Z_u	-.0955
	Z_w	-1.430
	Z_{δ_E}	69.8
	M_w	-.0235
	$M_{\dot{w}}$	-.0013
	M_q	-1.920
	M_{δ_E}	26.10
	M_u	0.0

Table III-1

Substituting these data into (III-1), (III-2), (III-3), and (III-4) yields the following set of equations:

(III-5)

$$\frac{u(s)}{\delta_E(s)} = \frac{0.1117s^2 - 810s - 1150}{(s^2 + 4.210s + 18.242)(s^2 + 0.00901s + 0.00396)}$$

$$\frac{\Delta\alpha(s)}{\delta_E(s)} = \frac{1}{U_o}\frac{w(s)}{\delta_E(s)} = \frac{69.8s^3 + 17343s^2 + 168.4s + 80.25}{(s^2+4.210s+18.242)(s^2+0.00901s+0.00396)}$$

$$\frac{\theta(s)}{\delta_E(s)} = \frac{26.01s^2 + 35.96s + 0.3502}{(s^2+4.210s+18.242)(s^2+0.00901s+0.00396)}$$

(III-5) are not written according to the convention selected for writing transfer functions; instead, they are to be written in the form:

$$\text{Transfer Function} = K\,G(s)$$

where K is the frequency invariant part, and G(s) the frequency dependent part, of the transfer function.

In the K G(s) form, (III-5) become:

(III-6) $$\frac{u(s)}{\delta_E(s)} = -15920\,\frac{\left(\frac{s}{-725.4}+1\right)\left(\frac{s}{1.44}+1\right)}{\left(\frac{s^2}{\omega_{n_p}^2}+\frac{2\zeta_p}{\omega_{n_p}}s+1\right)\left(\frac{s^2}{\omega_{n_{sp}}^2}+\frac{2\zeta_{sp}}{\omega_{n_{sp}}}s+1\right)}$$

(III-7) $$\frac{\Delta\alpha(s)}{\delta_E(s)} = 1110\,\frac{\left(\frac{s}{248.5}+1\right)\left[\frac{s^2}{(0.068)^2}+\frac{2(0.0713)}{0.068}s+1\right]}{\left(\frac{s^2}{\omega_{n_p}^2}+\frac{2\zeta_p}{\omega_{n_p}}s+1\right)\left(\frac{s^2}{\omega_{n_{sp}}^2}+\frac{2\zeta_{sp}}{\omega_{n_{sp}}}s+1\right)}$$

(III-8) $$\frac{\theta(s)}{\delta_E(s)} = 4.85\,\frac{\left(\frac{s}{1.372}+1\right)\left(\frac{s}{0.0098}+1\right)}{\left(\frac{s^2}{\omega_{n_p}^2}+\frac{2\zeta_p}{\omega_{n_p}}s+1\right)\left(\frac{s^2}{\omega_{n_{sp}}^2}+\frac{2\zeta_{sp}}{\omega_{n_{sp}}}s+1\right)}$$

where

$\omega_{n_{sp}} = 4.27$ $\omega_{n_p} = 0.0714$

$\zeta_{sp} = 0.493$ $\zeta_p = 0.0630$

Inspection of the roots of the characteristic equation (commonly called the "longitudinal stability quartic") for these degrees of freedom shows that the characteristic longitudinal motions consist of two oscillatory modes. One of these is a relatively well damped high frequency oscillation called the short period mode, and the other is a lightly damped relatively low frequency oscillation called the phugoid mode. Both are discussed later in more detail.

Figures III-1, III-2, and III-3 are Bode plots of (III-6), (III-7), and (III-8) respectively. By examining these plots, several conclusions can be drawn concerning the phugoid and short period modes of the transient response of the airframe.

Figure III-1 shows that the amplitude ratio, $\left|\frac{u}{\delta_E}\right|$, is much smaller at the natural frequency of the short period than at that of the phugoid. This indicates that relatively smaller changes in airspeed occur during the short period transient mode than during the phugoid transient oscillation.

By inspection of Figure III-2 or equation (III-7), it may be seen that a quadratic in the numerator of the $\frac{\Delta\alpha}{\delta_E}$ transfer function very nearly cancels the denominator quadratic which represents the phugoid oscillation. Consequently, there is almost no change in angle of attack during the phugoid oscillation.

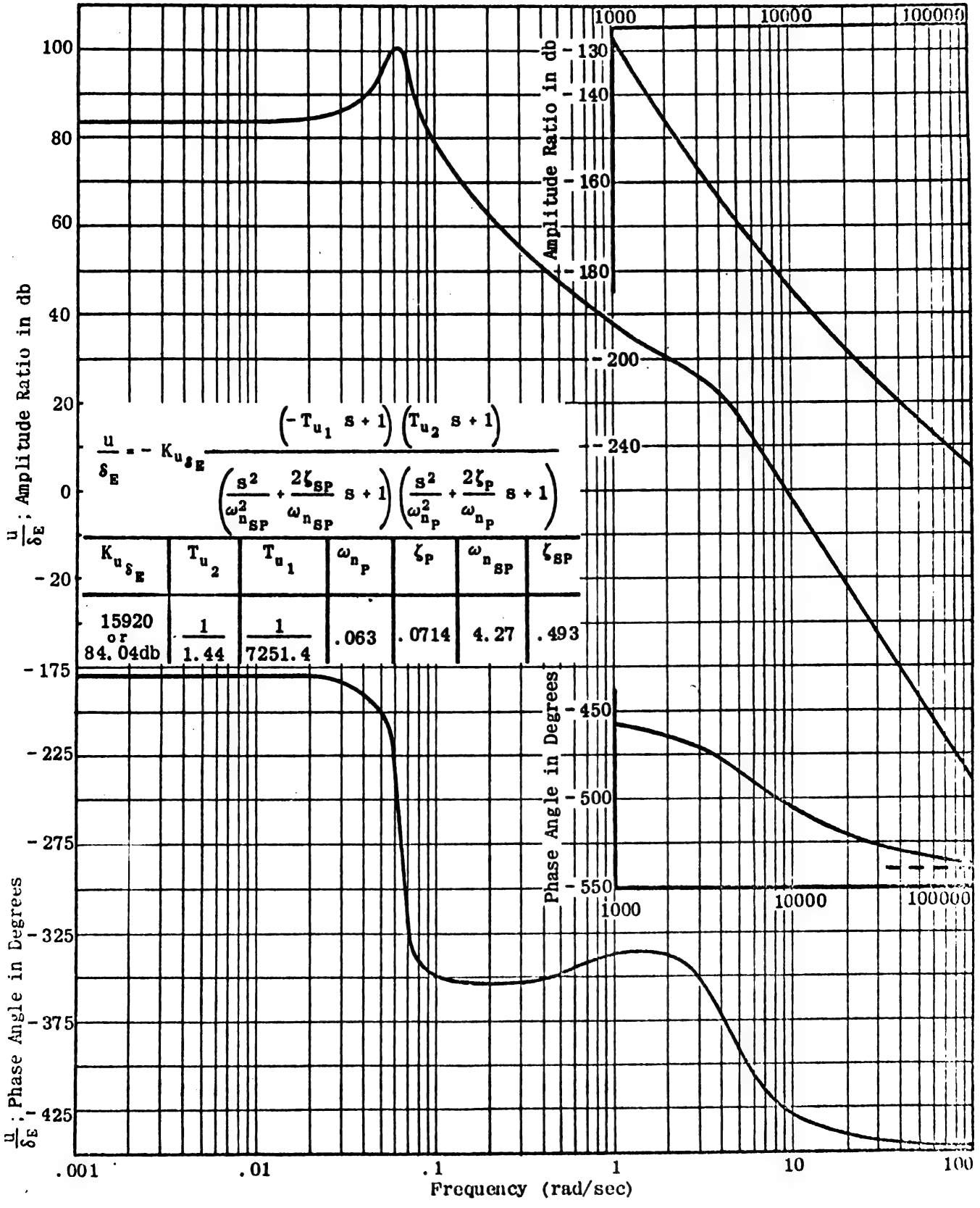

Figure III-1 Forward Speed Response to Elevator Deflection. Three Degree of Freedom

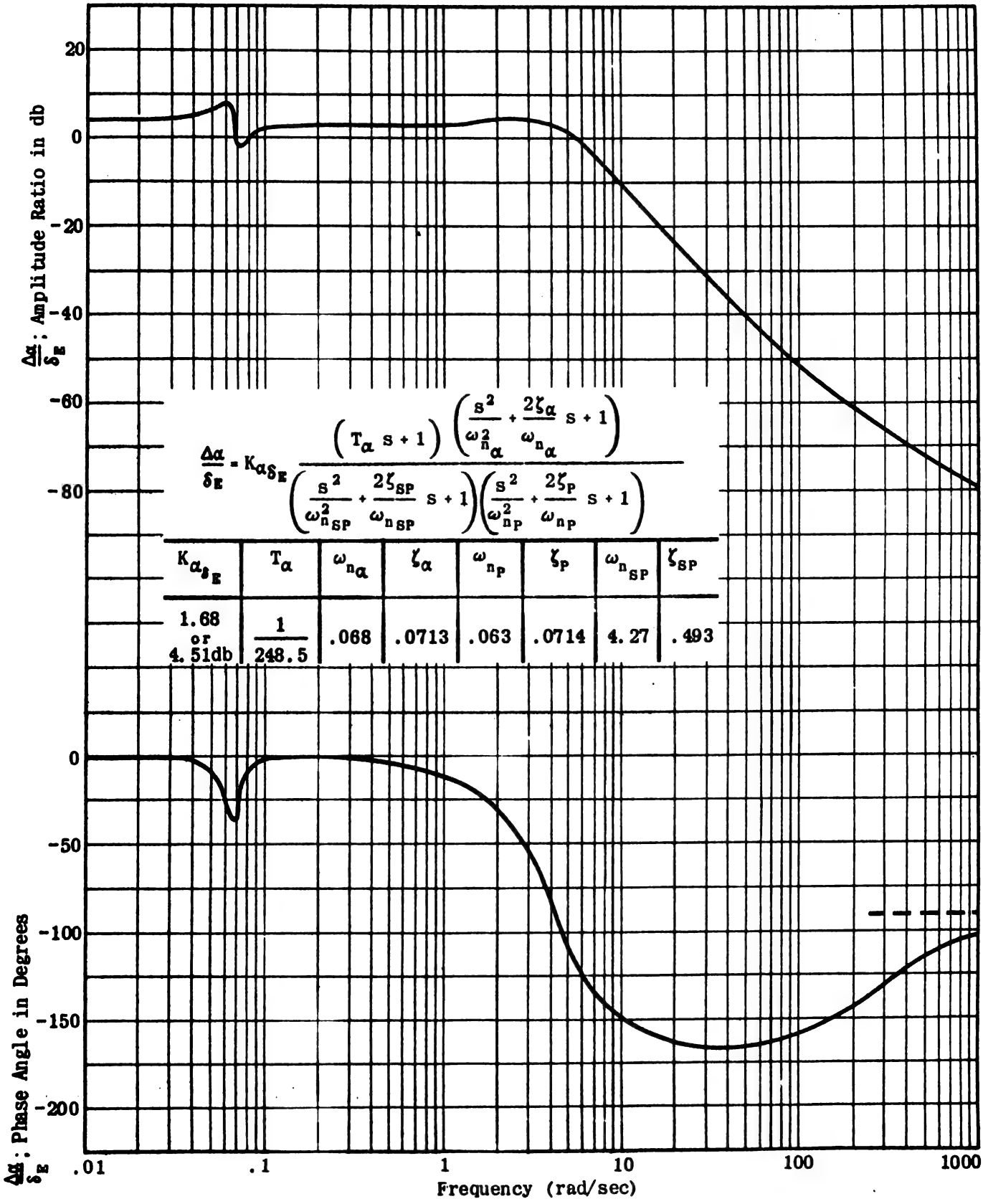

Figure III-2 Change in Angle of Attack Response to Elevator Deflection. Three Degree of Freedom

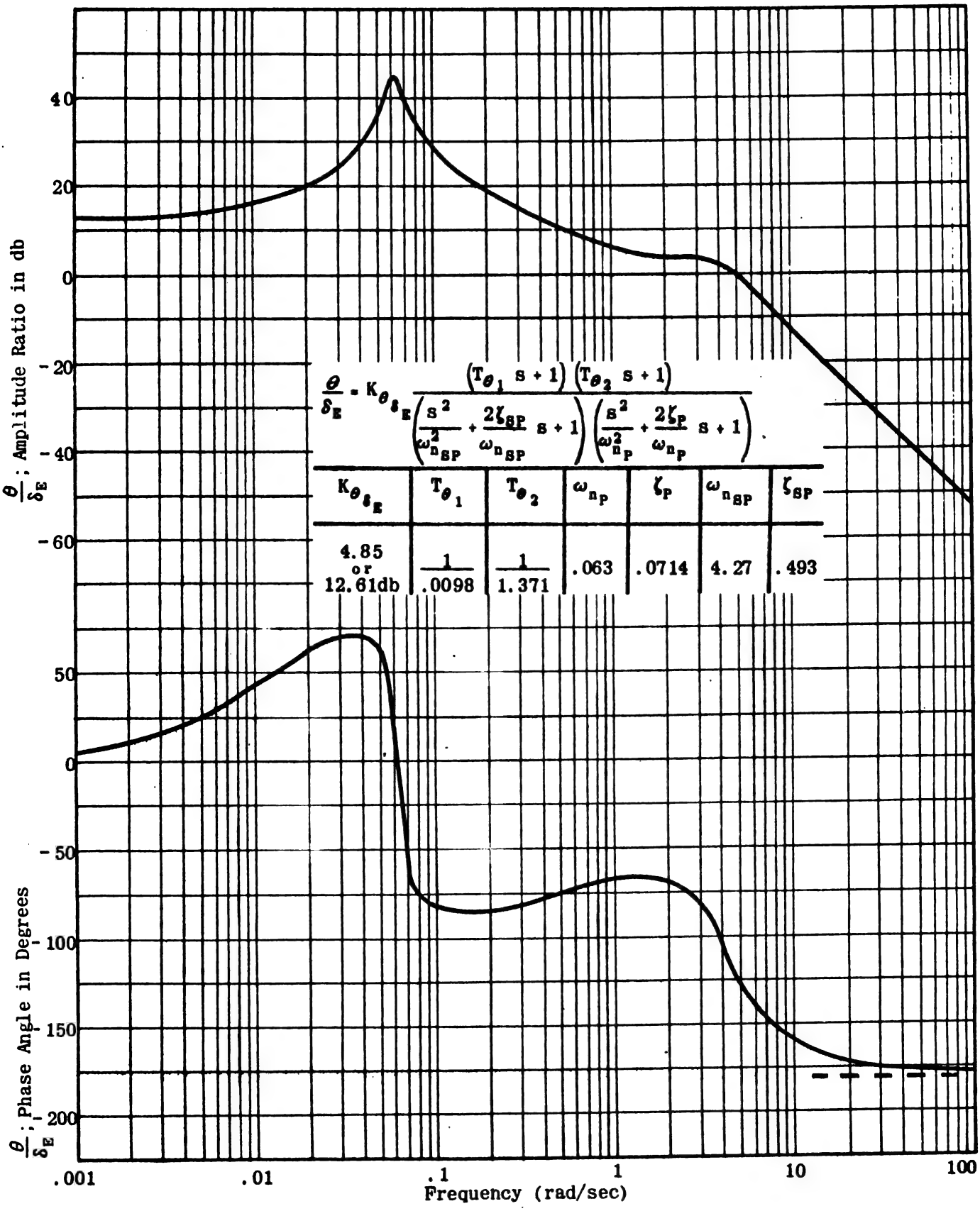

$$\frac{\theta}{\delta_E} = K_{\theta\delta_E} \frac{(T_{\theta_1} s + 1)(T_{\theta_2} s + 1)}{\left(\frac{s^2}{\omega_{n_{SP}}^2} + \frac{2\zeta_{SP}}{\omega_{n_{SP}}} s + 1\right)\left(\frac{s^2}{\omega_{n_P}^2} + \frac{2\zeta_P}{\omega_{n_P}} s + 1\right)}$$

$K_{\theta\delta_E}$	T_{θ_1}	T_{θ_2}	ω_{n_P}	ζ_P	$\omega_{n_{SP}}$	ζ_{SP}
4.85 or 12.61db	1 / .0098	1 / 1.371	.063	.0714	4.27	.493

Figure III-3 Pitch Angle Response to Elevator Deflection. Three Degree of Freedom

Figure III-3 shows that the values of the amplitude ratio, $|\frac{\theta}{\delta_E}|$, at the short period and the phugoid natural frequencies, are more nearly equal than those of $|\frac{u}{\delta_E}|$ at the same frequencies. This implies that the amplitudes of θ occurring in the characteristic modes are more nearly equal than those of u, for the same inputs. Inspection of the Bode plots shows that only relatively small amplitudes of u occur in the short period mode, and of α in the phugoid mode, whereas larger amplitudes of θ occur in both.

These observations indicate that good approximations to these modes can be obtained by considering that each of them consists of only two degrees of freedom: the phugoid, of u and θ degrees of freedom, and the short period, of α and θ.

Before the approximate transfer functions are discussed, these conclusions concerning the relative amplitudes are verified by inspection of analog computer results. Figure III-4 shows the appropriate analog computer traces.

From this figure, it can be seen that the maximum amplitude of u is very much smaller in the short period than in the phugoid, and that the maximum amplitude of $w(\cong U_o\alpha)$ during the phugoid is very nearly zero. Further, the maximum amplitudes of θ in each mode are comparable in magnitude. All these facts are in agreement with what was inferred from the Bode plots.

The characteristic response of an airplane to an impulse elevator deflection can be described as follows: When the elevator is deflected, the airplane undergoes a rapid change in both pitch angle and angle of attack. The angle of attack rapidly returns to approximately its initial value; the airplane then slowly oscillates in forward speed and pitch angle until the transient motion disappears and the airplane resumes its initial flight conditions.

On the basis of the analysis presented above, the equations of motion are now used to derive some approximate transfer functions. Equations (II-198) reduced by applying Assumptions VIII and IX and by considering only elevator deflection, are rewritten as:

(III-9)
$$(s - X_u)u(s) - X_w w(s) + g\theta(s) = 0$$
$$-Z_u u(s) + (s - Z_{\dot{w}})w(s) - sU_o\theta(s) = Z_{\delta_E}\delta_E(s)$$
$$M_u u(s) - (sM_{\dot{w}} + M_w)w(s) + (s - M_q)s\theta(s) = M_{\delta_E}\delta_E(s)$$

SECTION 4 – TWO DEGREE OF FREEDOM SHORT PERIOD MODE APPROXIMATIONS

The two degree of freedom approximation to the short period mode can be determined by setting the variation in forward velocity, u, equal to zero and deleting the first relation of (III-9). This is in accordance with the previous statements that u is of relatively small amplitude in the short period mode and that a suitable two degree of freedom approximation can be obtained by considering only the α(i.e., w) and θ relations.

(III-10)
$$(s - Z_{\dot{w}})w(s) - sU_o\theta(s) = Z_{\delta_E}\delta_E(s)$$
$$-(sM_{\dot{w}} + M_w)w(s) + (s - M_q)s\theta(s) = M_{\delta_E}\delta_E(s)$$

Solving this system of equations leads to the transfer functions:

(III-11)
$$\frac{\alpha(s)}{\delta_E(s)} = \frac{1}{U_o}\frac{w(s)}{\delta_E(s)} = \frac{1}{U_o}\frac{Z_{\delta_E}s + (U_oM_{\delta_E} - Z_{\delta_E}M_q)}{[s^2 - (U_oM_{\dot{w}} + Z_w + M_q)s + (M_qZ_w - U_oM_w)]}$$

(III-12)
$$\frac{\theta(s)}{\delta_E(s)} = \frac{(M_{\delta_E} + Z_{\delta_E}M_{\dot{w}})s + (Z_{\delta_E}M_w - M_{\delta_E}Z_w)}{s[s^2 - (U_oM_{\dot{w}} + Z_w + M_q)s + (M_qZ_w - U_oM_w)]}$$

The common part of the denominators of these transfer functions is of the form $s^2 + 2\zeta\omega_n s + \omega_n^2$, with:

(III-13)
$$\omega_n = \sqrt{M_qZ_w - U_oM_w}$$

and

(III-14)
$$\zeta = \frac{-(U_oM_{\dot{w}} + Z_w + M_q)}{2\omega_n}$$

Evaluating (III-11) and (III-12) for the numerical values of the stability derivatives from Table III-1, and arranging the results in the K G(s) form, yield:

(III-15)
$$\frac{\alpha(s)}{\delta_E(s)} = 1.44\,\frac{\frac{s}{248.5} + 1}{\frac{s^2}{\omega_{n_{sp}}^2} + \frac{2\zeta_{sp}}{\omega_{n_{sp}}}s + 1}$$

and

(III-16)
$$\frac{\theta(s)}{\delta_E(s)} = 1.955\,\frac{\frac{s}{1.371} + 1}{s\left(\frac{s^2}{\omega_{n_{sp}}^2} + \frac{2\zeta_{sp}}{\omega_{n_{sp}}}s + 1\right)}$$

where $\omega_{n_{sp}} = 4.27$ rad/sec. and $\zeta_{sp} = 0.493$

Figures III-5 and III-6 are Bode plots of (III-15) and (III-16) respectively. The analog computer solutions of the equations for the two degree of freedom approximation to the short period mode are shown in Figure III-7.

To check the accuracy of this two degree of freedom approximation, three comparisons are made: first, the numerical values of the appropriate ratios and natural frequencies in (III-6) and (III-16) are compared; second, the Bode charts of Figures III-2 and III-5, and of Figures III-3 and III-6 are superimposed; and third, the analog computer traces of the two and three degree of freedom solutions are compared.

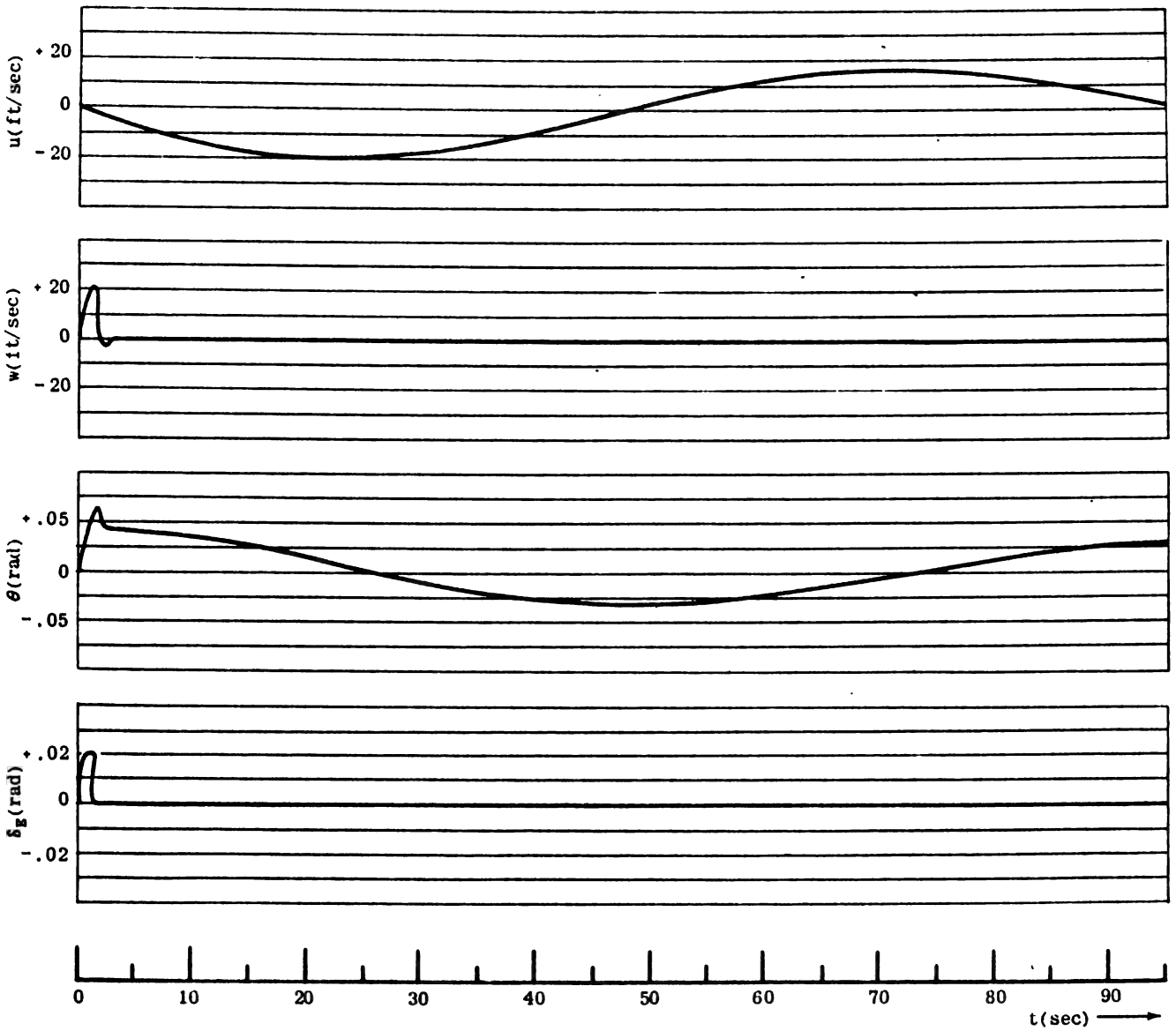

Figure III-4 Analog Computer Record of Time History for Pulse Elevator Deflection, Three Degree of Freedom

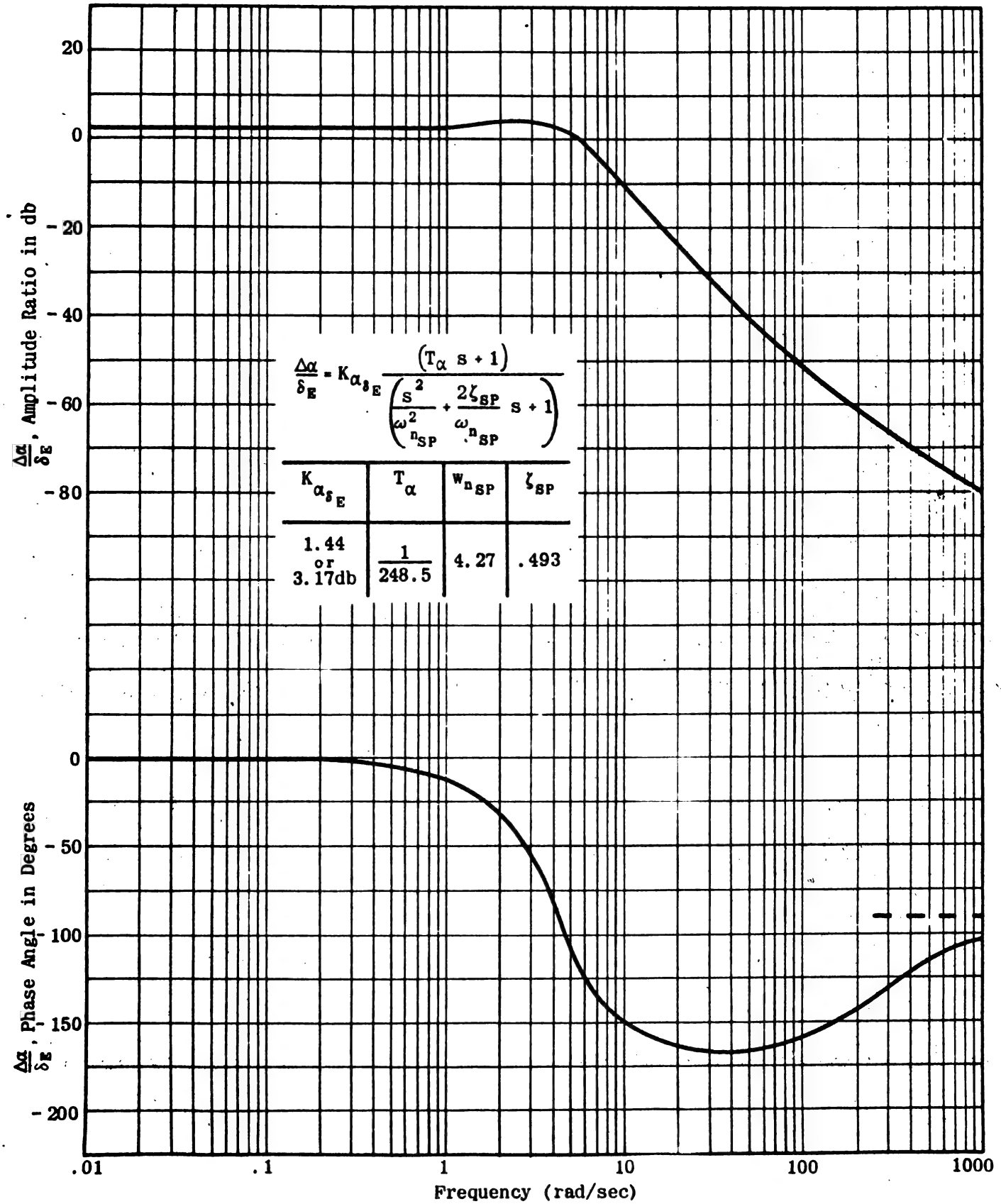

Figure III-5 Change in Angle of Attack Response to Elevator Deflection. Two Degree of Freedom, Short Period Mode

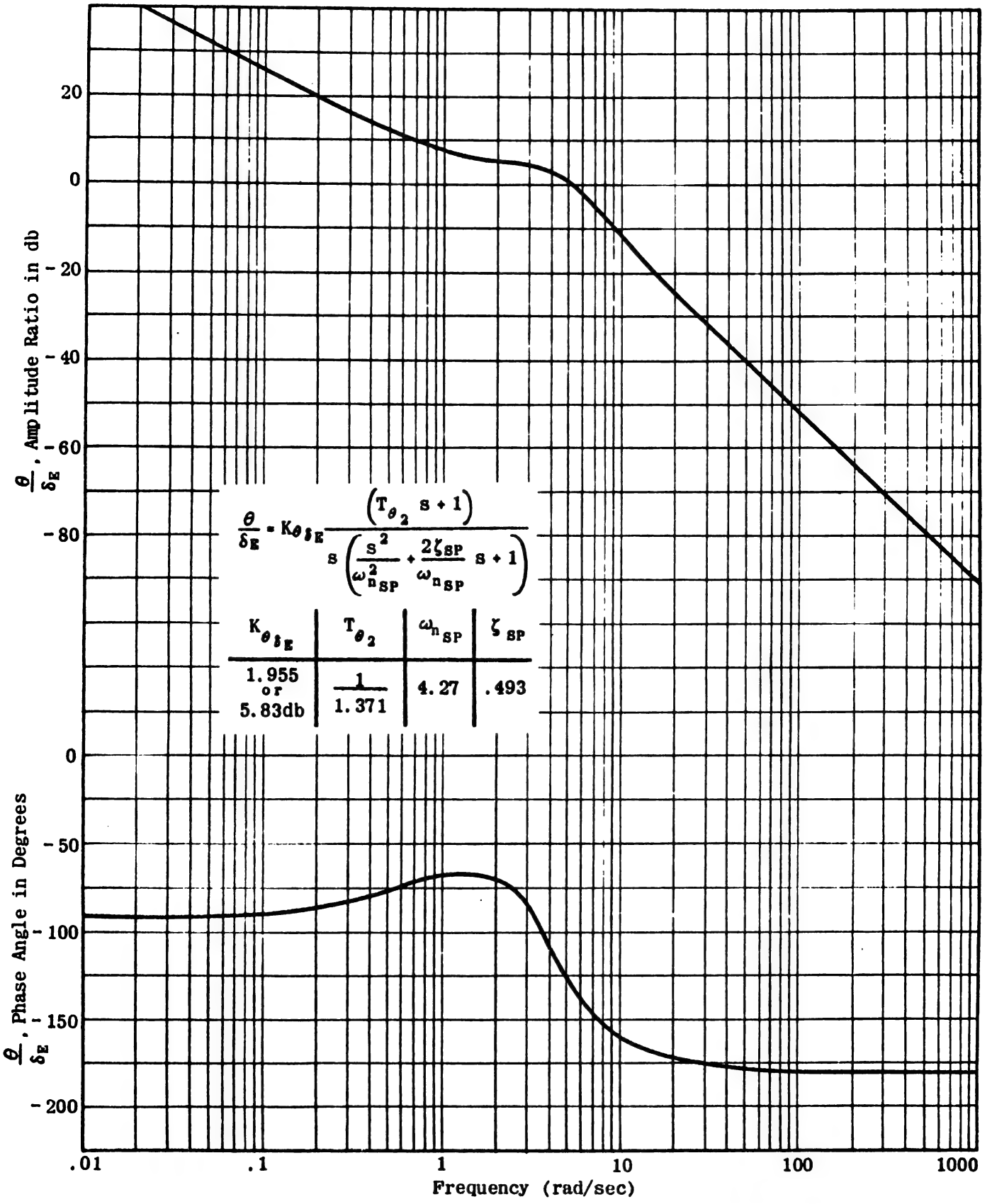

$$\frac{\theta}{\delta_E} = K_{\theta\delta_E} \frac{\left(T_{\theta_2} s + 1\right)}{s\left(\frac{s^2}{\omega_{n_{SP}}^2} + \frac{2\zeta_{SP}}{\omega_{n_{SP}}} s + 1\right)}$$

$K_{\theta\delta_E}$	T_{θ_2}	$\omega_{n_{SP}}$	ζ_{SP}
1.955 or 5.83db	$\frac{1}{1.371}$	4.27	.493

Figure III-6 Pitch Angle Response to Elevator Deflection. Two Degree of Freedom, Short Period Mode

Table III-2 contains the values of ζ_{sp} and $\omega_{n_{sp}}$ for both the two and three degree of freedom cases. It can be seen that these values check exactly.

SHORT PERIOD MODE		
	ζ	ω_n(rad/sec)
Two Degrees of Freedom	0.493	4.27
Three Degrees of Freedom	0.493	4.27

Comparison of ζ and ω_n of two degree and three degree of freedom short period mode.

TABLE III-2

In Figure III-8, the two degree of freedom $\Delta\alpha/\delta_E$ transfer function (from Figure III-5) and the three degree of freedom $\Delta\alpha/\delta_E$ transfer function (from Figure III-2) are plotted. Figure III-9 shows the plots of the three degree of freedom (from Figure III-3) and two degree of freedom (from Figure III-6) θ/δ_E transfer functions. In both cases, it can be seen that there is very good agreement in both phase and amplitude ratio in the vicinity of the short period natural frequency.

As a final check, the two and three degree of freedom solutions of the equations of motion from the analog computer are superimposed in Figure III-10, which shows that there is excellent agreement between them.

In summary, the two degree of freedom solution of the pitching moment and vertical force equations of motion is a very good approximation to the short period mode. For a typical flight condition, the short period mode can be considered to consist of changes only in angle of attack and in angle of pitch; the short period motion occurs before there is any appreciable change in forward speed.

SECTION 5 – TWO DEGREE OF FREEDOM PHUGOID MODE APPROXIMATIONS

As indicated in Section III-3, the quantity w, the incremental velocity in the z direction, is almost exactly zero, but u and θ undergo relatively large variations in amplitude during the phugoid motion.

These facts suggest that an approximation to the phugoid may be obtained by setting $w = 0$ in (III-9); the result of doing this is:

(III-17)
$$(s - X_u)u(s) + g\theta(s) = 0$$
$$-Z_u u(s) - sU_o\theta(s) = Z_{\delta_E}\delta_E(s)$$
$$-M_u u(s) + s(s - M_q)\theta(s) = M_{\delta_E}\delta_E(s)$$

Since three equations in two unknowns have no solution in general, it is necessary to eliminate one equation of (III-17); this can be done on the basis of physical reasoning.

In general, the stability derivative M_u is extremely small and is therefore usually assumed to be zero as it has been for the generic aircraft which provides the numerical values used in the present discussion. Further, the phugoid motion of an aircraft is so slow that the inertia forces acting during it can be assumed negligible. If both these assumptions are used, the last relation of (III-17) becomes:

(III-18)
$$-sM_q\theta(s) = M_{\delta_E}\delta_E(s)$$

If this last relation is combined with either of the first two of (III-17), the characteristic equations of these two approximate systems cannot have complex roots; that is, the systems represented by these pairs of equations cannot oscillate. To obtain an oscillatory solution, it is therefore necessary to use the first two equations of (III-17):

(III-19)
$$(s - X_u)u(s) + g\theta(s) = 0$$
$$-Z_u u(s) - sU_o\theta(s) = Z_{\delta_E}\delta_E(s)$$

The resulting transfer functions are of the form:

(III-20)
$$\frac{u(s)}{\delta_E(s)} = \frac{Z_{\delta_E}\, g}{U_o\left(s^2 - X_u s - \frac{Z_u g}{U_o}\right)}$$

and

(III-21)
$$\frac{\theta(s)}{\delta_E(s)} = \frac{-(s - X_u)Z_{\delta_E}}{U_o\left(s^2 - X_u s - \frac{Z_u g}{U_o}\right)}$$

and hence the natural frequency and damping ratio of the approximation to the phugoid are $\omega_{n_p} = \sqrt{-Z_u g/U_o}$ and $\zeta_p = -X_u/2\omega_{n_p}$ respectively.

By substituting the appropriate numerical values from Table III-1 into (III-20) and (III-21) and arranging the results in the KG(s) form, the transfer functions become:

(III-22)
$$\frac{u(s)}{\delta_E(s)} = 730\,\frac{1}{\left(\frac{s^2}{\omega_{n_p}^2} + \frac{2\zeta_p}{\omega_{n_p}}s + 1\right)}$$

and

(III-23)
$$\frac{\theta(s)}{\delta_E(s)} = 0.220\,\frac{-\left(\frac{s}{0.0097} + 1\right)}{\left(\frac{s^2}{\omega_{n_p}^2} + \frac{2\zeta_p}{\omega_{n_p}}s + 1\right)}$$

where $\begin{cases} \omega_{n_p} = 0.0683 \\ \zeta_p = 0.0710 \end{cases}$

Figures III-11 and III-12 are the Bode plots of (III-22) and (III-23), respectively. The analog computer solutions of the equations for the two degree of freedom approximation to the phugoid mode are shown in Figure III-13.

The accuracy of the two degree of freedom approximation to the phugoid mode can be checked in the same manner

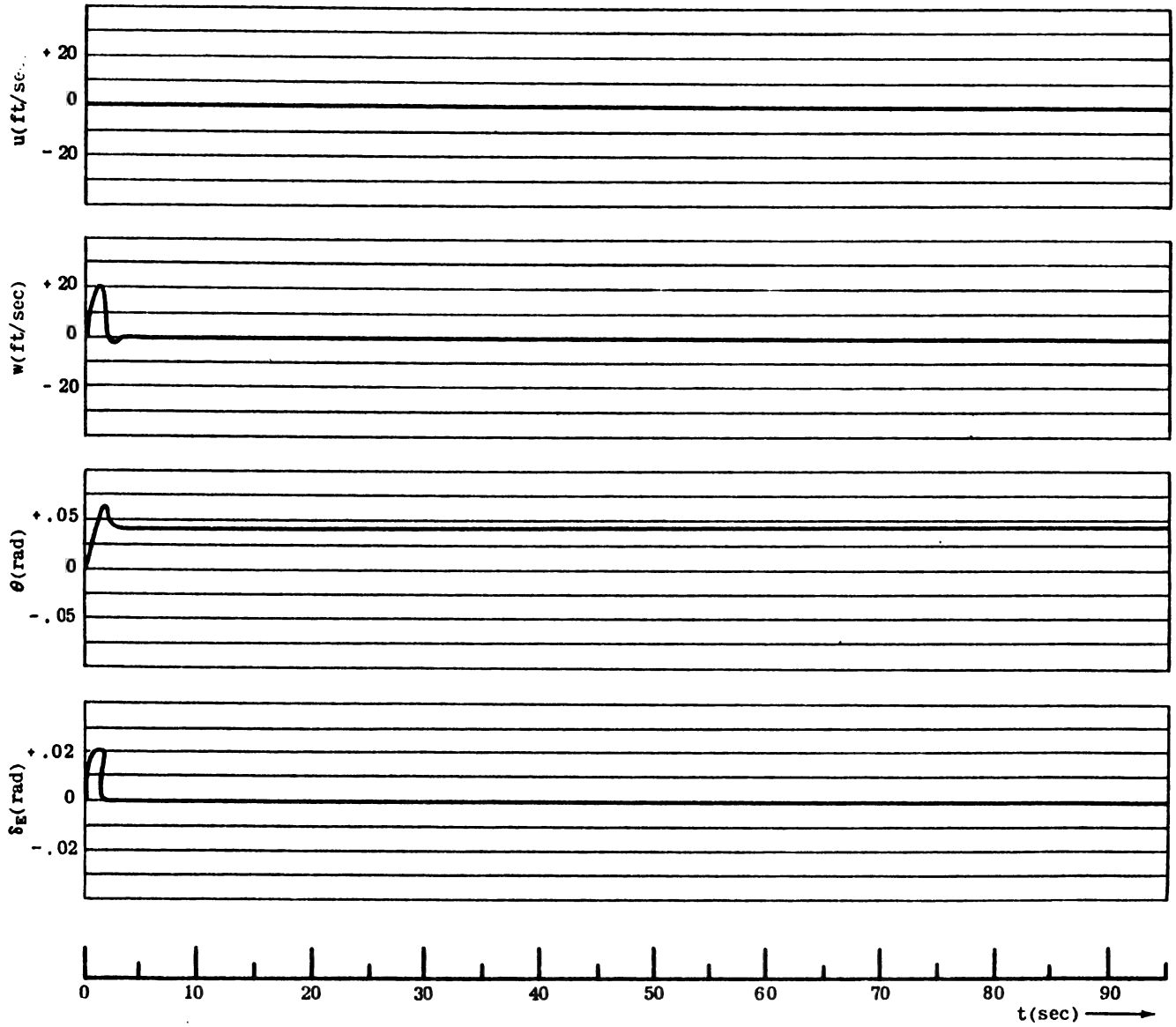

Figure III-7 Analog Computer Record of Time History for Pulse Elevator Deflection. Two Degree of Freedom, Short Period Mode

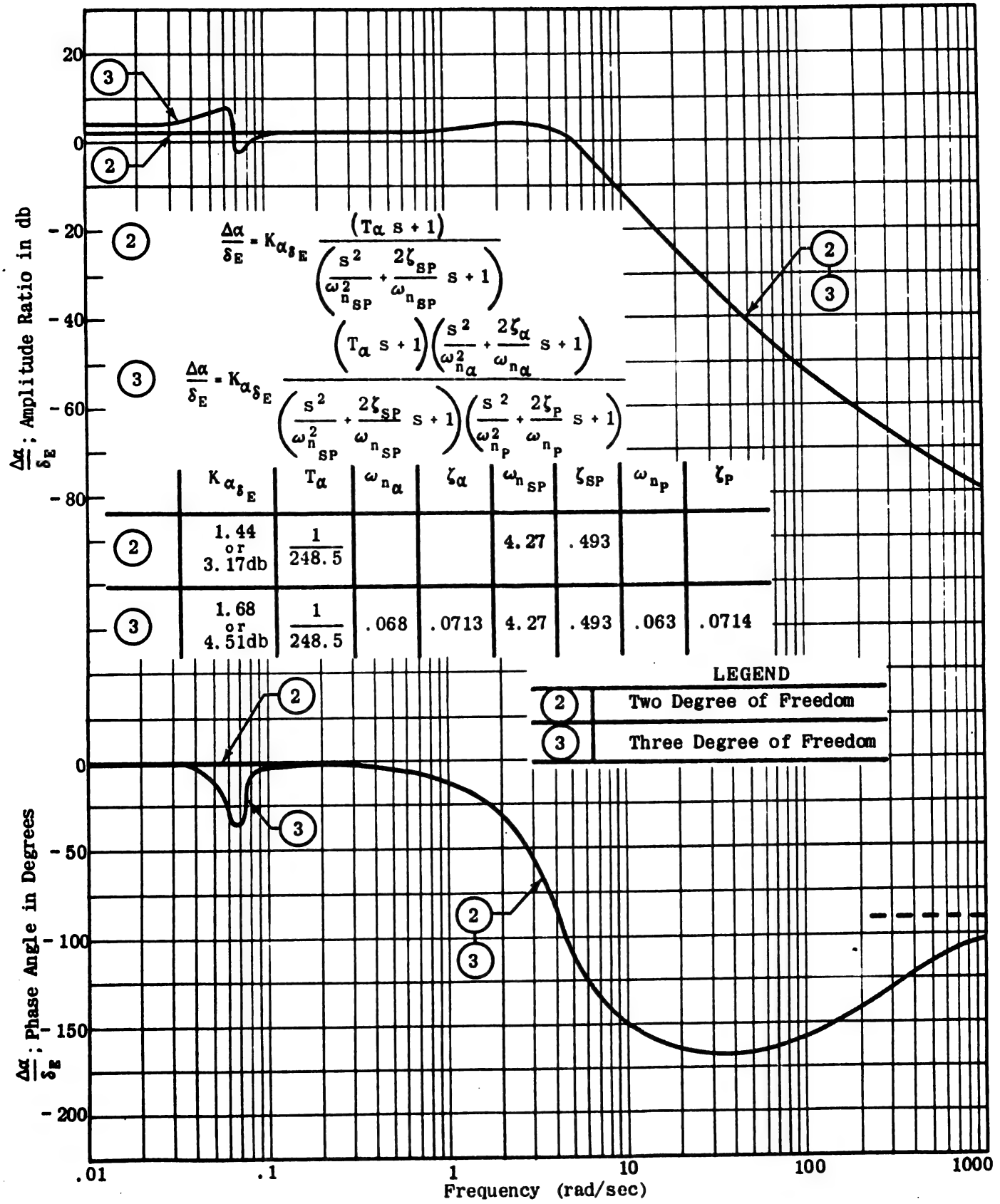

	$K_{\alpha_{\delta_E}}$	T_α	ω_{n_α}	ζ_α	$\omega_{n_{SP}}$	ζ_{SP}	ω_{n_P}	ζ_P
(2)	1.44 or 3.17db	$\frac{1}{248.5}$			4.27	.493		
(3)	1.68 or 4.51db	$\frac{1}{248.5}$	.068	.0713	4.27	.493	.063	.0714

Figure III-8 Change in Angle of Attack Response to Elevator Deflection. Two Degree of Freedom (Short Period) and Three Degree of Freedom Cases

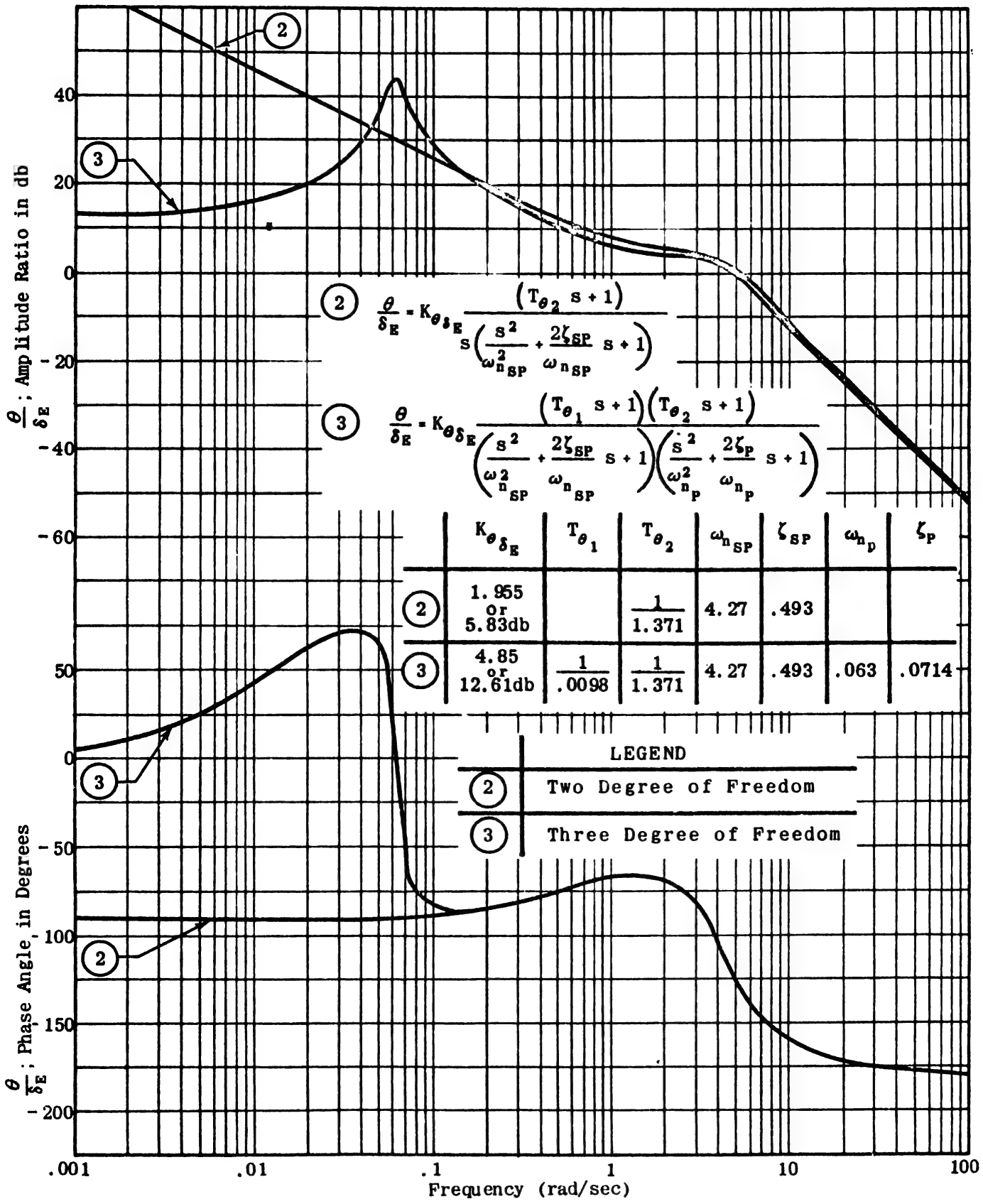

	$K_{\theta\delta_E}$	T_{θ_1}	T_{θ_2}	$\omega_{n_{SP}}$	ζ_{SP}	ω_{n_p}	ζ_p
(2)	1.955 or 5.83db		$\frac{1}{1.371}$	4.27	.493		
(3)	4.85 or 12.61db	$\frac{1}{.0098}$	$\frac{1}{1.371}$	4.27	.493	.063	.0714

Figure III-9 Pitch Angle Response to Elevator Deflection. Two Degree of Freedom (Short Period) and Three Degree of Freedom Cases

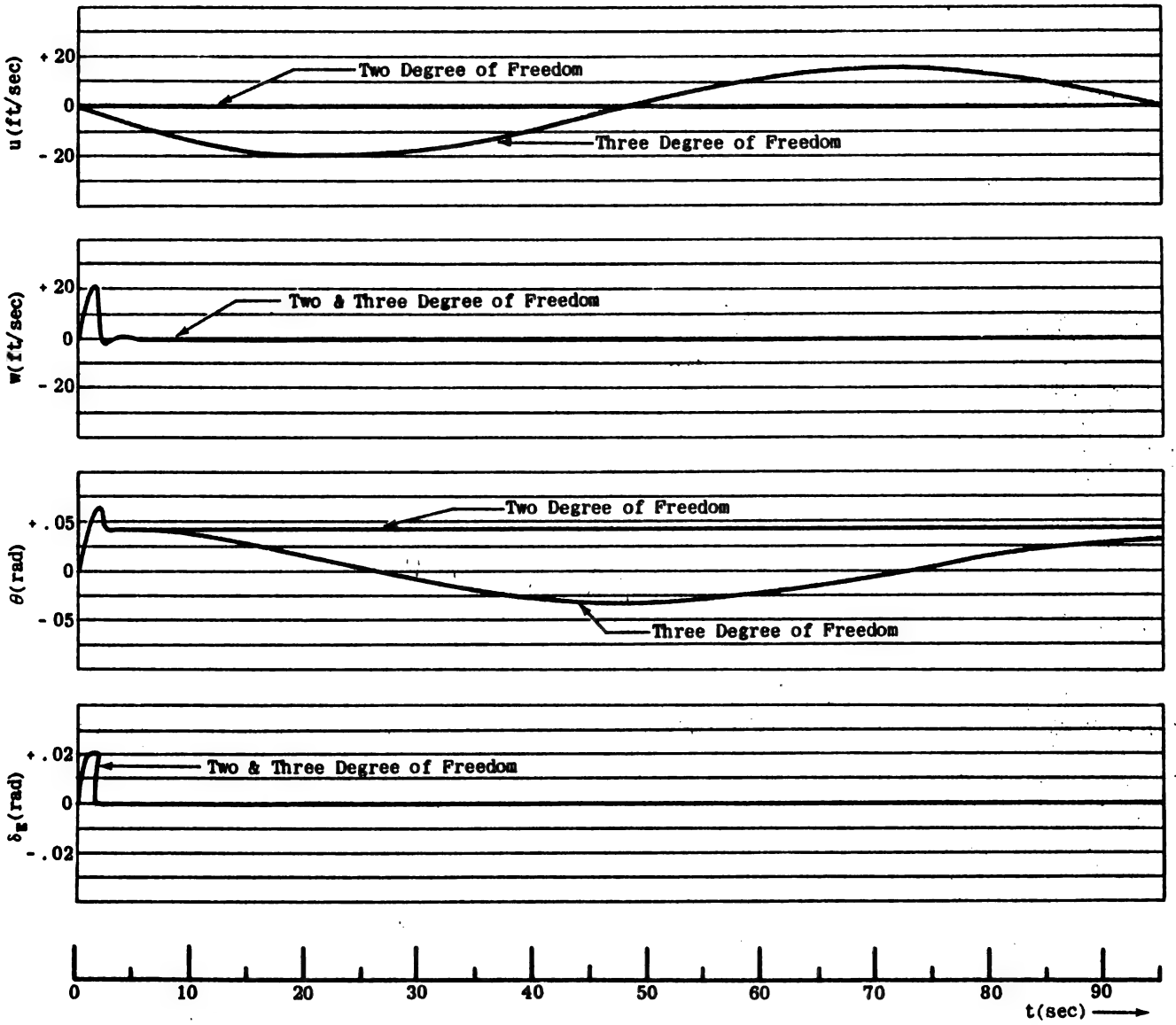

Figure III-10 Analog Computer Record of Time History for Pulse Elevator Deflection. Two Degree of Freedom (Short Period) and Three Degree of Freedom Superimposed

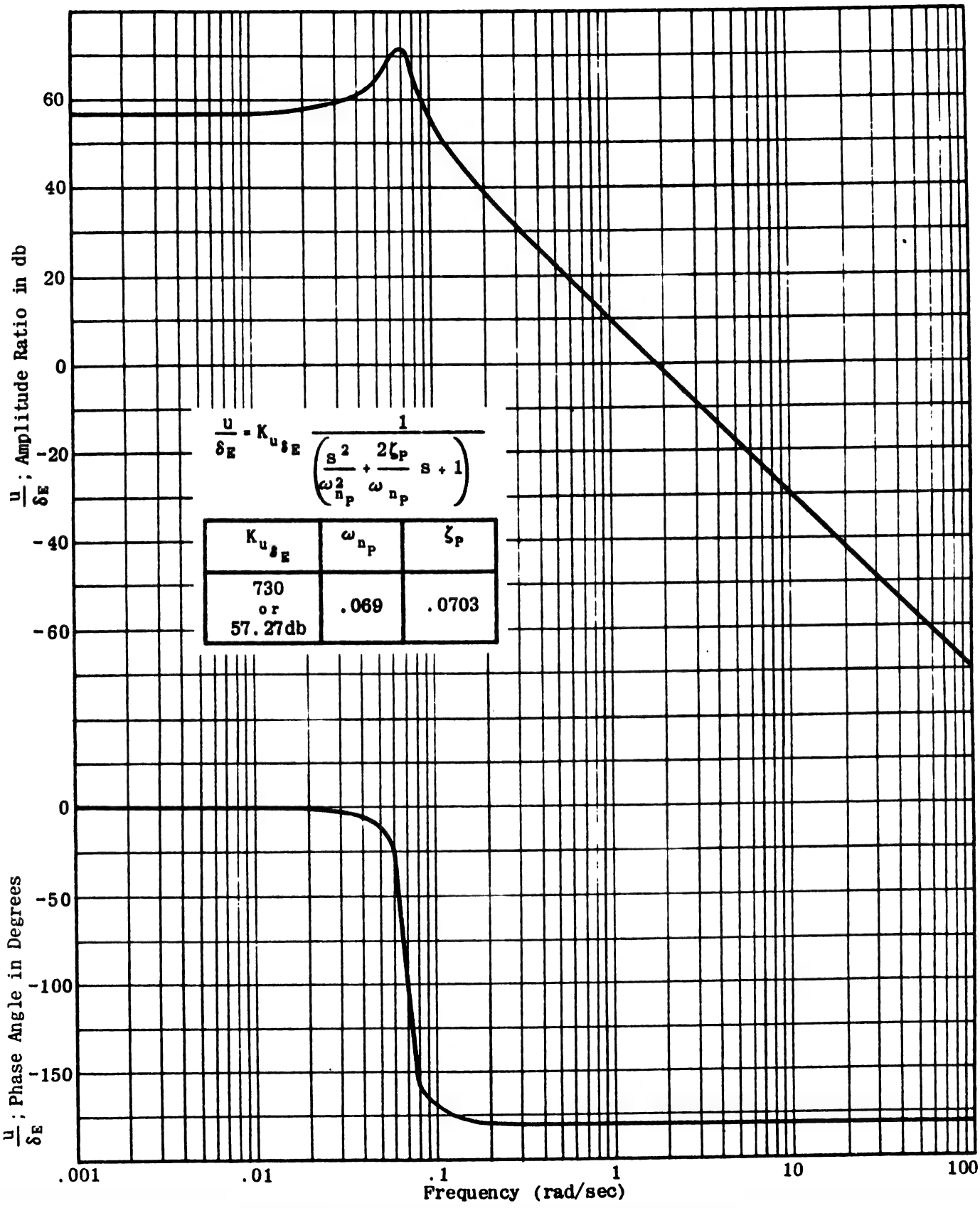

Figure III-11 Forward Speed Response to Elevator Deflection. Two Degree of Freedom, Phugoid Mode

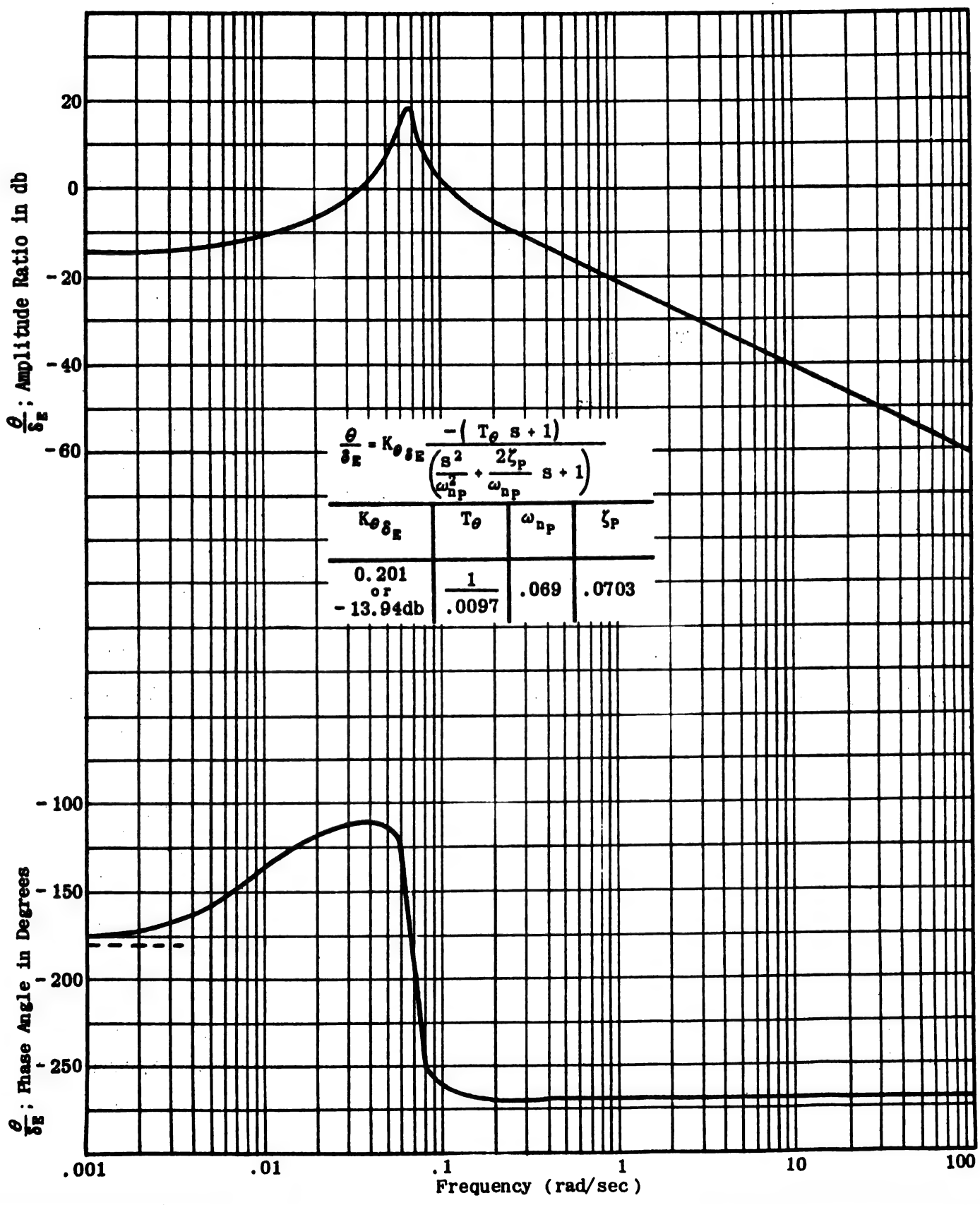

$$\frac{\theta}{\delta_E} = K_{\theta\delta_E} \frac{-(T_\theta s + 1)}{\left(\frac{s^2}{\omega_{n_P}^2} + \frac{2\zeta_P}{\omega_{n_P}} s + 1\right)}$$

$K_{\theta\delta_E}$	T_θ	ω_{n_P}	ζ_P
0.201 or -13.94db	$\frac{1}{.0097}$	.069	.0703

Figure III-12 Pitch Angle Response to Elevator Deflection. Two Degree of Freedom, Phugoid Mode

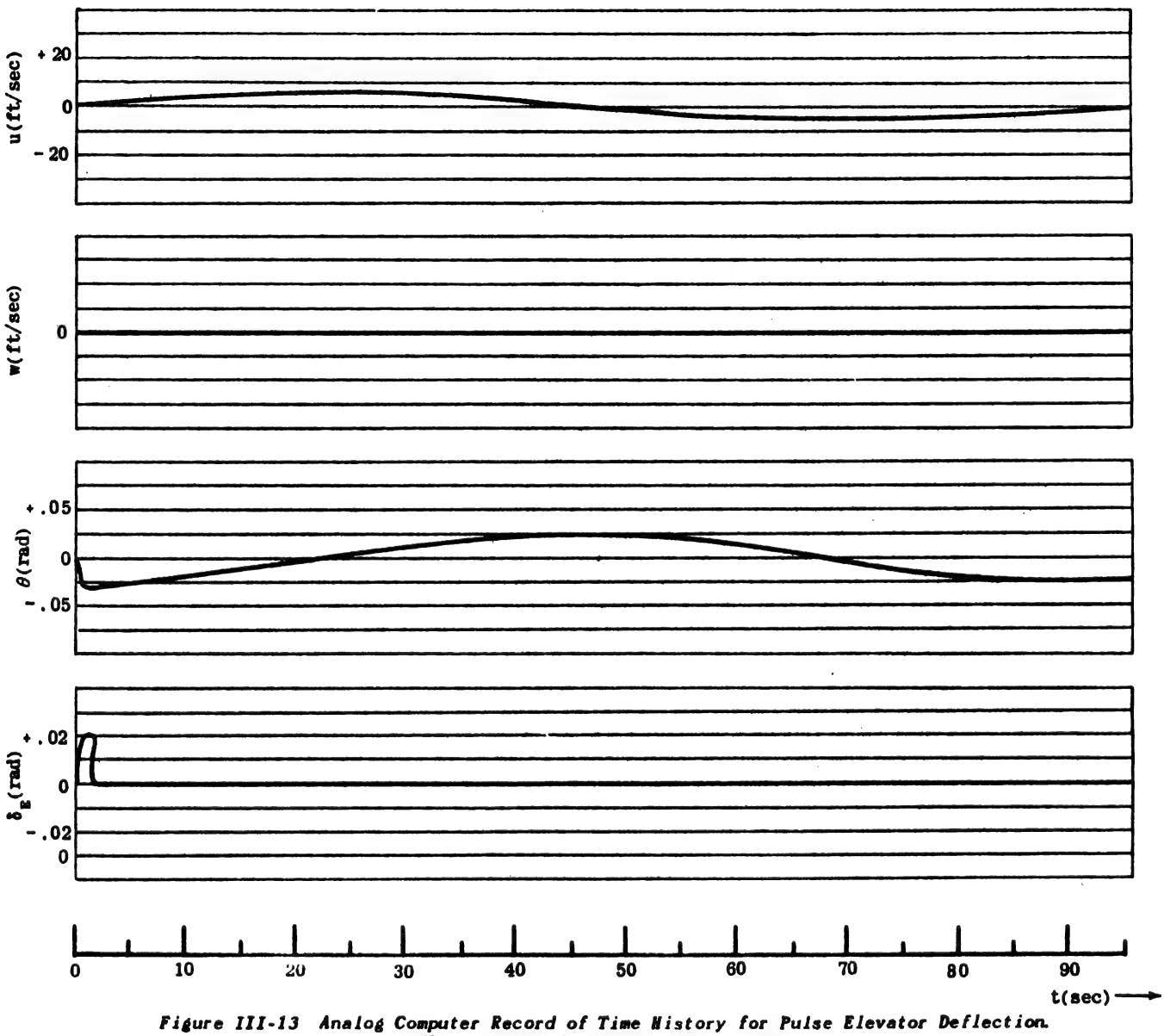

Figure III-13 Analog Computer Record of Time History for Pulse Elevator Deflection. Two Degree of Freedom, Phugoid Mode

as the short period approximation was checked in the preceding section. Table III-3 shows that there is reasonably good agreement between values of ζ_p and of ω_{n_p} for both the two and three degree of freedom cases.

PHUGOID MODE		
	ζ	ω_n (rad/sec)
Two Degrees of Freedom	0.0710	0.0683
Three Degrees of Freedom	0.0714	0.0630

Comparison of ζ and ω_n of Two Degree and Three Degree of Freedom Phugoid Mode.

TABLE III-3

Figure III-14 shows the two degree of freedom u/δ_E transfer function (from Figure III-11) and the similar three degree of freedom transfer function (from Figure III-1). The plots of the three and two degree of freedom θ/δ_E transfer functions are shown in Figure III-15 (from Figures III-3 and III-12 respectively).

Figures III-14 and III-15 indicate that both the u/δ_E and θ/δ_E two degree of freedom approximate phugoid transfer functions are of smaller amplitude than the equivalent three degree of freedom functions, and are shifted 180° in phase with respect to them. These differences can be explained by considering how the elevator deflection contributes to the motion.

In the three degree of freedom case, a positive elevator deflection causes the airplane to pitch in the positive direction (nose up) because of the relatively large positive M_{δ_E} and produces at the same time a small vertical force downward because of the relatively small Z_{δ_E}. The result of the pitching moment is an increase in pitch angle in phase with the elevator deflection, and the result of the vertical force is a small downward velocity producing a small positive increase in angle of attack also in phase with the elevator deflection. Since the lift increases in direct proportion to the angle of attack, these changes cause the airplane to climb with increasing pitch. As the pitch angle increases, the component of the force of gravity along the negative x axis increases, causing the airplane to decelerate. Therefore, the change in forward speed is out of phase with the elevator deflection.

In the two degree of freedom case, the change in angle of attack is set equal to zero. Since only the equations of the forces in the x and z directions are used in this two degree of freedom approximation, an elevator deflection is assumed to produce only the downward force due to Z_{δ_E}. For the angle of attack to remain zero, the airplane must pitch in the negative direction (nose down). This increases the component of the force of gravity along the positive x axis, and the airplane therefore accelerates. Thus, in the two degree of freedom case, the change in forward speed is in phase with the elevator deflection, whereas the change in pitch angle is out of phase with it. If the phases of both the θ/δ_E and u/δ_E approximate transfer function plots are shifted by 180°, they agree reasonably well, in the vicinity of the phugoid frequency, with the plot of the three degree of freedom transfer function.

Figure III-16 shows the analog computer solutions of the two and three degree of freedom equations superimposed. In each case, the two degree of freedom solutions have a smaller amplitude and a 180° phase shift compared to the three degree of freedom solutions, whereas the frequencies are in relatively good agreement.

In summary, it appears that the two degree of freedom approximation to the short period mode is in good agreement with the complete three degree of freedom short period mode, whereas the two degree of freedom approximation to the phugoid mode yields only reasonably good agreement with the exact value of the phugoid natural frequency and damping.

SECTION 6 – ACCELERATION TRANSFER FUNCTIONS

Transfer functions which relate to the acceleration, as measured by an accelerometer carried with an aircraft, are important because an accelerometer may be used as the sensing element in an autopilot.

However, the acceleration thus measured is not identical with the acceleration of the aircraft due to its flight path. For example, the resultant acceleration measured by an accelerometer located at the c.g. of the craft is the vector sum of the acceleration due to a curved flight path and the component of the gravitational acceleration along the axis with which the accelerometer is aligned. If the accelerometer is mounted so that it measures accelerations along the z-axis, it gives a reading even if the airplane is flying in horizontal, unaccelerated flight. This reading is due solely to the force of gravity.

Because accelerometers may be used as sensing elements, transfer functions relating the actually measured accelerations to control surface deflections are of more value to the systems engineer than are those given in terms of the accelerations undergone by the airframe due to its flight path. Therefore, this section is concerned with transfer functions relating specifically to quantities measured by accelerometers aligned along the x and z axes.

If the airframe is initially in unaccelerated horizontal flight and is then disturbed from this condition, the change in acceleration registered by an accelerometer located at the c.g. of the craft and aligned along the z axis, a_z, will be proportional to the acceleration of the airframe plus the change in the component of the gravitational acceleration along the z axis.

(II-63) show that the sum of these two changes is exactly the quantity on the left side of the second equation Modifying this relation in accordance with Assumptions

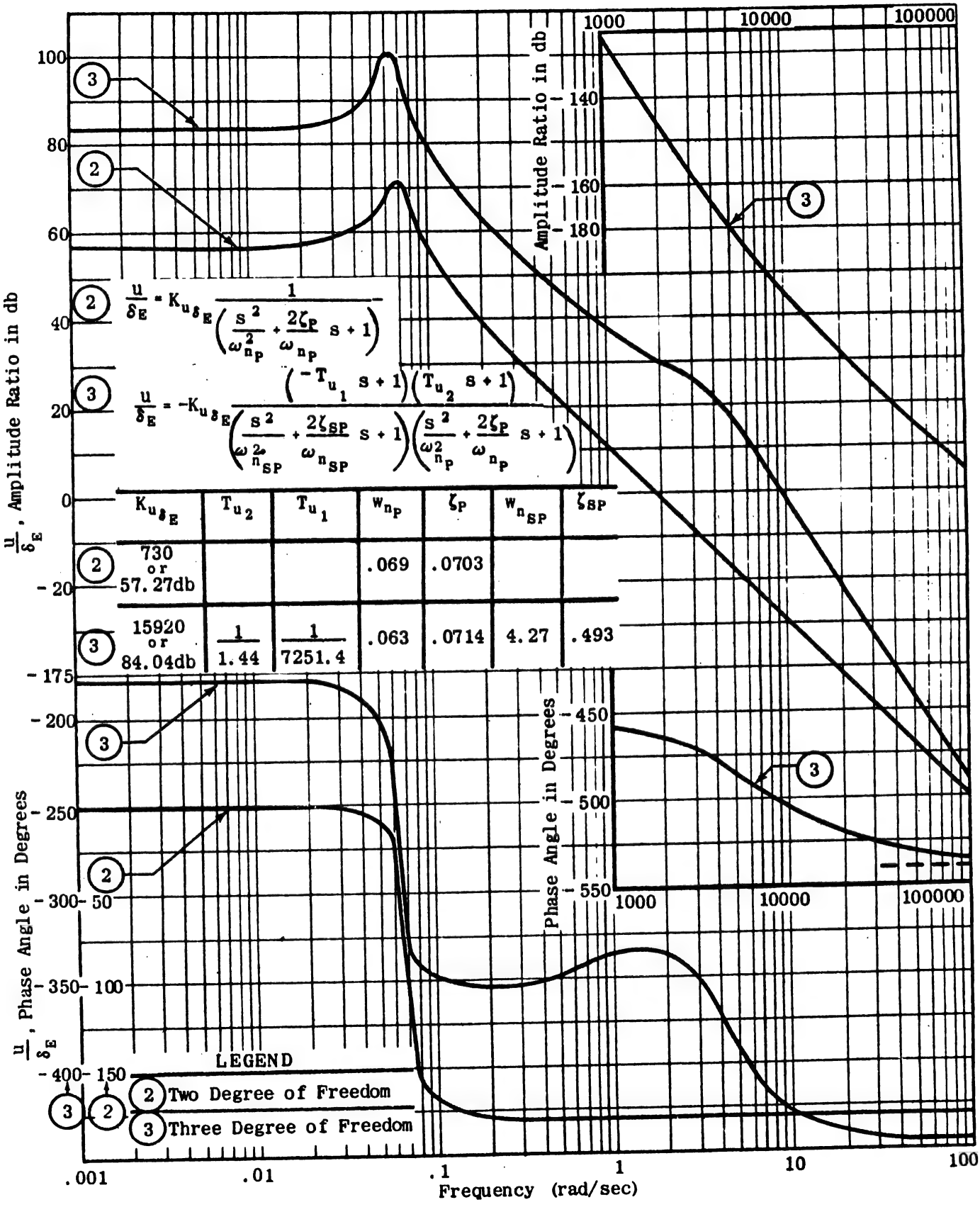

	$K_{u_{\delta_E}}$	T_{u_2}	T_{u_1}	w_{n_P}	ζ_P	$w_{n_{SP}}$	ζ_{SP}
2	730 or 57.27db			.069	.0703		
3	15920 or 84.04db	1/1.44	1/7251.4	.063	.0714	4.27	.493

Figure III-14 Forward Speed Response to Elevator Deflection. Two Degree of Freedom (Phugoid) and Three Degree of Freedom Cases

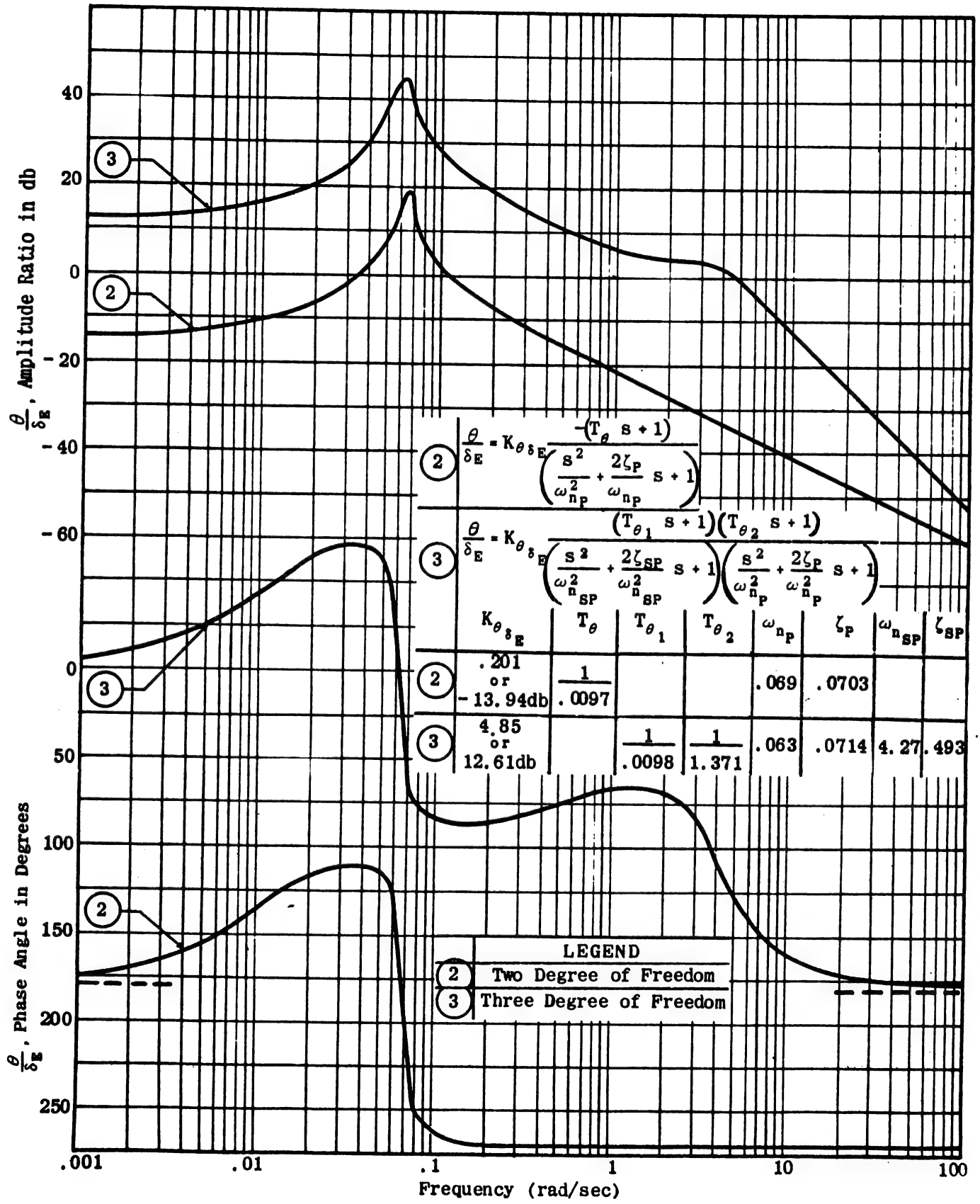

	$K_{\theta\delta_E}$	T_θ	T_{θ_1}	T_{θ_2}	ω_{n_P}	ζ_P	$\omega_{n_{SP}}$	ζ_{SP}
2	.201 or -13.94db	$\frac{1}{.0097}$			.069	.0703		
3	4.85 or 12.61db		$\frac{1}{.0098}$	$\frac{1}{1.371}$	.063	.0714	4.27	.493

Figure III-15 Pitch Angle Response to Elevator Deflection. Two Degree of Freedom (Phugoid) and Three Degree of Freedom Cases

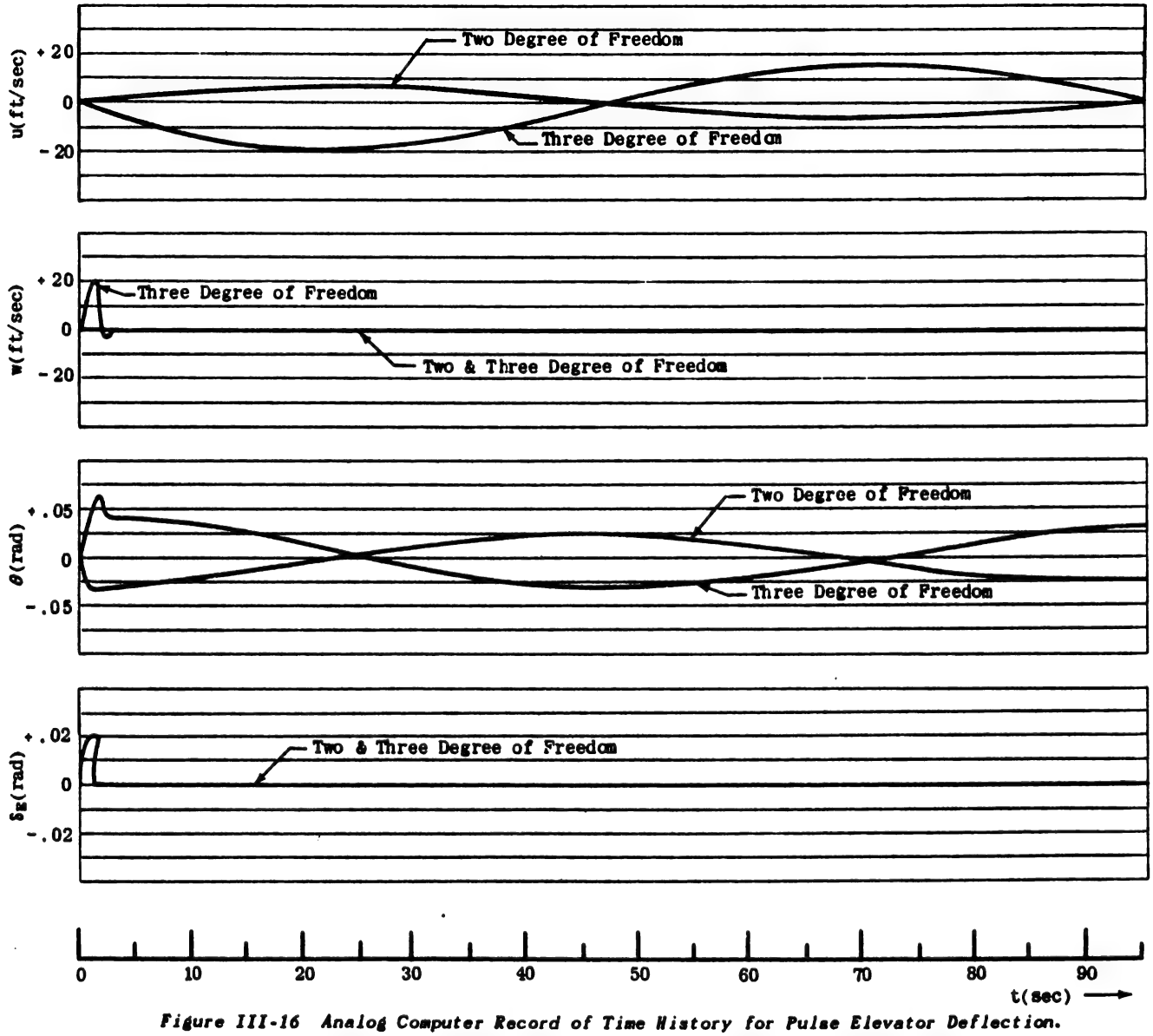

Figure III-16 Analog Computer Record of Time History for Pulse Elevator Deflection. Two Degree of Freedom (Phugoid) and Three Degree of Freedom Cases.

VIII and IX, the substance of the relevant equation may be written as:

(III-24) $$a_z = \dot{w} - U_o q = Z_w w + Z_u u + Z_{\delta_E}\delta_E$$

Since $\gamma_o = 0$, according to Assumption IX and the assumption of small perturbations, the change in the gravitational acceleration does not appear in the expression for a_z.

The acceleration recorded by an accelerometer located at the cg of the airframe and aligned with the x axis, a_x, can be obtained from the first equation of (II-63) simplified in accordance with Assumptions VIII and IX:

(III-25) $$a_x = \dot{u} + g\theta = X_u u + X_w w$$

The transfer functions $\frac{a_x}{\delta_E}$ and $\frac{a_z}{\delta_E}$ are:

(III-26) $$\frac{a_x}{\delta_E}(s) = X_u \frac{u}{\delta_E}(s) + X_w \frac{w}{\delta_E}(s)$$

(III-27) $$\frac{a_z}{\delta_E}(s) = Z_w \frac{w}{\delta_E}(s) + Z_u \frac{u}{\delta_E}(s) + Z_{\delta_E}$$

(III-26) and (III-27) can be expanded in terms of the stability derivatives by using (III-1), (III-2), and (III-3). The results are:

(III-28) $$\frac{a_x}{\delta_E} = \frac{A_{a_x}s^3 + B_{a_x}s^2 + C_{a_x}s + D_{a_x}}{D_1}$$

where
$$A_{a_x} = X_w Z_{\delta_E}$$
$$B_{a_x} = X_w(M_{\delta_E}U_o - M_q Z_{\delta_E})$$
$$C_{a_x} = -gX_u(M_{\delta_E} - M_{\dot{w}}Z_{\delta_E})$$
$$D_{a_x} = g[X_u(M_{\delta_E}Z_w - Z_{\delta_E}M_w) + X_w(M_u Z_{\delta_E} - M_{\delta_E}Z_u)]$$

(III-29) $$\frac{a_z}{\delta_E} = \frac{s(A_{a_z}s^3 + B_{a_z}s^2 + C_{a_z}s + D_{a_z})}{D_1}$$

where
$$A_{a_z} = Z_{\delta_E}$$
$$B_{a_z} = -Z_{\delta_E}(M_q + M_{\dot{w}}U_o + X_u)$$
$$C_{a_z} = M_{\delta_E}U_o Z_w + Z_{\delta_E}[X_u(M_q + U_o M_{\dot{w}}) - U_o M_w]$$
$$D_{a_z} = M_{\delta_E}[U_o(X_w Z_u - X_u Z_w) - gZ_u] + Z_{\delta_E}[U_o(M_w X_u - M_u X_w) + gM_u]$$

Inserting the numerical values of the stability derivatives from Table III-1 into (III-28) and (III-29) results in:

(III-30)
$$\frac{a_x(s)}{\delta_E(s)} = 154\,\frac{\left[\frac{s^2}{(0.637)^2} + \frac{2(0.228)}{0.637}s + 1\right]\left(\frac{s}{247.92} + 1\right)}{\left[\frac{s^2}{(0.063)^2} + \frac{2(0.0714)}{0.063}s + 1\right]\left[\frac{s^2}{(4.27)^2} + \frac{2(0.493)}{4.27}s + 1\right]}$$

(III-31)
$$\frac{a_z(s)}{\delta_E(s)} = 2060\,\frac{s\left(\frac{s}{0.0064} + 1\right)\left(\frac{s}{16.95} - 1\right)\left(\frac{s}{9.73} + 1\right)}{\left[\frac{s^2}{(0.063)^2} + \frac{2(0.0714)}{0.063}s + 1\right]\left[\frac{s^2}{(4.27)^2} + \frac{2(0.493)}{4.27}s + 1\right]}$$

The Bode plots of (III-30) and (III-31) are shown in Figures III-17 and III-18.

It should be noted that the change in altitude can be found directly from (III-24):

(III-32) $$\Delta h = \int\int a_z dt = \int\int (\dot{w} - U_o q)\, dt$$

and $$\frac{\Delta h}{\delta_E} = \frac{1}{s^2}\frac{a_z}{\delta_E}$$

SECTION 7 – APPROXIMATE FACTORS OF LONGITUDINAL TRANSFER FUNCTIONS

Since it is possible to find the roots of a quartic in terms of its coefficients, it is theoretically possible to express the roots of the longitudinal characteristic equation explicitly in terms of the stability derivatives. However, actually finding the roots by this method is wholly impracticable because of the amount of labor involved and the complex form of the end results.

It is possible and practicable, however, to derive an approximate factorization of the stability quartic, which provides good approximations to the natural frequencies and damping ratios under certain frequently occurring conditions (to be stated later).

In this section, approximate factors of both the numerators and the denominators of the transfer functions $\frac{u}{\delta_E}$, $\frac{w}{\delta_E}$, $\frac{\theta}{\delta_E}$, and $\frac{a_z}{\delta_E}$ are discussed, and the condition under which the approximations are valid is stated. The factors are presented as explicit functions of particular stability derivatives.

These approximate factors are valuable in obtaining a quick estimate of the exact factors. In addition, they give some insight into which stability derivatives are the major contributors to the time constants, to natural frequencies, and to damping ratios of the transfer functions.

An approximate factorization of the longitudinal characteristic equations, generally accredited to Bairstow, can be derived in the following manner.

The longitudinal characteristic equation is:

(III-33) $$D_1 = As^4 + Bs^3 + Cs^2 + Ds + E = 0$$

which can be written in factored form as:

(III-34) $$D_1 = \underbrace{(s^2 + as + b)}_{\text{short period}}\ \underbrace{(s^2 + \alpha s + \beta)}_{\text{phugoid}} = 0$$

In general, the quantities B and C are considerably larger than D and E. This is true when the short period natural frequency and damping ratio are much greater

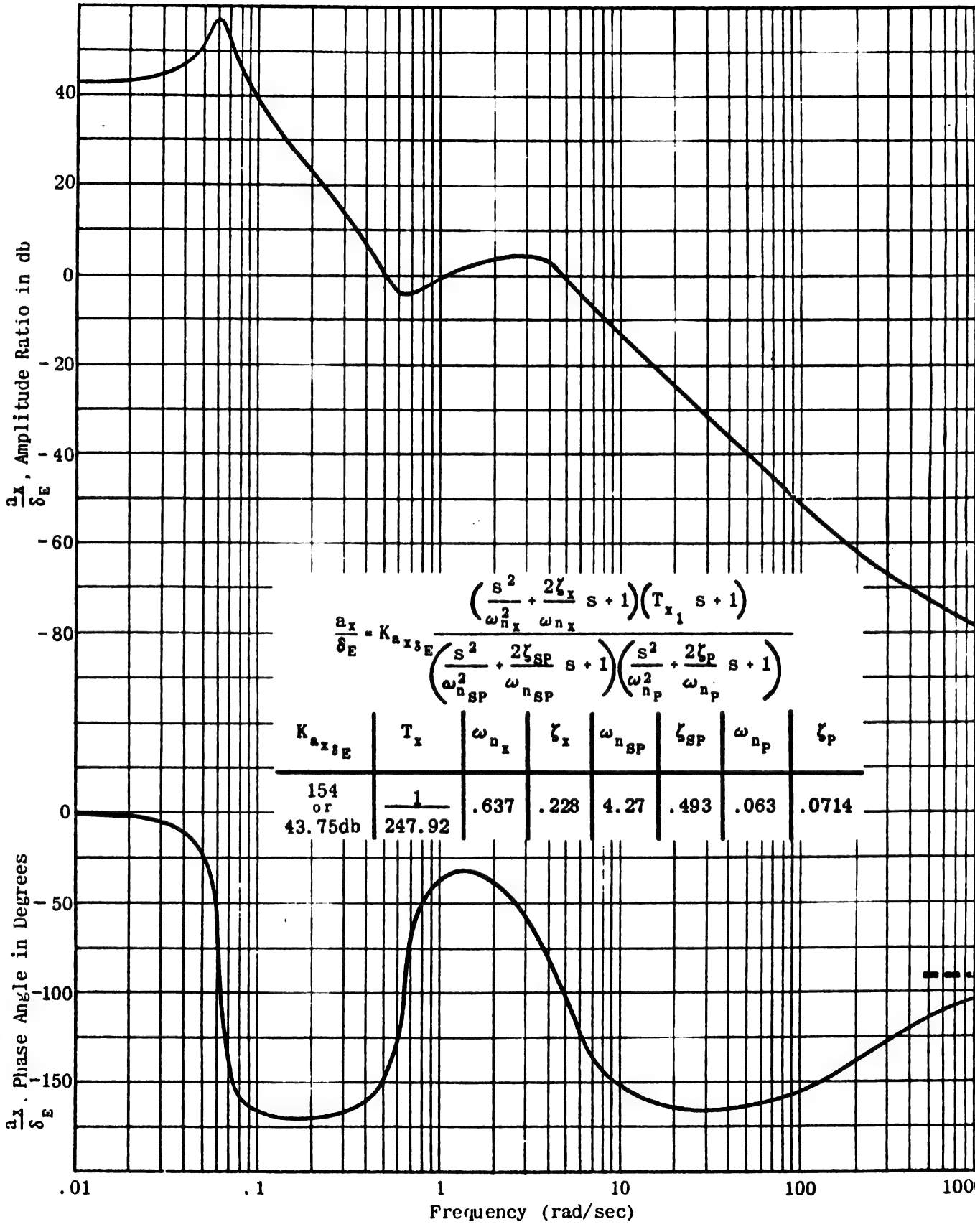

$$\frac{a_x}{\delta_E} = K_{a_{x_{\delta_E}}} \frac{\left(\frac{s^2}{\omega_{n_x}^2} + \frac{2\zeta_x}{\omega_{n_x}} s + 1\right)\left(T_{x_1} s + 1\right)}{\left(\frac{s^2}{\omega_{n_{SP}}^2} + \frac{2\zeta_{SP}}{\omega_{n_{SP}}} s + 1\right)\left(\frac{s^2}{\omega_{n_P}^2} + \frac{2\zeta_P}{\omega_{n_P}} s + 1\right)}$$

$K_{a_{x_{\delta_E}}}$	T_x	ω_{n_x}	ζ_x	$\omega_{n_{SP}}$	ζ_{SP}	ω_{n_P}	ζ_P
154 or 43.75db	$\frac{1}{247.92}$	.637	.228	4.27	.493	.063	.0714

Figure III-17 Forward Acceleration Response to Elevator Deflection. Three Degree of Freedom

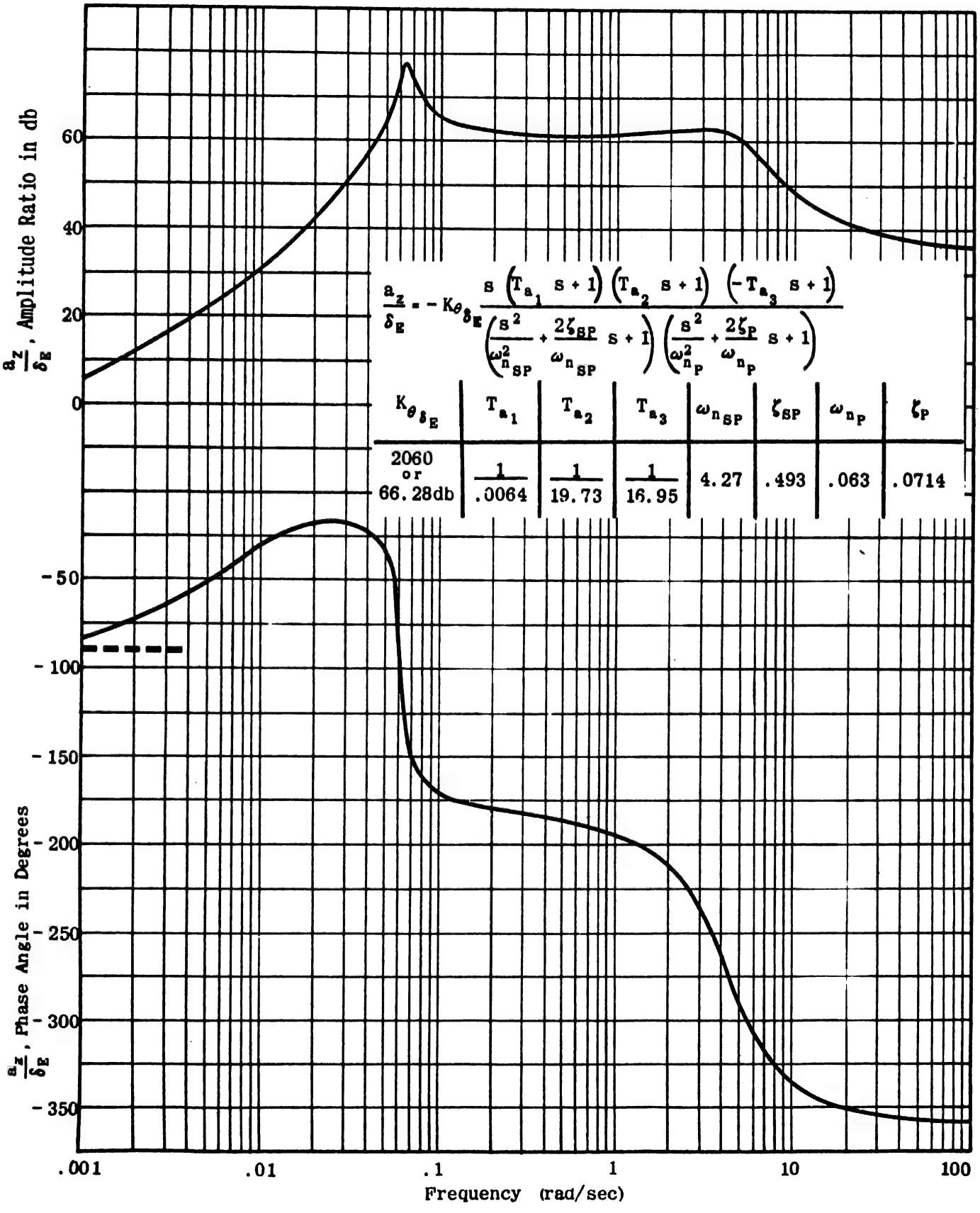

$$\frac{a_z}{\delta_E} = -K_{\theta\delta_E} \frac{s\left(T_{a_1}\, s + 1\right)\left(T_{a_2}\, s + 1\right)\left(-T_{a_3}\, s + 1\right)}{\left(\frac{s^2}{\omega_{n_{SP}}^2} + \frac{2\zeta_{SP}}{\omega_{n_{SP}}}\, s + 1\right)\left(\frac{s^2}{\omega_{n_P}^2} + \frac{2\zeta_P}{\omega_{n_P}}\, s + 1\right)}$$

$K_{\theta\delta_E}$	T_{a_1}	T_{a_2}	T_{a_3}	$\omega_{n_{SP}}$	ζ_{SP}	ω_{n_P}	ζ_P
2060 or 66.28db	$\frac{1}{.0064}$	$\frac{1}{19.73}$	$\frac{1}{16.95}$	4.27	.493	.063	.0714

Figure III-18 Vertical Acceleration Response to Elevator Deflection. Three Degree of Freedom

AIRFRAME APPROXIMATE COEFFICIENTS AND FACTORS—LONGITUDINAL TRANSFER FUNCTIONS *

$\frac{u}{\delta_E} = \frac{N_u}{D_1}$; $\frac{w}{\delta_E} = \frac{N_w}{D_1}$; $\frac{\theta}{\delta_E} = \frac{N_\theta}{D_1}$; $\frac{a_z}{\delta_E} = \frac{N_{a_z}}{D_1}$

*ASSUMPTIONS USED: LEVEL FLIGHT CONDITIONS.
$L_{\dot{x}} = L_x = Y_o = X_{\dot{w}} = X_q = Z_{\dot{w}} = X_{\delta_E} = T_u = 0$

DENOMINATOR D_1:

$$D_1 = A s^4 + B s^3 + C s^2 + D s + E \cong (s^2 + B s + C)\left(s^2 + \frac{DC - BE}{C^2} s + \frac{E}{C}\right)$$

$A \cong 1$

$B \cong -U_o M_{\dot{w}} - M_q - Z_w$

$C \cong M_q Z_w - U_o M_w$

$D \cong -X_u (M_q Z_w - U_o M_w) - M_u (X_w U_o - g)$

$E \cong g(Z_u M_w - M_u Z_w)$

$$D_1 \cong K_{D_1}\left(\frac{s^2}{\omega_{n_{SP}}^2} + \frac{2\zeta_{SP}}{\omega_{n_{SP}}} s + 1\right)\left(\frac{s^2}{\omega_{n_P}^2} + \frac{2\zeta_P}{\omega_{n_P}} s + 1\right)$$

short period — phugoid

$K_{D_1} \cong g(Z_u M_w - M_u Z_w)$

$\omega_{n_{SP}} \cong \sqrt{M_q Z_w - U_o M_w}$

$\zeta_{SP} \cong \left(1/2\omega_{n_{SP}}\right)(-U_o M_{\dot{w}} - Z_w - M_q)$

$\omega_{n_P} \cong \left(1/\omega_{n_{SP}}\right)\sqrt{g(M_w Z_u - M_u Z_w)}$

$\zeta_P \cong -\frac{X_u}{2\omega_{n_P}} - \frac{\zeta_{SP}\omega_{n_P}}{\omega_{n_{SP}}} - \frac{M_u(U_o X_w - g) - X_w Z_u M_q}{2\omega_{n_P}\omega_{n_{SP}}^2}$

$\zeta_P \cong -X_u/2\omega_{n_P}$

$\frac{w}{\delta_E}$:

$$N_w = A_w s^3 + B_w s^2 + C_w s + D_w = A_w(s^3 + B'_w s^2 + C'_w s + D'_w)$$
$$N_w \cong K'_w (s + \tau_1)[s + (\sigma \pm j\omega_D)]$$

$A_w \cong Z_{\delta_E}$

$B'_w = \frac{M_{\delta_E}}{Z_{\delta_E}}(U_o + Z_q) - M_q$

$C'_w \cong -\left[\frac{X_u M_{\delta_E}}{Z_{\delta_E}}(U_o + Z_q) - X_u M_q\right]$

$D'_w \cong \left(M_u - \frac{M_{\delta_E}}{Z_{\delta_E}} Z_u\right) g$

$K'_w = Z_{\delta_E}$

$\sigma = -\frac{X_u}{2}$

$\tau_1 = \frac{M_{\delta_E}}{Z_{\delta_E}}(U_o + Z_q) - M_q$

$$\omega_D = \sqrt{\frac{\left(M_u - \frac{M_{\delta_E}}{Z_{\delta_E}} Z_u\right) g}{\frac{M_{\delta_E}}{Z_{\delta_E}}(U_o + Z_q) - M_q}}$$

$$N_w \cong K_w (T_w s + 1)\left(\frac{s^2}{\omega_{n_1}^2} + \frac{2\zeta_1}{\omega_{n_1}} s + 1\right)$$

$K_w = \left(Z_{\delta_E} M_u - M_{\delta_E} Z_u\right) g$

$$T_w = \frac{Z_{\delta_E}}{M_{\delta_E}(U_o + Z_q) - M_q Z_{\delta_E}}$$

$$\zeta_1 = -\frac{X_u}{2}\sqrt{\frac{M_{\delta_E}(U_o + Z_q) - M_q Z_{\delta_E}}{g\left(M_u Z_{\delta_E} - M_{\delta_E} Z_u\right) + (X_u^2/4)\left[M_{\delta_E}(U_o + Z_q) - M_q Z_{\delta_E}\right]}}$$

$$\omega_{n_1} = \sqrt{\frac{g\left(M_u Z_{\delta_E} - Z_u M_{\delta_E}\right) + (X_u^2/4)\left[M_{\delta_E}(U_o + Z_q) - M_q Z_{\delta_E}\right]}{M_{\delta_E}(U_o + Z_q) - M_q Z_{\delta_E}}}$$

TABLE III - 4 (Sheet 1 of 2 Sheets)

$\frac{u}{\delta_E}$:

$$N_u = A_u s^3 + B_u s^2 + C_u s + D_u$$

$$A_u \cong 0$$
$$B_u \cong Z_{\delta_E} X_w$$
$$C_u \cong M_{\delta_E}[X_w(U_o + Z_q) - g]$$
$$D_u \cong M_{\delta_E} Z_w g$$

$$N_u \cong B_u s^2 + C_u s + D_u$$

$$N_u \cong K_u\left(T_{u_1} s + 1\right)\left(T_{u_2} s + 1\right)$$

$$K_u \cong M_{\delta_E} Z_w g \quad **$$

$$T_{u_1} \cong \frac{Z_{\delta_E}}{M_{\delta_E}\left[U_o + Z_q - (g/X_w)\right]}$$

$$T_{u_2} \cong \frac{(X_w/2)(U_o + Z_q) - 1}{Z_w}$$

$\frac{\theta}{\delta_E}$:

$$N_\theta = \left(A_\theta s^2 + B_\theta s + C_\theta = A_\theta(s^2 + B'_\theta s + C'_\theta)\right)$$

$$A_\theta \cong M_{\delta_E}$$
$$B'_\theta \cong -Z_w$$
$$C'_\theta \cong Z_w X_u - X_w Z_u$$

$$N_\theta \cong K_\theta\left(T_{\theta_1} s + 1\right)\left(T_{\theta_2} s + 1\right)$$

$$K_\theta = (Z_w X_u - X_w Z_u) M_{\delta_E}$$
$$T_{\theta_1} = -(1/Z_w)$$
$$T_{\theta_2} = \frac{Z_w}{X_w Z_u - Z_w X_u}$$

$\frac{a_z}{\delta_E}$:

$$N_{a_z} = s\left(A_{a_z} s^3 + B_{a_z} s^2 + C_{a_z} s + D_{a_z}\right)$$

$$A_{a_z} \cong Z_{\delta_E}$$
$$B_{a_z} \cong M_{\delta_E} Z_q - Z_{\delta_E} M_q$$
$$C_{a_z} \cong M_{\delta_E} U_o Z_w$$
$$D_{a_z} \cong -M_{\delta_E}[Z_u g + U_o(Z_w X_u - X_w Z_u)]$$

$$N_{a_z} \cong -K_{a_z} s\left(T_{a_1} s + 1\right)\left(T_{a_2} s + 1\right)\left(T_{a_3} s + 1\right)$$

$$K_{a_z} \cong M_{\delta_E}[Z_u g + U_o(Z_w X_u - X_w Z_u)]$$

$$T_{a_1} = \frac{-U_o Z_w}{Z_u g + U_o(Z_w X_u - X_w Z_u)}$$

$$T_{a_2} = \frac{2Z_{\delta_E}}{\left(M_{\delta_E} Z_q - Z_{\delta_E} M_q\right) + 2\sqrt{Z_{\delta_E} M_{\delta_E} U_o Z_w}}$$

$$T_{a_3} = \frac{2Z_{\delta_E}}{\left(M_{\delta_E} Z_q - Z_{\delta_E} M_q\right) - 2\sqrt{Z_{\delta_E} M_{\delta_E} U_o Z_w}}$$

**

NOTE:
DIVIDE BY K_{D_1} TO OBTAIN COMPLETE APPROXIMATE D.C. GAIN OF THE TRANSFER FUNCTION.
(THIS APPLIES TO ALL THE FACTORED NUMERATOR EQUATIONS.)

TABLE III - 4 (Sheet 2 of 2 Sheets)

than the corresponding quantities for the phugoid. Since this is generally true, a and b can be considered large in comparison with α and β.

Expanding (III-34) yields:

(III-35) $$D_1 = s^4 + (a + \alpha)\ s^3 + (b + a\alpha + \beta)\ s^2 + (ab + a\beta)s + b\beta$$

By equating coefficients of like terms in (III-33) and (III-35):

(III-36)
$$B = a + \alpha \qquad D = ab + a\beta$$
$$C = b + a\alpha + \beta \qquad E = b\beta$$

and by neglecting relatively small quantities on the right sides of (III-36):

(III-37)
$$B \cong a \qquad C \cong b$$
$$\beta = \frac{E}{b} \cong \frac{E}{C}$$
$$\alpha = \frac{D - a\beta}{b} \cong \frac{D - \frac{BE}{C}}{C} = \frac{DC - BE}{C^2}$$

where '$\cong$' means "is approximately equal to".

Then:

(III-38)
$$D_1 \cong \underbrace{(s^2 + Bs + C)}_{\text{short period}} \quad \underbrace{\left(s^2 + \frac{DC - BE}{C^2}\, s + \frac{E}{C}\right)}_{\text{phugoid}}$$

In this expression:

$$B = 2\zeta_{SP}\omega_{n_{SP}} \qquad C = \omega^2_{n_{SP}} \qquad \frac{DC - BE}{C^2} = 2\zeta_p\omega_{n_p}$$

or

$$\omega_{n_{SP}} = \sqrt{C}$$
$$\zeta_{SP} = \frac{B}{2\omega_{n_{SP}}} = \frac{B}{2\sqrt{C}}$$
$$\omega_{n_p} = \sqrt{\frac{E}{C}}$$
$$\zeta_p = \frac{DC - BE}{2C^2\omega_{n_p}} = \frac{DC - BE}{2\sqrt{C^3E}}$$

(III-38) is generally more useful when it is written in terms of damping ratios and natural frequencies:

(III-39)
$$D_1 \cong K_{D_1}\left(\frac{s^2}{\omega^2_{n_{SP}}} + \frac{2\zeta_{SP}}{\omega_{n_{SP}}}\, s + 1\right)\left(\frac{s^2}{\omega^2_{n_p}} + \frac{2\zeta_p}{\omega_{n_p}}\, s + 1\right)$$

where

$$K_{D_1} = \omega^2_{n_p}\ \omega^2_{n_{SP}}$$

By writing out the expressions for the coefficients in D_1 in terms of the stability derivatives, by substituting the results into the above expressions for the approximate natural frequencies and damping ratios, and by neglecting in the results all terms whose values are small in comparison with other terms to which they are added, the quantities $\omega_{n_{SP}}$, ω_{n_p}, ζ_{SP}, and ζ_p, are then given in terms of combinations of stability derivatives:

$$\omega_{n_{SP}} \cong \sqrt{M_qZ_w - U_oM_w}$$

$$\zeta_{SP} \cong \frac{-1}{2\omega_{n_{SP}}}\,(U_oM_w + Z_w + M_q)$$

$$\omega_{n_{SP}} \cong \frac{1}{\omega_{n_{SP}}}\sqrt{g(M_wZ_u - M_uZ_w)}$$

$$\zeta_p \cong -\frac{X_u + \zeta_{SP}\omega_{n_p}}{2\omega_{n_p}\ \omega_{n_{SP}}} - \frac{M_u(U_oX_w - g) - X_wZ_uM_q}{2\omega_{n_p}\ \omega^2_{n_{SP}}}$$

Approximate factors have also been derived for each of the numerators in the $\frac{u}{\delta_E}$, $\frac{\theta}{\delta_E}$, $\frac{w}{\delta_E}$, and $\frac{a_z}{\delta_E}$ transfer functions. These approximate factors have been checked with the exact factors of the transfer functions of a conventional cruciform configuration airplane at a variety of flight conditions and have yielded reasonably good agreement. The approximate factors are summarized in Table III-4 on pages III-26 and III-27.

SECTION 8 – EFFECT OF SINGLE DIMENSIONAL STABILITY DERIVATIVE VARIATION

In this section, the longitudinal characteristic equation is evaluated for numerical values of the stability derivatives for a particular flight condition. The effect of separately varying each of the stability derivatives in the characteristic equation is then presented in the form of plots of the natural frequencies, damping ratios, and time constants of the characteristic equation as functions of each derivative.

All plots presented are for one particular flight condition. Therefore, predictions and conclusions based on an examination of these plots are strictly applicable only to the given flight condition. However, it is felt that the results are general enough to indicate significant trends for a wide variety of flight conditions.

The following example shows how a particular stability derivative can be varied. If an airplane is equipped with a rate gyroscope aligned to measure the pitch rate and connected so that the elevator is deflected in proportion to the measured pitch rate, quantities denoted as ΔM_q and ΔZ_q are created. $\Delta M_q q$ and $\Delta Z_q q$ are incremental values of the angular and linear accelerations caused by deflecting the elevator.

(III-41) $$M_{q_T}q = M_qq + \Delta M_qq = (M_q + \Delta M_q)q$$

(III-42) $$M_{q_T} = M_q + \Delta M_q$$

Similarly:

(III-43) $$Z_{q_T} = Z_q + \Delta Z_q$$

In (III-42) and (III-43), the subscript "T" denotes "total", and the terms Z_q and M_q are the stability derivatives inherent in the airframe. The quantity ΔM_q can be expressed as:

(III-44) $$\Delta M_q = \frac{\delta_E}{q} M_{\delta_E} = K M_{\delta_E}$$

that is, the increment to the pitching moment due to pitch rate is proportional to the pitching moment due to elevator deflection. Similarly:

(III-45) $$\Delta Z_q = \frac{\delta_E}{q} Z_{\delta_E} = K Z_{\delta_E}$$

The coefficient "K" in (III-44) and (III-45) is referred to as the "gain". The magnitudes of ΔM_q and ΔZ_q increase directly with K. M_{q_T} and Z_{q_T} can be adjusted to have any value by selecting a suitable value for K.

M_{q_T} and Z_{q_T} can be considered the effective values of M_q and Z_q. If it were possible to create a value ΔZ_q without creating a value ΔM_q, the effect of changing Z_q would be determined by replacing the value Z_q in the characteristic equation by Z_{q_T} and then finding the roots of the equation. If this were done for enough values of Z_{q_T}, a plot of the parameters of the characteristic equation versus Z_{q_T} could be made.

Two assumptions are implicit in the plots of this section. The first is that a control surface can be deflected without lag proportionally to the instantaneous measured value of a given variable (the theoretical mechanism assumed capable of such performance is referred to as a "perfect autopilot"). The second assumption is that it is possible to change only one stability derivative at a time. In those cases where the movement of a particular control surface essentially alters more than one stability derivative, two or more of the attending plots must be superimposed to obtain the resultant trend.

Since many of the stability derivatives used in analytical work are not known exactly, these plots are also of value because the effect of a possible error in evaluating a given stability derivative can be predicted from these plots.

Figures III-19 to III-26 are now discussed and related to the approximate factors of the longitudinal characteristic equation derived in Section III-7, when this is practicable. In general, the trends predicted from the approximate factors and those from the plots are similar only for small variations of a given derivative about the base value of the derivative (that is, the unmodified value inherent in the airplane).

The approximate factors of the longitudinal characteristic equation are rewritten below for reference:

(III-46) $$\omega_{n_{SP}} \approx \sqrt{M_q Z_w - U_o M_w}$$

(III-47) $$\zeta_{SP} \approx \frac{-1}{2\omega_{n_{SP}}} (U_o M_w + Z_w + M_q)$$

(III-48) $$\omega_{n_p} \approx \frac{1}{\omega_{n_{SP}}} \sqrt{g(M_w Z_u - M_u Z_w)}$$

(III-49) $$\zeta_p \approx -\frac{X_u}{2\omega_{n_p}} - \frac{\zeta_{SP}\omega_{n_P}}{\omega_{n_{SP}}} - \frac{M_u(U_o Z_w - g) - X_w Z_u M_q}{2\omega_{n_p}\omega^2_{SP}}$$

The stability derivatives for the airframe at the flight condition used in this section are listed in Table III-5; the flight condition for which the stability derivatives have the values given in this table is referred to as the "base case".

Altitude (ft.)	20,000
Weight (lbs.)	36,300
Mach Number	.65
True Airspeed (ft/sec)	673.8
X_u	-.0093
X_w	.0169
Z_u	-.1223
Z_w	-1.24
Z_q	-7.46
M_w	-.0037
$M_{\dot{w}}$	.000178
M_q	-2.775
M_u	.00013

Table III-5

The factored form of the characteristic equation for the base case is:

(III-50) $$D_1 = \left[s^2 + 2\zeta_p\omega_{n_p} s + \omega^2_{n_p}\right]\left[s^2 + 2\zeta_{SP}\omega_{n_{SP}} s + \omega^2_{n_{SP}}\right]$$

$$D_1 = [s^2 + 2(.0728)(.0577)s + .00333]$$
$$[s^2 + 2(.8)(2.435)s + 5.929]$$

Figure III-19 shows the effect of varying X_u. It can be seen that the short period characteristics are relatively unaffected by changes in X_u. The principal effect of changing X_u is to alter the phugoid damping ratio, ζ_p, which increases almost linearly with X_u until the damping becomes greater than the critical value, $\zeta_p > 1$, when the phugoid oscillation splits up into two real roots. As X_u increases (i.e., moves in the positive direction), the degree of stability of the phugoid mode decreases; as X_u becomes more negative, this degree of stability increases. These effects are predicted by the approximate factors. Since X_u appears only in (III-49), which is the expression for the phugoid damping ratio, it is expected that X_u will not appreciably affect short period characteristics. X_u enters linearly into the approximate expression for ζ_p, and good correlation exists between the approximate factors and the trend predicted by Figure III-19.

The expression for X_u as given in (II-190) is rewritten as:

(III-52) $$X_u = -\frac{\rho S U}{m}\left(C_{D_u} + C_D\right)$$

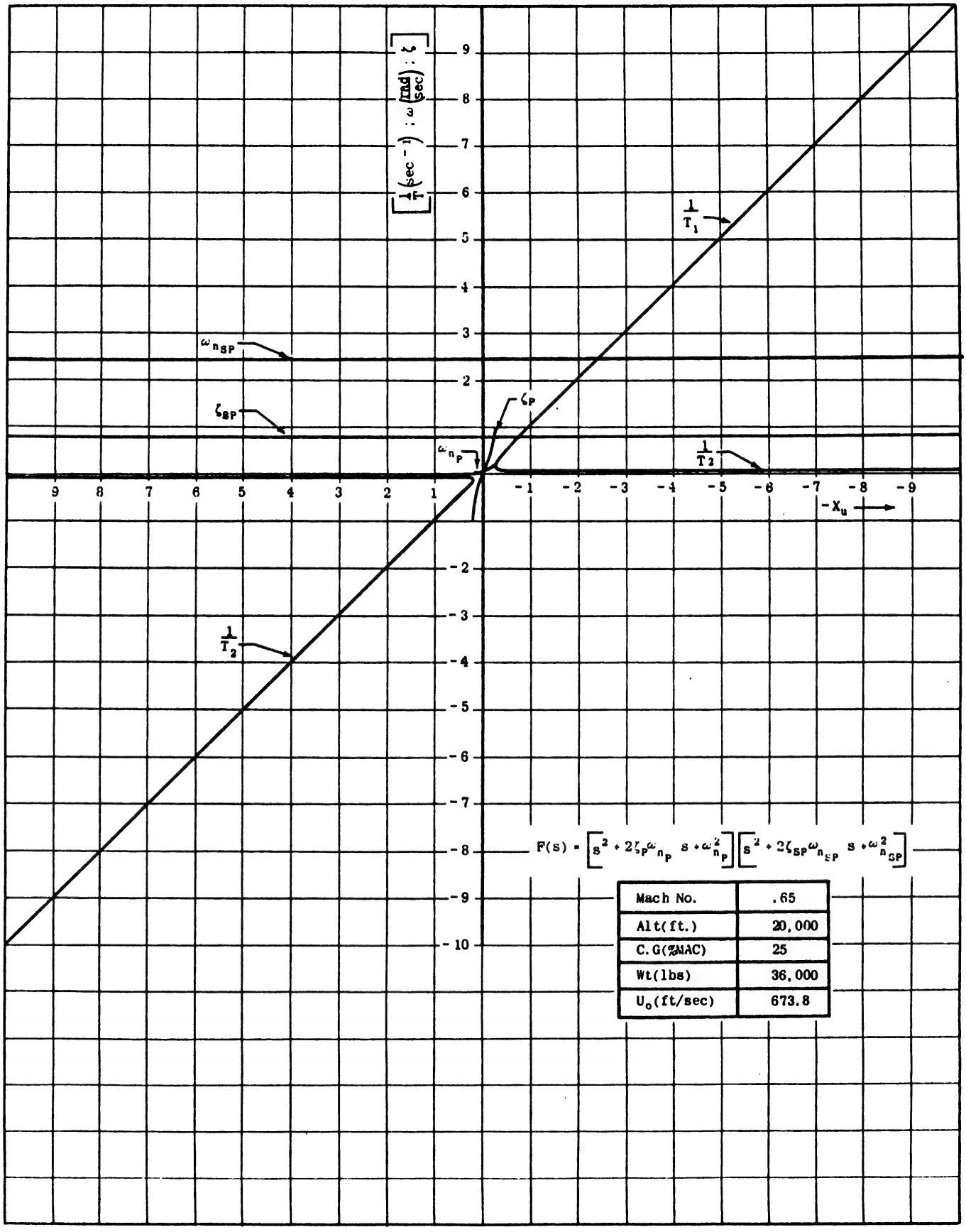

Mach No.	.65
Alt(ft.)	20,000
C.G(%MAC)	25
Wt(lbs)	36,000
U_o(ft/sec)	673.8

Figure III-19 Effect of X_u on Parameters of the Longitudinal Characteristic Equation Base Case Equation (X_u = -.0093)

This equation shows that X_u becomes more negative as the drag coefficient, C_D, of the airplane increases. Therefore, increasing the drag of the airplane (and hence X_u) tends to increase the degree of stability of the phugoid mode.

Figure III-20 shows the effect of varying X_w. As in the case of X_u, X_w appears to affect only the phugoid damping ratio. ζ_P varies linearly with X_w, indicating an increase in phugoid stability with an increase in the derivative X_w. X_w also appears linearly in the approximation to ζ_P, (III-49), and does not appear in the short period approximate factors.

For present purposes, (III-49) can be written as a linear term in X_w, plus a constant not dependent upon X_w:

(III-53) $$\zeta_P = K_1 + K_2 X_w$$

In this, K_2 is positive since the quantity $(Z_u M_q - M_u U_0)$ is positive. Therefore, the approximate factor for ζ_P indicates that ζ_P undergoes a positive linear increase with an increase in X_w.

The expression for X_w given in (II-190) is now rewritten as:

(III-54) $$X_w = \frac{\rho S U}{2m}\left(C_L - C_{D_\alpha}\right)$$

This relation shows that either an increase in C_L or a decrease in the drag curve slope would tend to contribute to the stability of the phugoid mode.

The effect of Z_u is shown in Figure III-21. Examination of this figure shows that changing Z_u primarily affects only the phugoid natural frequency and damping ratio. As Z_u becomes more negative, the phugoid natural frequency increases, but the phugoid damping ratio decreases. Z_u does not appear in the short period approximations, (III-46) and (III-47.

In the approximation of the phugoid natural frequency, (III-48), Z_u enters in the form of a factor of the product $M_w Z_u$. Since M_w is negative for the base case, as Z_u becomes larger in absolute value but still retains its negative sign, the product $Z_u M_w$ increases; as a result, the approximate phugoid natural frequency increases.

In (III-49), the second term on the right is negative. This term increases in magnitude proportionally to ω_{n_P}, and therefore ω_{n_P} causes this term to become more negative resulting in a decrease in the value of ζ_P. Consequently, analytical approximations verify the existence of the trends shown in Figure III-21.

Figure III-22 shows that as Z_w, in the neighborhood of the base value, -1.24, becomes more negative, the only essential change in the natural frequencies and damping ratios is that the short period natural frequency increases. This is in accordance with (III-46); since M_q is negative, as Z_w becomes more negative, $\omega_{n_{SP}}$ increases.

Z_w also appears in the approximate expressions for the short period damping ratio and the phugoid natural frequency, both of which appear in the phugoid damping ratio approximation. However, Z_w occurs in both the numerator and the denominator of the expressions for ζ_{SP}, and neither of these parameters is appreciably affected by reasonably large changes of Z_w about its base value. Hence, both Figure III-22 and the approximations can be used to predict that changes in Z_w principally affect only the short period natural frequency.

Figure III-23 shows that large changes in the value of Z_q have no appreciable effect on any of the parameters of the longitudinal characteristic equation. Since Z_q does not appear in any of the approximate factors, this result agrees with that which would be predicted from them.

The effects of varying M_u are shown in Figure III-24. This shows that changes in M_u drastically affect both short period and phugoid characteristics. The relation between the phugoid approximations of (III-48) and (III-49) and the trend predicted by Figure III-24 are discussed first.

(III-48) and (III-49) indicate that the phugoid natural frequency increases and the phugoid damping decreases as M_u increases in value, and also that as M_u moves in the negative direction, ω_{n_P} decreases and ζ_P increases. Figure III-24 verifies this.

Figure III-24 also shows that the short period natural frequency and damping ratio are affected by M_u, although the approximate expressions for these, (III-46) and (III-47), do not contain M_u. However, in arriving at the approximate factorization, it was assumed that $\omega_{n_{SP}} >> \omega_{n_P}$ and $\zeta_{SP} >> \zeta_P$. As M_u moves in either the positive or negative direction from its base value, the phugoid roots rapidly become of about the same magnitude as the short period roots, as shown in Figure III-24, so that the approximate factorization no longer holds.

Figure III-25 shows the effect of varying M_w. The phugoid characteristics are relatively unaffected. As M_w moves in the negative direction, an increase in the short period natural frequency and a decrease in the short period damping ratio result. An increase in M_w causes the short period mode to break up into two real roots. These effects can be predicted from (III-46) and (III-47).

As M_w becomes large and negative, the term $-U_0 M_w$ becomes large and positive, and thus $\omega_{n_{SP}}$ becomes large. Since $\omega_{n_{SP}}$ appears in the denominator of the approximation for ζ_{SP}, an increase in $\omega_{n_{SP}}$ results in a decrease in the short period damping ratio.

M_w enters into both the numerator and the denominator of the phugoid natural frequency approximation. Thus, changes in M_w are only slightly reflected in ω_{n_P}.

The first term on the right side of (III-49) contributes the major portion of the phugoid damping ratio. For large magnitudes of M_w (and therefore of $\omega_{n_{SP}}$), the second

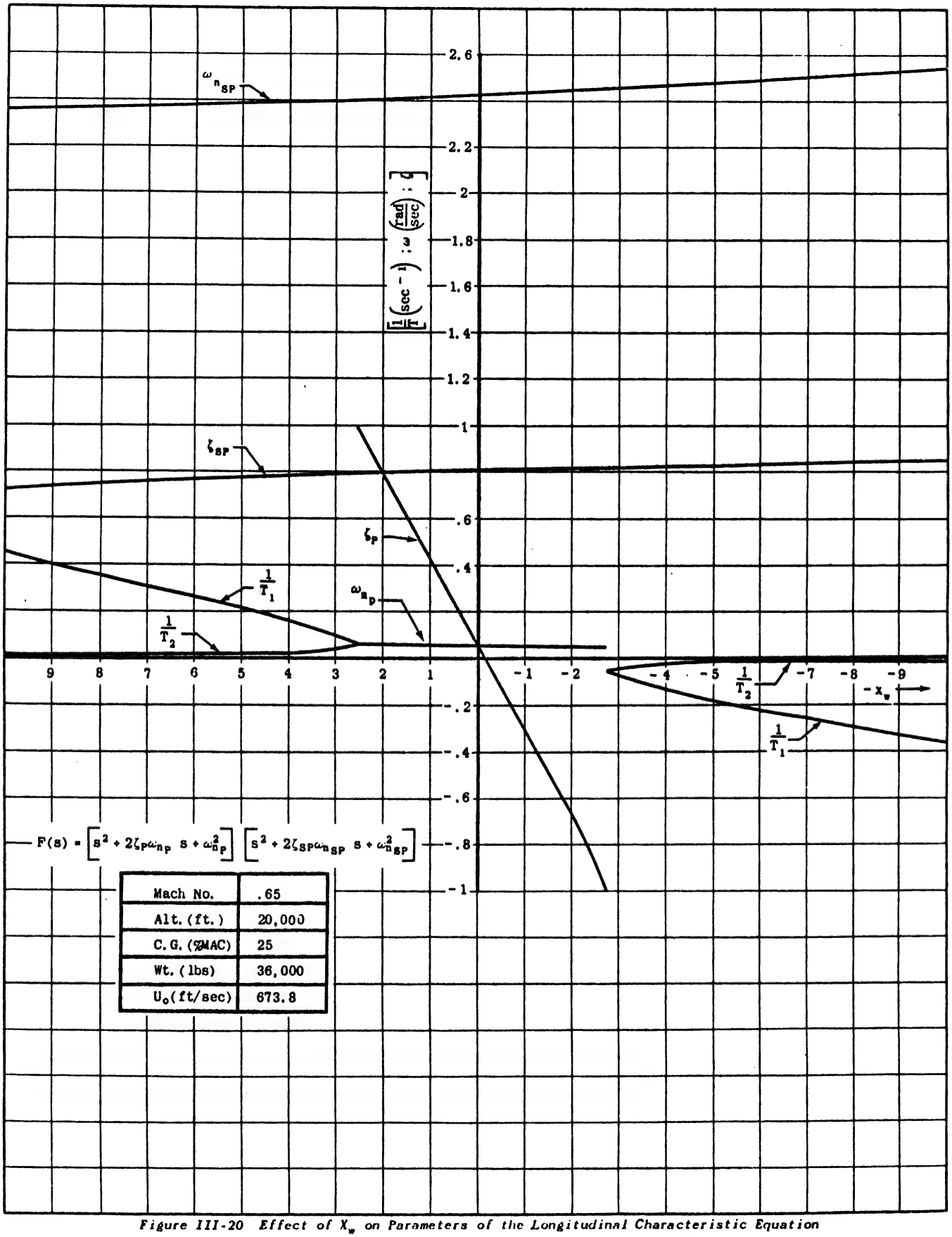

Mach No.	.65
Alt. (ft.)	20,000
C.G. (%MAC)	25
Wt. (lbs)	36,000
U_o (ft/sec)	673.8

Figure III-20 Effect of X_w on Parameters of the Longitudinal Characteristic Equation Base Case Equation (X_w = .0169)

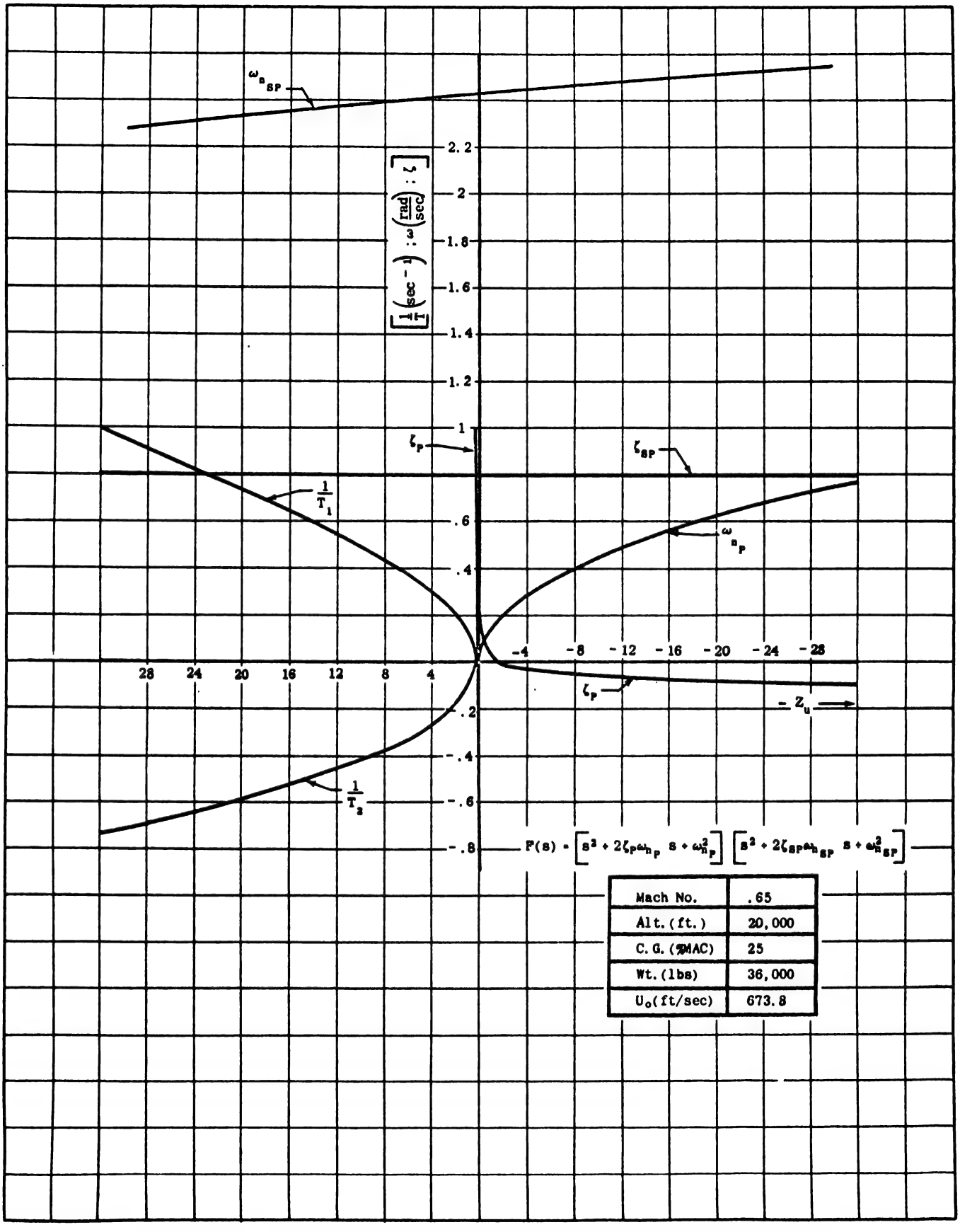

Mach No.	.65
Alt. (ft.)	20,000
C. G. (%MAC)	25
Wt. (lbs)	36,000
U_o (ft/sec)	673.8

Figure III-21 Effect of Z_u on Parameters of the Longitudinal Characteristic Equation Base Case Equation (Z_u = -.1223)

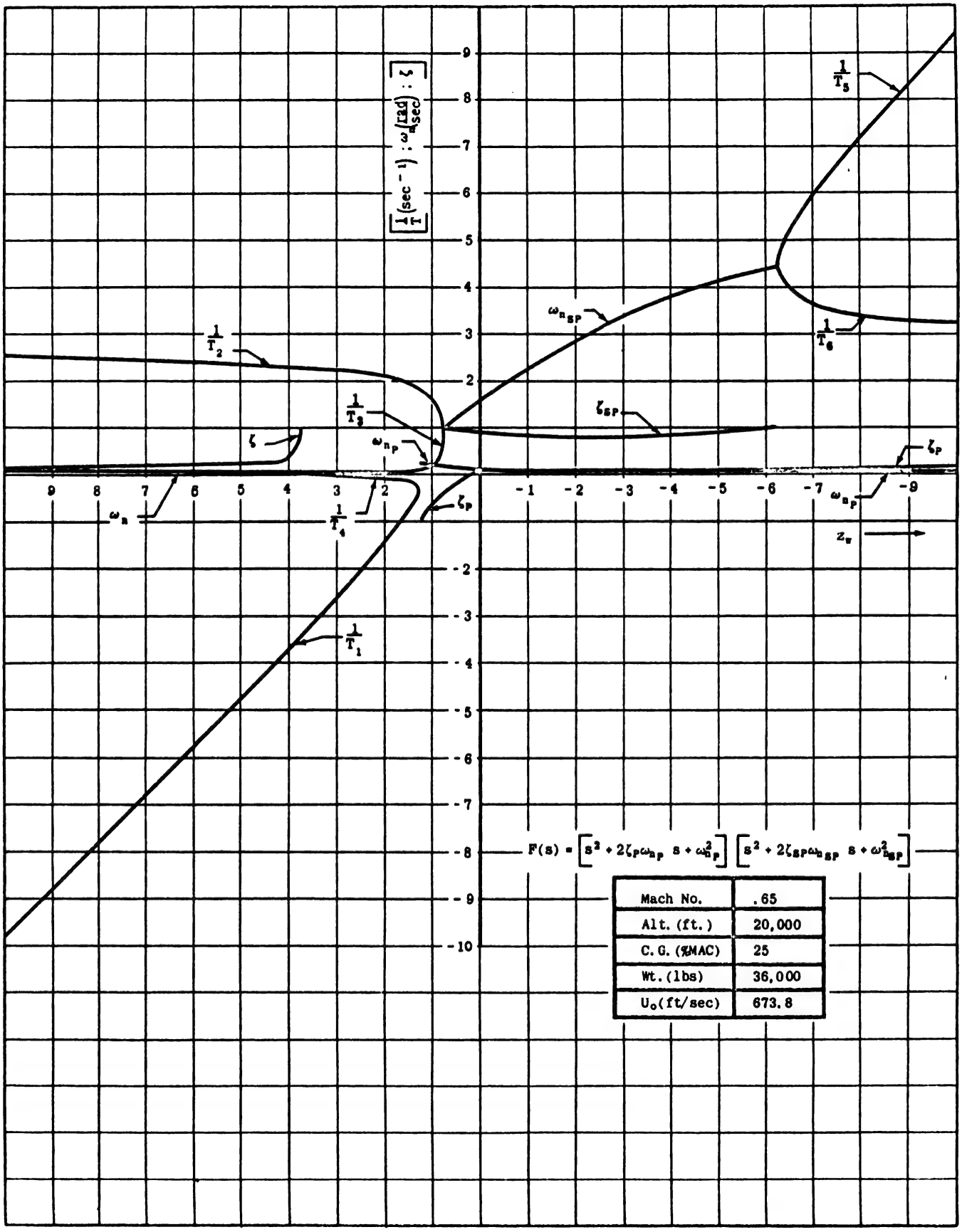

Mach No.	.65
Alt. (ft.)	20,000
C. G. (%MAC)	25
Wt. (lbs)	36,000
U_o(ft/sec)	673.8

Figure III-22 Effect of Z_w on Parameters of the Longitudinal Characteristic Equation Base Case Equation (Z_w = -1.24)

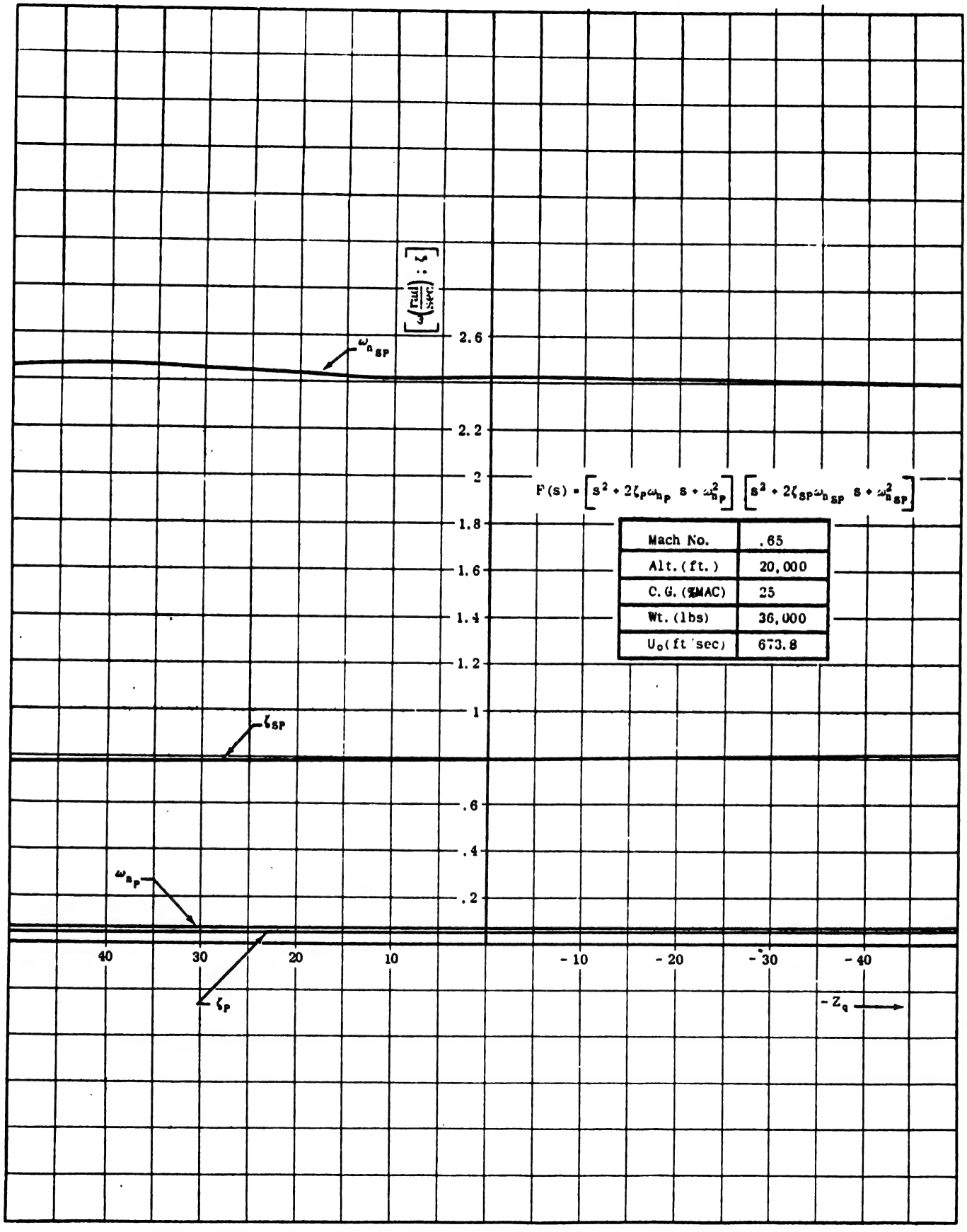

Figure III-23 Effect of Z_q on Parameters of the Longitudinal Characteristic Equation Base Case Equation ($Z_q = -7.46$)

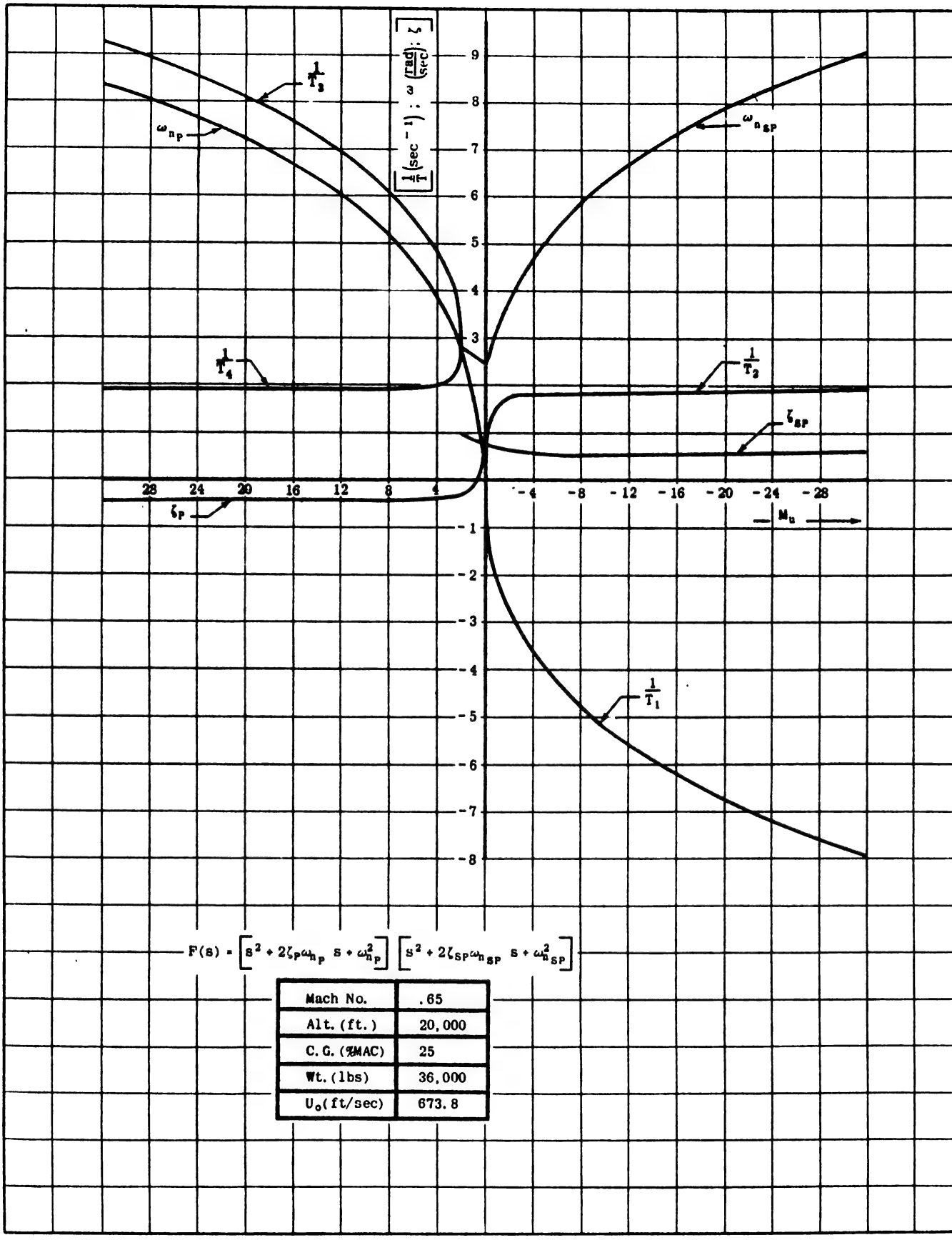

$$F(s) = \left[s^2 + 2\zeta_P\omega_{n_P}\, s + \omega_{n_P}^2\right]\left[s^2 + 2\zeta_{SP}\omega_{n_{SP}}\, s + \omega_{n_{SP}}^2\right]$$

Mach No.	.65
Alt. (ft.)	20,000
C. G. (%MAC)	25
Wt. (lbs)	36,000
U_o(ft/sec)	673.8

Figure III-24 Effect of M_u on Parameters of the Longitudinal Characteristic Equation Base Case Equation (M_u = .00013)

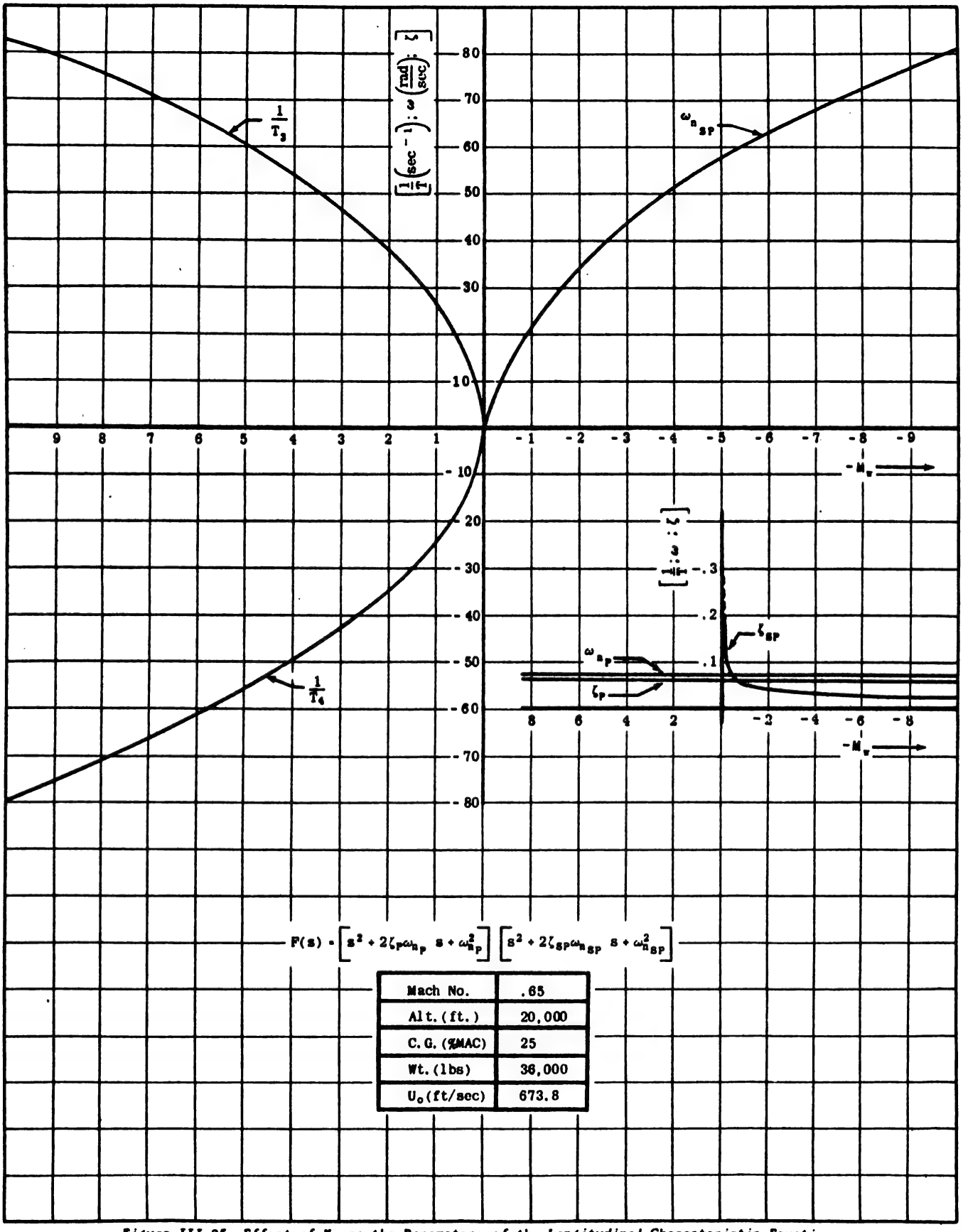

Mach No.	.65
Alt. (ft.)	20,000
C.G. (%MAC)	25
Wt. (lbs)	36,000
U_o (ft/sec)	673.8

Figure III-25 Effect of M_w on the Parameters of the Longitudinal Characteristic Equation Base Case Equation (M_w = -.0037)

and third terms on the right side of (III-49) become extremely small in comparison with the first term. Since these terms are relatively very small to start with, their decrease does not appreciably change the phugoid damping ratio.

The effect of varying M_q is shown in Figure III-26. Changes of M_q in the vicinity of the base value (-2.775) can be seen to affect principally the short period characteristics. A decrease in M_q increases both the short period damping ratio and the short period natural frequency, whereas increases in M_q decrease both $\omega_{n_{SP}}$ and ζ_{SP}. (III-46) and (III-47) show that these effects are accounted for in the approximations.

In summary, it appears that there is good correlation between the approximate factorization of the longitudinal characteristic equation and the curves presented in this section. It seems reasonable to conclude that both can be used in evaluating the effects of variations in the stability derivatives. In general, the curves are more reliable for predicting the effect of large variations in any of the derivatives on the resulting airplane motion, but it should be emphasized that neither the approximate factors nor the curves yield reliable predictions of trends for all flight conditions. However, since both the curves and the approximate factors are based on flight conditions that are more or less typical, their reliability is generally good.

SECTION 9 – APPROXIMATE FACTORS EXPRESSED AS FUNCTIONS OF THE BASIC NON-DIMENSIONAL STABILITY DERIVATIVES

In this section, the approximate factorization of the longitudinal characteristic equation is expressed in terms of the basic non-dimensional stability derivatives and other parameters of the airplane and the flight condition.

Aerodynamic data from wind tunnel tests, flight tests, and theoretical analyses are usually presented in the form of basic non-dimensional stability derivatives because correlation between different airplanes and different flight conditions is most easily attainable when the stability derivatives are in this form. For this reason, Chapter IV of the volume is devoted to a discussion of these basic non-dimensional stability derivatives.

Expressing the approximate factors in terms of the basic non-dimensional stability derivatives aids in determining the effect of varying these derivatives on airframe motions. These expressions should therefore help the reader relate the discussions of Chapter IV to material presented in the present chapter. With the approximate factors in this form, approximations to the airframe modes of motion can also be obtained without first calculating the dimensional stability derivatives.

To derive the desired expressions, the approximate quantities from (II-190) are substituted into (III-46) through (III-49). The last equation in (III-49) is simplified by using only the first term on the right side.

(It has been mentioned previously that this term is the major contributor to the phugoid damping ratio.) The resulting equations are: *

$$\text{(III-55)}\quad \omega_{n_{SP}} \approx \frac{1}{\tau}\left(\frac{c}{2k_{yy}}\right)\left[-\frac{C_{m_q}}{2}\left(C_{L_\alpha}+C_D\right)-2\mu_c\, C_{m_\alpha}\right]^{1/2}$$

$$\zeta_{SP} \approx \frac{-1}{2\omega_{n_{SP}}}\left(\frac{1}{\tau}\right)\left(\frac{c}{2k_{yy}}\right)^2\left[C_{m_{\dot\alpha}}+C_{m_q}-\frac{C_{L_\alpha}+C_D}{2\left(\frac{c}{2k_{yy}}\right)^2}\right]$$

$$\omega_{n_P} \approx \frac{1}{\omega_{n_{SP}}}\left(\frac{gc}{2k_{yy}^2}\right)^{1/2}\left(\frac{1}{\tau}\right)\left[\left(C_{m_u}+C_{m_\alpha}\right)\left(C_{L_\alpha}+C_L\right)-C_{m_\alpha}\left(C_{L_u}+C_L\right)\right]^{1/2}$$

$$\zeta_P \approx \frac{C_{D_u}+C_D}{2\tau\,\omega_{n_P}}$$

where $\mu_c = \frac{m}{\rho S c}$, $\tau = \frac{m}{\rho S U}$

* The quantities μ and τ were first introduced by A. Glauert, 'A Non-Dimensional Form of the Stability Equations of an Airplane,' Reports and Memoranda, R & M No. 1093, British Aeronautical Research Council, 1927.

SECTION 10 – EFFECT OF FLIGHT CONDITION ON THE LONGITUDINAL TRANSIENT RESPONSE OF AN AIRPLANE

Previous sections of this chapter have been devoted to the discussion of particular flight conditions. In this section, the effects of varying the flight condition on the transient response of an airplane are demonstrated by presenting analog computer traces of the solutions of the equations of motion for various flight conditions. Stability derivatives used in this analysis are theoretical values calculated for a hypothetical high-performance jet airplane of conventional cruciform configuration.

Plots which can be used to determine the damping ratio and the natural frequency of oscillatory modes from the transient response are also included in this section in addition to the derivation of a formula for the time required for an oscillatory mode to damp to one-half amplitude. Finally, some traces, which show the effect of varying a single dimensional stability derivative, are given.

Figure III-27, III-28, and III-29 can be used to determine the damping ratio of oscillatory modes. Since the damped period (T_D) can be read directly from the response curves, the natural frequency can be calculated from:

$$\text{(III-56)}\quad \omega_D = \frac{2\pi}{T_D} = \omega_n\sqrt{1-\zeta^2}$$

A parameter sometimes used to describe system performance is the time for an oscillatory mode to damp to one-half amplitude. This parameter is denoted by the symbol $T_{1/2}$. The equation for an oscillatory mode can be written in the form:

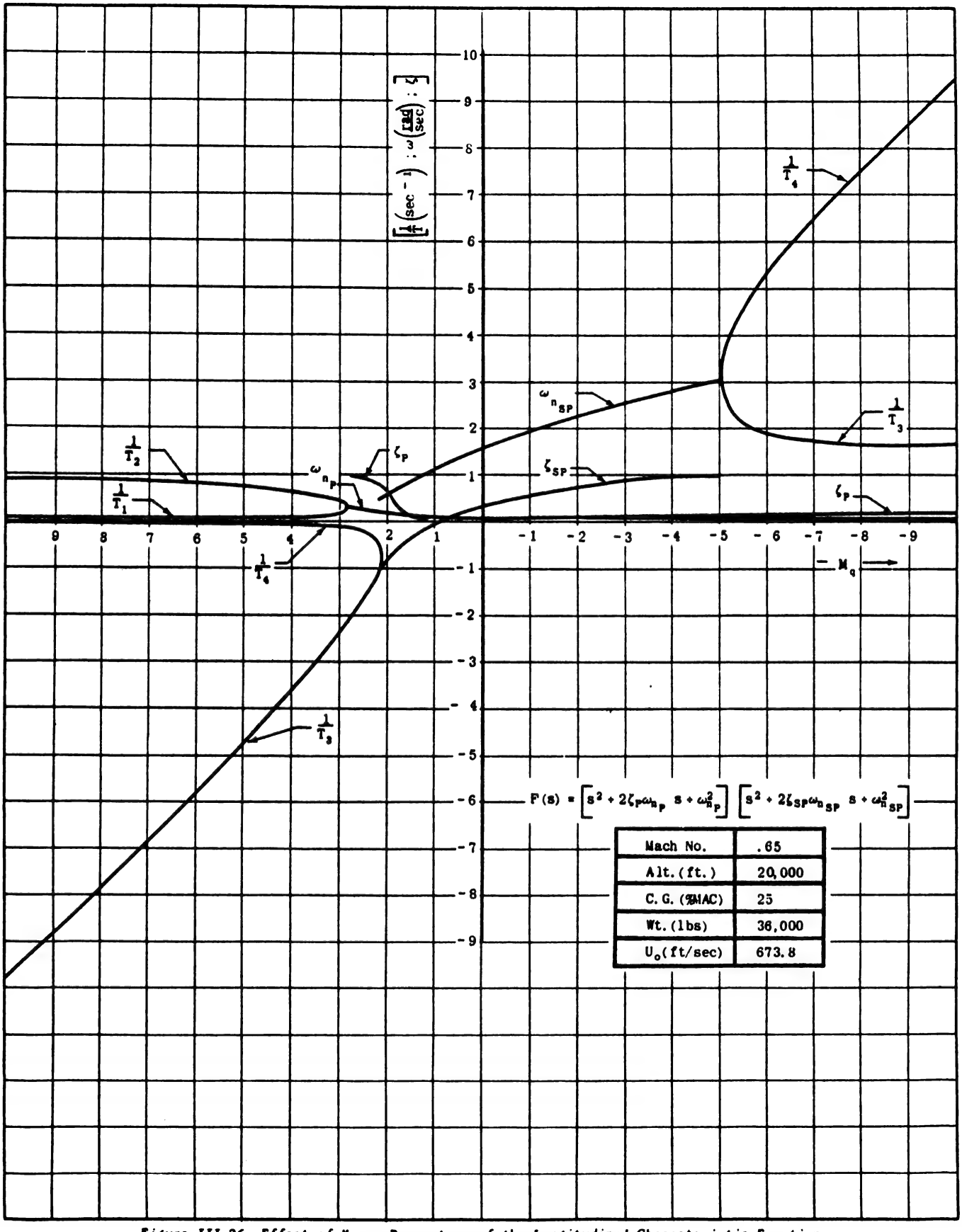

Mach No.	.65
Alt. (ft.)	20,000
C. G. (%MAC)	25
Wt. (lbs)	36,000
U_o (ft/sec)	673.8

Figure III-26 Effect of M_q on Parameters of the Longitudinal Characteristic Equation Base Case Equation (M_q = -2.775)

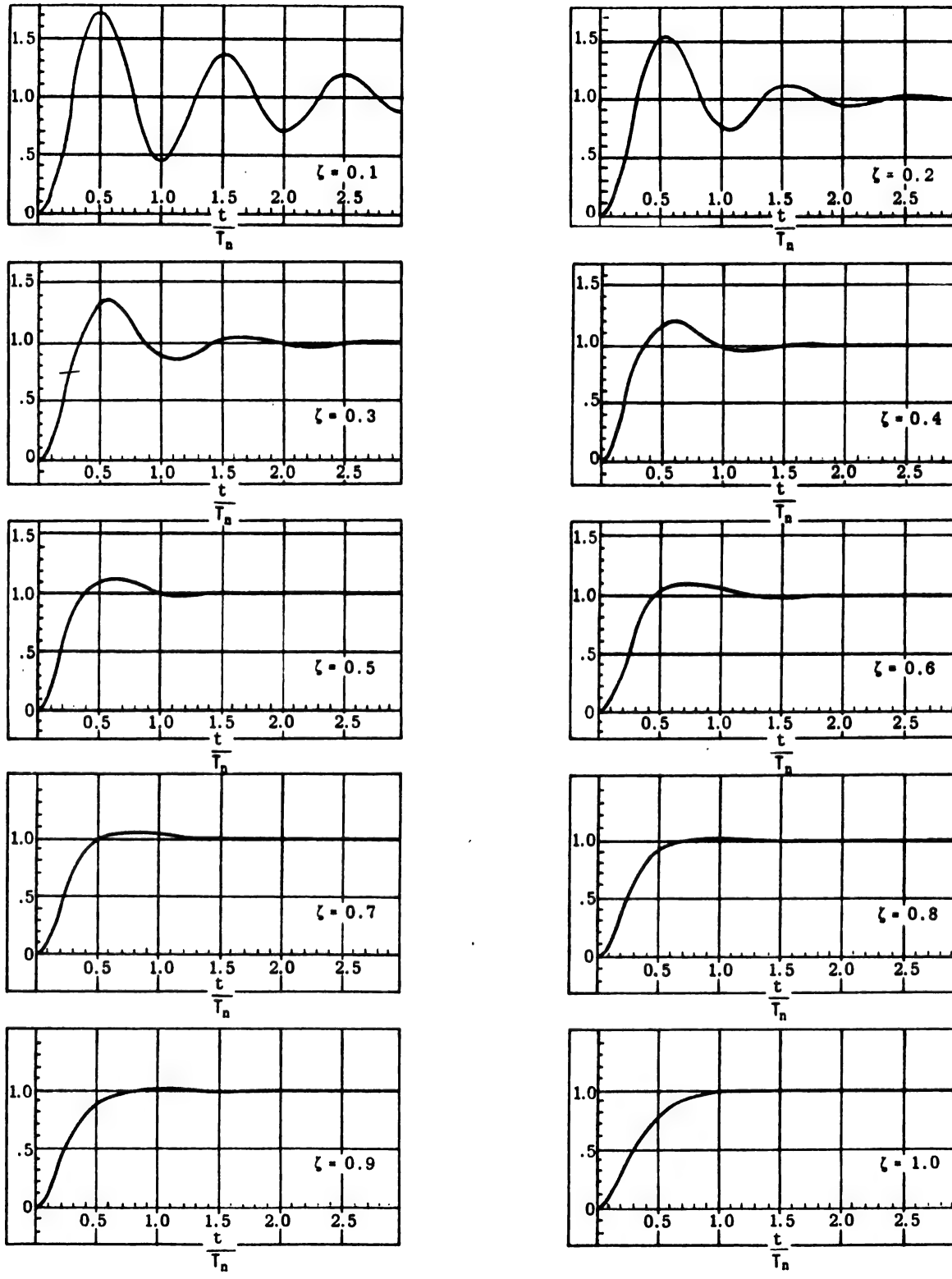

$$\frac{1}{s\left[\frac{s^2}{\omega_n^2} + \frac{2\zeta}{\omega_n} s + 1\right]} \qquad T_n = \frac{2\pi}{\omega_n}$$

Figure III-27 Typical Response Curves of Second Order System to Step Function Disturbance When Damping Ratio is Less than Critical ($\zeta < 1$)

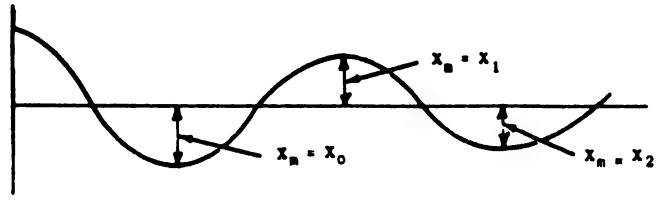

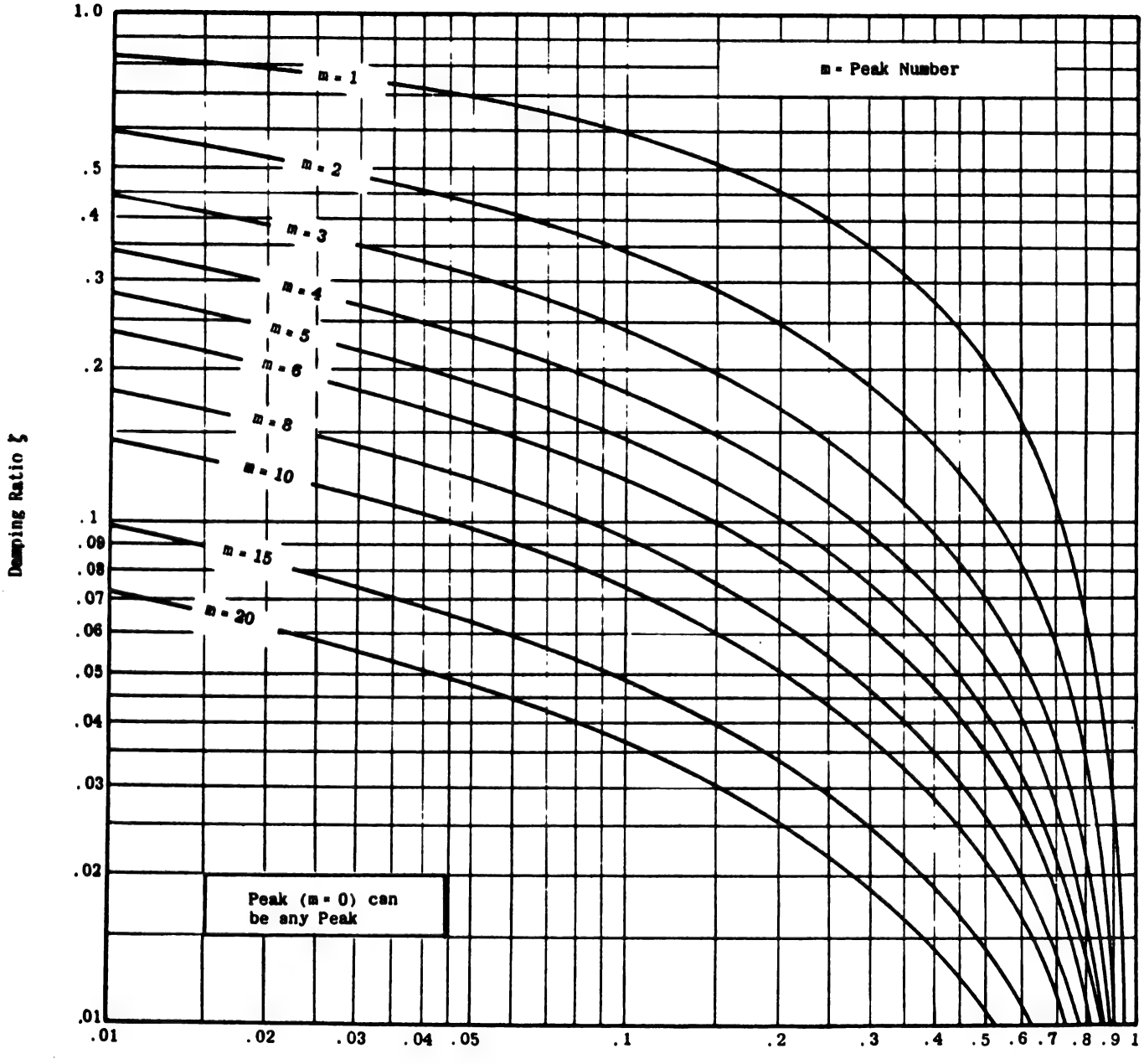

$$\frac{s}{\frac{s^2}{\omega_n^2} + \frac{2\zeta}{\omega_n} s + 1} \cdot \frac{1}{\frac{s^2}{\omega_n^2} + \frac{2\zeta}{\omega_n} s + 1} \cdot \frac{1}{s\left[\frac{s^2}{\omega_n^2} + \frac{2\zeta}{\omega_n} s + 1\right]}$$

Figure III-28 Damping Ratio of Oscillatory Transients as a Function of Subsidence Ratio for Second Order System

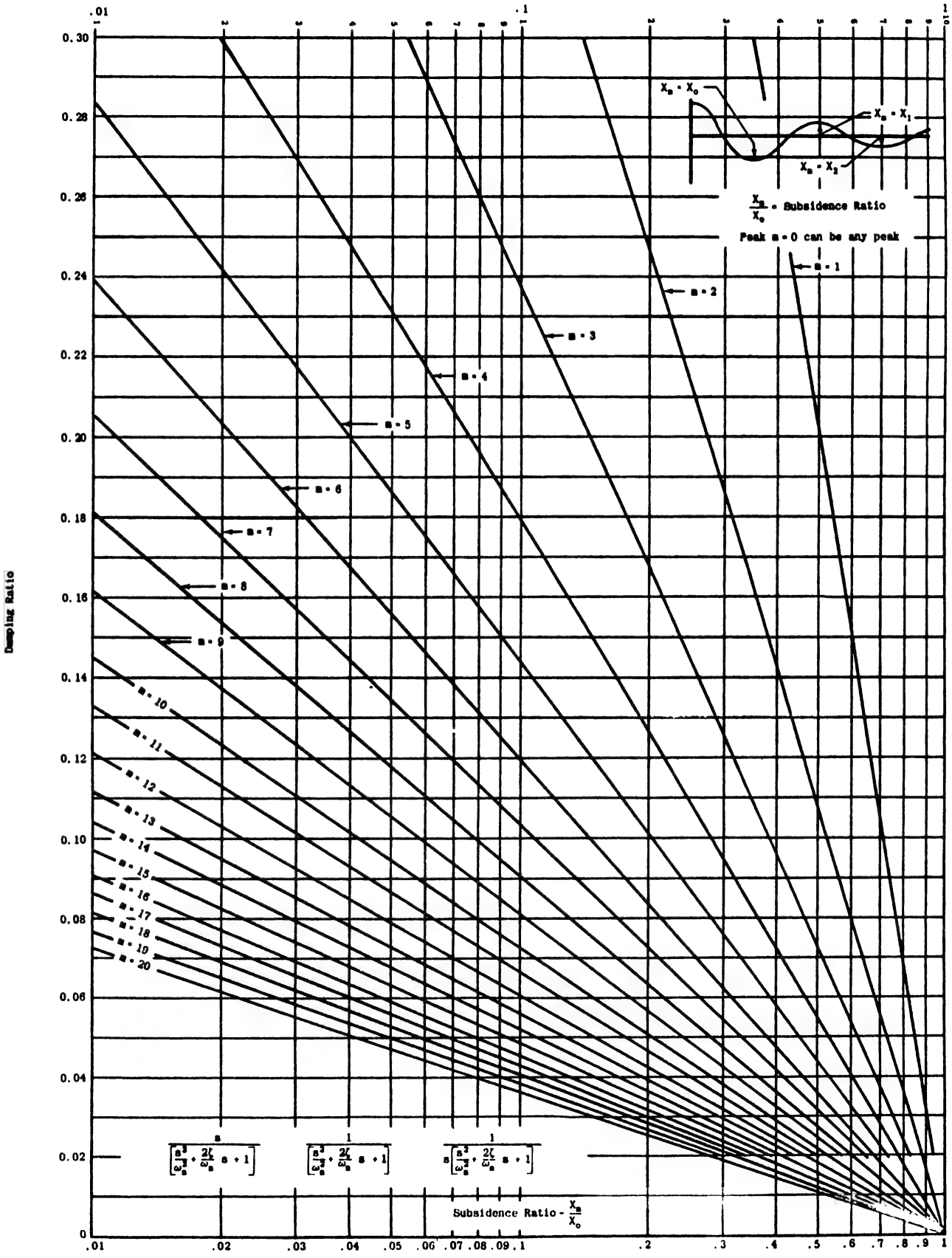

Figure III-29 Damping Ratio of Oscillatory Transients as a Function of Subsidence Ratio for Second Order Systems

(III-57)

$$X = Ae^{-\alpha t}\cos(\omega_D t + \phi)$$

where:

X = amplitude at any time t
α = damping constant $= \zeta\omega_n$
ω_D = damped natural frequency
A = maximum amplitude
ϕ = phase angle

A plot of (III-57) appears in Figure III-30. It can be seen from this figure that the curve $Ae^{-\alpha t}\cos(\omega_D t + \phi)$, that is, the magnitude of X at any time, t_1, cannot be greater than the value given by:

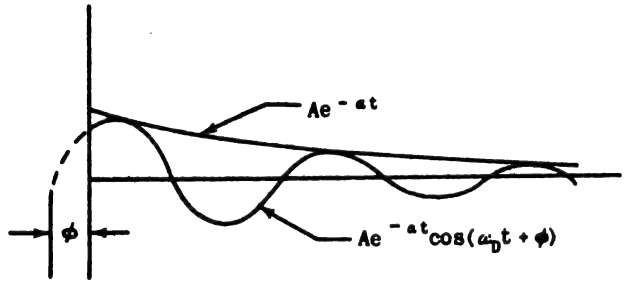

Figure III-30

(III-58) $$[X]_{t_1} = Ae^{-\alpha t_1}$$

and at time, t_2, the value of X must be less than, or at most can be equal to:

(III-59) $$[X]_{t_2} = Ae^{-\alpha t_2}$$

(III-58) and (III-59) can be used to determine the time required for $[X]_{t_2}$ to equal one-half $[X]_{t_1}$:

(III-60) $$\frac{[X]_{t_1}}{[X]_{t_2}} = 2 = \frac{Ae^{-\alpha t_1}}{Ae^{-\alpha t_2}}$$

(III-61) $$e^{-\alpha t_1} = 2e^{-\alpha t_2}$$

Taking the natural log of both sides of (III-61) and performing the indicated operations yield:

(III-62)

$$-\alpha t_1 = \ln 2 - \alpha t_2$$
$$\alpha(t_2 - t_1) = \ln 2$$
$$t_2 - t_1 = T_{\frac{1}{2}} = \frac{\ln 2}{\alpha}$$
$$T_{\frac{1}{2}} = \frac{.693}{\alpha}$$

and, since $\alpha = \zeta\omega_n$

(III-63) $$T_{\frac{1}{2}} = \frac{.693}{\zeta\omega_n}$$

(III-63) gives the value of the time required for a stable oscillatory mode to damp to one-half amplitude. If the system is unstable, (III-63) shows the value of the time required for the mode to double its amplitude. (This equation is not used in the following analysis. It is presented here solely because it is a parameter that appears frequently in literature dealing with aircraft stability and control.)

Figures III-31, III-32, III-33, and III-34 are analog computer traces of solutions of the equations of motion for a hypothetical high-performance jet aircraft flying at sea level at the indicated Mach numbers. From these curves, the natural frequency and damping ratio of each of the oscillatory modes can be obtained.

By computing enough such solutions, the values of the short period and phugoid natural frequencies and damping ratios could be obtained as functions of Mach number. The four curves actually shown are presented merely to indicate the expected variation of these parameters with Mach number. From these curves, certain facts can be readily determined: the short period has its highest frequency at maximum Mach number; the phugoid diverges at Mach numbers of 1.0 and 1.2; and the short period is more than critically damped and splits up into real roots at $M = 0.8$.

The effect of altitude variation is shown in the curves of Figures III-32, III-35, and III-36. As in the case of the traces showing Mach number variation, more complete information would be required to make statements of any significance. However, even with these few traces available, there are indications that the phugoid natural frequency and the short period damping ratio decrease with altitude, and that there is no uniform variation of any of the other parameters with altitude at the Mach number used.

Figures III-37, III-38, and III-39 show the effect of varying the stability derivative M_w. Figure III-37 is the solution for the flight condition of Table III-1. Figures III-38 and III-39 are solutions of the equations of motion that are identical with those corresponding to Figure III-37 except that the value of M_w has been changed as indicated on the figures.

In the discussion of the effect of variation of M_w in Section III-8, it was concluded that the primary effect of M_w in becoming more negative was to increase the short period natural frequency and to decrease the short period damping ratio. These same effects are illustrated in these figures.

To summarize, it should be stated that much of the information concerning the dynamic response of an airframe can be obtained mathematically only by rather lengthy computational methods, whereas the same information can be obtained with comparative simplicity by the use of an analog computer.

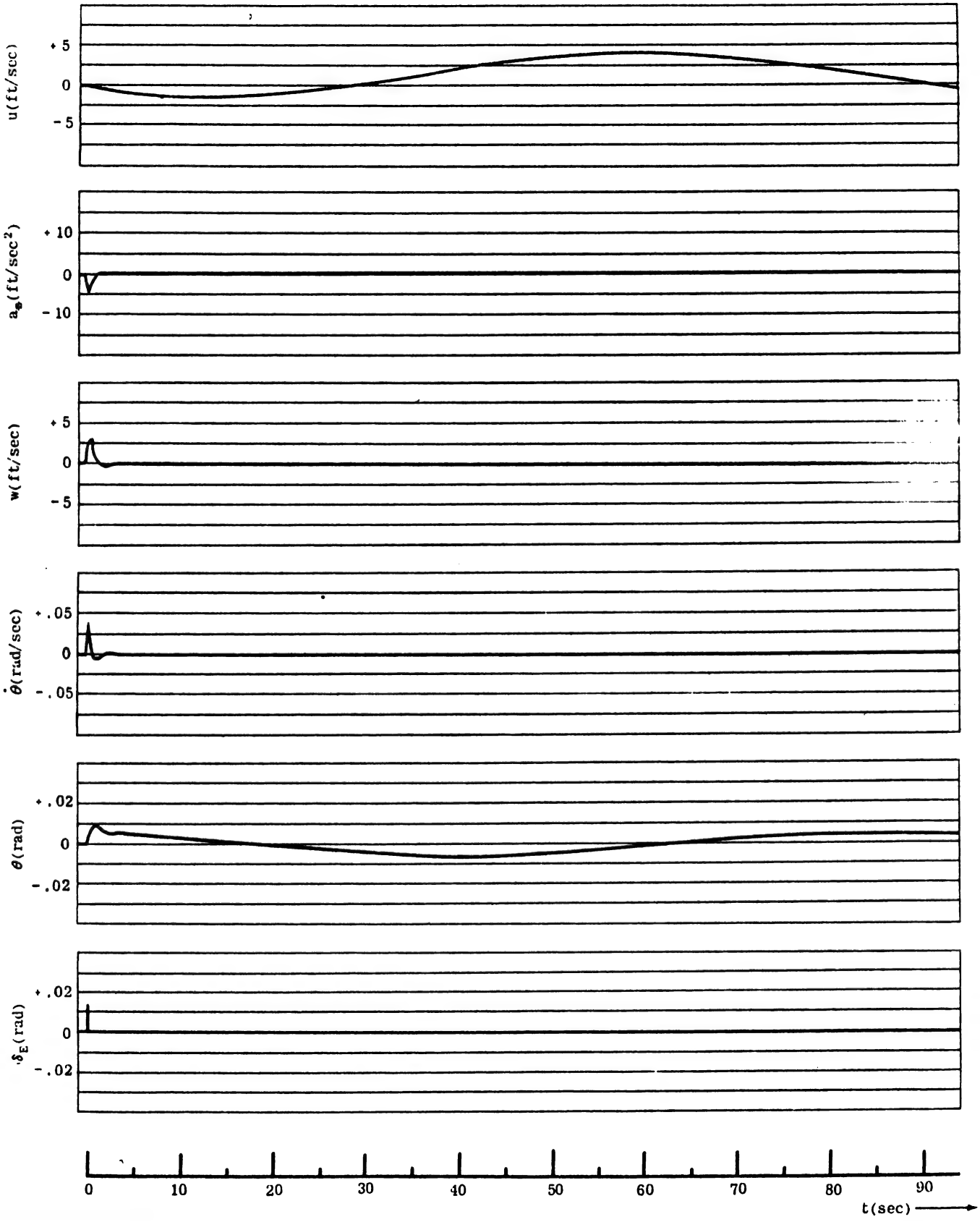

Figure III-31 Analog Computer Record of Time History for Pulse Elevator Deflection. Three Degree of Freedom (Mach No. = .4; Altitude = Sea Level)

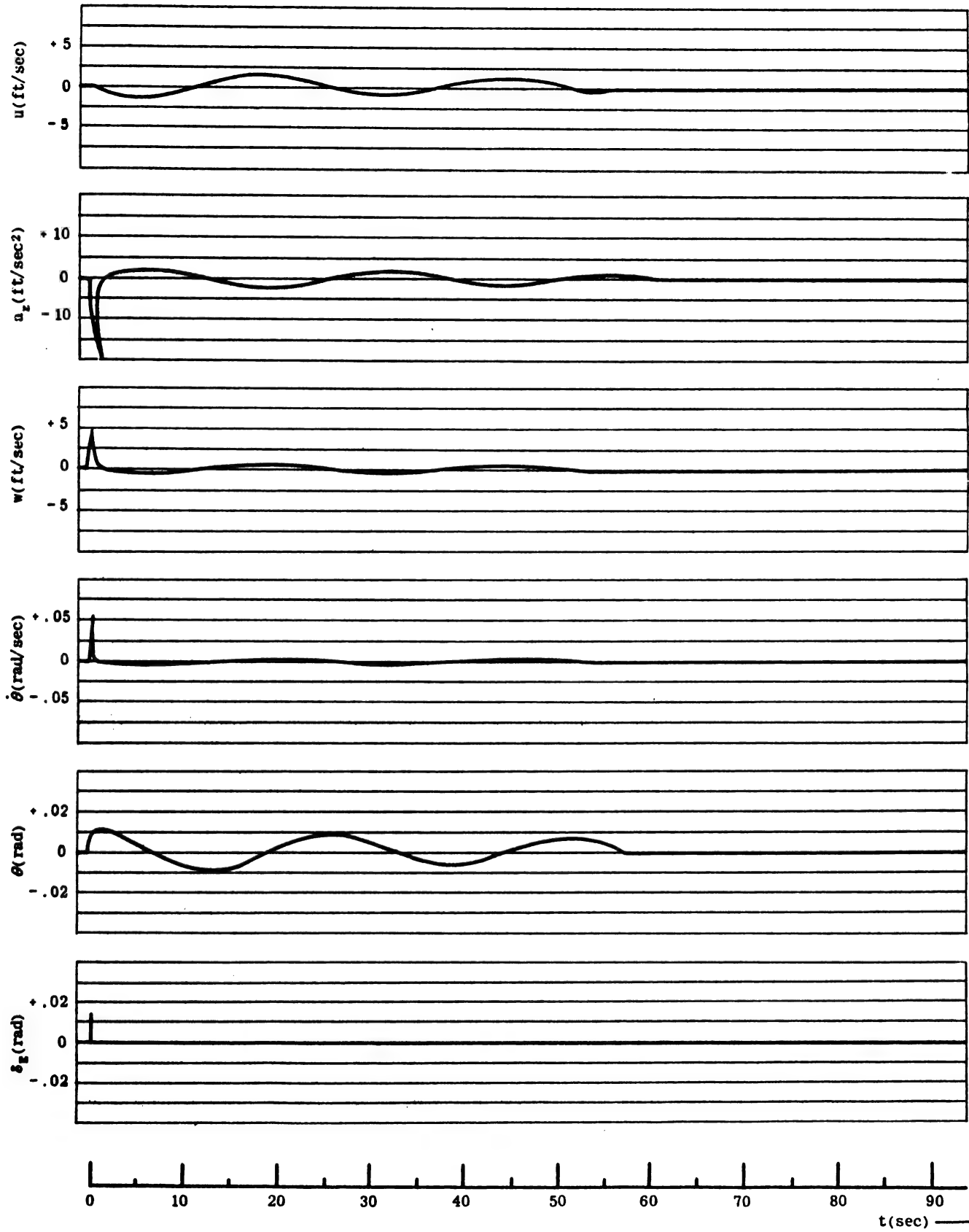

Figure III-32 Analog Computer Record of Time History for Pulse Elevator Deflection. Three Degree of Freedom (Mach No. = .8; Altitude = Sea Level)

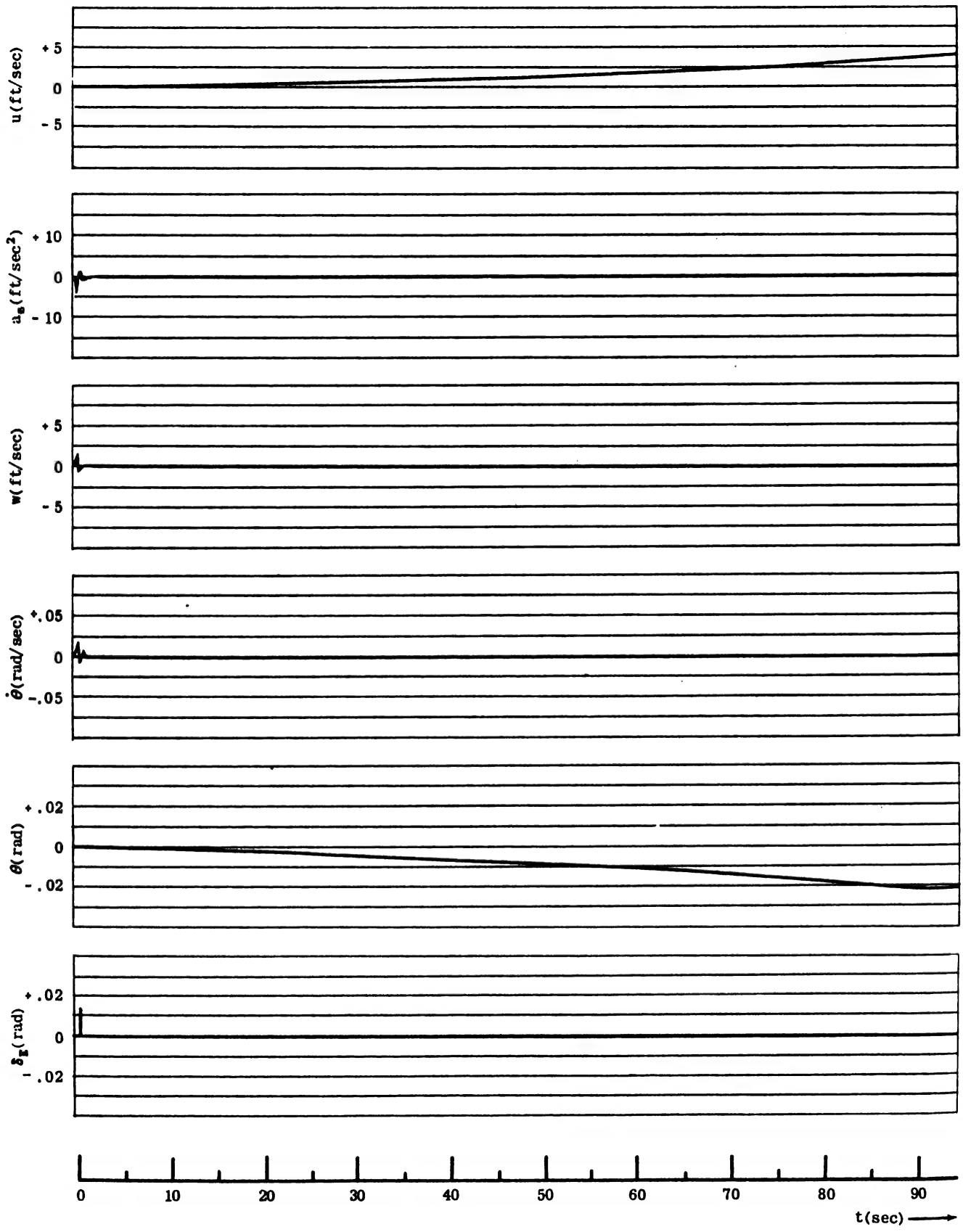

Figure III-33 Analog Computer Record of Time History for Pulse Elevator Deflection. Three Degree of Freedom (Mach No. = 1.0; Altitude = Sea Level)

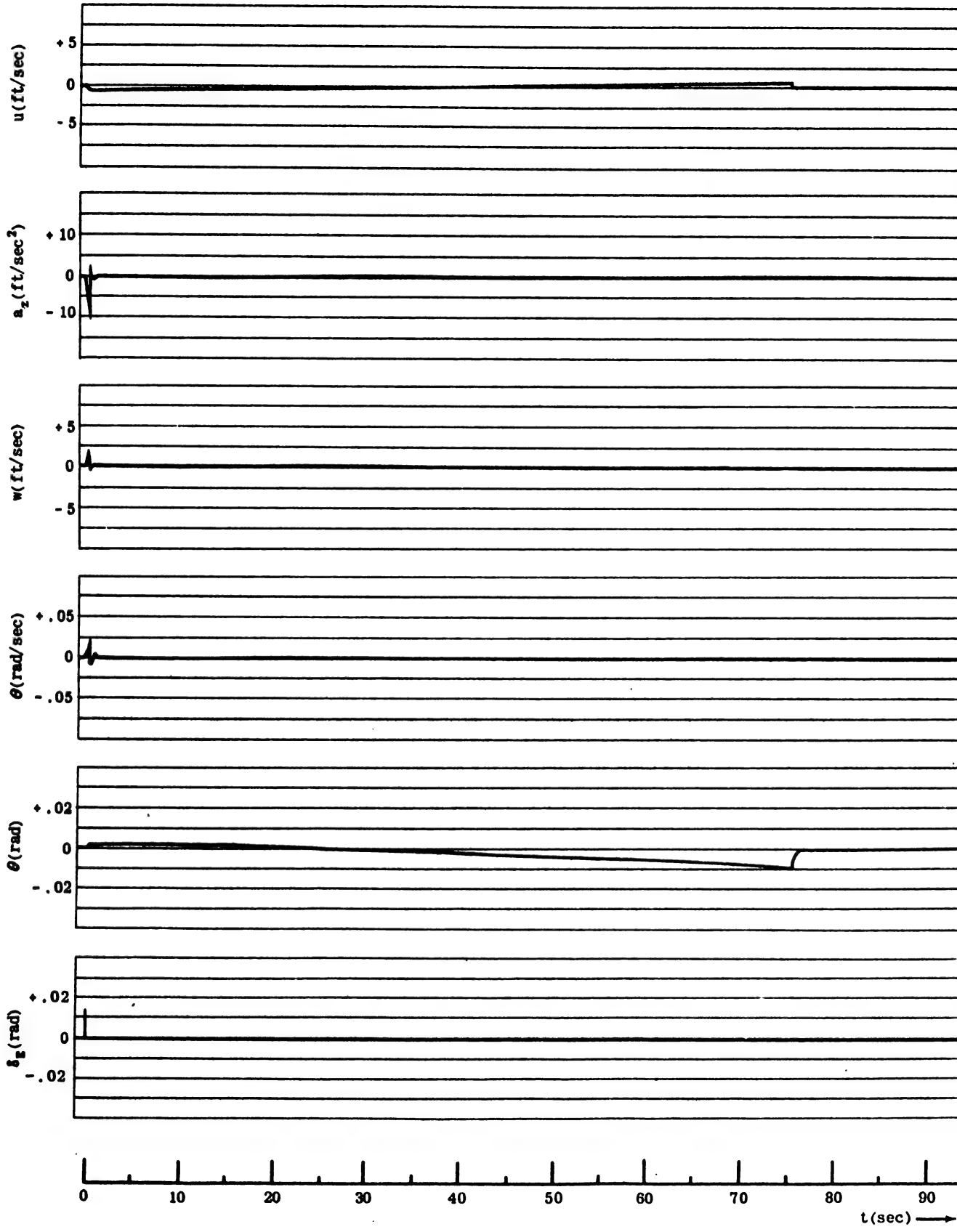

Figure III-34 Analog Computer Record of Time History for Pulse Elevator Deflection. Three Degree of Freedom (Mach No. = 1.2; Altitude = Sea Level)

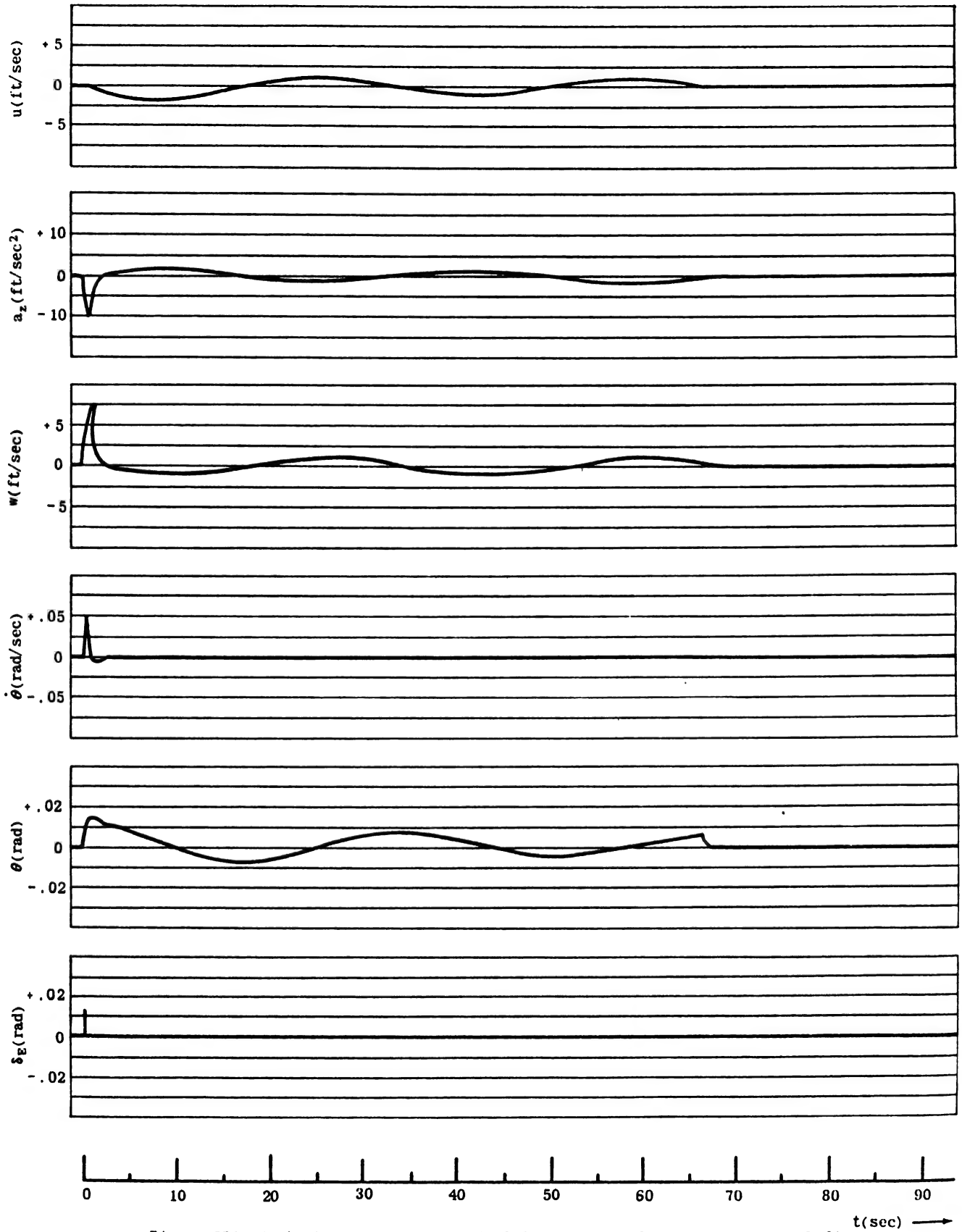

Figure III-35 Analog Computer Record of Time History for Pulse Elevator Deflection, Three Degree of Freedom (Mach No. = .8; Altitude = 30,000 Ft.)

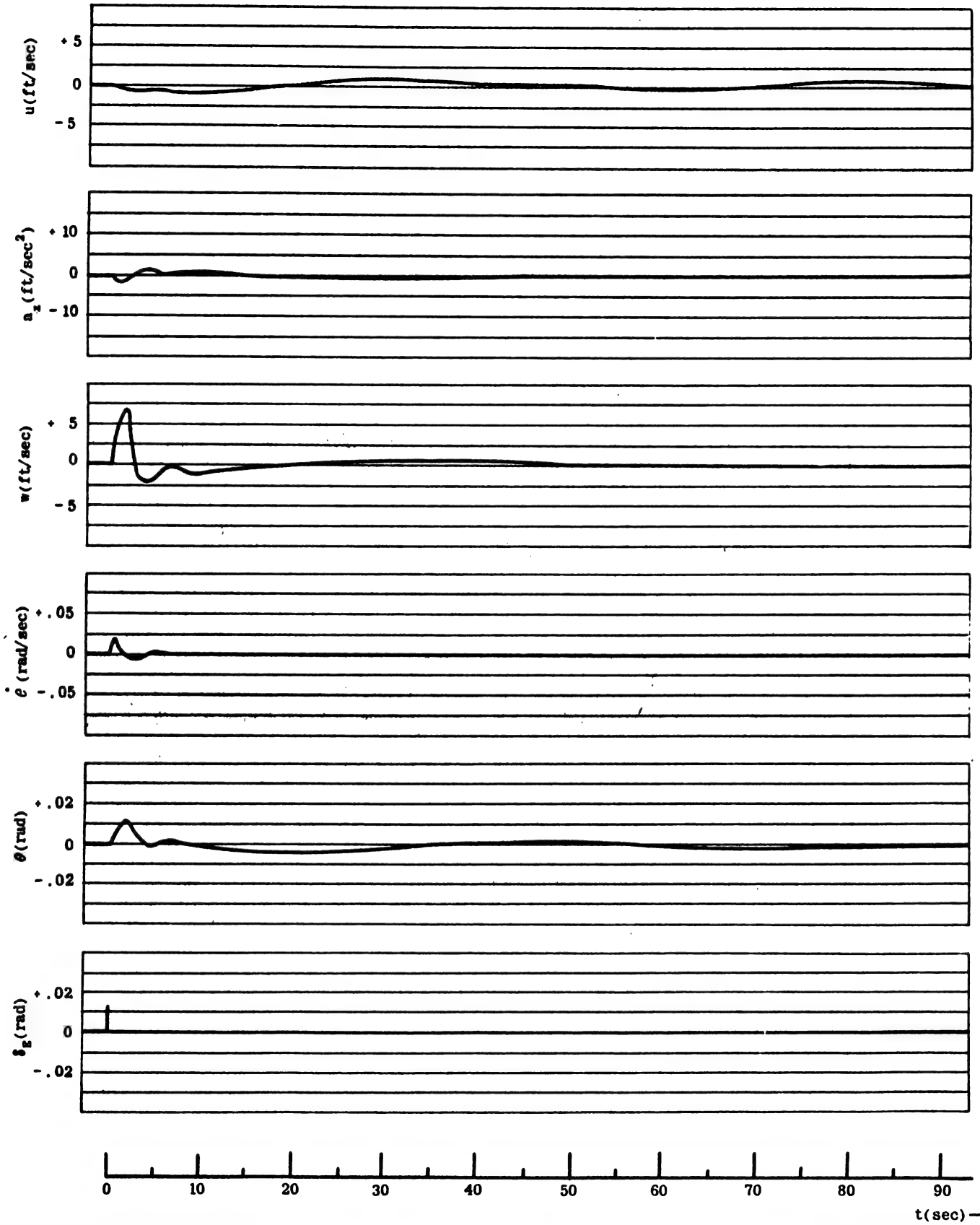

Figure III-36 Analog Computer Record of Time History for Pulse Elevator Deflection. Three Degree of Freedom (Mach No. = .8; Altitude = 60,000 Ft.)

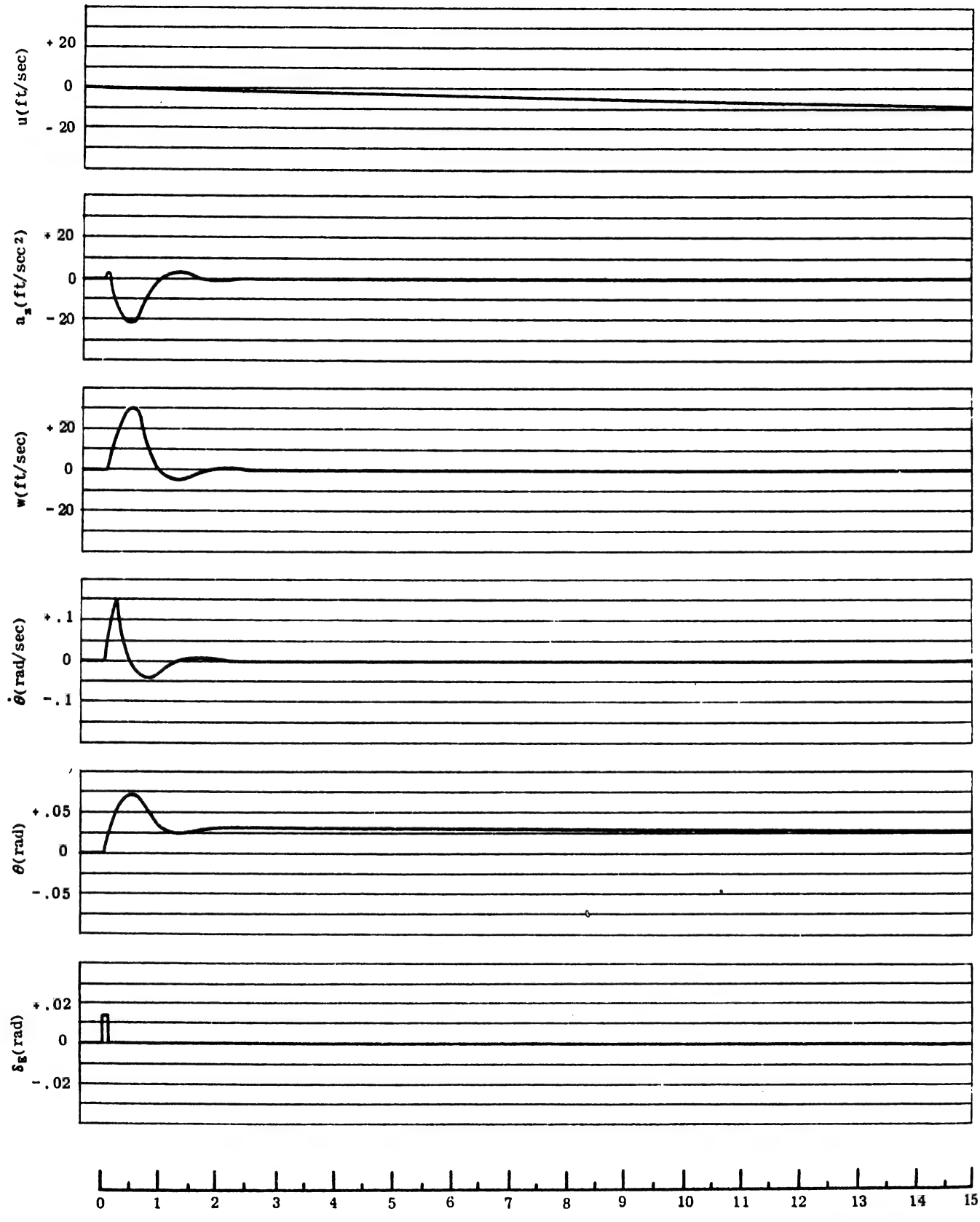

Figure III-37 Analog Computer Record of Time History for Pulse Elevator Deflection Three Degree of Frequency (M_w = -.0235; Mach No. = .6; Altitude = 20,000 Ft.)

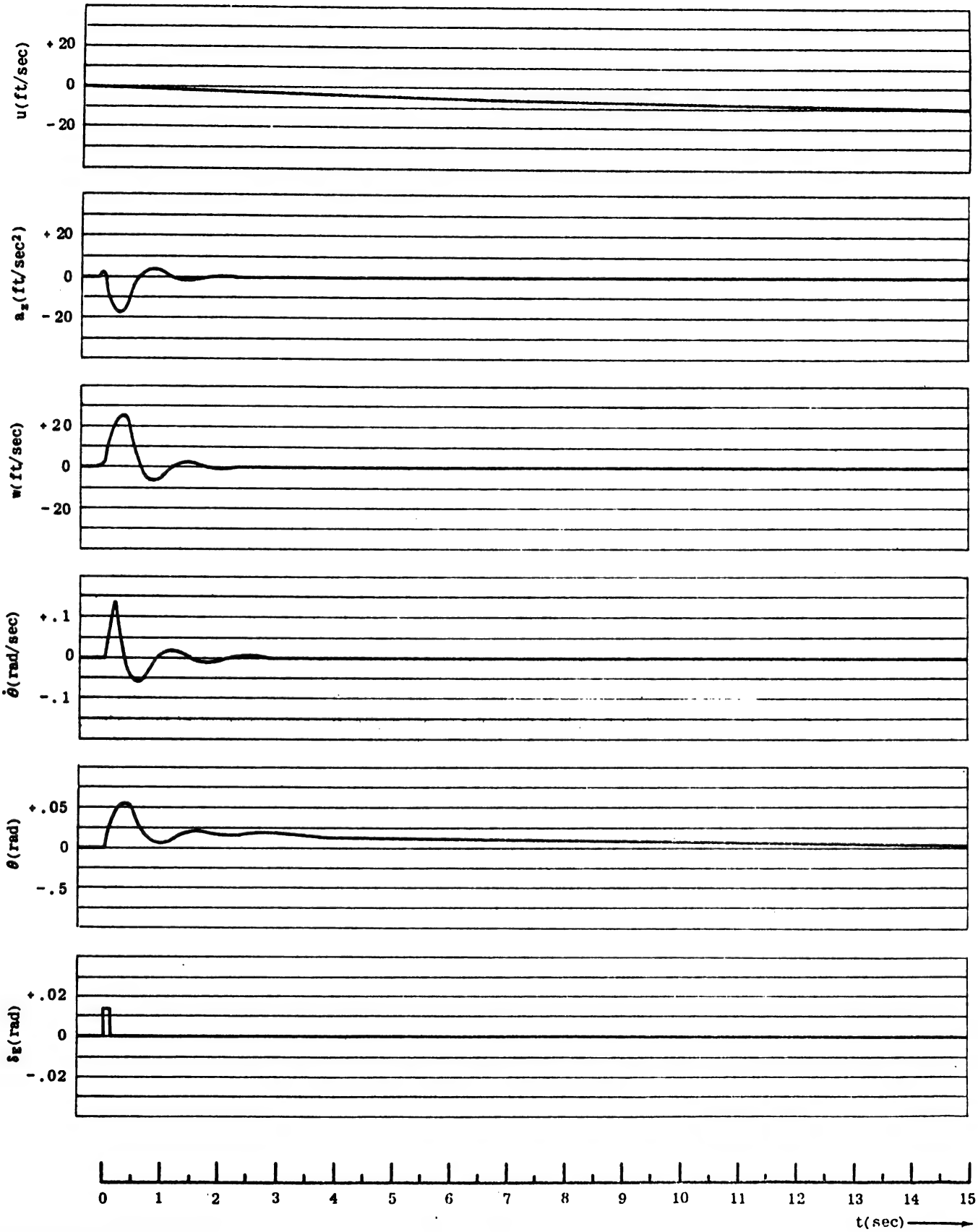

Figure III-38 Analog Computer Record of Time History for Pulse Elevator Deflection, Three Degree of Freedom (M_w = -.05; Mach No. = .6; Altitude = 20,000 Ft.)

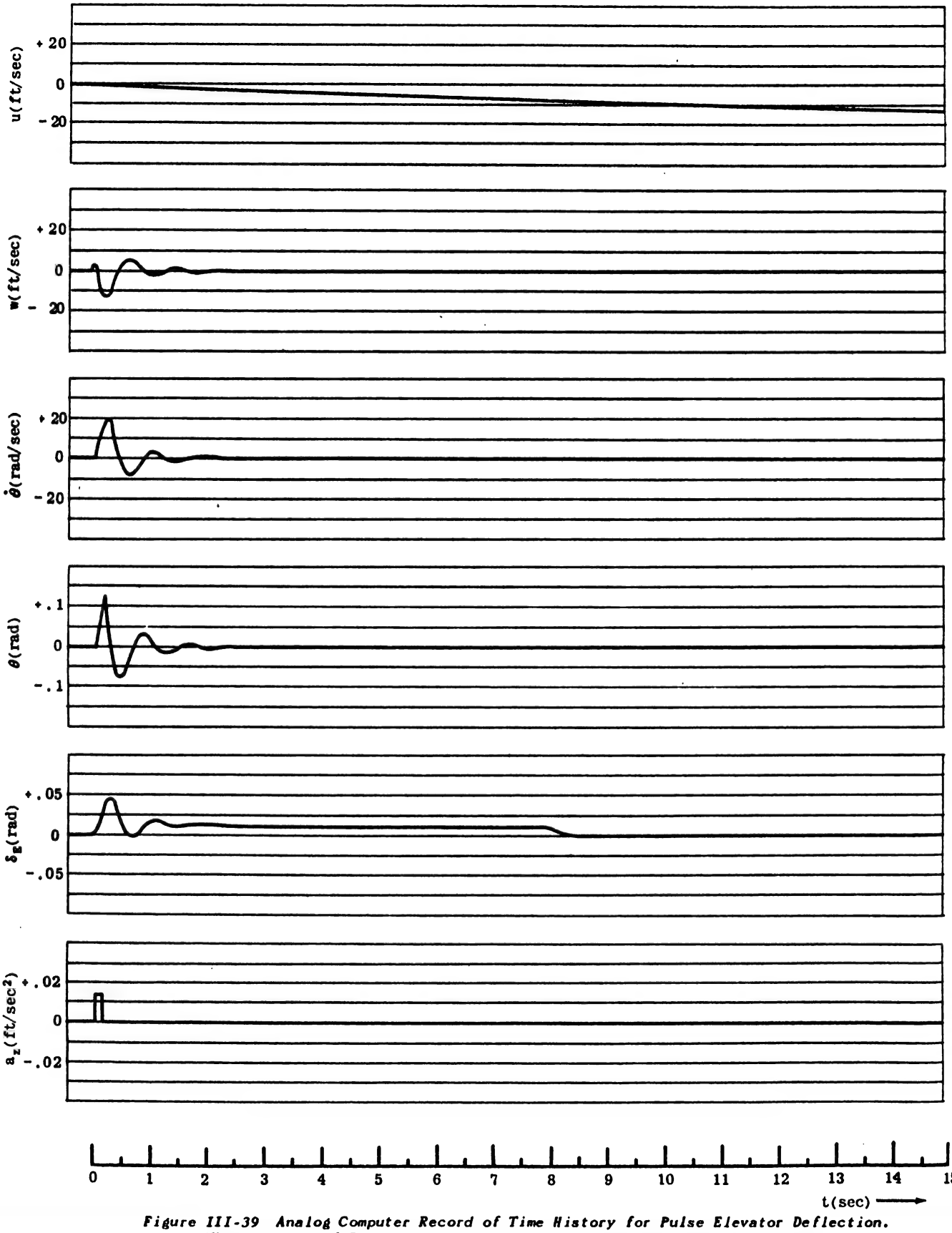

Figure III-39 Analog Computer Record of Time History for Pulse Elevator Deflection. Three Degree of Freedom ($M_w = -.1$; Mach No. = .6; Altitude = 20,000 Ft.)

LATERAL TRANSFER FUNCTIONS

SECTION 11 – AIRPLANE RESPONSE TO RUDDER DEFLECTION

The lateral transfer functions are treated in the same manner as the longitudinal ones were in the preceding pages. The response of an airplane to rudder deflection is examined first, and then the response to aileron deflection.

The lateral equations of motions, (II-197), are rewritten for reference as:

(III-64)

$$\dot{\beta} - Y_v\beta - Y_p^*p - \frac{g}{U_o}(\cos\gamma_o)\phi + r - Y_r^*r - \frac{g}{U_o}(\sin\gamma_o)\psi = Y_{\delta_A}^*\delta_A + Y_{\delta_R}^*\delta_R$$

$$-L_\beta\beta + \dot{p} - L_pp - \frac{I_{xz}}{I_{xx}}\dot{r} - L_rr = L_{\delta_A}\delta_A + L_{\delta_R}\delta_R$$

$$-N_\beta\beta - \frac{I_{xz}}{I_{zz}}\dot{p} - N_pp + \dot{r} - N_rr = N_{\delta_A}\delta_A + N_{\delta_R}\delta_R$$

(III-64) will be somewhat simplified before proceeding with the analysis.

ASSUMPTION X: Y_p^*p , Y_r^*r , and $Y_{\delta_A}^*\delta_A$ are assumed to be small enough in comparison with other terms in the Yforce equation that they can be neglected.

From Assumptions IX and X, the following quantities which occur in (III-64) can be equated to zero:

$$Y_p^* = Y_r^* = Y_{\delta_A}^* = \gamma_o = 0$$

(It should be pointed out that the derivatives set equal to zero in Assumption X are generally small and can be neglected in the analysis of most conventional airframes. However, this assumption is not always valid. The effect of each stability derivative should be evaluated before it is discarded as negligible.)

(III-64) then reduce to:

(III-65)
$$\dot{\beta} - Y_v\beta - \frac{g}{U_o}\phi + r = Y_{\delta_R}^*\delta_R$$

$$-L_\beta\beta + \dot{p} - L_pp - \frac{I_{xz}}{I_{xx}}\dot{r} - L_rr = L_{\delta_R}\delta_R + L_{\delta_A}\delta_A$$

$$-N_\beta\beta - \frac{I_{xz}}{I_{zz}}\dot{p} - N_pp + \dot{r} - N_rr = N_{\delta_R}\delta_R + N_{\delta_A}\delta_A$$

The transfer functions derived in Chapter II are thus reduced to:

(III-66)

$$D_2 = s(As^4 + Bs^3 + Cs^2 + Ds + E)$$
$$A = I - A_1B_1$$
$$B = -Y_v(1 - A_1B_1) - L_p - N_r - A_1N_p - B_1L_r$$
$$C = N_\beta + L_p(Y_v + N_r) + N_p(A_1Y_v - L_r) + Y_v(B_1L_r + N_r) + B_1L_\beta$$
$$D = -N_\beta(L_p + A_1g/U_o) + N_p(L_\beta + Y_vL_r) - L_pN_rY_v - L_\beta\, g/U_o$$
$$E = g/U_o(L_\beta N_r - N_rL_\beta)$$

where

$$A_1 = \frac{I_{xz}}{I_{xx}} \qquad B_1 = \frac{I_{xz}}{I_{zz}}$$

(III-67)

$$\frac{\beta(s)}{\delta_R(s)} = \frac{N_{(\beta/\delta_R)}}{D_2} = \frac{s(A_\beta s^3 + B_\beta s^2 + C_\beta s + D_\beta)}{D_2}$$

(where the notation $N_{(\beta/\delta_R)}$ indicates the transfer function numerator for sideslip angle caused by rudder deflection).

$$A_\beta = Y_{\delta_R}^*(1 - A_1B_1)$$
$$B_\beta = -Y_{\delta_R}^*(L_p + N_r + A_1N_p + B_1L_r) - L_{\delta_R}B_1 - N_{\delta_R}$$
$$C_\beta = Y_{\delta_R}^*(L_pN_r - N_pL_r) + L_{\delta_R}(\frac{g}{U_o} - N_p) + N_{\delta_R}(A_1\frac{g}{U_o} + L_p)$$
$$D_\beta = N_{\delta_R}\frac{g}{U_o}L_r - L_{\delta_R}\frac{g}{U_o}N_r$$

(III-68)

$$\frac{\phi(s)}{\delta_R(s)} = \frac{N_{(\phi/\delta_R)}}{D_2} = \frac{s(A_\phi s^2 + B_\phi s + C_\phi)}{D_2}$$

$$A_\phi = L_{\delta_R} + N_{\delta_R}A_1$$
$$B_\phi = Y_{\delta_R}^*(L_\beta + A_1N_\beta) - L_{\delta_R}(N_r + Y_v) + N_{\delta_R}(L_r - A_1Y_v)$$
$$C_\phi = -Y_{\delta_R}^*(L_rN_\beta + L_\beta N_r) + L_{\delta_R}(Y_vN_r + N_\beta) - N_{\delta_R}(L_\beta - Y_vL_r)$$

(III-69)

$$\frac{\psi(s)}{\delta_R(s)} = \frac{N_{(\psi/\delta_R)}}{D_2} = \frac{A_\psi s^3 + B_\psi s^2 + C_\psi s + D_\psi}{D_2}$$

$$A_\psi = N_{\delta_R} + B_1L_{\delta_R}$$
$$B_\psi = Y_{\delta_R}^*(N_\beta + B_1L_\beta) + L_{\delta_R}(N_p - B_1Y_v) - N_{\delta_R}(Y_v + L_p)$$
$$C_\psi = Y_{\delta_R}^*(L_\beta N_p - N_\beta L_p) - L_{\delta_R}Y_vN_p + N_{\delta_R}L_pY_v$$
$$D_\psi = \frac{g}{U_o}(L_{\delta_R}N_\beta - N_{\delta_R}L_\beta)$$

For the numerical analysis in this section, the data in Table III-6 are used.

Substituting the data from Table III-6 into (III-67), (III-68), and (III-69) yields:

(III-70)

$$\frac{\beta(s)}{\delta_R(s)} = 0.016\frac{(s - 0.00374)(s + 1.75)(s + 117.25)}{(s - 0.001355)(s + 1.777)(s^2 + 0.0912\,s + 3.525)}$$

$$\frac{\phi(s)}{\delta_R(s)} = 0.5744\frac{(s + 2.56)(s - 2.885)}{(s - 0.001355)(s + 1.777)(s^2 + 0.0912\,s + 3.525)}$$

$$\frac{\psi(s)}{\delta_R(s)} = -1.3584\frac{(s + 1.7767)(s^2 + 0.0033\,s + 0.08575)}{s(s - 0.001355)(s + 1.777)(s^2 + 0.0912s + 3.525)}$$

(III-70) are now arranged in the K G(s) form:

(III-71)

$$\frac{\beta(s)}{\delta_R(s)} = 1.049\frac{\left(\frac{s}{-0.00374} + 1\right)\left(\frac{s}{1.75} + 1\right)\left(\frac{s}{117.25} + 1\right)}{s\left(\frac{s}{-0.001355} + 1\right)\left(\frac{s}{1.777} + 1\right)\left(\frac{s^2}{\omega_{n_D}^2} + \frac{2\zeta_D}{\omega_{n_D}}s + 1\right)}$$

Altitude (ft.)		20,000
Weight (lbs.)		30,500
Mach Number		.638
True Airspeed (ft./sec.)		660
	Y_v	-.0829
	Y_{δ_R}	.0116
	L_β	-4.770
	L_p	-1.695
	L_r	.1776
	L_{δ_R}	.666
	L_{δ_A}	27.25
	N_p	-.0025
	N_r	-.0957
	N_{δ_R}	-1.383
	N_{δ_A}	-.615
	N_β	3.55
	$A_1 = \frac{I_{xz}}{I_{xx}}$	.0663
	$B_1 = \frac{I_{xz}}{I_{zz}}$	.0370

TABLE III-6

(III-72)

$$\frac{\varphi(s)}{\delta_R(s)} = 500\,\frac{\left(\frac{s}{2.561}+1\right)\left(\frac{s}{-2.885}+1\right)}{\left(\frac{s}{-0.001355}+1\right)\left(\frac{s}{1.777}+1\right)\left(\frac{s^2}{\omega_{n_D}^2}+\frac{2\zeta_D}{\omega_{n_D}}s+1\right)}$$

(III-73)

$$\frac{\psi(s)}{\delta_R(s)} = 24.35\,\frac{\left(\frac{s}{1.7767}+1\right)\left(\frac{s^2}{\omega_{n_1}^2}+\frac{2\zeta_1}{\omega_{n_1}}s+1\right)}{s\left(\frac{s}{-0.001355}+1\right)\left(\frac{s}{1.777}+1\right)\left(\frac{s^2}{\omega_{n_D}^2}+\frac{2\zeta_D}{\omega_{n_D}}s+1\right)}$$

where: $\omega_{n_1} = 0.293$ $\omega_{n_D} = 1.8775$
$\zeta_1 = 0.00563$ $\zeta_D = 0.0243$

In examining the analog traces, it must be kept in mind that each of these records the motion of the airframe in one degree of freedom; for instance, the β trace shows all the sideslip, i.e., the summation of the β motions of all three modes. And similarly, each mode will, in general, contribute to every trace; for example, the dutch roll impresses its oscillatory motion on the β, φ, and ψ trace. (The quantity $\dot{\psi}$, rather than ψ is recorded because it is $\dot{\psi}$ itself that enters the equations of motion.)

Figures III-40, III-41, and III-42 are Bode plots of (III-71), (III-72), and (III-73), respectively. Several conclusions can be drawn from inspection of these plots.

Since the amplitude ratios at the dutch roll natural frequency in Figures III-40, III-41, and III-42 are nearly equal, it may be concluded that comparable amplitudes of β, φ, and ψ occur in the dutch roll mode of the transient response when the airframe motion is excited by a rudder deflection.

From Figures III-40 and III-42, or from (III-71) and (III-73), it can be seen that the factor in the denominator which characterizes the rolling mode is almost exactly cancelled out by a numerator factor in these two relations.

From this it may be concluded that only relatively small amounts of ψ and β occur in the rolling mode. In other words, the rolling mode is almost totally composed of rolling motion. (This is, of course, the reason for calling it the rolling mode.)

The amplitude ratio at the spiral break point, ($\frac{1}{T}$), in Figure III-40 is much less than the amplitude ratios at the spiral break points in Figures III-41 and III-42. It may therefore be concluded that at any instant the magnitudes of ψ and φ in the divergent spiral mode are considerably greater than that of β. It follows that the spiral mode can be said to be composed mainly of roll and yaw.

Figure III-43 shows traces of the indicated variables obtained by an analog computer. The following facts can be determined from this figure: After the dutch roll oscillation has essentially died out, the roll angle, φ, diverges while the yaw rate, r, increases slightly in value; the sideslip angle, β, remains zero.

Since the divergent spiral is the only mode which remains after the roll subsidence and dutch roll modes have disappeared, it can be said that φ and r are the dominant degrees of freedom in the spiral mode. An increasing value of yaw rate, r, represents an increasing value of yaw angle, ψ. The divergent spiral mode is then composed mainly of increasing values of yaw and roll. This result agrees with the conclusion drawn from inspection of the Bode charts.

Figure III-43 also shows that the same order of magnitude of β, φ, and ψ occurs during the dutch roll. (It is sufficient to compute roughly the area under the curve of r during one-half the dutch roll period to get an approximation to the amount of yaw angle the exists at any given time.)

The rapid roll subsidence is indicated by the fact that the curve of the roll angle, φ, plotted against time, reaches an essentially constant mean value (except for the divergence due to the spiral) in a relatively short time. This effect is not evident in the curves for β and r. These facts verify the statement previously made that the rolling mode is composed principally of rolling motion.

The characteristic response of an airplane to an impulse rudder deflection can be summarized as follows: after the rudder is deflected, the airplane rapidly rolls, yaws, and sideslips. It then executes a damped oscillation in all three degrees of freedom (dutch roll). All during the oscillatory motion, the mean value of roll angle and yaw angle increases. This divergence continues even after the oscillatory mode has damped out. This latter motion is, of course, the spiral divergence.

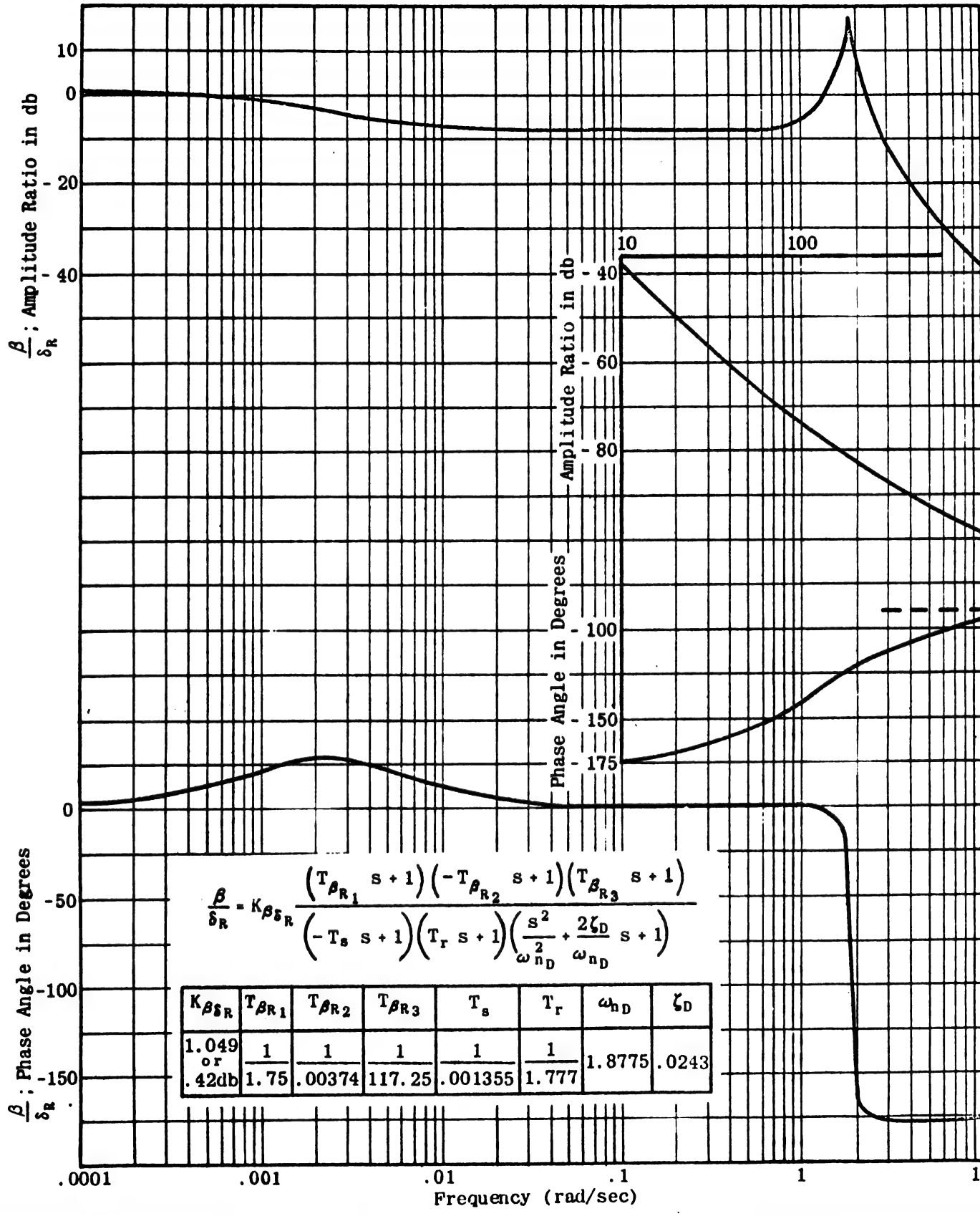

$$\frac{\beta}{\delta_R} = K_{\beta\delta_R} \frac{\left(T_{\beta_{R_1}} s + 1\right)\left(-T_{\beta_{R_2}} s + 1\right)\left(T_{\beta_{R_3}} s + 1\right)}{\left(-T_s s + 1\right)\left(T_r s + 1\right)\left(\frac{s^2}{\omega_{n_D}^2} + \frac{2\zeta_D}{\omega_{n_D}} s + 1\right)}$$

$K_{\beta\delta_R}$	$T_{\beta_{R_1}}$	$T_{\beta_{R_2}}$	$T_{\beta_{R_3}}$	T_s	T_r	ω_{n_D}	ζ_D
1.049 or .42db	1 / 1.75	1 / .00374	1 / 117.25	1 / .001355	1 / 1.777	1.8775	.0243

Figure III-40 Sideslip Angle Response to Rudder Deflection. Three Degree of Freedom

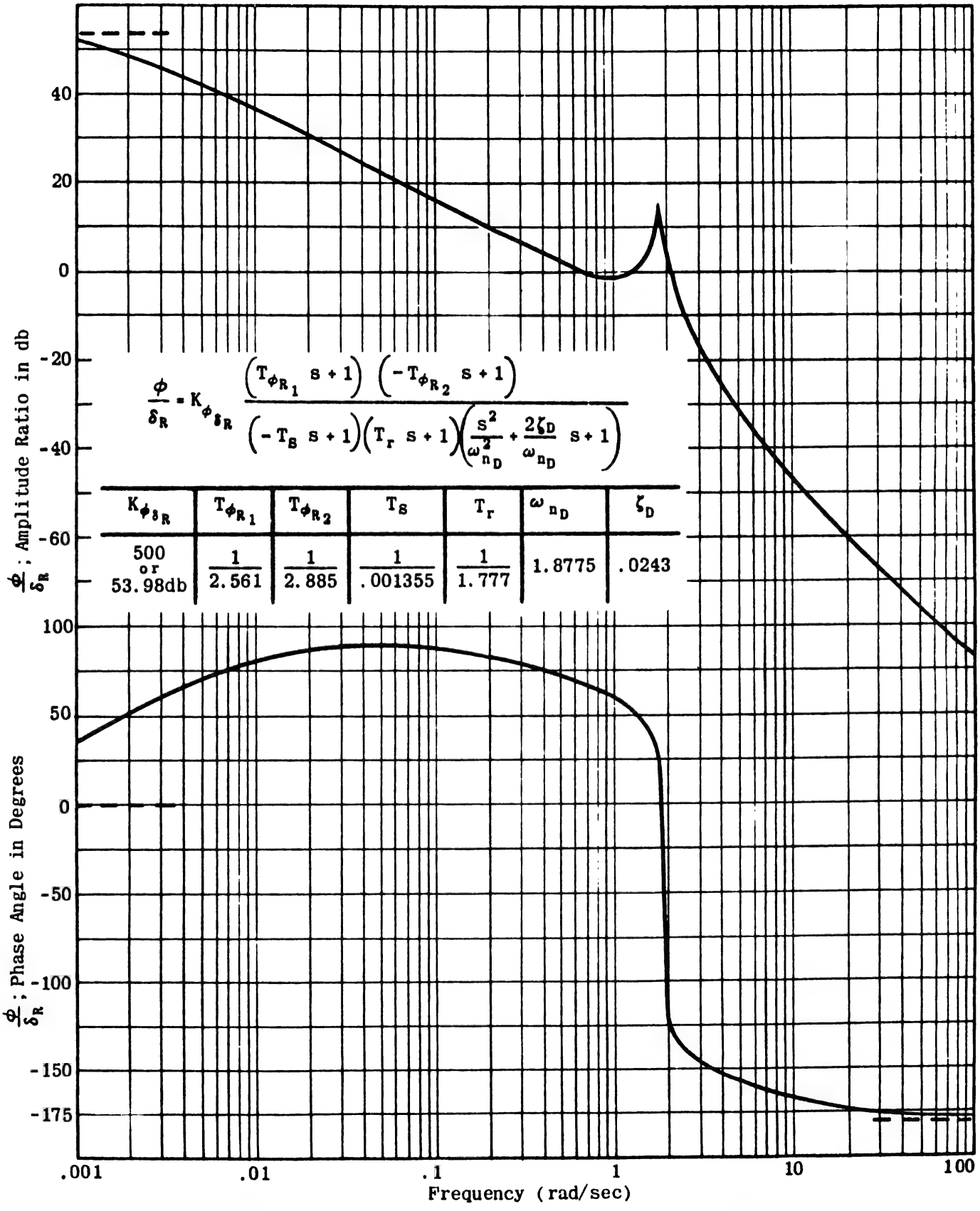

Figure III-41 Roll Angle Response to Rudder Deflection. Three Degree of Freedom

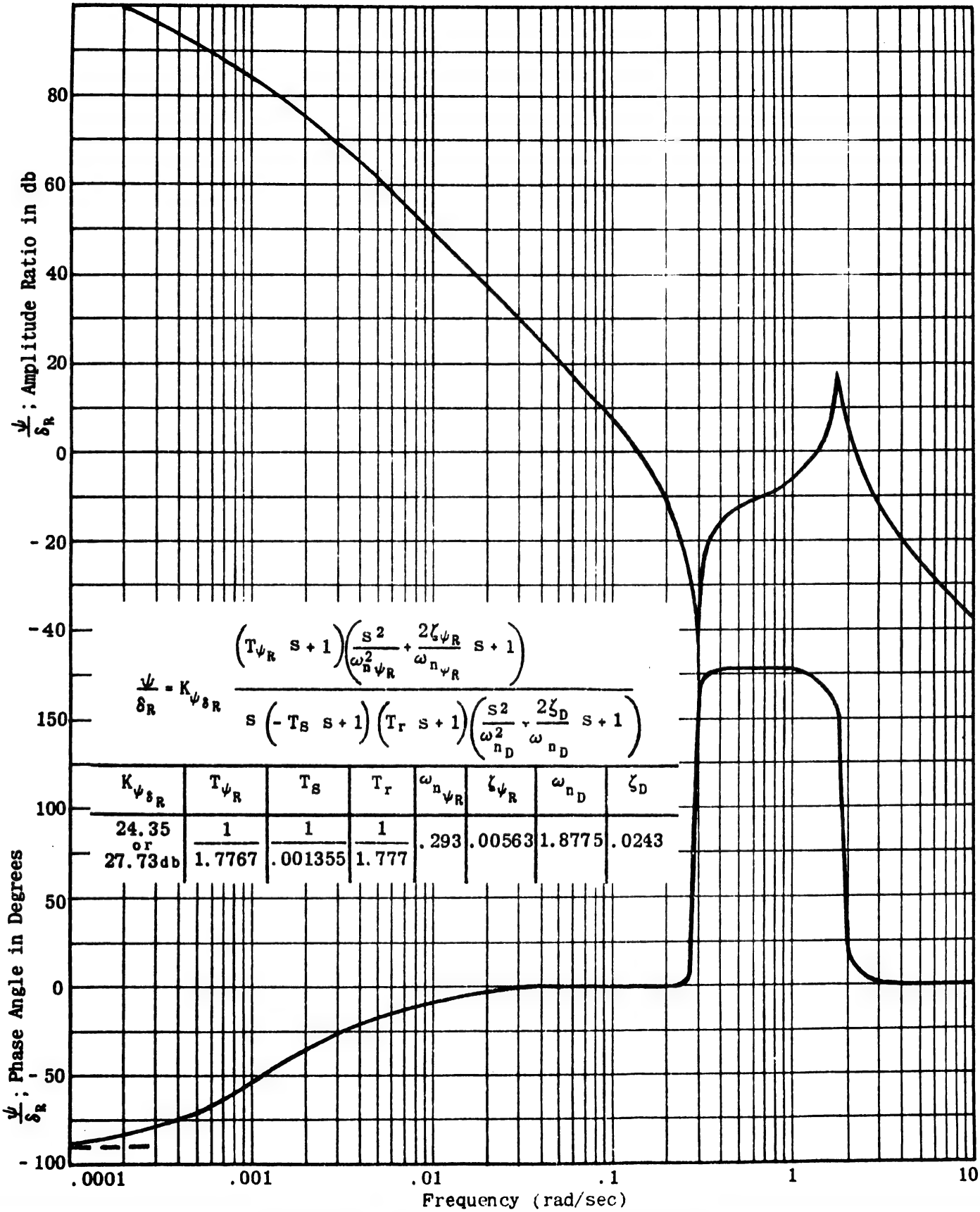

$$\frac{\psi}{\delta_R} = K_{\psi\delta_R} \frac{\left(T_{\psi_R}\, s + 1\right)\left(\frac{s^2}{\omega_{n\psi_R}^2} + \frac{2\zeta_{\psi_R}}{\omega_{n_{\psi_R}}}\, s + 1\right)}{s\left(-T_S\, s + 1\right)\left(T_r\, s + 1\right)\left(\frac{s^2}{\omega_{n_D}^2} + \frac{2\zeta_D}{\omega_{n_D}}\, s + 1\right)}$$

$K_{\psi\delta_R}$	T_{ψ_R}	T_S	T_r	$\omega_{n_{\psi_R}}$	ζ_{ψ_R}	ω_{n_D}	ζ_D
24.35 or 27.73db	$\frac{1}{1.7767}$	$\frac{1}{.001355}$	$\frac{1}{1.777}$	.293	.00563	1.8775	.0243

Figure III-42 Yaw Angle Response to Rudder Deflection. Three Degree of Freedom

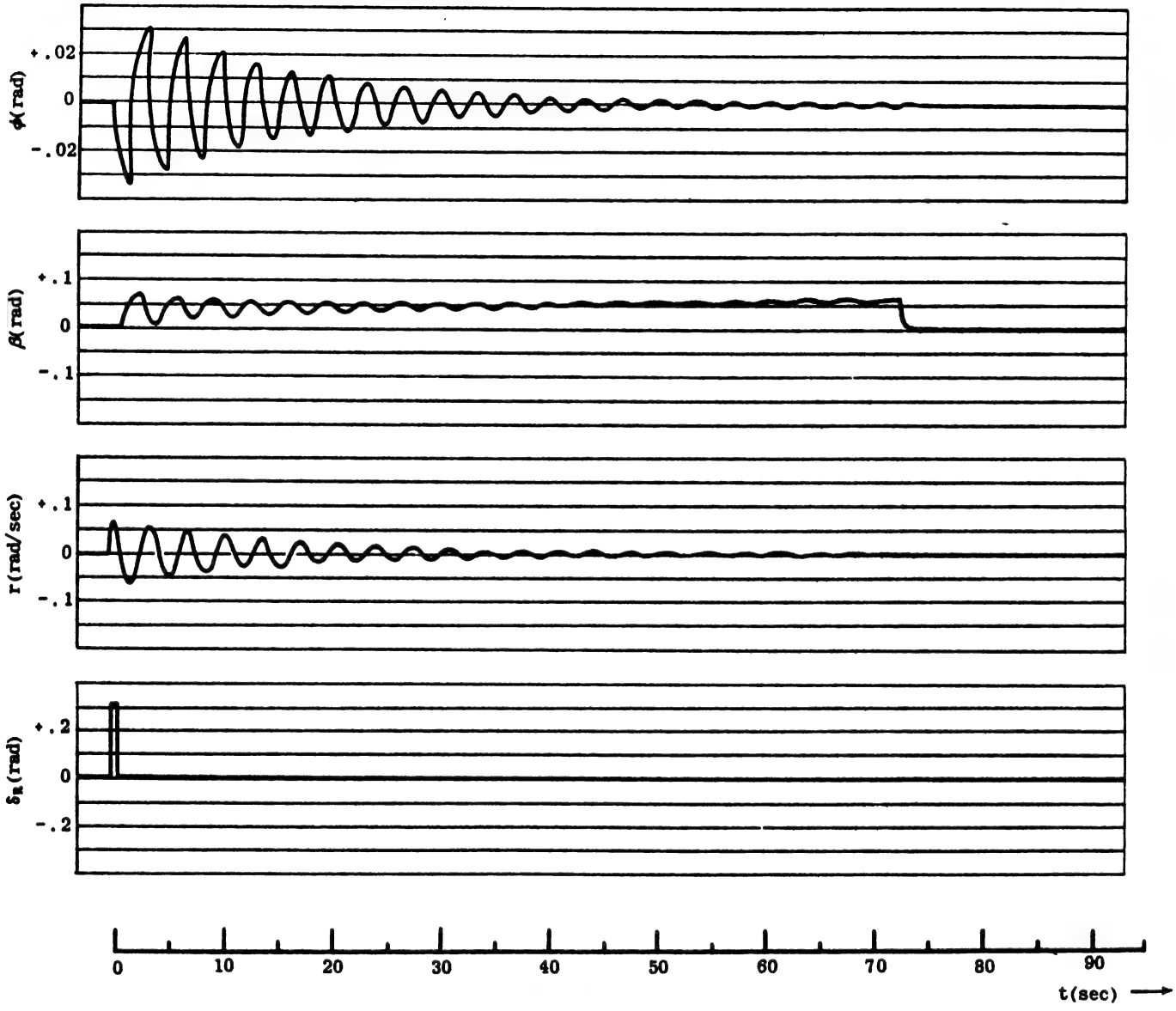

Figure III-43 Analog Computer Record of Time History for Pulse Rudder Deflection. Three Degree of Freedom

SECTION 12 – AIRPLANE RESPONSE TO AILERON DEFLECTION

It was mentioned in Chapter II that the transfer functions for rudder deflections can be altered to apply to aileron deflections merely by replacing δ_R by δ_A wherever δ_R appears; and by changing Y_{δ_R}, L_{δ_R}, and N_{δ_R} to Y_{δ_A}, L_{δ_A}, and N_{δ_A} respectively.

Making these changes and remembering that, according to Assumption X, $Y^*_{\delta_A} = 0$, the transfer functions (III-67), (III-68), and (III-69) become:

(III-74)

$$\frac{\beta(s)}{\delta_A(s)} = \frac{N_{(\beta/\delta_A)}}{D_2} = \frac{s(B_\beta s^2 + C_\beta s + D_\beta)}{D_2}$$

$$B_\beta = -L_{\delta_A} B_1 - N_{\delta_A}$$

$$C_\beta = L_{\delta_A}\left(\frac{g}{U_o} - N_p\right) + N_{\delta_A}\left(A_1 \frac{g}{U_o} + L_p\right)$$

$$D_\beta = N_{\delta_A} \frac{g}{U_o} L_r - L_{\delta_A} \frac{g}{U_o} N_r$$

(III-75)

$$\frac{\varphi(s)}{\delta_A(s)} = \frac{N_{(\phi/\delta_A)}}{D_2} = \frac{s(A_\phi s^2 + B_\phi s + C_\phi)}{D_2}$$

$$A_\phi = L_{\delta_A} + N_{\delta_A} A_1$$

$$B_\phi = -L_{\delta_A}(N_r + Y_v) + N_{\delta_A}(L_r - A_1 Y_v)$$

$$C_\phi = L_{\delta_A}(Y_v N_r + N_\beta) - N_{\delta_A}(+L_\beta - Y_v L_r)$$

(III-76)

$$\frac{\psi(s)}{\delta_A(s)} = \frac{N_{(\psi/\delta_A)}}{D_2} = \frac{s(A_\psi s^3 + B_\psi s^2 + C_\psi s + D_\psi)}{D_2}$$

$$A_\psi = N_{\delta_A} + B_1 L_{\delta_A}$$

$$B_\psi = L_{\delta_A}(N_p - B_1 Y_v) - N_{\delta_A}(Y_v + L_p)$$

$$C_\psi = -L_{\delta_A} Y_v N_p + N_{\delta_A} L_p Y_v$$

$$D = \frac{g}{U_o}(L_{\delta_A} N_\beta - N_{\delta_A} L_\beta)$$

Substituting the data from Table III-6 into (III-74), (III-75), and (III-76) yields:

(III-77)

$$\frac{\beta(s)}{\delta_A(s)} = -0.394 \frac{(s + 0.0495)(s - 6.250)}{(s - 0.001355)(s + 1.777)(s^2 + 0.0912s + 3.525)}$$

$$\frac{\varphi(s)}{\delta_A(s)} = 27.2 \frac{(s^2 + 0.01747\, s + 3.455)}{(s - 0.001355)(s + 1.777)(s^2 + 0.0912\, s + 3.525)}$$

$$\frac{\psi(s)}{\delta_A(s)} = 0.394 \frac{(s + 1.65)(s^2 - 4.398\, s + 7.07)}{s(s - 0.001355)(s + 1.777)(s^2 + 0.0912s + 3.525)}$$

(III-77) are now arranged in the K G(s) form:

(III-78)

$$\frac{\beta(s)}{\delta_A(s)} = -14.38 \frac{\left(\frac{s}{0.0495} + 1\right)\left(\frac{s}{-6.250} + 1\right)}{\left(\frac{s}{-0.001355} + 1\right)\left(\frac{s}{1.777} + 1\right)\left(\frac{s^2}{\omega^2_{n_D}} + \frac{2\zeta_D}{\omega_{n_D}} s + 1\right)}$$

(III-79)

$$\frac{\varphi(s)}{\delta_A(s)} = -11070 \frac{\left(\frac{s^2}{\omega^2_{n_2}} + \frac{2\zeta_2}{\omega_{n_2}} s + 1\right)}{\left(\frac{s}{-0.001355} + 1\right)\left(\frac{s}{1.777} + 1\right)\left(\frac{s^2}{\omega^2_{n_D}} + \frac{2\zeta_D}{\omega_{n_D}} s + 1\right)}$$

(III-80)

$$\frac{\psi(s)}{\delta_A(s)} = -543.7 \frac{\left(\frac{s}{1.65} + 1\right)\left(\frac{s^2}{\omega^2_{n_1}} + \frac{2\zeta_1}{\omega_{n_1}} s + 1\right)}{s\left(\frac{s}{-0.001355} + 1\right)\left(\frac{s}{1.777} + 1\right)\left(\frac{s^2}{\omega^2_{n_D}} + \frac{2\zeta_D}{\omega_{n_D}} s + 1\right)}$$

where: $\zeta_D = 0.0243$ $\quad \zeta_1 = -0.827$ $\quad \zeta_2 = 0.0047$

$\omega_{n_D} = 1.8775$ $\quad \omega_{n_1} = 2.659$ $\quad \omega_{n_2} = 1.871$

Figures III-44, III-45, and III-46 are Bode plots of (III-78), (III-79), and (III-80) respectively.

Examination of Figures III-44, III-45, and III-46 and equations (III-78), (III-79), and (III-80) leads to much the same conclusions that were drawn from the transfer functions and Bode plots for rudder deflection, with certain important exceptions.

Although (III-80) and Figure III-46 show that the roll root approximately cancels out of the $\frac{\psi}{\delta_A}$ transfer function as in the case of rudder deflection, there is no comparable cancellation of the roll root in the $\frac{\beta}{\delta_A}$ transfer function in (III-78). In addition, (III-79) or Figure III-45 shows that a numerator quadratic approximately cancels out the denominator quadratic representing the dutch roll mode in the $\frac{\varphi}{\delta_A}$ transfer function. These facts indicate that when the transient motion of the airplane is excited by an aileron deflection, there exists a relatively small amount of rolling in the dutch roll mode and some sideslip in the rolling mode. It has been shown that, in the case of rudder deflection, comparable magnitudes of β, ϕ, and ψ occur in the dutch roll mode, whereas the rolling mode consists of almost pure rolling motion.

It may then be concluded that the relative magnitudes of the degrees of freedom occurring in a particular mode of the transient response depend upon whether the transient is excited by an aileron or a rudder deflection. Further, in the case under consideration, there is a relatively smaller amount of ϕ in the dutch roll caused by aileron deflection than there is in that due to rudder deflection. (For instance, $\frac{\phi_{MAX}}{\beta_{MAX}}$ in the dutch roll due to aileron deflection will be smaller than $\frac{\phi_{MAX}}{\beta_{MAX}}$ in the dutch roll excited by rudder deflection.)

Figure III-47 shows the analog computer solution of the lateral equations of motion for an aileron pulse deflection. Comparison of Figure III-47 with Figure III-43 shows that the ratio of the maximum roll angle to the maximum sideslip angle in the dutch roll mode excited by aileron deflection is less than the similar ratio when the excitation is applied by deflecting the rudder.

This result should not be understood to be the general case; it should rather be considered an example of how transient characteristics maybe predicted from observation of the transfer function or Bode plot.

Even though there are certain differences in the transient motions for the lateral degrees of freedom, depending on which control surface is used to excite the transient, the ratios of the degrees of freedom in any of the modes are

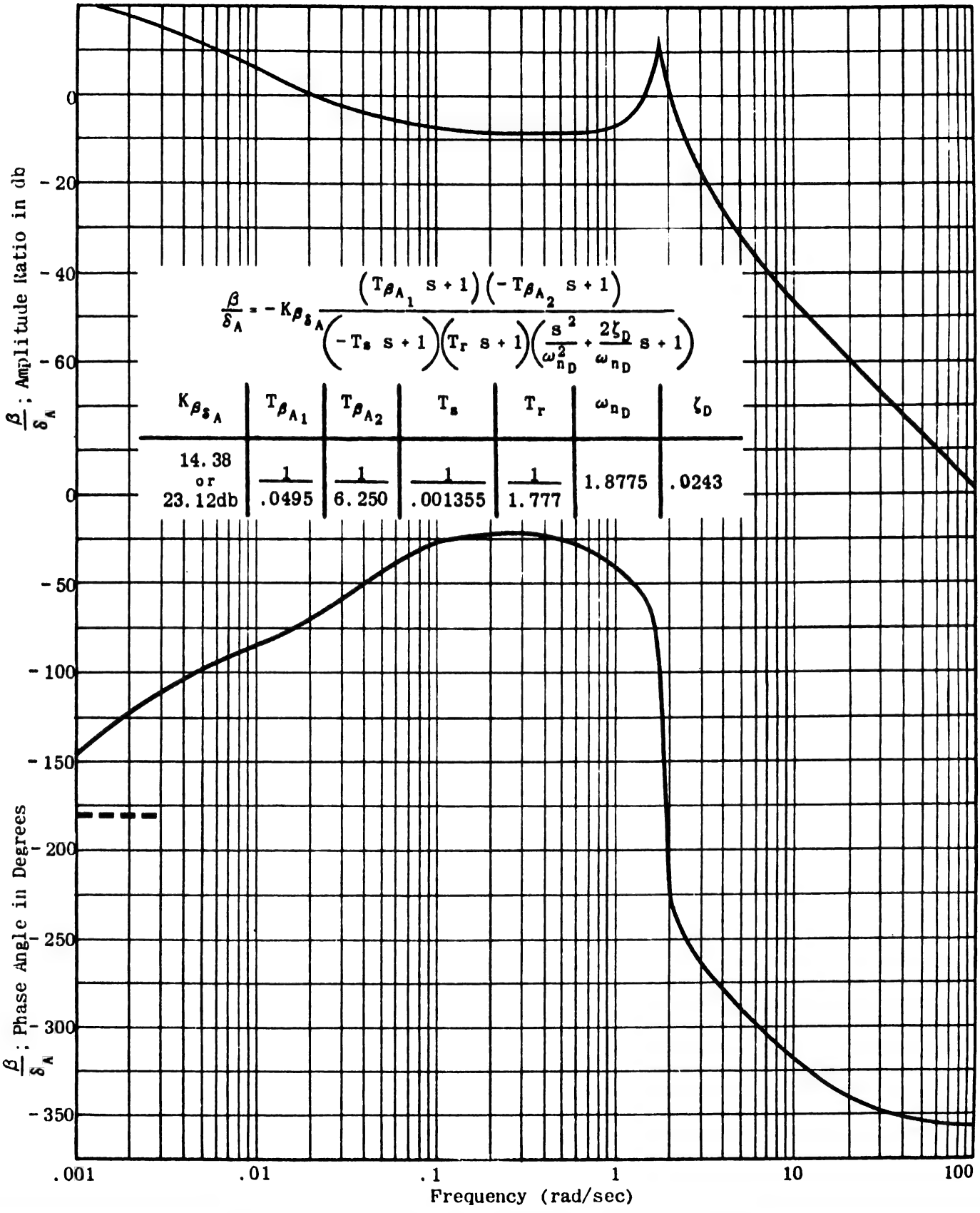

Figure III-44 Sideslip Angle Response To Aileron Deflection. Three Degree of Freedom

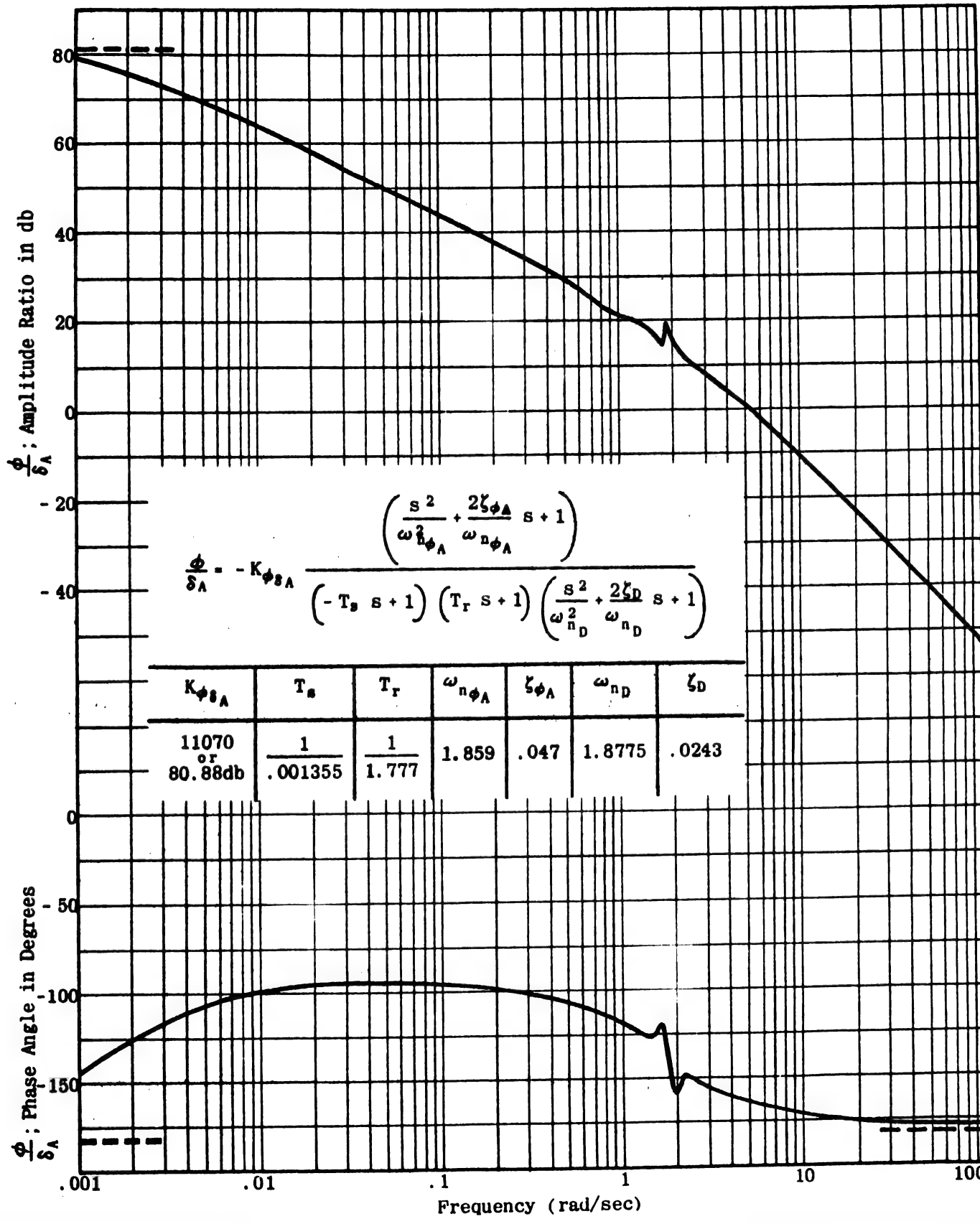

Figure III-45 Roll Angle Response to Aileron Deflection. Three Degree of Freedom

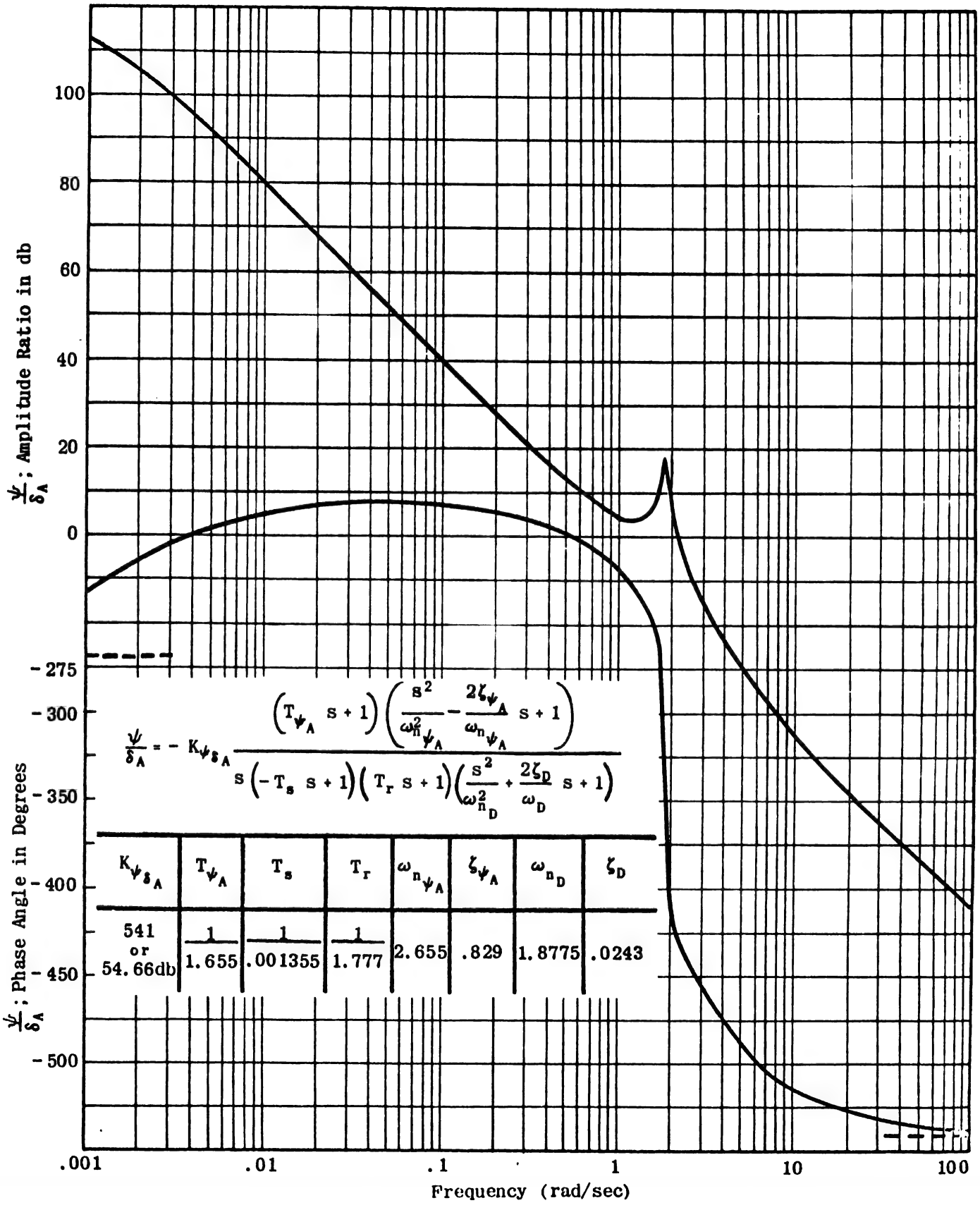

Figure III-46 Yaw Angle Response to Aileron Deflection. Three Degree of Freedom

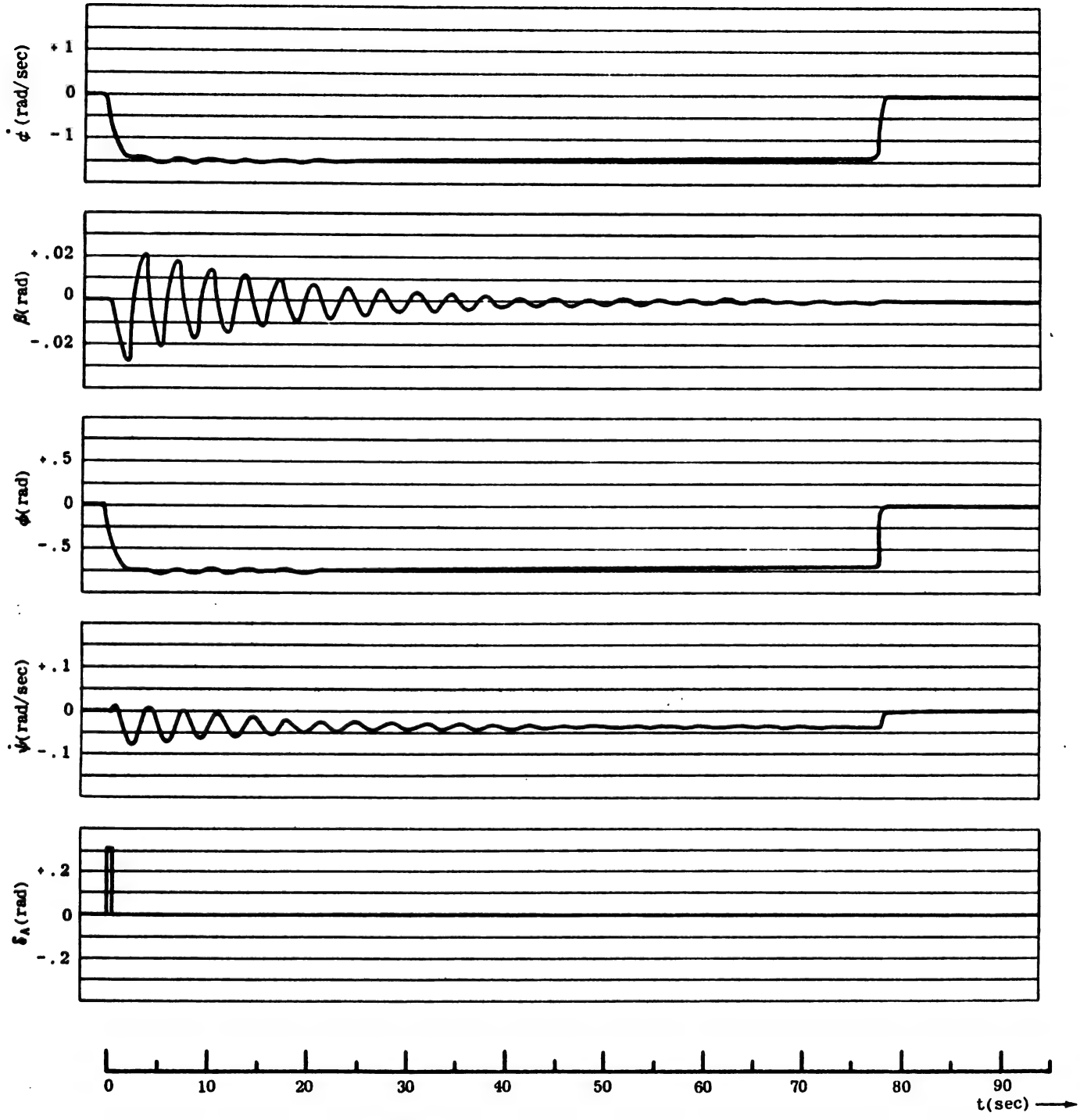

Figure III-47 Analog Computer Record of Time History for Pulse Aileron Deflection. Three Degree of Freedom

roughly the same.

In summary, the rolling mode is an almost pure rolling motion; the dutch roll mode contains roughly comparable amplitudes of rolling, yawing, and sideslip; and the spiral mode consists mostly of yawing and rolling.

SECTION 13 – APPROXIMATE TRANSFER FUNCTIONS

By taking into account the results of the above analysis, some useful approximate transfer functions can be determined.

Since the dutch roll mode approximately cancels out the $\frac{\phi}{\delta_A}$ transfer function, this mode is considered to consist solely of the sideslip and yaw degrees of freedom. Figures III-44 and III-46 show that the sideslip angle is approximately 180° out of phase with the yaw angle at the dutch roll natural frequency. This permits an additional simplification to be made by assuming that $\beta = -\psi$.

Under these assumptions, the dutch roll mode reduces to an oscillation during which the wings remain level and sideslip angle is equal but opposite in direction to the yaw angle, as shown in Figure III-48.

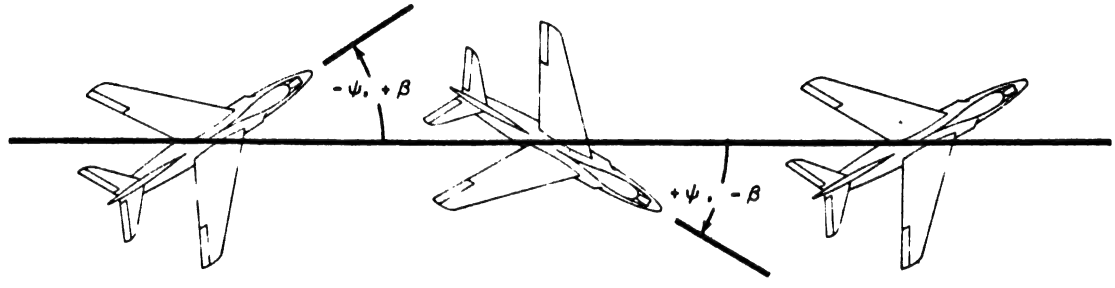

Figure III-48 One Degree of Freedom Dutch Roll

SECTION 14 – ONE DEGREE OF FREEDOM DUTCH ROLL MODE

A single degree of freedom approximation to the dutch roll mode of motion is now derived.

If, as stated above, this mode consists only of the sideslip and yaw degrees of freedom when it is excited by aileron deflection, the roll angle, ϕ, and its derivatives can be set equal to zero in the lateral equations (III-65) to arrive at this approximation. Further, since only the ailerons are to be used, δ_R may also be set equal to zero.

The relations (III-65) then become:

(III-81)

$$\dot{\beta} - Y_v\beta + \dot{\psi} = 0$$
$$-L_\beta\beta - (I_{xz}/I_{xx})\ddot{\psi} - L_r\dot{\psi} = L_{\delta_A}\delta_A$$
$$-N_\beta\beta + \ddot{\psi} - N_r\dot{\psi} = N_{\delta_A}\delta_A$$

The second of these relations can be eliminated from consideration by the fact that the roll angle and its derivatives, and therefore the sum of the rolling moments, must vanish.

When $\beta = -\psi$, the first equation of (III-81) becomes $-Y_v\beta = 0$ and is not applicable to the problem at hand.

The one degree of freedom approximation sought for must then arise from the third relation of (III-81). By substituting $\beta = -\psi$ into this equation and taking the Laplace transform:

$$(s^2 - N_r s + N_\beta)\,\beta(s) = -N_{\delta_A}\delta_A(s)$$

which leads to the approximate transfer function:

(III-82)

$$\frac{\beta(s)}{\delta_A(s)} = \frac{-N_{\delta_A}}{s^2 - N_r s + N_\beta}$$

Substituting numerical values from Table III-6 into (III-82) yields:

(III-83)

$$\frac{\beta(s)}{\delta_A(s)} = \frac{+0.615}{s^2 + 0.0957\,s + 3.55}$$

(III-84)

$$\frac{\beta(s)}{\delta_A(s)} = \frac{K}{\left(\frac{s^2}{\omega_n^2} + \frac{2\zeta}{\omega_n}s + 1\right)} = \frac{0.173}{\frac{s^2}{(1.883)^2} + \frac{2(0.0254)}{1.883}s + 1}$$

where: $\zeta = \dfrac{-N_r}{2\sqrt{N_\beta}} = 0.0254$

$\omega_n = \sqrt{N_\beta} = 1.883$

$K = -\dfrac{N_{\delta_A}}{N_\beta} = 0.173$

Figure III-49 shows the Bode plot of (III-84), and Figure III-50 shows the analog computer solution of the third

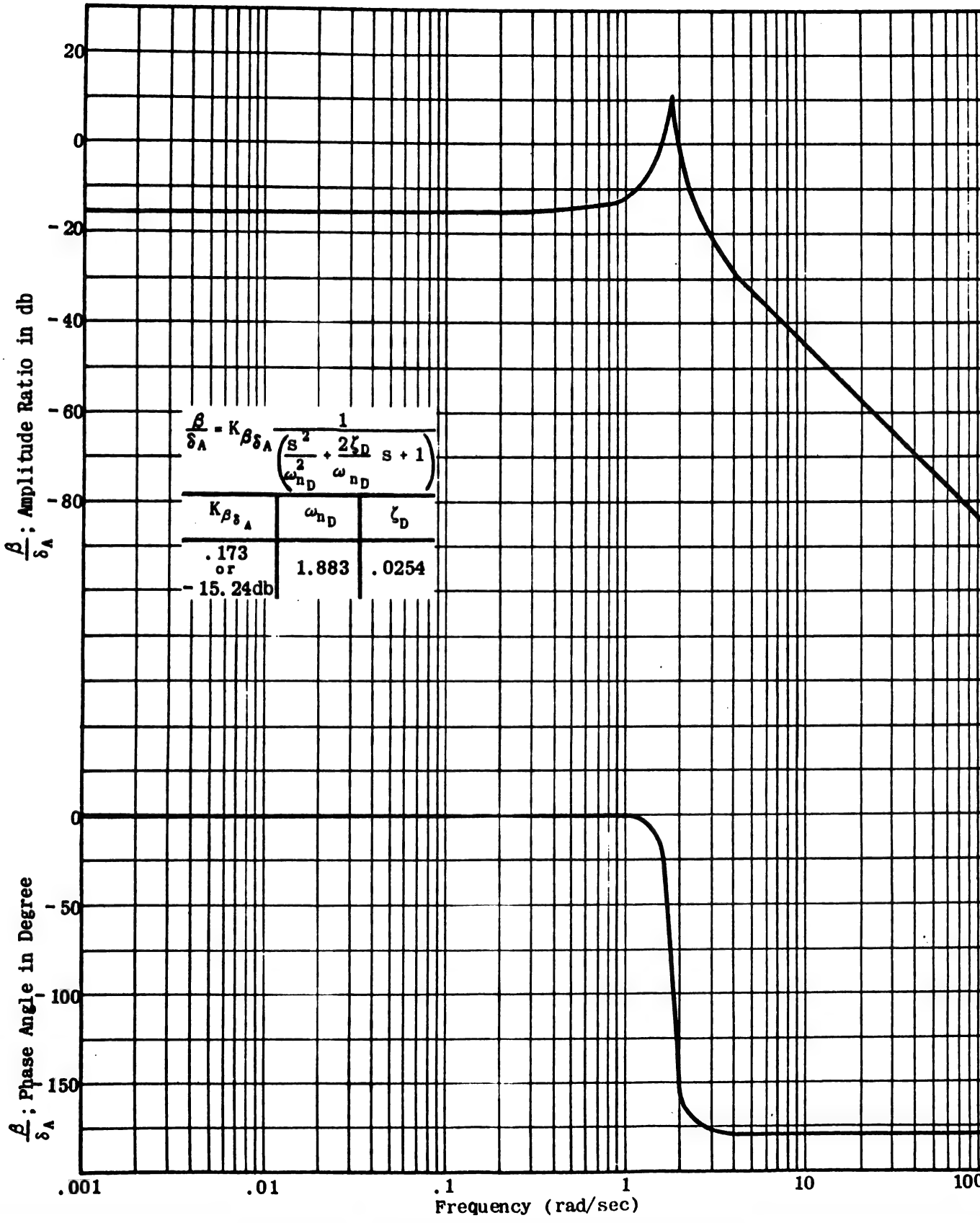

Figure III-49 Sideslip Angle Response to Aileron Deflection. One Degree of Freedom

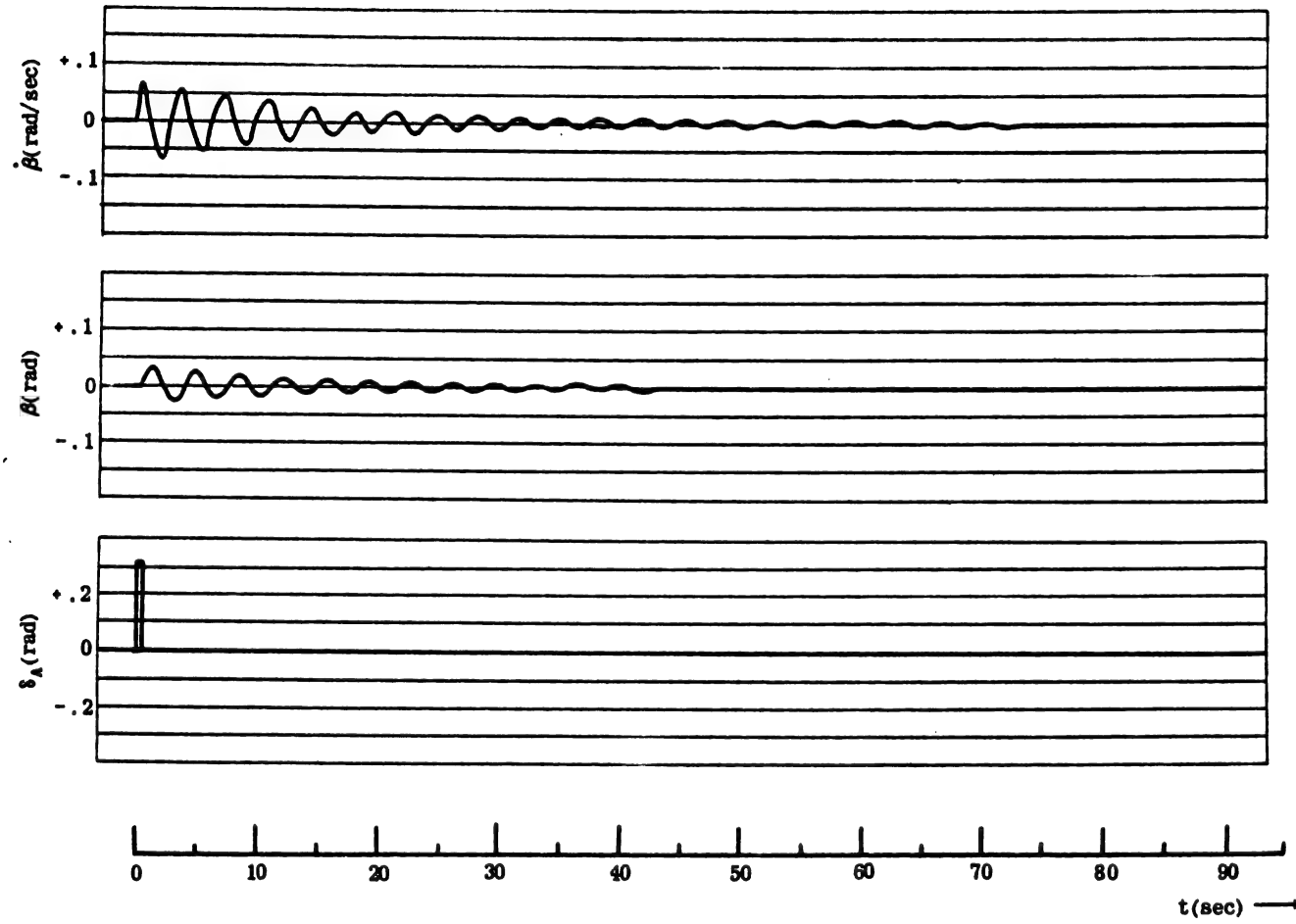

Figure III-50 Analog Computer Record of Time History for Pulse Aileron Deflection, One Degree of Freedom

equation of (III-81) with $\beta \rightarrow -\psi$, for an aileron pulse deflection.

To check the accuracy of the one degree of freedom approximation, three comparisons are made; the numerical values of the dampings and natural frequencies in (III-78) and (III-84) are compared; the Bode plots of Figures III-40 and III-49 are superimposed; and the analog computer traces of the one and three degree of freedom soultions are compared.

DUTCH ROLL MODE		
	ζ	ω_n (rad/sec)
One Degree of Freedom	.0254	1.833
Three Degree of Freedom	.0243	1.8775

Comparison of ζ and ω_n of one and three degree of Freedom Dutch Roll Mode

TABLE III-7

Table III-7 gives the values of ζ and ω_n for both the one and three degree of freedom cases. It can be seen that these values are very nearly the same.

In Figure III-51, the one degree of freedom $\frac{\beta}{\delta_A}$ transfer function (from Figure III-49) and three degree of freedom $\frac{\beta}{\delta_A}$ transfer function (from Figure III-44) are plotted. There is very good agreement in phase angle, natural frequency, and damping; but there is a considerable difference in amplitude ratio.

As a final check, the one and three degree of freedom solutions of the equations of motion from an analog computer are superimposed in Figure III-52. This figure shows that there is excellent agreement between the one and three degree of freedom solutions except for the amplitudes of the curves.

In summary, the one degree of freedom solution of the yawing moment equation is a very good approximation to the dutch roll mode. The approximation shows the dependence of dutch roll damping on the stability derivative N_r and the dependence of the dutch roll natural frequency on N'_β.

SECTION 15 – ONE DEGREE OF FREEDOM ROLLING MODE

A one degree of freedom approximation to the rolling mode is now developed.

Since the rolling mode consists almost entirely of rolling motion, the rolling moment equation with the sideslip angle and the yaw angle set equal to zero is used in the approximation.

(III-85) $$\dot{p} - L_p p = L_{\delta_A}\delta_A + L_{\delta_R}\delta_R$$

Only aileron deflection is considered; i.e., $\delta_R = 0$.

The transfer function for roll angle due to aileron deflection is:

(III-86) $$\frac{\phi(s)}{\delta_A(s)} = \frac{L_{\delta_A}}{s(s - L_p)}$$

Substituting numerical values of the stability derivatives into (III-86) yields:

(III-87) $$\frac{\phi(s)}{\delta_A(s)} = \frac{27.25}{s(s + 1.695)}$$

or, in the K G(s) form:

(III-88) $$\frac{\phi(s)}{\delta_A(s)} = \frac{16.1}{s\left(\frac{s}{1.695} + 1\right)}$$

Figure III-53 is the Bode plot of (III-88), and Figure III-54 is the analog computer solution of (III-85) for a pulse aileron deflection.

The magnitude of the roll root as given by the one degree of freedom approximation is very close to the exact value given in (III-79).

Figure III-55 consists of Figures III-53 and III-45 superimposed; similarly, Figure III-56 consists of Figures III-54 and III-47. Inspection of Figures III-55 and III-56 shows that there is very good agreement between the exact rolling mode and the one degree of freedom approximation. The conclusion that the rolling mode consists mainly of rolling motion appears to be valid for the case under consideration.

SECTION 16 – APPROXIMATE FACTORS OF LATERAL TRANSFER FUNCTIONS

As in the longitudinal case, the factors of the complete three degree of freedom lateral transfer functions cannot, in general, be expressed exactly in terms of the stability derivatives in any usable form.

In this section, approximate factors of the transfer functions, $\frac{\beta}{\delta_R}$, $\frac{\phi}{\delta_R}$, $\frac{\psi}{\delta_R}$, $\frac{\beta}{\delta_A}$, $\frac{\phi}{\delta_A}$, $\frac{\psi}{\delta_A}$, and $\frac{a_y}{\delta_R}$ and $\frac{a_y}{\delta_A}$, are presented.

An approximate factorization of the lateral characteristic equation can be developed in the following way.

The lateral characteristic equation is:

(III-89) $$D_2 = s(As^4 + Bs^3 + Cs^2 + Ds + E) = 0$$

Since the quantity in the parentheses generally factors into a quadratic and two first order roots, the characteristic equation can also be written as:

(III-90) $$D_2 = \underbrace{s\left(s + \frac{1}{T_s}\right)}_{\text{Spiral Mode}} \underbrace{\left(s + \frac{1}{T_R}\right)}_{\text{Rolling Mode}} \underbrace{\left(s^2 + 2\zeta_D\omega_{n_D}s + \omega_{n_D}^2\right)}_{\text{Dutch Roll Mode}}$$

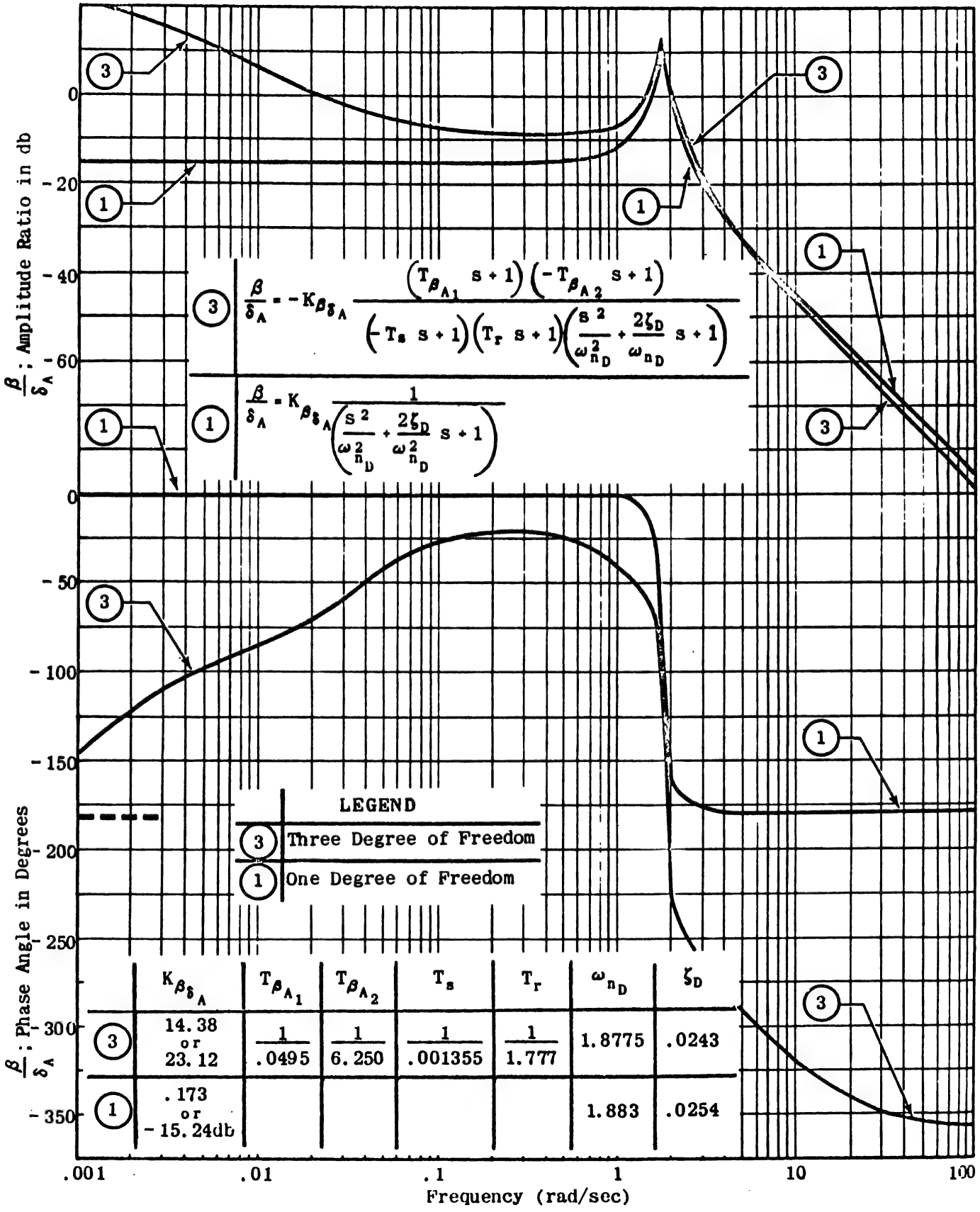

	$K_{\beta\delta_A}$	$T_{\beta_{A_1}}$	$T_{\beta_{A_2}}$	T_s	T_r	ω_{n_D}	ζ_D
3	14.38 or 23.12	1/.0495	1/6.250	1/.001355	1/1.777	1.8775	.0243
1	.173 or -15.24db					1.883	.0254

Figure III-51 Sideslip Angle Response to Aileron Deflection. One Degree of Freedom and Three Degree of Freedom Cases

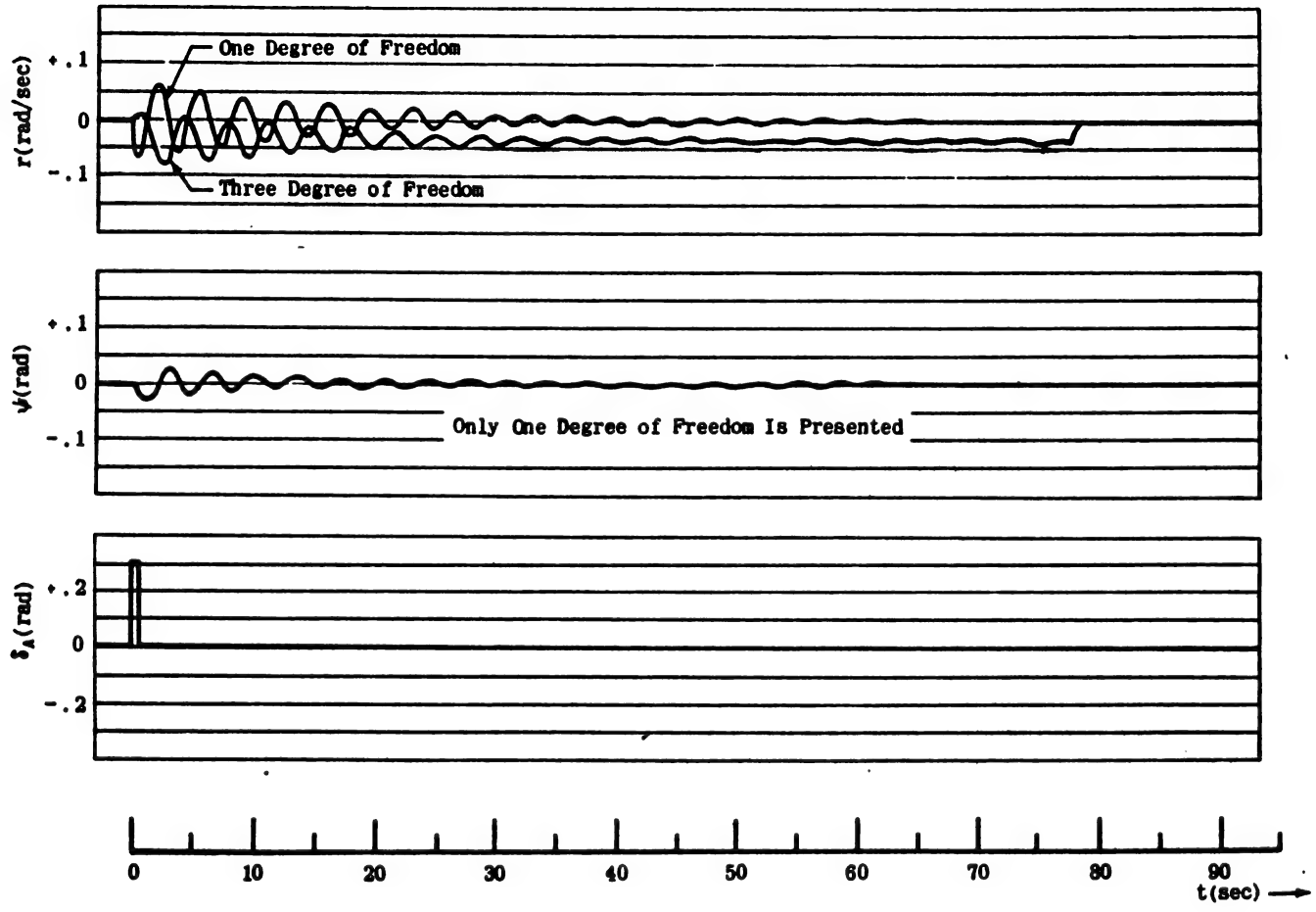

Figure III-52 Analog Computer Record of Time History for Pulse Aileron Deflection. One Degree of Freedom and Three Degree of Freedom Cases

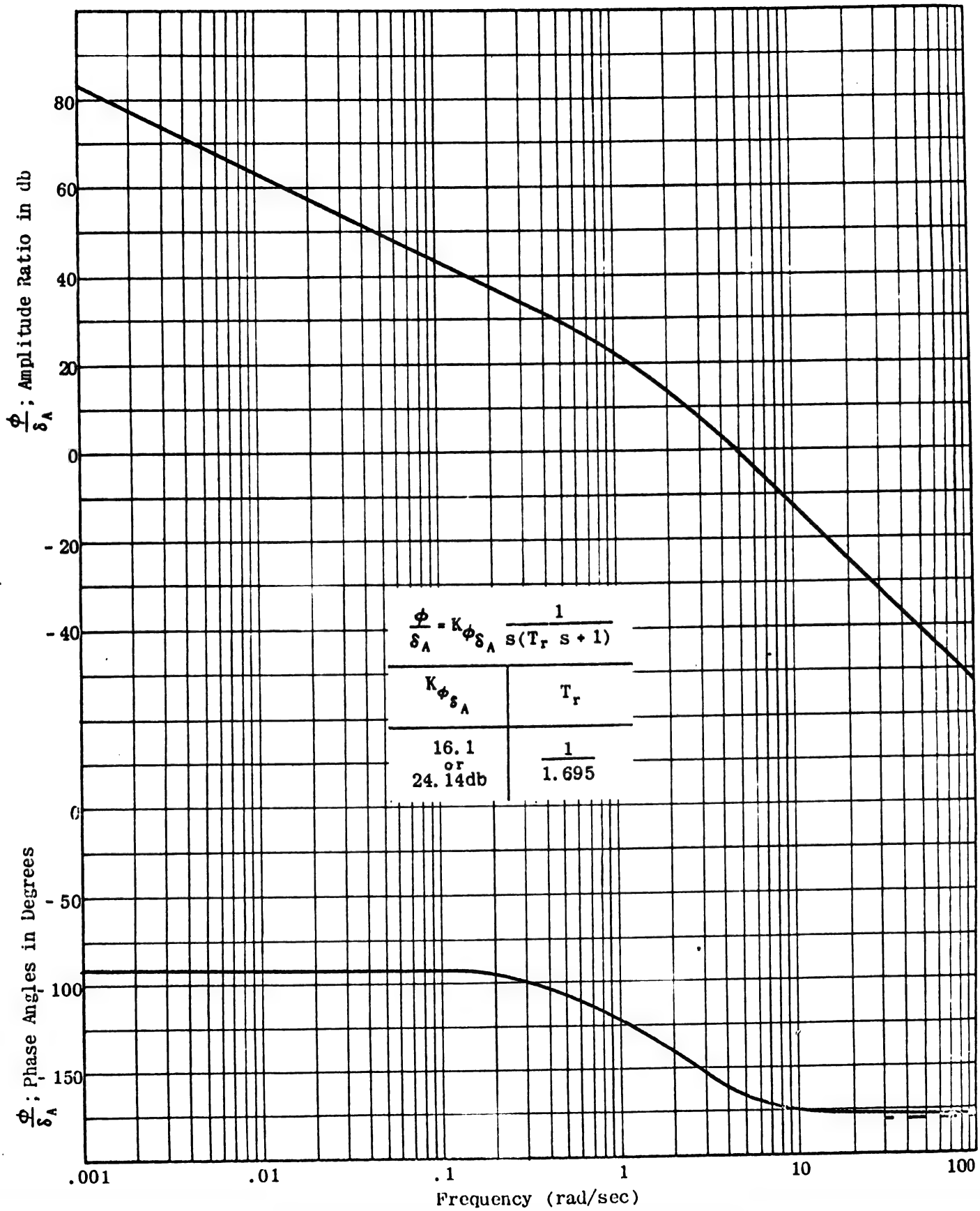

Figure III-53 Roll Angle Response to Aileron Deflection. One Degree of Freedom

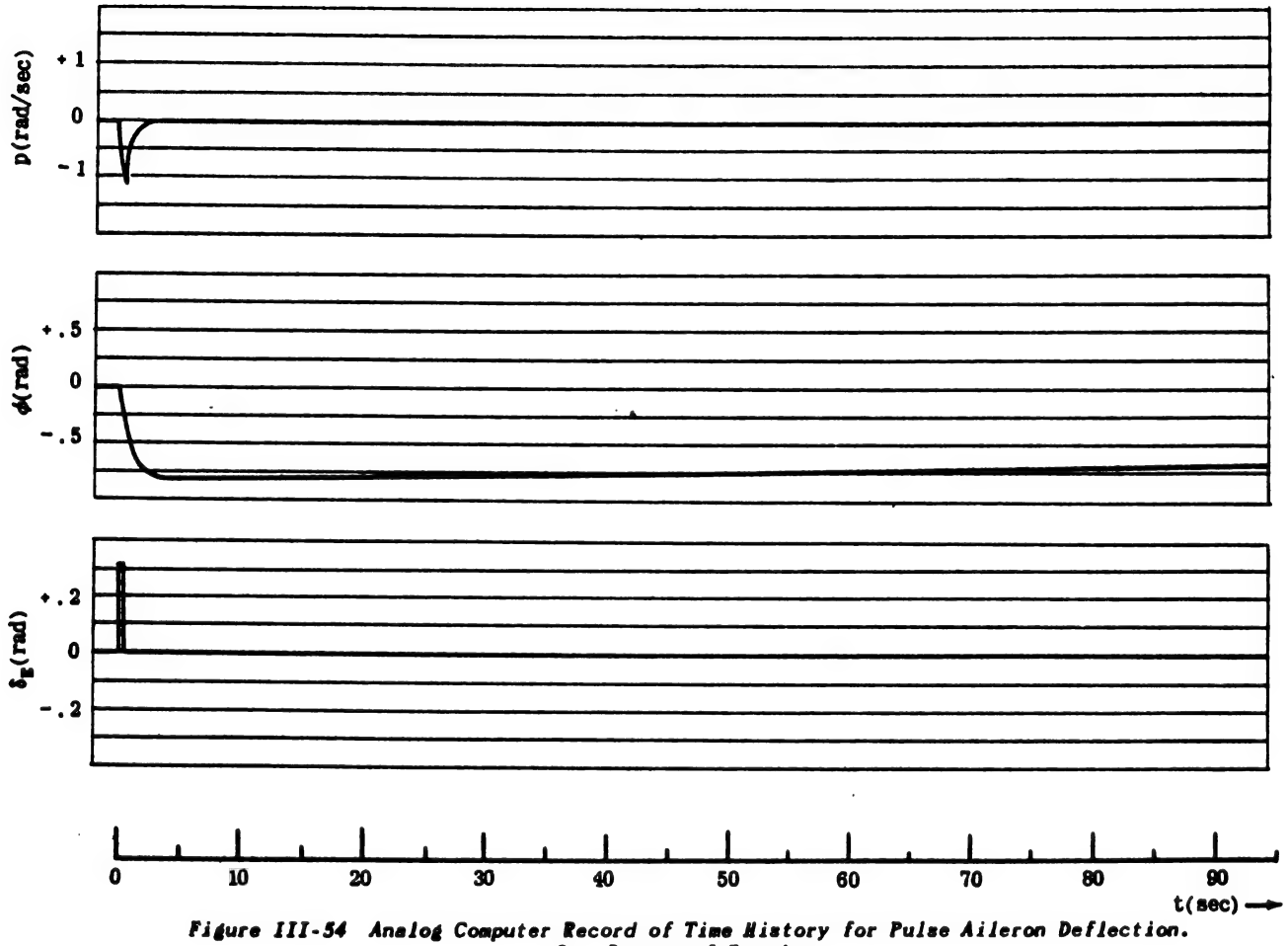

Figure III-54 Analog Computer Record of Time History for Pulse Aileron Deflection. One Degree of Freedom

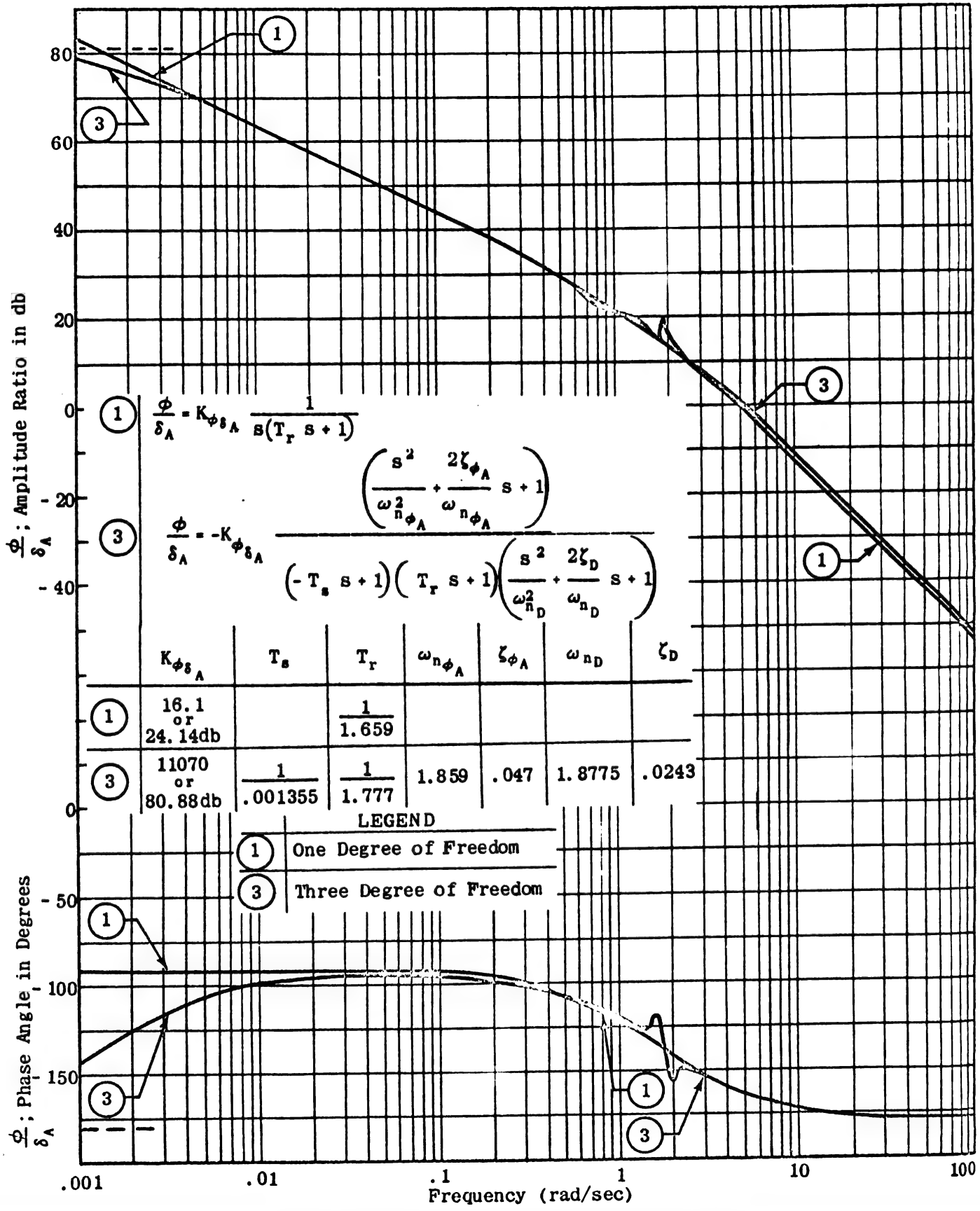

	$K_{\phi\delta_A}$	T_s	T_r	$\omega_{n\phi_A}$	ζ_{ϕ_A}	ω_{n_D}	ζ_D
1	16.1 or 24.14db		$\frac{1}{1.659}$				
3	11070 or 80.88db	$\frac{1}{.001355}$	$\frac{1}{1.777}$	1.859	.047	1.8775	.0243

Figure III-55 Roll Angle Response to Aileron Deflection. One Degree of Freedom and Three Degree of Freedom Cases

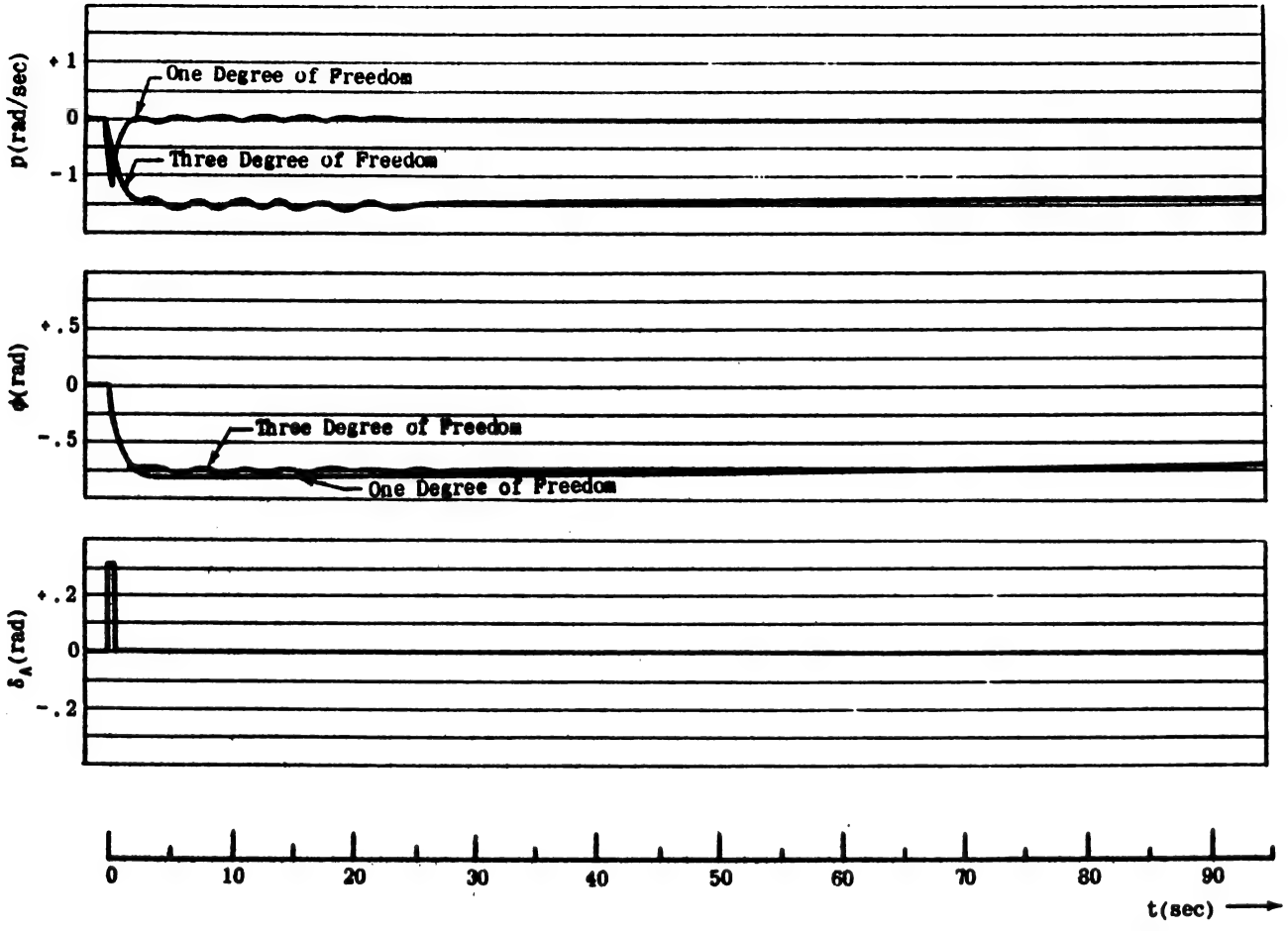

Figure III-56 Analog Computer Record of Time History for Pulse Aileron Deflection. One Degree of Freedom and Three Degree of Freedom Superimposed.

AIRFRAME APPROXIMATE COEFFICIENTS AND FACTORS—LATERAL TRANSFER FUNCTIONS*

$$\frac{\beta}{\delta_A} = \frac{N_{(\beta/\delta_A)}}{D_2} \; ; \; \frac{\phi}{\delta_A} = \frac{N_{(\phi/\delta_A)}}{D_2} \; ; \; \frac{\psi}{\delta_A} = \frac{N_{(\psi/\delta_A)}}{D_2} \; ;$$

$$\frac{\beta}{\delta_R} = \frac{N_{(\beta/\delta_R)}}{D_2} \; ; \; \frac{\phi}{\delta_R} = \frac{N_{(\phi/\delta_R)}}{D_2} \; ; \; \frac{\psi}{\delta_R} = \frac{N_{(\psi/\delta_R)}}{D_2} \; ; \; \frac{a_Y}{\delta_R} = \frac{N_{(a_Y/\delta_R)}}{D_2}$$

*ASSUMPTIONS USED: LEVEL FLIGHT CONDITIONS

$$L_x = L_z = Y_p = Y_R = Y_{\delta_A} = \gamma_o = \alpha_o = 0$$

D_2 :

$$D_2 = s(As^4 + Bs^3 + Cs^2 + Ds + E)$$

$$D_2 = K_{D_2}(-T_s s + 1)(T_r s + 1)\left(\frac{s^2}{\omega_{n_2}^2} + 2\frac{\zeta_2}{\omega_{n_2}} s + 1\right)(s)$$

$$A \cong 1$$
$$B \cong -(Y_v + L_p + N_r)$$
$$C \cong N_\beta$$
$$D \cong -Y_v(L_pN_r) - L_pN_\beta - L_\beta g/U_o$$
$$E \cong (g/U_o)(L_\beta N_r - L_r N_\beta)$$

$$K_{D_2} \cong (g/U_o)(L_\beta N_r - L_r N_\beta)$$

$$T_s \cong \frac{Y_v(L_pN_r) + L_pN_\beta + L_\beta g/U_o}{(g/U_o)(L_\beta N_r - L_r N_\beta)}$$

$$T_r \cong \frac{N_\beta}{-Y_v(L_pN_r) - L_pN_\beta - L_\beta g/U_o}$$

$$\omega_{n_2} \cong \sqrt{N_\beta}$$

$$\zeta_2 \cong \frac{-(Y_v + L_p + N_r) - (1/T_r) + (1/T_s)}{2\sqrt{N_\beta}}$$

$\frac{\beta}{\delta_A}$: $N_{(\beta/\delta_A)} = s\left(A_\beta s^2 + B_\beta s + C_\beta\right)$

$$A_\beta \cong -\left(L_{\delta_A}\frac{I_{xz}}{I_{xx}} + N_{\delta_A}\right)$$

$$B_\beta \cong (N_{\delta_A}L_p - L_{\delta_A}N_p) + L_{\delta_A}g/U_o$$

$$C_\beta \cong (N_{\delta_A}L_r - L_{\delta_A}N_r)g/U_o$$

$$N_{(\beta/\delta_A)} \cong K_\beta s(T_{\beta_{a_1}} s + 1)(T_{\beta_{a_2}} s + 1)$$

** $K_\beta = (N_{\delta_A}L_r - L_{\delta_A}N_r)g/U_o$

$$T_{\beta_{a_1}} = \frac{L_{\delta_A} + (N_{\delta_A}L_p - L_{\delta_A}N_p)U_o/g}{(N_{\delta_A}L_r - L_{\delta_A}N_r)}$$

$$T_{\beta_{a_2}} = -\frac{N_{\delta_A} + L_{\delta_A}I_{xz}/I_{xx}}{(N_{\delta_A}L_p - L_{\delta_A}N_p) + L_{\delta_A}g/U_o}$$

** DIVIDE BY K_{D_2} TO OBTAIN COMPLETE D.C. GAIN OF THE TRANSFER FUNCTION (THIS APPLIES TO ALL THE FACTORED NUMERATOR EQUATIONS)

$\frac{\beta}{\delta_R}$: $N_{(\beta/\delta_R)} \cong s(A'_\beta s^3 + B'_\beta s^2 + C'_\beta s + D'_\beta)$

$$A'_\beta \cong Y_{\delta_R}$$

$$B'_\beta \cong -N_{\delta_R}$$

$$C'_\beta \cong N_{\delta_R}L_p$$

$$D'_\beta \cong \frac{g}{U_o}(N_{\delta_R}L_r - L_{\delta_R}N_r)$$

$$N_{(\beta/\delta_R)} \cong K'_\beta s(T_{\beta_{r_1}} s + 1)(T_{\beta_{r_2}} s + 1)(T_{\beta_{r_3}} s + 1)$$

$$K'_\beta = \frac{g}{U_o}(N_{\delta_R}L_r - L_{\delta_R}N_r)$$

$$T_{\beta_{r_1}} = \frac{U_o}{g}\left(\frac{N\delta_R\ L_p}{N_{\delta_R} - L_{\delta_R}N_r}\right)$$

$$T_{\beta_{r_2}} = -\frac{1}{L_p}$$

$$T_{\beta_{r_3}} = -\frac{Y_{\delta_R}}{N_{\delta_R}}$$

$\frac{\phi}{\delta_A}$: $N_{(\phi/\delta_A)} = s(A_\phi s^2 + B_\phi s + C_\phi) = A_\phi s(s^2 + B'_\phi + C'_\phi)$

$$A_\phi \cong L_{\delta_A}$$

$$B_\phi \cong -(N_r + Y_v)$$

$$C_\phi \cong N_\beta$$

$$N_{(\phi/\delta_A)} \cong K_\phi\left(\frac{s^2}{\omega_{n_3}^2} + 2\frac{\zeta_3}{\omega_{n_3}} s + 1\right)$$

$$K_\phi = N_\beta L_{\delta_A}$$

$$\zeta_3 = \frac{-(N_r + Y_v)}{2\sqrt{N_\beta}}$$

$$\omega_{n_3} = \sqrt{N_\beta}$$

TABLE III-8 (Sheet 1 of 2 Sheets)

$\frac{\phi}{\delta_R}$:

$$N_{(\phi/\delta_R)} = s(A_\phi s^2 + B_\phi s + C_\phi)$$

$$A_\phi \simeq N_{\delta_R}\frac{I_{xz}}{I_{xx}} + L_{\delta_R}$$

$$B_\phi \simeq Y_{\delta_R}L_\beta + N_{\delta_R}L_r + L_{\delta_A}(-N_r - Y_v)$$

$$C_\phi \simeq L_{\delta_R}N_\beta - N_{\delta_R}L_\beta$$

$$N_{(\phi/\delta_R)} \simeq K_\phi s(T_{\phi_{r_1}}s + 1)(T_{\phi_{r_2}}s + 1)$$

$$K_\phi = L_{\delta_R}N_\beta - N_{\delta_R}L_\beta$$

$$T_{\phi_{r_1}} = \frac{2L_{\delta_R}}{N_{\delta_R}L_r - 2L_{\delta_R}\sqrt{\frac{N_{\delta_R}L_\beta - L_{\delta_R}N_\beta}{L_{\delta_R} + N_{\delta_R}(I_{xz}/I_{xx})}}}$$

$$T_{\phi_{r_2}} = \frac{2L_{\delta_R}}{N_{\delta_R}L_r + 2L_{\delta_R}\sqrt{\frac{N_{\delta_R}L_\beta - L_{\delta_R}N_\beta}{L_{\delta_R} + N_{\delta_R}(I_{xz}/I_{xx})}}}$$

$\frac{\psi}{\delta_A}$:

$$N_{(\psi/\delta_A)} = A_\psi s^3 + B_\psi s^2 + C_\psi s + D_\psi$$

$$A_\psi \simeq N_{\delta_A} + L_{\delta_A}\frac{I_{xz}}{I_{xz}}$$

$$B_\psi \simeq -N_{\delta_A}L_p$$

$$C_\psi \simeq Y_v(N_{\delta_A}L_p - L_{\delta_A}N_p)$$

$$D_\psi \simeq L_{\delta_A}N_\beta\frac{g}{U_o}$$

$\frac{\psi}{\delta_R}$

$$N_{(\psi/\delta_R)} \simeq K_\psi(T_{\psi_r}s + 1)\left(\frac{s^2}{\omega_{n_\delta}^2} + 2\frac{\zeta_\delta}{\omega_{n_\delta}}s + 1\right)$$

$$K_\psi = \frac{g}{U_o}(L_{\delta_R}N_\beta - L_\beta N_{\delta_R})$$

$$T_{\psi_r} = -1/L_p$$

$$\omega_{n_\delta} = \sqrt{\frac{(g/U_o)(L_{\delta_R}N_\beta - N_{\delta_R}L_\beta)}{-L_pN_{\delta_R}}}$$

$$\zeta_\delta = \frac{L_p(N_{\delta_R}Y_v - Y_{\delta_R}N_\beta) + \frac{g}{U_o}\frac{(L_{\delta_R}N_\beta - N_{\delta_R}L_\beta)}{L_p}}{2\sqrt{(-N_{\delta_R}L_p)(g/U_o)(L_{\delta_R}N_\beta - N_{\delta_R}L_\beta)}}$$

$\frac{a_y}{\delta_R}$:

$$N\left(a_y/\delta_R\right) = s\left(A_{a_y}s^4 + B_{a_y}s^3 + C_{a_y}s^2 + D_{a_y}s + E_{a_y}\right) \simeq K_{a_y}s\left(-T_{a_{y_{r_1}}}s + 1\right)\left(T_{a_{y_{r_2}}}s + 1\right)\left(T_{a_{y_{r_3}}}s + 1\right)\left(-T_{a_{y_{r_4}}}s + 1\right)$$

$$A_{a_y} \simeq U_oY_{\delta_R}$$

$$B_{a_y} \simeq -L_pU_oY_{\delta_R}$$

$$C_{a_y} \simeq U_o(Y_{\delta_R}N_\beta - Y_vN_{\delta_R})$$

$$D_{a_y} \simeq U_oL_p(Y_vN_{\delta_R} - Y_{\delta_R}N_\beta) - gY_{\delta_R}L_\beta$$

$$E_{a_y} \simeq gY_v(N_{\delta_R}L_r - L_{\delta_R}N_r) + gY_{\delta_R}(L_\beta N_r - L_rN_\beta)$$

$$K_{a_y} = U_oL_p(Y_vN_{\delta_R} - Y_{\delta_R}N_\beta) + gY_{\delta_R}(L_\beta N_r - L_rN_\beta)$$

$$T_{a_{y_{r_1}}} = \frac{U_o}{g}\left[\frac{L_p(Y_vN_{\delta_R} - Y_{\delta_R}N_\beta)}{L_R(Y_vN_{\delta_R} - Y_{\delta_R}N_\beta) + N_r(Y_{\delta_R}L_\beta - Y_vL_{\delta_R})}\right]$$

$$T_{a_{y_{r_2}}} = -\frac{1}{L_p}$$

$$T_{a_{y_{r_3}}} \simeq T_{a_{y_{r_4}}} \simeq \sqrt{\frac{Y_{\delta_R}}{N_{\delta_R}Y_v - Y_{\delta_R}N_\beta}}$$

TABLE III - 8 (Sheet 2 of 2 Sheets)

Multiplying together the last three factors on the right of (III-90) yields:

$$(III\text{-}91)\quad D_2 = s\left\{s^4 + \left[2\zeta_D\omega_{n_D} + \frac{1}{T_s} + \frac{1}{T_R}\right]s^3 + \left[\frac{1}{T_s}\frac{1}{T_R} + 2\zeta_D\omega_{n_D}\left(\frac{1}{T_s} + \frac{1}{T_R}\right) + \omega_{n_D}^2\right]s^2 + \left[2\zeta_D\omega_{n_D}\frac{1}{T_s}\frac{1}{T_R} + \omega_{n_D}^2\left(\frac{1}{T_s} + \frac{1}{T_R}\right)\right]s + \omega_{n_D}^2\frac{1}{T_s}\frac{1}{T_R}\right\}$$

Since the right sides of (III-89) and (III-91) must be identically the same, the coefficients of like powers of s in them can be equated:

$$(III\text{-}92)\quad A = 1$$
$$B = 2\zeta_D\omega_{n_D} + \frac{1}{T_s} + \frac{1}{T_R}$$
$$C = \frac{1}{T_s}\frac{1}{T_R} + 2\zeta_D\omega_{n_D}\left(\frac{1}{T_s} + \frac{1}{T_R}\right) + \omega_{n_D}^2$$
$$D = 2\zeta_D\omega_{n_D}\frac{1}{T_s}\frac{1}{T_R} + \omega_{n_D}^2\left(\frac{1}{T_s} + \frac{1}{T_R}\right)$$
$$E = \frac{1}{T_s}\frac{1}{T_R}\omega_{n_D}^2$$

Both $\frac{1}{T_s}$ and ζ_D are generally very small in comparison with either of $\frac{1}{T_R}$ and ω_{n_D}, which are of the same order of magnitude. In view of this fact, the following assumptions can be made:

$$(III\text{-}93)\quad \omega_{n_D}^2 >> \frac{1}{T_s}\frac{1}{T_R} + 2\zeta_D\omega_{n_D}\left(\frac{1}{T_s} + \frac{1}{T_R}\right)$$
$$\omega_{n_D}^2\frac{1}{T_R} >> \omega_{n_D}^2\frac{1}{T_s} + 2\zeta_D\omega_{n_D}\frac{1}{T_s}\frac{1}{T_R}$$

(III-92) then reduce to:

$$(III\text{-}94)\quad A \approx 1$$
$$B \approx 2\zeta_D\omega_{n_D} + \frac{1}{T_R} + \frac{1}{T_s}$$
$$C \approx \omega_{n_D}^2$$
$$D \approx \omega_{n_D}^2\frac{1}{T_R}$$
$$E \approx \omega_{n_D}^2\frac{1}{T_s}\frac{1}{T_R}$$

(III-94) can now be used to express ζ_D, ω_{n_D}, $\frac{1}{T_s}$, and $\frac{1}{T_R}$ as functions of the coefficients of the quartic in (III-89):

$$(III\text{-}95)\quad \frac{1}{T_s} \approx \frac{E}{D} \qquad \frac{1}{T_R} \approx \frac{D}{C}$$
$$\omega_{n_D} \approx \sqrt{C}$$
$$\zeta_D \approx \frac{B - \frac{E}{D} - \frac{D}{C}}{2\sqrt{C}} \approx \frac{B - \frac{1}{T_s} - \frac{1}{T_R}}{2\omega_{n_D}}$$

The coefficients A through E of the stability quartic, (III-89), can be simplified by neglecting relatively small stability derivatives, and combinations of them, in the expressions following (III-66). The results are:

$$(III\text{-}96)\quad A \approx 1 \qquad C \approx N_\beta$$
$$B \approx -Y_v - L_p - N_r \qquad D \approx -Y_v L_p N_r - L_p N_\beta - \frac{g}{U_o}L_\beta$$
$$E \approx -\frac{g}{U_o}(N_\beta L_r - L_\beta N_r)$$

Expressed in terms of the combinations of stability derivatives given in (III-96), (III-95) become:

$$(III\text{-}97)\quad \frac{1}{T_s} \approx \frac{g/U_o\,(N_\beta L_r - L_\beta N_r)}{Y_v L_p N_r + L_p N_\beta + g/U_o L_\beta}$$
$$\frac{1}{T_R} \approx \frac{Y_v L_p N_r + L_p N_\beta + g/U_o L_\beta}{-N_\beta}$$
$$\omega_{n_D} \approx \sqrt{N_\beta} \qquad \zeta_D \approx \frac{-Y_v - L_p - N_r - \frac{1}{T_R} - \frac{1}{T_s}}{2\sqrt{N_\beta}}$$

Approximate factors have also been derived for each of the numerators of the lateral transfer functions. As in the longitudinal case, checking these approximate factors with the exact factors of transfer functions of a conventional cruciform configuration airplane at a variety of flight conditions has yielded reasonably good agreement. The approximate factors are summarized in Table III-8.

SECTION 17 - LATERAL ACCELERATION TRANSFER FUNCTION

The lateral acceleration that would be recorded by an accelerometer mounted at the center of gravity of an airframe and aligned with the Y axis is given by the first relation of (III-65), here rewritten as:

$$(III\text{-}98)\quad \dot{\beta} - \frac{g}{U_o}\phi + r = Y^*_{\delta_R}\delta_R + Y_v\beta$$

From this:

$$(III\text{-}99)\quad a_y = U_o\left(\dot{\beta} + r - \frac{g}{U_o}\phi\right) = U_o\left(Y_v\beta + Y^*_{\delta_R}\delta_R\right)$$

In (III-99), $U_o(\dot{\beta} + r)$ is the acceleration sensed by the accelerometer because the airframe is in accelerated motion, and $-g\phi$ is the acceleration sensed by the accelerometer because of the component of gravity which acts along the Y axis when the wings of the airframe are not level.

The transfer function $\frac{a_y}{\delta_R}$ is:

$$(III\text{-}100)\quad \frac{a_y(s)}{\delta_R(s)} = U_o Y_v\frac{\beta(s)}{\delta_R(s)} + U_o Y^*_{\delta_R}$$

Expressing the relation (III-100) in terms of the stability derivatives yields:

$$(III\text{-}101)\quad \frac{a_y(s)}{\delta_R(s)} = \frac{s\left(A_{a_y}s^4 + B_{a_y}s^3 + C_{a_y}s^2 + D_{a_y}s + E_{a_y}\right)}{D_2}$$

where

$$A_{a_y} = U_o Y^*_{\delta_R} (1 - A_1 B_1)$$

$$B_{a_y} = U_o Y^*_{\delta_R} (-L_p - N_r - A_1 N_p - B_1 L_r)$$

$$C_{a_y} = U_o Y^*_{\delta_R} \left[N_\beta + L_p N_r - N_p L_r + Y_v B_1 L_\beta\right] + U_o Y_v \left[-L_{\delta_R} B_1 - N_{\delta_R}\right]$$

$$D_{a_y} = U_o Y^*_{\delta_R} \left[-N_\beta \left(L_p + A_1 \frac{g}{U_o}\right) + N_p L_\beta - L_\beta \frac{g}{U_o}\right] + U_o Y_v \left[L_{\delta_R} \left(\frac{g}{U_o} - N_p\right) + N_{\delta_R} \left(A_1 \frac{g}{U_o} + L_p\right)\right]$$

$$E_{a_y} = g\left\{Y^*_{\delta_R} \left[(L_\beta N_r - N_\beta L_r) + Y_v \left(N_{\delta_R} L_r - L_{\delta_R} N_r\right)\right]\right\}$$

(III-101), numerically evaluated for the flight condition in Table III-6, becomes:

(III-102)

$$\frac{a_y(s)}{\delta_R(s)} = \frac{7.637(s+0.000725)(s+1.705)(s+2.551)(s-2.468)}{(s-.001355)(s+1.777)(s^2+.0912s+3.525)}$$

and, in the KG(s) form, becomes:

(III-103)

$$\frac{a_y(s)}{\delta_R(s)} = 700 \frac{\left(\frac{s}{.000725}+1\right)\left(\frac{s}{1.705}+1\right)\left(\frac{s}{2.551}+1\right)\left(\frac{-s}{2.468}+1\right)}{\left(\frac{-s}{.001355}+1\right)\left(\frac{s}{1.777}+1\right)\left(\frac{s^2}{1.877^2}+2\frac{(0.0243)}{1.877}s+1\right)}$$

Figure III-57 is the Bode plot of (III-103).

SECTION 18 – EFFECT OF SINGLE DIMENSIONAL STABILITY DERIVATIVE VARIATION

In this section, the effects of variations in individual stability derivatives on the natural frequencies and damping ratios of the lateral equations are discussed.

Some comments were made in Section III-8 concerning methods of obtaining such variations physically and on the significance of the results obtained from this type of analysis. The material contained in Section III-8 should therefore be read before that presented here.

The values of the stability derivatives for the base case used in the following analyses are contained in Table III-9.

Altitude (ft)	0	N_r	-.0937
Weight (lbs)	38,100	N_p	-.00616
Mach Number	.6	L_β	-4.706
True Airspeed (ft/sec)	669.7	N_β	3.5581
$A_1 = I_{xz}/I_{xx}$	.0358	Y_v	-.1327
$B_1 = I_{xz}/I_{zz}$	.0259	Y_p	-.00009
L_r	.2485	Y_r	.0012
L_p	-1.7605		

Table III-9

The approximate factors of the lateral characteristic equation are rewritten below for convenience in reference:

(III-104)
$$\frac{1}{T_s} \approx \frac{\frac{g}{U_o}\left(N_\beta L_r - L_\beta N_r\right)}{Y_v L_p N_r + L_p N_\beta + \frac{g}{U_o} L_\beta}$$

(III-105)
$$\frac{1}{T_R} \approx -\frac{Y_v L_p N_r + L_p N_\beta + \frac{g}{U_o} L_\beta}{N_\beta}$$

(III-106)
$$\omega_{n_D} \approx \sqrt{N_\beta}$$

(III-107)
$$\zeta_D \approx \frac{-Y_v - L_p - N_r - \frac{1}{T_s} - \frac{1}{T_R}}{2\sqrt{N_\beta}}$$

Figure III-58 shows that the effects on the lateral frequencies and damping ratios of varying Y_v through values in the vicinity of the base value, $Y_v = -0.1327$, are negligible; except that ζ_D, the dutch roll damping ratio, takes on larger positive values as Y_v becomes more negative. (III-107) shows that this variation in Y_v is to be expected. The quantity Y_v also occurs in the numerator of the expression for $\frac{1}{T_R}$, (III-105), and in the denominator of that for $\frac{1}{T_s}$, (III-104); but the Y_v term is much smaller than those containing L_β and N_β in these expressions, and hence the effects of variations in Y_v on $\frac{1}{T_R}$ and $\frac{1}{T_s}$ are unimportant. Since, in addition, ω_{n_D} is not a function of Y_v, moderate variations in Y_v are appreciably reflected only in ζ_D.

Figure III-59 shows the effect of Y_p which is generally a very small number and consequently does not appear in the approximate factors. Y_p also is not very amenable to artificial variation. It has been included here for the sake of completeness.

Figure III-60 shows the effect of Y_r which, like Y_p, is generally a very small number and therefore does not appear in the approximate factors, but it is somewhat more susceptible to artificial variation. As Y_r becomes more negative, the dutch roll natural frequency increases in Y_r cause the dutch roll to split into two real roots, one of which is divergent.

The effects of changing L_β are indicated by the curves in Figure III-61, which contains plots of: $\frac{1}{T_R}$, the reciprocal of the roll time constant; $\frac{1}{T_s}$, the reciprocal of the spiral time constant; ζ_D, the dutch roll damping ratio; and ω_{n_D}, the dutch roll natural frequency, as functions of L_β.

It is shown by this figure that as L_β moves in the negative direction, $\frac{1}{T_R}$ and $\frac{1}{T_s}$ both increase, but that ζ_D tends to move toward more negative values. It can be seen that ω_{n_D} does not depend upon L_β.

These variations with L_β are confirmed by examination of the relations which set forth the approximations to these parameters, (III-104) through (III-107).

(III-105) shows that the approximation to $\frac{1}{T_R}$ should increase as L_β becomes more negative, since the quantity $-(g/U_o)/L_\beta$ is a positive number increasing in magnitude when L_β is negative and its numerical value increases.

(III-104) can be used to show that the behavior of $\frac{1}{T_s}$, as L_β moves in the negative direction, is similar to that of $\frac{1}{T_R}$. L_β occurs in both the numerator and the denomina-

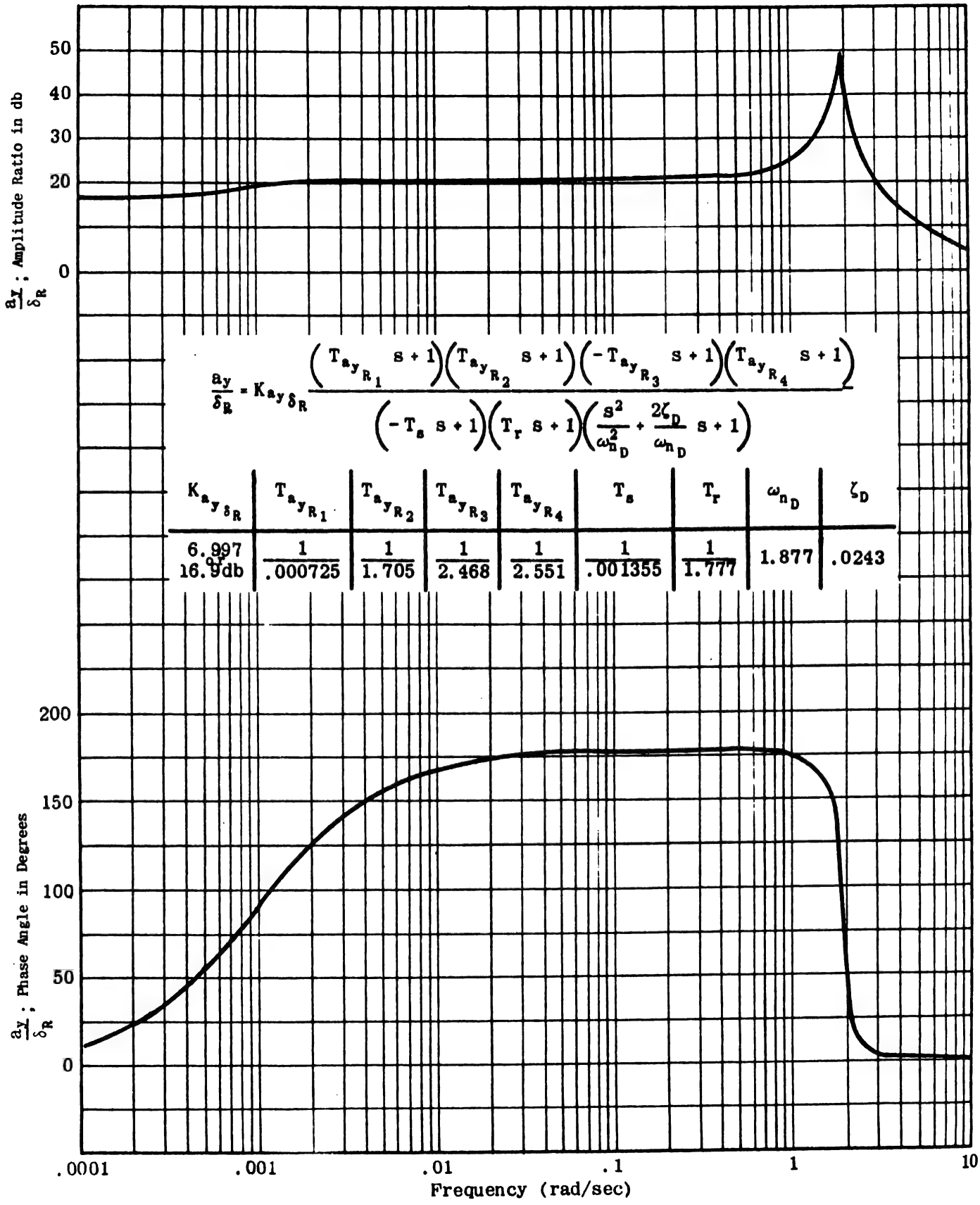

Figure III-57 Side Acceleration Response to Rudder Deflection. Three Degree of Freedom

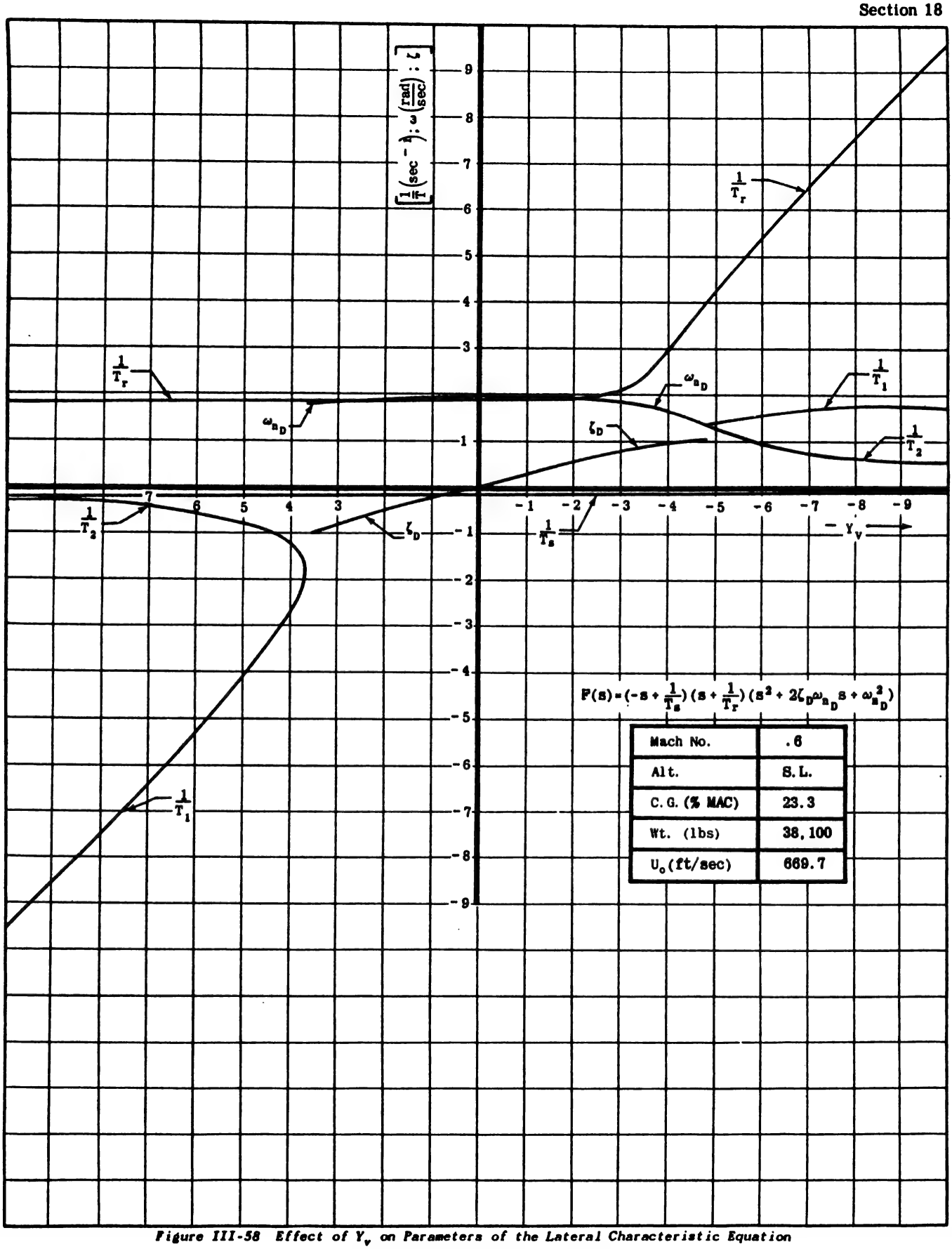

Mach No.	.6
Alt.	S.L.
C.G. (% MAC)	23.3
Wt. (lbs)	38,100
U_o (ft/sec)	669.7

Figure III-58 Effect of Y_v on Parameters of the Lateral Characteristic Equation

Base Case Equation ($Y_v = -.1327$)

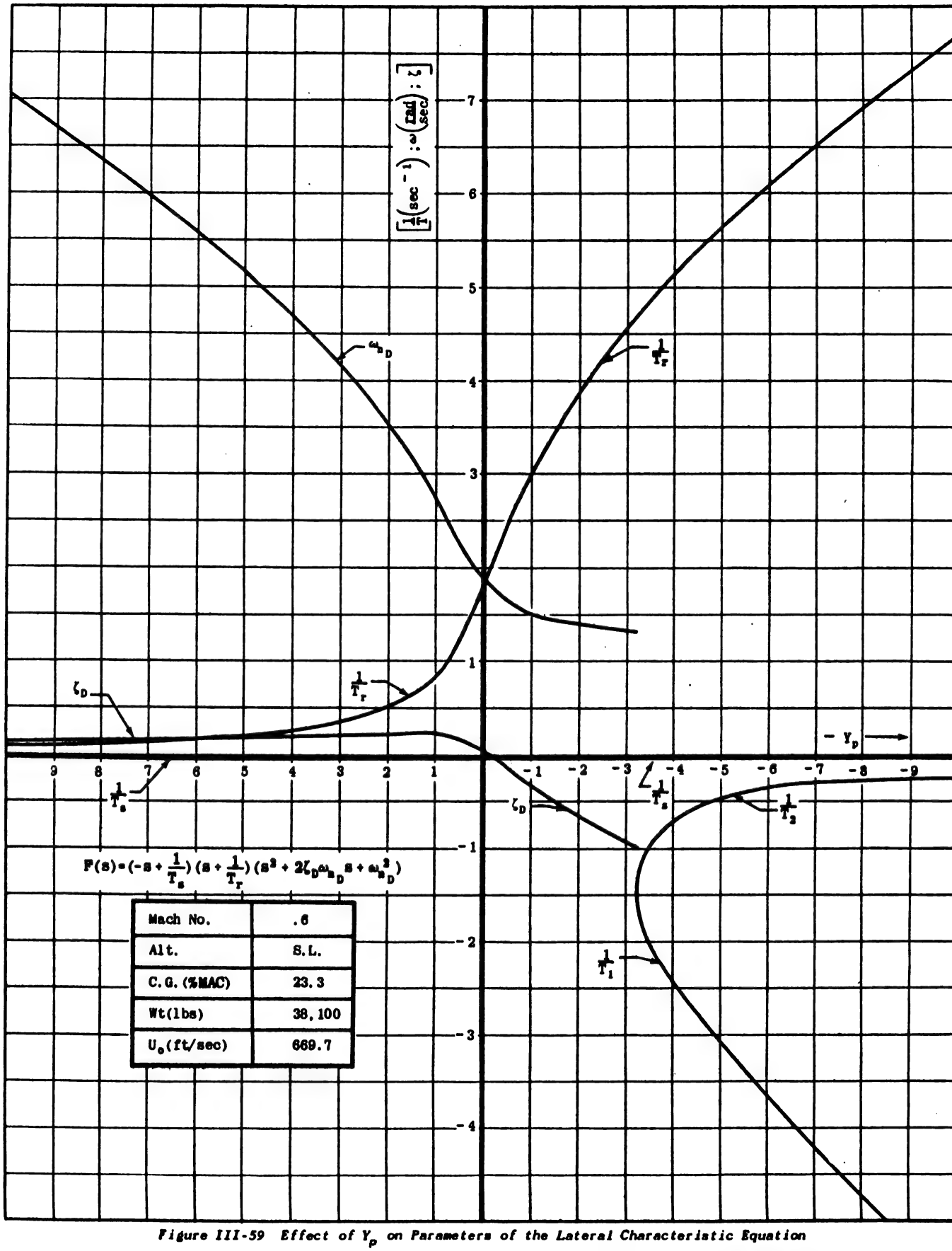

Mach No.	.6
Alt.	S.L.
C.G. (%MAC)	23.3
Wt(lbs)	38,100
U_o(ft/sec)	669.7

Figure III-59 Effect of Y_p on Parameters of the Lateral Characteristic Equation

Base Case Equation (Y_p = -.00009)

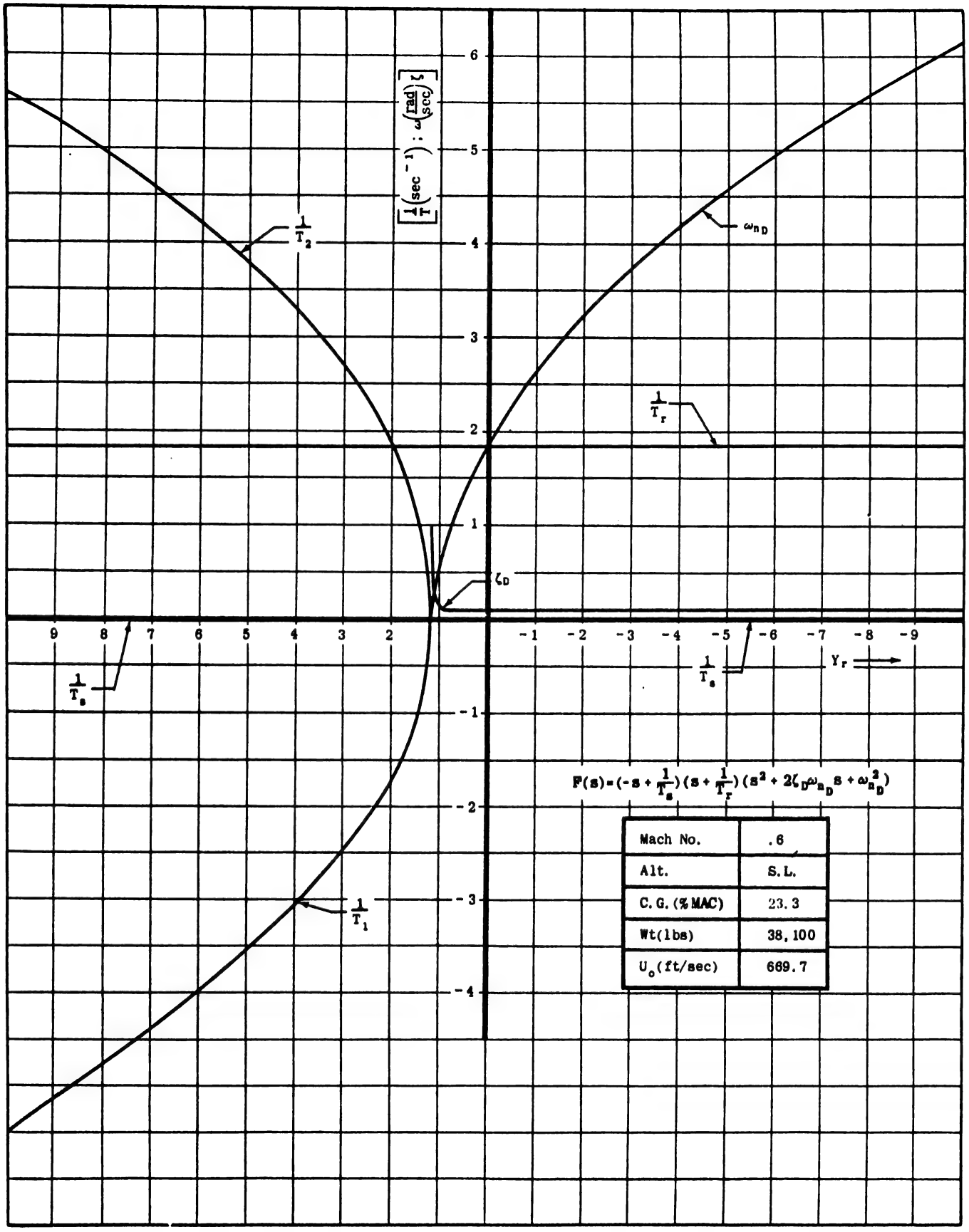

Figure III-60 Effect of Y_r on Parameters of the Lateral Characteristic Equation
Base Case Equation (Y_r = .0012)

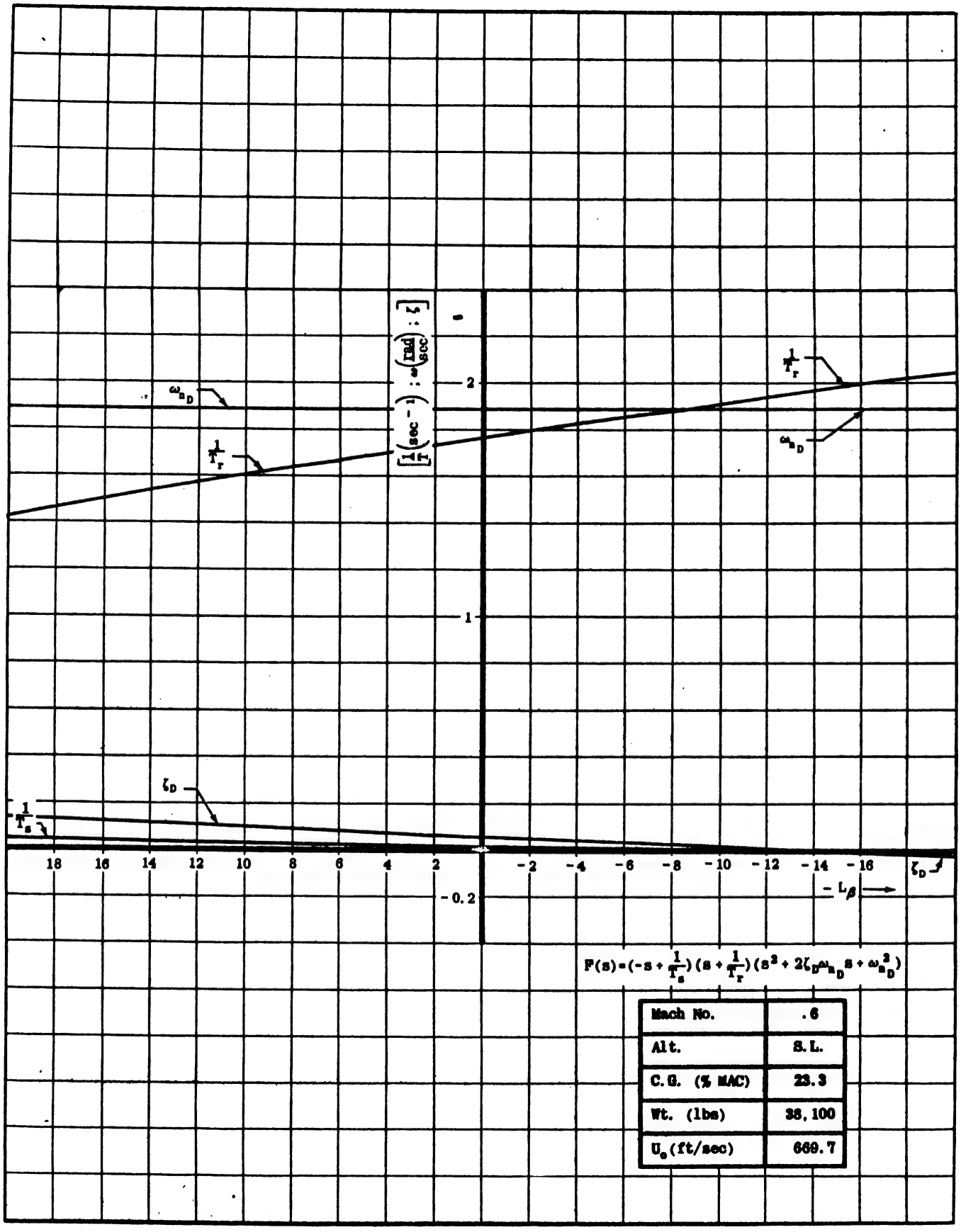

Mach No.	.6
Alt.	S.L.
C.G. (% MAC)	23.3
Wt. (lbs)	38,100
U_o (ft/sec)	669.7

Figure III-61 Effect of L_β on Parameters of the Lateral Characteristic Equation
Base Case Equation ($L_\beta = 4.706$)

tor of the approximate expression for $\frac{1}{T_s}$; however, the term in L_β in the denominator is small in comparison with the other terms there, so that variation of L_β has little effect upon the value of the denominator. For the base case under consideration, the numerator is positive and the denominator negative; therefore at the base condition, $\frac{1}{T_s}$ is negative. This checks the conclusion that the approximate spiral mode is a divergence. As L_β becomes more negative, the numerator quantity decreases in magnitude and becomes less positive. The over-all effect is that as L_β moves in a negative direction, $\frac{1}{T_s}$ becomes more positive; and eventually, as L_β becomes large enough in magnitude, but still of negative sign, the divergence becomes a subsidence.

The increase in the dutch roll damping, ζ_D, as L_β moves positively, can be inferred from a consideration of (III-107) and the remarks above concerning $1/T_s$ and $1/T_R$.

(III-107) is of the form $\zeta_D = \frac{1}{A}\left(B - \frac{1}{T_s} - \frac{1}{T_R}\right)$ where A and B (for this base case) are positive quantities which are not functions of L_β; $1/T_s$ and $1/T_R$, of course, depend upon L_β.

Since $1/T_s$ is a negative quantity near the base value of L_β, ζ_D can be written equivalently as $\zeta_D = \frac{1}{A}\left(B + \left|\frac{1}{T_s}\right| - \frac{1}{T_R}\right)$ As L_β becomes more negative in this region, $\left|1/T_s\right|$ becomes less in magnitude; under these conditions, ζ_D decreases in value.

The conclusion may then be drawn that as L_β moves in the negative direction, ζ_D tends to become less, due to the variation in $1/T_s$; that is, a decrease in the reciprocal of the spiral time constant tends to increase the dutch roll damping.

By similar reasoning, taking into account the fact the $\frac{1}{T_R}$ is a positive quantity, an increase in the value of $\frac{1}{T_R}$ tends to decrease the dutch roll damping. As stated above, such an increase in $\frac{1}{T_R}$ occurs as L_β becomes more negative.

Summarizing, it may be seen that as L_β moves in the negative direction, its variation tends to increase ζ_D through its effect on $\frac{1}{T_s}$ and to decrease ζ_D through its effect on $\frac{1}{T_R}$.

Figure III-61 shows that for the same variation in L_β, the magnitude of the change in $\frac{1}{T_R}$ is greater than that in $\frac{1}{T_s}$; therefore, the net effect on ζ_D is that the dutch roll damping ratio increases as L_β becomes more negative.

The effect of changing L_p is shown in Figure III-62. It appears that L_p has a relatively small effect on all the parameters except $\frac{1}{T_R}$, the reciprocal of the roll time constant, which increases linearly as L_p moves in the negative direction.

(III-105) clearly shows the reason for this change in $\frac{1}{T_R}$, since the equation is of the form: $\frac{1}{T_R} = AL_p + B$, where A and B are combinations of other stability derivatives but do not depend upon L_p. For the base case, A is negative, so that $\frac{1}{T_R}$ becomes more positive as L_p moves in the negative direction.

The effect of changing L_p is not reflected in the approximation for ζ because L_p and $\frac{1}{T_R}$ essentially cancel out of (III-107) if all quantities involved are held constant, except for L_p. That changes in L_p have some effect on $\frac{1}{T_s}$ can be predicted from (III-104), but the effect of varying L_p in this relation is small.

Figure III-63 shows that the principal effect of changing L_r is to vary $\frac{1}{T_s}$, the reciprocal of the spiral time constant. As L_r moves in the negative direction, $\frac{1}{T_s}$ moves positively; that is, as L_r becomes more negative, the spiral mode becomes more unstable. This can be seen from (III-104): the denominator of the expression on the right of this relation is negative in almost all cases, and as L_r becomes more negative, the quantity $N_\beta L_r$, and therefore the numerator, also becomes a negative number of larger absolute value. The ratio of numerator to denominator, that is, $1/T_s$, then becomes a positive number of increasing magnitude as L_r becomes more negative.

The effects of changing N_β are shown in Figure III-64. The principal effect of increasing N_β is an increase in the Dutch roll natural frequency. (III-106) also indicates this trend.

The term L_pN_β in the numerator of (III-105) and also in the denominator of (III-104) is very large, in comparison with the other terms in these expressions, for values of N_β in the vicinity of the base value, $N_\beta = 3.5581$, or when the absolute magnitude of N_β is large. Consequently, for these values of N_β, L_pN_β essentially cancels out of both (III-104) and (III-105), indicating that only the dutch roll natural frequency and damping ratio will be appreciably affected by variations of N_β around its base balue. Figure III-64 shows that the dutch roll damping ratio increases with a negative movement of N_β. This trend is also indicated in (III-107).

Figure III-65 shows the effects of varying N_p. Since N_p is generally very small, it does not appear in the approximate factors. N_p is usually negative; however, at flight near the stall, it can become positive. The most important effect of an increase of N_p is to cause the usually very stable rolling mode to become divergent. As N_p becomes more negative, the dutch roll damping ratio decreases toward instability, and $\frac{1}{T_R}$ and the dutch roll natural frequency increase.

The effects of changing N_r are shown in Figure III-66. Changes in N_r in the vicinity of its base value are reflected principally in the dutch roll damping ratio and in the reciprocal of the spiral time constant, $\frac{1}{T_s}$. It can

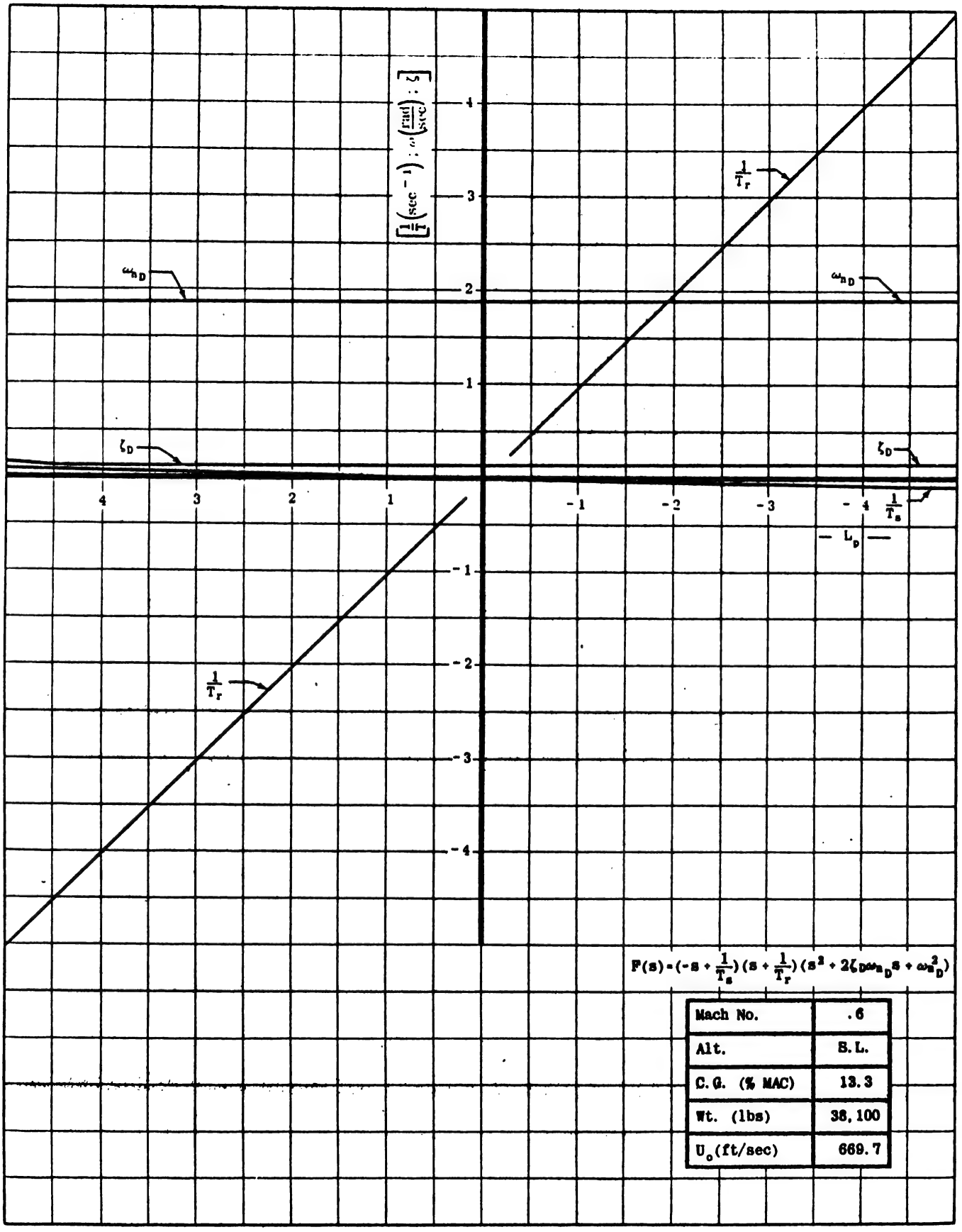

Figure III-62 Effect of L_p on Parameters of the Lateral Characteristic Equation Base Case Equation (L_p = -1.7605)

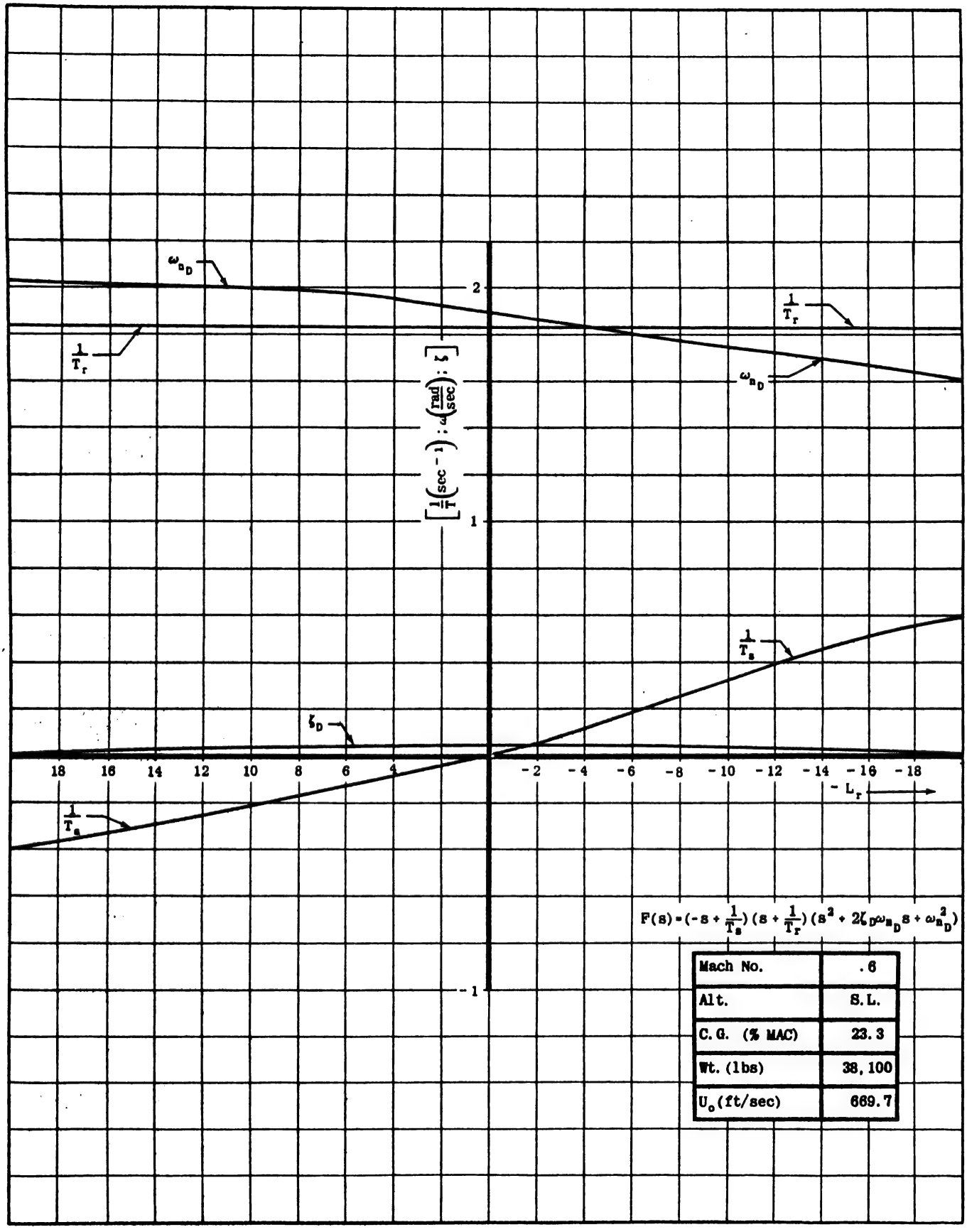

Mach No.	.6
Alt.	S.L.
C.G. (% MAC)	23.3
Wt. (lbs)	38,100
U_o (ft/sec)	669.7

Figure III-63 Effect of L_r on Parameters of the Lateral Characteristic Equation
Base Case Equation (L_r = .2485)

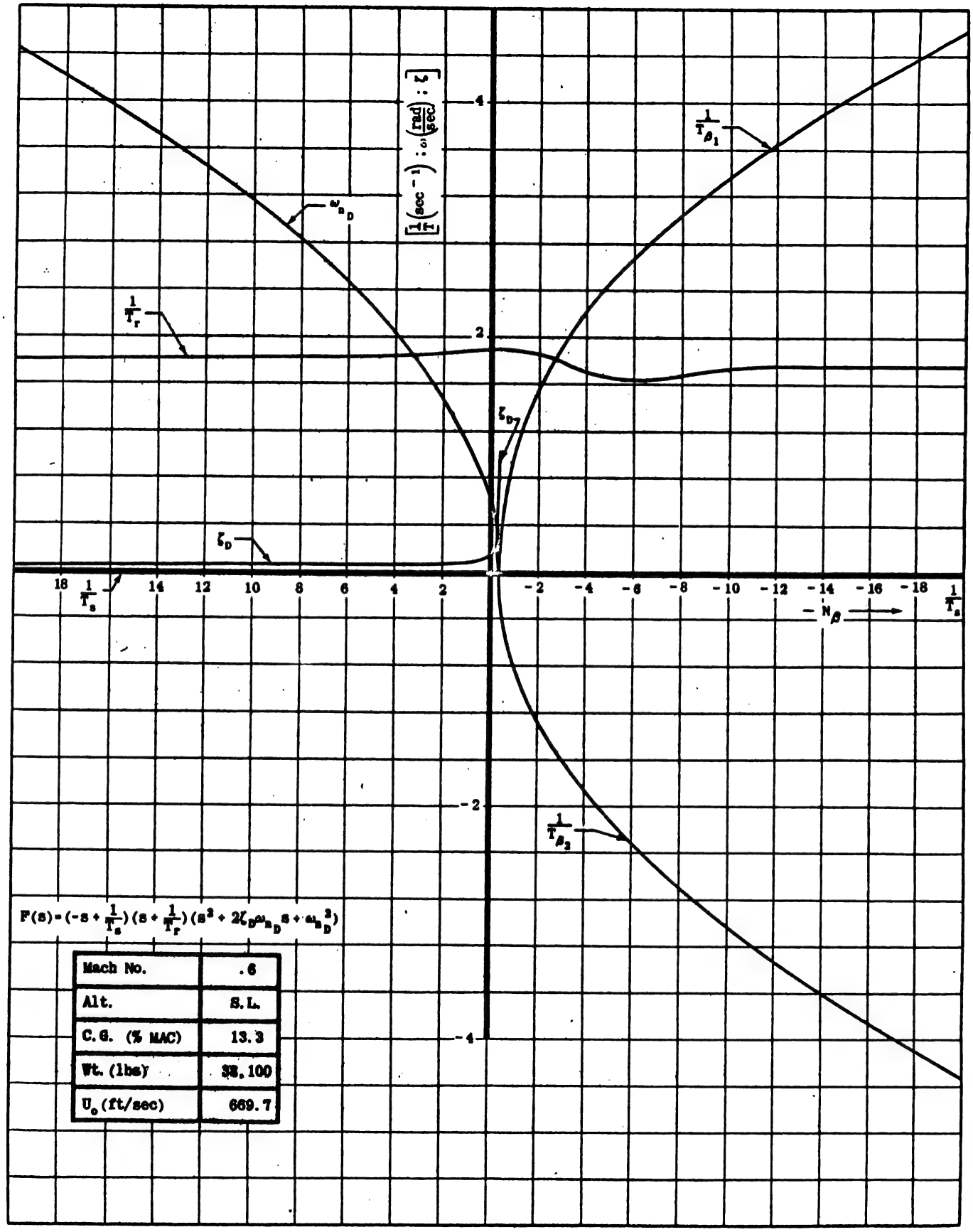

Mach No.	.6
Alt.	S.L.
C.G. (% MAC)	13.3
Wt. (lbs)	38,100
U_o (ft/sec)	669.7

Figure III-64 Effect of N_β on Parameters of the Lateral Characteristic Equation

Base Case Equation ($N_\beta = 3.5581$)

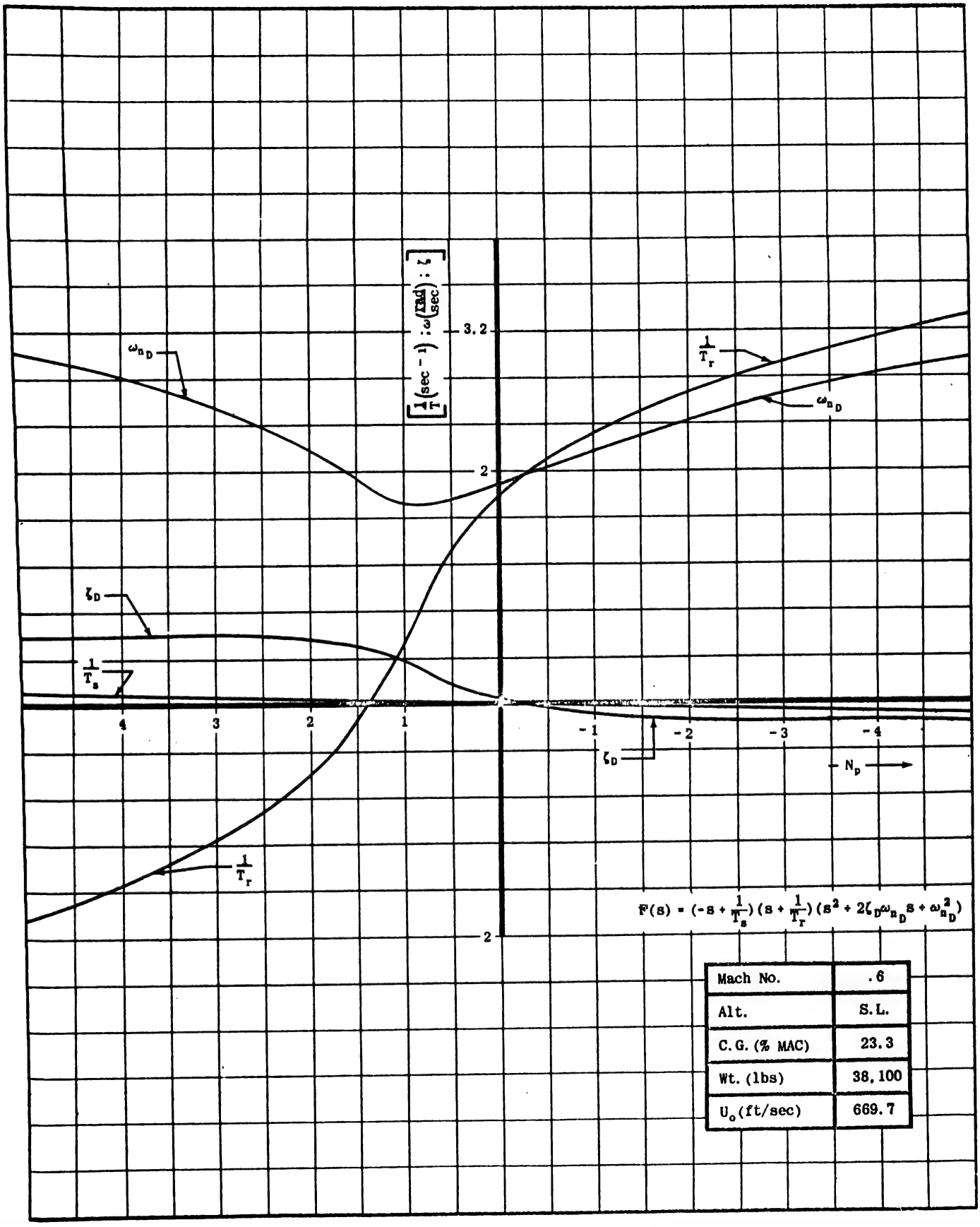

Mach No.	.6
Alt.	S.L.
C.G. (% MAC)	23.3
Wt. (lbs)	38,100
U_o (ft/sec)	669.7

Base Case Equation (N_p = -.00616)

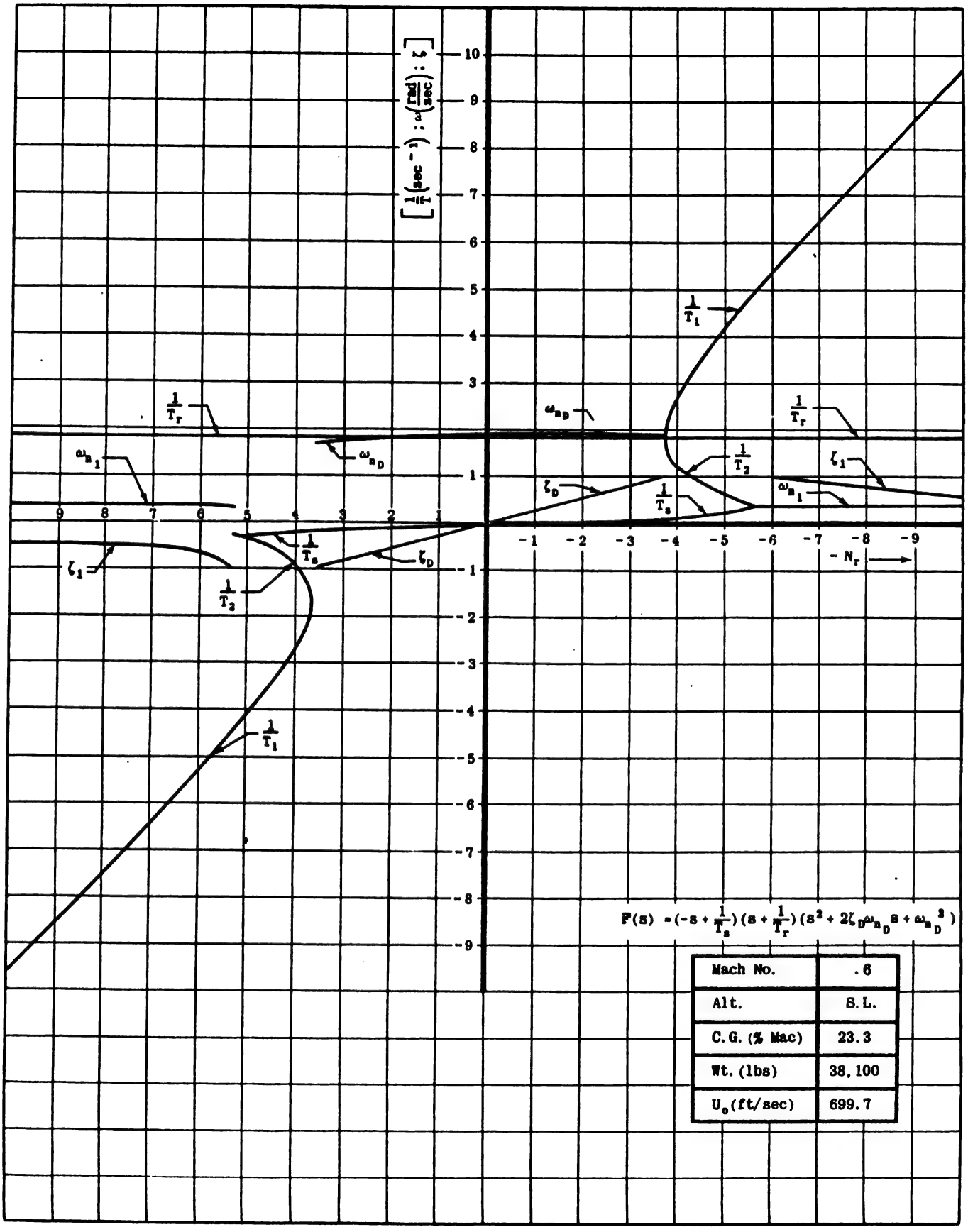

Figure III-66 Effect of N_r on Parameters of the Lateral Characteristic Equation Base Case Equation (N_r = -.0937)

be seen that ζ_D increases linearly as N_r becomes more negative in the vicinity of its base value. This effect is also plainly indicated in (III-107).

As N_r moves negatively, the spiral mode becomes more stable. N_r enters into both the numerator and the denominator of (III-104), but since $L_p N_\beta$ is generally much greater than $Y_v L_p N_r$, small changes in N_r do not appreciably affect the denominator on the right of (III-104). On the other hand, since $N_\beta L_r$ and $-L_\beta N_r$ are generally of the same order of magnitude and are of opposite sign, comparatively small changes in N_r become important here; hence the effect on the spiral mode of changing N_r can be determined by consideration of the numerator alone. This numerator becomes more negative with similar variation in N_r. Since the denominator of (III-104) is negative for the base case, $\frac{1}{T_s}$ increases as N_r becomes more negative. Therefore, (III-104) and Figure III-66 agree as to the effect on $\frac{1}{T_s}$ of varying N_r.

Figures III-67 and III-68 show that small variations in the values of $\frac{I_{xz}}{I_{xx}}$ and $\frac{I_{xz}}{I_{zz}}$ do not have any appreciable effect on any of the parameters of the lateral characteristic equation.

In summary, good correlation exists between the lateral approximate factors and the curves presented. However, it should again be emphasized that caution must be used in attempting to extend these results to other flight conditions, particularly if they differ considerably from the one used in this section.

SECTION 19 – APPROXIMATE FACTORS EXPRESSED AS FUNCTIONS OF THE BASIC NON-DIMENSIONAL STABILITY DERIVATIVES

In this section, the approximate factors of the lateral characteristic equation are expressed in terms of the basic non-dimensional stability derivatives and other parameters of the airframe and the flight condition. The usefulness of approximate factors in this form is discussed in Section III-9.

To derive the desired expressions, the appropriate quantities of (II-191) are substituted into (III-107). The approximation for ζ_D given in (III-107) is simplified to:

(III-108) $$\zeta_D \approx -\frac{N_r}{2\sqrt{N_\beta}}$$

(III-108) was shown in Section III-14 to be a relatively good approximation to the dutch roll damping ratio.

Performing the above substitutions yields:

(III-109) $$\frac{1}{T_s} \approx \left(\frac{g}{U_o}\right) \frac{\left(C_{n_\beta} C_{l_p} - C_{l_\beta} C_{n_r}\right)}{\left[(1/4\mu_b) C_{y_\beta} C_{l_p} C_{n_r} + C_{l_p} C_{n_\beta} + (g/U_o)(4\tau)\left(k_{zz}/b\right)^2 C_{l_\beta}\right]}$$

(III-110) $$\frac{1}{T_R} \approx -\frac{1}{4\tau}\left(\frac{b}{k_{xx}}\right)^2 \frac{\left[\frac{1}{4\mu_b} C_{y_\beta} C_{l_p} C_{n_r} + C_{l_p} C_{n_r} + \frac{g}{U_o}(4\tau)\left(\frac{k_{zz}}{b}\right)^2 C_{l_\beta}\right]}{C_{n_\beta}}$$

(III-111) $$\omega_{n_D} \approx \frac{1}{\tau}\left(\frac{b}{k_{zz}}\right)\sqrt{\frac{\mu_b}{2} C_{n_\beta}}$$

(III-112) $$\zeta \approx -\frac{1}{8}\left(\frac{b}{k_{zz}}\right) \frac{C_{n_r}}{\sqrt{\frac{\mu_b}{2} C_{n_\beta}}}$$

where:

$$\mu_b = \frac{m}{\rho S b} \quad \text{and} \quad \tau = \frac{m}{\rho S U}$$

SECTION 20 – EFFECT OF FLIGHT CONDITION ON THE LATERAL TRANSIENT RESPONSE OF AN AIRPLANE

In this section, traces of the solutions of the equations of motion obtained from an analog computer are presented; these records show the effect of flight condition on the transient response of an airplane. Also included are some analog computer solutions showing the effects of single dimensional stability derivative variation. The stability derivatives used in this analysis are theoretical values calculated for a hypothetical high-performance jet airplane of conventional cruciform configuration.

Figures III-69, III-70, III-71, and III-72 show the effect of Mach number variations at constant altitude. Several trends are indicated in these plots. The dutch roll natural frequency increases with Mach number while the dutch roll damping ratio remains roughly constant. At least for subsonic Mach numbers, these trends are generally reliable, and C_{n_r} and C_{n_β} can be considered roughly constant. Thus, (III-111) and (III-112) can be used to predict that ω_{n_D} increases with Mach number and that ζ_D is independent of Mach number.

Figures III-70, III-73, and III-74 show the effect of altitude variation at constant Mach number. These graphs indicate that the dutch roll damping ratio decreases with increasing altitude and actually becomes unstable at 60,000 feet. This effect can be predicted from equation (III-112): since the density appears in the numerator, ζ_D decreases as the altitude increases.

Figures III-75, III-76, and III-77 show the effect of changing N_r and indicate that the principal effect of N_r in becoming more negative is to increase the dutch roll damping ratio. This result checks with the conclusion drawn in Section III-18.

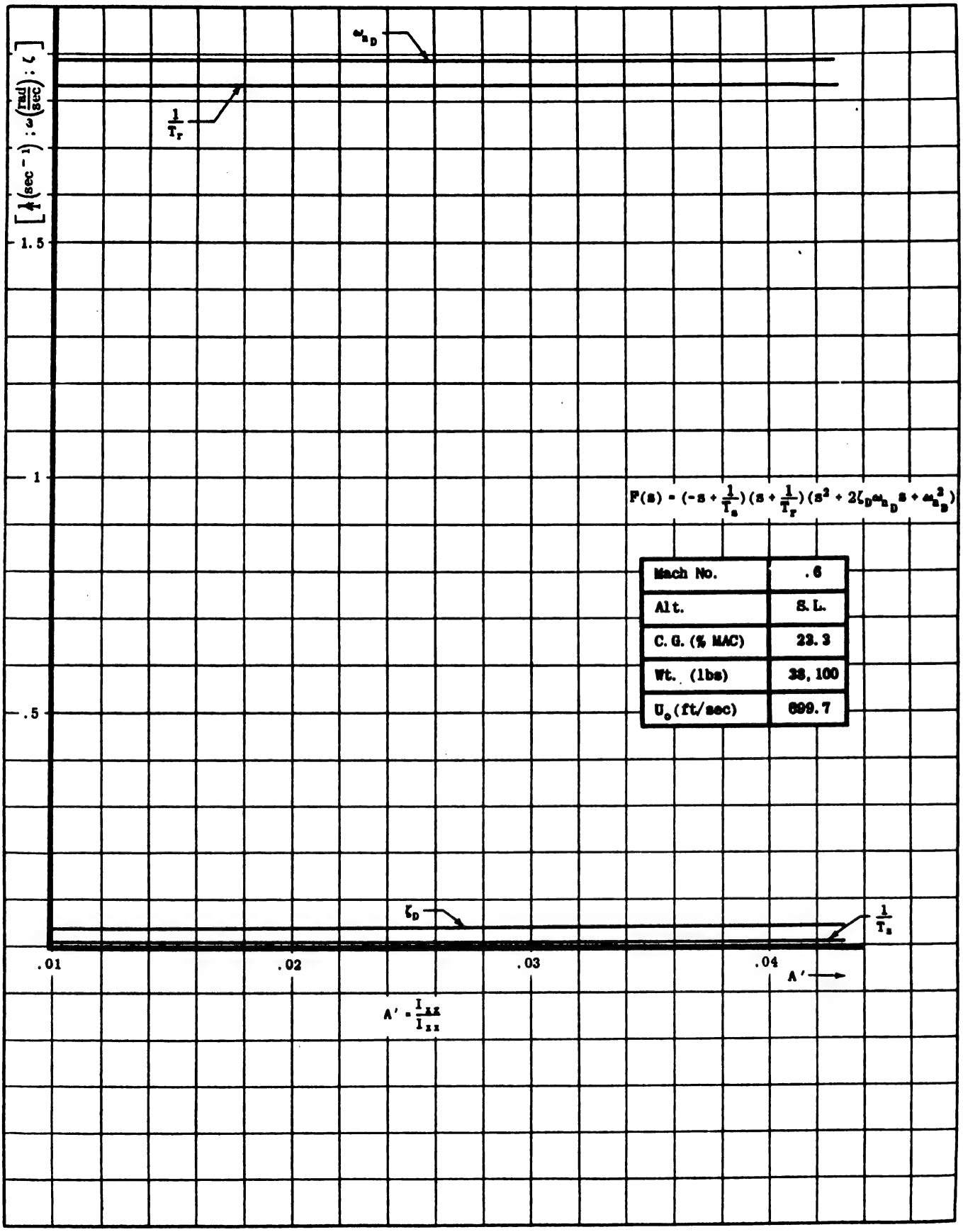

Figure III-67 Effect of A' on Parameters of the Lateral Characteristic Equation
Base Case Equation (A' = .0358)

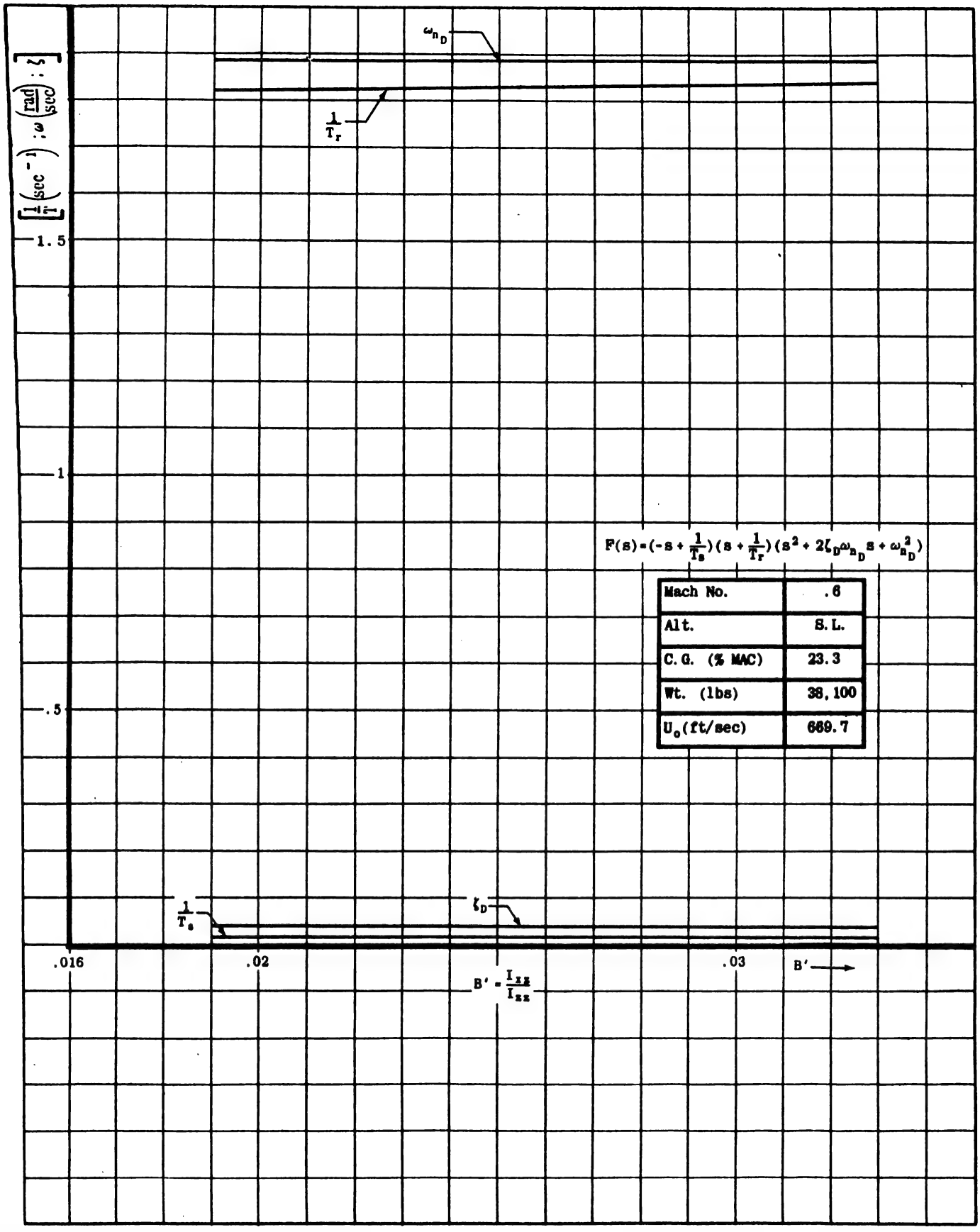

Figure III-68 Effect of B' on Parameters of the Lateral Characteristic Equation
Base Case Equation (B' = .0259)

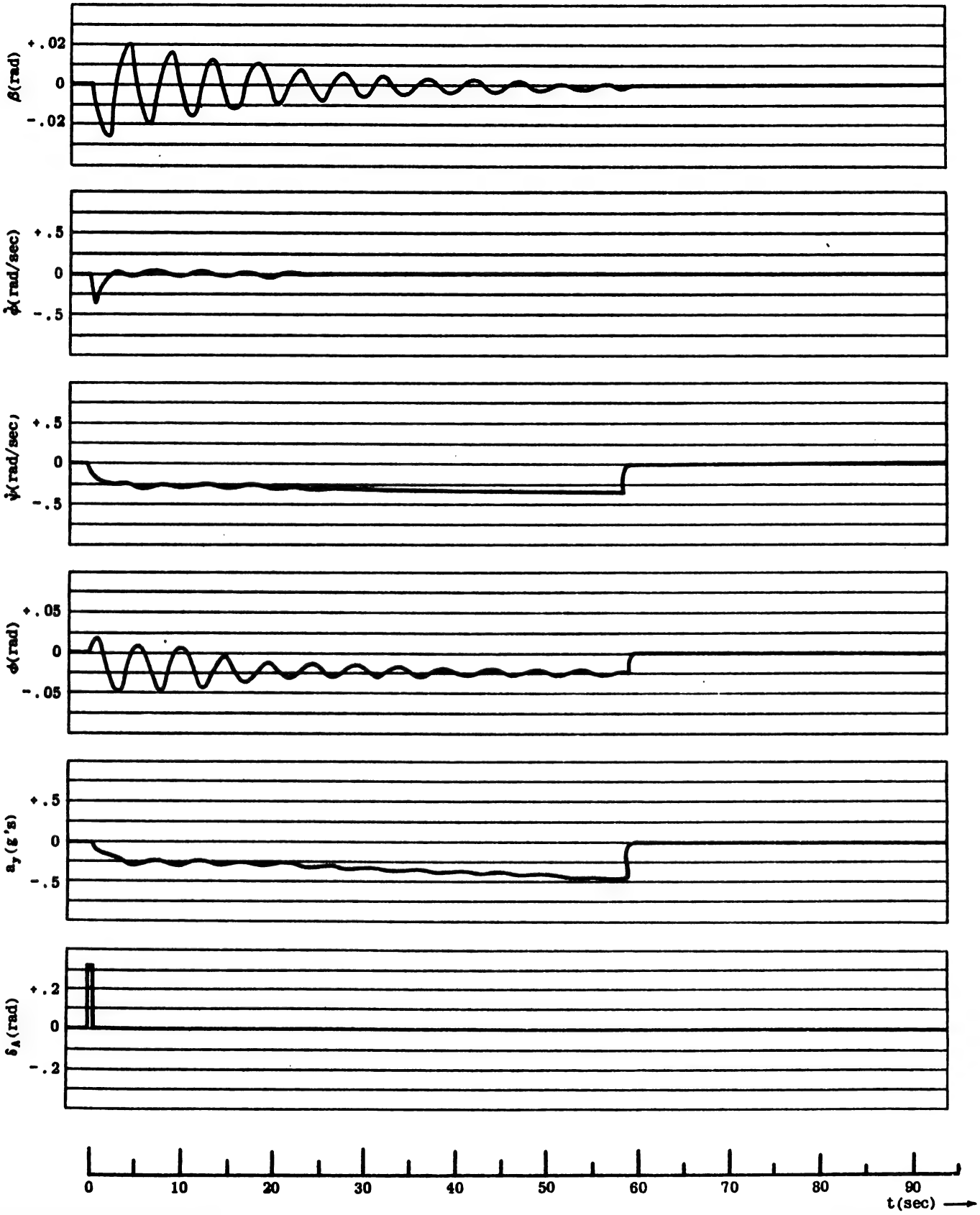

Figure III-69 Analog Computer Record of Time History for Pulse Aileron Deflection. Three Degree of Freedom (Mach No. = .4; Altitude = Sea Level)

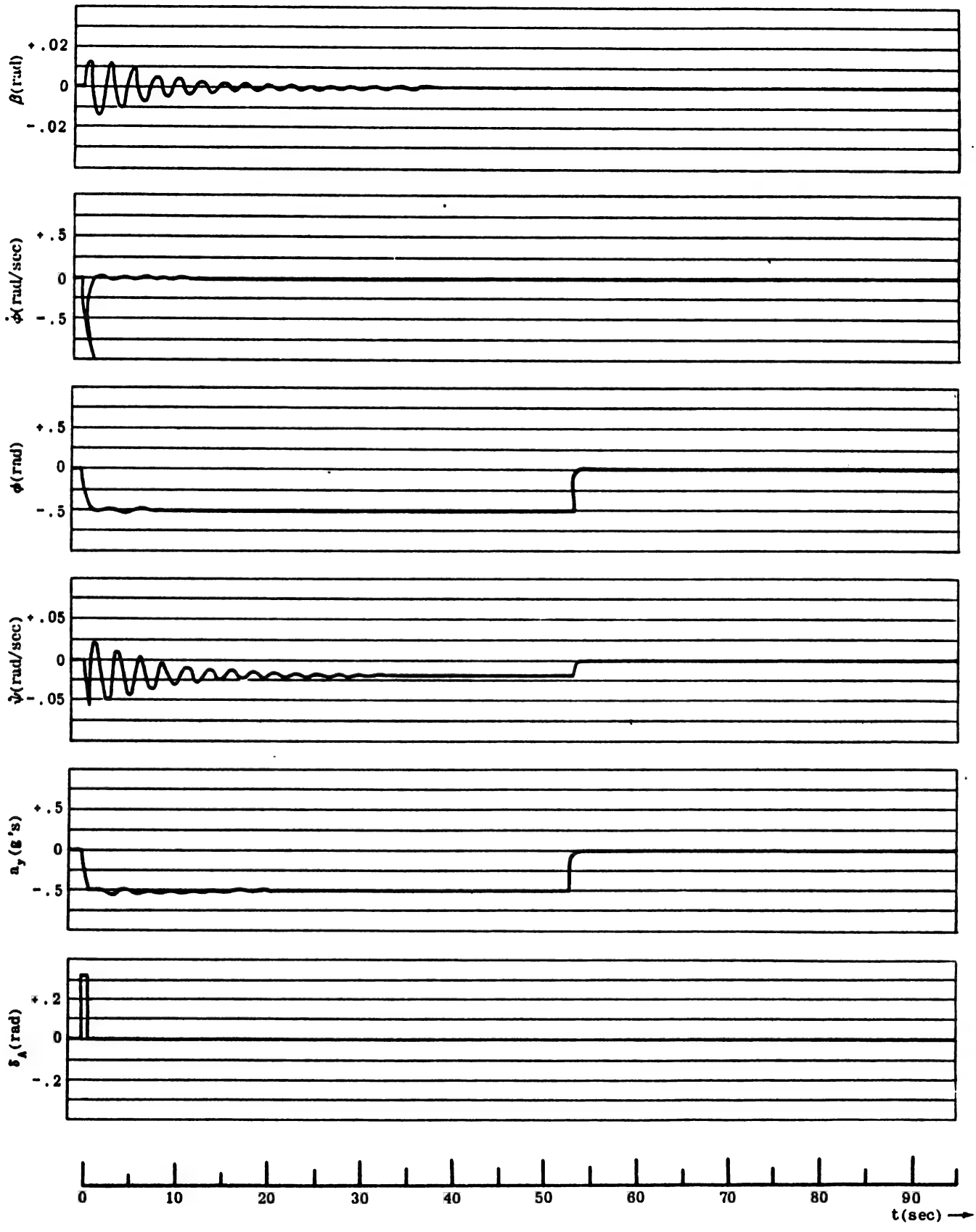

Figure III-70 Analog Computer Record of Time History for Pulse Aileron Deflection. Three Degree of Freedom (Mach No. = .8; Altitude = Sea Level)

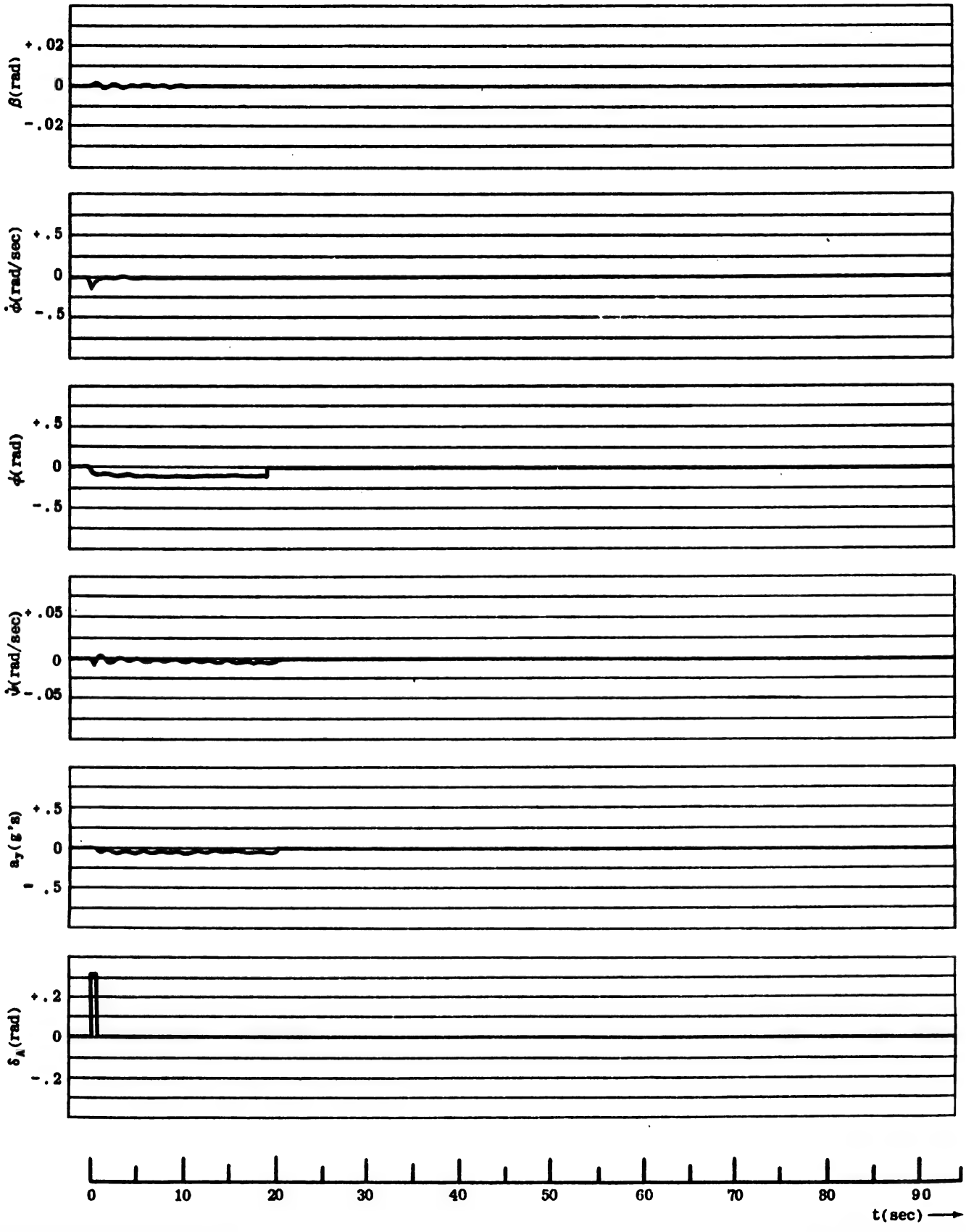

Figure III-71 Analog Computer Record of Time History for Pulse Aileron Deflection. Three Degree of Freedom (Mach No. = 1.0; Altitude = Sea Level)

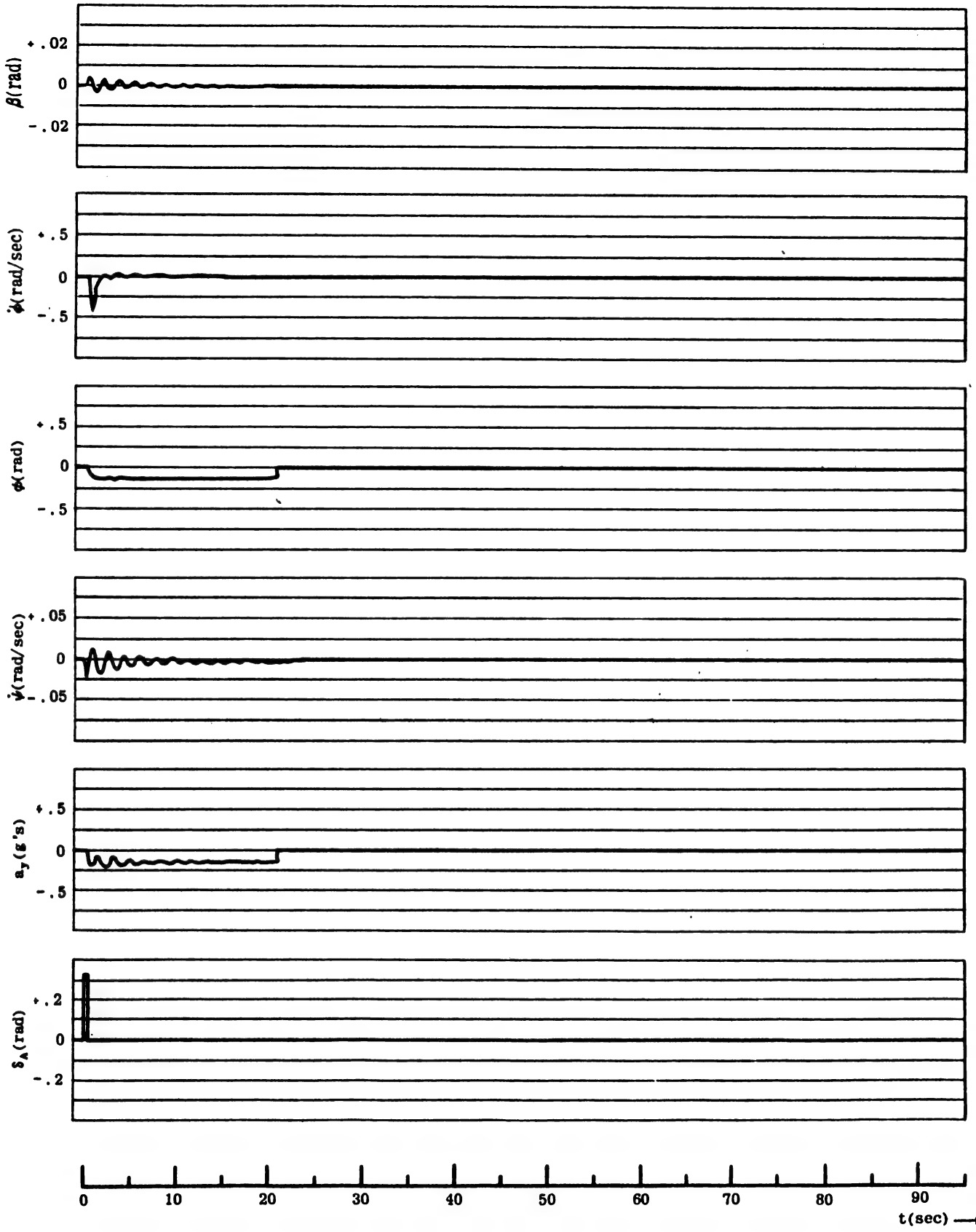

Figure III-72 Analog Computer Record of Time History for Pulse Aileron Deflection. Three Degree of Freedom (Mach No. = 1.2; Altitude = Sea Level)

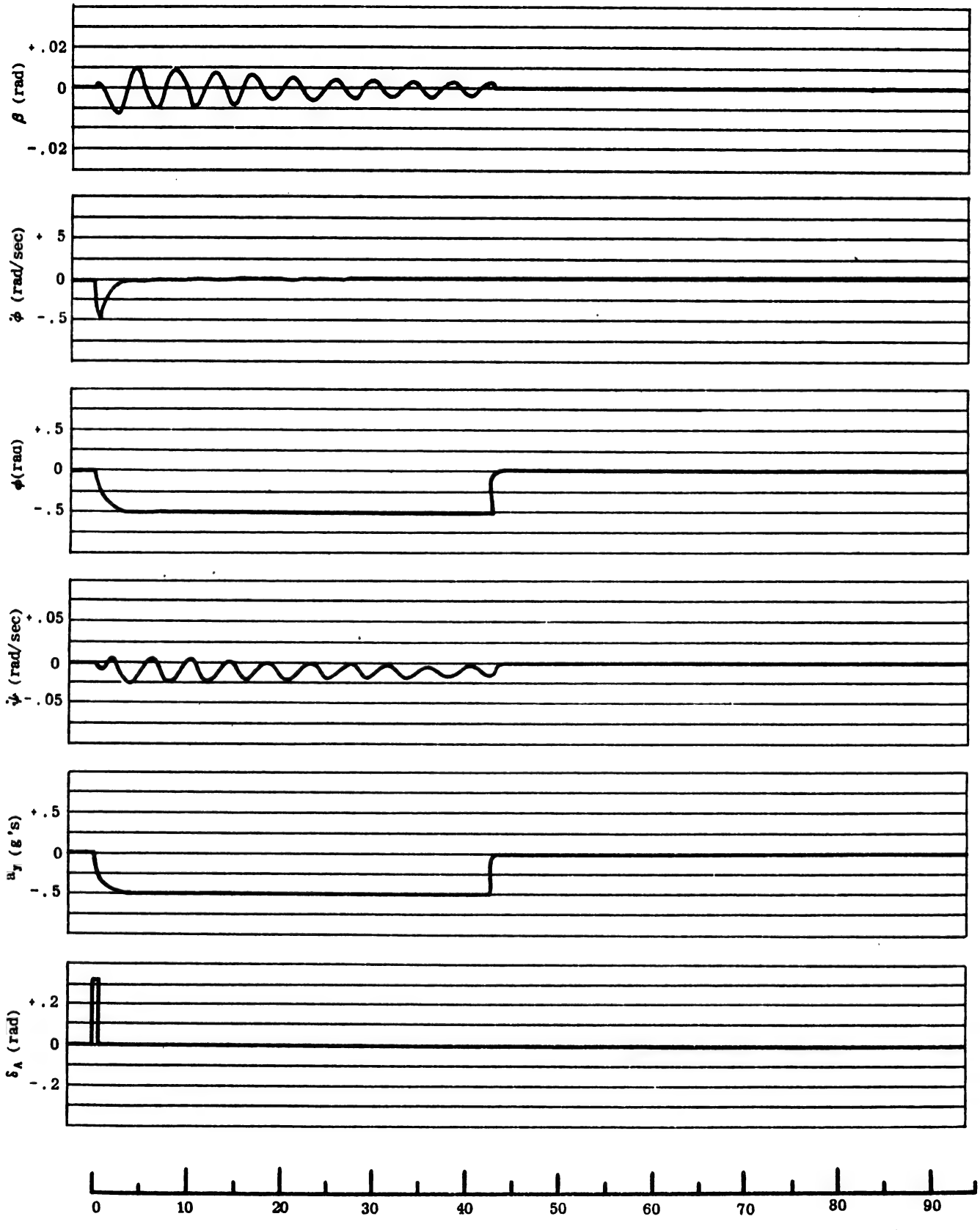

Figure III-73 Analog Computer Record of Time History for Pulse Aileron Deflection. Three Degree of Freedom (Mach No. = .8; Altitude = 30,000 Ft.)

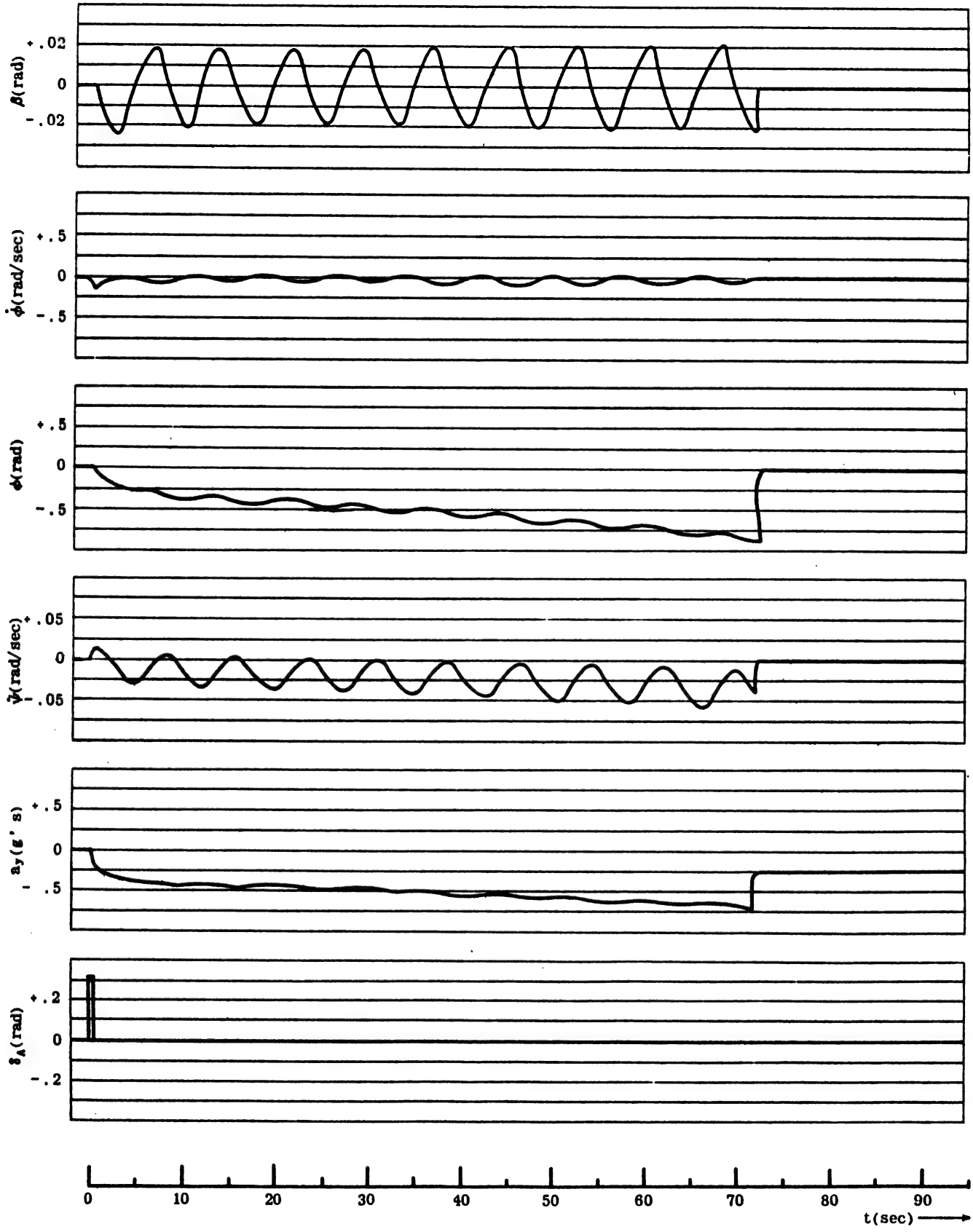

Figure III-74 Analog Computer Record of Time History for Pulse Aileron Deflection. Three Degree of Freedom (Mach No. = .8; Altitude = 60,000 Ft.)

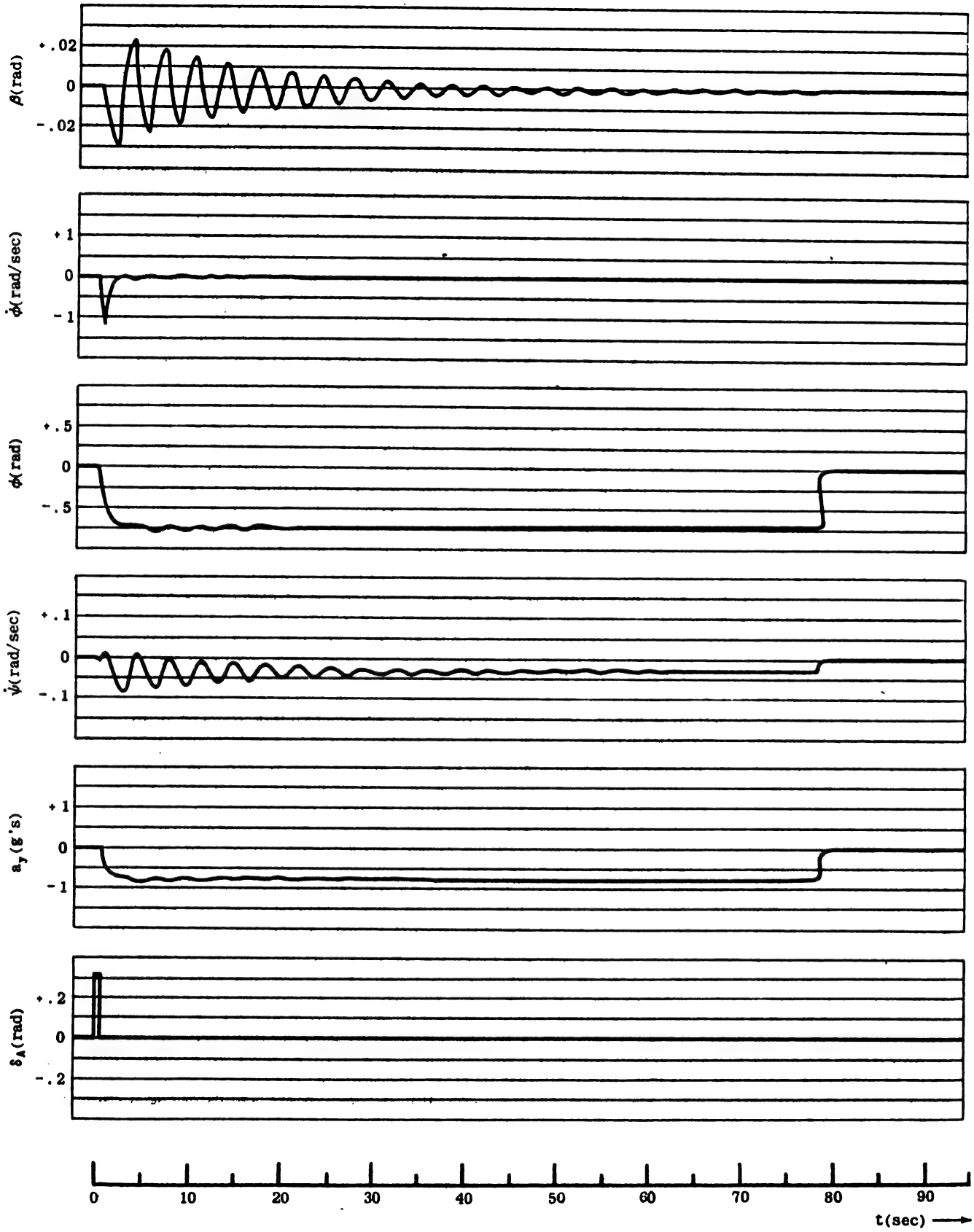

Figure III-75 Analog Computer Record of Time History for Pulse Aileron Deflection. Three Degree of Freedom (Mach No. = .638; Altitude = 20,000 Ft; N_r = -.0957)

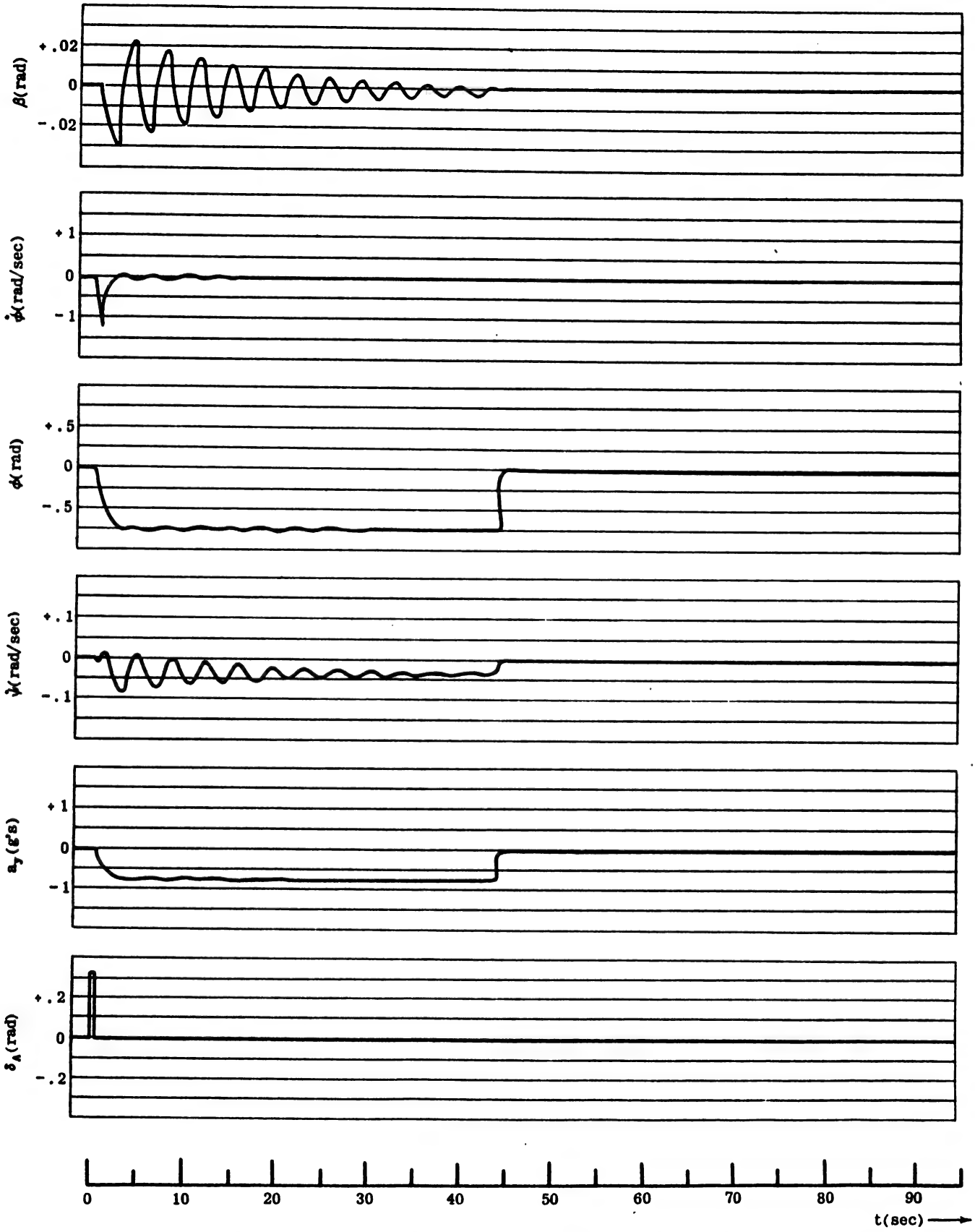

Figure III-76 Analog Computer Record of Time History for Pulse Aileron Deflection. Three Degree of Freedom (Mach No. = .638; Altitude = 20,000 Ft; N_r = -.1053)

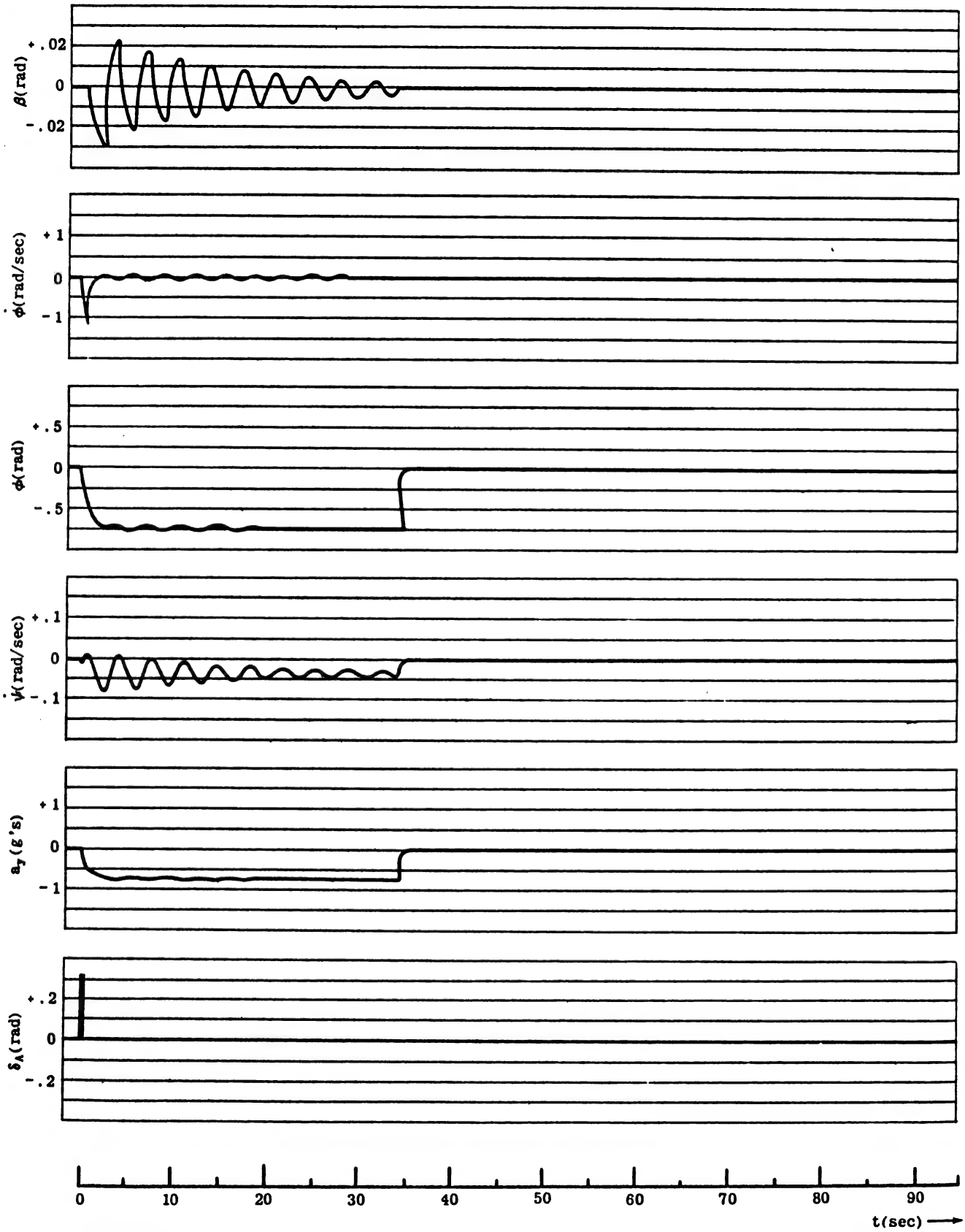

Figure III-77 Analog Computer Record of Time History for Pulse Aileron Deflection. Three Degree of Freedom (Mach No. = .638; Altitude = 20,000 Ft; N_r = -.1148)

Figures III-78, III-79, and III-80 show that the main effect of increasing N_β is to increase the dutch roll natural frequency. This result also checks with that found in Section III-18.

In summary, the basic purpose of presenting the material contained in this section is to demonstrate that much of the information concerning the dynamic response of an airplane can be obtained mathematically only by rather lengthy computational methods and that the same information can be rather simply obtained with the aid of an analog computer.

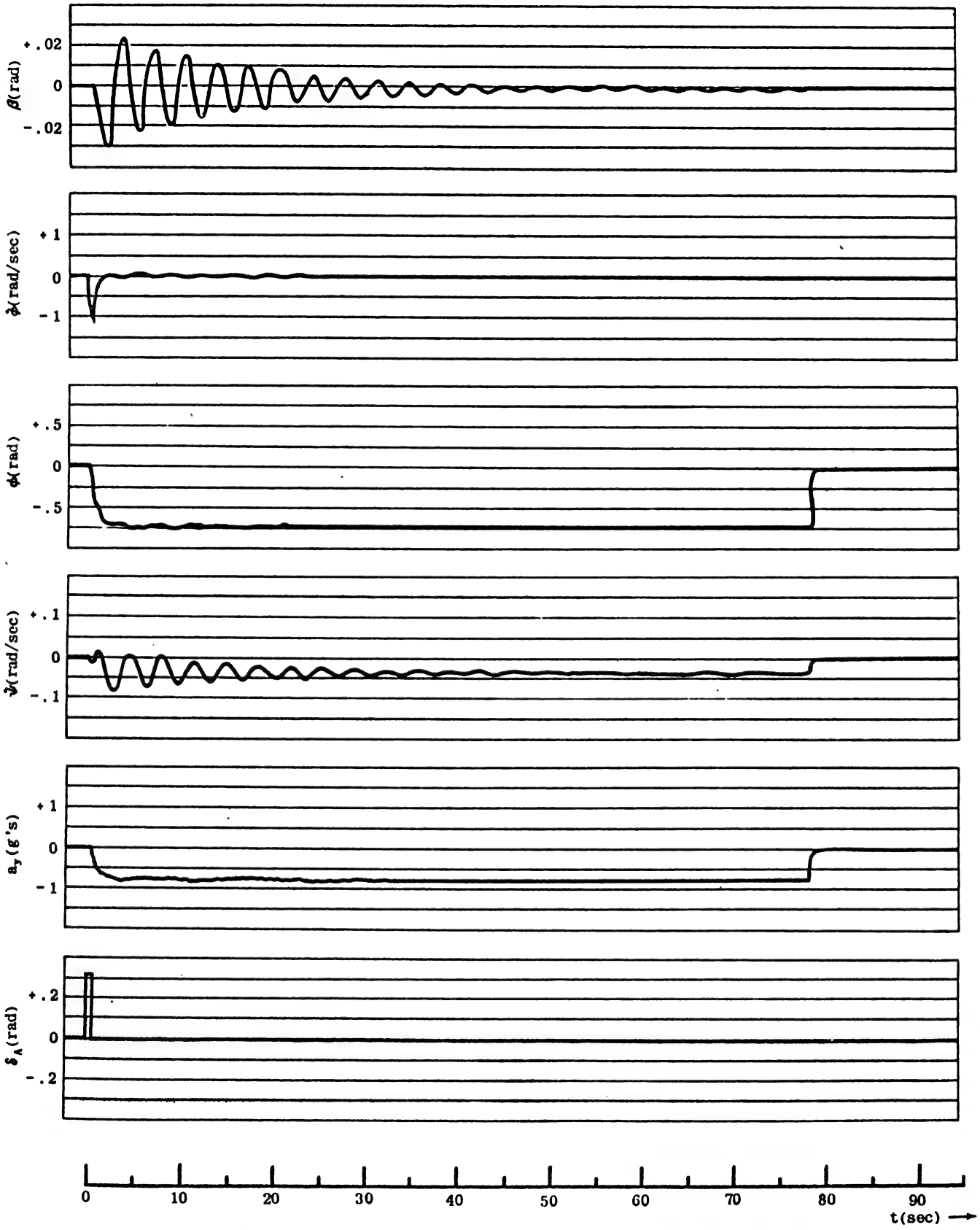

Figure III-78 Analog Computer Record of Time History for Pulse Aileron Deflection. Three Degree of Freedom (Mach No. = .638; Altitude = 20,000 Ft; N_β = 3.55)

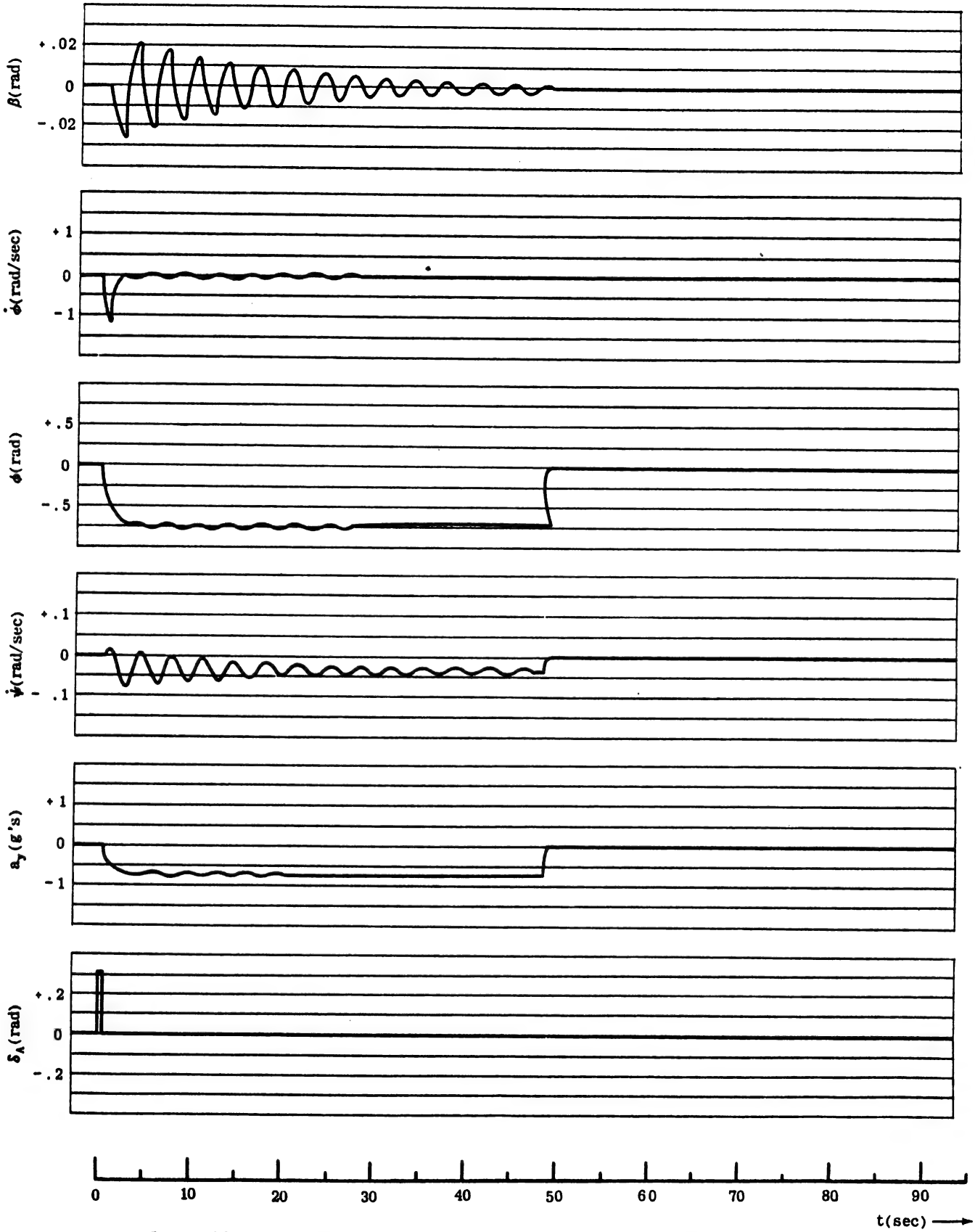

Figure III-79 Analog Computer Record of Time History for Pulse Aileron Deflection. Three Degree of Freedom (Mach No. = .638; Altitude = 20,000 Ft; N_β = 3.91)

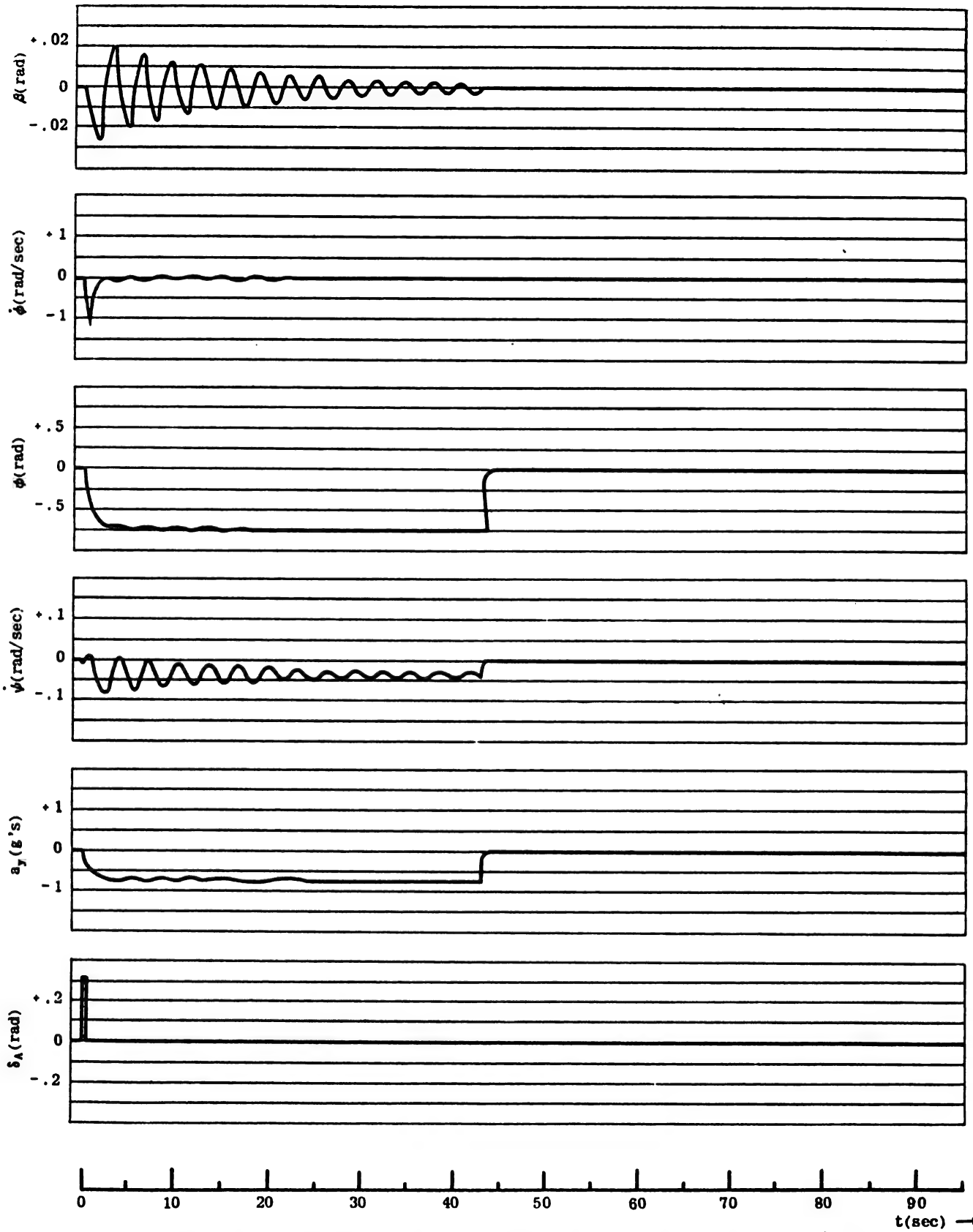

Figure III-80 Analog Computer Record of Time History for Pulse Aileron Deflection. Three Degree of Freedom (Mach No. = .638; Altitude = 20,000 Ft; N_β = 4.26)

CHAPTER IV

DISCUSSION OF STABILITY DERIVATIVES

SECTION 1 – INTRODUCTION

In the preceding chapters of this volume, the coefficients in the airframe transfer functions have been shown to depend almost wholly upon the stability derivatives; that is, upon aerodynamic partial derivatives. The numerical examples previously cited show that small changes in the values of some of these derivatives can produce pronounced effects on the airframe response to disturbances.

A knowledge of the values of stability derivatives is therefore very important in designing an integrated airframe-autopilot-controls system. Chapter IV discusses stability derivatives in greater detail than does the preceding material of this volume, so that the necessary background for an appreciation of their effects on airframe response may be acquired.

The plan for this chapter is first, in Section 2, to discuss the various forms of stability derivatives and to show the importance and application of each form; next, in Section 3, to treat each derivative separately and in detail; and finally, in Sections 4 and 5, to enumerate and to discuss the various factors that affect the values of stability derivatives, such as airframe geometry, Mach number, and dynamic pressure.

No attempt is made here to provide a general handbook for evaluating or estimating stability derivatives with a particular airframe in mind. Present day design trends are toward aircraft of unconventional geometry which are operated in the transonic region and subjected to great aeroelastic effects. The resulting complexity of factors involved in particular applications makes it necessary to consult many detailed references, and at present the services of a competent aerodynamicist are required.

SECTION 2 – THE DIFFERENT FORMS OF STABILITY DERIVATIVES

Preceding sections have shown that the requirements of particular applications often make it convenient to deal with the equations of motion in several different forms. The equations may be dimensional or non-dimensional in conjunction with different axis systems, and a corresponding set of stability derivatives is associated with each form of the equations.

The stability derivatives used in the design stage of an airframe are usually obtained from various unrelated theoretical reports, from wind tunnel data on models, and from flight test data on similar full-scale aircraft. Consequently, the available data are found in varying forms and may be expressed with respect to any one of the three common axis systems. It is therefore extremely important, when making use of these unrelated data, to examine the form of the stability derivatives given in each source and to make the conversion, if necessary, to the one consistent form which corresponds to that of the equations of motion to be used in setting up the airframe transfer functions.

(a) DIMENSIONAL AND NON-DIMENSIONAL FORMS

In the literature relating to aircraft stability and control, four different forms of stability derivatives appear, but little or no distinction in terminology is made among them; all are referred to as "stability derivatives" regardless of the particular form. For purposes of discussion and for clarification, it is convenient to illustrate what these four general forms are as they are used in this manual.

Example 1. Basic dimensional stability derivatives:

$$\frac{\partial L}{\partial p}$$

Example 2. Dimensional stability derivative parameters:

$$L_p = \left(\frac{1}{I_x}\right)\left(\frac{\partial L}{\partial p}\right)$$

Example 3. Basic non-dimensional stability derivatives:

$$C_{l_p} = \frac{\partial C_l}{\partial\left(\frac{pb}{2U}\right)} = \left(\frac{1}{qSb}\right)\left[\frac{\partial L}{\partial\left(\frac{pb}{2U}\right)}\right]$$

Example 4. Non-dimensional stability derivative parameters:

$$l_p = \left(\frac{1}{4}\right)\left(\frac{b}{k_x}\right)^2 C_{l_p}$$

It may be seen from the examples that the dimensional form (examples 1 and 2) is concerned with direct forces, moments, and velocities, whereas the non-dimensional form (examples 3 and 4) is concerned with force and moment coefficients and with non-dimensional velocities (e.g., $pb/2U$ is the non-dimensionalized form of the rolling velocity, p). It may also be seen that the basic

stability derivatives (examples 1 and 3) do not involve moments of inertia, whereas the stability derivative parameters (examples 2 and 4) are functions not only of moments of inertia but of the basic stability derivatives. Conversion relations between these four general forms and also specific mathematical definitions of individual derivatives are given in Appendix IV-1 (Tables IV-1 to IV-4).

It must be emphasized that the specific notation and the specific definitions used in this manual are not necessarily employed by all writers on the subject. For example, Durand, in a basic aerodynamic reference work (Reference 4), uses the notation L_p to signify the partial derivative $\partial L/\partial p$, whereas most of the present-day writers use L_p (or $L_{\dot{\phi}}$) to represent the stability derivative parameter $(1/I_x)(\partial L/\partial p)$. On the other hand, almost everyone uses the same notation for such basic non-dimensional stability derivatives as C_{l_p}, C_{L_α}, and C_{m_q}.

Today only two of the four forms listed above appear to be of practical importance; these are the basic non-dimensional stability derivative (e.g., C_{l_p}) and the dimensional stability derivative parameter (e.g., L_p).

The basic non-dimensional form (C_{l_p}) is important because correlation between the performance of different airframes or the same airframe at different flight conditions is most easily attained with these stability derivatives; as a result, aerodynamic stability derivative data from wind tunnel tests, flight tests, and theoretical analyses are usually presented in the basic non-dimensional form.

The dimensional stability derivative parameter form (L_p) is important because stability derivatives in this form can be used directly as numerical coefficients in the sets of simultaneous differential equations describing the dynamics of the airframe, when the equations are based on real time. Thus, stability derivatives in this form are useful in determining the analytic transfer functions of the airframe and in setting up the mathematical model of the airframe on an analog computer in preparation for synthesis with auto-pilot and controls systems.

In this volume, then, most of the discussion dealing with the evaluation of stability derivatives makes use of the basic non-dimensional stability derivative form (C_{l_p}), and the discussion dealing with airframe transfer functions, with airframe synthesis with other components, and with analog computer techniques makes use of the dimensional stability derivative parameter form (L_p).

(b) STABILITY DERIVATIVE REFERENCE AXES

In addition to establishing the form of stability derivative to be used, any particular form of the equations of motion also establishes the reference axis system for the associated stability derivatives. For example, when dealing with equations of motion based on the stability axis system, stability derivatives based on this system should be used. Similarly, when dealing with equations of motion based on principal axes, stability derivatives based on principal axes should be used.

It was shown in Chapter II that the stability axis system is probably the most generally useful, mainly because the evaluation of derivatives from wind tunnel tests and from theoretical considerations is easier with this axis system.

It must be remembered, of course, that there are some instances where other axis systems are used as bases for evaluation. "Wind tunnel" axes, for example, are usually employed as the reference system for obtaining derivative data in low speed wind tunnel tests. On the other hand, for high speed wind tunnel tests, stability derivative data are usually obtained with respect to body axes oriented by a convenient longitudinal reference line of the airplane, such as the fuselage reference line or the wing chord line. Again, in the supersonic range, theoretical derivatives are also easier to evaluate with respect to body axes for which the x-axis lies parallel to the wing chord. Finally, stability derivatives obtained from flight tests are usually oriented with respect to body axes; here the x-axis is determined by the instrument alignment in the airplane.

If, as in this volume, the stability axis system is chosen as the basic system, then stability derivative data based on "wind tunnel" or on body axes should be converted to the stability axis system. Whether this conversion is actually required for any particular case depends upon the particular axis system involved, the magnitude of the angular displacement between the systems, and the desired accuracy of the stability derivatives for the stability axis system. As a general rule, however, it is necessary to make sure that all data are expressed in the same axis system.

SECTION 3 – DETAILED ANALYSIS OF THE BASIC NON-DIMENSIONAL DERIVATIVES

This section gives a short physical explanation of how each stability derivative arises, its importance in the overall stability and control problem, and a qualitative estimate of desirable values for design purposes.

The plan is to consider each derivative in turn, starting with the longitudinal derivatives pertaining to the drag, lift, and pitching moment coefficients, C_D, C_L, and C_m, and then progressing to the lateral derivatives related to the side force, yawing moment, and rolling moment coefficients, C_y, C_n, C_l.

It is apparent from this plan that certain limits have been imposed upon the scope of this discussion. A more complete analysis would include a detailed discussion of the effect of airframe configuration, Mach number, aeroelasticity, unsteady flow, etc., upon each derivative, rather than the general discussion of such factors which appears in Section 4 of this chapter. In addition, a more complete analysis would include means of esti-

mating values of stability derivatives for airframe configurations in the preliminary design stage, and finally it would supply a means of evaluating the probable accuracies of these values. Only with a complete knowledge of all the variables that affect stability derivatives could the generalized problem of an optimum airframe-autopilot-controls system be solved.

Even if sufficient information were available for a complete detailed analysis of the basic non-dimensional stability derivatives applicable to all airframes operated at any flight condition, the final product, although it might be of great benefit to the aerodynamicist, would be far too unwieldy and detailed to be of use to all those concerned with an integrated airframe-autopilot-controls system. It is hoped, therefore, that the following pages succeed in their basic purpose of providing a physical "feel" for stability derivatives. This purpose may seem modest in the light of the overall problem, but if it is achieved, considerable progress will have been made in broadening the outlook of the various specialists concerned with this problem of optimization.

It is appropriate at this point to enumerate the specific limitations in the analysis and interpretation of the material in this section:

1. The derivatives are discussed with reference to jet fighter type aircraft having wings of aspect ratio less than 6.0 and operating up to Mach numbers of approximately 2.0. Some of the statements and conclusions may not be entirely applicable to bomber type or high aspect ratio wing type of aircraft.
2. Unless otherwise mentioned, all statements relate to an airframe alone or to the airplane plus human pilot. Some of the statements do not necessarily apply to the airframe-plus-autopilot combinations.
3. Unless otherwise mentioned, all statements are for an inelastic airframe.
4. Unless otherwise mentioned, all statements are for an airframe in the aerodynamically clean configuration.
5. Unless otherwise mentioned, all statements are for unstalled flight.

In addition to recognizing these specific limitations upon the following material, it may be helpful if certain terms are explained before proceeding with the discussion of the stability derivatives themselves.

In certain instances a distinction is made between directional and lateral modes. Directional modes involve sideslip and yawing motion only. Lateral modes, used in this particular sense, involve rolling motion only. However, both directional and lateral modes are involved in the so-called lateral motions used in a general sense to distinguish them from longitudinal motions.

Reference is made to the two classes of stability derivatives: static and dynamic. The static derivatives arise from the position of the airframe with respect to the relative wind, and include such derivatives as C_{L_α}, C_{m_α}, C_{n_β}, and C_{l_β}. The dynamic derivatives arise from the motion (velocities) of the airframe, and include such derivatives as C_{m_q}, $C_{m_{\dot\alpha}}$, C_{n_r}, and C_{l_p}. Although the derivative $C_{n_{\dot\beta}}$ is discussed, no reference is made to the associated derivatives $C_{y_{\dot\beta}}$ and $C_{l_{\dot\beta}}$ because little is known about them.

In discussing desirable values of stability derivatives, there are usually three considerations involved: performance, stability, and control. In selecting values for derivatives where these three considerations have mutually conflicting requirements, it should be pointed out that in present design practice performance considerations come first, followed by control, and then stability.

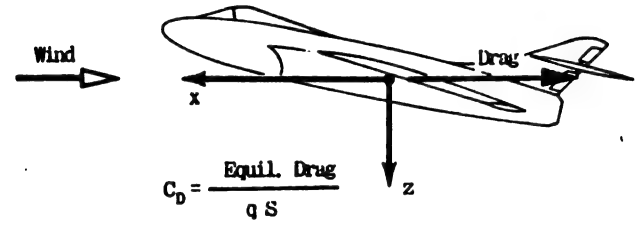

Figure IV-1 Equilibrium Drag Coefficient

C_D

Although not referred to as a stability derivative in the usual sense, the equilibrium drag coefficient, C_D, is the main contributor to the dimensional stability derivative parameter X_u*, the change in fore and aft force with forward velocity, and a minor contributor to the dimensional stability derivative parameter Z_w**, the change in vertical force with angle of attack.

In general, any portion of the airframe in contact with the external airstream contributes to the airframe drag. The fuselage, engine nacelles, external stores, tail surfaces, and internal engine ducts all contribute relatively small increments in comparison with the wing which contributes the major portion of the drag, especially at high angles of attack or high Mach numbers.

By definition, the drag coefficient is always measured along the direction of the relative wind; hence the equilibrium drag coefficient is measured along the negative equilibrium x-axis in the stability axis system (Figure IV-1) and is always positive in sign. In contrast, it should be pointed out that the derivative X_u is at all times measured along the x-axis and is always negative in sign.

As far as the performance of an airframe is concerned—range, speed, rate of climb, etc.—the drag coefficient is one of the most important parameters. It is apparent, then, that a desirable value of C_D is one which is as

* $X_u = \rho \frac{SU}{m}\left[-C_D - C_{D_u}\right]$

** $Z_w = \rho \frac{SU}{2m}\left[-C_{L_\alpha} - C_D\right]$

small as possible.

On the other hand, when airframe dynamics are considered, C_D is the main contributor to the damping of the phugoid mode, and the larger the value of C_D, the better the damping. However, flight experience has shown that the damping of the phugoid is of little importance in determining satisfactory flying qualities of an airframe as far as the pilot is concerned. Clearly then, performance requirements rather than flying qualities should dictate the design value of C_D.

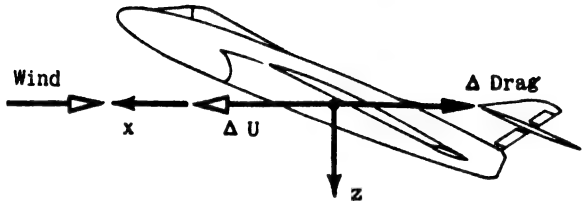

$$C_{D_u} = \frac{U}{2}\frac{\partial C_D}{\partial U} = \frac{U}{2qS}\frac{\partial (Drag)}{\partial U}$$

Figure IV-2 Drag Coefficient Change Due to Variation in Forward Velocity

C_{D_u}

The stability derivative C_{D_u} is the change in drag coefficient with varying forward velocity, the angle of attack and the altitude remaining constant. To non-dimensionalize this derivative, C_{D_u} in this manual is defined mathematically as $(U/2)(\partial C_D/\partial u)$, a term which appears as a part of the dimensional derivative parameter X_u^*, the change in fore and aft force with change in forward velocity.

C_{D_u} can arise from two sources: Mach number effects and aeroelastic effects. In most cases C_{D_u} arising from the latter of these is zero or very small and can be neglected. C_{D_u} arising from Mach number effects is very small for low subsonic Mach numbers but sometimes reaches a considerable positive value near the critical Mach number of an airframe $(.8<M<1.0)$, where a large increase in drag occurs.

The effect of a positive value of C_{D_u} on longitudinal dynamics is an increase in the damping of the phugoid mode. However, as pointed out under the discussion of C_D, this damping is believed to be of little importance as far as satisfactory flying qualities of an airframe are concerned. From a performance viewpoint, the smallest possible value of C_{D_u} is desirable because of the low rise in drag associated with it.

Until the relatively recent advent of high Mach number flight, the derivative C_{D_u} was seldom mentioned in stability and control literature. There is evidence in the current literature that some consideration is being given it, but until further results are published, definitive information regarding the importance of C_{D_u} in longitudinal dynamics will not be available.

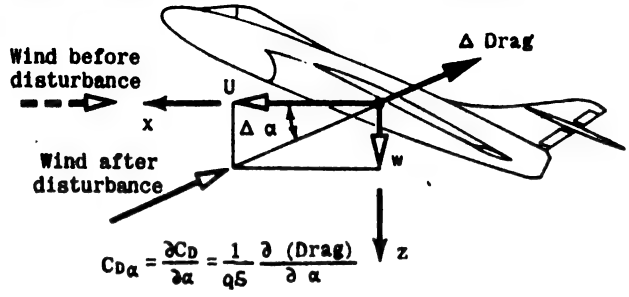

$$C_{D_\alpha} = \frac{\partial C_D}{\partial \alpha} = \frac{1}{qS}\frac{\partial (Drag)}{\partial \alpha}$$

Figure IV-3 Drag Coefficient Change Due to Variation in Angle of Attack

C_{D_α}

The stability derivative C_{D_α} is the change in drag coefficient with varying angle of attack. When the angle of attack of an airframe increases from the equilibrium condition, the total drag will increase; hence C_{D_α} will normally be positive in sign. By far the largest contribution to C_{D_α} comes from the wing, but there are small contributions from the horizontal tail and the fuselage. It is to be kept in mind that drag is always measured with respect to the relative wind and not along the x-axis in the stability axis system. However, the dimensional derivative parameter X_w^{**}, of which C_{D_α} is a part, is measured along the x-axis.

The derivative C_{D_α} is usually unimportant in airframe dynamics. It affects mostly the phugoid mode, where a decrease in C_{D_α} increases stability; however, this effect is slight, mainly because the changes in angle of attack occurring in phugoid motion are small.

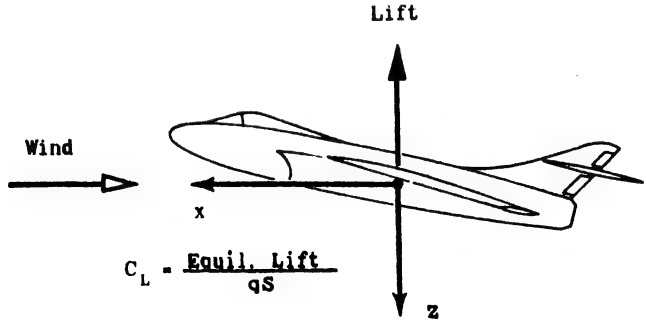

$$C_L = \frac{\text{Equil. Lift}}{qS}$$

Figure IV-4 Equilibrium Lift Coefficient

$$^* X_u = \rho\frac{SU}{m}\left[-C_D - \frac{U}{2}\frac{\partial C_D}{\partial U}\right]$$

$$^{**} X_w = \rho\frac{SU}{2m}\left[C_L - C_{D_\alpha}\right]$$

C_L

Although not referred to as a stability derivative in the usual sense, the equilibrium lift coefficient, C_L, contributes the major portion of the dimensional stability derivative parameter Z_u*, the change in vertical force with varying forward velocity, and X_w, the change in fore and aft force with varying angle of attack.

By definition, lift coefficient is always measured perpendicular to the relative wind and is positive upward (Figure IV-4) and so the equilibrium lift coefficient is measured along the negative equilibrium z-axis of the stability axis system. On the other hand, Z_u is always measured along the positive z-axis and is positive downward.

The equilibrium lift coefficient must be distinguished from the transient lift coefficient, the value of which can change during a disturbance. Normally, the equilibrium lift coefficient of an airframe is positive in sign; however, the transient lift coefficient can be of negative sign during push-over type maneuvers or in gusty weather flight.

The equilibrium lift coefficient, C_L, is one of the basic parameters used to specify the flight condition of an airframe. Low values of C_L are associated with low angles of attack and high speeds, whereas high values of C_L are associated with high angles of attack and low speeds.

In longitudinal dynamics, variations in the equilibrium lift coefficient principally affect the phugoid mode, with both the damping and the period decreasing with an increase in C_L. In addition, because many of the lateral derivatives are functions of C_L, the lateral dynamics are also affected; the main effect is a decrease in Dutch roll damping with an increase in C_L.

Although low values for C_L are therefore preferable for stability, more important performance considerations usually take precedence in determining the desirable values of this derivative.

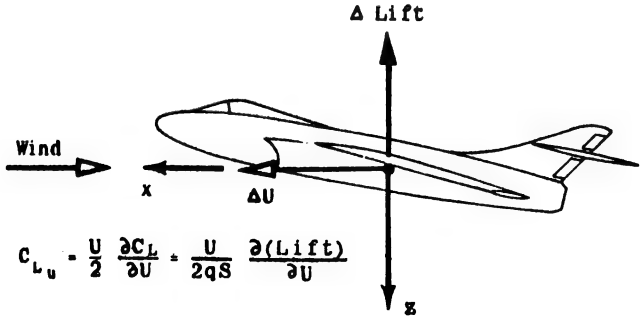

Figure IV-5 Lift Coefficient Change Due to Variation in Forward Velocity

* $Z_u = \rho \frac{SU}{m}\left[-C_L - C_{L_u}\right]$

As far as performance is concerned, a large range of equilibrium lift coefficients is desirable because a low value of C_L and its associated low drag is desirable to attain high cruising speeds, and yet a high value of C_L is desirable to permit low landing speeds.

C_{L_u}

The stability derivative C_{L_u} is the change in lift coefficient with variations in forward velocity, angle of attack and altitude remaining constant. To non-dimensionalize this derivative, C_{L_u} in this volume is defined as $(U/2)(\partial C_L/\partial U)$, a term which appears as a part of the dimensional derivative parameter Z_u**, the change in vertical force with varying forward velocity.

C_{L_u} arises from two sources: Mach number effects and aeroelastic effects. The magnitude of the total C_{L_u} can vary considerably and its sign can change, depending not only upon the airframe geometry and its elastic properties, but also upon the Mach number and dynamic pressure at which it is flying. The magnitude of C_{L_u} is negligibly small for low speed flight, but it may reach a considerable value near the critical Mach number of the airframe.

Until recently, the derivative C_{L_u} was given little or no consideration in stability and control research, and because of the present lack of published information concerning it, the relative importance of C_{L_u} has not been established. It is believed, however, that the effect of C_{L_u} on longitudinal stability and control is quite small, and that it mainly affects the phugoid mode in such a manner that a positive value of C_{L_u} decreases the period of the phugoid.

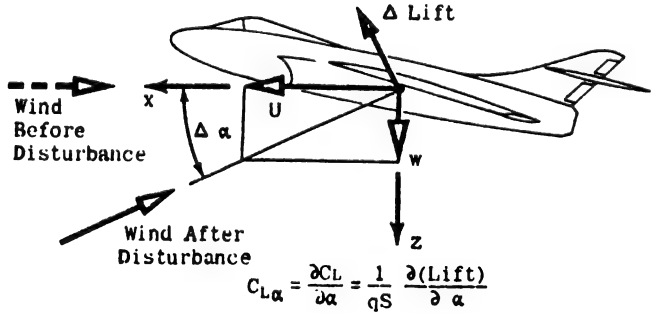

Figure IV-6 Lift Coefficient Change Due to Variation in Angle of Attack

** $Z_u = \rho \frac{SU}{m}\left[-C_L - \frac{U}{2}\frac{\partial C_L}{\partial U}\right]$

C_{L_α}

The stability derivative C_{L_α} is the change in lift coefficient with varying angle of attack. C_{L_α} is commonly known as the "lift curve slope." When the angle of attack of the airframe is increased, the lift force will increase more or less linearly until the wing stalls. The derivative C_{L_α} is therefore always positive in sign at angles of attack below the stall. It should be pointed out that the aerodynamic lift force by convention is always measured perpendicular to the relative wind (flight path).

The total airframe C_{L_α} is made up of contributions from the wing, the fuselage, and the horizontal tail. Ordinarily the wing accounts for about 80% to 90% of the total C_{L_α}, although the wing contribution becomes less if the size of the fuselage is large in comparison with the size of the wing.

The derivative C_{L_α} is very important to the equilibrium flight condition of an airframe; it is also important in dynamic considerations.

In the equilibrium flight condition, a high value of C_{L_α} is desirable because, for a given angle of attack, the airframe with the higher value of C_{L_α} will usually have a lower drag, and therefore better performance. C_{L_α} is also important in establishing the attitude of the airframe at landing and take-off; when the value of C_{L_α} is low, the airframe must land and take-off at a relatively high angle of attack. If this has to be done, pilot visibility is impaired, and difficulty in designing the landing gear is aggravated.

As far as dynamic stability is concerned, this derivative makes an important contribution to the damping of the longitudinal short period mode for all aircraft and especially for tailless aircraft because in this case almost all the damping of the short period mode comes from C_{L_α}.

A high value of C_{L_α} would therefore be desirable on all counts were it not for the fact that such values of C_{L_α} are necessarily associated with a high aspect-ratio unswept wing—a configuration which is contrary to present design trends; consequently this high C_{L_α} is not always realized in practice.

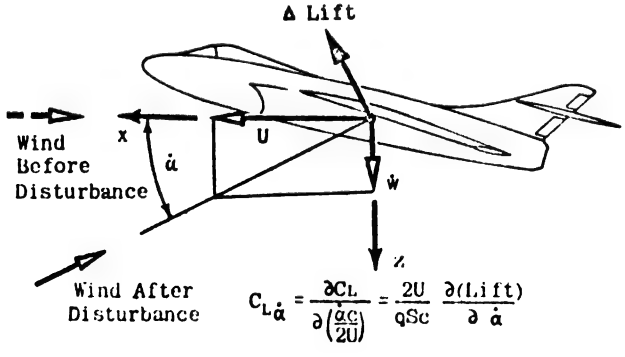

Figure IV-7 Lift Coefficient Change Due to Variation in Rate of Change of Angle of Attack

$C_{L_{\dot\alpha}}$

The stability derivative $C_{L_{\dot\alpha}}$ is the change in lift coefficient with variation in rate of change of angle of attack. This derivative is sometimes referred to as $C_{L_{\dot w}}$, the change in lift coefficient with vertical acceleration. The relation between these two forms is given by $C_{L_{\dot\alpha}} = U C_{L_{\dot w}}$ since $\dot\alpha = \dot w/U$. These derivatives arise from a so-called "plunging" type of motion along the z-axis, in which the angle of pitch, θ, remains zero during the disturbance.

The derivative $C_{L_{\dot\alpha}}$ arises essentially from two independent sources: an aerodynamic time lag effect and various "dead-weight" aeroelastic effects. For low speed flight, $C_{L_{\dot\alpha}}$ arises mostly from the aerodynamic lag effect, and its sign is positive. For high speed flight the sign of $C_{L_{\dot\alpha}}$ can be positive or negative, depending on the nature of the aeroelastic effects.

The horizontal tail of a conventional airframe is immersed in the downwash field of the wing and is mounted some distance aft of the wing. Whenever the wing undergoes a change in angle of attack, the downwash field is altered; and since it takes a finite length of time before this downwash alteration arrives at the tail, the resulting lift on the tail lags the motion of the aircraft and creates the derivative $C_{L_{\dot\alpha}}$. Even for tailless aircraft $C_{L_{\dot\alpha}}$ apparently has a value due to the fact that the wing must accelerate the air mass in its path as it accelerates (apparent mass effect).

Since the type of motion under consideration is an acceleration ($\dot w$), $C_{L_{\dot\alpha}}$ can also arise from aeroelastic effects such as wing twisting due to the dead weight moment caused by nacelles projecting in front of the wing, and from fuselage bending caused by the dead weight of the aft fuselage and empennage section, both of which change the effective angle of attack of the horizontal tail.

The derivative $C_{L_{\dot\alpha}}$ is usually unimportant in longitudinal dynamics. The effect of $C_{L_{\dot\alpha}}$ on longitudinal dynamics is essentially the same as if the airframe's mass or inertia were changed in the equation relating the forces in the z direction. This effect is very small, and for this reason $C_{L_{\dot\alpha}}$ is sometimes neglected in longitudinal dynamic analysis.

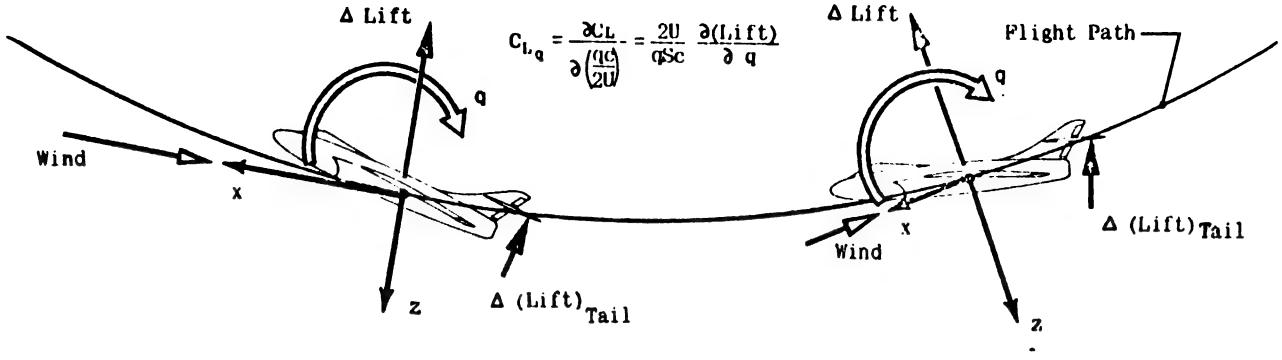

Figure IV-8 Lift Coefficient Change Due to Variation in Pitching Velocity

C_{L_q}

The stability derivative C_{L_q} is the change in lift coefficient with no change of angle of attack of the airplane as a whole with varying pitching velocity. As the airframe pitches about its center of gravity, the angle of attack of the horizontal tail changes, and a lift force is developed on the horizontal tail producing a contribution to the derivative C_{L_q}. The sign of this contribution is positive.

There is also a contribution to C_{L_q} because of various "dead weight" aeroelastic effects. Since the airframe is moving in a curved flight path due to its pitching, a centrifugal force is developed on all the components of the airframe. This force can cause the wing to twist as a result of the dead weight moment of overhanging nacelles, and can cause the horizontal tail angle of attack to change as a result of fuselage bending due to the weight of the tail section.

In low speed flight, C_{L_q} comes mostly from the effect of the curved flight path on the horizontal tail and its sign is positive. In high speed flight the sign of C_{L_q} can be positive or negative, depending on the nature of the aeroelastic effects.

In past experience, the effect of C_{L_q} on longitudinal stability has usually been very small and it has therefore been neglected in dynamic analyses, but because of the possibility of great aeroelastic effects, especially at high Mach number flight, the magnitude of C_{L_q} may be increased considerably and it is not certain that it can be neglected.

$C_{L_{\delta_E}}$

The stability derivative $C_{L_{\delta_E}}$ is the change in lift coefficient with changes in elevator deflection. When the elevator is deflected upward a negative increment in lift on the horizontal tail results; hence the derivative $C_{L_{\delta_E}}$ is normally negative in sign.

On conventional aircraft with the horizontal tail mounted at an appreciable distance aft of the center of gravity, $C_{L_{\delta_E}}$ is usually very small and its effect is unimportant; however on tailless aircraft, $C_{L_{\delta_E}}$ is comparatively large, and cannot be neglected.

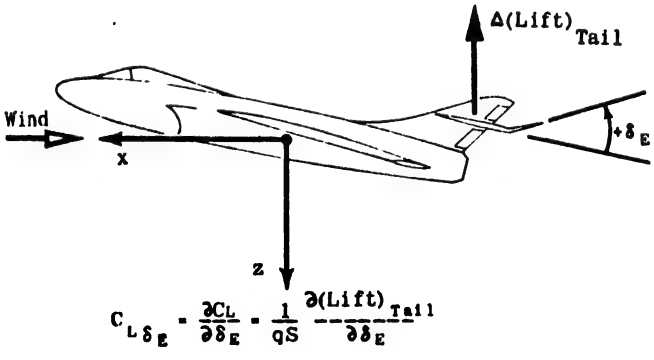

Figure IV-9 Lift Coefficient Change Due to Variation in Elevator Deflection

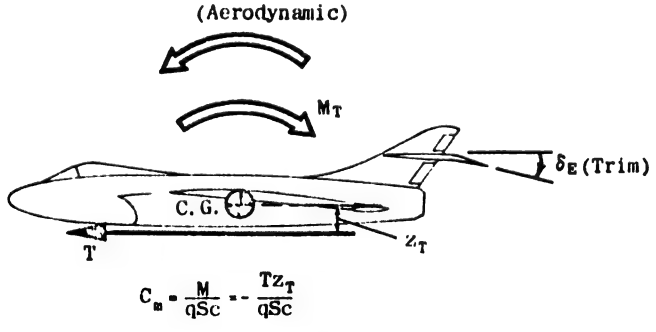

Figure IV-10 Aerodynamic Pitching Moment Coefficient in Equilibrium Flight

C_m

C_m is the aerodynamic pitching moment coefficient about the c.g. required to balance the moment coefficient due to thrust when the airframe is in the equilibrium flight

condition. It is not usually referred to as a stability derivative although it appears in the dimensional stability derivative M_u*.

It will be shown later that the thrust moment coefficient is given by $C_{m_T} = Tz_T/qSc$ where T is the thrust and z_T is its moment arm about the c.g. (Figure IV-10). In order to balance out this thrust moment coefficient in the equilibrium condition the required aerodynamic moment coefficient (which would come mostly from a trim elevator deflection) must be the same magnitude but of opposite sign:

$$C_m = -C_{m_T} = -\frac{Tz_T}{qSc}$$

The sign of C_m is negative when the line of thrust is below the c.g.

From the above expression it is apparent that the value of C_m will be zero only if the thrust is zero (gliding flight), or if the thrust moment arm, z_T, is zero. It is important to point out that in most of the literature dealing with the classical equations of motion gliding flight has been assumed, and C_m has therefore been zero. When considering powered flight, however, the equilibrium value of C_m is not necessarily zero, and should be included in dynamic longitudinal stability studies.

The importance of C_m in airframe dynamics has not been definitely established. It principally affects the longitudinal phugoid mode where positive values of C_m will tend to decrease the period of the oscillation.

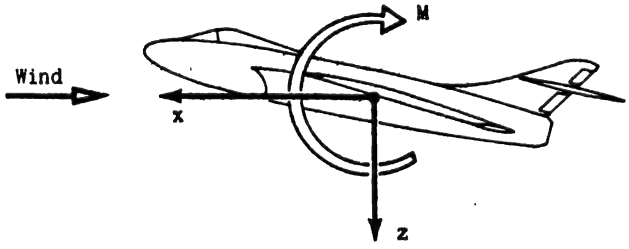

Figure IV-11 Pitching Moment Change Due to to Variation in Forward Velocity

C_{m_u}

The stability derivative C_{m_u} is the change in pitching moment coefficient with variation in forward velocity, angle of attack and altitude remaining constant. In order to non-dimensionalize this derivative, C_{m_u} in this volume is defined as $(U/2)(\partial C_m/\partial U)$.

The magnitude of C_{m_u} can vary considerably and the sign can change, depending upon such factors as the airframe's geometry and its elastic properties, and the Mach number and dynamic pressure at which it is flying. This derivative can arise from three sources: thrust or power effects, Mach number effects, and aeroelastic effects.

In the past, the literature has treated C_{m_u} only as a power effect arising from the propwash of propeller-driven aircraft. Today, however, because of the use of jet engines and the associated alleviation of power effects on dynamic stability, the C_{m_u} from thrust effects is probably small. (The thrust effects themselves are discussed more thoroughly in part 5 (g) of Section 4.) On the other hand, the contributions to C_{m_u} due to Mach number and aeroelastic effects are becoming more and more important, and it is believed that these effects should no longer be neglected when evaluating C_{m_u}.

The importance of the derivative C_{m_u} in airframe dynamics has not been definitely established. It principally affects the longitudinal phugoid mode, where positive values of C_{m_u} will tend to decrease both the period and the damping of the oscillation. This effect can become quite objectionable, especially when the phugoid motion is lightly damped. It appears therefore that zero, or at most, very small values of C_{m_u} are desirable.

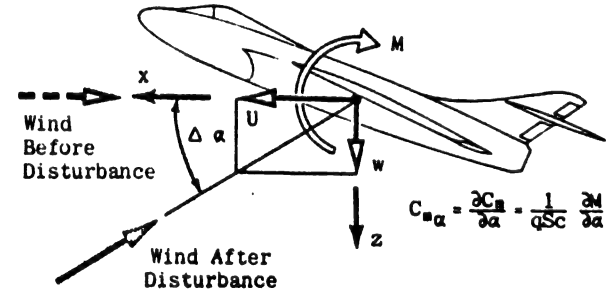

Figure IV-12 Pitching Moment Coefficient Change Due to Variation in Angle of Attack

C_{m_α}

The stability derivative C_{m_α} is the change in pitching moment coefficient with varying angle of attack and is commonly referred to as the longitudinal static stability derivative. When the angle of attack of the airframe increases from the equilibrium condition, the increased lift on the horizontal tail causes a negative pitching moment about the center of gravity of the airframe. Simultaneously, the increased lift of the wing causes a positive or negative pitching moment, depending on the fore and aft location of the lift vector with respect to the center of gravity. These contributions together with the pitching moment contribution of the fuselage are combined to establish the derivative C_{m_α}.

The magnitude and sign of the total C_{m_α} for a particular airframe configuration are thus a function of the center of gravity position, and this fact is very important in

* $M_u = \frac{\rho S U c}{I_y}\left[C_m + C_{m_u}\right]$

longitudinal stability and control. The aerodynamic center of the airframe is the fore and aft location along the airframe where the increment of lift due to a change in angle of attack effectively acts. If the center of gravity is ahead of the aerodynamic center, the value of C_{m_α} is negative, and the airframe is said to possess static longitudinal stability. Conversely, if the center of gravity is aft of the aerodynamic center, the value of C_{m_α} is positive, and the airframe is then statically unstable.

C_{m_α} is perhaps the most important derivative as far as longitudinal stability and control are concerned. C_{m_α} primarily establishes the natural frequency of the short period mode, and is a major factor in determining the response of the airframe to elevator motions and to gusts. In general, a large negative value of C_{m_α} (i.e., large static stability) is desirable for good flying qualities. However, if C_{m_α} is too large, the required elevator effectiveness for satisfactory control may become unreasonably high. A compromise is thus necessary in selecting a design range for C_{m_α}.

Design values of static stability are usually expressed not in terms of C_{m_α}, but rather in terms of the derivative

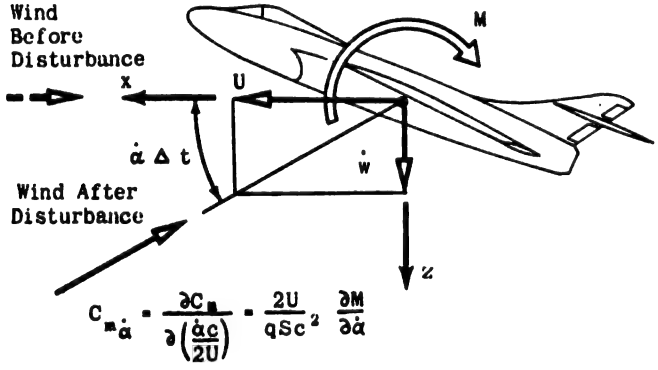

Figure IV-13 Pitching Moment Coefficient Change Due to Variation in Rate of Change of Angle of Attack

$C_{m_{C_L}}$, where the relation is: $C_{m_\alpha} = C_{m_{C_L}} C_{L_\alpha}$.

It should be pointed out that $C_{m_{C_L}}$ in the above expression is actually a partial derivative for which the forward speed remains constant.

$C_{m_{\dot{\alpha}}}$

The stability derivative $C_{m_{\dot{\alpha}}}$ is the change in pitching moment coefficient with variation in rate of change of angle of attack. This derivative is sometimes referred to as $C_{m_{\dot{w}}}$, the change in pitching moment coefficient with change in vertical acceleration. The relation between these two forms is given by $C_{m_{\dot{\alpha}}} = UC_{m_{\dot{w}}}$, since $\dot{\alpha} \approx \dot{w}/U$. These derivatives arise from a so-called "plunging" type of motion along the z-axis, in which the angle of pitch, θ, remains zero during the disturbance.

The derivative $C_{m_{\dot{\alpha}}}$ arises essentially from two independent sources: an aerodynamic time lag effect and various "dead weight" aeroelastic effects. For low speed flight $C_{m_{\dot{\alpha}}}$ will come mostly from the aerodynamic lag effect and its sign will be negative. For high speed flight the sign of $C_{m_{\dot{\alpha}}}$ can be positive or negative, depending on the nature of the aeroelastic effects.

The horizontal tail of a conventional aircraft is mounted some distance aft of the wing and is immersed in the downwash field of the wing. Whenever the wing undergoes a change in angle of attack, the downwash field is altered, and since it takes a finite length of time before this downwash alteration arrives at the tail, the resulting lift on the tail, and consequently the resulting pitching moment on the airframe, lags the motion and creates the derivative $C_{m_{\dot{\alpha}}}$. Even for tailless aircraft there apparently exists a value for $C_{m_{\dot{\alpha}}}$ due to the fact that the wing must accelerate the air mass in its path as it accelerates (apparent mass effect).

Since the type of motion under consideration is an acceleration ($\dot{w}$), $C_{m_{\dot{\alpha}}}$ can also arise from aeroelastic effects such as wing twisting due to the dead weight moment caused by the projection of the nacelles in front

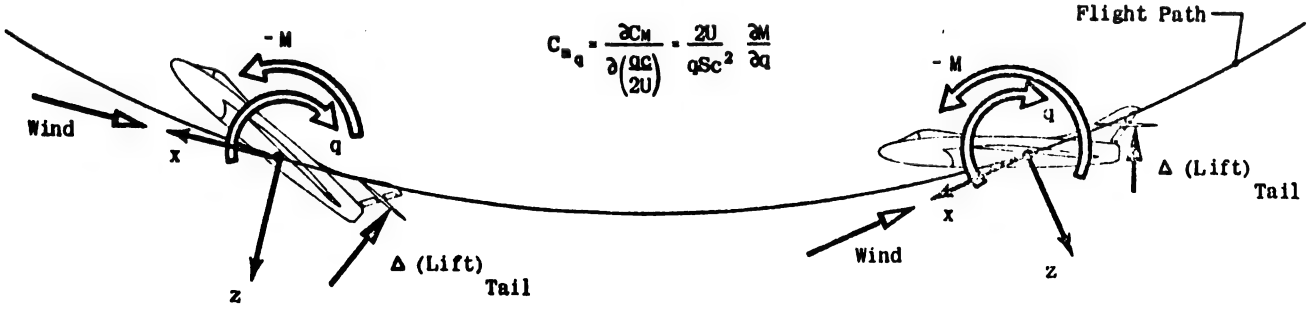

Figure IV-14 Pitching Moment Coefficient Due to Variation in Pitching Velocity

of the wing, and bending of the fuselage caused by the dead weight of the aft fuselage and empennage section. This twisting and bending changes the effective angle of attack of the horizontal tail.

The derivative $C_{m_{\dot{\alpha}}}$ is quite important in longitudinal dynamics because it is involved in the damping of the short period mode. A negative value of $C_{m_{\dot{\alpha}}}$ increases the damping of this mode; consequently, high negative values of this derivative are desirable.

C_{m_q}

The stability derivative C_{m_q} is the change in pitching moment coefficient with varying pitch velocity and is commonly referred to as the pitch damping derivative. As the airframe pitches about its center of gravity path, the angle of attack of the horizontal tail changes, and a lift force is developed on the horizontal tail producing a negative pitching moment on the airframe and hence a contribution to the derivative C_{m_q}.

There is also a contribution to C_{m_q} because of various "dead weight" aeroelastic effects. Since the airframe is moving in a curved flight path due to its pitching, a centrifugal force is developed on all the components of the airframe. The force can cause the wing to twist as a result of the dead weight moment of overhanging nacelles, and can cause the horizontal tail angle of attack to change as a result of fuselage bending due to the weight of the tail section.

In low speed flight, C_{m_q} comes mostly from the effect of the curved flight path on the horizontal tail and its sign is negative. In high speed flight the sign of C_{m_q} can be positive or negative, depending on the nature of the aeroelastic effects.

The derivative C_{m_q} is very important in longitudinal dynamics because it contributes a major portion of the damping of the short period mode for conventional aircraft. As pointed out, this damping effect comes mostly from the horizontal tail. For tailless aircraft, the magnitude of C_{m_q} is consequently small; this is the main reason for the usually poor damping of this type of configuration. C_{m_q} is also involved to a certain extent in the damping of the phugoid mode. In almost all cases, high negative values of C_{m_q} are desirable.

Usually C_{m_q} is not considered as a preliminary design parameter except perhaps in tailless aircraft configurations. In the light of the present design trend toward larger radii of gyration in pitch and higher altitude flight, it is believed that consideration of C_{m_q} is necessary in the preliminary design stage.

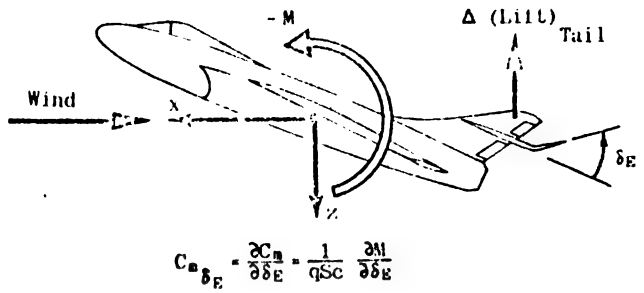

Figure IV-15 Pitching Moment Coefficient Change Due to Variation in Elevator Deflection

$C_{m_{\delta_E}}$

The stability derivative $C_{m_{\delta_E}}$ is the change in pitching moment coefficient with changes in elevator deflection and is commonly referred to as the elevator effectiveness (or elevator power). When the elevator is deflected upward, the resultant increment in lift on the horizontal tail creates a positive pitching moment about the center of gravity of the airframe; hence the derivative $C_{m_{\delta_E}}$ is normally positive in sign.

The primary function of the elevator is to control the angle of attack of the airframe both in equilibrium flight and in maneuvers. This function is usually considered to be the most important of all the control functions about the three axes, and so the elevator control effectiveness, $C_{m_{\delta_E}}$ is of great importance in airframe design.

The design value of $C_{m_{\delta_E}}$ is essentially determined by the anticipated fore and aft center of gravity travel of an airframe. The larger the center of gravity range, the larger the required value of $C_{m_{\delta_E}}$ will be. To keep the size of the elevator within practical bounds, the center of gravity range must be held as small as possible. Thus in many cases of design, the maximum practical $C_{m_{\delta_E}}$ determines the allowable center of gravity range, and in other cases the center of gravity range determines the value of $C_{m_{\delta_E}}$. A desirable value of $C_{m_{\delta_E}}$ cannot be stated in general, for each design case must be analyzed separately.

C_{y_β}

The stability derivative C_{y_β} is the change in side force coefficient with changing sideslip angle. It can be referred to as the "side force damping derivative." When the airframe sideslips, the relative wind strikes the airframe obliquely, creating a side force, Y, on the vertical tail, the fuselage, and the wing. It must be remembered that this side force is measured along the y-axis, which is fixed to the airframe during the steady flight condition and moves with the airframe during a disturbance.

The major portion of C_{y_β} usually comes from the ver-

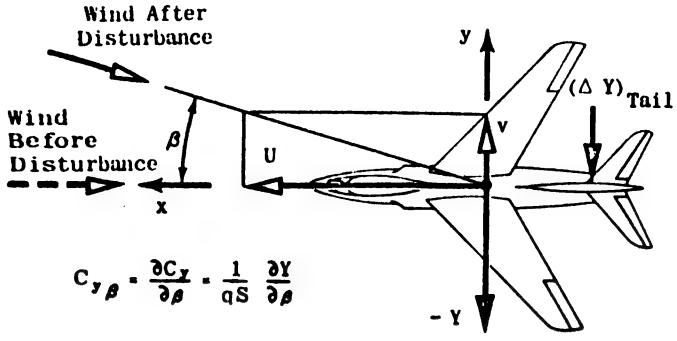

Figure IV-16 Side Force Coefficient Change Due to Variation in Sideslip Angle

tical tail, with smaller contributions from the fuselage and wing. It is always negative in sign for practical airframe configurations.

The derivative C_{y_β} is fairly important in lateral dynamics. Because it contributes to the damping of the Dutch roll mode, a large negative value of this derivative would appear desirable; however, a large negative value of C_{y_β} may create an undesirable lag effect in the airplane's response when an attempt is made to hold the wings level in rough air, or to perform aileron maneuvers.

Usually, C_{y_β} is not taken as an important parameter in the preliminary design of an airframe. C_{y_β} comes mostly from the vertical tail, and the design of the vertical tail is dictated primarily by the directional stability $\left(C_{n_\beta}\right)$ requirements. However, reconsideration of the importance of C_{y_β} may be necessary if some types of autopilots are to be installed in the airframe.

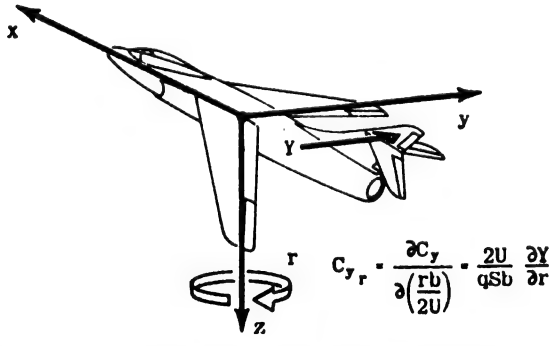

Figure IV-17 Side Force Coefficient Change Due to Variation in Yawing Velocity

C_{y_r}

The stability derivative C_{y_r} is the change in side force coefficient with variation in yawing velocity. Since the vertical tail is mounted at some distance behind the airframe's center of gravity, whenever the airframe is rotating at a yaw velocity, r, there is an effective side force developed on the tail, and this force gives the main contribution to the derivative C_{y_r}, which will be positive and quite small.

C_{y_r} is of little importance in lateral dynamics; consequently, it is common practice to neglect this derivative in lateral calculations.

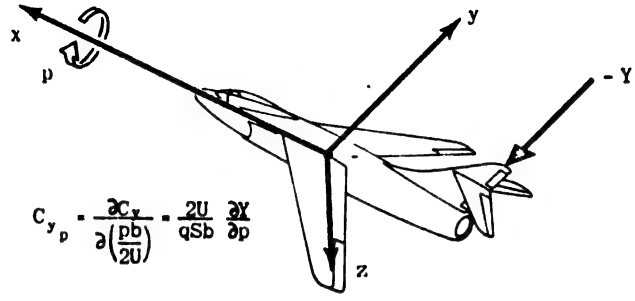

Figure IV-18 Side Force Coefficient Change Due to Variation in Rolling Velocity

C_{y_p}

The stability derivative C_{y_p} is the change in side force coefficient with variation in rolling velocity. It arises mainly from the vertical tail, although for some airframe configurations there is also an appreciable contribution from the wing. A side force is produced on the vertical tail when the airframe has a rolling velocity, p, about the x-axis, if the vertical tail is located either above or below the x-axis; this is caused by the effective angle of attack on the tail, due to p. The sign of C_{y_p} can be positive or negative, depending on the vertical tail geometry, the sidewash from the wing, and the equilibrium angle of attack of the airframe.

Since C_{y_p} is of very little importance in lateral dynamics, it is common practice to neglect this derivative in lateral dynamic calculations.

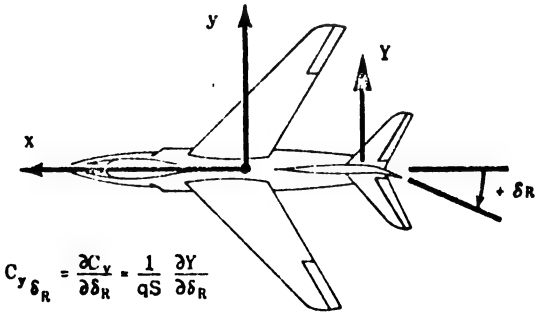

Figure IV-19 Side Force Coefficient Change Due to Variation in Rudder Deflection

$C_{y_{\delta_R}}$

The stability derivative $C_{y_{\delta_R}}$ is the change in side force coefficient with variation in rudder deflection. According to the sign convention adopted in this volume, a positive rudder deflection gives a positive side force, hence the derivative $C_{y_{\delta_R}}$ is positive in sign.

If the airframe alone is considered, the effect of the derivative $C_{y_{\delta_R}}$ is unimportant in lateral stability and control. For this reason it is usually neglected in lateral dynamic analyses. However, when the installation of an autopilot is considered, $C_{y_{\delta_R}}$ should not be neglected in the design analyses because its influence on the combined airframe plus autopilot system stability may not be negligible.

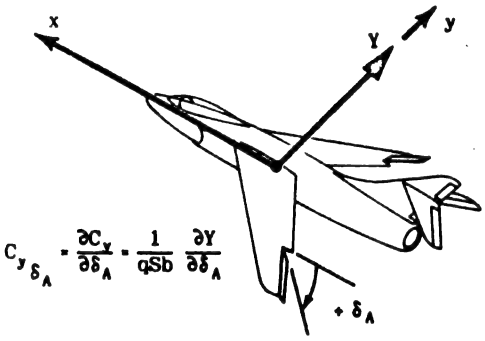

Figure IV-20 Side Force Coefficient Change Due to Variation in Aileron Deflection

$C_{y_{\delta_A}}$

The stability derivative $C_{y_{\delta_A}}$ is the change in side force coefficient with aileron deflection. For most conventional airframe configurations, the magnitude of this derivative is zero; however, for certain aircraft with highly swept wings of low aspect ratio, a value for this derivative other than zero may exist.

The effect $C_{y_{\delta_A}}$ on lateral stability and control is not known, but it is believed to be negligibly small.

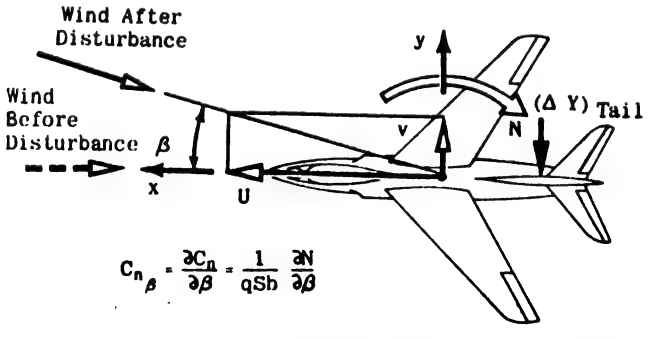

Figure IV-21 Yawing Moment Coefficient Change Due to Sideslip

C_{n_β}

The stability derivative C_{n_β} is the change in yawing moment coefficient with variation in sideslip angle. It is usually referred to as the static directional derivative or the "weathercock" derivative. When the airframe sideslips, the relative wind strikes the airframe obliquely, creating a yawing moment, N, about the center of gravity. The major portion of C_{n_β} comes from the vertical tail, which stabilizes the body of the airframe just as the tail feathers of an arrow stabilize the arrow shaft. The C_{n_β} contribution due to the vertical tail is positive, signifying static directional stability, whereas the C_{n_β} due to the body is negative, signifying static directional instability. There is also a contribution to C_{n_β} from the wing, the value of which is usually positive but very small compared to the body and vertical tail contributions.

The derivative C_{n_β} is very important in determining the dynamic lateral stability and control characteristics. Most of the references concerning full-scale flight tests and free-flight wind tunnel model tests agree that C_{n_β} should be as high as possible for good flying qualities. A high value of C_{n_β} aids the pilot in effecting coordinated turns and prevents excessive sideslip and yawing motions in extreme flight maneuvers and in rough air. C_{n_β} primarily determines the natural frequency of the Dutch roll oscillatory mode of the airframe, and it is also a factor in determining the spiral stability characteristics.

Because of its important effect on the lateral characteristics, C_{n_β} is considered to be an important preliminary design parameter. To take into account airframe configurations with very high wing loadings and very short wing spans, Reference 1 recommends the following formula in determining a desirable order of magnitude of C_{n_β} for any piloted aircraft:

$$\text{Desirable} \quad C_{n_\beta} \geq +.0286 \frac{\sqrt{W}}{b}$$

According to present design tends, this formula appears to be quite appropriate for airframe plus the human pilot, but for airframes with autopilot installations, the magnitude of airframe C_{n_β}, indicated by the above formula may become unimportant. For instance, there is evidence that it may be advantageous to design an airframe with a relatively small vertical tail and yet achieve satisfactory flying qualities by artificially adding C_{n_β} by means of the autopilot.

$C_{n_{\dot\beta}}$

The stability derivative $C_{n_{\dot\beta}}$ is the change in yawing moment coefficient with variations in rate of change of sideslip angle. If the airframe is undergoing a rate of change of sideslip angle, $\dot\beta$, a yawing moment can be produced on the airframe by the vertical tail because of the sidewash time lag effects from the wing and fuselage.

Although a derivative $C_{n_{\dot\beta}}$ is known to exist, very little

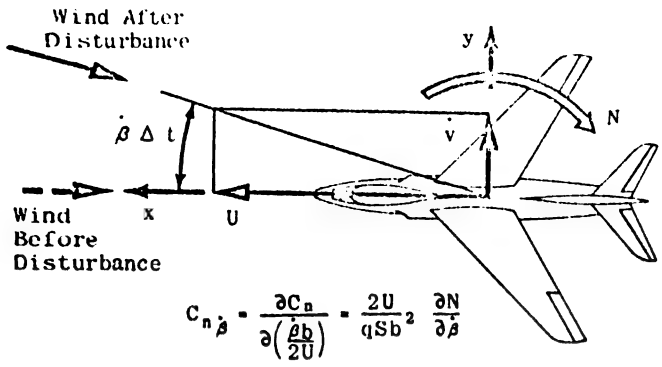

Figure IV-22 Yawing Moment Coefficient Change Due to Variation in Rate of Change of Sideslip

can be stated about its magnitude or algebraic sign because of the wide variations in opinion and in interpretation of experimental data concerning it. For most airframe configurations, $C_{n_{\dot\beta}}$ is apparently of rather small magnitude and can probably be neglected in lateral dynamic calculations. For some configurations, however, $C_{n_{\dot\beta}}$ may be of the same order of magnitude as C_{n_r} and, of course, should not be neglected. The difficulty is that there are insufficient data at present to indicate for which configurations $C_{n_{\dot\beta}}$ may or may not be of importance.

The derivative $C_{n_{\dot\beta}}$ must be distinguished from the derivative C_{n_r}. All stability derivatives are partial derivatives; that is, they are taken with respect to one independent variable at a time, the rest of the independent variables remaining fixed. Thus, $C_{n_{\dot\beta}}$ arises from a transient motion in which the sideslip angle is increasing with time but the rate of yaw remains zero, whereas C_{n_r} arises from a motion where yaw angle is increasing with time but the change in sideslip angle remains zero. During the Dutch roll oscillation of an airframe and during yaw oscillation tests on wind tunnel models, the yaw angle and the sideslip angle are both changing; consequently both $C_{n_{\dot\beta}}$ and C_{n_r} are involved in these motions.

When $C_{n_{\dot\beta}}$ cannot be neglected for a particular configuration, its effect on lateral dynamics will appear mainly in the Dutch roll damping characteristics. To increase this damping, positive values of $C_{n_{\dot\beta}}$ are desired.

C_{n_r}

The stability derivative C_{n_r} is the change in yawing moment coefficient with change of yawing velocity. It is known as the yaw damping derivative. When the airframe is yawing at an angular velocity r, a yawing moment is produced which opposes the rotation. C_{n_r} is made up of contributions from the wing, the fuselage, and the vertical tail, all of which are negative in sign. The contribution from the vertical tail is by far the largest, usually amounting to about 80% or 90% of the total C_{n_r} of the airframe.

The derivative C_{n_r} is very important in lateral dynamics because it is the main contributor to the damping of the Dutch roll oscillatory mode. It also is important to the spiral mode. For each mode, large negative values of C_{n_r} are desired.

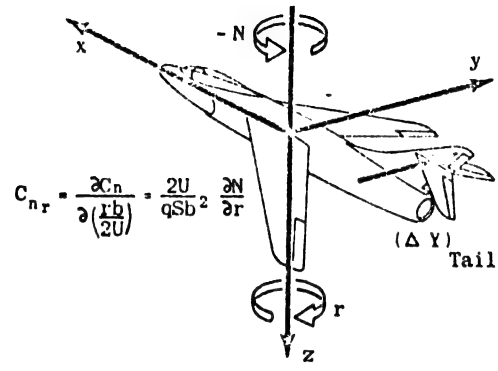

Figure IV-23 Yawing Moment Coefficient Change Due to Variation in Yawing Velocity

In the past, C_{n_r} was not considered an important design parameter because a vertical tail design which produced a reasonable value of static directional stability (C_{n_β}) was almost certain to give adequate Dutch roll damping. Today, however, because of design trends toward higher wing loadings and higher radii of gyrations in yaw in conjunction with high altitude flight, it is apparent that the vertical tail alone cannot provide sufficient C_{n_r} for the damping of the Dutch roll mode.

For present airframes without autopilots, C_{n_r} must therefore be considered of major importance in preliminary design. Adequate Dutch roll damping can be obtained by effectively adding to the derivative C_{n_r}.

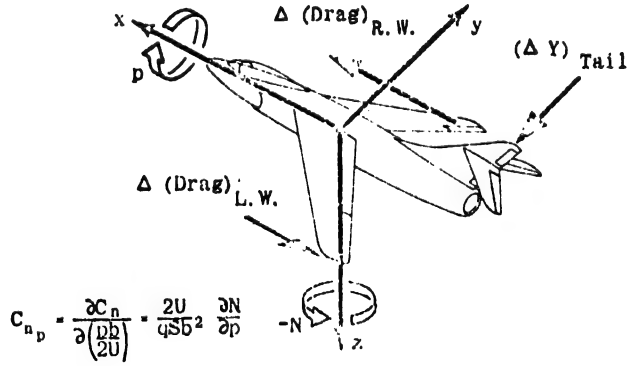

Figure IV-24 Yawing Moment Coefficient Change Due to Variation in Rolling Velocity

C_{n_p}

The stability derivative C_{n_p} is the change in yawing moment coefficient with varying rolling velocity. It

arises from two main sources: the wing and the vertical tail. A negative yawing moment is developed on the airframe because of the unsymmetrical lift distribution causing a difference between the drag on the right wing and that on the left wing when the airframe is rolling. The contribution from the vertical tail can be either positive or negative depending on the vertical tail geometry, the sidewash from the wing, and the equilibrium angle of attack of the airframe.

The derivative C_{n_p} is fairly important in lateral dynamics because of its influence on Dutch roll damping. It is usually negative in sign, and for most airframe configurations, the larger its negative value, the greater the reduction in Dutch roll damping. Therefore, positive values of C_{n_p} are to be desired. For the airframe alone, C_{n_p} is not generally considered to be an important preliminary design parameter; however, if an autopilot is installed to create effective C_{n_p}, this derivative may become quite important in lateral dynamics.

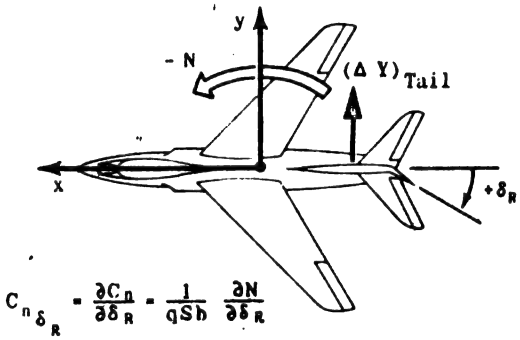

Figure IV-25 Yawing Moment Coefficient Change Due to Variation in Rudder Deflection

$C_{n_{\delta_R}}$

The stability derivative $C_{n_{\delta_R}}$ is the change in yawing moment coefficient with variation in rudder deflection. This derivative is commonly referred to as the rudder effectiveness (or rudder power). When the rudder is deflected positively, that is, to the left, a negative yawing moment is created on the airplane; hence the derivative $C_{n_{\delta_R}}$ is negative.

The importance of $C_{n_{\delta_R}}$ in determining lateral and directional control qualities varies considerably with different types of airframes.

The design value of $C_{n_{\delta_R}}$ for a jet-powered airframe is usually determined by considering such requirements as counteracting adverse yaw in rolling maneuvers, directional control in crosswind take-offs and landings, antisymmetric power, and spin recovery control. An additional factor which can be influential in establishing a design value for $C_{n_{\delta_R}}$ is introduced when an autopilot operates through the rudder.

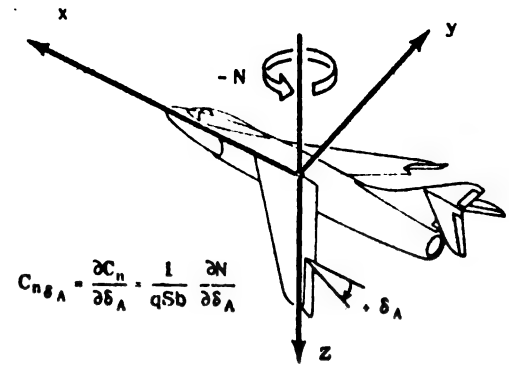

Figure IV-26 Yawing Moment Coefficient Change Due to Variation in Aileron Deflection

$C_{n_{\delta_A}}$

The stability derivative $C_{n_{\delta_A}}$ is the change in yawing moment coefficient with change of aileron deflection. This derivative arises from the difference in drag due to the down aileron compared to the drag of the up aileron. The sign of $C_{n_{\delta_A}}$ depends mainly upon the rigging of the ailerons and the angle of attack of the airframe. If negative, as it usually is, $C_{n_{\delta_A}}$ is called the "adverse yaw coefficient due to ailerons" because it causes the airframe to yaw initially in a direction opposite to that desired by the pilot when he deflects the ailerons for a turn. If positive, it produces favorable yaw in the turning maneuver.

The derivative $C_{n_{\delta_A}}$ is quite important in determining the lateral control qualities of an airframe. For good response to aileron deflection, $C_{n_{\delta_A}}$ should be zero or of a very small positive value.

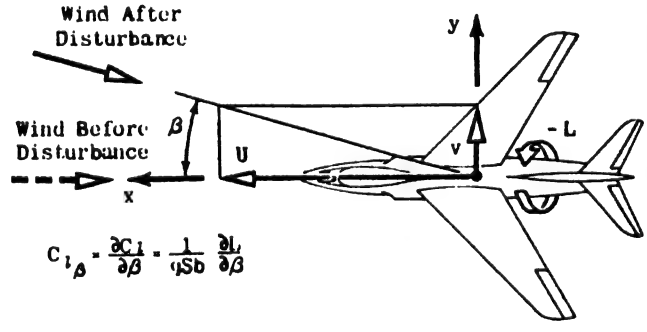

Figure IV-27 Rolling Moment Coefficient Change Due to Variation in Sideslip

C_{l_β}

The stability derivative C_{l_β} is the change in rolling moment coefficient with variation in sideslip angle and is usually referred to as the "effective dihedral derivative." When the airframe sideslips, a rolling moment is developed because of the dihedral effect of the wing and because of the usual high position of the vertical tail relative to the equilibrium x-axis (Figure IV-27). No general statements can be made concerning

the relative magnitudes of the contributions to C_{l_β} from the vertical tail and from the wing since these contributions vary considerably from airframe to airframe and for different angles of attack of the same airframe. C_{l_β} is nearly always negative in sign, signifying a negative rolling moment for a positive sideslip.

Some confusion in nomenclature may arise here because a pilot often speaks of an airplane having "positive dihedral effect" if the right wing tends to rise (negative rolling moment) when the airplane is side-slipped to the right (positive sideslip). A "positive dihedral effect" implies that the derivative C_{l_β} is negative. In the design stage, the value of C_{l_β} for a particular airframe can be adjusted at will within a large range by merely changing the amount of built-in wing dihedral.

The derivative C_{l_β} is very important in lateral stability and control, and it is therefore usually considered in the preliminary design of an airframe. It is involved in damping both the Dutch roll mode and the spiral mode. It is also involved in the maneuvering characteristics of an airframe, especially with regard to lateral control with the rudder alone, near stall.

To improve the Dutch roll damping characteristics of an airframe, small negative values of C_{l_β} are desired, but to improve the spiral stability, large negative values are desired. Since at least some "positive dihedral effect" is considered necessary for good maneuvering qualities, the design value of C_{l_β} must be more or less of a compromise between the static lateral requirement of "positive dihedral effect" and the dynamic lateral requirements of satisfying Dutch roll damping and spiral stability. Most of the references concerned with full scale and model flight tests agree that the best flying qualities are obtained when the effective dihedral is kept rather small.

The compromise in C_{l_β} mentioned above may be necessary only when considering the airframe plus human pilot combination. For an airframe with an autopilot installation, the selection of a design C_{l_β} for the airframe alone will probably be less critical.

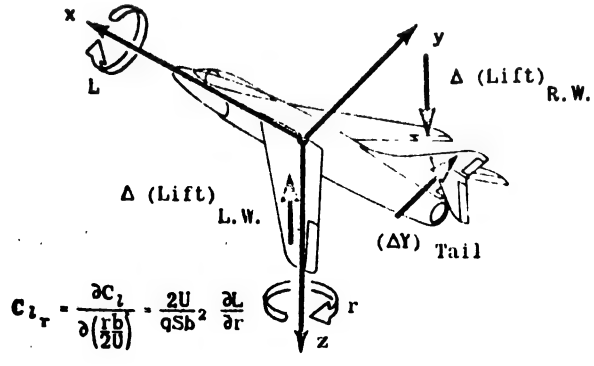

Figure IV-28 Rolling Moment Coefficient Change Due to Variation in Yawing Velocity

C_{l_r}

The stability derivative C_{l_r} is the change in rolling moment coefficient with change in yawing velocity. If the airframe is yawing at the rate r about the vertical axis, the left wing panel will move faster than the right, producing more lift on the left panel and consequently a positive rolling moment. In addition to this major wing contribution, the vertical tail will also contribute to C_{l_r} if it is located either above or below the x-axis. Its contribution can therefore be positive or negative, depending upon the vertical tail geometry and the equilibrium angle of attack of the airframe. The sign of C_{l_r} is usually positive.

The derivative C_{l_r} is of secondary importance in lateral dynamics, but, it should not be neglected in lateral dynamic calculations. For a conventional airframe configuration, changes in C_{l_r} of reasonable magnitude show only slight effect on the Dutch roll damping characteristics. In the spiral mode, however, C_{l_r} has a considerable effect. For stability in this mode, it is desirable that the positive value of C_{l_r} be as small as possible. C_{l_r} is not usually considered as a preliminary design parameter.

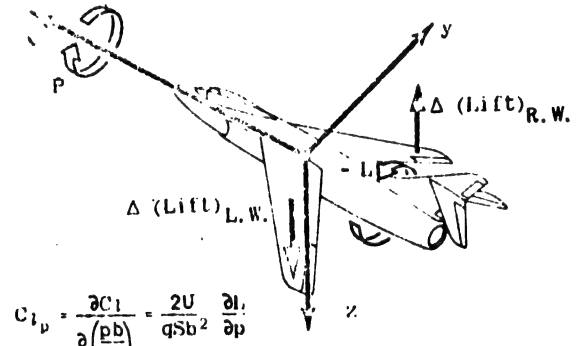

Figure IV-29 Rolling Moment Coefficient Change Due to Variation in Rolling Velocity

C_{l_p}

The stability derivative C_{l_p} is the change in rolling moment coefficient with change in rolling velocity and is usually known as the roll damping derivative. When the airframe rolls at an angular velocity p a rolling moment is produced as a result of this velocity; this moment opposes the rotation. C_{l_p} is composed of contributions, negative in sign, from the wing and the horizontal and vertical tails. However, unless the size of the tails is unusually large in comparison with the size of the wing, the major portion of the total C_{l_p} comes from the wing.

The derivative C_{l_p} is quite important in lateral dynamics because essentially C_{l_p} alone determines the damping in roll characteristics of the aircraft. Normally, it appears that small negative values of C_{l_p} are more desirable than large ones because the airframe will

respond better to a given aileron input and will suffer fewer flight perturbations due to gust inputs.

The derivative C_{l_p} is not usually considered a preliminary design parameter. Its value is more or less given by the wing planform geometry which is determined by other more important design criteria. The value of C_{l_p} does directly affect the design of the ailerons, however, since C_{l_p} in conjunction with $C_{l_{\delta_A}}$ establishes the airframe's maximum available rolling velocity; this is an important criterion of flying quality.

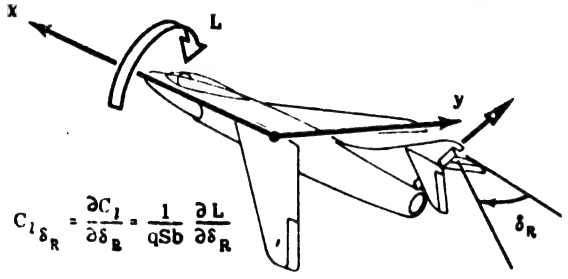

Figure IV-30 Rolling Moment Coefficient Change Due to Variation in Rudder Deflection

$C_{l_{\delta_R}}$

The stability derivative $C_{l_{\delta_R}}$ is the change in rolling moment coefficient with variation in rudder deflection. Because the rudder is usually located above the x-axis, a positive rudder deflection will create a positive rolling moment. $C_{l_{\delta_R}}$ is therefore usually positive in sign; however, it can be negative, depending on the particular airframe configuration and the angle of attack at which it is flying.

The derivative $C_{l_{\delta_R}}$ is usually of only minor importance in the lateral control qualities of conventional aircraft, and it is sometimes neglected in analyses. When dealing with airframe-plus-autopilot synthesis of a particular configuration, however, it is believed that this derivative should be included until further research shows that it can be neglected for that case.

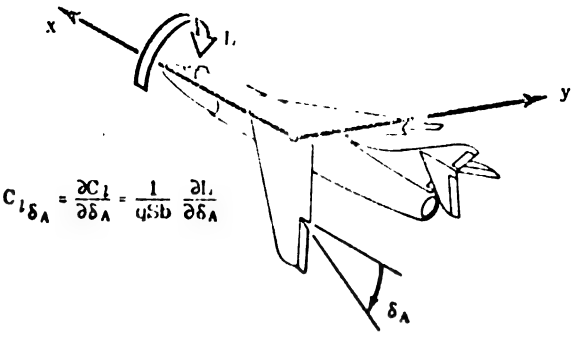

Figure IV-31 Rolling Moment Coefficient Change Due to Variation in Aileron Deflection

$C_{l_{\delta_A}}$

The stability derivative $C_{l_{\delta_A}}$ is the change in rolling moment coefficient with change in aileron deflection. It is commonly referred to as the aileron effectiveness (or aileron power). According to the definition used in this volume, left aileron down is a positive deflection. This produces a rolling moment to the right which is positive; $C_{l_{\delta_A}}$ is therefore positive.

As far as lateral dynamics are concerned, the derivative $C_{l_{\delta_A}}$ is the most important of the control surface derivatives. The aileron effectiveness in conjunction with the damping in roll (C_{l_p}) establishes the maximum available rate of roll of an airframe, which is a very important consideration in fighter combat tactics at high speed. The aileron effectiveness is also very important in low speed flight during take-offs and landings where adequate lateral control is necessary to counteract asymmetric gusts tending to roll the aircraft.

Desirable values of $C_{l_{\delta_A}}$ for a particular fighter airframe configuration can be determined by use of the Navy and Air Force specification that the value of the wing tip helix angle during a rolling maneuver for full aileron deflection should be at least such that $\frac{pb}{2U} = .09$.

SECTION 4 – FACTORS THAT DETERMINE THE BASIC NON-DIMENSIONAL STABILITY DERIVATIVES IN GENERAL

The purpose of this section is to present a general discussion of all the various factors that determine or influence the basic non-dimensional stability derivatives and to point out their relative importance.

A thorough knowledge of these factors is important to the servomechanist, to the control system designer, and to all the others concerned with optimizing the integrated airframe-autopilot-controls system. Not only must they be aware that changes in these factors produce changes in the stability derivatives; but, they must also know which factors produce important changes and which negligible ones. Such information is especially important to the aerodynamicist, for when he is given a particular airframe configuration at a particular flight condition, he must carefully consider each factor in establishing numerical values for the stability derivatives.

The two primary factors which establish the basic non-dimensional stability derivatives for any airframe are (1) the configuration of the airframe and (2) its flight condition; in general, the first is the more important.

In the lists which follow, each of these primary factors is divided into various contributing factors listed in order of decreasing importance within each group.

Airframe Configuration

(a) Basic airframe geometry: wing and tail

planforms, tail sizes and moment arms, wing dihedral, fuselage size, etc.
(b) Alterable airframe geometry: wing trailing edge and leading edge flaps, speed brakes, landing gear extension, etc.
(c) Alterable airframe weight distribution: center of gravity position.

Flight Condition

(d) Mach number.
(e) Angle of attack (lift coefficient).
(f) Dynamic pressure (aeroelasticity).
(g) Power (thrust).
(h) Unsteady flow.

This order of importance within each group is based upon data derived from a typical high-performance jet fighter and is presented to give a general idea concerning the relative importance of the factors involved, but it must be remembered that this order may vary slightly for different airframes and for different individual stability derivatives.

So many factors are involved in determining the stability derivatives for a particular airframe under all flight conditions that it would obviously be a tremendous task for the aerodynamicist to consider all these factors in detail before arriving at final stability derivative estimates. Fortunately, when the airframe is in the preliminary design stage, fairly good estimates of most stability derivatives important to dynamic stability and control qualities can be made by considering the three factors listed in the Airframe Configuration group and a fourth, Mach number, from the Flight Condition group. Once the values of stability derivatives have been obtained by considering these four factors, the effects of the rest can be considered merely as additions or refinements; consequently, rough estimates of their values will usually suffice.

In the following pages, each of these eight factors is discussed in detail.

(a) EFFECT OF AIRFRAME BASIC GEOMETRY

Of all the contributing factors that determine the basic non-dimensional stability derivatives, the most important is the basic airframe geometry. The term "basic airframe geometry" as used here refers to the geometrical characteristics of the airframe when it is in the aerodynamic "clean" configuration; that is, with flaps, speed brakes, landing gear, etc., all retracted.

Not only is basic airframe geometry the most important factor, but more theoretical and experimental data are available on its effects than on the effects of any of the others. With the aid of such basic reports as References 1 to 5 of Chapter V, most of the low-speed stability derivatives can be evaluated to a fair degree of accuracy merely from an examination of a three-view drawing of an airframe. Some of the major effects of the geometry of various airframe components can be briefly outlined:

The wing planform has a great influence on many derivatives. The aspect ratio and sweepback of the wing are the main elements establishing derivatives related to lift, drag, and rolling moment, such as C_{L_α}, C_{D_α}, C_{l_p}, and C_{l_r}. The wing planform in conjunction with the amount of dihedral angle also establishes the value of C_{l_β}.

The size and geometry of the horizontal tail and its moment arm from the center of gravity establish the longitudinal pitching moment derivatives C_{m_α} and C_{m_q}, and provide a large contribution to C_{m_α}. Similarly, the size and geometry of the vertical tail and its moment arm from the center of gravity have a major effect on the side force and yawing moment derivatives C_{y_β}, C_{n_β}, $C_{n_{\dot\beta}}$, C_{y_r}, and C_{n_r}.

The size and shape of the fuselage and of the nacelles have a great effect on C_{n_β}, and a somewhat smaller effect on C_{m_α}. The positioning of the wing, the horizontal tail, and the vertical tail on the fuselage is quite important in determining not only mutual interference effects, but downwash and sidewash effects on the tails. These interference effects sometimes have a considerable influence on the pitching moment, side force, and yawing moment derivatives such as C_{m_α}, $C_{m_{\dot\alpha}}$, C_{y_β}, C_{n_β}, $C_{n_{\dot\beta}}$, and C_{n_r}.

(b) EFFECT OF ALTERABLE AIRFRAME GEOMETRY

The term "alterable airframe geometry" is used here to refer to any of the retractable or disposable aerodynamic devices; such as wing leading edge flaps, wing trailing edge flaps, speed brakes, landing gear, and droppable external stores; which are used for special flight conditions and which render the configuration different from its usual "clean" configuration. However, the term does not apply to conventional control surfaces which are considered part of the "clean" configuration.

Extension of wing leading edge and trailing edge flaps enables the airframe to reach a higher lift coefficient and produces a great increase in the drag coefficient, but the effects on the other longitudinal stability derivatives are usually small, except that C_{m_α} and C_{D_α} may be affected in some cases of highly swept wing configurations. Extension of wing trailing edge flaps, however, drastically changes some lateral derivatives, especially C_{n_r} and C_{l_β}.

Extension of speed brakes increases the drag coefficient of the airframe but usually does not appreciably affect any of the other stability derivatives. But if the speed brakes are of the wing split-flap type, a great increase in C_{n_r} will result, and if the wing is highly swept, there may also be considerable changes in C_{y_β}

and C_{l_β}.

Extension of the landing gear usually does not have an appreciable effect on any of the stability derivatives although it does affect the drag coefficient.

The addition of wing pedestal tanks or tip tanks to an airframe can produce appreciable changes in such derivatives as C_{L_α}, C_{D_α}, C_{l_p}, $C_{l_{\delta_A}}$, and C_{n_β}, depending upon the particular configuration. Unfortunately, data of a general nature concerning external store configurations are rather scarce at the present time; it is therefore difficult to estimate the resulting effects on all the stability derivatives.

(c) EFFECT OF ALTERABLE AIRFRAME WEIGHT DISTRIBUTION

As a particular airframe is operated throughout its flight regime, the burning of fuel, the firing of ammunition, and the dropping of external stores change the weight distribution. The most important effect of this is the resulting fore and aft shift in the center of gravity, which produces a very great change in the airframe's longitudinal static stability derivative C_{m_α}. (This situation is explained more thoroughly in the discussion of C_{m_α} in Section IV-3.)

In addition, as the position of the center of gravity shifts, there is a consequent change in the moment arm of the horizontal tail, resulting in changes in the pitching moment derivatives $C_{m_{\dot\alpha}}$, C_{m_q}, and $C_{m_{\delta_E}}$. However, the per cent change in these derivatives is usually negligibly small except for some tailless configurations where the effective tail moment arm is rather short.

Finally, since the airframe is not completely rigid but is subject to elastic distortion, weight distribution can cause appreciable deformation of the airframe configuration and so affect certain stability derivatives. For example, large nacelles and external stores mounted on the wing can change the wing bending and torsional characteristics enough to affect some of the stability derivatives, mainly $C_{m_{\dot\alpha}}$, C_{m_q}, and C_{l_β}. The magnitude of these effects depends on the particular geometry and elastic properties of the airframe concerned.

(d) EFFECT OF MACH NUMBER

The effect of Mach number on basic stability derivatives is, in general, second in importance only to the effect of airframe configuration. Every derivative is changed to an appreciable extent as the Mach number varies throughout the speed range of supersonic aircraft.

The magnitude of the change in stability derivatives as the Mach number is varied from 0 to about 1.4 is primarily a function of the airframe's basic geometry. A configuration which has a high aspect ratio unswept wing and tail, both with thick airfoil sections, will show large and abrupt changes (of the order of 50% or more) in its stability derivatives. Conversely, a configuration which has a low aspect ratio highly swept wing and tail, both with very thin airfoil sections, will show only small and relatively smooth changes in the stability derivatives over the same Mach number range.

The slopes of the lift curve of the wing and of the horizontal tail are of fundamental importance in the evaluation of many of the derivatives. A brief examination of a particular derivative (C_{L_α}) will demonstrate fairly typical effects of Mach number on stability derivatives in general.

Figure IV-32 shows the effects of different wing planforms on C_{L_α} vs. Mach number. Aspect ratio and sweepback have a pronounced influence on C_{L_α} for subsonic Mach numbers, and an even greater influence in the transonic region. But for Mach numbers greater than about 1.6, the effect of the wing geometry diminishes as shown by the converging trend of the family of curves in the diagram. (For high supersonic Mach numbers, theory shows that C_{L_α} is given by the single expression $C_{L_\alpha} = \frac{4}{\sqrt{M^2-1}}$ and is independent of wing geometry.) This reduction in the importance of airframe geometry in supersonic Mach number regimes is fairly typical for most of the stability derivatives.

If any one effect of Mach number is more important than the rest, it is probably the effect on the longitudinal static stability derivative C_{m_α}. The wing contribution to C_{m_α} depends on the distance between the center of pressure of the air load and the center of gravity of the airframe. For relatively low aspect ratio wings the center of pressure gradually moves forward as the Mach number increases from 0 to about .8 or .9, producing a positive increment to C_{m_α} and thus making the airframe less stable. As the Mach number is increased through the transonic region and into the supersonic region, the center of pressure shifts aft, causing a large negative increment to C_{m_α} and thus greatly increasing the static stability of the airframe.

Another very important effect of Mach number is its great influence upon the primary control effectiveness derivatives $C_{m_{\delta_E}}$, $C_{l_{\delta_A}}$, $C_{n_{\delta_R}}$, and upon the related secondary derivatives such as $C_{L_{\delta_E}}$, $C_{n_{\delta_A}}$, $C_{y_{\delta_A}}$, and $C_{l_{\delta_R}}$. For the conventional trailing edge flap type of control, an increase in Mach number from 0 to .8 or .9 usually augments the control effectiveness by an appreciable amount. As the Mach number is further increased through the transonic region, however, the control effectiveness decreases rapidly, so that at supersonic speeds it approaches a value about one half that at low subsonic Mach numbers.

(e) EFFECT OF ANGLE OF ATTACK

The values of some basic non-dimensional stability de-

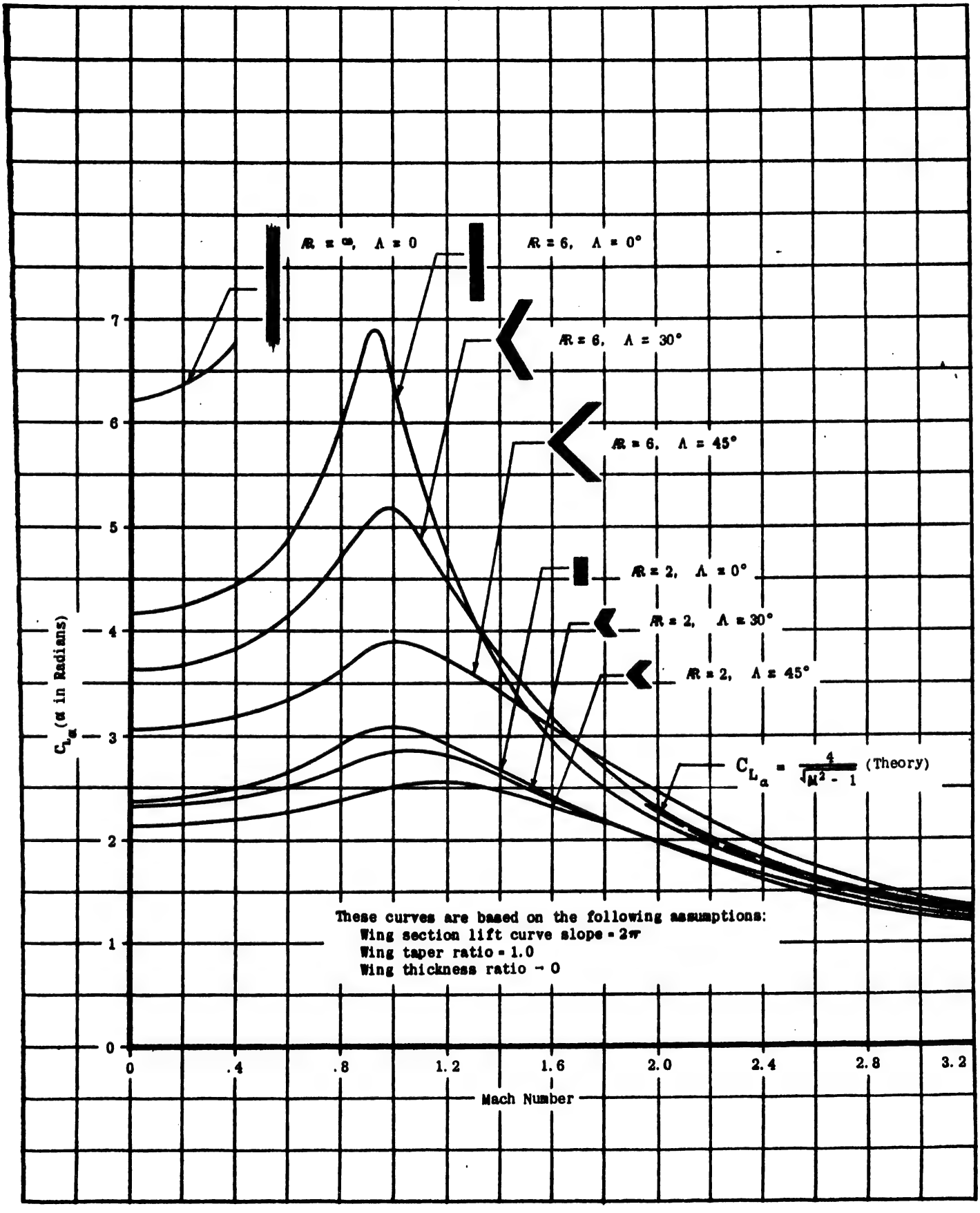

Figure IV - 32 Effect of Mach Number and Wing Geometry on C_{L_α}

rivatives depend on the angle of attack, or lift coefficient, of the airframe, whereas other derivatives are relatively unaffected.

Usually there are only a few longitudinal derivatives that are primarily functions of angle of attack: C_{D_α}, C_{D_u}, C_{L_u}, and C_{m_u}. Of course the equilibrium lift and drag coefficients C_L and C_D also depend on α. If the wing of the airframe is of low aspect ratio or highly swept, the curves of C_L and C_m versus α which are usually considered to be straight-line relationships in classical aerodynamics, are likely to become nonlinear; thus causing the longitudinal derivatives C_{L_α} and C_{m_α}, the slopes of these curves, to be functions of angle of attack.

Many of the lateral derivatives change with angle of attack: the ones that change the most are C_{l_β}, C_{l_r}, C_{y_p}, C_{n_p}, $C_{l_{\delta_R}}$, and $C_{n_{\delta_A}}$; the ones that usually change only slightly are C_{y_β}, C_{n_β}, $C_{y_{\delta_R}}$, $C_{n_{\delta_R}}$, and C_{n_p}. A few of the lateral derivatives, such as C_{l_p} and $C_{l_{\delta_A}}$, remain fairly constant with angle of attack, at least up to the stall.

Although most of the derivatives mentioned above are actually functions of α, they are usually evaluated at an equilibrium angle of attack corresponding to a given equilibrium flight condition and are thereafter assumed to remain constant during any angle of attack perturbation from the equilibrium condition. This assumption must be made to maintain the linearity of the equations of motion. It is clear that the validity of this assumption depends; first, on how much the derivatives change with a small change in α; and second, on how much these changes in the derivatives affect the airframe dynamics. For instance, the derivative C_{L_α} may exhibit a large nonlinear effect with α, but if only the dynamics of the phugoid are of interest, the perturbation in α, $\Delta\alpha$, is small, and thus the effective contribution of this derivative to the motion, given by the product $C_{L_\alpha}\Delta\alpha$, is small. Consequently, the nonlinear effects of C_{L_α} with α can be safely neglected for this case.

Although such nonlinear effects of angle of attack are usually quite small and can be neglected there is one derivative, C_{m_α}, which requires special attention in certain cases. The curve of C_m versus α is usually a straight line; however, for highly swept wings of moderate aspect ratio this curve can exhibit some rather abrupt nonlinearities. This means that C_{m_α}, the slope of this curve, can show a large change in magnitude over a relative small range of α. It is clear that in equilibrium flight condition in the vicinity of this nonlinearity, there may be a large error in the calculated longitudinal dynamics if the effect of angle of attack on C_{m_α} is not taken into account.

This sort of nonlinearity can be handled on an analog computer by using two or more straight lines to approximate the C_m versus α curve, or, better still, by a cam describing the nonlinear curve exactly.

(f) EFFECT OF AEROELASTICITY

Until a few years ago, the only aeroelastic effect on the dynamics of aircraft considered important was the reduction in maximum attainable rate of roll; that is, the reduction in the aileron effectiveness derivative $C_{l_{\delta_A}}$ and the roll damping derivative C_{l_p}. Since that time, because thinner wings have aggravated the structural problems, aeroelastic effects on many of the other derivatives have become appreciable. Today, aeroelastic effects on stability and control are so important that it is imperative for the aerodynamicist to consider them in evaluating stability derivatives.

Aeroelastic effects on stability derivatives can arise from any of the following considerations:

1. Wing torsion and bending due to:
   a. Airloads in equilibrium flight.
   b. Aileron deflection.
   c. "Dead weight" distribution when the aircraft is subjected to a normal acceleration increment, Δn.
2. Horizontal tail torsion and bending due to:
   a. Airloads in equilibrium flight.
   b. Elevator deflection.
3. Vertical tail torsion and bending due to rudder deflection.
4. Fuselage bending and torsion due to:
   a. Airloads on the horizontal tail.
   b. Airloads on the vertical tail.
5. Fuselage bending due to "dead weight" distribution when the aircraft is subject to a normal acceleration increment, Δn.

This list is quite general but may or may not be complete for a particular airframe. Its main purpose is to create an awareness in all those concerned with an optimum airframe-autopilot-control system of the many possible sources of aeroelastic effects on airframe stability derivatives.

The magnitude of aeroelastic effects for any particular airframe configuration at a particular flight condition depends upon the following factors:

1. Dynamic pressure.
2. Airframe geometry.
3. Mach number.
4. Structural rigidity.
5. Normal acceleration.

A brief discussion of each of these five factors follows.

1. Dynamic Pressure

Aeroelastic effects are primarily a function of dynamic pressure, q. By definition, the value of the dynamic pressure is: $q = \frac{1}{2}\rho U^2$, where ρ is the density of the air and U is the true forward velocity of the aircraft. Thermodynamically, q can be expressed as $.7pM^2$, where p is the ambient static pressure of the atmosphere. Since p decreases as altitude increases, it is clear that dynamic pressure increases as the Mach number increases and as the altitude decreases. And if it is assumed that the effects of aeroelasticity increase with dynamic pressure (which is generally the case), then it can be concluded that the magnitude of aeroelastic effects are largest when the aircraft is flying at high speeds and at low altitudes.

For most stability and control investigations, the change in altitude during a maneuver is either zero or small enough to be neglected. Therefore, when the forward speed changes (i.e., when the Mach number changes), as it does for example during a phugoid oscillation, the dynamic pressure changes, and the forces and moments due to aeroelastic deflection are altered, affecting the values of the stability derivatives C_{D_u}, C_{L_u}, and C_{m_u}. The effect upon C_{m_u} is the most important one and should be appraised when estimating stability derivatives.

2. Airframe Geometry

The magnitude and, more importantly, the sign of aeroelastic corrections to the "rigid" stability derivatives depend to a large extent upon the airframe geometry, especially upon the geometry of the wing. As an example, consider the lift curve slope, C_{L_α}. In Figure IV-33, the ratio of elastic C_{L_α} to rigid C_{L_α} is plotted as a function of dynamic pressure.

The effect of aeroelastic deflection is to increase C_{L_α} for a sweptforward wing and to decrease it for a sweptback wing. For a straight wing, C_{L_α} is first increased, then decreased as q is increased thru the transonic region. Similar effects can be observed for other stability derivatives; consequently it is essential to know the specific airframe configuration before any aeroelastic effects can be calculated.

3. Mach Number

In addition to its primary effect in determining the dynamic pressure, the flight Mach number itself is quite important in establishing aeroelastic corrections to stability derivatives. Since the distribution of the air load on the wing and horizontal tail is altered as the Mach number is changed, the resulting aeroelastic deflections are also affected and are especially noticeable in the transonic region. In Figure IV-32, for example, the odd behavior of the curves in the transonic region results from a rearward shift of the center of pressure of the air loads on the wing as the Mach number increases.

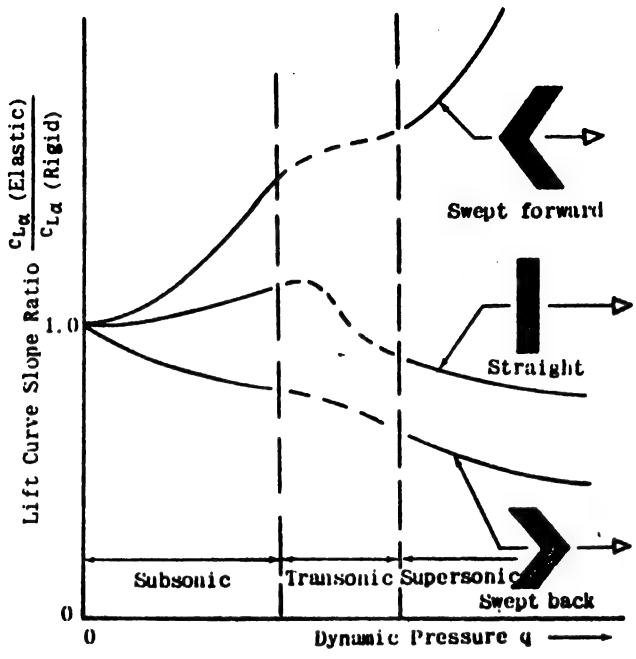

Figure IV-33 Effect of Wing Geometry on Aeroelastic C_{L_α} (Altitude Assumed Constant)

For subsonic flight the line of the centers of pressure for a straight wing with average aspect ratio is located approximately at .25 MAC, a position normally ahead of the elastic axis of the wing. As the Mach number is increased through the transonic and into the supersonic region, this line of centers of pressure moves aft to about .50 MAC, a position normally aft of the elastic axis. As a result, the torsional deflection of the wing about its elastic axis will actually change direction as the transonic region is traversed. This phenomenon is clearly demonstrated by the action of the straight wing curve of Figure IV-33.

4. Structural Rigidity

Structural rigidity is of course very important in determining the magnitude of the aeroelastic effects on stability derivatives. The more rigid the structure, the more it can resist the air loads, and the less it is subject to aeroelastic deformations. But the amount of rigidity possible is limited by considerations of weight and aerodynamics. For example, very thin wings are considered necessary for supersonic aircraft because they make possible a reduction in aerodynamic drag. However, a very thin wing inevitably means a wing which is weak in resistance to torsion even if it is constructed of solid material. This lack of rigidity results in great aeroelastic effects on the derivatives $C_{l_{\delta_A}}$ and C_{l_p}. In addition, a thin wing will probably bend spanwise easily producing a great effect on C_{l_β}. The most usual way of minimizing these effects is to use a wing plan-

form of low aspect ratio.

In addition to the torsional and bending deflections of the wing, the structural rigidity of the horizontal tail and of the rear portion of the fuselage can produce serious aeroelastic problems because the pitching moment contribution to the airframe from the horizontal tail depends not only upon the aeroelastic bending and torsion of the horizontal tail itself, but also upon the flexibility of the fuselage as a link between the tail and the rest of the airframe. The aft fuselage is subjected to a moment from the tail as well as to a vertical force. Usually the vertical force is the predominant effect, so that the fuselage deflects in a direction to relieve the load on the tail, thus reducing the horizontal tail effectiveness. This effect has serious aerodynamic consequences because all the pitching moment stability derivatives, C_{m_u}, C_{m_α}, $C_{m_{\dot\alpha}}$, C_{m_q}, and $C_{m_{i_g}}$, depend on the horizontal tail effectiveness, and most of them are very important to longitudinal stability and control characteristics.

5. Normal Acceleration

Depending on the particular geometry and structural rigidity of an airframe, aeroelastic effects can be important under flight conditions involving normal acceleration other than one "g." For instance, consider an aircraft with large engine nacelles mounted outboard along the wing span and with the center of gravity of the nacelles forward of the elastic axis of the wing. When this aircraft is subjected to change in normal acceleration, Δn, the "dead weight" of the nacelles produces both torsional and bending deflections of the wing.

Actually, the correct method for introducing these aeroelastic effects into the dynamics of the airframe is to provide equations of motion to account for the elastic degrees of freedom, in addition to the conventional equations of motion which are written with respect to the center of gravity of the rigid airframe. For the aircraft described in the last paragraph, for example, two more equations are necessary to account for the wing tip rotation and for its deflection relative to the center of gravity of the airframe.

However, if the motions of the airframe are assumed to be rather slow in comparison with the natural frequencies of the elastic portions of the airframe, the inertia effects of various concentrated masses relative to the entire mass of the airframe can be neglected, and only the "steady state" aerodynamic effects caused by structural deformations need be considered.

Assume that the airframe is subjected to an incremental normal acceleration, Δn, which does not change with time—for instance, during a stabilized turn or a constant speed pull up maneuver. For this stabilized normal acceleration the change in airload on the wing caused by the torsional and bending deflections produces increments in lift and pitching moment which can be expressed by the partial derivatives $\frac{\partial C_L}{\partial \Delta n}$ and $\frac{\partial C_m}{\partial \Delta n}$. It may be concluded that in the particular case of stabilized normal acceleration, no additional elastic equations of motion are required, and aeroelastic effects can be taken into account in the conventional equations of motion for a rigid airframe by adding terms of the form $\frac{\partial C_m}{\partial \Delta n}\Delta n$ and $\frac{\partial C_L}{\partial \Delta n}\Delta n$.

But instead of using these new stability derivatives in this form in the equations of motion, it is convenient to split each of them into components which are, in effect, contributions to more common stability derivatives. That is, $\frac{\partial C_L}{\partial \Delta n}$ is transformed into contributions to $C_{L_{\dot\alpha}}$ and C_{L_q}, and $\frac{\partial C_m}{\partial \Delta n}$ is transformed into contributions to $C_{m_{\dot\alpha}}$ and C_{m_q}. These transfers can be made because $\Delta n = \frac{U}{g}(\dot\theta - \dot\alpha)$ at all times for the rigid airplane equations.

For example, consider the pitching moment equation expressed in non-dimensional stability derivatives including the derivative $\frac{\partial C_m}{\partial \Delta n}$:

$$C_m = \frac{\partial C_m}{\partial \alpha}\Delta\alpha + \frac{\partial C_m}{\partial\left(\frac{\dot\alpha c}{2U}\right)}\frac{\dot\alpha c}{2U} + \frac{\partial C_m}{\partial\left(\frac{qc}{2U}\right)}\frac{\dot\theta c}{2U} + \frac{\partial C_m}{\partial \Delta n}\Delta n + \dots$$

Substituting $\Delta n = \frac{U}{g}(\dot\theta - \dot\alpha)$ and collecting terms,

$$C_m = \frac{\partial C_m}{\partial \alpha}\Delta\alpha + \left[\frac{\partial C_m}{\partial\left(\frac{\dot\alpha c}{2U}\right)} - \frac{2U^2}{cg}\frac{\partial C_m}{\partial \Delta n}\right]\frac{\dot\alpha c}{2U} + \left[\frac{\partial C_m}{\partial\left(\frac{qc}{2U}\right)} + \frac{2U}{cg}\frac{\partial C_m}{\partial \Delta n}\right]\frac{\dot\theta c}{2U} + \dots$$

which can be written,

$$C_m = C_{m_\alpha}\Delta\alpha + C_{m_{\dot\alpha}}\frac{\dot\alpha c}{2U} + C_{m_q}\frac{\dot\theta c}{2U} + \dots$$

where both $C_{m_{\dot\alpha}}$ and C_{m_q} consist of two parts, the basic portion arising from the aerodynamics of the airframe, and the other part arising from the elastic deflection caused by normal acceleration.

It may be seen, therefore, that when the aeroelastic effects of "dead weight" items are due to steady state normal acceleration, they can be taken into account merely by adding their effective contributions to the derivatives $C_{L_{\dot\alpha}}$, C_{L_q}, $C_{m_{\dot\alpha}}$, and C_{m_q}. This sort of aeroelastic contribution to stability derivatives is not too difficult to evaluate, especially if static deflection data from stress static loading tests on the prototype airplane are available, giving experimental values for $\frac{\partial C_L}{\partial \Delta n}$ and $\frac{\partial C_m}{\partial \Delta n}$.

When the derivatives $\frac{\partial C_L}{\partial \Delta n}$ and $\frac{\partial C_m}{\partial \Delta n}$ are introduced into the equations of motion of the airframe, an approximate expression for Δn is sometimes used: $\Delta n = \frac{C_{L_\alpha}\Delta\alpha}{C_L}$, where $\Delta\alpha$ is the perturbation angle of attack and C_L is the equilibrium lift coefficient. This expression for Δn is true only for the steady state portion of constant speed pull-up type maneuvers where the pitching velocity q is constant and where the rate of change of angle of attack,

$\dot{\alpha}$, is zero. This expression also neglects the effects of such derivatives as $C_{L_{\delta_E}}$, $C_{L_{\dot{\alpha}}}$, and C_{L_q}. If this approximate expression for Δn is used, aeroelastic contributions to the stability derivatives C_{L_α} and C_{m_α} are obtained instead of contributions to $C_{L_{\dot{\alpha}}}$, C_{L_q}, $C_{m_{\dot{\alpha}}}$, and C_{m_q}, as was demonstrated above. Although this technique yields reasonably practical answers, it must be realized that the approximations involved lead to greater inaccuracy than if the correct expression for Δn is used.

By considering the motion of the airframe restricted to steady normal accelerations (that is, when Δn is not a function of time) it has been shown that aeroelastic effects due to normal acceleration can be included in the conventional equations of motion, and that, as a result, the complications of introducing additional elastic equations of motion have been avoided. The question is whether or not this technique can be used when the motions of the airplane are not steady, as during the response to an elevator pulse or to a sinusoidal elevator input. Although no flight test data are available to substantiate the conclusion, this technique is believed to yield satisfactory results for low frequencies, say from 0 up to 8 radians per second.

The main assumptions involved are that the inertia characteristics of the various elastic portions of the airframe moving relative to the c.g. of the airframe, and the higher order aerodynamic derivatives caused by the relative motion are both neglected.

In practice, most jet fighters of today are of sufficient rigidity and of such configuration that this sort of aeroelastic effect resulting from normal acceleration is of secondary importance in dynamic stability and control. In other words, the magnitudes of $\frac{\partial C_m}{\partial \Delta n}$ and $\frac{\partial C_L}{\partial \Delta n}$ are usually small enough that their contributions to $C_{L_{\dot{\alpha}}}$, C_{L_q}, $C_{m_{\dot{\alpha}}}$, and C_{m_q} can be ignored. However, at least one case is known where these aeroelastic contributions cannot be neglected; it is therefore recommended that for any given configuration under consideration these effects be evaluated.

In some cases the effects of aeroelasticity cannot be considered as simple additions and corrections to the usual stability derivatives, and additional equations of motion with entirely new stability derivatives are required to define the aeroelastic motion.

For example, consider a straight wing aircraft with a very thin airfoil section and with heavy external stores mounted on the wing tips. The natural frequency in bending (and perhaps in torsion) of this system can be low enough to effect the design of a longitudinal autopilot for this aircraft, and consequently this aeroelastic effect must be considered as an additional degree of freedom. This example differs from the previous one in that the natural frequency of the present elastic system is assumed relatively low and close to the frequency of the longitudinal short period mode.

This sort of aeroelastic deformation may affect not only the stability but also the flutter characteristics. Flutter problems are usually concerned with the coupling of the natural modes of the elastic airframe with aerodynamic unsteady flow effects, and in general, the frequencies involved are too high to cause any effect on aircraft-plus-autopilot stability. But there is an intermediate frequency range between the high frequencies involved in flutter and the relatively low frequencies involved in dynamic stability, and in this range there can be elastic effects without unsteady flow (such as that described in the example in the previous paragraph), or conversely, there can be unsteady flow effects without elastic changes.

As another example of aeroelastic effects due to acceleration which may require additional equations of motion, consider an airplane in which the rear part of the fuselage is relatively flexible and the aft fuselage-empennage system has a natural frequency close to either the longitudinal short period or to the Dutch roll natural frequencies.

In summary, not only are aeroelastic effects important in establishing the values of stability derivatives for equilibrium flight, but in some cases they can be important in transient and steady state oscillatory considerations of aircraft dynamics in the frequency range lower than those of classical flutter.

Techniques for arriving at suitable equations of motion for fuselage bending and wing bending are available.*

Derivatives important to aircraft stability and control and most likely to be affected by aeroelasticity are: C_{m_α}, $C_{m_{\delta_E}}$, C_{m_u}, $C_{m_{\dot{\alpha}}}$, C_{m_q}, C_{L_α}, $C_{l_{\delta_A}}$, C_{l_p}, $C_{n_{\delta_A}}$, C_{l_β} and $C_{n_{\delta_R}}$.

(g) Effect of Power

Although very few experimental data are available concerning the effects of jet power on stability derivatives, it is not too difficult to calculate or estimate the major effects theoretically. Such investigations have shown that, in general, power effects on the basic stability derivatives are rather small (Reference 3); consequently, most dynamic stability analyses neglect jet power effects. It must not be assumed that jet power effects can be neglected when considering longitudinal equilibrium or trim conditions, for the moment due to a thrust line not passing through the center of gravity of an airframe may be quite large.

It is usually necessary to mount the tail surfaces of a jet-powered airframe at a safe distance from the jet blast because of the very high temperature. As a result, jet power-on stability problems are much simpler than those of the propeller-driven airframe as the latter

*Pai, S.I., and Sears, W.R., 'Some Aeroelastic Properties of Swept Wings,' Journal of the Aeronautical Sciences, XVI, No. 2 (February 1949), 105-115, 119; White, R.J., 'Investigation of Lateral Dynamic Stability in the XB-47 Airplane,' Journal of the Aeronautical Sciences, XVII, No. 3 (March 1950), 133-148.

is subject to power effects that can be quite large because the tail surfaces are frequently immersed in the propeller slip-stream.

There are three major contributions from the jet power plant to the equilibrium (trim) and dynamic stability of the airframe:

1. Direct thrust effects.
2. Direct normal force effects at the air duct inlet.
3. Induced downwash at the tail due to the inflow to the jet blast.

(A fourth jet effect, that is sometimes considered, may be termed a Coriolis effect, and involves the forces and moments on the airframe produced by the interaction between the linear fore and aft internal mass flow along the length of the jet engine and an angular velocity of the airframe itself. For conventional turbojet fighters it appears that this effect is small enough to be neglected, but for rocket powered missiles it can become significant.*)

1. Direct Thrust Effects

Consider the direct thrust effect on the pitching moment. When the thrust vector (T) passes through the center of gravity of the airplane, there can be no resultant pitching moment acting on the airplane. However, the thrust can act along an axis located some distance (arm z_T) from the center of gravity Figure IV-34.

The jet thrust moment M_T, is given by:

$$M_T = Tz_T$$

Converting M_T to a moment coefficient:

$$C_{m_T} = \frac{Tz_T}{qSc}$$

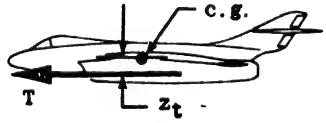

Figure IV-34 Jet Thrust Moment

This thrust moment coefficient, C_{m_T}, must be balanced out by an aerodynamic moment coefficient, C_m, when the airframe is in an equilibrium flight condition, thus creating a contribution to the stability derivative parameters m_u and M_u**. Hence this direct thrust effect influences the longitudinal dynamics of the airframe.

Another direct thrust effect arises because the thrust output of a jet engine at a constant throttle setting changes with the forward speed of the engine, creating the basic dimensional stability derivative $\frac{\partial T}{\partial u}$. The value of this derivative can be obtained from engine performance curves of the type shown in Figure IV-35.

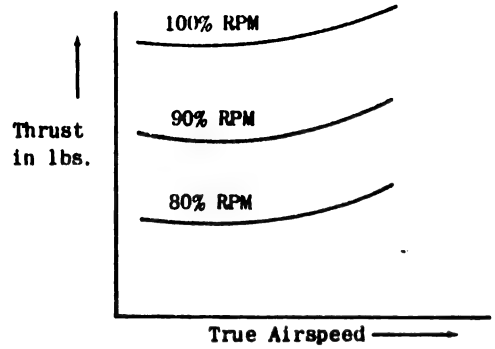

Figure IV-35 Typical Effect of Speed on Jet Engine Thrust (altitude assumed constant)

$\frac{\partial T}{\partial u}$ is given by the slope of these curves, and it can be seen that its magnitude is quite small since the curves are relatively flat. This is characteristic of present-day jet engines, and consequently, the thrust stability derivative $\frac{\partial T}{\partial u}$ is usually neglected in dynamic stability analyses.

If jet engines are mounted outboard along the wing span of an airframe, a contribution to the lateral stability derivative C_{n_p} arises because of the difference in thrust resulting from the different effective forward speeds of engines mounted on opposite sides. Similarly jet engines mounted above or below the center of gravity of an airframe contribute to the longitudinal stability derivative C_{m_q}. However, both these contributions are functions of the engine characteristics shown in Figure IV-35, and it has already been concluded that these characteristics produce negligible effects. For example, calculations were made of the direct thrust effect on C_{n_r} for the Northrop YB-49 Flying Wing Bomber; eight jet engines were mounted along the wing at relatively large distances from the center of gravity, and even in this rather extreme case, the change in C_{n_r} due to this jet effect was only of the order of a few percent.*

2. Direct Normal Force Effects at the Air-Duct Inlet

If the airframe is flying at some attitude, either in the equilibrium condition or during a disturbance, where the local flow entering the air duct inlet must be deflected to flow into and along the duct axis (Figure IV-36), the resulting momentum change of the air stream causes a force normal to the airframe velocity to act at the nose or lip of the inlet. The magnitude of this normal force is given by

*Statler, I.C., 'Dynamic Stability at High Speeds from Unsteady Flow Theory,' Journal of the Aeronautical Sciences, XVII, No. 4 (April 1950), 232-242, 255.

**$m_u = \frac{1}{2}\left(\frac{c}{k_y}\right)\left(C_m + C_{m_u}\right)$, $M_u = \frac{\rho SUc}{I_y}\left(C_m + C_{m_u}\right)$

*Koerner, W.G., 'Dynamic Lateral Stability - YB-49,' Northrop Aircraft Report A-119, Northrop Aircraft, Inc., Hawthorne, Calif., 1949.

Normal Force = $\dot{m}U \sin \delta$

where $\dot{m}$ is the air mass flow into the engine and δ is the angle through which the local flow must be deflected to flow into the air duct inlet.

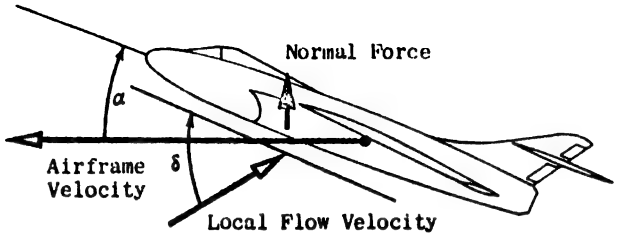

Figure IV-36 Normal Force at Air Duct Inlet

Wind tunnel tests were performed on an isolated nacelle to verify the presence of this normal force and to determine the point of application along the length of the nacelle.* These tests confirmed the magnitude of the normal force given by the above equation and showed that when the nacelle was mounted on a wing, the normal force at the air duct inlet due to the air mass flow was about twice as high as for the isolated nacelle. This difference was caused by the upwash ahead of the entry, due to the wing (see Figure IV-36). Thus, in calculating the normal force at the air duct entry, it is important to deal with the local flow at that position, and not merely with the relative wind vector associated with the complete airframe.

Since the air duct inlet is usually ahead of the center of gravity, this normal force gives rise to a nose-up pitching moment which increases with angle of attack, thus creating a positive increment of the derivative C_{m_α}; this change tends to be statically destabilizing. The small positive increment to C_{L_α} due to this effect is negligible.

A similar condition exists in sideslip, where the force at the air duct entry increases the magnitude of the stability derivative C_{y_β} and normally decreases the derivative C_{n_β}; these changes are in a direction to make the craft statically less stable. Calculations on the eight-jet flying wing YB-49 showed that the maximum increase in C_{y_β} was of the order of 10% when considering this flow deflection effect, but the decrease in C_{n_β} was negligible for this configuration because of the short effective moment arm.

Depending upon the airframe configuration, other stability derivatives may be affected by this airduct inlet normal force effect. If the jet engines are mounted at relatively large distances from the center of gravity of the airframe, forces and moments will be developed at the air duct entries when the airframe is undergoing pitching, rolling, and yawing velocities, leading to contributions to such derivatives as $C_{m_{\dot{q}}}$, C_{l_p}, and C_{n_r}. For most cases, however, these contributions are negligibly small.

*Squire, H.B., 'Jet Flow and Its Effects on Aircraft,' Aircraft Engineering (British), XXII, No. 253 (March 1950), 62-67.

3. Induced Downwash at the Tail Due to Jet Inflow

The third contribution of the jet engine unit to the airframe stability is the effect of the jet-induced downwash at the horizontal tail. This is caused by the high-velocity jet exit stream sucking in the slower-moving air in the vicinity of the jet.

In practice, this effect need be considered only for those configurations where the jet blast passes under or over the horizontal tail surface. On airframe configurations where the jet exit is located in the extreme rear of the fuselage and the tail surfaces are ahead of the jet exit, this flow effect may be neglected.

The resulting change in downwash varies with angle of attack of the airframe and with the jet velocity.

As far as affecting any of the stability derivatives used in dynamics is concerned, the jet-induced downwash modifies primarily the static stability derivative C_{m_α} since the jet deflection is a function of angle of attack. However, as stated, this is found to be small. No doubt there would also be contributions to derivatives such as $C_{m_{\dot{\alpha}}}$ and C_{m_q}, but no pertinent information seems available at present.

When an airframe is sideslipping there is an asymmetric inflow into the blast of the jet or jets which induces a sidewash at the vertical tail. For instance, for an aircraft configuration similar to the Gloster Meteor, where the jet engines are mounted outboard along the wing, the lateral derivative C_{n_β} is reduced because of this jet-induced sidewash effect; however, no information on the magnitude of the reduction is available.

(h) EFFECT OF UNSTEADY FLOW

Although the effect of unsteady flow on stability derivatives has been taken into consideration for many years in aerodynamic flutter, only recently has this effect become important in stability and control considerations, mainly as a result of the higher operating speeds of today's aircraft.

Most unsteady flow effects arise from the fact that the final steady lift caused by an abrupt change in angle of attack of a lifting surface does not occur instantaneously. This is illustrated in Figure IV-37, for a two-dimensional wing. The time to reach 90% of the final lift value, Δt, varies roughly between .01 and .2 of a second, depending on the geometry of the wing and the speed at which it is flying.

For an oscillating wing, where the angle of attack is varying sinusoidally, the lift will follow sinusoidally but

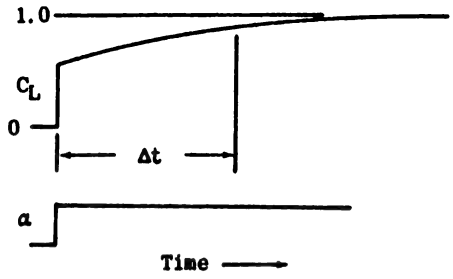

Figure IV-37 Lift Build-up Due to an Abrupt Change in Angle of Attack

its magnitude will be smaller than that of the non-oscillating wing; in addition there will be a phase difference between lift and angle of attack. This unsteady flow effect is a function of the frequency of the oscillation and also of the Mach number at which the oscillation is occurring.

Before examining this, however, it is necessary to understand how unsteady flow effects are introduced into the equations of motion. In accordance with the practice adopted in this chapter of writing aerodynamic forces and moments in terms of conventional stability derivatives, the latter must be considered as functions of frequency because of unsteady flow effects. For example,

$$C_L(\alpha) = C_{L_\alpha}\,\alpha + C_{L_{\dot\alpha}}\,\dot\alpha + C_{L_{\ddot\alpha}}\,\ddot\alpha + C_{L_q}\,q + C_{L_{\dot q}}\,\dot q + C_{L_{\delta_E}}\,\delta_E + C_{L_{\dot\delta_E}}\,\dot\delta_E + C_{L_{\ddot\delta_E}}\,\ddot\delta_E$$

where the derivatives C_{L_α}, $C_{L_{\dot\alpha}}$, $C_{L_{\ddot\alpha}}$, etc. are various functions of frequency.

To represent frequency-dependent stability derivatives mathematically for use in the equations of motion, it is convenient to express them as complex numbers. For instance,

$$C_{L_\alpha}(\omega) = RC_{L_\alpha}(\omega) + iIC_{L_\alpha}(\omega)$$

where R and I indicate the magnitude of the real and imaginary components respectively, of the complex number $C_{L_\alpha}(\omega)$. When the frequency of the oscillation is zero, the imaginary part, $IC_{L_\alpha}(\omega)$, is zero and $C_{L_\alpha}(\omega) = RC_{L_\alpha}(\omega)$, indicating that the derivative C_{L_α} is acting exactly in phase with α. This is the usual concept of a stability derivative when unsteady flow effects are neglected.

As an illustration of the effects of frequency and Mach number on stability derivatives as far as unsteady flow effects are concerned, consider Figure IV-38.

By referring to Figure IV-38b, it may be seen that when the reduced frequency, $\omega c/2U$, has the value 0.10, the magnitude of C_{L_α} is reduced to about 90% of the steady flow value ($\omega c/2U = 0$), and C_{L_α} has a phase lag of about 16^0 compared to α. Notice also that a component of C_{L_α} along the imaginary axis can be considered a contribution to the derivative $C_{L_{\dot\alpha}}$; a contribution which in this case enters the oscillating system as an undamping effect, since it represents a force 180^0 out of phase with the angular velocity of the system. Moreover, even though the magnitude of this imaginary component may be small compared with the original vector of C_{L_α}, it can contribute a large percentage change to $C_{L_{\dot\alpha}}$. A comparison of plot (a) with plot (b) shows that an increase in the Mach number from .5 to .8 accentuates the effect of reduced frequency.

In general, all the aerodynamic derivatives of an airframe behave in a similar manner. It is clear therefore that the effect of unsteady flow on conventional stability is to change them from real numbers to complex numbers, the real and imaginary parts of which are functions of the frequency of the oscillation and the Mach number at which the oscillation is occurring.

The question is this: at what values of frequency and Mach number do unsteady flow effects become so im-

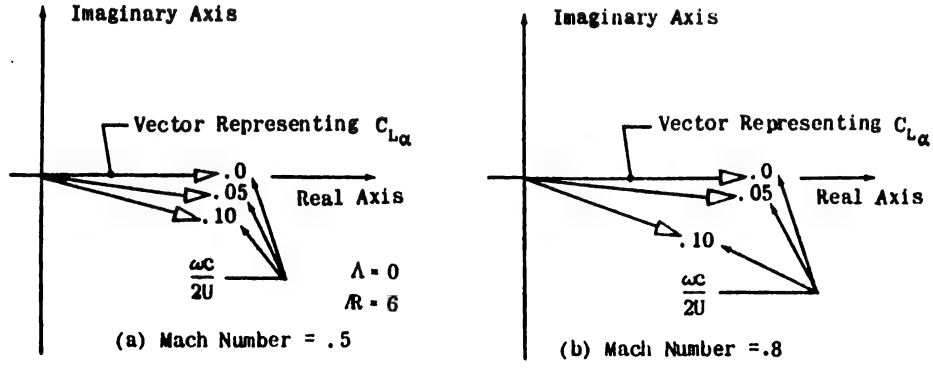

Figure IV-38 Effect of Reduced Frequency and Mach Number on C_{L_α} of a Wing (Reference 7)

portant that they must be considered in evaluating stability derivatives? Theoretical calculations on the longitudinal short period mode of a typical jet fighter airplane (F-80) indicate that the contributions of unsteady flow and the inclusion of higher order derivatives in the equations of motion are not important for subsonic speeds in the frequency range of 0 to 8 radians per second. * Flight test data on this airplane have subsequently verified this conclusion.

Other theoretical calculations on the longitudinal short period mode agree with these results for conventional aircraft with horizontal tails; however, for tailless aircraft or aircraft with short tail arms unsteady flow may be quite important. Pinsker shows that the deterioration in pitch damping of tailless aircraft is particularly severe when c.g. positions are forward. **

Pinsker also shows that a rapid deterioration of directional damping due to unsteady flow occurs at Mach numbers beyond 0.6 for conventional aircraft. Although his presentation of flight test data on the British Meteor seems to substantiate this conclusion, flight test data on various other jet fighters and transonic research aircraft do not indicate so detrimental an effect.

*Statler, I.C., 'Dynamic Stability at High Speeds from Unsteady Flow Theory,' Journal of the Aeronautical Sciences, XVII, No. 4 (April 1950), 232-242, 255.

** Pinsker, W.J.G., 'A Note on the Dynamic Stability of Aircraft at High Subsonic Speeds when Considering Unsteady Flow,' Royal Aircraft Establishment Report No. Aero. 2378, Farnborough, Hants, May 1950.

In spite of the great progress in unsteady flow research, it appears that no definite conclusions can be drawn at present concerning the conditions under which unsteady flow should or should not be considered in evaluating stability derivatives. The following digest of findings by Milliken (Reference 2) and others, summarizes the present status.

For conventional aircraft configurations (i.e., those not too heavily swept), unsteady flow effects in the reduced frequency range $0 < \frac{\omega c}{2U} < \approx .10$ are unimportant in the entire subsonic range for the longitudinal case. This conclusion essentially applies in the supersonic range except that the downwash lag derivative $C_{m_{\dot{\alpha}}}$ and possibly the horizontal tail lift curve slope must be considered in complex form. In the transonic range ($\approx .85 < M < \approx 1.2$) some theoretical considerations suggest great effects, but no supporting practical evidence is available. For aircraft configurations without horizontal tails or with short tail arms, unsteady flow effects are probably much more important.

Although little research in unsteady flow has been done for directional oscillations, it is conjectured that the same general conclusions as were reached in the longitudinal case are applicable here.

In evaluating the effect of unsteady flow on stability derivatives, there is one final word of caution. Most of the available literature is restricted to the special case of steady state sinusoidal oscillations. Numerical values of stability derivatives obtained from these references are not applicable either to damped sinusoidal oscillations or to aircraft responses to arbitrary control motions which are not sinusoidal in shape.

SECTION - 5. FACTORS THAT DETERMINE THE DIMENSIONAL STABILITY DERIVATIVE PARAMETERS

Once the aerodynamicist has evaluated the basic non-dimensional stability derivatives for a particular airframe configuration, these derivatives must be converted to the dimensional parameter form to be used in the dimensional equations of motion.

Reference to the conversion tables (IV-3 and IV-4 in the Appendix to this Chapter) will show that the multiplying factors used to convert the basic non-dimensional derivatives to the dimensional parameter form consist of various combinations of the following variables:

1. c, b, S (airframe geometry)
2. m, I_x, I_y, I_z (airframe mass and mass distribution)
3. ρ, U (flight condition)

For example:

$$M_q = \frac{\rho S U c^2}{4 I_y} \left(C_{m_q} \right)$$

It can be concluded that, in general, dimensional stability derivative parameters are direct functions of airframe geometry, of mass and mass distribution, and of flight conditions, in addition to being functions of the basic non-dimensional stability derivatives which are in turn implicit functions of airframe geometry, mass distribution, and flight condition.

In Section IV-4 it was shown that, in determining the values of the basic non-dimensional derivatives, the airframe configuration is usually the primary factor, with flight conditions and especially the Mach number being of secondary importance and merely modifying the primary value established by the airframe configuration. In determining the dimensional stability derivative parameters, however, notice that the values depend directly on the flight conditions ρ and U. This is important, because the effect of flight conditions is so great that, in general, the values of the dimensional stability derivative parameters can be said to be functions of both the airframe configuration and its flight condition, since these effects are of equal importance as far as the above parameters are concerned.

In numerous general investigations of aircraft stability and control of the past, the variables in the multiplying factors listed at the beginning of this section were grouped into such forms as:

$\tau = \frac{m}{\rho S U}$ Aerodynamic time (airsec)

$\mu_c = \frac{m}{\rho S c}$ Longitudinal relative airplane density

$\mu_b = \frac{m}{\rho S b}$ Lateral relative airplane density

By the use of these parameters, τ, μ_c, and μ_b, it was shown how certain stability and control characteristics of aircraft could be generalized. However, in most of these investigations, the basic non-dimensional derivatives were tacitly considered independent of all the factors discussed in Section 4, such as Mach number and dynamic pressure. In other words, they were not considered functions of τ, μ_c, and μ_b.

Today, because of the increased importance of Mach number and aeroelastic effects, the dependence of the basic non-dimensional stability derivatives on flight conditions can no longer be ignored, and the validity of these rather simple generalized studies when applied to modern jet aircraft is questionable. Therefore, it is felt that the once popular forms τ, μ_c, and μ_b have lost much of their significance. A consideration of some of the simpler combinations of the variables appears to be in order in generalized studies.

Some of the common combinations suitable for general studies are:

$AR = \frac{b^2}{S}$ Wing aspect ratio

$\frac{W}{S}$ Wing loading

$q = \frac{\rho}{2} U^2$ Dynamic pressure

$C_L = \frac{n}{q}\left(\frac{W}{S}\right)$ Lift coefficient

$\left(\frac{b}{K_x}\right)^2 \cdot \left(\frac{b}{K_z}\right)^2 \cdot \left(\frac{c}{K_y}\right)^2$ Non-dimensional inertia parameters

It is also convenient to express the flight conditions in terms of Mach number, M, and pressure altitude, h, rather than in terms of ρ and U.

BIBLIOGRAPHY

1. Perkins, Courtland D, and Hage, Robert E., 'Airplane Performance Stability and Control,' John Wiley & Sons, Inc., New York, 1949.

2. Milliken, W. F., Jr., 'Dynamic Stability and Control Research,' Cornell Aeronautical Laboratory, Inc., Report No. Cal-39, Cornell Research Foundation, Buffalo, N.Y. (Paper presented at the Third International Joint Conference of the R. Ae. S.-I. A. S., Brighton, England, September 3-14, 1951.)

3. Campbell, John P., and McKinney, Marion O., 'Summary of Methods for Calculating Dynamic Lateral Stability and Response and for Estimating Lateral Stability Derivatives,' NACA Technical Note, TN 2409, Langley Memorial Aeronautical Laboratory, Langley Field, Va., July 1951.

4. Durand, William, F., ed., 'Aerodynamic Theory': Volume 5, 'Dynamics of the Airplane,' by B. Melvill Jones, Durand Reprinting Committee, California Institute of Technology, 1943.

5. Pearson, Henry A., and Jones, Robert T., 'Theoretical Stability and Control Characteristics of Wings with Various Amounts of Taper and Twist,' NACA Technical Report, TR No. 635, Langley Memorial Aeronautical Laboratory, Langley Field, Va., 1938.

6. Jones, Arthur L., 'The Theoretical Lateral-Stability Derivatives for Wings at Supersonic Speeds,' Journal of the Aeronautical Sciences, XVII, No. 1 (January 1950), 39-46, 59.

7. Statler, I.C., 'Handbook for Computing Non-Stationary Flow Effects on Subsonic Dynamic Longitudinal Response Characteristics of an Airplane,' Cornell Aeronautical Laboratory, Report No. TB-495-F-12, Cornell Research Foundation, Inc., Buffalo, N.Y., March 1, 1950.

APPENDIX – CHAPTER IV

TABLE IV-1

LONGITUDINAL NON-DIMENSIONAL STABILITY DERIVATIVES

(STABILITY AXIS SYSTEM)

BASIC NON-DIMENSIONAL STABILITY DERIVATIVES			NON-DIMENSIONAL STABILITY DERIVATIVE - PARAMETERS
TOTAL AIRFRAME		THEORETICAL HORIZONTAL TAIL CONTRIBUTION	
DEFINITIONS	UNIT		
$C_D = \frac{DRAG}{qS}$	$\frac{1}{1}$		
$C_{D_u} = \frac{U}{2}\frac{\partial C_D}{\partial U}$	$\frac{1}{1}$		$x_u = (-C_D - C_{D_u})$
$C_{D_\alpha} = \frac{\partial C_D}{\partial \alpha}$	$\frac{1}{rad}$		$x_w = \frac{1}{2}(C_L - C_{D_\alpha})$
$C_{D_{\delta_E}} = \frac{\partial C_D}{\partial \delta_E}$	$\frac{1}{rad}$		$x_{\delta_E} = \frac{-1}{2} C_{D_{\delta_E}}$
$C_L = \frac{Lift}{qS}$	$\frac{1}{1}$		
$C_{L_u} = \frac{U}{2}\frac{\partial C_L}{\partial U}$	$\frac{1}{1}$		$z_u = (-C_L - C_{L_u})$
$C_{L_\alpha} = \frac{\partial C_L}{\partial \alpha}$	$\frac{1}{rad}$	$\left[C_{L_\alpha}\right]_H = C_{L_{\alpha_H}} \frac{q_H}{q}\frac{S_H}{S}\left(1 - \frac{\partial \epsilon}{\partial \alpha}\right)$	$z_w = \frac{1}{2}(-C_{L_\alpha} - C_D)$
$C_{L_{\dot\alpha}} = \frac{\partial C_L}{\partial\left(\frac{\dot\alpha c}{2U}\right)}$	$\frac{1}{rad}$	$\left[C_{L_{\dot\alpha}}\right]_H = 2C_{L_{\alpha_H}} \frac{q_H}{q}\frac{S_H}{S}\frac{l_H}{c}\frac{\partial \epsilon}{\partial \alpha}$	$z_{\dot w} = \frac{-1}{4} C_{L_{\dot\alpha}}$
$C_{L_q} = \frac{\partial C_L}{\partial\left(\frac{qc}{2U}\right)}$	$\frac{1}{rad}$	$\left[C_{L_q}\right]_H = 2C_{L_{\alpha_H}} \frac{q_H}{q}\frac{S_H}{S}\frac{l_H}{c}$	$z_q = \frac{-1}{4} C_{L_q}$
$C_{L_{\delta_E}} = \frac{\partial C_L}{\partial \delta_E}$	$\frac{1}{rad}$	$C_{L_{\delta_E}} = C_{L_{\alpha_H}} \frac{q_H}{q}\frac{S_H}{S}\frac{\partial \alpha_H}{\partial \delta_E}$	$z_{\delta_E} = -\frac{1}{2} C_{L_{\delta_E}}$
$C_m = \frac{M}{qSc}$	$\frac{1}{1}$		
$C_{m_u} = \frac{U}{2}\frac{\partial C_m}{\partial U}$	$\frac{1}{1}$		$m_u = \frac{1}{2}\left(\frac{c}{k_y}\right)^2 (C_m + C_{m_u})$
$C_{m_\alpha} = \frac{\partial C_m}{\partial \alpha}$	$\frac{1}{rad}$	$\left[C_{m_\alpha}\right]_H = -\frac{l_H}{c}\left[C_{L_\alpha}\right]_H$	$m_w = \frac{1}{2}\left(\frac{c}{k_y}\right)^2 C_{m_\alpha}$
$C_{m_{\dot\alpha}} = \frac{\partial C_m}{\partial\left(\frac{\dot\alpha c}{2U}\right)}$	$\frac{1}{rad}$	$\left[C_{m_{\dot\alpha}}\right]_H = \frac{-l_H}{c}\left[C_{L_{\dot\alpha}}\right]_H$	$m_{\dot w} = \frac{1}{4}\left(\frac{c}{k_y}\right)^2 C_{m_{\dot\alpha}}$
$C_{m_q} = \frac{\partial C_m}{\partial\left(\frac{qc}{2U}\right)}$	$\frac{1}{rad}$	$\left[C_{m_q}\right]_H = -\frac{l_H}{c}\left[C_{L_q}\right]_H$	$m_q = \frac{1}{4}\left(\frac{c}{k_y}\right)^2 C_{m_q}$
$C_{m_{\delta_E}} = \frac{\partial C_m}{\partial \delta_E}$	$\frac{1}{rad}$	$C_{m_{\delta_E}} = -\frac{l_E}{c} C_{L_{\delta_E}}$	$m_{\delta_E} = \frac{1}{2}\left(\frac{c}{k_y}\right)^2 C_{m_{\delta_E}}$

APPENDIX - CHAPTER IV

TABLE IV-2

LATERAL NON-DIMENSIONAL STABILITY DERIVATIVES

(STABILITY OR BODY AXIS SYSTEMS)

BASIC NON-DIMENSIONAL STABILITY DERIVATIVES			NON-DIMENSIONAL STABILITY DERIVATIVE PARAMETERS
TOTAL AIRFRAME		THEORETICAL VERTICAL TAIL CONTRIBUTION	
DEFINITIONS	UNIT		
$C_{y_\beta} = \frac{\partial C_y}{\partial \beta}$	$\frac{1}{\text{rad}}$	$\left[C_{y_\beta}\right]_v = -C_{L_{\alpha_v}} \frac{q_v}{q} \frac{S_v}{S} \left(1 - \frac{\partial \sigma}{\partial \beta}\right)$	$y_v = \frac{1}{2} C_{y_\beta}$
$C_{y_{\dot\beta}} = \frac{\partial C_y}{\partial \left(\frac{\dot\beta b}{2U}\right)}$	$\frac{1}{\text{rad}}$	UNKNOWN	$y_{\dot v} = \frac{1}{4} C_{y_{\dot\beta}}$
$C_{y_r} = \frac{\partial C_y}{\partial \left(\frac{rb}{2U}\right)}$	$\frac{1}{\text{rad}}$	$\left[C_{y_r}\right]_v = 2C_{L_{\alpha_v}} \frac{q_v}{q} \frac{S_v}{S} \frac{l_v}{b} \left(1 - \frac{U}{l_v} \frac{\partial \sigma}{\partial r}\right)$	$y_r = \frac{1}{4} C_{y_r}$
$C_{y_p} = \frac{\partial C_y}{\partial \left(\frac{pb}{2U}\right)}$	$\frac{1}{\text{rad}}$	$\left[C_{y_p}\right]_v = 2C_{L_{\alpha_v}} \frac{q_v}{q} \frac{S_v}{S} \frac{h_v}{b} \left(1 - \frac{U}{h_v} \frac{\partial \sigma}{\partial p}\right)$	$y_p = \frac{1}{4} C_{y_p}$
$C_{y_{\delta_R}} = \frac{\partial C_y}{\partial \delta_R}$	$\frac{1}{\text{rad}}$	$C_{y_{\delta_R}} = C_{L_{\alpha_v}} \frac{q_v}{q} \frac{S_v}{S} \frac{\partial \alpha_v}{\partial \delta_R}$	$y_{\delta_R} = \frac{1}{2} C_{y_{\delta_R}}$
$C_{y_{\delta_A}} = \frac{\partial C_y}{\partial \delta_A}$	$\frac{1}{\text{rad}}$		$y_{\delta_A} = \frac{1}{2} C_{y_{\delta_A}}$
$C_{n_\beta} = \frac{\partial C_n}{\partial \beta}$	$\frac{1}{\text{rad}}$	$\left[C_{n_\beta}\right]_v = -\frac{l_v}{b} \left[C_{y_\beta}\right]_v$	$n_v = \frac{1}{2} \left(\frac{b}{k_z}\right)^2 C_{n_\beta}$
$C_{n_{\dot\beta}} = \frac{\partial C_n}{\partial \left(\frac{\dot\beta b}{2U}\right)}$	$\frac{1}{\text{rad}}$	$\left[C_{n_{\dot\beta}}\right]_v = -\frac{l_v}{b} \left[C_{y_{\dot\beta}}\right]_v$	$n_{\dot v} = \frac{1}{4} \left(\frac{b}{k_z}\right)^2 C_{n_{\dot\beta}}$
$C_{n_r} = \frac{\partial C_n}{\partial \left(\frac{rb}{2U}\right)}$	$\frac{1}{\text{rad}}$	$\left[C_{n_r}\right]_v = -\frac{l_v}{b} \left[C_{y_r}\right]_v$	$n_r = \frac{1}{4} \left(\frac{b}{k_z}\right)^2 C_{n_r}$
$C_{n_p} = \frac{\partial C_n}{\partial \left(\frac{pb}{2U}\right)}$	$\frac{1}{\text{rad}}$	$\left[C_{n_p}\right]_v = -\frac{l_v}{b} \left[C_{y_p}\right]_v$	$n_p = \frac{1}{4} \left(\frac{b}{k_z}\right)^2 C_{n_p}$
$C_{n_{\delta_R}} = \frac{\partial C_n}{\partial \delta_R}$	$\frac{1}{\text{rad}}$	$\left[C_{n_{\delta_R}}\right]_v = -\frac{l_R}{b} C_{y_{\delta_R}}$	$n_{\delta_R} = \frac{1}{2} \left(\frac{b}{k_z}\right)^2 C_{n_{\delta_R}}$
$C_{n_{\delta_A}} = \frac{\partial C_n}{\partial \delta_A}$	$\frac{1}{\text{rad}}$		$n_{\delta_A} = \frac{1}{2} \left(\frac{b}{k_z}\right)^2 C_{n_{\delta_A}}$
$C_{l_\beta} = \frac{\partial C_l}{\partial \beta}$	$\frac{1}{\text{rad}}$	$\left[C_{l_\beta}\right]_v = \frac{h_v}{b} \left[C_{y_\beta}\right]_v$	$l_v = \frac{1}{2} \left(\frac{b}{k_x}\right)^2 C_{l_\beta}$
$C_{l_{\dot\beta}} = \frac{\partial C_l}{\partial \left(\frac{\dot\beta b}{2U}\right)}$	$\frac{1}{\text{rad}}$	$\left[C_{l_{\dot\beta}}\right]_v = \frac{h_v}{b} \left[C_{y_{\dot\beta}}\right]_v$	$l_{\dot v} = \frac{1}{4} \left(\frac{b}{k_x}\right)^2 C_{l_{\dot\beta}}$
$C_{l_r} = \frac{\partial C_l}{\partial \left(\frac{rb}{2U}\right)}$	$\frac{1}{\text{rad}}$	$\left[C_{l_r}\right]_v = \frac{h_v}{b} \left[C_{y_r}\right]_v$	$l_r = \frac{1}{4} \left(\frac{b}{k_x}\right)^2 C_{l_r}$
$C_{l_p} = \frac{\partial C_l}{\left(\frac{pb}{2U}\right)}$	$\frac{1}{\text{rad}}$	$\left[C_{l_p}\right]_v = \frac{h_v}{b} \left[C_{y_p}\right]_v$	$l_p = \frac{1}{4} \left(\frac{b}{k_x}\right)^2 C_{l_p}$
$C_{l_{\delta_R}} = \frac{\partial C_l}{\partial \delta_R}$	$\frac{1}{\text{rad}}$	$C_{l_{\delta_R}} = \frac{h_r}{b} C_{y_{\delta_R}}$	$l_{\delta_R} = \frac{1}{2} \left(\frac{b}{k_x}\right)^2 C_{l_{\delta_R}}$
$C_{l_{\delta_A}} = \frac{\partial C_l}{\partial \delta_A}$	$\frac{1}{\text{rad}}$		$l_{\delta_A} = \frac{1}{2} \left(\frac{b}{k_x}\right)^2 C_{l_{\delta_A}}$

APPENDIX – CHAPTER IV

TABLE IV-3

LONGITUDINAL DIMENSIONAL STABILITY DERIVATIVE PARAMETERS

(STABILITY AXIS SYSTEM)

QUANTITY	IN TERMS OF BASIC STABILITY DERIVATIVES			IN TERMS OF NON-DIMENSIONAL STABILITY DERIVATIVE PARAMETERS
	DIMENSIONAL		NON-DIMENSIONAL	
	DEFINITIONS	UNIT		
X_u	$-\frac{1}{m}\frac{\partial X}{\partial u}$	$\frac{1}{sec}$	$-\frac{\rho SU}{m}\left(-C_D - C_{D_u}\right)$	$-\frac{1}{\tau} x_u$
X_w	$-\frac{1}{m}\frac{\partial X}{\partial w}$	$\frac{1}{sec}$	$-\frac{\rho SU}{2m}\left(C_L - C_{D_\alpha}\right)$	$-\frac{1}{\tau} x_w$
X_{δ_E}	$-\frac{1}{m}\frac{\partial X}{\partial \delta_E}$	$\frac{ft}{sec^2 rad}$	$-\frac{\rho SU^2}{2m}\left(-C_{D_{\delta_E}}\right)$	$-\frac{U}{\tau} x_{\delta_E}$
Z_u	$-\frac{1}{m}\frac{\partial Z}{\partial u}$	$\frac{1}{sec}$	$-\frac{\rho SU}{m}\left(-C_L - C_{L_u}\right)$	$-\frac{1}{\tau} z_u$
Z_w	$-\frac{1}{m}\frac{\partial Z}{\partial w}$	$\frac{1}{sec}$	$-\frac{\rho SU}{2m}\left(-C_{L_\alpha} - C_D\right)$	$-\frac{1}{\tau} z_w$
$Z_{\dot{w}}$	$-\frac{1}{m}\frac{\partial Z}{\partial \dot{w}}$	$\frac{1}{1}$	$-\frac{\rho Sc}{4m}\left(-C_{L_{\dot{\alpha}}}\right)$	$-\frac{c}{\tau U} z_{\dot{w}}$
Z_q	$-\frac{1}{m}\frac{\partial Z}{\partial q}$	$\frac{ft}{sec\text{-}rad}$	$-\frac{\rho SUc}{4m}\left(-C_{L_q}\right)$	$-\frac{c}{\tau} z_q$
Z_{δ_E}	$-\frac{1}{m}\frac{\partial Z}{\partial \delta_E}$	$\frac{1}{sec^2 rad}$	$-\frac{\rho SU^2}{2m}\left(-C_{L_{\delta_E}}\right)$	$-\frac{U}{\tau} z_{\delta_E}$
M_u	$-\frac{1}{I_y}\frac{\partial M}{\partial u}$	$\frac{1}{sec\text{-}ft}$	$-\frac{\rho SUc}{I_y}\left(C_m + C_{m_u}\right)$	$-\frac{2}{\tau c} m_u$
M_w	$-\frac{1}{I_y}\frac{\partial M}{\partial w}$	$\frac{1}{sec\text{-}ft}$	$-\frac{\rho SUc}{2I_y} C_{m_\alpha}$	$-\frac{1}{\tau c} m_w$
$M_{\dot{w}}$	$-\frac{1}{I_y}\frac{\partial M}{\partial \dot{w}}$	$\frac{1}{ft}$	$-\frac{\rho Sc^2}{4I_y} C_{m_{\dot{\alpha}}}$	$-\frac{1}{\tau U} m_{\dot{w}}$
M_q	$-\frac{1}{I_y}\frac{\partial M}{\partial q}$	$\frac{1}{sec\ rad}$	$-\frac{\rho SUc^2}{4I_y} C_{m_q}$	$-\frac{1}{\tau} m_q$
M_{δ_E}	$-\frac{1}{I_y}\frac{\partial M}{\partial \delta_E}$	$\frac{1}{sec^2 rad}$	$-\frac{\rho SU^2 c}{2I_y} C_{m_{\delta_E}}$	$-\frac{U}{\tau c} m_{\delta_E}$

APPENDIX – CHAPTER IV

TABLE IV-4

LATERAL DIMENSIONAL STABILITY DERIVATIVE PARAMETERS

(STABILITY OR BODY AXES SYSTEMS)

QUANTITY	IN TERMS OF BASIC STABILITY DERIVATIVES			IN TERMS OF NON-DIMENSIONAL STABILITY DERIVATIVE PARAMETERS
	DIMENSIONAL		NON-DIMENSIONAL	
	DEFINITIONS	UNIT		
Y_v	$-\frac{1}{mU}\frac{\partial Y}{\partial \beta}$	$\frac{1}{\text{sec-rad}}$	$-\frac{\rho SU}{2m} C_{y_\beta}$	$-\frac{1}{\tau} y_v$
$Y_{\dot{v}}$	$-\frac{1}{mU}\frac{\partial Y}{\partial \dot{\beta}}$	$\frac{1}{\text{rad}}$	$-\frac{\rho Sb}{4m} C_{y_{\dot{\beta}}}$	$-\frac{b}{\tau U} y_{\dot{v}}$
Y_r	$-\frac{1}{mU}\frac{\partial Y}{\partial r}$	$\frac{1}{\text{rad}}$	$-\frac{\rho Sb}{4m} C_{y_r}$	$-\frac{b}{\tau U} y_r$
Y_p^*	$-\frac{1}{mU}\frac{\partial Y}{\partial p}$	$\frac{1}{\text{rad}}$	$-\frac{\rho Sb}{4m} C_{y_p}$	$-\frac{b}{\tau U} y_p$
$Y_{\delta_R}^*$	$-\frac{1}{mU}\frac{\partial Y}{\partial \delta_R}$	$\frac{1}{\text{sec-rad}}$	$-\frac{\rho SU}{2m} C_{y_{\delta_R}}$	$-\frac{1}{\tau} y_{\delta_R}$
$Y_{\delta_A}^*$	$-\frac{1}{mU}\frac{\partial Y}{\partial \delta_A}$	$\frac{1}{\text{sec-rad}}$	$-\frac{\rho SU}{2m} C_{y_{\delta_A}}$	$-\frac{1}{\tau} y_{\delta_A}$
N_β	$-\frac{1}{I_z}\frac{\partial N}{\partial \beta}$	$\frac{1}{\text{sec}^2\text{rad}}$	$-\frac{\rho SU^2 b}{2I_z} C_{n_\beta}$	$-\frac{U}{\tau b} n_v$
$N_{\dot{\beta}}$	$-\frac{1}{I_z}\frac{\partial N}{\partial \dot{\beta}}$	$\frac{1}{\text{sec-rad}}$	$-\frac{\rho SUb^2}{4I_z} C_{n_{\dot{\beta}}}$	$-\frac{1}{\tau} n_{\dot{v}}$
N_r	$-\frac{1}{I_z}\frac{\partial N}{\partial r}$	$\frac{1}{\text{sec-rad}}$	$-\frac{\rho SUb^2}{4I_z} C_{n_r}$	$-\frac{1}{\tau} n_r$
N_p	$-\frac{1}{I_z}\frac{\partial N}{\partial p}$	$\frac{1}{\text{sec-rad}}$	$-\frac{\rho SUb^2}{4I_z} C_{n_p}$	$-\frac{1}{\tau} n_p$
N_{δ_R}	$-\frac{1}{I_z}\frac{\partial N}{\partial \delta_R}$	$\frac{1}{\text{sec}^2\text{rad}}$	$-\frac{\rho SU^2 b}{2I_z} C_{n_{\delta_R}}$	$-\frac{U}{\tau b} n_{\delta_R}$
N_{δ_A}	$-\frac{1}{I_z}\frac{\partial N}{\partial \delta_A}$	$\frac{1}{\text{sec}^2\text{rad}}$	$-\frac{\rho SU^2 b}{2I_z} C_{n_{\delta_A}}$	$-\frac{U}{\tau b} n_{\delta_A}$
L_β	$-\frac{1}{I_x}\frac{\partial L}{\partial \beta}$	$\frac{1}{\text{sec}^2\text{rad}}$	$-\frac{\rho SU^2 b}{2I_x} C_{l_\beta}$	$-\frac{U}{\tau b} l_v$
$L_{\dot{\beta}}$	$-\frac{1}{I_x}\frac{\partial L}{\partial \dot{\beta}}$	$\frac{1}{\text{sec-rad}}$	$-\frac{\rho SUb^2}{4I_x} C_{l_{\dot{\beta}}}$	$-\frac{1}{\tau} l_{\dot{v}}$
L_r	$-\frac{1}{I_x}\frac{\partial L}{\partial r}$	$\frac{1}{\text{sec-rad}}$	$-\frac{\rho SUb^2}{4I_x} C_{l_r}$	$-\frac{1}{\tau} l_r$
L_p	$-\frac{1}{I_x}\frac{\partial L}{\partial p}$	$\frac{1}{\text{sec-rad}}$	$-\frac{\rho SUb^2}{4I_x} C_{l_p}$	$-\frac{1}{\tau} l_p$
L_{δ_R}	$-\frac{1}{I_x}\frac{\partial L}{\partial \delta_R}$	$\frac{1}{\text{sec}^2\text{rad}}$	$-\frac{\rho SU^2 b}{2I_x} C_{l_{\delta_R}}$	$-\frac{U}{\tau b} l_{\delta_R}$
L_{δ_A}	$-\frac{1}{I_x}\frac{\partial L}{\partial \delta_A}$	$\frac{1}{\text{sec}^2\text{rad}}$	$-\frac{\rho SU^2 b}{2I_x} C_{l_{\delta_A}}$	$-\frac{U}{\tau b} l_{\delta_A}$

CHAPTER V

METHODS OF OBTAINING STABILITY DERIVATIVES

SECTION 1 – INTRODUCTION

The purposes of this chapter are to present a brief description of various methods and techniques in use today for the determination of numerical values of stability derivatives and to discuss the relative accuracies of these methods. The primary reason for the inclusion of this material is its value to the designers of the airframe, the control surfaces, the control actuators, and the autopilot. These engineers must necessarily be concerned with the interpretation of aerodynamic stability data and with the evaluation of the accuracy of these data if they are to arrive at an integrated system design.

Considerations relating to the accuracy with which aerodynamic data are known are of extreme importance in the integration of system design. For example, it is quite possible that the estimated stability derivatives for a given airframe may be known to be inaccurate, perhaps due to insufficient or questionable basic information from which to compute the derivatives; this is particularly true, of course, in the transonic region. If the designers of the specialized components are all alert to this situation, their various apparatus can then be designed with sufficient tolerances to take into account the potential inaccuracies of the derivatives.

In general, there are three methods of obtaining stability derivatives which can be listed in the following order of increasing accuracy:

1. Estimating from theory and related empirical data.
2. Model testing.
3. Full-scale flight testing.

Each of these three methods will be considered in the following pages.

SECTION 2 – ESTIMATING FROM THEORY AND RELATED EMPIRICAL DATA

In the preliminary design stage of an integrated airframe-autopilot-controls system, the exact configuration of the airframe is not known; consequently, stability derivatives must be estimated in a rather general manner to establish their ranges of values. Since it is impractical to perform model tests on all the various configurations which may arise at this stage of the design, the necessary stability derivative data can be obtained only from theory and from related empirical data on similar airframe configurations.

In general, the recommended procedure is to assume, first of all, a certain airframe configuration or a strictly limited range of configurations. Then, by consulting a few basic theoretical reports, stability derivatives for the low subsonic region can be estimated. References 1 and 2 are very useful in determining the characteristics of the wing alone. References 3 and 4 provide a means of estimating the longitudinal derivatives for the complete airframe, and Reference 5 summarizes rather completely the lateral derivatives for the complete airframe.

The next step is to estimate the effect of Mach number on the stability derivatives in the subsonic region ($0<M<.9$) by applying the Prandtl-Glauert rule of compressibility. This method consists of modifying the lift curve slopes of the wing and the horizontal and vertical tails as functions of Mach number. References 5 and 6 provide methods of procedure and design charts for this modification.

For the transonic and the low supersonic region ($.9<M<1.5$), theoretical methods of determining stability and control derivatives for the complete airframe are practically non-existent. As a result, the designer must resort to various empirical data on similar airframe configurations. But because there is no theory which can be used as a guide, the trends indicated by empirical data are difficult to correlate, and this problem is further complicated by the fact that the data obtained by all the various techniques applicable to transonic investigations may be unreliable or inaccurate or both. Apparently the best method of estimating stability derivative values in the transonic region at present is to use correlation plots showing the variation of the stability derivatives with Mach number, for various types of aircraft.

For the supersonic region ($M > 1.5$), limited theoretical methods are again available for estimating values of stability derivatives. In general, the higher the supersonic Mach number, the more reliable the theory. References 5 and 7 present very good summaries and bibliographies of available literature for estimating

supersonic derivatives of wing-alone configurations. Theoretical research relating to complete airframe configurations of wing, body, and tail, and to the associated mutual interference effects, has been very limited, and the designer must again resort to empirical data and to correlation plots.

After the designer has estimated the Mach number effects on the stability derivatives, he should consider the important effects of any of the other factors discussed in Section 5 of Chapter IV. For example, with a sweptback wing of moderate aspect ratio, aeroelastic effects on the stability derivatives are quite important and must be taken into account.

Generalized design procedures for evaluating the effect of these factors on stability derivatives are not available. Each effect must be investigated in the light of its particular application.

SECTION 3 – MODEL TESTING

To increase the accuracy of the stability derivative estimates based upon theory and related empirical data, models duplicating the geometry of the contemplated full-scale airframe are usually built and tested. In fact, model testing has become such an important science that it is now considered indispensable to aircraft development.

In applying the results of model tests to the full-scale airplane, there is an important scale relationship which must be taken into account in the interpretation of data. This scale relationship of geometrically similar objects is given by the non-dimensional parameter $\rho V l/\mu$, which is called the Reynolds number of the particular scale-flow combination. In this parameter, ρ is the density and μ the viscosity of the medium (air) through which the body moves; V is the forward velocity of the body with respect to the medium; and l is some characteristic length of the body (usually the mean aerodynamic chord of the wing) measured in the direction of the air stream.

When the Reynolds numbers of two flows are equal, the flow characteristics are dynamically similar. Assuming a model and a full-scale aircraft operating at the same speed in the same atmospheric conditions, ρ, V, and μ are the same, but the Reynolds number of the model-flow combination is lower than the Reynolds number of the airplane-flow combination in direct proportion to the size of the model.

Full-scale aircraft operate in a Reynolds number range of 6,000,000 to 100,000,000, whereas model testing is done in a Reynolds number range of 500,000 to 10,000,000. Stability derivative data based on model tests performed at Reynolds numbers of 6,000,000 or more may be considered directly applicable to the full-scale airplane, but if the model tests are performed at Reynolds numbers of less than 6,000,000, it is likely that the stability derivative values will require modification before they can be applied to the full-scale airplane. One of the difficulties in using model test data is that the effects of Reynolds number are in most cases quantitatively unpredictable, and the correct interpretation of the data is largely a matter of judgment based on experience.

There are two general types of model testing: wind tunnel testing and model flight testing. These types are considered in detail in the following pages.

(a) WIND TUNNEL TEST

The present day wind tunnel is generally recognized as being almost indispensable in obtaining aerodynamic information concerning specific aircraft design configurations. Many different kinds of wind tunnels are in use throughout the country, each of which has its particular advantages for certain types of testing. Most of them can be classified as "conventional type tunnels."

1. Conventional Tunnel

In general, the conventional wind tunnel consists of a tubular channel forming a closed circuit through which air is circulated at high velocities.

During tests in this type of tunnel, the model remains stationary, and the various aerodynamic forces and moments acting on the model are measured by means of a balance system or by strain gages mounted on struts to which the model is attached.

Conventional wind tunnel testing is concerned with determining the derivatives which are not rates of change with time, the so-called "static" stability derivatives. The usual practice is to obtain six basic data; three forces, lift, drag, and side forces; and three moments, pitching, yawing, and rolling moments.

In the longitudinal case, the coefficients C_L, C_D and C_m are functions of angle of attack α; therefore, the static derivatives C_{L_α}, C_{D_α}, and C_{m_α} are obtained from wind tunnel data.

In the lateral case, the coefficients C_y, C_n, and C_l are a function of sideslip angle β; therefore, the derivatives C_{y_β}, C_{n_β} and C_{l_β} are obtained from wind tunnel data.

Also obtainable from these tests are the control effectivenesses and the related derivatives such as: $C_{L_{\delta_E}}$ and $C_{m_{\delta_E}}$ for the elevator; $C_{y_{\delta_R}}$, $C_{n_{\delta_R}}$, and $C_{l_{\delta_R}}$ for the rudder; and $C_{y_{\delta_A}}$, $C_{n_{\delta_A}}$ and $C_{l_{\delta_A}}$ for the aileron. Moreover, the control surface hinge moment parameters can be obtained, such as:

$$\frac{\partial C_{h_E}}{\partial \delta_E}, \quad \frac{\partial C_{h_E}}{\partial \alpha}, \quad \frac{\partial C_{h_R}}{\partial \delta_R}, \quad \frac{\partial C_{h_R}}{\partial \beta}, \quad \frac{\partial C_{h_A}}{\partial \delta_A}, \quad \frac{\partial C_{h_A}}{\partial \alpha}$$

Finally, the majority of testing programs involving

airframe configurations in conventional wind tunnels include the determination of the characteristics of alterable airframe geometry; such as flaps, slats, speed brakes, landing gear, and so forth. In addition, the effects of power and free controls are sometimes obtained.

Wind tunnel data are not always as accurate as might be desired and the results must be interpreted by experienced personnel. For some stability derivatives, such as C_{L_α}, the experimental results provide satisfactorily accurate values; in cases such as C_D, C_{m_α}, $C_{m_{\delta_E}}$, $C_{l_{\delta_A}}$, the wind tunnel data may not be directly applicable to the full-scale airframe because of Reynolds number and aeroelastic effects.

Some of the sources of error in conventional wind tunnel testing are:

a. Scale effects due to the low Reynolds number of the test.
b. Choking phenomena at high subsonic Mach numbers.
c. Inaccurate corrections to the data, such as tare and alignment corrections and wall corrections.
d. Incorrect duplication of power effects.
e. Inaccurate representation of drag by omission of some protuberances.
f. Use of solid wood models having lower percentage structural deflections under load than does the airplane.
g. Mechanical and instrumentation discrepancies involved in the measurement of forces and moments.
h. Human errors that are likely to occur in the testing and data reduction.

An understanding of the sources, the importance, and the correction of errors is essential for interpreting the results of wind tunnel tests. Reynolds number effects appear to be prominent among these sources of error. For example, at low Reynolds numbers, there is a tendency for boundary layer separation to occur at a lower angle of attack on the model than on the full-scale airplane, thereby causing earlier changes in such derivatives as C_{m_α}, C_{L_α}, and C_{l_β}, as functions of equilibrium angle of attack.

In spite of such limitations, wind tunnel testing is a powerful tool in the hands of the designer if he exercises great care in test procedures and in data interpretation.

2. Rolling Flow Tunnel

The basic purpose of the rolling flow tunnel is to duplicate, as accurately as possible, the flow pattern conditions which exist around the airframe when it executes a pure rolling motion in actual flight. The rolling flow technique can give experimental values for the three stability derivatives due to rolling velocity, p ; they are: the side force coefficient due to roll, C_{y_p} ; the yawing moment coefficient due to roll, C_{n_p} ; and the roll damping derivative, C_{l_p}.

There are two different testing techniques used to simulate the rolling motion of the airplane. The first of these has been developed at Langley Field where NACA has constructed a stability tunnel having a balance system which can be rotated. The model to be tested is mounted upon a support which is free to rotate, and a small auxiliary controllable-pitch airfoil, which is attached to an arm on the model, creates the force needed to rotate the model. This technique is called the "rolling-wing" method.

In the second technique, also developed by NACA, the model is held stationary and the airstream in which the model is immersed is rotated by means of a rotor equipped with a series of curved vanes. This technique is called the "rolling-flow" method.

One advantage of the rolling-flow technique over the rolling-wing technique is that it permits all forces and moments to be measured with the model mounted on a conventional balance system. But on the other hand, this method does not exactly simulate the conditions of an airplane in steady roll or of a model in forced rotation, for there is a buildup of static pressure near the tunnel walls due to centrifugal force acting on the rotating air, which results in a pressure variation along any radius, a condition which does not exist when an airplane rotates. However, this pressure variation effect probably does not play an important part in most tests.

Both these techniques appear to be attractive methods of obtaining rolling moment derivatives; data obtained from tests show them to be in consistent agreement, and in addition, such data check closely with calculated values of C_{l_p}.*

3. Curved Flow Tunnel

The curved flow technique of measuring stability derivatives due to yawing velocity, r , and to pitching velocity, q , is somewhat similar in principle to the rolling-flow technique. The air flow in the wind tunnel follows a curved path in the vicinity of the model and has a velocity variation normal to the circular arc streamlines in direct proportion to the local radius of curvature of the flow. Such a flow is made possible by using a curved test section in combination with a variable-mesh screen designed to form a reduced velocity region on the inner side of the curved section.

* MacLachlan, Robert, and Letko, William, 'Correlation of Two Experimental Methods of Determining the Rolling Characteristics of Unswept Wings,' NACA Technical Note, TN 1309, Langley Memorial Aeronautical Laboratory, Langley Field, Va., May 1947.

The model is fixed to a conventional balance system, and the forces and moments acting on the model are measured as functions of either yawing velocities or pitching velocities depending upon the orientation of the model with respect to the curved flow. By this means it is possible to determine the stability derivatives C_{y_r}, C_{n_r}, C_{l_r}, C_{l_q}, and C_{m_q}.

The curved flow technique does not exactly reproduce the conditions of an airplane flying in a curved path, since, for the model, there is a static pressure gradient created by the centrifugal forces on the air mass in rotation, which causes an apparent lateral buoyancy. Corrections for this effect can be calculated and applied. This static pressure gradient also produces a tendency for boundary layer air on the model to flow toward the center of rotation, a tendency opposite to that in actual flight. This effect cannot be evaluated accurately at present, but it is known to be of secondary importance. Turbulence is also a secondary complication not readily amenable to mathematical analysis.

Reasonably good agreement has been reported among the curved-flow technique, the free oscillation technique, and the calculated results.* In general, data obtained from the curved flow tunnel tests indicate satisfactory measurement of the rotary characteristics caused by yawing or pitching velocity, and the accuracy attained is considered superior to that of such other techniques; as the various oscillation and whirling arm methods.

4. Oscillation Tests

Another method of attacking the problem of evaluating the rotary damping derivatives is the model oscillation technique. This method requires either (a) free oscillation or (b) forced oscillation of the model. In either case, the model is mounted in a conventional wind tunnel on a single strut and is free to rotate essentially as a one-degree-of-freedom system in either pitch or yaw.

In the free oscillation method, a torsion spring provides restoring moment, so that a damped oscillation results from merely displacing and releasing the model. An oscillograph or high-speed motion picture camera records the resulting motion. The total damping is then evaluated from the decay of the amplitude of the oscillation.

The forced oscillation method is somewhat more complex, for it requires a mechanism designed to maintain a steady oscillation by applying a sinusoidally varying yawing or pitching moment. Oscillograph or photograph records are analyzed for angle of pitch or sideslip, angular acceleration, and applied moment. From these data, the moments acting on the model at zero acceleration can be determined, and from these moments, in turn, the damping derivatives can be obtained.

Data derived by the forced oscillation procedure are not expected to be as accurate as those obtained by the free oscillation technique because of the difficulty in obtaining records free from random disturbances. On the other hand, forced oscillation enables one to determine results in the high lift coefficient range where difficulty is experienced with free oscillation.

It should be pointed out that either of these oscillation techniques gives the total damping of the system which in the longitudinal case (pitching) is $(C_{m_q} + C_{m_{\dot{\alpha}}})$ and in the lateral case (yawing) is $(C_{n_r} - C_{n_{\dot{\beta}}})$. Thus, the individual values of the damping derivatives C_{m_q}, $C_{m_{\dot{\alpha}}}$, C_{n_r}, and $C_{n_{\dot{\beta}}}$ cannot be determined from oscillation tests alone, since the total damping obtained is composed of the sum of the respective pairs.

If the values of C_{n_r} and C_{m_q} are determined for a particular model by means of the curved flow technique, it is theoretically possible to determine the derivatives $C_{n_{\dot{\beta}}}$ and $C_{m_{\dot{\alpha}}}$ by performing oscillation tests on the same model.

In practice, however, the use of this procedure may be somewhat limited by the inaccuracy of the data involved in the two types of testing.

Comparisons of free oscillation and curved flow techniques indicate satisfactory agreement for moderate lift; however, at high lift coefficients, differing values of C_{n_r} are obtained by these two methods.**

Further comparisons of the results obtained from both free and forced oscillation techniques with those from curved flow techniques indicate satisfactory agreement.*

5. Free-Flight Tunnel

In the free-flight tunnel technique, the model is not attached to any sort of balance system, but is allowed to move freely within the test section of the tunnel. The model has movable control surfaces, and its motions

* Bird, John D., Jaquet, Byron M., and Cowan, John W., 'Effect of Fuselage and Tail Surfaces on Low-Speed Yawing Characteristics of a Swept-Wing Model as Determined in Curved-Flow Test Section of Langley Stability Tunnel,' NACA Technical Note, TN 2483, Langley Memorial Aeronautical Laboratory, Langley Field, Va., October 1951.

**Goodman, Alex, and Feigenbaum, David, 'Preliminary Investigation at Low Speeds of Swept Wings in Yawing Flow,' NACA Research Memorandum, RM L7109, Langley Memorial Aeronautical Laboratory, Langley Field, Va., February 4, 1948.

can be controlled by a human "pilot" who flies the model as he would a full-scale aircraft.

The free-flight tunnel is not used primarily to obtain specific numerical values of stability derivatives, but rather to study the general stability and control behavior with reference to desirable flying qualities from a pilot's viewpoint. However, it is possible to obtain quantitative stability derivative data by analyzing motion picture records of the response of the model to control inputs.

The advantage of this free-flight technique is that the low speed overall dynamics and handling qualities of a particular aircraft configuration can be investigated in the preliminary design stage. Various characteristics can be determined, such as elevator required to trim, damping and period of the longitudinal and lateral oscillatory modes, spiral stability, response to control inputs, and stall behavior.

Some of the data from free-flight testing have been found to conflict with full-scale test data.* The earlier boundary layer separation on the model due to the lower Reynolds number very likely accounts for the largest portion of the disagreement. Stall characteristics are not too clearly demonstrated by the free-flight model, and spiral stability is difficult to measure; but the test is useful for comparisons between different flight conditions and different configurations. Considerable scatter in observations is inevitable because steady conditions cannot be obtained before application of the controls.

These various inconsistencies and quantitative disagreements with full-scale data are appreciable, but it is believed that, with an understanding of their nature and magnitude, correct general conclusions can be drawn from the model data regarding the stability and control of the airplane represented, particularly where an evaluation of the relative merits of different modifications is desired.

6. Whirling Arm

The whirling arm was one of the earliest experimental methods devised for testing models. In this technique, the model and its balance system are attached to a long arm, and the whole assembly is rotated at high speeds. By this means, yawing (or pitching) motion of an airplane is flight is simulated, and it is possible to determine values of derivatives such as C_{y_r}, C_{n_r}, C_{l_r}, C_{l_q}, and C_{n_q}.

Unfortunately, the model operates in the turbulent wake created from each previous revolution of the apparatus and this imposes a severe limitation on the accuracy and consistency of the data obtained. In addition, the balance system is subjected to centrifugal force due to the rotation, and large corrections must be applied to account for this effect.

For these reasons, the whirling arm technique is no longer widely used; it has been replaced by the more accurate curved flow tunnel technique.

7. Transonic Bump Tests

Wind tunnel testing in the transonic range is extremely difficult and unreliable in conventional tunnels because of choking phenomena between the model and the tunnel walls.

One method of obtaining data in the transonic region is to modify existing high subsonic wind tunnel test sections with a suitably contoured bump on which small reflection plane (half-span) models can be mounted. Even though the tunnel is operating at subsonic speeds, the increase in flow velocity over the bump creates a localized area of transonic and supersonic Mach numbers. Because of the small size of the model used, tunnel choking phenomena are avoided.

One disadvantage of this method is that the local increase in velocity over the bump is not uniform; there is a velocity gradient as a function of distance away from the surface of the bump. This means that the model is subjected to a Mach number gradient in the direction of the span.

Another disadvantage of this method is that the data are obtained at low Reynolds numbers because the models of necessity must be very small – approximately six inches in half-span.

The Mach number gradient and the low Reynolds numbers of the tests are the inevitable penalties for the avoidance of choking, and they sometimes constitute sufficient reason for skeptical attitudes toward bump model test results.

From transonic bump tests only static longitudinal stability derivative data can be obtained such as C_{D_α}, C_{D_u}, C_{l_α}, C_{l_u}, $C_{L_{\delta_E}}$, C_{m_α}, C_{m_u}, and $C_{m_{\delta_E}}$.

Because half-span models are used, no static directional stability derivative data are obtainable.

8. Supersonic Tunnel

At the present time, the design trend for supersonic tunnels is toward the conventional tunnel arrangement through which the air or any special gaseous working fluid is circulated continuously in a closed circuit. Other arrangements have been or are being used, however. In the "blow down" type tunnel, for example, the air is pumped under pressure into a large reservoir before the test and is released during the test to atmospheric pressure through a model test section in which supersonic velocities are attained.

The models are usually sting mounted, and the forces

* Shortal, Joseph A., and Osterhout, Clayton J., 'Preliminary Stability and Control Tests in the NACA Free-Flight Tunnel and Correlation with Full-Scale Flight Tests,' NACA Technical Note, TN 810, Langley Memorial Aeronautical Laboratory, Langley Field, Va., June 1941.

and moments are measured by means of electrical strain gages. Both static longitudinal data and directional stability data can be obtained.

Because of the large amounts of power required to drive the air at very high velocities in the conventional tunnel arrangement, the size of the tunnel must, in practice, be kept small, a restriction which in turn places severe limitations upon the size of the models to be tested. The resulting large difference in Reynolds number between the models and the full-scale aircraft makes the interpretation and application of most supersonic wind tunnel data on stability derivatives difficult.

(b) MODEL FLIGHT TEST

1. Transonic Wing Flow

The NACA wing flow method is similar in principle to the bump test model method because the manner of inducing supersonic flow is the same; in this case the wing of a full-scale airplane serves as the "bump."

The model, which must be very small, is placed on the wing of an airplane in the vicinity of the maximum thickness; the manner of mounting is similar to that of the bump method. A motor-driven device for rotating the model and a mechanism for measuring forces and moments on the model are incorporated in the wing. When the airplane is flown at high subsonic speeds, the model is immersed in the increased velocity zone on the upper surface of the wing.

The testing procedure consists of diving the airplane from some predetermined high altitude so that the Mach number on the wing varies through the transonic range. During the run, recording instruments provide a continuous sequence of airplane flight data and model test data.

In addition to providing static longitudinal, and lateral stability derivative data, the wing flow method can also be used to obtain directional dynamic characteristics in a manner similar to that of the model oscillation technique described earlier. When the wing flow method is used with half-span models as is ordinarily done, only static longitudinal data are obtainable.

The wing flow method is subject to somewhat greater limitations than the bump test method. Only one configuration can be tested during a particular flight because the airplane must return to the ground for changes in the model configuration. This procedure is costly and time-consuming for a systematic investigation of a large family of configurations. However, for tests on a particular model configuration, the method appears to be somewhat more practical.

Another limitation is the difficulty of maintaining steady test conditions on the model. During the dive of the airplane, the motion of its controls must be kept to a minimum, and atmospheric turbulence must be avoided. Sideslip angle and rolling velocity of the airplane can significantly affect the flow pattern over the model, and in some cases devices for measuring the local flow direction have been employed to correct for these effects. Sharp deviations from steady flight conditions can render the data inapplicable. Of course, none of these factors enters into the ordinary procedures of wind tunnel testing.

Up to the present time, comparisons with results from actual test flights show that the wing flow data are frequently too inaccurate for application to full-scale design. Here again, accuracy is lost because of the great departure from full-scale Reynolds number, a parameter which is necessarily low in most experimental work on models. In a fixed Mach number range, the only two variables affecting Reynolds number that the designer is at liberty to vary are the size of the model and the density of the air mass. The model size is limited by the physical dimensions of the transonic flow field over the wing, and density is determined by the altitude selected for the test and by the temperature of the atmosphere. The wind tunnel bump test method, on the other hand, allows the density to be increased considerably in variable-density type tunnels. Considering all these factors, it appears that the bump test method has some advantages over the wing flow method.

2. Ballistic Tests

The techniques involved in the study of projectiles fired from guns have been adapted to test missile and airplane configurations. The model, constructed of solid metal and carrying no power or instrumentation, is launched or fired from a special gun, and during its flight, it passes a series of photograph stations which provide a shadowgraph history of the trajectory. From these photographs, the spacial orientation of the model is obtained; and from this orientation, the linear and angular velocities can be derived.

This technique has been used successfully in studying the rolling characteristics of certain model configurations and in obtaining the aileron effectiveness derivative $C_{l_{\delta_A}}$ and the roll damping derivative C_{l_p} *.

An advantage of this technique is that the models are flown through undisturbed air; the main disadvantage is that the models are small, resulting in very low test Reynolds number.

3. Free-Fall Model Tests

One method which has been used to attain transonic Mach numbers in model testing consists of carrying the model to high altitudes and then dropping it to earth, thus using gravity as the source of power. During its descent, the model is tracked by radar and optical tracking equipment to determine its general flight path. The model can be equipped with radio-operated controls and with instrumentation for determining the response of the model to

* Balz, Ray E., and Nicolaides, John D., 'A Method of Determining Some Aerodynamic Coefficients from Supersonic Free-Flight Tests of a Rolling Missile,' Journal of the Aeronautical Sciences, XVII, No. 10 (October 1950), 609-621.

the control inputs. These response data are telemetered to ground stations.

The chief advantage of this method is that large models can be made to pass gradually through the transonic region under truly free-air conditions; its main disadvantage is that the model and its costly instrumentation are destroyed upon impact with the ground.

This method has been used mainly to study lift and drag characteristics of various wing configurations on missiles. The application of the free-fall technique to determining dynamic characteristics of models has not been developed to any great extent, and it appears that any developmental work along these lines has been superseded by the rocket-powered model technique.

4. Rocket-Powered Model Tests

The most promising of the free-flight model techniques is that employing rocket-powered models. This technique does not differ greatly from the drop-test method except that the model carries its own power in the form of a rocket. The model is accelerated to supersonic speeds by means of a booster rocket, which then separates from the model, permitting the model to coast back through the transonic region. In some cases the model itself carries a small additional rocket motor which extends the testing run time.

The model contains instrumentation to pick up its dynamic motions, and these data are telemetered to ground stations. Provisions are made either to pulse the controls of the model or to fire very small rockets aligned in a direction perpendicular to the center line of the model, thus producing input disturbances.

The rocket-powered model technique shares with the free-fall technique the important advantage that large models can be tested with correspondingly large test Reynolds number. But it also shares the disadvantage that the costly model is destroyed upon impact after the test run is completed.

If the instrumentation and telemetering equipment is sufficiently accurate, static and dynamic stability derivative data can be obtained from these tests in a manner similar to that for full-scale dynamic flight testing techniques described in the next section.

Aeroelastic effects on stability derivatives can be obtained by this method if two models constructed of different materials are used; for example, if one is constructed of steel and the other of aluminum.

SECTION 4 – FULL-SCALE FLIGHT TESTING

After the full-scale prototype of a particular airplane has been built, the estimates of stability derivatives from theory and model testing can be verified and refined by means of full-scale flight tests. However, such a testing program is rarely carried out because the time, effort, and special equipment involved make it a very costly procedure. Optimum flight test techniques and data reduction methods applicable to all aircraft have not been worked out; consequently, a large part of a flight test program must necessarily be devoted to the development of techniques for testing a particular airplane. In addition, the instrumentation of the airplane to be used in determining the frequency response and stability derivatives must be of higher quality than that required merely to demonstrate satisfactory flying qualities. In the past, the need for such a flight test program, except for academic purposes, has hardly been great enough to justify the expense.

The main reason why these costs have not been incurred is that the specifications which have been set up by the military services for piloted aircraft do not explicitly require that stability derivatives be obtained from flight testing. These specifications are based to a considerable extent upon a large number of opinions expressed by pilots concerning desirable or undesirable flying qualities of all types of military aircraft. Consequently, most of the full-scale flight testing for stability and control is carried out for the one purpose of demonstrating that the contractor's particular airplane meets these specifications.

However, these specifications do require that certain special flight test techniques be used and that certain maneuvers be executed, and from these, the values of some derivatives could be obtained. For example, in demonstrating the rolling response of the airplane due to aileron deflection, the derivatives $C_{l_{\delta_A}}$ and C_{l_p} could be obtained, and in demonstrating the Dutch roll damping characteristics of the airplane, the frequency of the oscillation could be measured to give the value C_{n_β}.

The important point remains that the military services do not require that flight tests be conducted to obtain all the stability derivatives or to obtain the frequency response of the airplane to control inputs from which stability derivatives could be derived, and consequently this sort of flight testing is not usually carried out.

At the present time, it is believed that flight testing of the full-scale airplane for the purpose of obtaining stability derivatives and frequency response data is of much more than purely academic interest and should be considered necessary not only because of the stringent requirements of the autopilot system and the control feel system in attaining desirable flying qualities but because today's aircraft are operating in the transonic region where aerodynamic stability and control data from estimation procedures and model tests are unreliable.

In general, there are three flight test techniques from which stability derivatives can be obtained: (1) steady flight technique, (2) transient response technique, and (3) sinusoidal oscillation technique. Each of these methods is discussed in the following pages.

(a) STEADY FLIGHT TECHNIQUES

The steady flight techniques described here consist of

steady-straight and steady-turning flight and are to be distinguished from the sinusoidal oscillation technique which is sometimes referred to as the steady state oscillation technique. In general, the steady-straight techniques determine only static stability derivatives; whereas, steady-turning type maneuvers permit several dynamic derivatives, such as C_{m_q} and C_{l_p}, to be obtained.

By first stabilizing the airplane in straight and level flight at different airspeeds and at different center of gravity locations, and then measuring the elevator required for trim, it is possible to obtain numerical values for certain combinations of stability derivatives made up of such derivatives as C_{D_α}, C_{L_α}, C_{m_α}, $C_{L_{\delta_E}}$, and $C_{m_{\delta_E}}$. In many cases, however, the explicit value of each derivative cannot be obtained separately unless the values of the other derivatives can be assumed or estimated from model tests or a different flight test technique.

If steady pull-up type maneuvers are performed at constant forward speed the value of C_{m_q} can be roughly evaluated, if $C_{m_{\delta_E}}$ is known, since the additional elevator deflection over that required for trim can be measured.

Steady sideslips yield data both on the static directional derivatives C_{y_β}, C_{n_β}, and C_{l_β}, and on the control derivatives $C_{y_{\delta_R}}$, $C_{n_{\delta_R}}$, $C_{n_{\delta_A}}$, and $C_{l_{\delta_A}}$. Here again, however, as with the longitudinal case, none of the derivatives can be evaluated explicitly unless values of some of the others are assumed. This procedure is not as difficult as it may at first appear. Flight test values of C_{n_β} can be easily obtained by measuring the period of the Dutch roll oscillation; and aileron effectiveness, $C_{l_{\delta_A}}$, can be estimated fairly accurately from model tests and rate of roll flight tests. If C_{n_β}, and $C_{l_{\delta_A}}$ are known, the remainder of the static directional derivatives can be evaluated from the simple steady flight side force, yawing moment, and pitching moment equations:

$$C_{y_{\delta_R}} \delta_R + C_{L_p} p = -C_{y_\beta} \beta$$

$$C_{n_{\delta_R}} \delta_R + C_{n_{\delta_A}} \delta_A = -C_{n_\beta} \beta$$

$$C_{l_{\delta_R}} \delta_R + C_{l_{\delta_A}} \delta_A = -C_{l_\beta} \beta$$

$$C_{m_{\delta_R}} = -\frac{l_{\delta_R}}{\bar{c}} C_{y_{\delta_R}}$$

where l_{δ_R}, the effective rudder arm from the cg of the airplane, can be estimated from the airplane's geometry.

If a steady rate of roll can be established for a given step function aileron deflection, measurements of the steady rolling velocity and of the aileron deflection required yield the ratio of the derivative C_{l_p} to $C_{l_{\delta_A}}$ from the simple relation:

$$\frac{C_{l_p}}{C_{l_{\delta_A}}} = \frac{\delta_A}{p} \cdot \frac{2U}{b}$$

All the maneuvers which are used in these steady flight techniques are prescribed as part of the contractor's demonstration that his airplane meets military stability and control requirements. These data will therefore be readily available for all prototype military aircraft. It may be seen, however, that these techniques yield little information on many of the dynamic derivatives; either the sinusoidal oscillation technique or the transient response technique must be used to obtain such data.

(b) SINUSOIDAL OSCILLATION TECHNIQUE

The sinusoidal oscillation technique is the most elaborate method of establishing the transfer function of the airplane. Although stability derivatives cannot be obtained directly by this method, it is possible to derive values of certain combinations of derivatives from plots of the transfer function.

Since this flight test technique consists of measuring the sinusoidal response of the airplane to a sinusoidal control input, some sort of sine wave generator equipment is required to actuate the control surface in the desired manner. If the aircraft has an autopilot, it is relatively a simple task to feed the output of a sine wave generator into the autopilot servo motor.

The advantage of the sinusoidal oscillation technique in establishing transfer functions is that it gives fairly accurate results over a wide range of frequencies. It is useful in certain frequency ranges where the exact form of the transfer function is in question. It can also be quite useful in establishing the existence of unsteady flow phenomena or in correlating theoretical predictions of unsteady flow phenomena, since most unsteady flow theory available at the present time is based on steady state sinusoidal oscillations.

The disadvantage of the sinusoidal oscillation technique is that it requires much more flight testing time than the transient technique because the airplane must be stabilized at each value of input frequency, and many stabilized points are required to define the complete transfer function of the airframe over the frequency range of interest.

To obtain stability derivatives from sinusoidal oscillation testing, the response data are plotted on log modulus-frequency charts (Bode charts) which are then examined for the position of first and second order break points. (One is aided here by correlation with theoretically derived transfer functions.) Since these break points are determined by various specific combinations of stability derivatives, called "transfer function coefficients," the value of each derivative cannot be established separately. However, if the values of some of the derivatives can be obtained from wind tunnel estimates or from steady state flight techniques, the rest can then be determined from the transfer function coefficient values. There is

no precise method known for obtaining stability derivatives in general from frequency response plots; it is at best a trial-and-error procedure, the usefulness of which depends upon the familiarity of the analyst with the particular frequency response and the particular airframe involved.

For certain special cases, however, several important techniques have been developed. In the longitudinal motions of conventional aircraft, for instance, it can be shown that for frequencies greater than the natural frequency of the phugoid the forward speed remains constant during maneuvers. Consequently, in the range of frequencies involved in the longitudinal short period motions, the equations of motion are reduced to two degrees of freedom, and the resulting frequency response describes a simple second order system. This has led to the concept of simple effective spring and damping constants, k and b, which contain specific combinations of static and dynamic stability derivatives.

The most obvious way of determining the effective spring and damping constants, k and b, is to analyze the free oscillation response of the aircraft to any sort of control input. The spring constant k and the damping constant b are determined respectively by the period of the oscillation and the rate of decay in amplitude of oscillation. This analysis technique, which is known as the "transient inspection method," does not, of course, imply the use of the forced oscillation flight technique under discussion at the moment, but it should be regarded as a possible source for obtaining k and b.

The second analysis technique assumes that forced sinusoidal oscillation tests have been conducted and that the data have been plotted in the form of log-modulus frequency response charts. For the special case of an assumed second order system, a complete set of transparent templates can be constructed which show the effect of different values of k and b on the frequency response of the general second order system. These templates are then compared with the frequency response data obtained from flight tests, and appropriate values of k and b are determined by a trial-and-error matching process.

The third method of obtaining k and b utilizes forced oscillation flight test data plotted in the form of a "circle diagram." In this method, the vector describing the ratio of the maximum amplitude of the output to that of the input and the corresponding phase angle are plotted as a function of frequency. For an ideal second order system, the shape of this plot is a circle, and from certain geometric properties of the circle, k and b can be determined. (This method is described in detail in Reference 8.) Although the circle diagram technique has been used with some success in the past, the newer methods of analysis have proved to be more convenient.

(c) TRANSIENT RESPONSE TECHNIQUE

The transient response technique appears to be the most practical flight test method for determining both the stability derivatives and the transfer functions of the airframe. In this technique, some measurable input is applied to the airframe, and stability derivatives and transfer functions are determined from the resulting transient response data.

The advantages of the transient technique over the sinusoidal flight testing technique are that much less actual flight time is required and that stability derivatives can be obtained directly from the transient data without performing a frequency response analysis. Further, the frequency response of an airframe can be derived mathematically from transient flight data by an application of Fourier transform methods.

One of the limitations of the transient technique is that the form of the equations of motion of the airframe must be known or assumed when stability derivatives are to be derived directly from transient data. The problem then usually arises as to whether or not higher order derivatives, unsteady flow effects, and aeroelastic modes should be included. It is theoretically possible to include all such effects and to determine which of them will turn out to be negligible This, however, appears to be impracticable because accurate values for derivatives making small contributions to the total effect cannot be obtained by such a process.

The airframe input which excites the transient response can be imparted by various means; motion of the aerodynamic control surfaces, change in thrust, firing of rockets of known impulse to produce yawing and pitching moments, and dropping of weights from wing tips to produce known rolling moments.

The input magnitude, duration, and form are important. Step inputs are useful when the airframe is able to reach a steady state value corresponding to the new trim flight conditions imposed by the input. When the airplane response cannot reach a steady state value, but diverges, a pulse input is more practical and also has the advantage that the duration and shape of the pulse can be chosen to produce a response whose major contribution lies in the frequency range of interest. Arbitrary or random inputs can also be used, but analysis of the results then becomes more laborious. Simplified response approximations, which exist for step and impulse inputs, are not available for more complex inputs, and insight into the problem may be lost in the complexity of the analysis.

Once transient flight data are available, there are at present three general methods of extracting stability derivative information from them:

1. Transient inspection method
2. Response curve fitting method
3. Fourier transform method

1. Transient Inspection Method

If the aircraft response to a pulse input contains an oscillatory component whose frequency and damping are such that the time, $T_{\frac{1}{2}}$, for the oscillations to damp to half-amplitude, and the period, P, of the oscillations may both be measured from the response records, the

equivalent spring constant, k , and damping, b , corresponding to this particular mode, can be determined from the following equations (see Reference 10):

$$k = \frac{0.48}{(T_{\frac{1}{2}})^2} + \frac{38.48}{P^2}$$

$$b = \frac{1.386}{T_{\frac{1}{2}}}$$

The numerical values of k and b thus obtained from flight test data may then be used in conjunction with the approximate equations describing the airframe's characteristic modes (see Chapter III) to obtain values of certain combinations of static and dynamic stability derivatives.

Because of the restrictive assumptions and approximations that may have to be made to get stability derivatives by this method, the results can be relied upon only to the extent that these assumptions and approximations have been established as applicable to a given case.

The chief advantage of the transient inspection method is that it permits the order of magnitude of certain stability derivatives, such as C_{n_β}, C_{m_α}, $(C_{n_r} - C_{n_{\dot\beta}})$, and $(C_{m_q} + C_{m_{\dot\alpha}})$, to be established quickly and easily without resorting to complex analytic procedures.

2. Response Curve-Fitting Methods

The response curve-fitting methods consist basically of matching transient responses by assuming the form of the equations of motion of the system to be known; the unknown coefficients of the various terms in the equations are then evaluated to match the transient data as well as possible.

One of the simplest forms of this method is to set up the equations of motion on an analog computer and, by a trial-and-error procedure, to determine values of the coefficients (stability derivatives) which best match the transient response. The success of this technique depends upon how accurately the values of stability derivatives are known prior to the flight testing, and to a certain extent, upon the experience of the person performing the analysis.

The analog computer technique of matching flight test transients is also useful in refining stability derivative values which have been obtained by any of the other flight test reduction techniques.

Various mathematical techniques have been devised to get stability derivatives directly from transient flight data. At present, it appears that the most useful of these methods are Greenberg's "derivative method," Prony's method, and Shinbrot's iteration method. (These methods are discussed in detail in References 9 and 10.)

In the "derivative method" (Reference 9) a sufficient number of values of the independent and dependent variables (such as δ, $\dot\theta$, $\ddot\theta$, α, $\dot\alpha$, etc., for the longitudinal case) are measured during the flight test transient so that when they are inserted in the assumed equations of motion, a set of equations will result which may then be solved simultaneously for all the stability derivatives.

Prony's method (Reference 10) consists of fitting a sum of exponentials to the response at a number of equally spaced time ordinates; this method can be used to obtain the transfer function coefficients (which are combinations of stability derivatives) from a step or impulse input.

Shinbrot's iteration method (Reference 10) uses the results of the derivative method or Prony's method as a first approximation; a more accurate set of values is then obtained by expansion in a Taylor's series and an iterative procedure for obtaining better approximations.

Successive approximations are possible, of course, with any of the methods mentioned, but this refinement may not be justified at the present time.

Nearly all these mathematical techniques utilize some form of least squares fit of the theoretical motion to the flight test data. The statistical principle of least squares states that the most probable value of an unknown parameter is one which will cause the sum of the squares of the errors (the difference between the measured and calculated values) to be a minimum. As pointed out in Reference 7, the least squares method can only be viewed as a mathematical means of "fairing" the experimental data. Since it nearly always introduces additional complications, the justification of its use in preference to simple visual fairing methods is not apparent for some cases.

In general, it appears that more work is required on the practicability of the various mathematical techniques and on the related problem of statistical fairing of redundant flight data before an optimum curve-fitting technique can be developed.

3. Fourier Transform Method

In the Fourier transform method, the transient response flight data are converted mathematically to frequency response form by application of the Fourier integral (Reference 9). These frequency response data can then be analyzed for values of the transfer function coefficients by any of the methods discussed in the section devoted to the sinusoidal oscillation technique.

One of the advantages of this method is that the frequency response obtained as an intermediate step in the computation of transfer function coefficients by this procedure is often itself of interest in problems of automatic stabilization. Another advantage is that the form of the equations of motion of the system need not be assumed as it does for the curve-fitting methods.

However, the Fourier transform method has the disadvantage that stability derivatives cannot be derived singly, for they occur in combinations as transfer function coefficients. A further limitation is that the size and shape of the input used in the flight test have a considerable influence on the accuracy with which the fre-

quency response can be derived, and also upon the range of frequencies for which that response is valid. For a pulse input, for example, it appears that the frequency response derived from the transient data will be applicable only to a limited range of frequencies on either side of the fundamental frequency of the pulse.

In Reference 11, the Fourier transform method is used successfully in obtaining transfer functions of a particular aircraft; however, no attempt is made to obtain transfer function coefficients or stability derivatives from the transfer function data.

SUMMARY

In the preliminary design stage of an airframe, the most expedient method of obtaining stability derivatives is by estimating from theory and making use of empirical data from similar airframe configurations.

In the subsonic region ($0 < M < .9$), stability derivatives can be estimated fairly well from theory by using the geometry of the airframe and applying the Prandtl-Glauert rule to account for compressibility.

In the high supersonic region ($1.5 < M < 10$), fairly good estimates of some of the stability derivatives can be made from theory. In general, the higher the supersonic Mach number, the more accurate the theory. Theoretical supersonic values are not available, however, for all the derivatives, especially for the various possible combinations of wing, body, and tail configurations.

In the transonic and low supersonic region ($.9 < M < 1.5$) theoretical methods are practically non-existent for determining stability and control derivatives of complete airframe configurations. Therefore, in estimating stability derivatives in this Mach number regime, empirical data on similar airframe configurations must be used; but the amount of such data is discouragingly small. In the transonic region the method of omphaloskepsis has been used successfully in estimating stability derivatives.

Aeroelastic effects on the more important stability and control derivatives can be calculated by theoretical means.

Generally, then, methods for obtaining stability derivatives by theory and by estimating from empirical data on similar airframes is fairly good in the subsonic region, but poor in the transonic and supersonic region.

When the design of the airframe has been determined to a certain extent, various wind tunnel tests, such as those described in Section 3 of this chapter, can be performed. Low speed conventional wind tunnel tests on a large model can be used to refine the theoretical estimates and to obtain the stability derivatives for the landing configuration. High subsonic wind tunnel tests can be used to refine the estimates on compressibility effects. Aeroelastic models can be used to verify the theoretically calculated aeroelastic trends. Because of the limited accuracy of theoretical estimates in the transonic and supersonic regions, it is almost imperative that transonic and supersonic tests be performed on the particular configuration either in the wind tunnel or by the rocket-firing technique.

If such a thorough model testing program is conducted, the accuracy of the original estimates of stability and control data should be increased so that it is entirely adequate for the subsonic region and fairly good for the transonic and supersonic regions.

At this stage of the airframe design, a full-scale prototype will probably be ready. If past procedures are followed, it is unlikely that more work will be performed to obtain improved values of stability derivatives unless the airplane exhibits particularly bad flying qualities. However, because of the stringent requirements imposed upon the autopilot system and control feel system in attaining desirable flying qualities, it is believed that the refinement of aerodynamic derivatives should not stop at this point, but rather that a certain portion of the prototype flight testing should be devoted to this end.

In general, the accuracy of the values of derivatives obtained from flight testing is considered better than that from any other method. The degree of accuracy obtained depends upon the flight test technique, the quality of the instrumentation, the data analysis technique, and, since some sort of averaging process must be applied, the total number of samples taken.

Many of the static stability derivatives can be obtained by means of steady flight testing techniques, provided that values of some of the derivatives can be adequately estimated from theory or wind tunnel test results. All the stability derivatives can be obtained with varying degrees of accuracy by matching the airplane's response to pulse control inputs by a least square curve fitting method, if the form of the equations of motion is known, or assumed.

Certain combinations of stability derivatives (transfer function coefficients) can be obtained from log frequency response (Bode) plots of the airframe by the trial-and-error curve fitting technique or by the circle diagram method. These log frequency response plots can be obtained directly by sinusoidal oscillation flight testing or indirectly by analyzing airplane transient responses to pulse inputs by application of the Fourier integral.

Because of the large amount of information obtained from a relatively small amount of flight time, the method of obtaining the transient response to a pulse input appears to offer the most advantages as far as the flight testing technique is concerned. In obtaining stability derivatives from these transient data, it is not known whether the direct method of least squares curve fitting to the transient, or the indirect method of first converting to frequency response plots and then to stability derivatives is the better.

BIBLIOGRAPHY

1. Toll, Thomas A., and Queijo, M.J., 'Approximate Relations and Charts for Low-Speed Stability Derivatives of Swept Wings,' NACA Technical Note, TN 1581, Langley Memorial Aeronautical Laboratory, Langley Field, Va., May 1948.

2. Pearson, Henry A., and Jones, Robert T., 'Theoretical Stability and Control Characteristics of Wings with Various Amounts of Taper and Twist,' NACA Technical Report, TR 635, Langley Memorial Aeronautical Laboratory, Langley Field, Va., 1938.

3. Zimmerman, Charles H., 'An Analysis of Longitudinal Stability in Power-Off Flight with Charts for Use in Design,' NACA Technical Report, TR 521, Langley Memorial Aeronautical Laboratory, Langley Field, Va., December 13, 1934.

4. Lyon, H. M., Truscott, P. M., Auterson, E. I., and Whatham, J., 'A Theoretical Analysis of Longitudinal Dynamic Stability in Gliding Flight,' Aeronautical Research Council, Reports and Memoranda, R & M No. 2075, July 1942.

5. Campbell, John P., and McKinney, Marion O., 'Summary of Methods for Calculating Dynamic Lateral Stability and Response and for Estimating Lateral Stability Derivatives,' NACA Technical Note, TN 2409, Langley Memorial Aeronautical Laboratory, Langley Field, Va., July 1951.

6. DeYoung, John, 'Theoretical Additional Span Loading Characteristics of Wings with Arbitrary Sweep, Aspect Ratio, and Taper Ratio,' NACA Technical Note, TN 1491, Ames Aeronautical Laboratory, Moffett Field, Calif., December 1947.

7. Milliken, W.F., Jr., 'Dynamic Stability and Control Research,' Cornell Aeronautical Laboratory, Inc., Report No. CAL-39, Cornell Research Foundation, Buffalo, N.Y. (Paper presented at the Third International Joint Conference of the R. Ae. S. - I. A. S., Brighton, England, September 3-14, 1951.)

8. Milliken, W.F., Jr., 'Dynamic Longitudinal Stability and Control Flight Tests of a B-25J Airplane. Forced Oscillation and Step Function Response Methods, Utilizing an A-12 Automatic Pilot,' Cornell Aeronautical Laboratory, Inc., Report No. TB-405-F-3, April 15, 1947.

9. Greenberg, Harry, 'A Survey of Methods for Determining Stability Parameters of an Airplane from Dynamic Flight Measurements,' NACA Technical Note, TN 2340, Ames Aeronautical Laboratory, Moffett Field, Calif., April 1951.

10. Shinbrot, Marvin, 'A Least Squares Curve Fitting Method with Applications to the Calculation of Stability Coefficients from Transient Response Data,' NACA Technical Note, TN 2341, Ames Aeronautical Laboratory, Moffett Field, Calif., April 1951.

11. Smaus, Louis H., Gore, Marvin R., and Waugh, Merle G., 'A Comparison of Predicted and Experimentally Determined Longitudinal Dynamic Responses of a Stabilized Airplane,' NACA Technical Note, TN 2578, Ames Aeronautical Laboratory, Moffett Field, Calif., December 1951.

Bureau of Aeronautics

FLIGHT CONTROL SYSTEM MANUALS

VOL. I, "METHODS OF ANALYSIS AND SYNTHESIS OF PILOTED AIRCRAFT FLIGHT CONTROL SYSTEMS" AE-61-1 Navy No. 1 (251 pages, 459 figures; $4.00)

Chapters – Fundamental Concepts, Analysis, Synthesis, Optimum Synthesis Methods, Non-linearities, Machine Methods, Analog Computer, Mathematical Background.

VOL. II, "DYNAMICS OF THE AIRFRAME" AE-61-4 II (185 pages, 178 figures; $4.25) Addendum to Vol. II (27 figures; $1.50)

Chapters – Derivation of the Airframe Transfer Functions, Discussion of Transfer Functions, Discussion of Stability Derivatives, Methods of Obtaining Stability Derivatives.

VOL. III, "THE HUMAN PILOT" AE-61-4 III (157 pages, 55 figures; $3.50)

Chapters – Fundamental Aspects – Sensing and Actuating Processes of a Human Pilot, Approximate Methods Predicting Responses of a Human Pilot.

VOL. IV, "THE HYDRAULIC SYSTEM" AE-61-4 IV (224 pages, 63 figures; $4.25)

Chapters – General Considerations, Analysis of the Generalized Hydraulic Servo Actuator, A Generalized Hydraulic Control System, The Fully Powered Hydraulic Control System, The Power Boost Hydraulic Control System, Special Considerations in Hydraulic Control System Design and Analysis, Component Design Factors, Influence of Servomechanisms on the Flutter of Servo-Controlled Aircraft, Methods of Analysis of Servo Flutter Interaction.

VOL. V, "THE ARTIFICIAL FEEL SYSTEM" AE-61-4- V (152 pages, 103 figures; $3.00)

Chapters – The Control Feel Problem, Design Procedure, Design Criteria.

VOL. VI, "AUTOMATIC FLIGHT CONTROL SYSTEMS FOR PILOTED AIRCRAFT" AE-61-4 VI (339 pages, 138 figures; $6.00)

Chapters – Automatic Flight Control Systems Past and Present, Components of Automatic Flight Control Systems, Design Methods, Systems Engineering and Other Design Considerations, Appendix.

The volumes listed above complete the series of Flight Control System Manuals presently available, and are identical in content to the original contract publications.

To order one or more of these volumes, contact:

NORAIR, 1001 E. Broadway, Hawthorne, Calif.
Attn: Dept. 3730

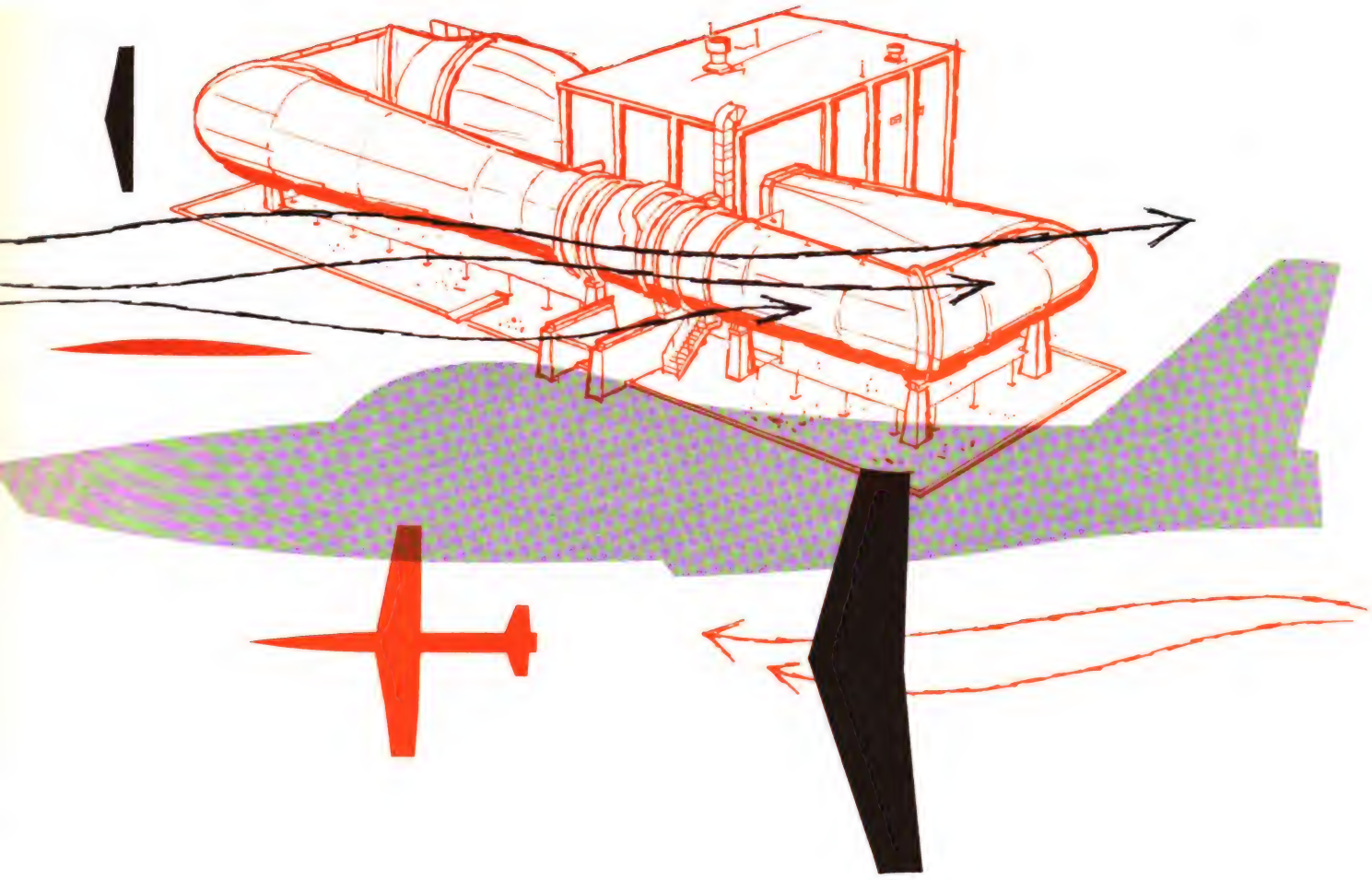

DYNAMICS OF THE AIRFRAME ADDENDUM

AE-6-4-II

NORAIR A DIVISION OF NORTHROP CORPORATION

BUREAU OF AERONAUTICS
FLIGHT CONTROL SYSTEM MANUALS

This series was originally prepared by Norair under Bureau of Aeronautics sponsorship to correlate the new and expanding techniques of automatic, powered control systems.

Continuing interest in these manuals, expressed by educational and industrial agencies, affirms the need for authoritative documents presenting technology of this scientific area.

In response Norair is offering, with Bureau of Aeronautics permission and encouragement, special reprints of the entire series of manuals to all interested individuals and agencies. Our objective is to contribute to understanding and advancing the state-of-the-art.

A list of the other volumes in this series, including printing costs, may be found on the last page of this manual.

BU AER
Report AE – 61 – 4 II

DYNAMICS OF THE AIRFRAME

ADDENDUM

BASIC VOLUME
WRITTEN AND EDITED BY SERVOMECHANISMS
SECTION AND AERODYNAMICS SECTION
NORTHROP AIRCRAFT, INC.

CONTRIBUTIONS TO VOLUME
BY OTHER AUTHORS
ARE NOTED IN INDIVIDUAL SECTIONS
IN ACCORDANCE WITH "IMPORTANT NOTE"
ON FOLLOWING PAGE

PREPARATION OF VOLUME
SPONSORED BY
BUREAU OF AERONAUTICS, NAVY DEPARTMENT

SEPTEMBER, 1952

The material of this addendum forms part of Report AE-61-4II, which together with Report AE-61-4I, has been written under BuAer Contract NOas 51-514(c), "Fundamentals of Design of Piloted Aircraft Flight Control Systems." These form part of a series of manuals being written for the purpose of providing a unified approach to problems of control system design.

For the sake of securing as wide a distribution as possible, Report AE-61-4I, "Methods of Analysis and Synthesis," which is Volume I of this series, and the part, "Dynamics of the Airframe" (Vol. II), of AE-61-4II which precedes this confidential addendum, have been issued in an unclassified status, in accordance with one of the general intents of the series to provide a source of information to be used by engineers in bridging the gap between their collegiate training and the more advanced topics of system engineering.

Since the figures of this addendum contain classified data, they could not be included in the body of this Report, but are presented here in order to include the maximum usable information available at this time. Because of the disparity in level of classification, no mention of this addendum has been made in the body of this Report, but the information herein is to be considered in conjunction with the contents of Chapter IV.

The numerical values and the ranges of values of derivatives shown on the following charts are estimates, based on trends shown by flight tests, wind tunnel tests, and theory; they apply only to fighter type piloted aircraft of today and the near future. They do not apply to missile configurations where the wing is quite small compared to the body, for in these configurations the range of values of non-dimensional derivatives can become very large. (Pitkin, Marvin, and Ankenbruck, Herman O., "Estimation of Range of Stability Derivatives for Current and Future Pilotless Aircraft," NACA Research Memorandum, RM L7E29, Langley Memorial Aeronautical Laboratory, Langley Field, Va., October 8, 1947.)

The following notation has been used in the graphs of this portion of this Report:

A solid line (————————) has been used for straight wing aircraft; a broken line (— — — —), for swept wing; and a dotted line (------) for delta wing.

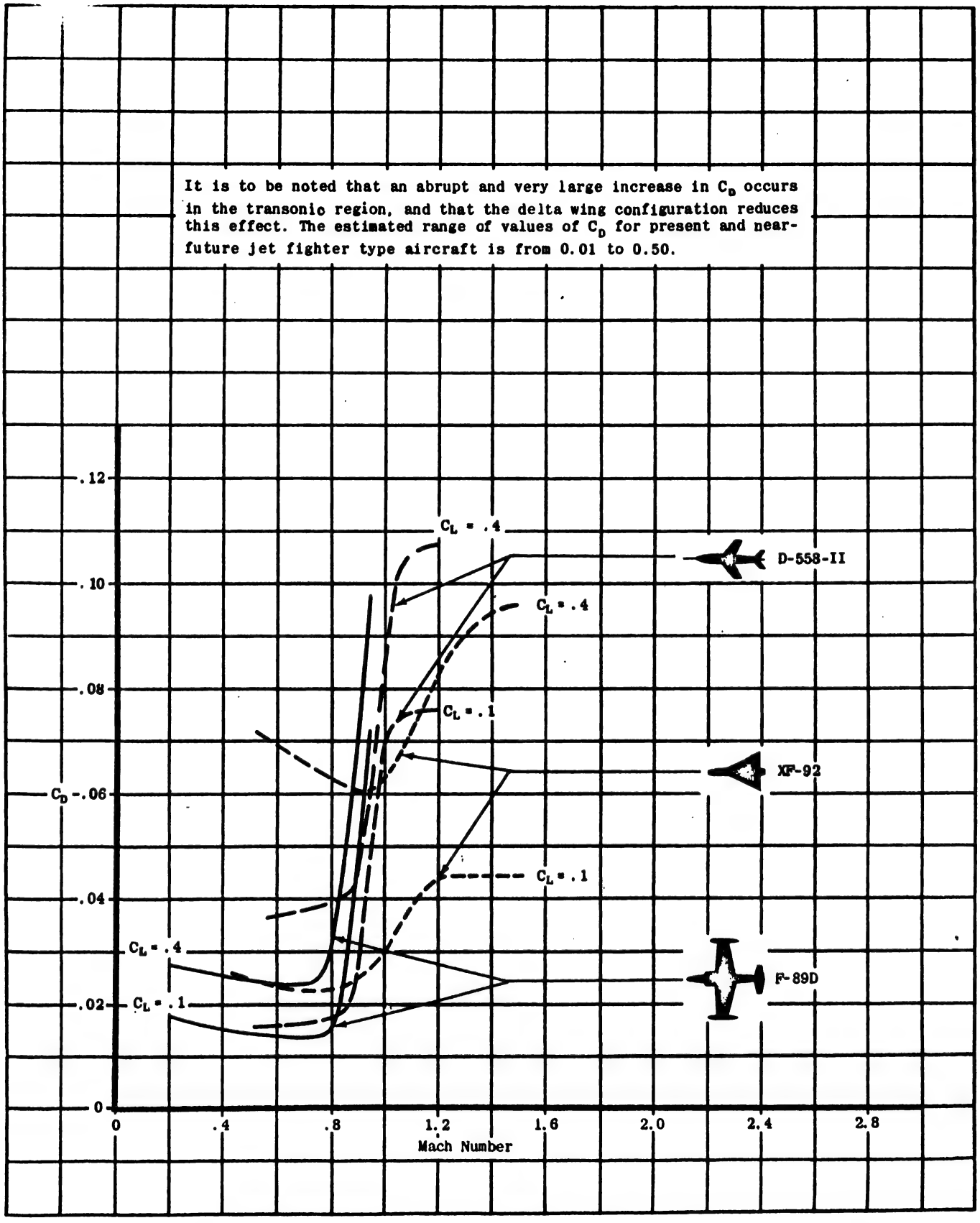

Figure A - 1 Variation of C_D with Mach Number for Several High Speed Jet Aircraft

It may be seen that C_{D_u} is approximately zero up to the critical Mach number region at which point it rises abruptly to large positive values, but that the abruptness of the rise and the magnitude which C_{D_u} attains are much less for the delta wing configuration. The estimated range of values of C_{D_u} for present and near-future jet fighter type aircraft is from - 0.01 to 0.50.

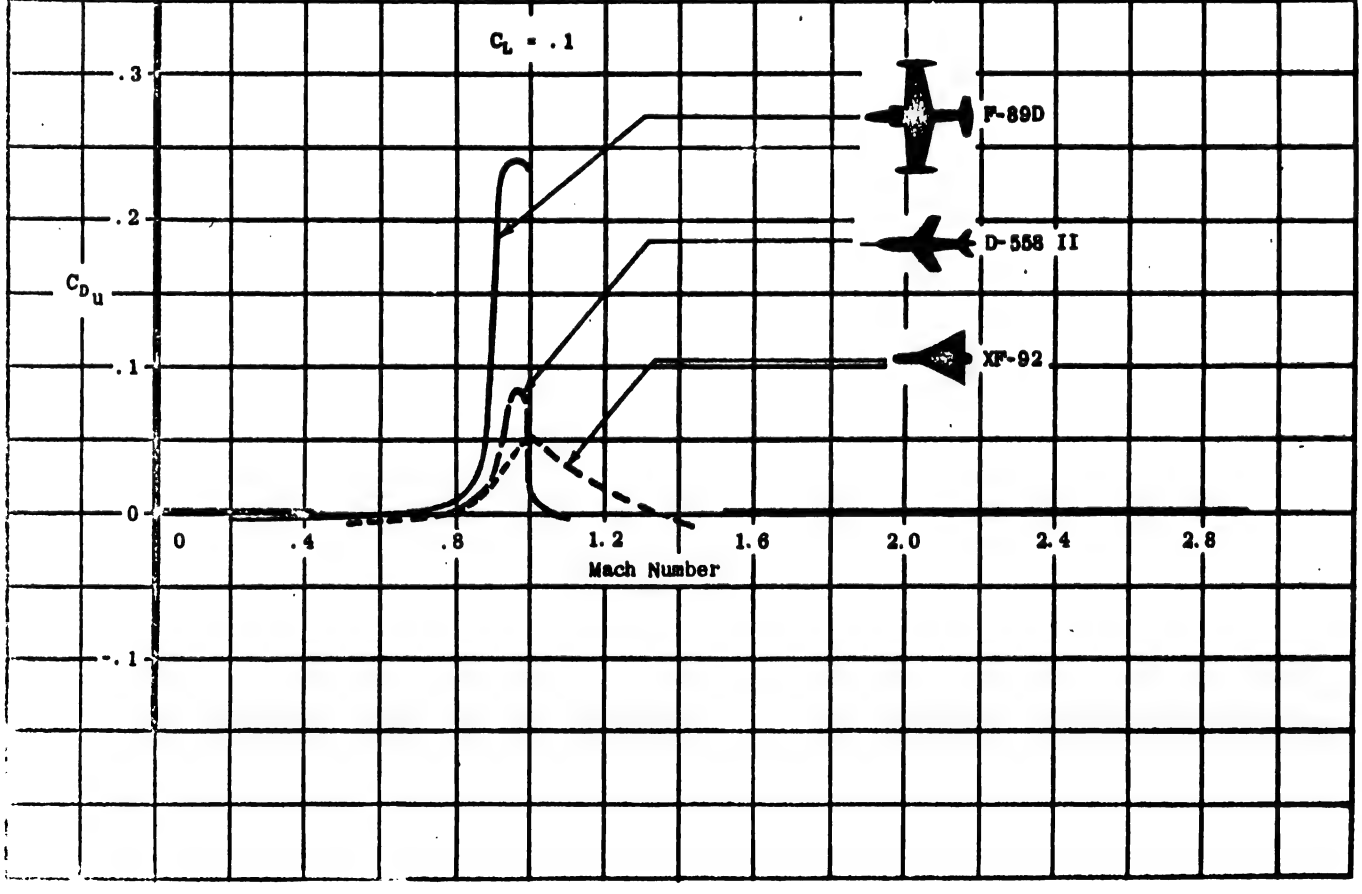

Figure A-2 Variation of C_{D_u} with Mach Number for Several High Speed Jet Aircraft

The values for all three airframe configurations show large variations with Mach number in the transonic region. The level of values in the low subsonic region is primarily a function of the equilibrium lift coefficient. The estimated range of values of C_{D_α} for present and near-future jet fighter type aircraft is from 0.02 to 0.20.

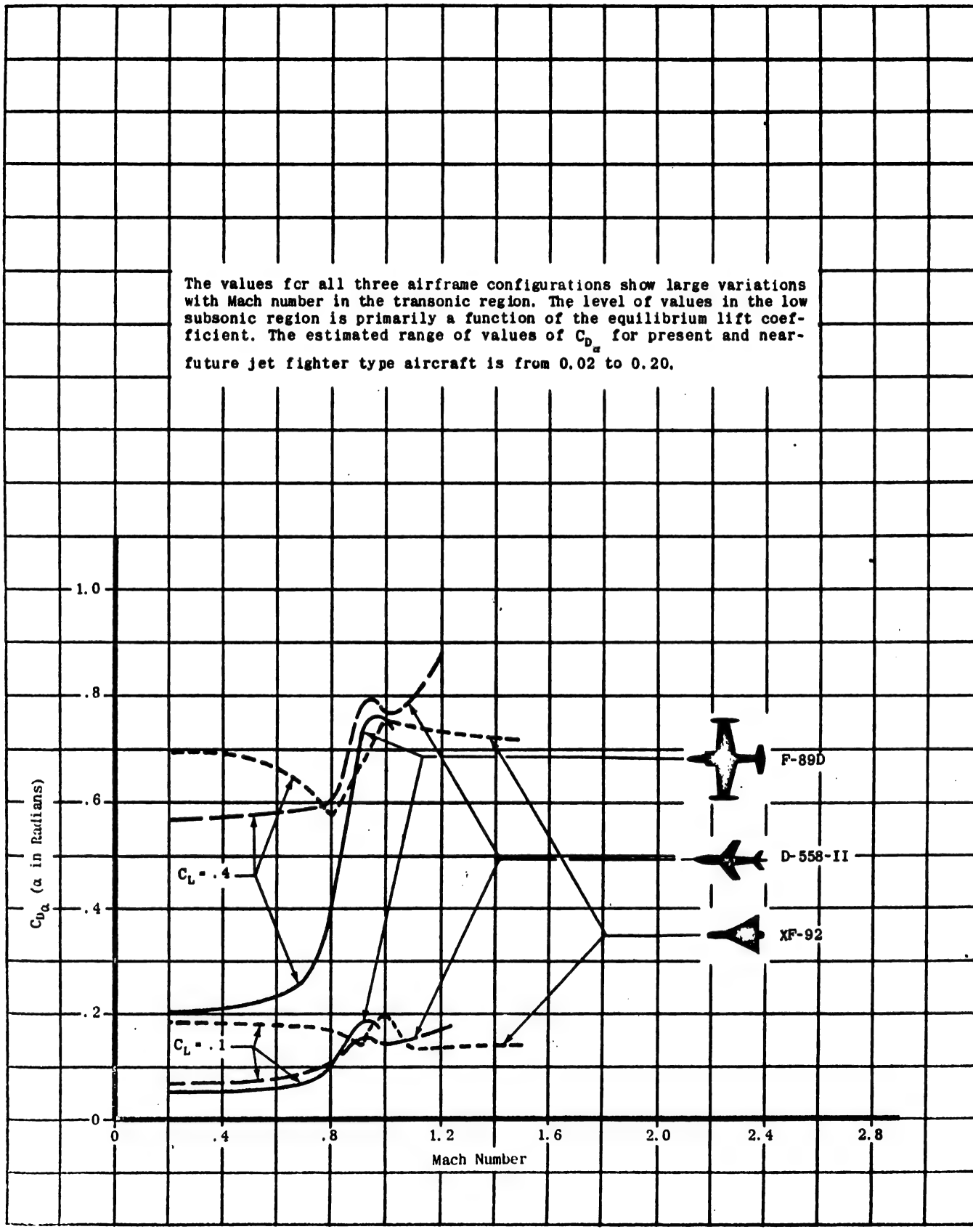

Figure A - 3 Variation of C_{D_α} with Mach Number for Several High Speed Jet Aircraft

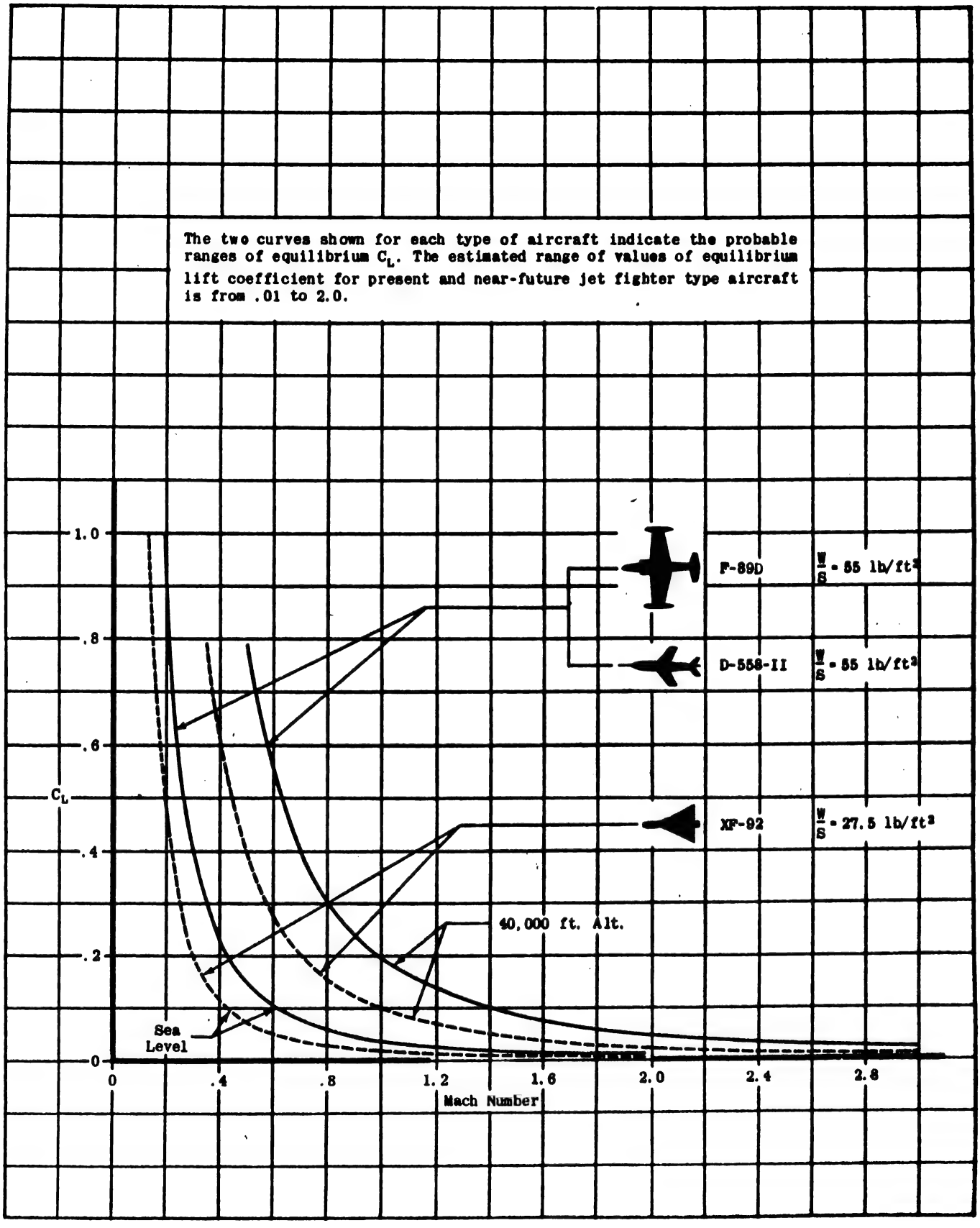

Figure A - 4 Variation of Equilibrium Lift Coefficient for Level Flight with Mach Number for Several High Speed Jet Aircraft

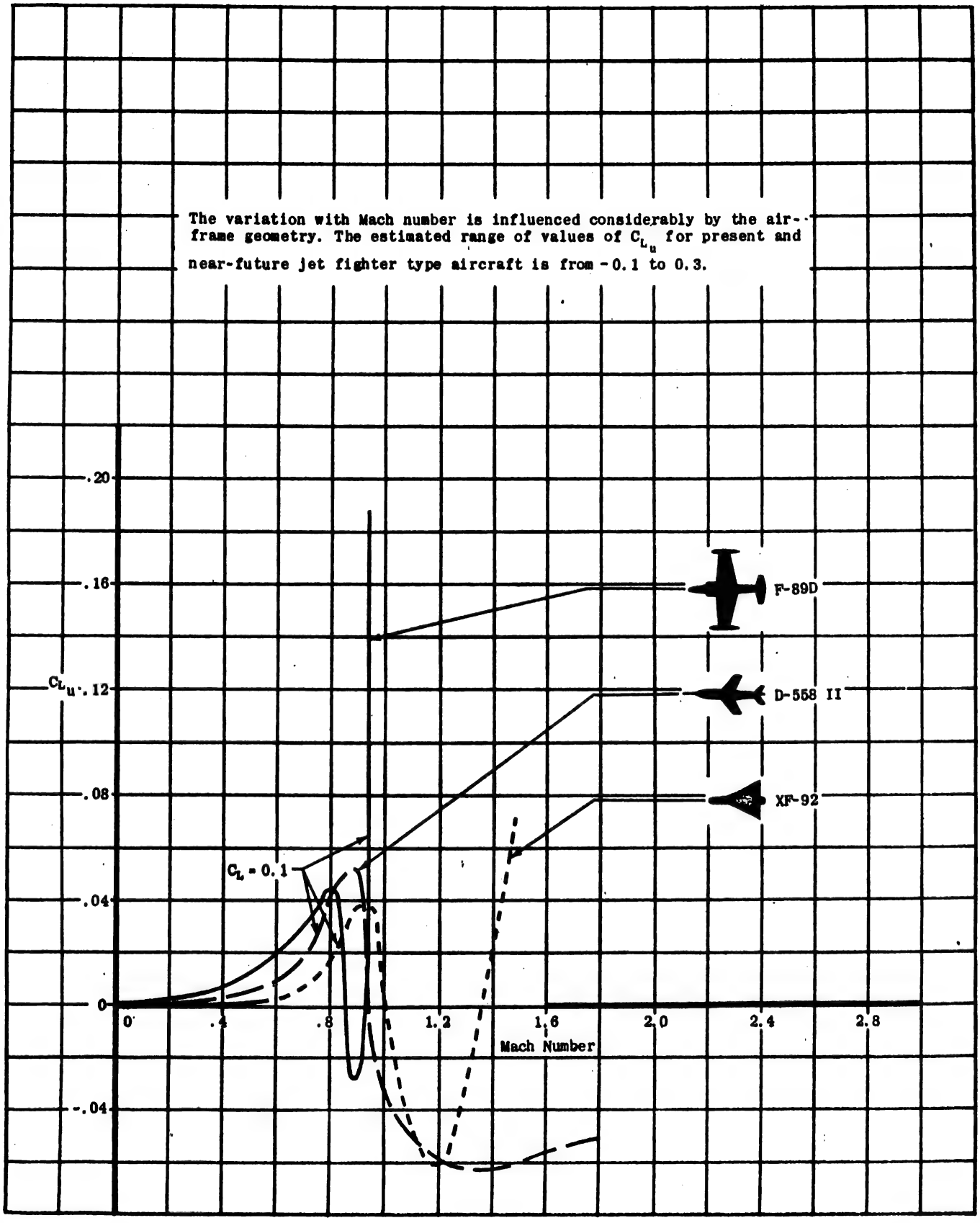

Figure A - 5 Variation of C_{L_u} with Mach Number for Several High Speed Jet Aircraft

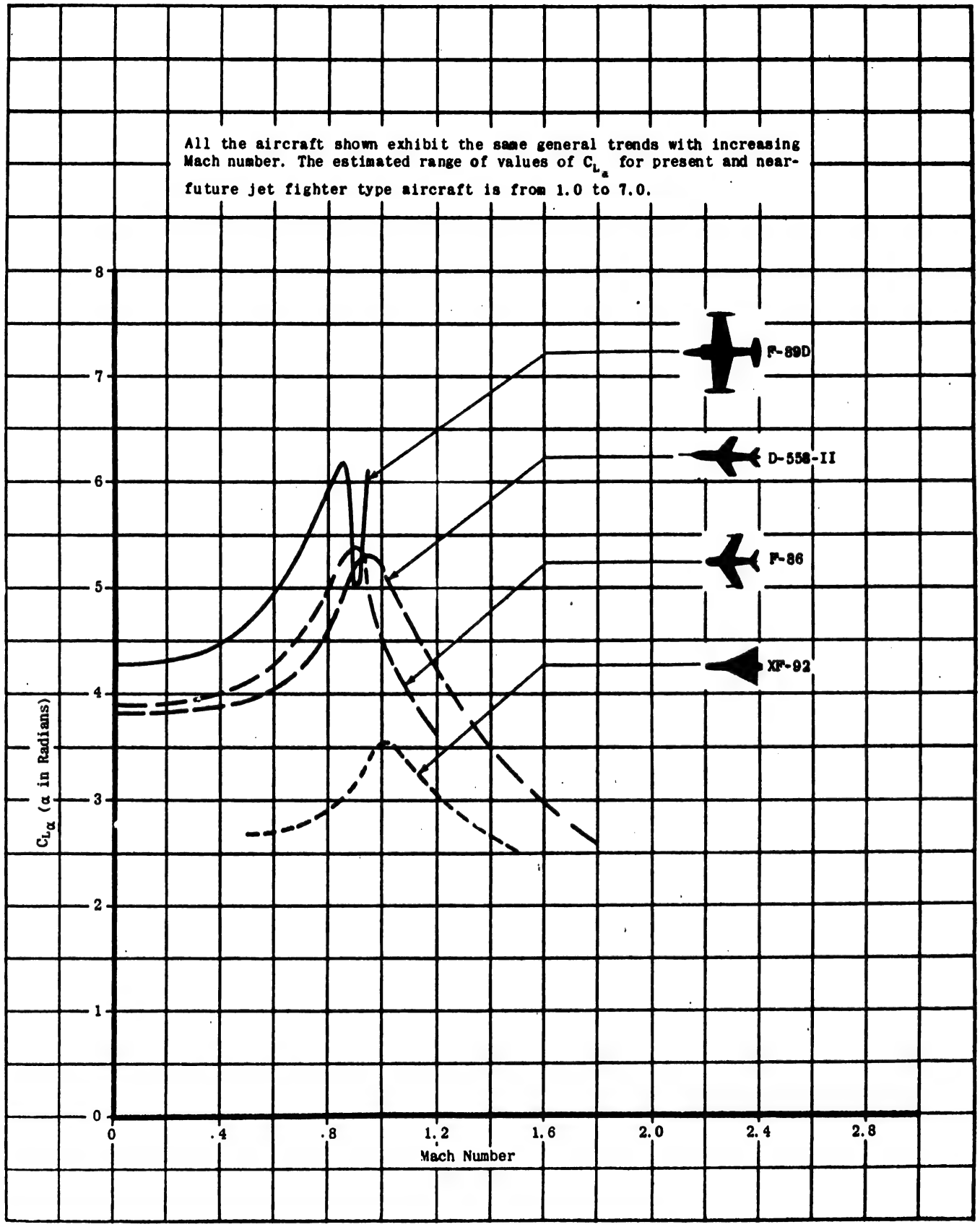

Figure A - 6 Variation of C_{L_α} with Mach Number for High Speed Jet Aircraft

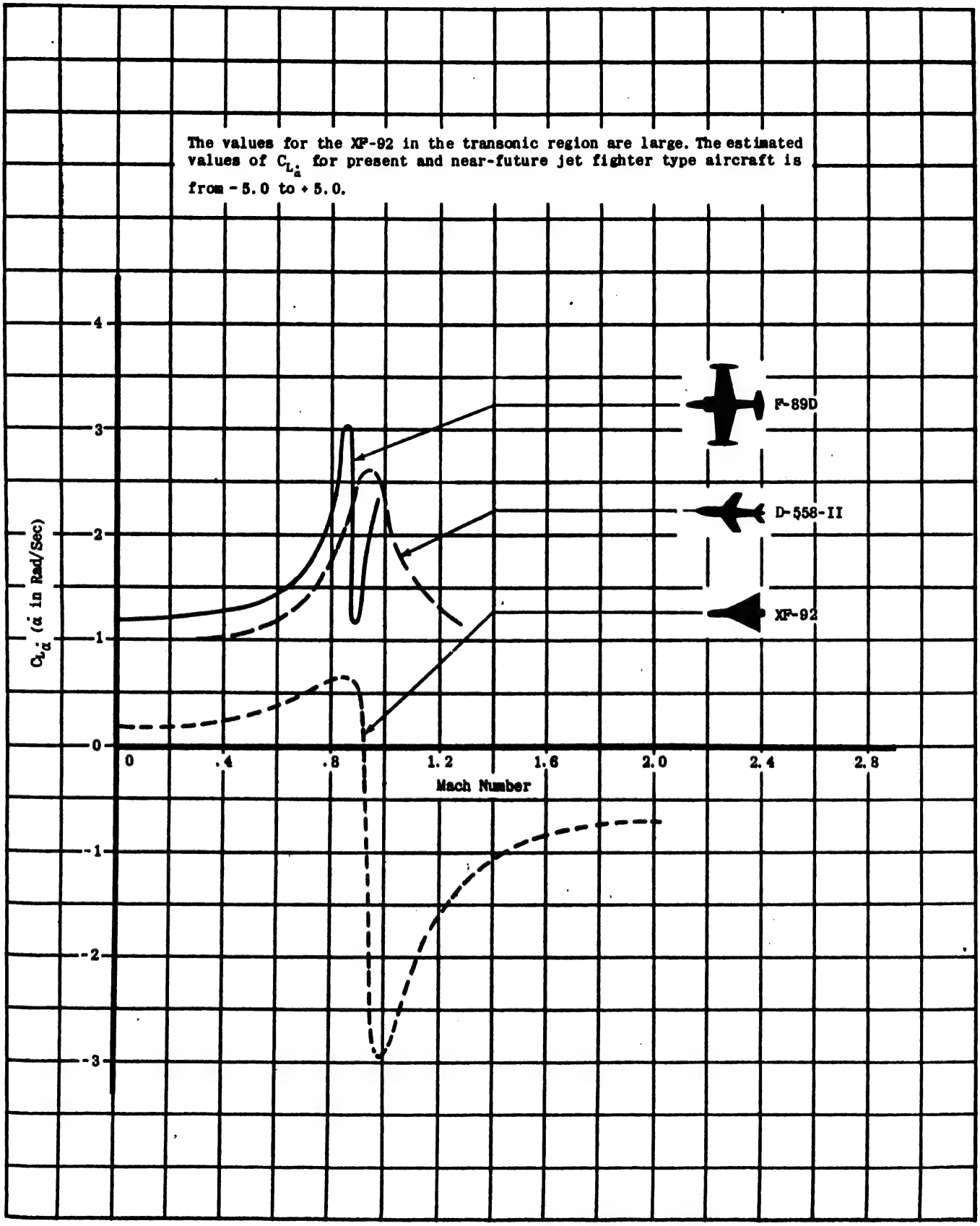

Figure A - 7 Variation of $C_{L_{\dot{\alpha}}}$ with Mach Number for Several High Speed Jet Aircraft

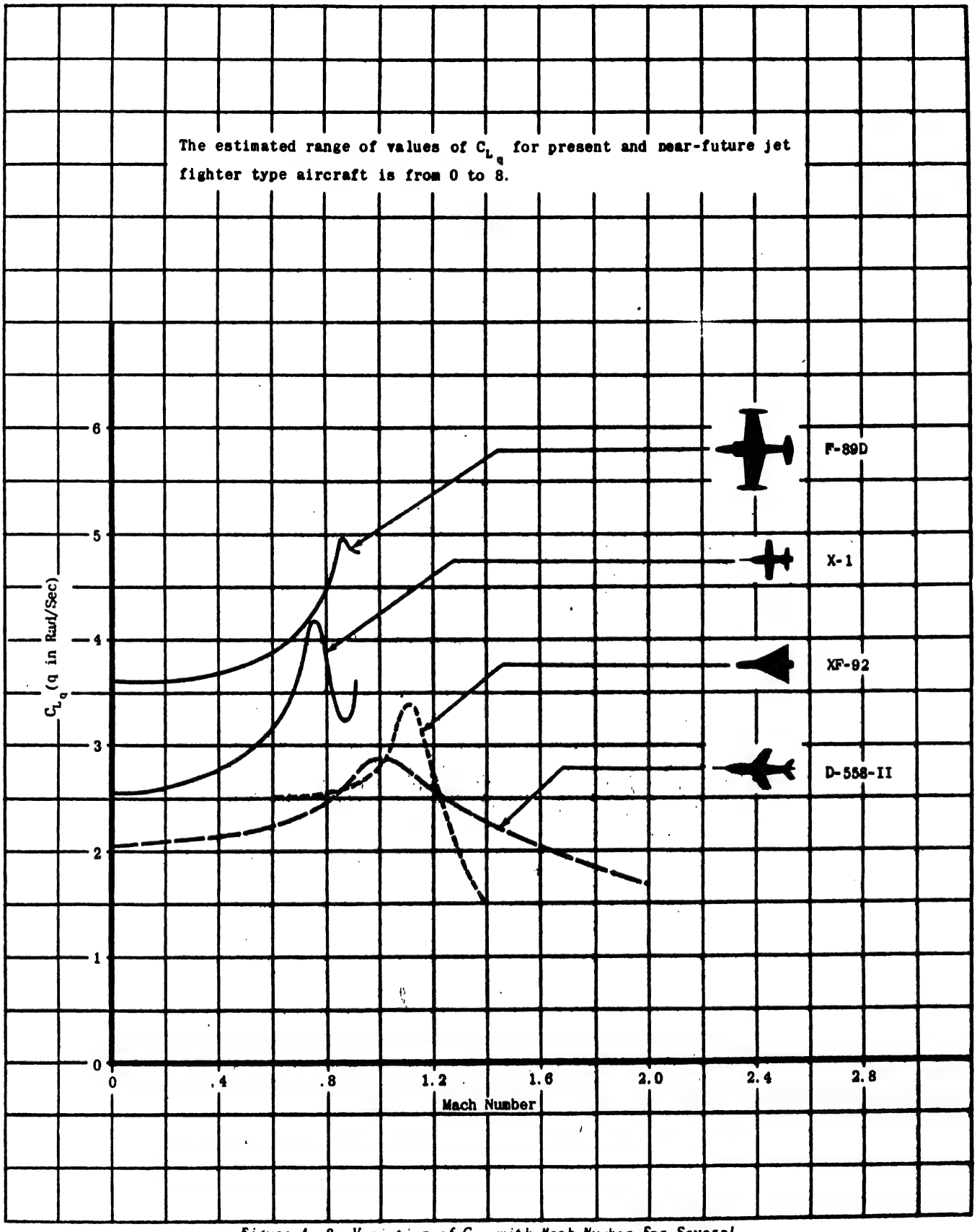

Figure A-8 Variation of C_{L_q} with Mach Number For Several High Speed Jet Aircraft

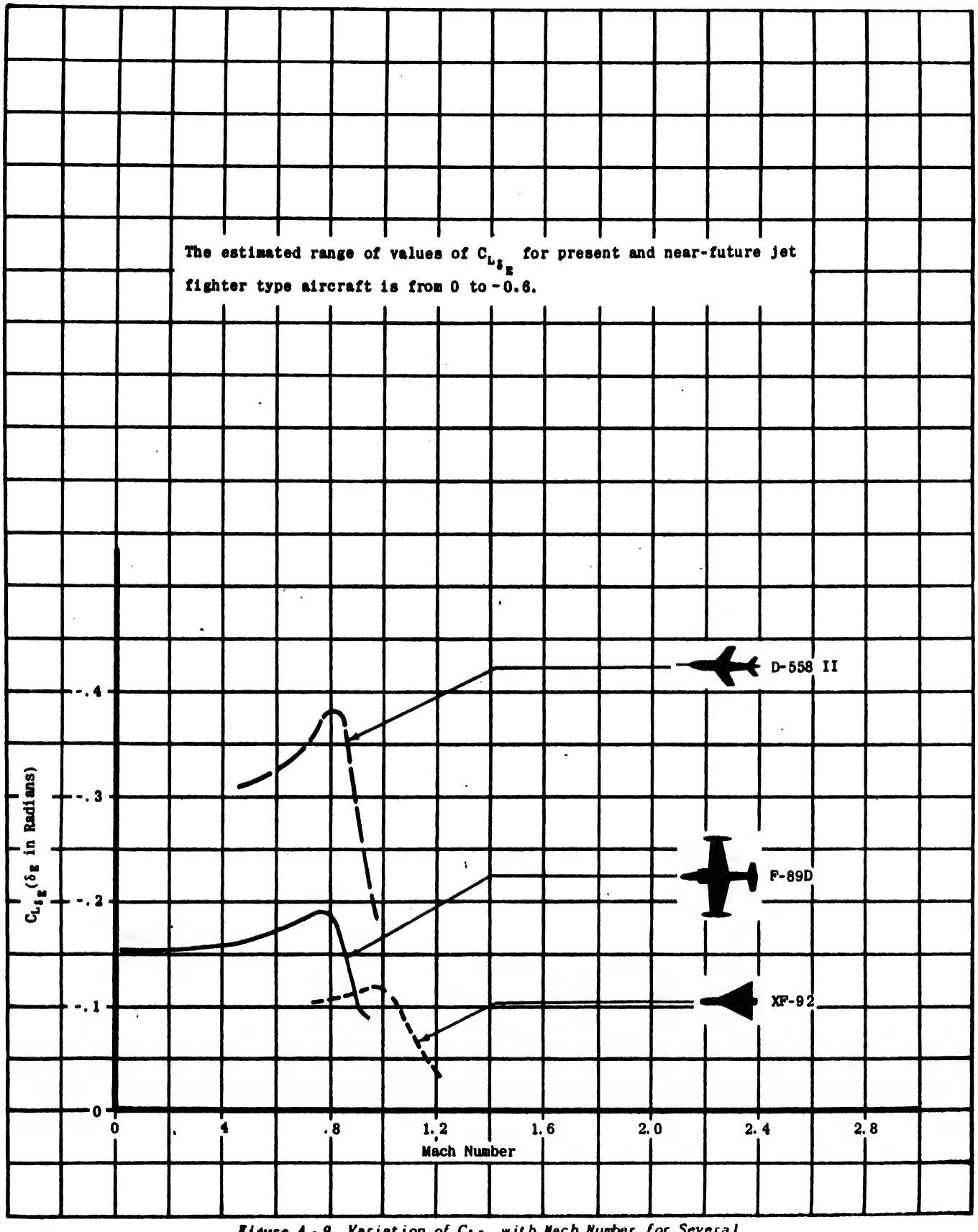

Figure A-9 Variation of $C_{L_{\delta_E}}$ with Mach Number for Several High Speed Jet Aircraft

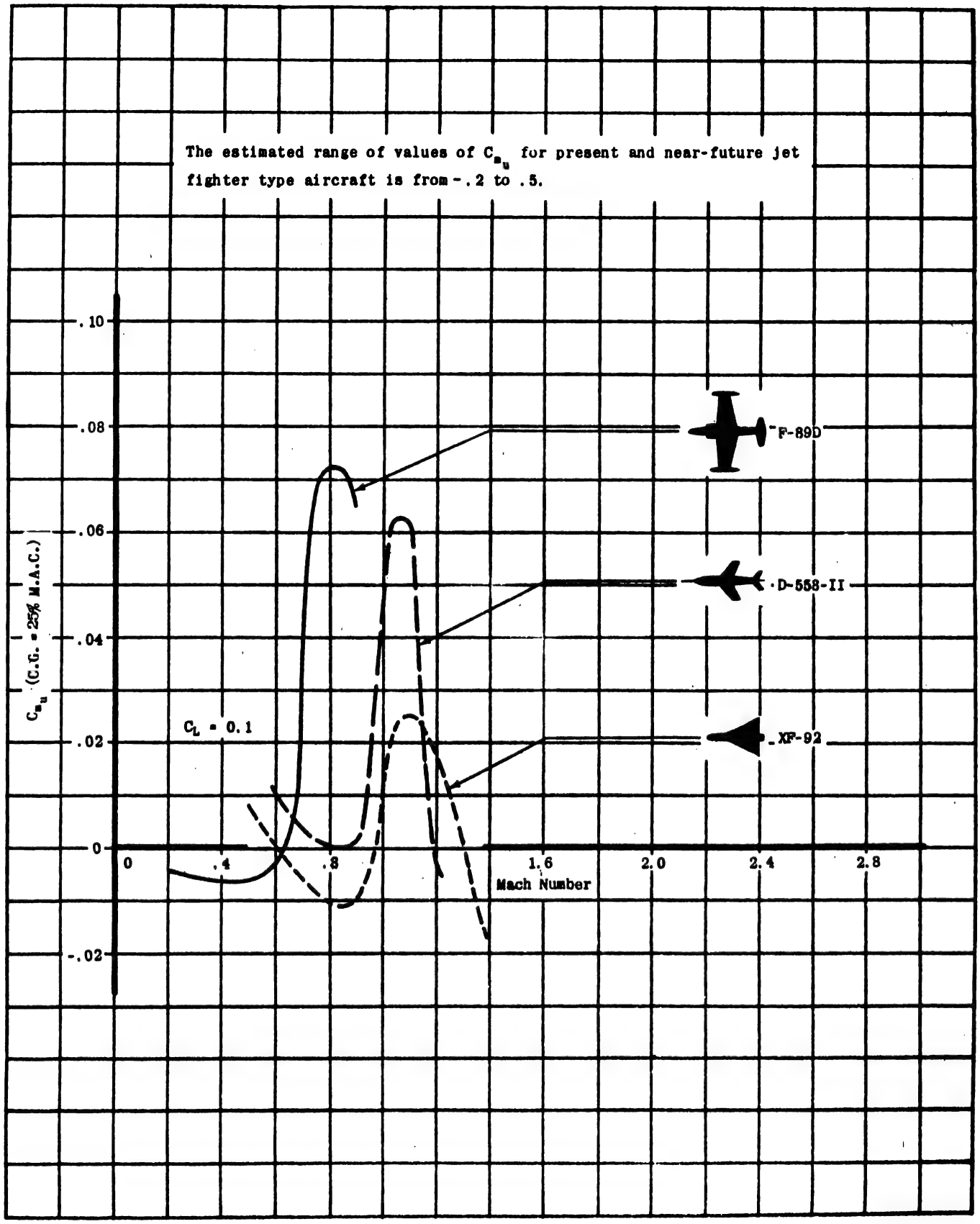

Figure A - 10 Variation of C_{m_u} with Mach Number for Several High Speed Jet Aircraft

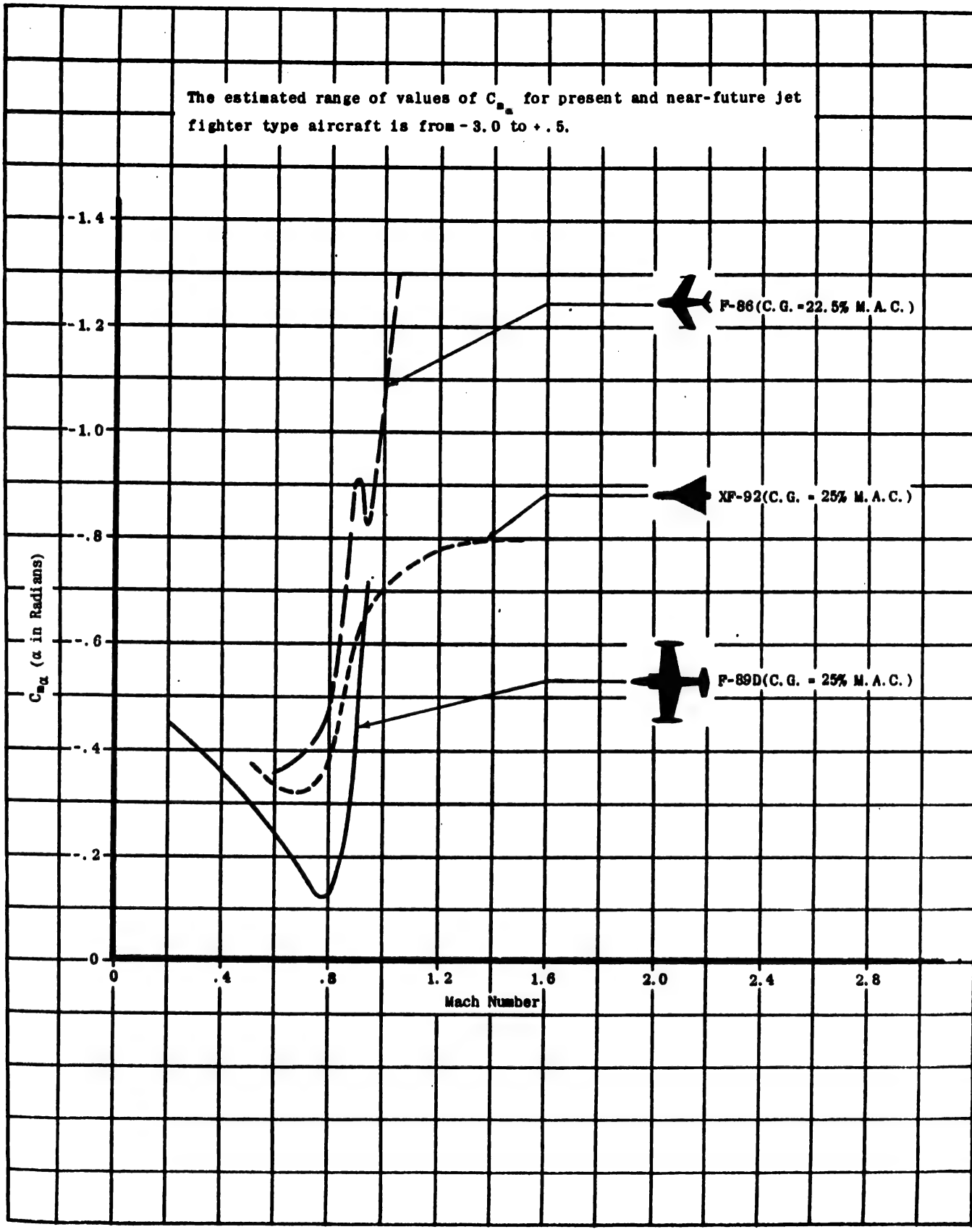

Figure A-11 Variation of C_{m_α} with Mach Number for Several High Speed Jet Aircraft

For the XF-92, positive values are attained in the transonic and supersonic region. Although data concerning the performance of the other airplanes in the transonic region are scarce, it is probable that some of these configurations would exhibit positive values also. The estimated range of values of $C_{m_{\dot{\alpha}}}$ for present and near-future jet fighter type

for present and near-future jet fighter type aircraft is from - 10 to +3.

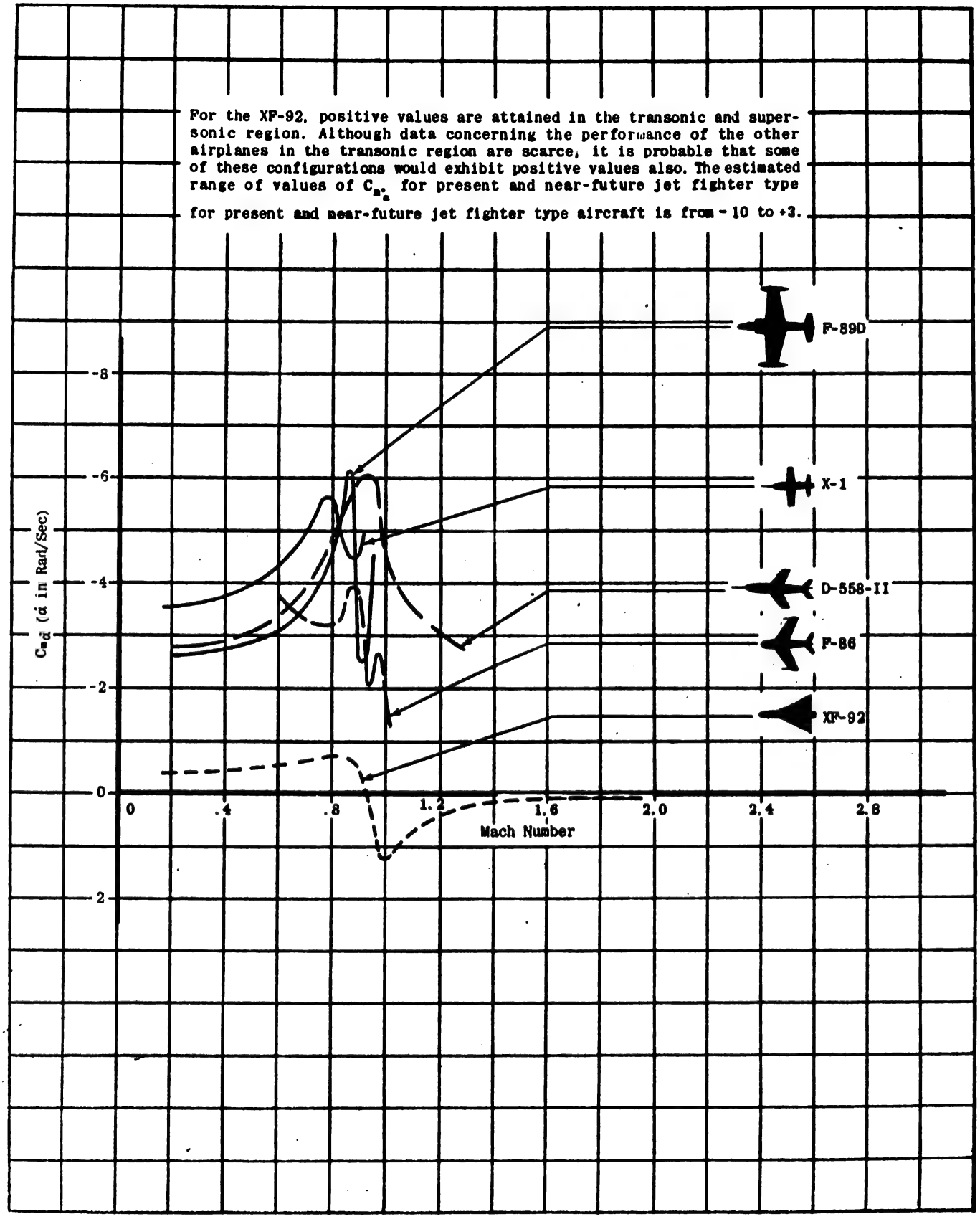

Figure A - 12 Variation of $C_{m_{\dot{\alpha}}}$ with Mach Number for Several High Speed Jet Aircraft

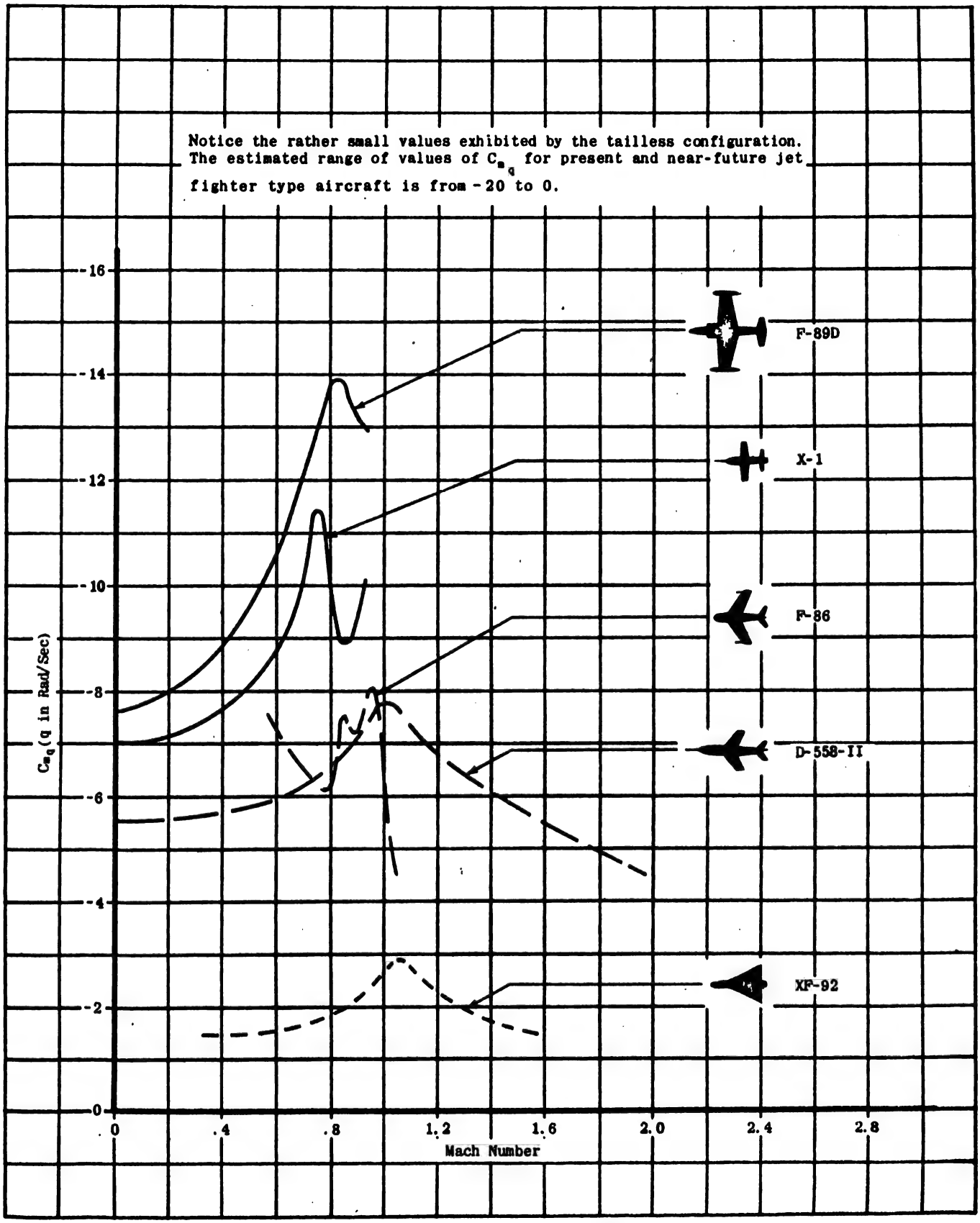

Figure A - 13 Variation of C_{m_q} with Mach Number for Several High Speed Jet Aircraft

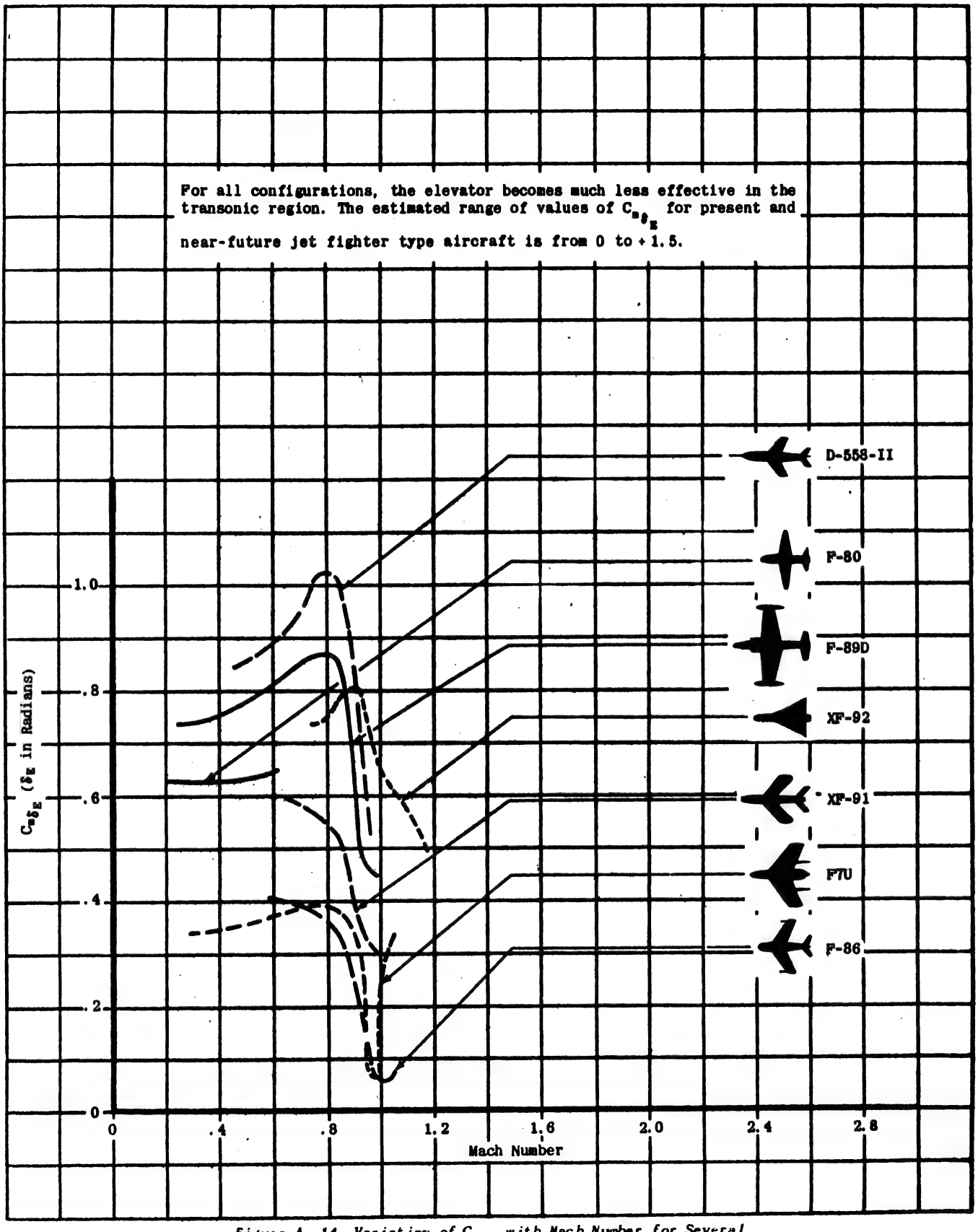

Figure A - 14 Variation of $C_{m_{\delta_E}}$ with Mach Number for Several High Speed Jet Aircraft

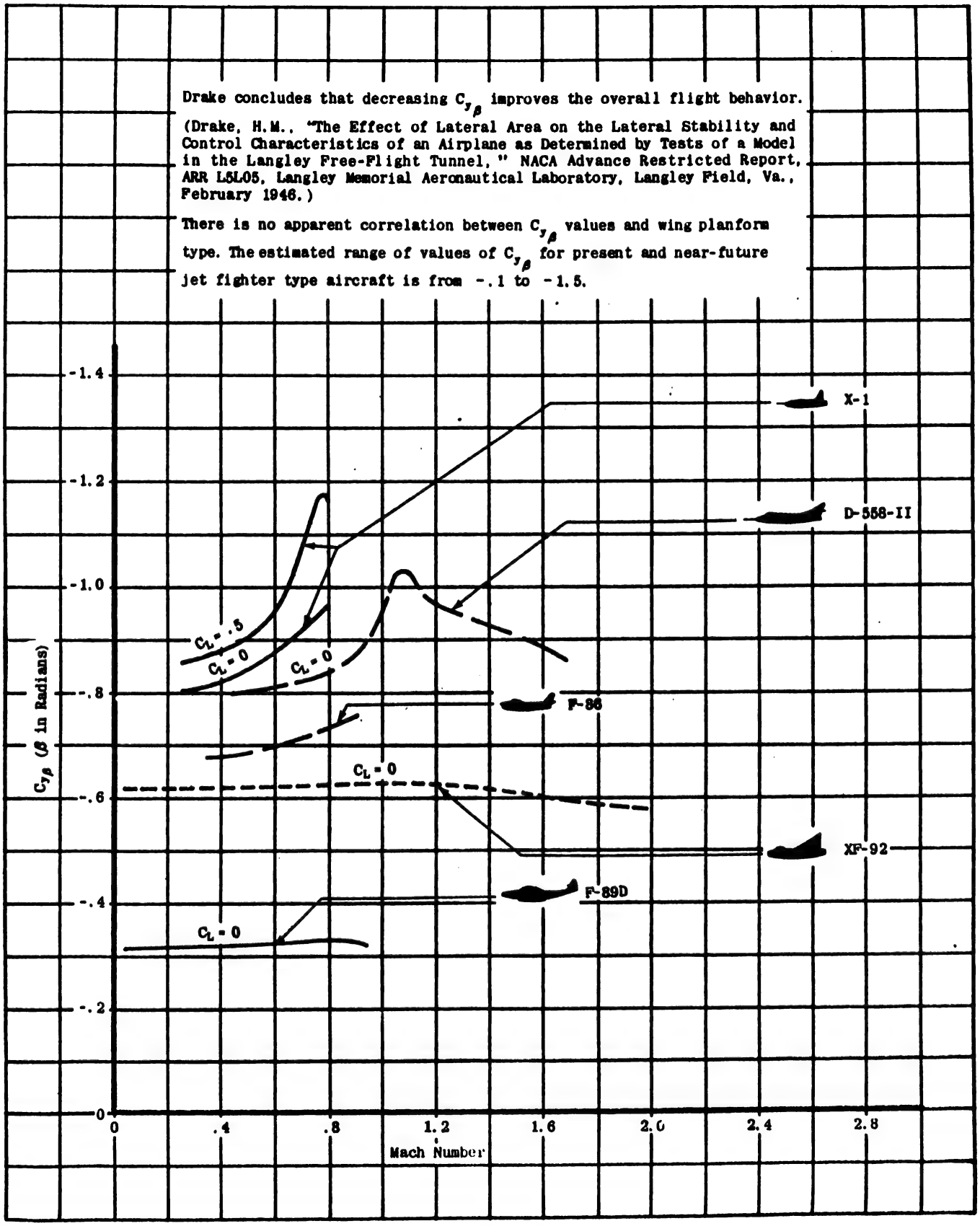

Figure A - 15 Variation of C_{y_β} with Mach Number for Several High Speed Jet Aircraft

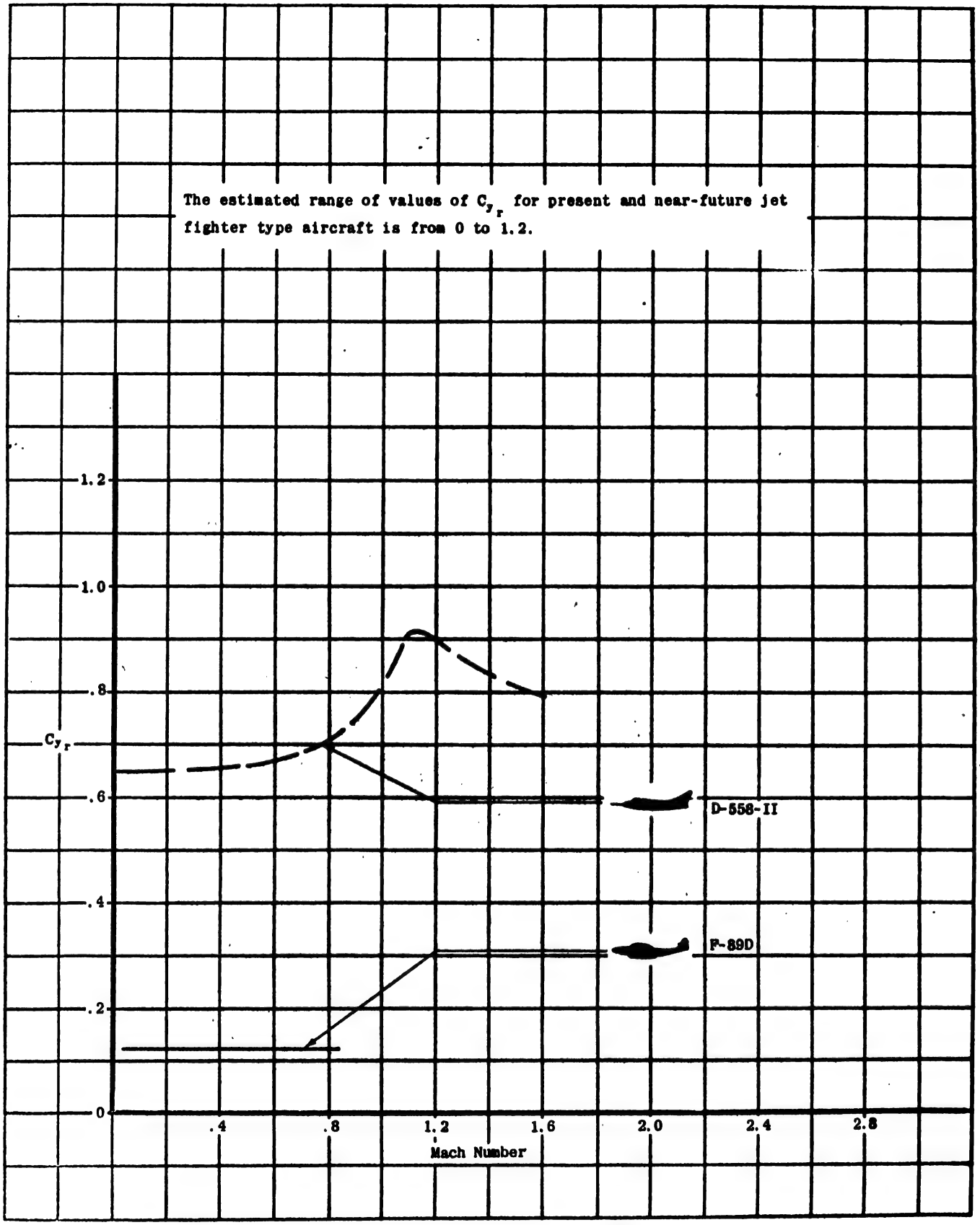

Figure A - 16 Variation of C_{y_r} with Mach Number for Several High Speed Jet Aircraft

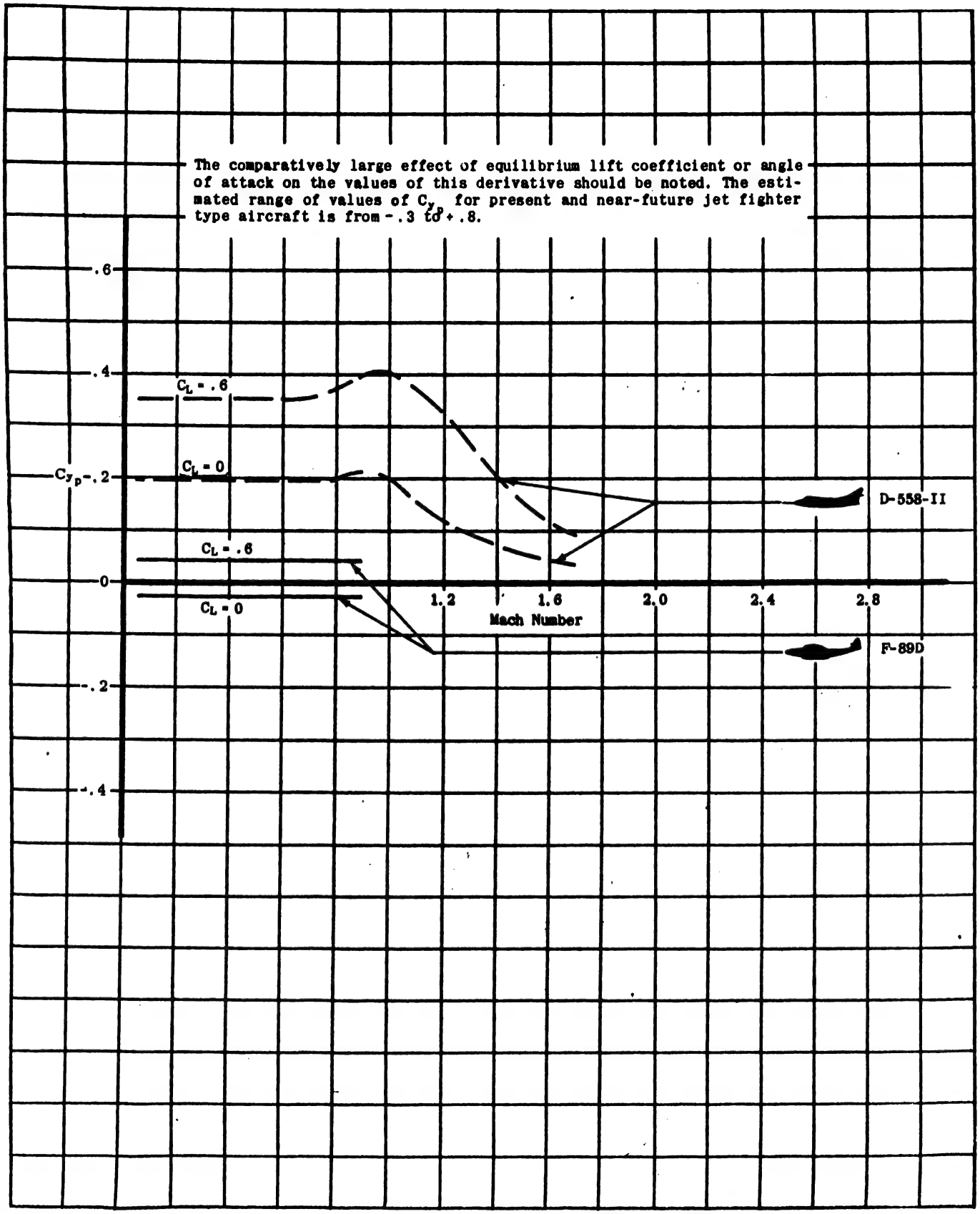

Figure A - 17 Variation of C_{y_p} with Mach Number for Several High Speed Jet Aircraft

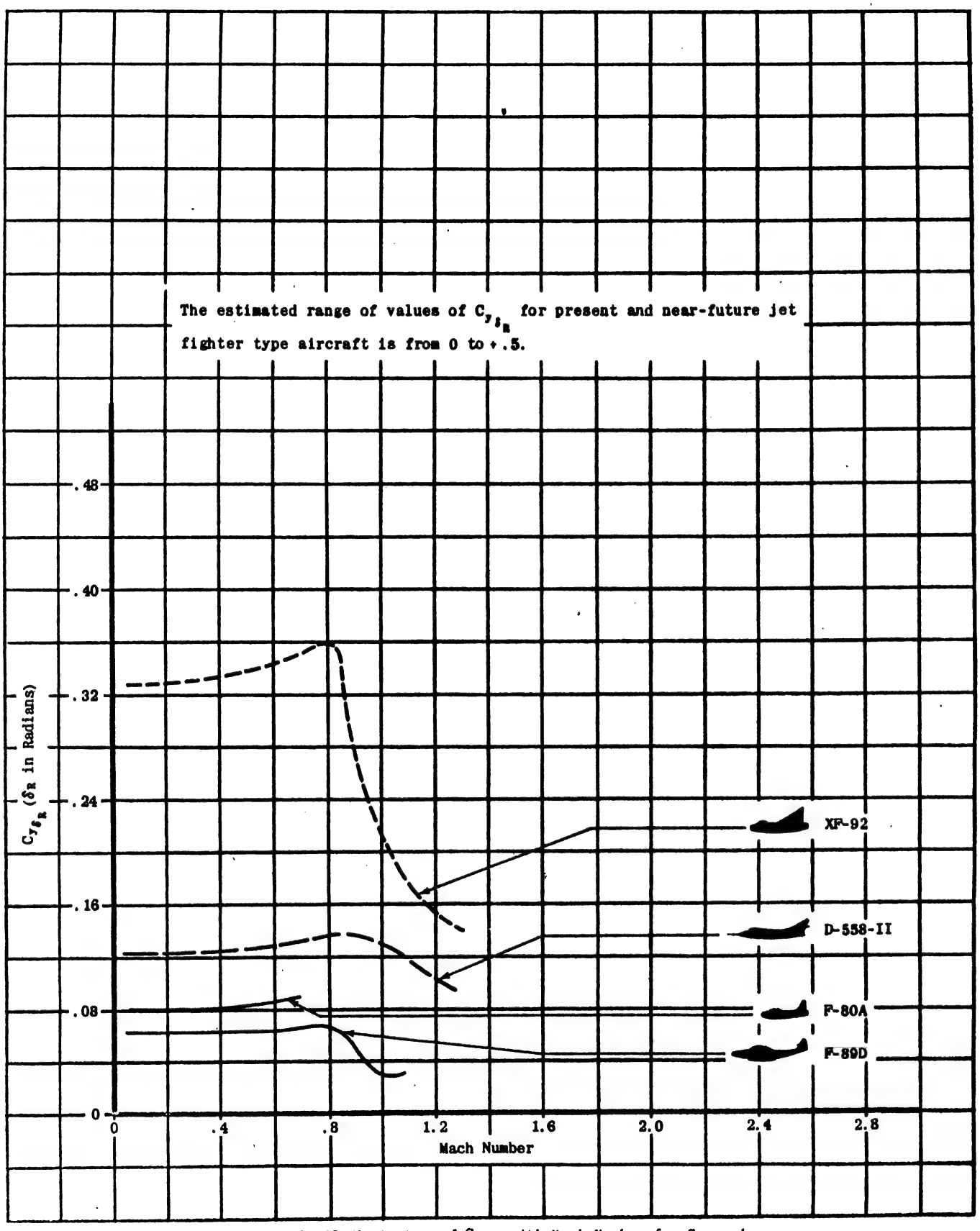

Figure A - 18 Variation of Cy_{δ_R} with Mach Number for Several High Speed Jet Aircraft

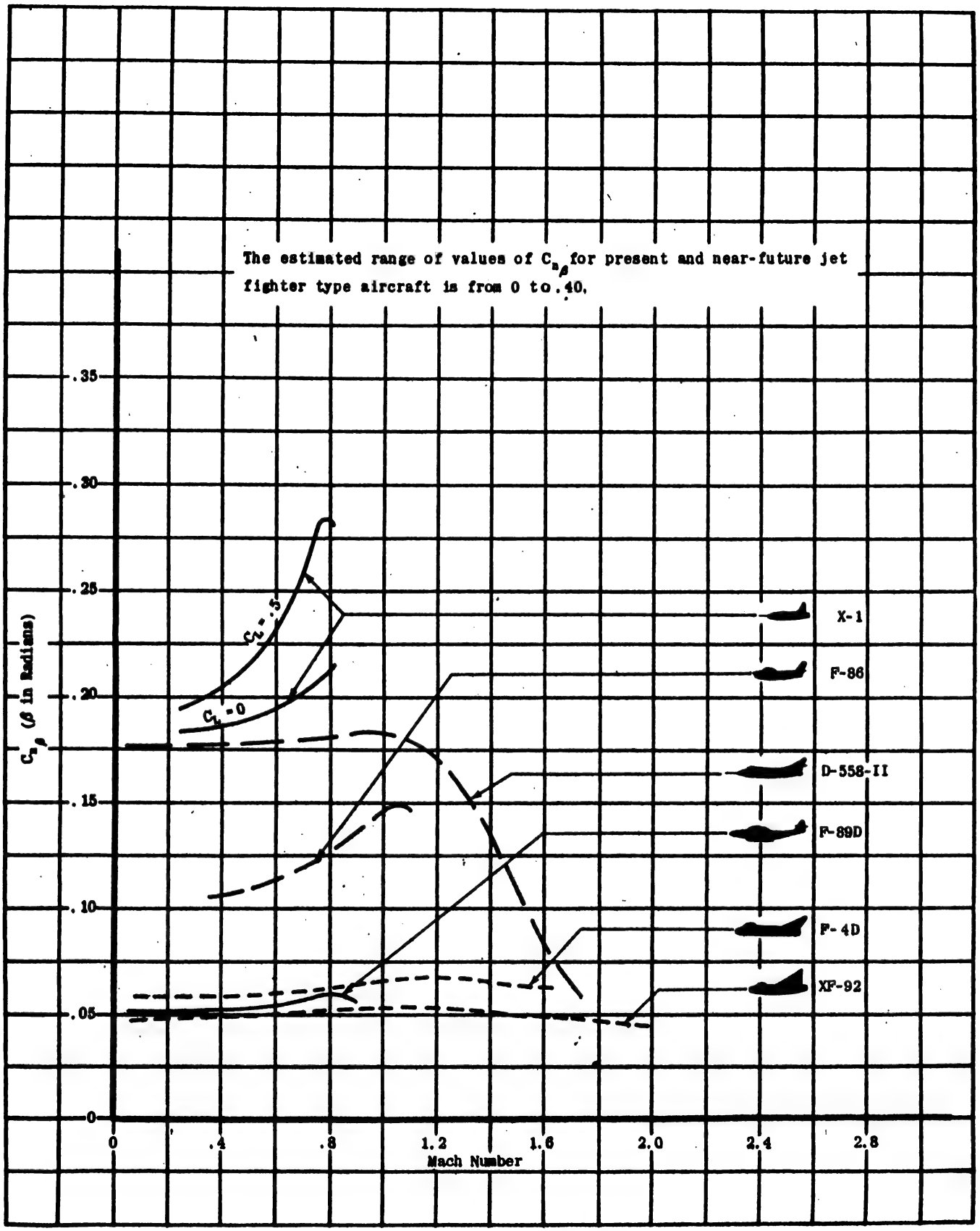

Figure A - 19 Variation of C_{n_β} with Mach Number for Several High Speed Jet Aircraft

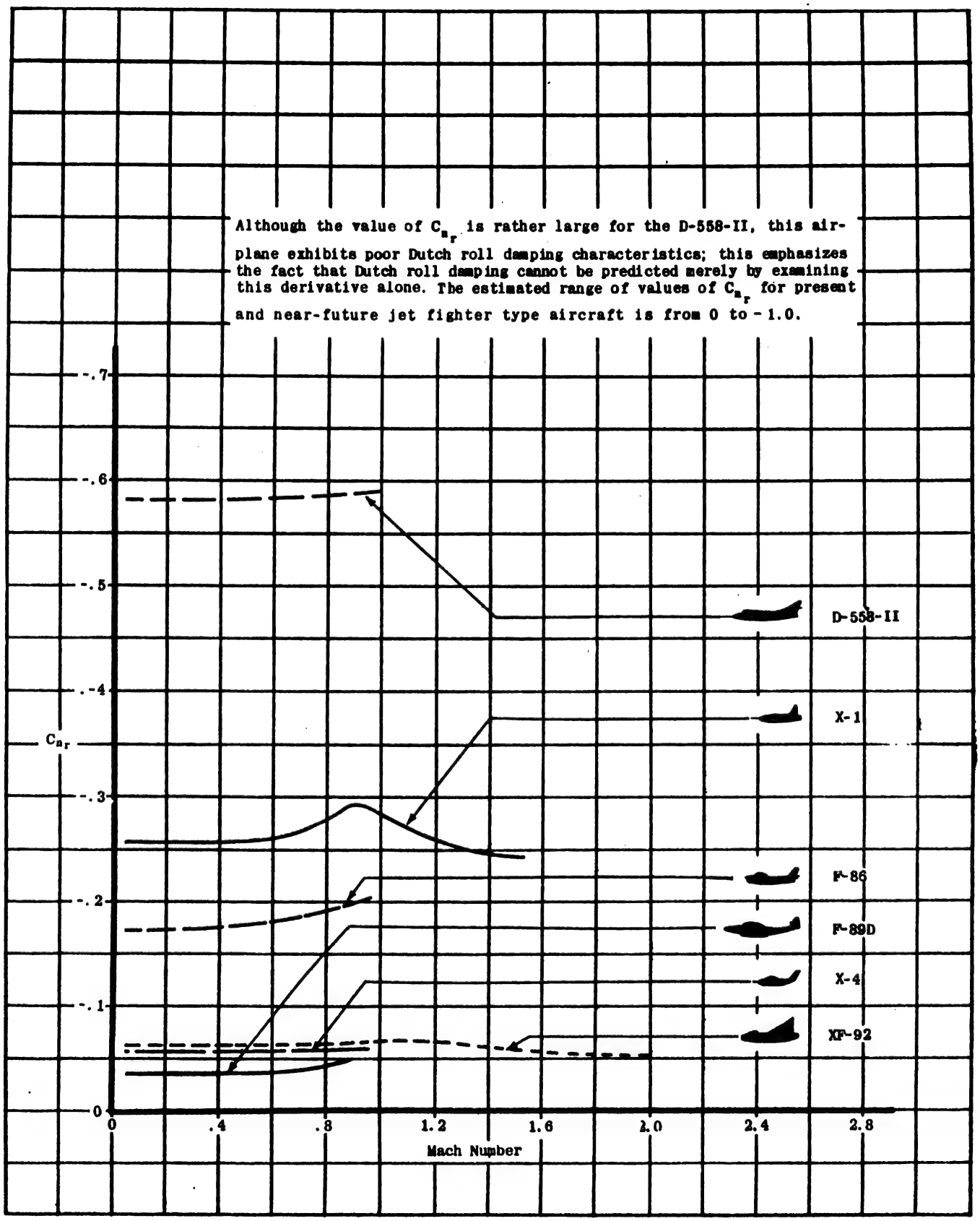

Figure A - 20 Variation of C_{n_r} with Mach Number for Several High Speed Jet Aircraft

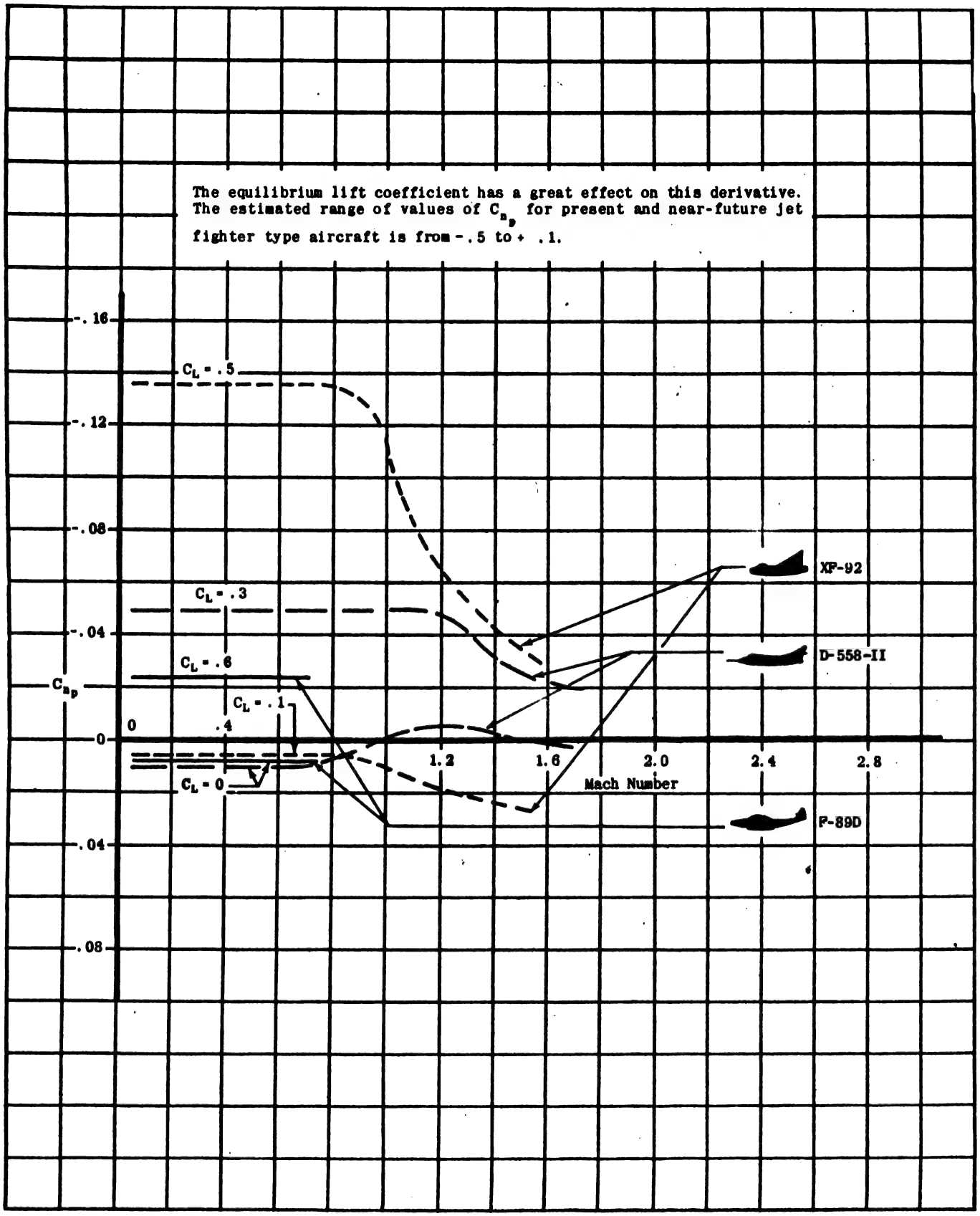

Figure A - 21 Variation of C_{n_p} with Mach Number for Several High Speed Jet Aircraft

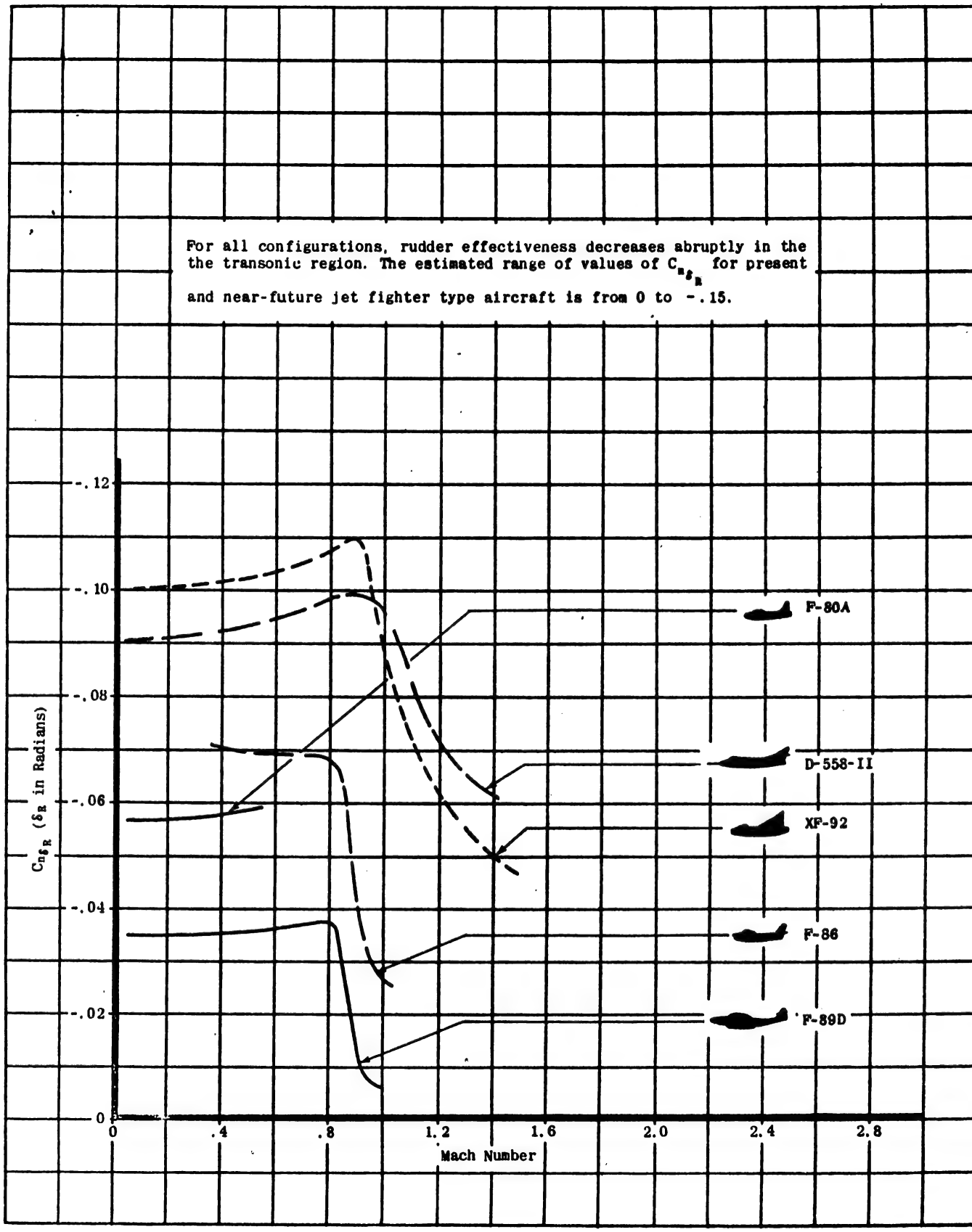

Figure A - 22 Variation of $C_{n_{\delta_R}}$ with Mach Number for Several High Speed Jet Aircraft

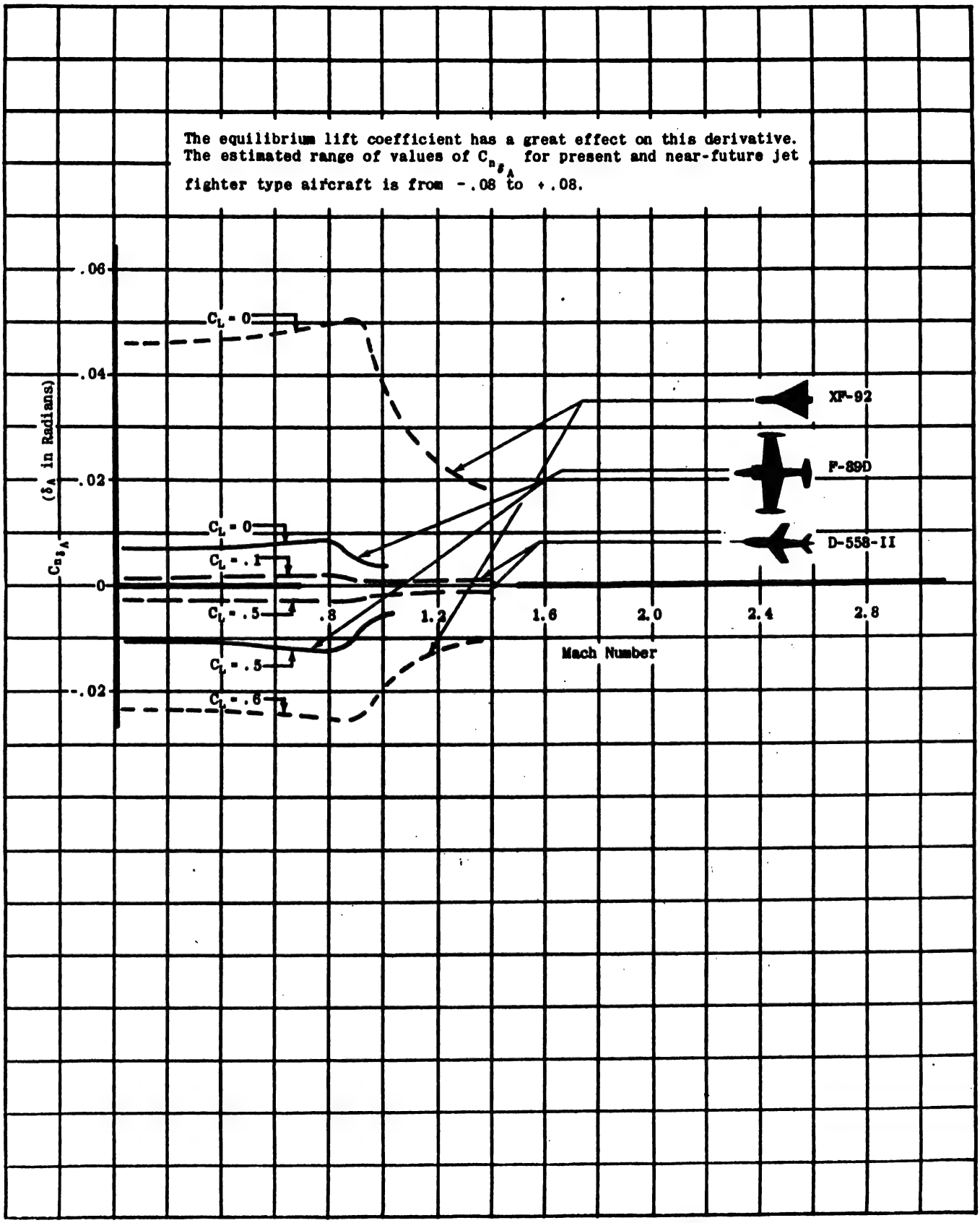

Figure A - 23 Variation of $C_{n_{\delta_A}}$ with Mach Number for Several High Speed Jet Aircraft

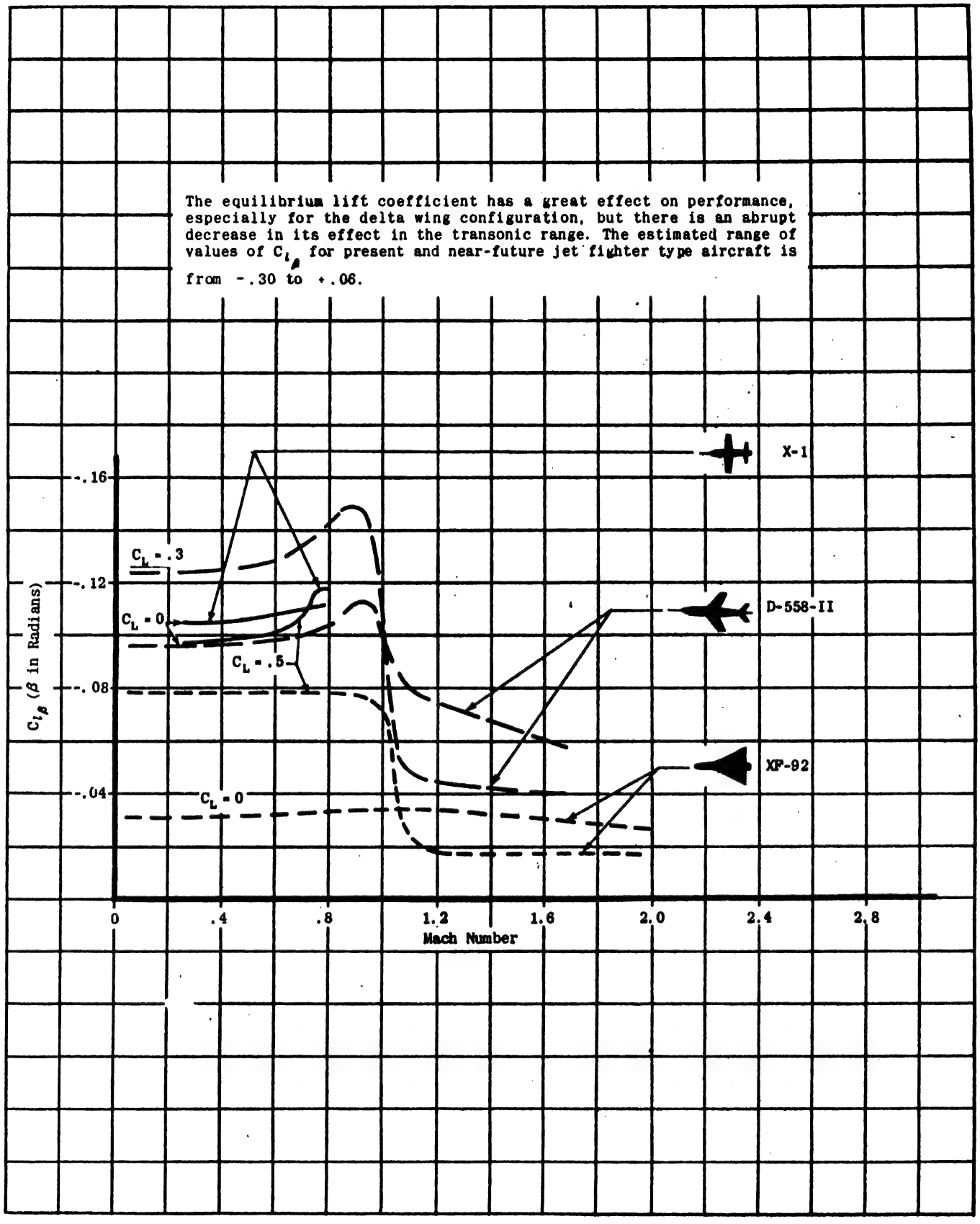

Figure A - 24 Variation of C_{l_β} with Mach Number for Several High Speed Jet Aircraft

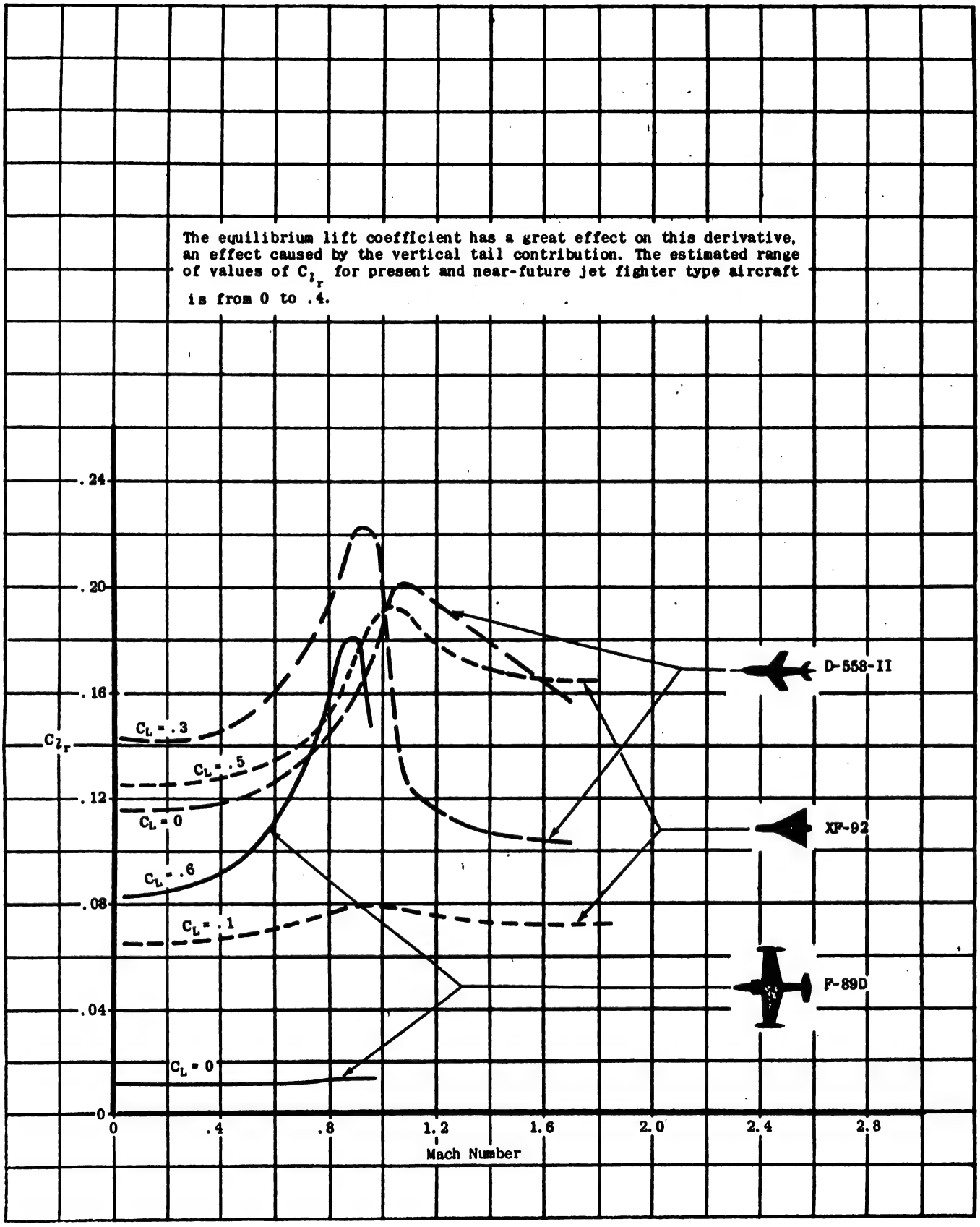

Figure A - 25 Variation of Cl_r with Mach Number for Several High Speed Jet Aircraft

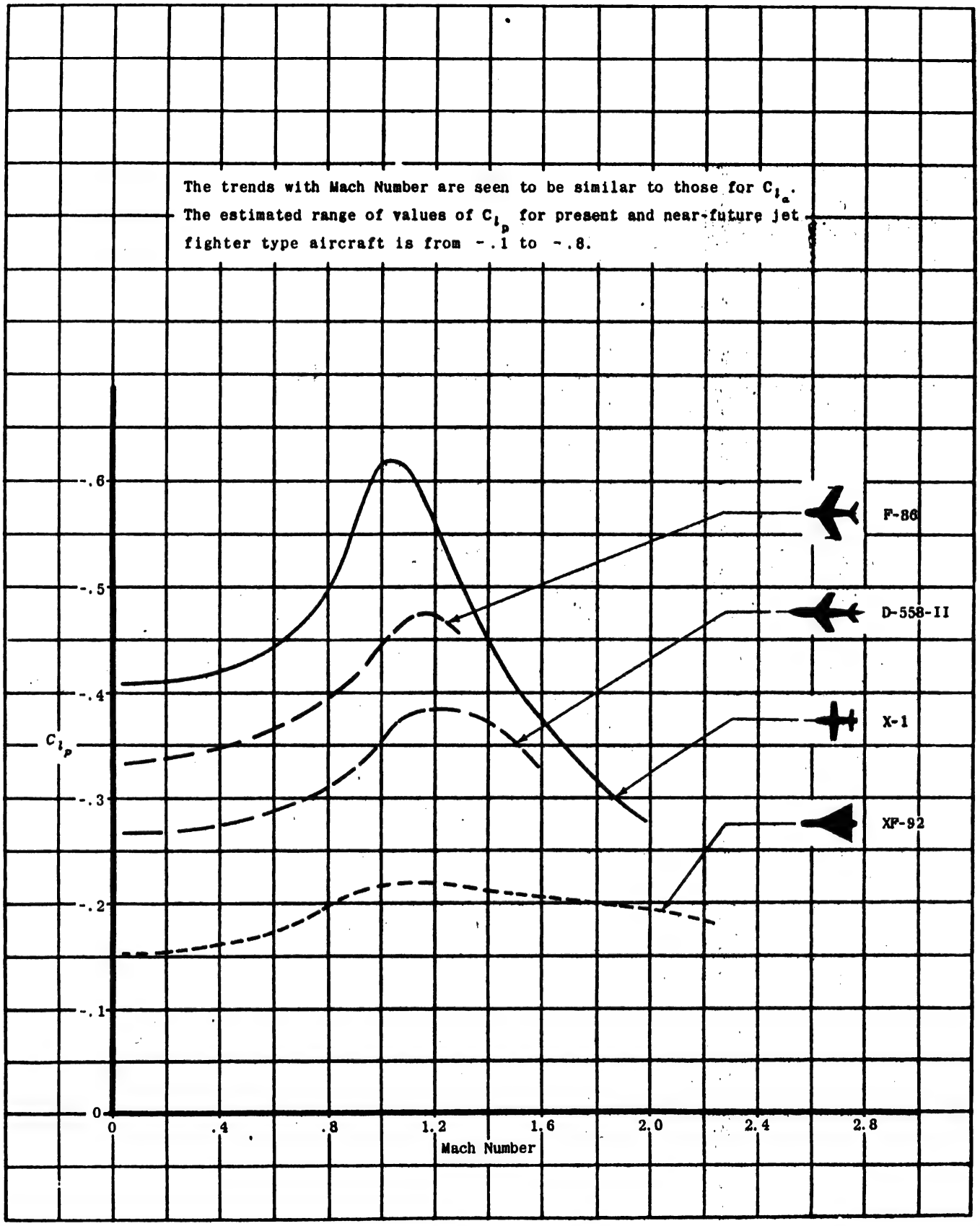

Figure A - 26 Variation of C_{l_p} with Mach Number for Several High Speed Jet Aircraft

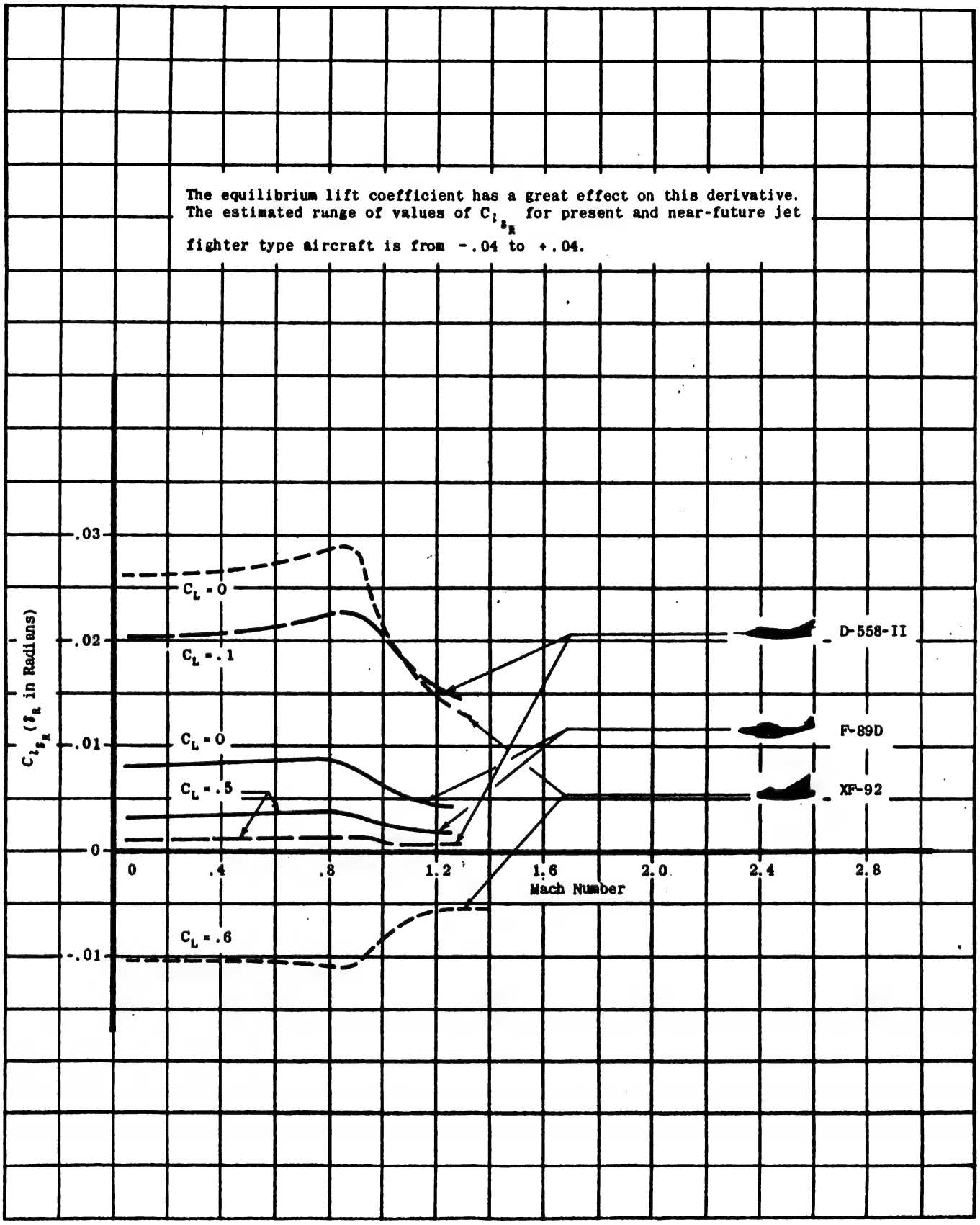

Figure A - 27 Variation of $C_{l_{\delta_R}}$ with Mach Number for Several High Speed Jet Aircraft

There is a considerable decrease in aileron effectiveness in the transonic region. Although not indicated in this figure, this decrease is more pronounced when aeroelastic effects are taken into account. The estimated range of values of $C_{l_{\delta_A}}$ for present and near-future jet fighter type aircraft is from 0 to .30.

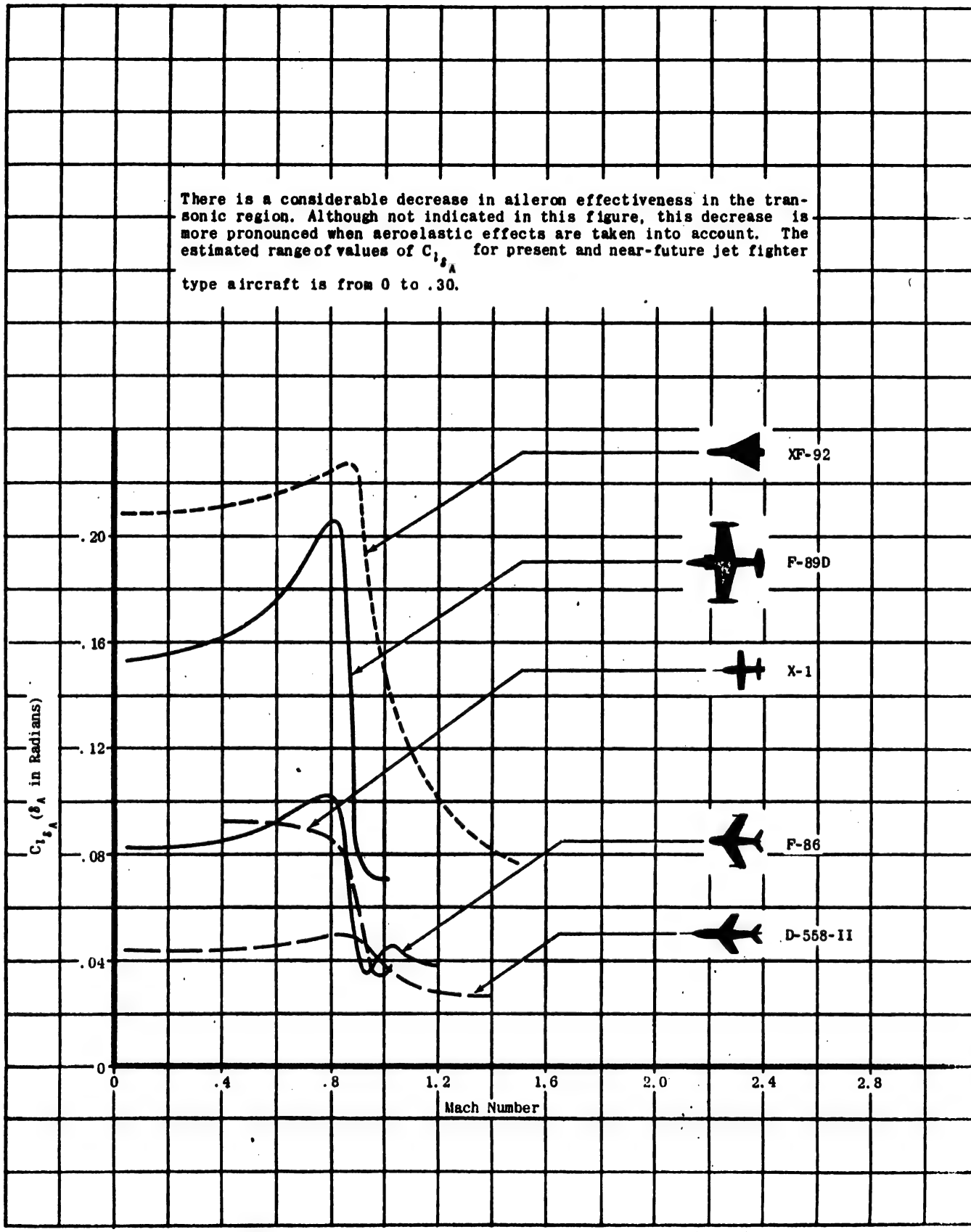

Figure A - 28 Variation of $C_{l_{\delta_A}}$ with Mach Number for Several High Speed Jet Aircraft

Bureau of Aeronautics

FLIGHT CONTROL SYSTEM MANUALS

VOL. I, "METHODS OF ANALYSIS AND SYNTHESIS OF PILOTED AIRCRAFT FLIGHT CONTROL SYSTEMS" AE-61-1 Navy No. 1 (251 pages, 459 figures; $4.00)

Chapters – Fundamental Concepts, Analysis, Synthesis, Optimum Synthesis Methods, Non-linearities, Machine Methods, Analog Computer, Mathematical Background.

VOL. II, "DYNAMICS OF THE AIRFRAME" AE-61-4 II (185 pages, 178 figures; $4.25) Addendum to Vol. II (27 figures; $1.50)

Chapters – Derivation of the Airframe Transfer Functions, Discussion of Transfer Functions, Discussion of Stability Derivatives, Methods of Obtaining Stability Derivatives.

VOL. III, "THE HUMAN PILOT" AE-61-4 III (157 pages, 55 figures; $3.50)

Chapters – Fundamental Aspects – Sensing and Actuating Processes of a Human Pilot, Approximate Methods Predicting Responses of a Human Pilot.

VOL. IV, "THE HYDRAULIC SYSTEM" AE-61-4 IV (224 pages, 63 figures; $4.25)

Chapters – General Considerations, Analysis of the Generalized Hydraulic Servo Actuator, A Generalized Hydraulic Control System, The Fully Powered Hydraulic Control System, The Power Boost Hydraulic Control System, Special Considerations in Hydraulic Control System Design and Analysis, Component Design Factors, Influence of Servomechanisms on the Flutter of Servo-Controlled Aircraft, Methods of Analysis of Servo Flutter Interaction.

VOL. V, "THE ARTIFICIAL FEEL SYSTEM" AE-61-4- V (152 pages, 103 figures; $3.00)

Chapters – The Control Feel Problem, Design Procedure, Design Criteria.

VOL. VI, "AUTOMATIC FLIGHT CONTROL SYSTEMS FOR PILOTED AIRCRAFT" AE-61-4 VI (339 pages, 138 figures; $6.00)

Chapters – Automatic Flight Control Systems Past and Present, Components of Automatic Flight Control Systems, Design Methods, Systems Engineering and Other Design Considerations, Appendix.

The volumes listed above complete the series of Flight Control System Manuals presently available, and are identical in content to the original contract publications.

To order one or more of these volumes, contact:

NORAIR, 1001 E. Broadway, Hawthorne, Calif.
Attn: Dept. 3730